4-19-2012 12:00 AM

Mass Spectrometry-Based Proteomics Analysis of the Matrix Microenvironment in Pluripotent Stem Cell Culture

Christopher Hughes
The University of Western Ontario

Supervisor
Dr. Gilles Lajoie
The University of Western Ontario

Graduate Program in Biochemistry
A thesis submitted in partial fulfillment of the requirements for the degree in Doctor of Philosophy

Mass Spectrometry-Based Proteomics Analysis of the Matrix Microenvironment in Pluripotent Stem Cell Culture

(Spine title: Proteomics of Human Stem Cell Derived Matrices)

(Thesis format: Integrated-Article)

by

Christopher S. Hughes

Graduate Program in Biochemistry

A thesis submitted in partial fulfillment
of the requirements for the degree of
Doctor of Philosophy

The School of Graduate and Postdoctoral Studies
The University of Western Ontario
London, Ontario, Canada

THE UNIVERSITY OF WESTERN ONTARIO
SCHOOL OF GRADUATE AND POSTDOCTORAL STUDIES

CERTIFICATE OF EXAMINATION

Supervisor	Examiners
_____	_____
Dr. Gilles Lajoie	Dr. Cheryle Séguin
	_____
Supervisory Committee	Dr. David Litchfield
_____	_____
Dr. Lars Konermann	Dr. Lars Konermann
_____	_____
Dr. Lynne-Marie Postovit	Dr. Daniel Figeys

The thesis by

Christopher S. Hughes

entitled:

Mass Spectrometry-Based Proteomics Analysis of the Matrix Microenvironment in Pluripotent Stem Cell Culture

is accepted in partial fulfillment of the
requirements for the degree of
Doctor of Philosophy

Date_____ _____
Chair of the Thesis Examination Board

Abstract

The stem cell microenvironment contains soluble factors, support cells, and components of the extracellular matrix (ECM) that combine to effect cellular behavior. Mass spectrometry based proteomics offers the opportunity to directly assay components of extracellular microenvironments, thereby providing a sensitive means for obtaining insight into the stem cell niche. In this study we present the generation and analysis of human embryonic stem cell (hESC) and human induced pluripotent stem cell (hiPSC) matrix microenvironments using an MS-based proteomics approach.

One of the primary limitations in the proteomics analysis of hESCs and hiPSCs is the reproducible generation of sufficient cell numbers amenable to experimentation. In Chapter 2 we develop reliable methods for the maintenance and proliferation of hESCs in metabolic labeling medium for use in stable isotope labeling with amino acids in cell culture (SILAC) experiments. Previously, the application of SILAC with hESCs was hindered by the use of medium insufficient for their reproducible culture and the problematic conversion of isotopically labeled arginine to proline. To address these issues, we demonstrate the culture of hESCs, hiPSCs, and mouse ESCs in SILAC conditions using a serum-replacement mixture and alternatively in defined medium. In these optimized conditions we show that the problematic conversion of arginine to proline can be eliminated through the simple addition of exogenous proline to the culture medium.

Within the *in vitro* microenvironment, the ECM plays a significant role in the maintenance and regulation of hESCs and hiPSCs. In order to better understand the

communication between hESCs and hiPSCs and the extracellular matrix, we focused our investigation on this portion of the microenvironment. To facilitate the proteomic analysis of complex ECM mixtures, in Chapter 3 we describe methods for the fractionation and MS-based proteomics analysis of these matrices. Application to a variety of cell-derived and recombinant growth matrices demonstrates not only the effectiveness of our methods, but also the utility of directly assaying matrices used in hESC culture for the determination of factors beneficial for the maintenance of self-renewal and pluripotency.

Through combination of the SILAC growth (Chapter 2) and matrix analysis (Chapter 3) methods, the protein compositions of conditioned matrices from multiple pluripotent stem cell lines are determined (Chapter 4). Within these matrices, numerous antagonists of core pluripotency pathways are identified, such as soluble frizzled related protein (sFRP) 1 and 2. In Chapter 5 we focus on characterizing the functions of sFRP1 and sFRP2 in hESC self-renewal and pluripotency. Taken together, the work presented here illustrates the utility of assaying interactions between stem cells and their matrix microenvironment for the determination of pathways involved in the regulation of the pluripotent phenotype.

Key Words: human embryonic stem cells, microenvironment, mass spectrometry, proteomics, extracellular matrix, protein digestion, peptide sequencing, pluripotency, differentiation, induced pluripotent stem cell

Co-Authorship Statement

Chapter 1

Hughes, C.S.*, Nuhn, A.*, Postovit, L.M., Lajoie, G.A.. (2011) “Proteomics of Human Embryonic Stem Cells”. *Proteomics*. 11;4:675 – 690

CSH and AN contributed equally to this manuscript. Both authors along with GL and LMP were involved in the generation of concepts to be presented and the drafting and revisions of the manuscript. All authors contributed to revisions and discussion of concepts.

Hughes, C.S., Ma, B., Lajoie, G.A.. (2010) “De Novo Sequencing Methods in Proteomics”. *Methods in Molecular Biology*. 604:105 - 121

CSH wrote the complete initial draft of the manuscript. Generation and discussion of concepts as well as revisions were completed by all authors.

Chapter 2

Bendall, S.C.*, Hughes, C.S.*, Stewart, M.H., Doble, B., Bhatia, M., Lajoie, G.A.. (2008) “Prevention of Amino Acid Conversion in SILAC Experiments with Embryonic Stem Cells”. *Molecular and Cellular Proteomics*. 7:1587 – 1597

SCB and CSH contributed equally to this manuscript. SCB and CSH were involved in experimental design, data interpretation, and manuscript preparation. The remaining authors were involved with aspects of experimental design, manuscript revision, and discussion of concepts.

Chapter 3

Hughes, C.S., Postovit, L.M., Lajoie, G.A.. (2010) “Matrigel: A Complex Protein Mixture Required for Optimal Growth of Cell Culture”. *Proteomics*. 10;9:1886 – 1890

CSH designed and performed experiments, interpreted data, and prepared the manuscript. Revisions were completed by all authors, as well as generation and discussion of concepts.

Hughes, C.S., Radan, L., Betts, D., Postovit, L.M., Lajoie, G.A.. (2011) “Proteomic Analysis of Extracellular Matrices used in Stem Cell Culture”. *Proteomics*. 11;20:3983 – 3991

CSH designed and performed experiments, interpreted data, and prepared the manuscript. LR also contributed to experimental work. All authors were involved in revisions of the manuscript and the generation and discussion of concepts.

Chapters 4 & 5 & 6

Hughes, C.S., Radan, L., Stanford, W., Betts, D., Postovit, L.M., Lajoie, G.A.. (2012) “Mass Spectrometry-Based Proteomics Analysis of the Matrix Microenvironment in Pluripotent Stem Cell Culture”. (In Preparation)

CSH designed and performed experiments, interpreted data, and prepared the manuscript. LR also contributed to experimental design as well as work. All other authors were involved with manuscript revisions as well as generation and discussion of concepts. WS donated iPSC lines used in the experiments.

Dedication

I would like to dedicate this firstly to my family for always being supportive of my endeavors and especially of my never-ending schooling. You have always been there when I have needed you and for that you will always have my appreciation. You have given me everything I have needed to become who I am today, for which I hope one day I can repay you.

Secondly, I would like to give thanks to all of my friends who have stuck with me through thick and thin. Especially Ryan, Jerry, and Jesse, no one knows me like you guys do. Although we don't live as close as we used to, we will always be lifelong bros. Jonathan, although I've only known you for a few years now we have had some awesome times, and I'm sure that will continue. Thank you for always being there, even if I only required someone to kill grubs with. Last but not least, Lida. You have been a never-ending source of support and good-will to me and for that I will forever owe you thanks. There is not much I can put here because you and I both know that you know me better than I know myself.

Thanks to all of you. This would not have been possible without your support.

Acknowledgements

Firstly I would like to thank everyone from the Lajoie lab. Sean, you were my mentor when I arrived at the lab and taught me a great deal about research and how to be a good scientist before you left. Paula, you always fought the never ending instrument battle with me and kept me afloat on the Global for my entire time in the lab. I hope that one day you finally find that piece of data analysis software that just does what you want with a click of a button and works it every time. Lastly, thank you Gilles for your support and knowledge throughout my graduate degree. You always gave me the space to work in a very independent fashion but were always there when I needed your help. You taught me a lot during my time here and were instrumental in developing me into the scientist I have become today.

Thank you to all the members from the Postovit lab. Scott, Daniela, Guihua, Michael, Padmalaya, Krista, Alia, and Dylan, you always provided the answers to questions, experimental advice, or training I required to stay afloat in the molecular biology world whenever I needed it. Lynne, even though you were never officially my supervisor you certainly were an excellent mentor. Although I guzzled reagents like crazy, you were always available to me for the scientific advice I needed to get through my graduate work. I would not have accomplished what I did without your help.

Thank you to the Betts lab. You welcomed me into your lab as one of your own and did anything you could to facilitate my work. Lastly, thank you to Courtney Brooks from the lab of Dr. Cheryle Seguin. The never ending supply of MEFs, hESCs, and MEF-CM you provided me with was critical to my work.

Table of Contents

List of Tables

List of Figures

List of Appendices

List of Abbreviations

1D SDS PAGE	one dimensional sodium dodecyl sulfate polyacrylamide gel electrophoresis
2D SDS PAGE	two dimensional sodium dodecyl sulfate polyacrylamide gel electrophoresis
7AAD	7-amino-actinomycin D
AA	amino acid
Ab	antibody
ABC	ammonium bicarbonate
ACN	acetonitrile
AFP	alpha-feto protein
ANOVA	analysis of variation
AS	ammonium sulfate
BME	beta mercaptoethanol
BMP	bone morphogenetic protein
BSA	bovine serum albumin
CapLC	capillary liquid chromatography
cDNA	complementary DNA
CDX	caudal type homeobox 2
CFU	colony forming unit
CID	collisional induced dissociation
CM	conditioned media
CMTX	conditioned matrix
CMV	cytomegalovirus
CTGF	connective tissue growth factor
DDA	data directed analysis
DMEM	Dulbecco's modified Eagle minimal essential medium
DMSO	dimethyl sulfoxide
DNA	deoxyribonucleic acid
DKK	dickkopf

DTT	dithiothreitol
EB	embroid body
EC	embryonal carcinoma
ECD	electron capture dissociation
ECL	enhanced chemiluminescence
ECM	extracellular matrix
EDTA	ethylenediaminetetraacetic acid
EGF	epidermal growth factor
ESC	embryonic stem cell
ESI	electrospray ionization
ETD	electron transfer dissociation
FA	formic acid
FACS	fluorescence activated cell sorting
FBS	fetal bovine serum
FGF	fibroblast growth factor
FGFR	fibroblast growth factor receptor
GAPDH	glyceraldehyde-3-phosphate dehydrogenase
GATA	gata-binding protein
GeLC	gel enhanced liquid chromatography
GFP	green fluorescent protein
GFR	growth factor reduced
GO	gene ontology
GSC	goosecoid
HARV	high aspect ratio vessel
hdF	hESC derived fibroblast
HDGF	hepatoma derived growth factor
HEK	human embryonic kidney
HGF	hepatocyte growth factor
hESC	human embryonic stem cell

hiPSC	human induced pluripotent stem cell
HPLC	high performance liquid chromatography
HRP	horse radish peroxidase
HSC	hematopoetic stem cell
ICAT	isotope-coded affinity tag
ICC	immunocytochemical
ICM	inner cell mass
ICR	ion cyclotron resonance
IE	iterative exclusion
IE-LC MS/MS	iterative exclusion liquid chromatography tandem mass spectrometry
IEF	isoelectric focusing
IGF	insulin-like growth factor
IGF1R	type 1 insulin-like growth factor recetor
IGFBP	insulin-like growth factor binding protein
IPI	International Protein Index
iPSC	induced pluripotent stem cell
ISCI	International Stem Cell Initiative
iTRAQ	isotope tags for relative and absolute quantification
Klf	Kruppel-like factor
KOSR	knockout serum replacement
LC	liquid chromatography
LC MS/MS	liquid chromatography tandem mass spectrometry
Lefty	left-right determination factor
LIF	leukemia inhibitory factor
LIT	linear ion trap
LOD	limit of detection
m/z	mass to charge ratio
MALDI	matrix assisted laser desorption ionization
MEF	mouse embryonic fibroblast

mESC	mouse embryonic stem cell
MIXL1	mix paired homeobox-like 1
MS	mass spectrometry
MS/MS	tandem mass spectrometry
MudPIT	multidimensional protein identification technology
MW	molecular weight
Myc	myelocytomatosis
NaOH	sodium hydroxide
NEAA	non-essential amino acids
NH4OH	ammonium hydroxide
NGF	nerve growth factor
N-GFR	non-growth factor reduced
Oct	octamer
ORF	open-reading frame
PAX	paired-box protein
PCR	polymerase chain reaction
Pkl	peak list
PDGF	platelet derived growth factor
PEDF	pigment epithelium derived factor
PI	propidium iodide
PLGS	protein lynx global server
PMSF	phenylmethylsulphonylfluoride
PTM	post-translational modification
PVDF	polyvinylidene fluoride
Q	quadrupole
QToF	quadrupole time of flight
RGD	Arg-Gly-Asp
RNA	ribonucleic acid
RPLPO	ribosomal protein, large, PO

RPM	revolutions per minute
RPMI	Roswell Park Memorial Institute medium
RT	retention time
RTK	receptor tyrosine kinase
RT-PCR	real-time polymerase chain reaction
SAX	strong anion exchange
SCX	strong cation exchange
SD	standard deviation
SDS	sodium dodecyl sulfate
SEM	standard error of the mean
SF	serum free
sFRP	soluble frizzed related protein
shRNA	short hairpin RNA
SILAC	stable isotope labeling with amino acids in cell culture
SOX	SRY (sex-determining region Y)-box
SPARC	secreted protein acidic and rich in cysteine
SSEA	stage specific embryonic antigen
TBST	tris buffered saline with tween
TGF	transforming growth factor
TIC	total ion chromatograph
TMT	tandem mass tags
ToF	time of flight
Tris	tris(hydroxymethyl) aminomethane
UniProt	Universal Protein Resource
UPLC	ultra performance liquid chromatography
VEGF	vascular endothelial growth factor
WB	western blot
WT	wild type

Ala	(A)	alanine
Arg	(R)	arginine
Asn	(N)	asparagine
Asp	(D)	aspartic acid
Cys	(C)	cysteine
Gln	(Q)	glutamine
Glu	(E)	glutamic acid
Gly	(G)	glycine
His	(H)	histidine
Ile	(I)	isoleucine
Leu	(L)	leucine
Lys	(K)	lysine
Met	(M)	methionine
Phe	(F)	phenylalanine
Pro	(P)	proline
Ser	(S)	serine
Thr	(T)	threonine
Trp	(W)	tryptophan
Tyr	(Y)	tyrosine
Val	(V)	valine

Chapter 1

Introduction

1.0 Pluripotency and Stem Cells

Stem cells are broadly defined by two primary characteristics: (i) the ability to self-renew, generating daughter cells equal to the parent and (ii) the unique capacity to differentiate into an array of cellular sub-types. Stem cells can provide valuable insight into human development and disease, have exciting potential in regenerative medicine, and can be used as models for drug discovery and toxicity analyses (reviewed in [1]). These properties have prompted the initiation of numerous research studies using stem cells as a model system with the goal of potentially unlocking the molecular mechanisms behind the regulation of the stem cell phenotype.

This chapter contains excerpts with permission from the following papers:

Hughes, C.S.*, Nuhn, A.*, Postovit, L.M., Lajoie, G.A.. (2011) “Proteomics of Human Embryonic Stem Cells”. *Proteomics*. 11;4:675 – 690

Hughes, C.S., Ma, B., Lajoie, G.A.. (2010) “De Novo Sequencing Methods in Proteomics”. *Methods in Molecular Biology*. 604:105 - 121

*Denotes equal author contribution

Stem cells can be further characterized by their differentiation capabilities and tissue-type of origin. A variety of cell and tissue types can give rise to cells of varying developmental potential. In mammals, pioneering work with teratocarcinomas established the presence of an undifferentiated cell type within these germ-line tumors (reviewed in [2]). These embryonal carcinoma (EC) cells were later cultured in a pluripotent state *in vitro* [3]. EC cells were later observed to have the capacity to differentiate *in vitro* through the formation of embryoid bodies (EB) [4]. Similar work *in vivo* demonstrated the ability of EC cells to generate chimeras and populate the germline in mice [5]. Together these findings suggested the similarity of EC cells to those that populate the inner cell mass (ICM) and contributed towards the discovery of embryonic stem cells (ESC).

Utilizing many of the findings gained from the study of EC cells, the derivation of ESCs from mice was demonstrated by Evans and Martin [6, 7]. ESCs are classified as being pluripotent, meaning they have the ability to differentiate into derivatives of the three primary germ layers (Figure 1.1). *In vitro*, pluripotency is conventionally demonstrated using an EB formation assay as previously mentioned for EC cells. These EBs can be assayed for the presence of markers delineating the three primary germ layers as indicators of differentiation capacity. More stringent tests of pluripotency are carried out *in vivo* using teratoma, chimera, or tetraploid complementation assays. Using a chimera assay to illustrate the ability to contribute to the germ line of injected mice, the *in vivo* pluripotency of mESCs was later demonstrated [8, 9].

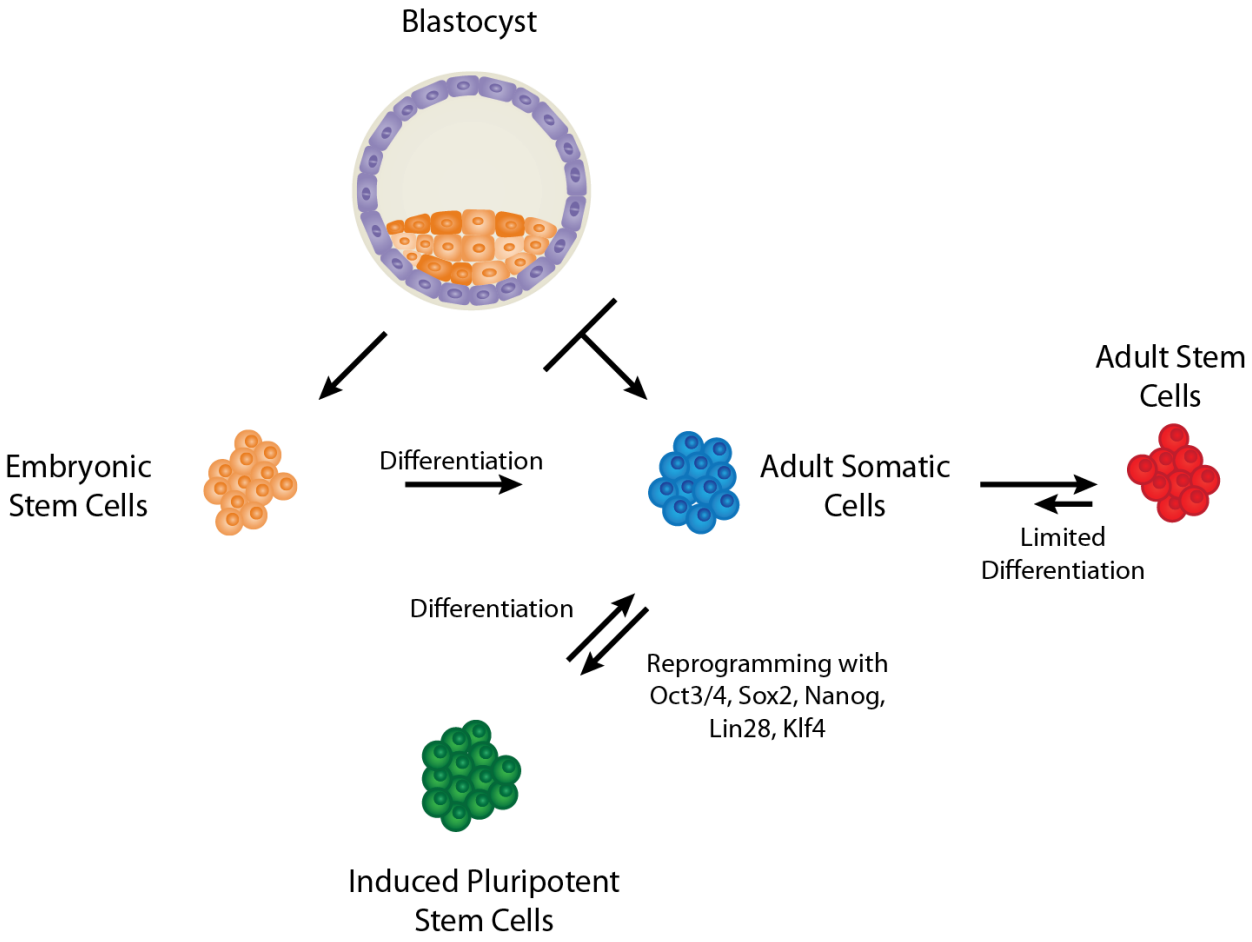

Figure 1.1. Derivation and distinction between stem cell types. Embryonic stem cells are the pluripotent derivatives of the inner cell mass of the blastocyst. Embryonic stem cells can be differentiated into any of the cells comprising the three primary germ layers. Adult somatic cells will contain tissue-specific populations of adult stem cells that are considered multipotent. Adult somatic cells derived from normal development can be reprogrammed using different combinations of transcription factors to generate induced pluripotent cells. These stem cells are also considered pluripotent and can mimic the differentiation capabilities of their embryonic counterparts. It is currently unknown whether embryonic and induced pluripotent cells are truly equivalent.

Soon after the work in mouse, derivation of pluripotent stem cells from the ICM of blastocyst stage embryos was demonstrated in humans (Figure 1.1) [10]. These hESCs shared the key properties of mESCs in that they could multiply indefinitely and generate cells of the three primary germ layers. Pluripotency could be assayed *in vitro* and *in vivo* using EB and teratoma formation respectively, but due to ethical concerns chimera and tetraploid complementation assays could not be undertaken. Since this time, alternative methods for the derivation of hESCs have been demonstrated, such as from biopsied blastomeres [11, 12].

Comparisons of mouse and human ESC lines have revealed several defining characteristics for each cell type. Identification of an undifferentiated colony is typically performed through the examination of intracellular and cell surface markers. mESCs and hESCs are both known to have strong expression for the nuclear cell markers Oct3/4 and Nanog [13]. On the cell surface, mESCs can be identified by the stage-specific embryonic antigen marker – 1 (SSEA-1) and the absence of SSEA-3 and -4. In hESCs, SSEA-3 and -4 mark undifferentiated cells whereas SSEA-1 is only present on those that have differentiated. Additional differences are observed when examining culture conditions for mESCs and hESCs. mESCs can be maintained in an undifferentiated and pluripotent state on a minimal matrix with supplementation of leukemic inhibitor factor (LIF) and bone morphogenic protein (BMP), whereas hESCs cannot [14, 15]. hESCs are typically grown on a layer of mitotically inactivated mouse feeder (MEF) cells in media supplemented with fibroblast growth factor 2 (FGF2 or basic FGF) [10]. Recent work has suggested that hESCs share several properties with mouse epiblast derived stem cells, whereas mESCs are indicative of a more naïve state

of the ICM [16, 17]. These findings have recently been advanced by the generation of naïve hESCs that share many of the defining properties of mESCs *in vitro* [18].

In contrast to embryonic, adult stem cells (ASC) are classified as being multipotent, meaning they can typically only generate differentiated cells that are a sub-type specific for the lineage to which they already belong (Figure 1.1). In addition to their limited differentiation capacity, ASCs are also have limited self-renewal capacity in culture, making their study difficult. Adult stem cells are thought to act as reservoirs of multipotent progenitors serving to regenerate cellular sub-types residing within specific tissues. This was originally validated in pioneering work with hematopoietic stem cells by Till and McCulloch where it was demonstrated that bone marrow cells could give rise to different types of blood cells [19, 20]. Since this time ASCs have been identified from heart, lung, skin, fat, and liver tissues (reviewed in [21]).

1.1 Inducing Pluripotency in Somatic Cells

The ability to reprogram somatic cells to induced pluripotent stem cells (iPSC) was first demonstrated in mice by Takahashi and Yamanaka [22]. The retroviral introduction of *POU5F1* (herein referred to as Oct3/4), Nanog, Sox 2, and c-Myc into mouse fibroblasts generated cells that shared the characteristic morphology of embryonic stem cells (Figure 1.1). However, due to deficiencies in their developmental potential, they were not classified as pluripotent. Reprogrammed fibroblasts that had the developmental potential of ESCs and were germline competent were later demonstrated in mouse [23, 24]. Shortly after the demonstration of mouse iPSCs, human fibroblasts were

reprogrammed by using different combinations of Oct3/4, Nanog, Sox 2, c-Myc, Lin28, and Klf4 [25-27]. These hiPSCs shared similar gene expression patterns and *in vitro* differentiation capabilities to their ESC counterparts.

Since these original discoveries, research on the reprogramming factors and methods for transgene introduction have been extensive (reviewed in [28]). Currently, the only factor that is verified to be absolutely essential for reprogramming is Oct3/4. Removal of unnecessary reprogramming factors, such as c-Myc, is deemed necessary for reducing the potential tumorigenicity of iPSCs to facilitate their use in therapeutic applications. Alternative methods for transgene introduction that have been demonstrated include: retroviral, adenoviral, lentiviral, Epstein-Barr Virus, piggyBAC transposase, recombinant protein, and synthetic RNA [28]. The main focus of these alternative methods is the generation of 'footprint' free iPSCs that do not contain any exogenous genetic material resulting from methods used for transgene expression. Using methods such as recombinant proteins and synthetic RNAs, fibroblasts can be efficiently reprogrammed to generate iPSCs free of exogeneous genetic material [28].

The observation that somatic cells can be reprogrammed to an embryonic-like state was a groundbreaking step forward in the stem cell field. The ability to generate embryonic-like cells in the lab side-stepped many of the ethical concerns surrounding stem cell research, and brought the prospect of cell-based therapeutics closer to reality. Tissue specific material could now be generated using a patient's own cells, overcoming immunocompatibility concerns. However, the risk of tumor formation in humans has to be eliminated before any significant *in vivo* studies can be carried out. In addition to any

potential clinical applications, these cells also provide new avenues for the study of stem cells and significantly increase the accessibility to this research area. However, due to limited information on the equivalency of induced pluripotent and embryonic stem cells, iPSCs are currently not yet recognized as a suitable replacement for hESCs in research.

1.2 Genomic and Proteomic Characterization of hESCs

Since the establishment of the first hESC line in 1998 by Thomson *et al*., a significant amount of research on hESC biology has been published [10]. In an effort to better characterize this cell type, many of these studies employed large screens directed at the identification of genes that regulate the pluripotent state [29-36]. Comparisons of gene expression patterns between hESCs, other pluripotent cells, or their differentiated derivatives, have led to the identification of growth and transcription factors that are hallmarks of hESC pluripotency, such as Oct 3/4, Nanog, and Sox 2 (Figure 1.2) [29, 32, 34-42]. The largest of these screens was undertaken by the International Stem Cell Initiative (ISCI). This group undertook characterization of 59 different hESC lines using a variety of analysis methods to identify hallmarks of pluripotency that are cell line independent [13, 43]. When global gene expression patterns were compared with that of the core pluripotency factor Nanog, a positive correlation was observed for many known hESC markers, such as Oct4, Nodal, LIN28, and DNMT3B. The findings of this global analysis led to the discovery of a set of genes that exhibited minimal variance across hESC lines that can be used as true markers of pluripotency. However, with the

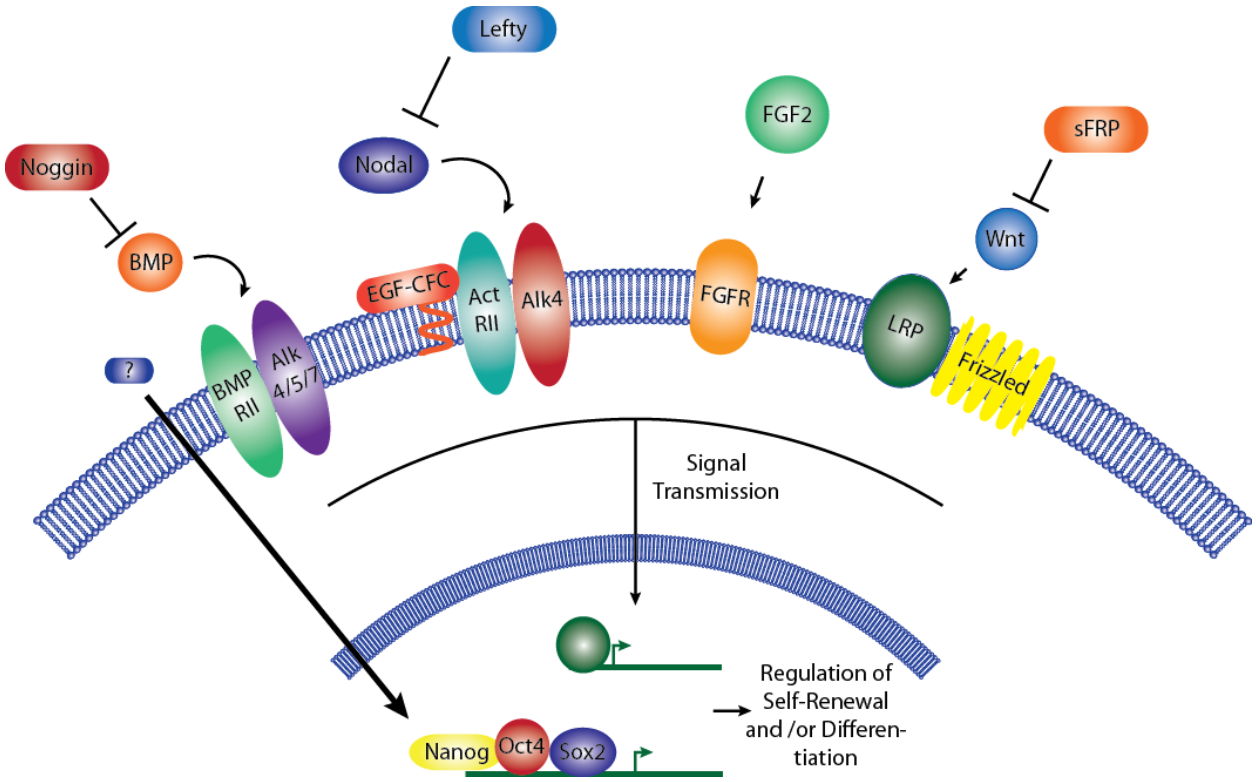

Figure 1.2. Regulation of human embryonic stem cell self-renewal and pluripotency. The pathways shown represent those believed to play the most significant roles in the regulation of hESCs *in vitro* based on current knowledge. FGF and Activin/Nodal pathways are key regulators required for maintenance of an undifferentiated state and as such is commonly supplemented into culture medium. BMP signaling is known to promote mESC maintenance but induces hESC differentiation. Canonical Wnt signaling has been shown to promote both differentiation and the maintenance of pluripotency. Oct4/Sox2/Nanog are critical for hESC pluripotency, however little is known about their regulation outside of the nucleus or cell itself. The bulk of the knowledge concerning these key pathways has been derived from comparative genomic and proteomic screens of differentiated and undifferentiated stem cells.

rapid generation of new hESC and hiPSC lines, reconciling heterogeneity across populations remains a challenge, especially in proteomics (reviewed in [44]).

Since proteins are the effectors of cellular processes, it is important to investigate how stem cells are regulated by changes at the protein level in addition to genomic analyses. Post-translational modifications (PTM), such as phosphorylation, may influence the activity of pivotal proteins, and this information can only be determined by studying the proteome. The importance of the analysis of the proteome is further emphasized by the fact that changes in RNA abundance do not always correspond to those in their respective proteins. This discordance is the result of post-transcriptional factors, such as stability of mRNA and the rates of translation and protein degradation [45-49]. Discordance between RNA and protein abundance has been observed in the analysis of stem cell populations [45-49]. In one of the first studies to analyze both mRNA and protein abundance levels in stem cells, Fathi *et al.* utilized mass spectrometry (MS)-based proteomics and qRT-PCR genomics approaches to characterize differences between hESCs and EBs [50]. When the proteomic and genomic data were compared there was minimal correlation between the two sets. These findings highlight the necessity for complementary genomic and proteomic analyses in order to fully validate observations made when studying hESC populations.

Technological advances in protein and peptide fractionation techniques, mass spectrometers, and quantitative methods have greatly increased the capacity to analyze and extract biological information from complex cellular samples. With recent advances in the ability to proliferate hESCs to numbers amenable to proteomic experiments, there

have been a surge of proteomic studies looking at hESCs (reviewed in [51-53]). Initial efforts focused on the analysis of the cellular proteomes of hESCs using 2D-SDS-PAGE methods coupled with MS for protein identification [50, 54]. However, these studies were limited in the depth of proteome coverage due to the use of methods that hindered the detection of low abundance proteins. Since this time, multiple large-scale analyses of the proteomes of hESCs and hiPSCs have been completed through utilization of high-resolution MS platforms coupled to multi-dimensional fractionation chromatography [55-57]. Although these studies provide valuable resources, in order to extract greater biological significance from their data and facilitate comparative analysis of hESCs with their differentiated counterparts, researchers have turned to quantitative proteomic methods [58-63]. Quantitative studies have also been applied to the direct analysis of the hESC phosphoproteome during maintenance and differentiation [64-67]. The results of these studies have provided valuable information on the dynamic state of the proteome in hESCs. Collectively, the genomic and proteomic studies that have been completed on hESCs to date have revealed and characterized many of the intracellular pathways currently considered to be critical for pluripotency (Figure 1.2).

1.3 Mass Spectrometry-based Proteomics

The goal of proteomics is to study the entire protein complement of cells or tissues. This not only encompasses the quantitative and qualitative analysis of protein abundance and turnover, but also their PTMs. Reaching this goal has conventionally relied upon technologies such as two-dimensional gel electrophoresis and western blotting. However, these methods offer limited information on a global proteome scale.

Although techniques for obtaining high-resolution and throughput genomic data sets have been available for some time, methods for the acquisition of complementary proteome data have lagged behind.

1.3.1 Mass Spectrometry-based Proteomics - In the field of proteomics, MS has become a central technology for the analysis of protein and peptide samples. This is due to the ability of MS instrumentation to rapidly acquire high quality spectra for thousands of peptides from a single sample injection. MS-based proteomics experiments are typically done in a 'bottom-up' approach, in which proteins are enzymatically digested to peptides prior to fractionation and analysis. Analysis of these complex peptide mixtures can yield high resolution and sensitivity data on the protein composition of a sample of interest. Greater instrument capabilities and new software advancements have resulted in the emergence of "top-down" experiments, in which intact proteins are analyzed (reviewed in [68, 69]). Until very recently, top-down experiments had not been amenable to large-scale analyses [70].

1.3.2 Mass Spectrometry of Proteins and Peptides - A typical MS analysis takes place in three steps. First, the mass of the intact peptide ions entering an MS in a given time window is measured. In the second step, specific precursor ions are selected in the first mass analyzer (e.g., Quadrupole 1), typically based on their relative abundance to one another, and fragmented in a collision cell (Quadrupole 2). The mass, or more accurately the mass-to-charge ratio (m/z), of each fragment ion is detected in a second mass analyzer (e.g., Time of Flight, Linear Ion Trap, Orbitrap, Ion Cyclotron Resonance cell), for each of the previously selected precursors. This type of experiment is referred

to as a tandem MS, or MS/MS analysis. Detailed investigation of the product ion masses within an MS/MS spectrum provides information on the sequence of the peptide selected for fragmentation and, by inference, identification of the protein to which it belongs.

Early forms of MS were not amenable to the analysis of protein samples. Ionization techniques such as electron and chemical ionization would cause high levels of in-source fragmentation for biomolecules. The development of soft ionization techniques, such as matrix-assisted laser desorption ionization (MALDI) and electrospray ionization (ESI), revolutionized the analysis of biomolecules by MS [71-73]. Both of these ionization types are classified as 'soft' techniques because there is little in-source fragmentation of the ionized species, such that the mass of the intact molecular ion can be measured. ESI and MALDI sources can be interfaced to a variety of mass analyzers and instrument architectures compatible with proteomics experiments. The most frequently used designs in proteomics are hybrid instruments that contain a combination of mass analyzers, such as: time of flight (TOF) [74, 75], quadrupole (Q), ion trap (LIT) [76], Fourier transform ion cyclotron resonance (FT-ICR) [77], and Orbitrap [78]. All of these platforms have advantages and disadvantages, for a comprehensive review of instruments types and their characteristics see ([76, 79]).

1.3.3 Proteomic Analysis of Complex Mixtures - Even with advancements in instrument scan speed, mass spectrometers can only detect a limited number of ions in a given period of time. To spread the components of an injected sample across a wider time window, chromatographic methods of separation are used prior to MS (Figure 1.3). The

conventional method of fractionation utilized prior to MS analysis is separation with a reversed phase (RP) column that partitions based on the hydrophobic character of the sample components. It is becoming increasingly common for researchers to employ a secondary orthogonal fractionation method prior to RP, such as strong cation exchange (SCX) or 1D-SDS-PAGE. The decrease in fraction complexity and complementary nature of these methods aids in providing an increase in depth of proteome coverage [80, 81]. One distinct advantage of ESI is its compatibility with a number of these on-line separation techniques employed prior to MS analysis.

1.3.4 Peptide Identification from Mass Spectra - In order to obtain information on the amino acid series of ions that enter the MS, sequence ions can be generated through fragmentation of the peptide parent ion in an MS collision cell. Each peptide ion dissociates in one place along the backbone so that the difference in mass between the resulting fragment ions potentially corresponds to the mass of an amino acid (reviewed in [82]). The most common form of fragmentation found in MS instrumentation is collision induced dissociation (CID) [83-85]. In CID, peptide ions are induced to fragment through collisions with inert gas molecules. Aside from CID, electron capture (ECD) and electron transfer dissociation (ETD) have been implemented in more recent mass spectrometers [86-88]. The combination of CID and ETD is now available on instrument platforms such as Orbitrap and qFT-ICR mass spectrometers. This allows for the acquisition of spectra from the same sample using two fragmentation techniques generating complementary series of fragment ions [89].

The identification of peptides from fragment ion data relies on spectral interpretation software (Figure 1.3). Conventional search engines perform comparisons between observed and theoretical peptide spectra from an *in silico* digest of a sequence database (reviewed in [90]). Search engines will score peptide matches based on a variety of metrics designed to generate a score representative of the quality of match between the observed and theoretical spectra [90, 91]. However, there has been a recent emergence in software designed to search peptide spectra against a database of previously acquired MS/MS experimental spectra identification [92]. These search engines offer greater sensitivity and speed, but are limited by the content of the experimental spectral databases.

An alternative to the previously mentioned database-dependent approaches are *de novo* methods that make use of computerized methods for determining the sequences of peptides directly from MS/MS spectra [93]. *De novo* methods use the knowledge of the fragmentation methods employed in the MS and basic search parameters input by the user to rebuild the peptide ion series [94-101]. *De novo* sequencing approaches hold a lot of potential due to their ability to identify previously unknown peptide sequences and post-translational modifications. However, utilizing a combination of multiple search engine strategies has been shown to be beneficial to achieving greater depth of coverage in proteomics experiments [102-104].

1.3.5 Quantitative Proteomics - To increase the biological significance of their data, quantitative proteomic strategies are frequently used to compare different cellular states or conditions (Figure 1.3). Mass spectrometers are not strictly quantitative, so

quantitative labeling is often used; however, label-free techniques are becoming increasingly popular (reviewed in [105, 106]). Application of the quantitative label can be done at the protein or peptide level, prior to analysis on the MS (Figure 1.3).

Reagents that are applied at the peptide level normally target primary amines to obtain complete sample coverage. In methods such as isobaric tags for relative and absolute quantification (iTRAQ) and tandem mass tags (TMT), samples are tagged following proteolytic digestion [107] (Figure 1.3). Peptides in different experimental conditions can be distinguished and quantified in MS/MS spectra based on the label applied. Dimethyl labeling approaches for peptide tagging have also been employed successfully, with the added advantage of minimal reagent expense [108, 109].

The most common alternatives to peptide tagging approaches are based on metabolic incorporation of isotopically labeled amino acids. One such isotopic labeling method, termed stable isotope labeling with amino acids in cell culture (SILAC) involves metabolic incorporation of ^{13}C and ^{15}N containing amino acids into a cell's proteome [110, 111]. Other methods based on metabolic incorporation of ^{15}N have been widely applied both *in vitro* and *in vivo* [112]. Both methods rely on the depletion of native versions of the targeted amino acids or elements and re-supplementation of isotopically labeled versions that can be incorporated into newly synthesized proteins. Metabolic incorporation can also be achieved through the feeding of labeled populations of cells to higher organisms [113]. In all mentioned metabolic approaches, differentially labeled samples are mixed at a defined ratio, and the relative abundance of proteins can be compared quantitatively based on the relative intensities of the peptide forms in MS

Figure 1.3. Conventional methods used in proteomics analysis of *in vitro* cell populations. Comparison of multiple experimental conditions can be performed separately or together. Separate sample analysis is conventionally done using 2D-SDS-PAGE fractionation followed by quantification of spot intensity on the gel. Spots that exhibit changes in intensity can be extracted from the gel and subjected to enzymatic digestion and subsequent identification through MS analysis. Alternatively, separate samples can be quantified in a label-free manner based on peptide abundance in the mass spectrum. When an isotopic label is used, samples from separate experimental conditions can be combined for analysis. When metabolic labeling with SILAC is used samples can be combined prior to fractionation and digestion. Alternatively, if iTRAQ or TMT approaches are used samples must remain separate until after enzymatic digestion and labeling. In both cases, peptides are analyzed and quantified in the mass spectrometer in a single analysis. For SILAC, quantification is completed at the MS level, whereas iTRAQ and TMT are performed in the MS/MS spectrum.

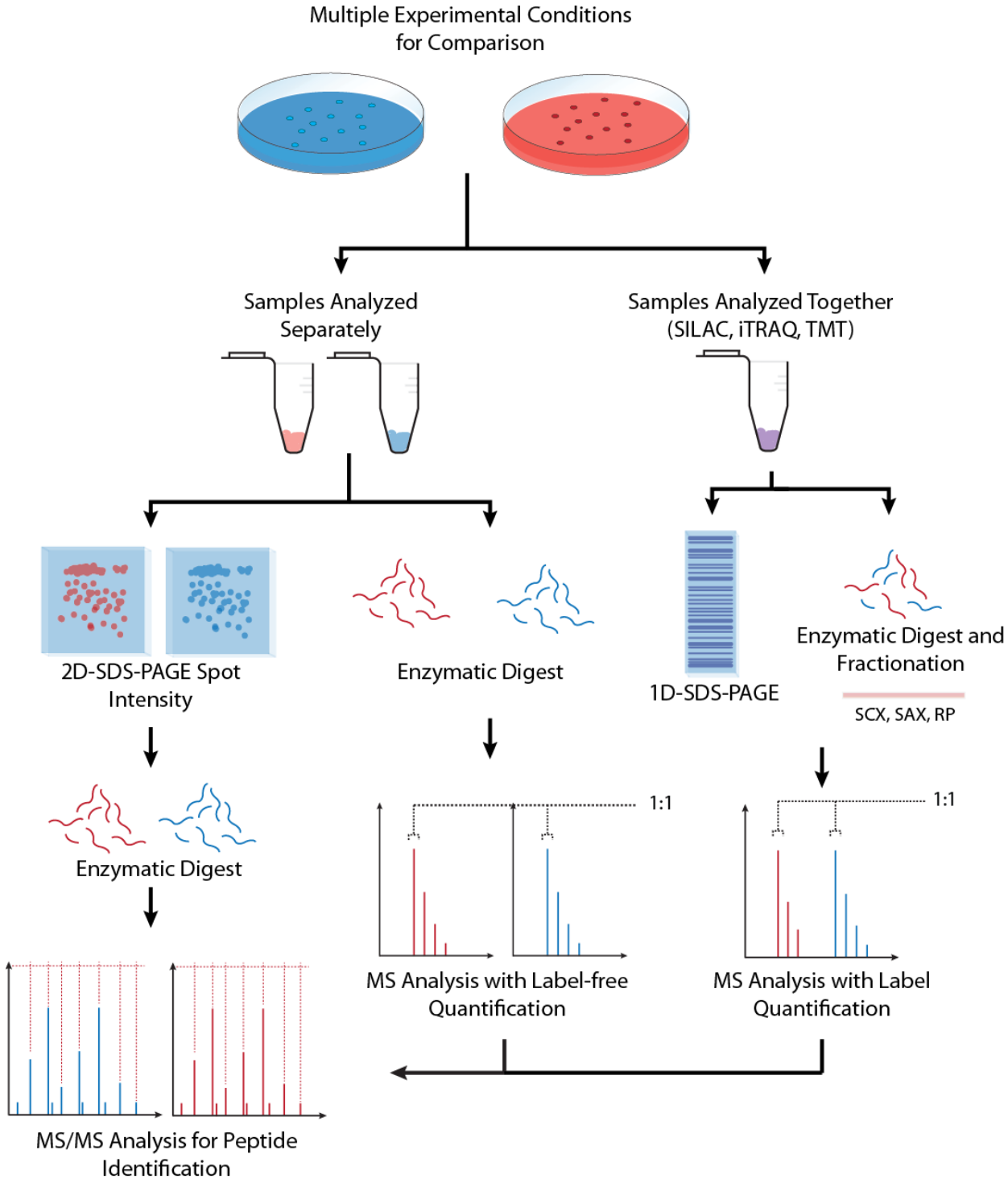
Multiple Experimental Conditions
for Comparison
Samples Analyzed
Separately
Samples Analyzed Together
(SILAC, iTRAQ, TMT)
2D-SDS-PAGE Spot
Intensity
Enzymatic Digest
1D-SDS-PAGE
Enzymatic Digest and
Fractionation
SCX, SAX, RP
Enzymatic Digest
1:1
1:1
MS Analysis with Label-free
Quantification
MS Analysis with Label
Quantification
MS/MS Analysis for Peptide
Identification

spectra. Isotopic labeling using any of the previously mentioned methods offer powerful tools for researchers to directly compare minute changes between cellular states over time (Figure 1.3).

1.4 *In Vitro* Culture of hESCs

Many experiments and therapeutic applications of hESCs require the cells to be pluripotent and free of non-human contamination. A major limitation to the use of hESCs in medical research is that they can undergo spontaneous differentiation in culture if proper conditions for retaining pluripotency are not maintained. At present, there is limited information about which culture conditions effectively maintain differentiated hESCs *in vitro*, and this restricts the amount of suitable material that can be generated for analysis [114-116]. One reason for this is that many advances in culture conditions for mouse embryonic stem cells are not applicable to hESCs [117].

Since the correct mixture of factors that maintains hESC pluripotency is unknown, hESCs are often derived on a feeder layer of MEF cells (Figure 1.4). This layer provides a growth substrate and secretes various growth factors, cytokines, and adhesion related proteins that promote pluripotency [118, 119]. Other human fibroblasts have also been shown to be supportive of sustained pluripotent hESC growth [120-124]. Due to the potential variability that culture on feeder layers presents and the risk of xeno-transmission from non-human sources, there has been a shift in the field to feeder-free growth of hESCs on defined matrices (Figure 1.4). A significant step forward in hESC culture methods was the discovery by Xu *et al.* that hESCs can be maintained on a layer of basement membrane matrix called Matrigel™™, in medium

that has been conditioned by irradiated MEFs (MEF-CM) [125]. Matrigel™™, which is extracted from Englebreth-Holm-Swarm tumors in mice, is a complex mixture of extracellular matrix (ECM) proteins that is composed primarily of laminin, collagen-IV, and enactin [126-128]. Matrigel™ has proven to be effective as a growth matrix for a wide variety of hESC lines using a variety of media formulations [129]. However, concerns regarding the composition and complexity of Matrigel™ and its suitability in research applications have been raised [126, 128, 130-132]. To overcome these limitations, a variety of ECM proteins or synthetic matrices have been evaluated for their ability to support hESC proliferation [133-148].

In parallel to matrix development, there have been numerous advances towards the generation of defined culture medium for hESC growth [149, 150]. All formulations contain growth factors designed to promote the maintenance of pluripotent hESCs, such as bFGF and Activin. In order to elucidate factors essential for the maintenance of hESCs, analyses of the secretomes of supportive feeder layers have been performed [151-154]. Factors supportive of the maintenance of hESC pluripotency, such as pigment epithelium derived factor (PEDF), have been identified through examination of these datasets. It was later demonstrated that PEDF can maintain undifferentiated hESCs without the addition of other exogenous supplements [155]. Other factors, such as Activin A and TGF-β1, were also identified in screens of conditioned media, both of which have been shown to promote the feeder-independent growth of hESCs in the absence of pre-conditioning with MEF layers [115, 156, 157]. Although these screens provide valuable information on extracellular regulation of hESC fate *in vitro*, our

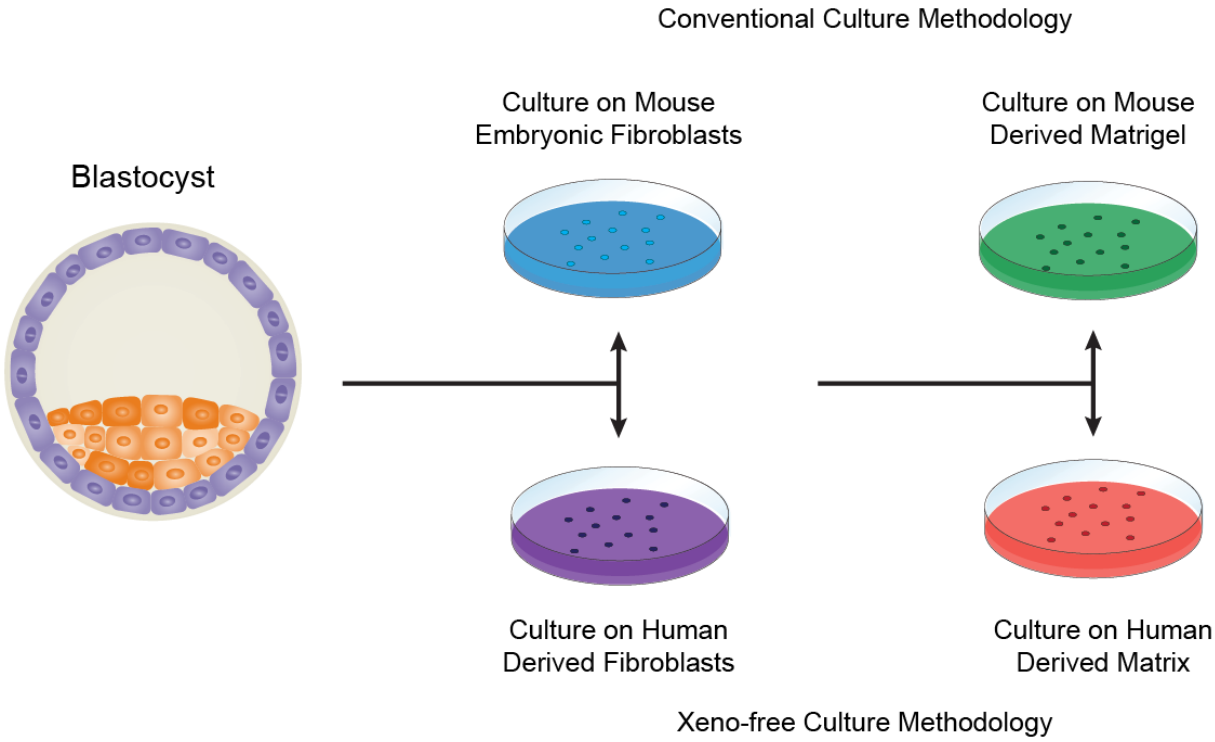

Figure 1.4. Derivation and culture of human embryonic stem cells. hESCs derived from the inner cell mass of the blastocyst are conventionally cultured on a layer of mouse embryonic fibroblast feeder cells in medium supplemented with FGF2. Alternatively, hESCs can be derived in xeno-free conditions by culturing them on human derived feeders, such as foreskin fibroblasts. hESCs derived in either condition can be passaged to feeder-free conditions where a culture matrix is substituted as the growth surface. The most commonly employed matrix is Matrigel™ in combination with culture media that has been conditioned on a mouse or human feeder-cell layer. If xeno-free conditions are desired, human cell-derived or recombinant protein matrices can be substituted and used in combination with defined culture medium.

understanding of how these pathways exact this control, alone or in combination, remains inadequate.

1.5 *In Vitro* Microenvironment and hESC Cell Fate

Based on advances in our knowledge regarding the optimal conditions for hESC culture *in vitro*, it is clear that extracellular processes are critical for maintaining the delicate balance between self-renewal and differentiation. Control over these extracellular processes is governed by a dynamic interplay between the various contributors to the microenvironment. This supportive environment is often referred to as the 'niche' and consists of a combination of accessory support cells, extracellular structure, and autocrine/paracrine signals (Figure 1.5). In stem cells, the concept of the niche was first defined for the hematopoietic system in mammals [158]. Additional evidence from Drosophila and C. *elegans* contributed to the development of the understanding of the stem cell niche (reviewed in [159, 160]). Research in mouse has contributed to the bulk of our current insight into the stem cell niche in mammalian systems. An example of this is recent work where the ability of mESCs to interact to form local microenvironments within single colonies that regulate cell-fate decisions dependent on the presence or absence of exogenous factors was demonstrated [161]. Studies such as these provide detailed insight into niche control of stem cells *in vitro*.

Studies directed at the analysis of the hESC niche have been limited due to the complexity its analysis presents. However, as illustrated by the intricate requirements for efficient proliferation *in vitro*, proteomic characterization of the microenvironment

from human stem cells should be a fruitful source of information. The necessity for supplementation of multiple exogenous factors illustrates the dynamic array of extracellular processes that combine to create a suitable hESC niche *in vitro*. Recent work using a global proteomics approach has demonstrated the valuable data that can yield from analysis of this soluble environment [162]. In addition to the components supplemented or secreted into the microenvironment, in this study it was observed that hESCs generate fibroblast cells supportive of self-renewal [162]. From proteomic analysis comparing the secretome of MEF feeders and hESCs, a novel mechanism was proposed wherein the supportive fibroblast cells responded to FGF supplementation to secrete factors that aided in the prevention of cellular differentiation [163, 164]. Although this was not the first global analysis of the hESC secretome, it generated the greatest depth of coverage leading to the identification of numerous stem cell regulatory proteins in the extracellular space.

In order to obtain a complete understanding of the hESC *in vitro* microenvironment, analysis of components other than soluble media components is required. Although numerous studies have focused on analysis of the soluble portion of the microenvironment, the interactions between hESCs and ECM in the niche is poorly understood. The ECM is known to provide structural support for processes such as cell attachment and migration. Moreover, it is widely postulated that the ECM interacts with an array of growth factors, acting to provide sustained release or co-factors required for activation (reviewed in [165]). The complex matrix requirements for the efficient culture of hESCs *in vitro* emphasize the importance of the ECM and the necessity for analysis of this contributor to the niche. Moreover, it was recently observed that metastatic cells

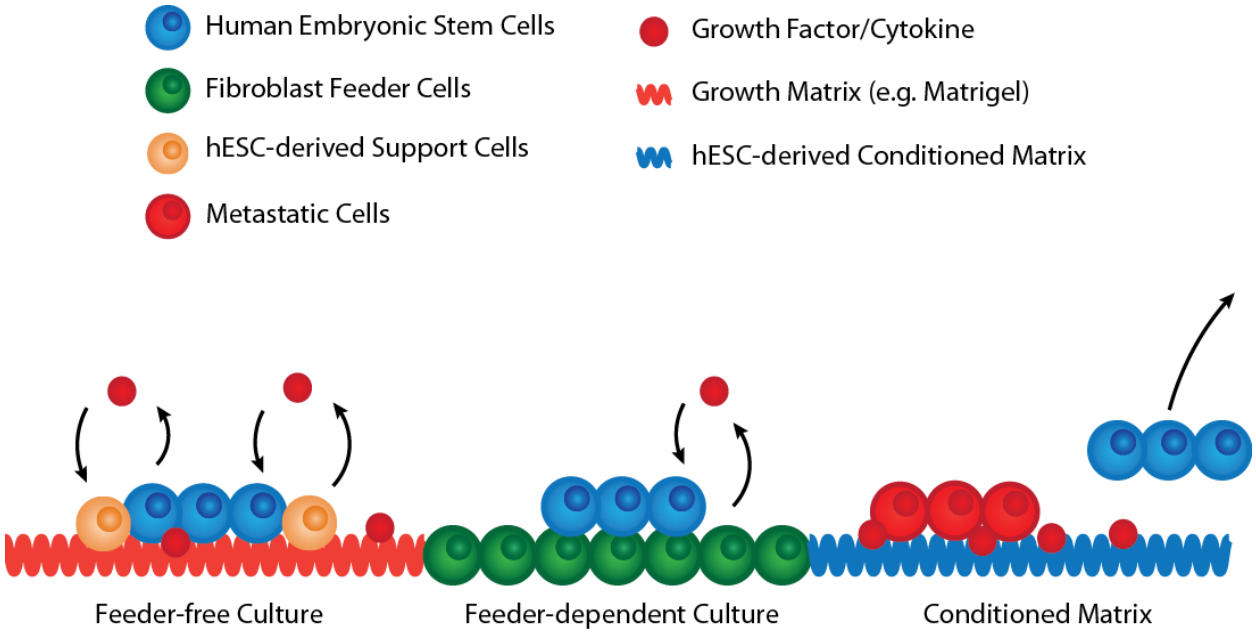

Figure 1.5. Maintenance of human embryonic stem cells in a dynamic microenvironment. Cultures maintained on Matrigel™ have been observed to contain hESC-derived cells that support stem cell maintenance through paracrine signaling pathways. On mouse or human fibroblast layers, maintenance of pluripotency is maintained through paracrine signaling with the feeder cells. Alternatively, on Matrigel™ or other matrices, hESCs can be maintained in medium that contains supportive factors secreted from feeder cells during conditioning. Many studies have focused on analysis of factors secreted during conditioning to elucidate hESC supportive pathways. Recent work has demonstrated the ability of hESC conditioned matrices to reprogram metastatic cells. This observation highlights the potential importance of the interactions between hESCs and the growth matrix used *in vitro*. However, few studies have focused on the elucidation of these interactions or the identification of hESC-derived factors in conditioned matrix.

could be ‘reprogrammed’ to a state that resembled their non-metastatic counterparts following exposure to an hESC conditioned matrix [166]. This observation was dependent on contact with the matrix portion of the microenvironment, and was not observed after exposure to hESC conditioned medium [167]. Studies such as these illustrate the potentially complex interactions between hESCs and the ECM *in vitro*. However, this area of the hESC microenvironment remains poorly understood as a result of the difficulty analysis of the ECM and its interactions presents.

1.6 Thesis Objective

With the potential wealth of information that can be extracted from the analysis of the hESC microenvironment, studies directed at the large-scale analysis of this dynamic environment needs to be undertaken. Critical to these studies will be the development of efficient methods for the analysis of the in-solution and matrix portions of the microenvironment. Moreover, integration of data obtained through the analysis of secreted factors with that of other supportive components of the microenvironment will be paramount for a more comprehensive understanding hESC regulation *in vitro*. With the recent observation that matrix deposited factors have the potential to reprogram metastatic melanoma cells, the ECM component of the hESC microenvironment necessitates further analysis [168]. To this end, one of the goals of this thesis will be directed at creating proteomic methods to facilitate the analysis of hESC and hiPSC conditioned matrices, as well as functional validation of identified candidates of interest.

In working towards these objectives we first develop methods for the efficient growth of hESCs in conditions amenable to SILAC experimentation *in vitro* (Chapter 2). We demonstrate that mouse and human ESCs can be maintained in an undifferentiated and pluripotent state in medium containing isotopically labeled arginine and lysine. We also extend this protocol to the feeder-free growth of hESCs and hiPSCs in SILAC medium that is completely defined. For both of these media formulations, we are able to overcome conversion of isotopically labeled arginine into proline, a typical occurrence in SILAC experiments. Application of these culture methods facilitated the expansion of labeled hESCs for further proteomic experimentation.

In order to extract information on the composition of hESC-derived matrices, proteomic methods directed at the fractionation and analysis of complex ECM-like mixtures were required. To this end, we developed methods aimed at the analysis of the complex ECM Matrigel™ (Chapter 3). By employing a range of fractionation and digestion protocols we demonstrate the complex proteomic profile of Matrigel™. Following this, we applied these methods to other cell-derived and recombinant matrix mixtures commonly used in hESC culture. These analyses revealed commonalities between matrices used in hESC culture. Based on the proteomics data, fibronectin was found to be enriched in all of the cell-derived hESC supportive matrices. To validate the ability of our proteomics approach to identify components critical for the maintenance of hESCs *in vitro*, we exhibit the maintenance of an undifferentiated and pluripotent state for cells grown on fibronectin as a sole matrix support.

After validation of our culture (Chapter 2) and matrix analysis methods (Chapter 3), we applied these conditions to the characterization of hESC and hiPSC conditioned matrices (Chapter 4). From our proteomics screen, we identify over 80 extracellular proteins in matrix conditioned by hESCs and hiPSCs. Comparative analyses with published stem cell secretome datasets aided in the identification of hESC regulatory proteins from our dataset. Based on the ability of the hESC-derived CMTX to enhance the maintenance of an undifferentiated state, we carry out functional validation of candidates identified in the CMTX to determine their roles in hESC pluripotency (Chapter 5). Focusing on the candidate soluble frizzled-related protein 1 & 2 (sFRP) proteins, we utilize a combination of approaches to elucidate their effects on hESC behavior. Taken together, our improved culture methods, matrix analysis protocols, and detailed composition of hESC derived matrices provide an effective toolbox for obtaining a more comprehensive understanding of how this dynamic cell type is regulated *in vitro*.

1.7 References

[1] Ahn, S.-M., Simpson, R., Lee, B., Genomics and proteomics in stem cell research: the road ahead. *Anat Cell Biol* 2010, *43*, 1-14.
[2] Andrews, P. W., Teratocarcinomas and human embryology: pluripotent human EC cell lines. Review article. *Apmis* 1998, *106*, 158-167; discussion 167-158.
[3] Finch, B. W., Ephrussi, B., Retention of Multiple Developmental Potentialities by Cells of a Mouse Testicular Teratocarcinoma During Prolonged Culture In Vitro and Their Extinction Upon Hybridization with Cells of Permanent Lines. *Proc Natl Acad Sci U S A* 1967, *57*, 615-621.
[4] Martin, G. R., Evans, M. J., Differentiation of clonal lines of teratocarcinoma cells: formation of embryoid bodies in vitro. *Proc Natl Acad Sci U S A* 1975, *72*, 1441-1445.
[5] Mintz, B., Illmensee, K., Normal genetically mosaic mice produced from malignant teratocarcinoma cells. *Proc Natl Acad Sci U S A* 1975, *72*, 3585-3589.
[6] Evans, M. J., Kaufman, M. H., Establishment in culture of pluripotential cells from mouse embryos. *Nature* 1981, *292*, 154-156.
[7] Martin, G. R., Isolation of a pluripotent cell line from early mouse embryos cultured in medium conditioned by teratocarcinoma stem cells. *Proc Natl Acad Sci U S A* 1981, *78*, 7634-7638.
[8] Bradley, A., Evans, M., Kaufman, M. H., Robertson, E., Formation of germ-line chimaeras from embryo-derived teratocarcinoma cell lines. *Nature* 1984, *309*, 255-256.
[9] Nagy, A., Rossant, J., Nagy, R., Abramow-Newerly, W., Roder, J. C., Derivation of completely cell culture-derived mice from early-passage embryonic stem cells. *Proc Natl Acad Sci U S A* 1993, *90*, 8424-8428.
[10] Thomson, J. A., Itskovitz-Eldor, J., Shapiro, S. S., Waknitz, M. A., Swiergiel, J. J., Marshall, V. S*., et al.*, Embryonic stem cell lines derived from human blastocysts. *Science* 1998, *282*, 1145-1147.
[11] Klimanskaya, I., Chung, Y., Becker, S., Lu, S. J., Lanza, R., Human embryonic stem cell lines derived from single blastomeres. *Nature* 2006, *444*, 481-485.
[12] Klimanskaya, I., Chung, Y., Becker, S., Lu, S. J., Lanza, R., Derivation of human embryonic stem cells from single blastomeres. *Nat Protoc* 2007, *2*, 1963-1972.
[13] Andrews, P. W., Benvenisty, N., McKay, R., Pera, M. F., Rossant, J., Semb, H*., et al.*, The International Stem Cell initiative: toward benchmarks for human embryonic stem cell research. *Nature Biotechnology* 2005, *23*, 795-797.
[14] Xu, R. H., Chen, X., Li, D. S., Li, R., Addicks, G. C., Glennon, C*., et al.*, BMP4 initiates human embryonic stem cell differentiation to trophoblast. *Nat Biotechnol* 2002, *20*, 1261-1264.
[15] Williams, R. L., Hilton, D. J., Pease, S., Willson, T. A., Stewart, C. L., Gearing, D. P*., et al.*, Myeloid leukaemia inhibitory factor maintains the developmental potential of embryonic stem cells. *Nature* 1988, *336*, 684-687.
[16] Tesar, P. J., Chenoweth, J. G., Brook, F. A., Davies, T. J., Evans, E. P., Mack, D. L*., et al.*, New cell lines from mouse epiblast share defining features with human embryonic stem cells. *Nature* 2007, *448*, 196-199.
[17] Silva, J., Smith, A., Capturing pluripotency. *Cell* 2008, *132*, 532-536.
[18] Hanna, J., Cheng, A. W., Saha, K., Kim, J., Lengner, C. J., Soldner, F*., et al.*, Human embryonic stem cells with biological and epigenetic characteristics similar to those of mouse ESCs. *Proceedings of the National Academy of Sciences of the United States of America* 2010, *107*, 9222-9227.
[19] Till, J. E., Mc, C. E., A direct measurement of the radiation sensitivity of normal mouse bone marrow cells. *Radiat Res* 1961, *14*, 213-222.
[20] Till, J. E., McCulloch, E. A., Siminovitch, L., A Stochastic Model of Stem Cell Proliferation, Based on the Growth of Spleen Colony-Forming Cells. *Proc Natl Acad Sci U S A* 1964, *51*, 29-36.
[21] Mezey, E., Adult Stem Cell Plasticity Revisited. *Adult Stem Cells: Biology and Methods of Analysis* 2011, 113-131.
[22] Takahashi, K., Yamanaka, S., Induction of pluripotent stem cells from mouse embryonic and adult fibroblast cultures by defined factors. *Cell* 2006, *126*, 663-676.
[23] Maherali, N., Sridharan, R., Xie, W., Utikal, J., Eminli, S., Arnold, K*., et al.*, Directly reprogrammed fibroblasts show global epigenetic remodeling and widespread tissue contribution. *Cell Stem Cell* 2007, *1*, 55-70.

[24] Okita, K., Ichisaka, T., Yamanaka, S., Generation of germline-competent induced pluripotent stem cells. *Nature* 2007, *448*, 313-U311.
[25] Yu, J., Vodyanik, M. A., Smuga-Otto, K., Antosiewicz-Bourget, J., Frane, J. L., Tian, S.*, et al.*, Induced pluripotent stem cell lines derived from human somatic cells. *Science* 2007, *318*, 1917-1920.
[26] Park, I. H., Zhao, R., West, J. A., Yabuuchi, A., Huo, H. G., Ince, T. A.*, et al.*, Reprogramming of human somatic cells to pluripotency with defined factors. *Nature* 2008, *451*, 141-U141.
[27] Takahashi, K., Tanabe, K., Ohnuki, M., Narita, M., Ichisaka, T., Tomoda, K.*, et al.*, Induction of pluripotent stem cells from adult human fibroblasts by defined factors. *Cell* 2007, *131*, 861-872.
[28] Leeb, C., Jurga, M., McGuckin, C., Moriggl, R., Kenner, L., Promising New Sources for Pluripotent Stem Cells. *Stem Cell Reviews and Reports* 2010, *6*, 15-26.
[29] Bhattacharya, B., Miura, T., Brandenberger, R., Mejido, J., Luo, Y., Yang, A. X.*, et al.*, Gene expression in human embryonic stem cell lines: unique molecular signature. *Blood* 2004, *103*, 2956-2964.
[30] Boiani, M., Scholer, H. R., Regulatory networks in embryo-derived pluripotent stem cells. *Nat Rev Mol Cell Biol* 2005, *6*, 872-884.
[31] Boyer, L. A., Lee, T. I., Cole, M. F., Johnstone, S. E., Levine, S. S., Zucker, J. R.*, et al.*, Core transcriptional regulatory circuitry in human embryonic stem cells. *Cell* 2005, *122*, 947-956.
[32] Brandenberger, R., Khrebtukova, I., Thies, R. S., Miura, T., Jingli, C., Puri, R.*, et al.*, MPSS profiling of human embryonic stem cells. *BMC Dev Biol* 2004, *4*, 10.
[33] Carpenter, M. K., Rosler, E., Rao, M. S., Characterization and differentiation of human embryonic stem cells. *Cloning and Stem Cells* 2003, *5*, 79-88.
[34] Richards, M., Tan, S. P., Tan, J. H., Chan, W. K., Bongso, A., The transcriptome profile of human embryonic stem cells as defined by SAGE. *Stem Cells* 2003, *22*, 51-64.
[35] Sperger, J. M., Chen, X., Draper, J. S., Antosiewicz, J. E., Chon, C. H., Jones, S. B.*, et al.*, Gene expression patterns in human embryonic stem cells and human pluripotent germ cell tumors. *Proc Natl Acad Sci U S A* 2003, *100*, 13350-13355.
[36] Wei, C. L., Miura, T., Robson, P., Lim, S. K., Xu, X. Q., Lee, M. Y. C.*, et al.*, Transcriptome profiling of human and murine ESCs identifies divergent paths required to maintain the stem cell state. *Stem Cells* 2005, *23*, 166-185.
[37] Heins, N., Englund, M. C. O., Sjoblom, C., Dahl, U., Tonning, A., Bergh, C.*, et al.*, Derivation, characterization, and differentiation of human embryonic stem cells. *Stem Cells* 2004, *22*, 367-376.
[38] Chen, H. F., Kuo, H. C., Chien, C. L., Shun, C. T., Yao, Y. L., Ip, P. L.*, et al.*, Derivation, characterization and differentiation of human embryonic stem cells: comparing serum-containing versus serum-free media and evidence of germ cell differentiation. *Human Reproduction* 2007, *22*, 567-577.
[39] Miura, T., Luo, Y., Khrebtukova, I., Brandenberger, R., Zhou, D., Thies, R. S.*, et al.*, Monitoring early differentiation events in human embryonic stem cells by massively parallel signature sequencing and expressed sequence tag scan. *Stem Cells Dev* 2004, *13*, 694-715.
[40] Lagarkova, M. A., Volchkov, P. Y., Lyakisheva, A. V., Philonenko, E. S., Kiselev, S. L., Diverse epigenetic profile of novel human embryonic stem cell lines. *Cell Cycle* 2006, *5*, 416-420.
[41] Bhattacharya, B., Puri, S., Puri, R. K., A review of gene expression profiling of human embryonic stem cell lines and their differentiated progeny. *Curr Stem Cell Res Ther* 2009, *4*, 98-106.
[42] Mitsui, K., Tokuzawa, Y., Itoh, H., Segawa, K., Murakami, M., Takahashi, K.*, et al.*, The homeoprotein Nanog is required for maintenance of pluripotency in mouse epiblast and ES cells. *Cell* 2003, *113*, 631-642.
[43] Adewumi, O., Aflatoonian, B., Ahrlund-Richter, L., Amit, M., Andrews, P. W., Beighton, G.*, et al.*, Characterization of human embryonic stem cell lines by the International Stem Cell Initiative. *Nat Biotechnol* 2007, *25*, 803-816.
[44] Gundry, R. L., Burridge, P. W., Boheler, K. R., Pluripotent stem cell heterogeneity and the evolving role of proteomic technologies in stem cell biology. *Proteomics* 2011, *11*, 3947-3961.
[45] Abreu, R. D., Penalva, L. O., Marcotte, E. M., Vogel, C., Global signatures of protein and mRNA expression levels. *Molecular Biosystems* 2009, *5*, 1512-1526.
[46] Ghaemmaghami, S., Huh, W. K., Bower, K., Howson, R. W., Belle, A., Dephoure, N.*, et al.*, Global analysis of protein expression in yeast. *Nature* 2003, *425*, 737-741.
[47] Gygi, S. P., Rochon, Y., Franza, B. R., Aebersold, R., Correlation between protein and mRNA abundance in yeast. *Molecular and Cellular Biology* 1999, *19*, 1720-1730.

[48] Schwanhausser, B., Busse, D., Li, N., Dittmar, G., Schuchhardt, J., Wolf, J.*, et al.*, Global quantification of mammalian gene expression control. *Nature* 2011, *473*, 337-342.
[49] Vogel, C., Abreu, R. D., Ko, D. J., Le, S. Y., Shapiro, B. A., Burns, S. C.*, et al.*, Sequence signatures and mRNA concentration can explain two-thirds of protein abundance variation in a human cell line. *Molecular Systems Biology* 2010, *6*.
[50] Fathi, A., Pakzad, M., Taei, A., Brink, T. C., Pirhaji, L., Ruiz, G.*, et al.*, Comparative proteome and transcriptome analyses of embryonic stem cells during embryoid body-based differentiation. *Proteomics* 2009, *9*, 4859-4870.
[51] Van Hoof, D., Mummery, C. L., Heck, A. J., Krijgsveld, J., Embryonic stem cell proteomics. *Expert Rev Proteomics* 2006, *3*, 427-437.
[52] Baharvand, H., Fathi, A., van Hoof, D., Salekdeh, G. H., Concise review: trends in stem cell proteomics. *Stem Cells* 2007, *25*, 1888-1903.
[53] Van Hoof, D., Heck, A. J., Krijgsveld, J., Mummery, C. L., Proteomics and human embryonic stem cells. *Stem Cell Res* 2008, *1*, 169-182.
[54] Baharvand, H., Hajheidari, M., Ashtiani, S. K., Salekdeh, G. H., Proteomic signature of human embryonic stem cells. *Proteomics* 2006, *6*, 3544-3549.
[55] Van Hoof, D., Passier, R., Ward-Van Oostwaard, D., Pinkse, M. W., Heck, A. J., Mummery, C. L.*, et al.*, A quest for human and mouse embryonic stem cell-specific proteins. *Mol Cell Proteomics* 2006, *5*, 1261-1273.
[56] Phanstiel, D. H., Brumbaugh, J., Wenger, C. D., Tian, S. L., Probasco, M. D., Bailey, D. J.*, et al.*, Proteomic and phosphoproteomic comparison of human ES and iPS cells. *Nature Methods* 2011, *8*, 821-U884.
[57] Pera, M. F., The proteomes of native and induced pluripotent stem cells. *Nature Methods* 2011, *8*, 807-808.
[58] Tian, R., Wang, S., Elisma, F., Li, L., Zhou, H., Wang, L.*, et al.*, Rare Cell Proteomic Reactor Applied to Stable Isotope Labeling by Amino Acids in Cell Culture (SILAC)-based Quantitative Proteomics Study of Human Embryonic Stem Cell Differentiation. *Mol Cell Proteomics*, *10*, M110 000679.
[59] Chaerkady, R., Kerr, C. L., Kandasamy, K., Marimuthu, A., Gearhart, J. D., Pandey, A., Comparative proteomics of human embryonic stem cells and embryonal carcinoma cells. *Proteomics* 2010.
[60] Chaerkady, R., Kerr, C. L., Marimuthu, A., Kelkar, D. S., Kashyap, M. K., Gucek, M.*, et al.*, Temporal Analysis of Neural Differentiation Using Quantitative Proteomics. *Journal of Proteome Research* 2009, *8*, 1315-1326.
[61] Yocum, A. K., Gratsch, T. E., Leff, N., Strahler, J. R., Hunter, C. L., Walker, A. K.*, et al.*, Coupled global and targeted proteomics of human embryonic stem cells during induced differentiation. *Molecular & Cellular Proteomics* 2008, *7*, 750-767.
[62] Graumann, J., Hubner, N. C., Kim, J. B., Ko, K., Moser, M., Kumar, C.*, et al.*, Stable isotope labeling by amino acids in cell culture (SILAC) and proteome quantitation of mouse embryonic stem cells to a depth of 5,111 proteins. *Mol Cell Proteomics* 2008, *7*, 672-683.
[63] Collier, T. S., Sarkar, P., Rao, B., Muddiman, D. C., Quantitative Top-Down Proteomics of SILAC Labeled Human Embryonic Stem Cells. *Journal of the American Society for Mass Spectrometry* 2010, *21*, 879-889.
[64] Prokhorova, T. A., Rigbolt, K. T., Johansen, P. T., Henningsen, J., Kratchmarova, I., Kassem, M.*, et al.*, Stable isotope labeling by amino acids in cell culture (SILAC) and quantitative comparison of the membrane proteomes of self-renewing and differentiating human embryonic stem cells. *Mol Cell Proteomics* 2009, *8*, 959-970.
[65] Brill, L. M., Xiong, W., Lee, K. B., Ficarro, S. B., Crain, A., Xu, Y.*, et al.*, Phosphoproteomic analysis of human embryonic stem cells. *Cell Stem Cell* 2009, *5*, 204-213.
[66] Van Hoof, D., Munoz, J., Braam, S. R., Pinkse, M. W., Linding, R., Heck, A. J.*, et al.*, Phosphorylation dynamics during early differentiation of human embryonic stem cells. *Cell Stem Cell* 2009, *5*, 214-226.
[67] Rigbolt, K. T. G., Prokhorova, T. A., Akimov, V., Henningsen, J., Johansen, P. T., Kratchmarova, I.*, et al.*, System-Wide Temporal Characterization of the Proteome and Phosphoproteome of Human Embryonic Stem Cell Differentiation. *Science Signaling* 2011, *4*.
[68] Kelleher, N. L., Top-down proteomics. *Analytical Chemistry* 2004, *76*, 196a-203a.
[69] Siuti, N., Kelleher, N. L., Decoding protein modifications using top-down mass spectrometry. *Nature Methods* 2007, *4*, 817-821.

[70] Tran, J. C., Zamdborg, L., Ahlf, D. R., Lee, J. E., Catherman, A. D., Durbin, K. R.*, et al.*, Mapping intact protein isoforms in discovery mode using top-down proteomics. *Nature*.
[71] Fenn, J. B., Mann, M., Meng, C. K., Wong, S. F., Whitehouse, C. M., Electrospray ionization for mass spectrometry of large biomolecules. *Science* 1989, *246*, 64-71.
[72] Karas, M., Hillenkamp, F., Laser desorption ionization of proteins with molecular masses exceeding 10,000 daltons. *Anal Chem* 1988, *60*, 2299-2301.
[73] Whitehouse, C. M., Dreyer, R. N., Yamashita, M., Fenn, J. B., Electrospray interface for liquid chromatographs and mass spectrometers. *Anal Chem* 1985, *57*, 675-679.
[74] Chernushevich, I. V., Loboda, A. V., Thomson, B. A., An introduction to quadrupole-time-of-flight mass spectrometry. *J Mass Spectrom* 2001, *36*, 849-865.
[75] Roepstorff, P., MALDI-TOF mass spectrometry in protein chemistry. *EXS* 2000, *88*, 81-97.
[76] Yost, R. A., Boyd, R. K., Tandem Mass-Spectrometry - Quadrupole and Hybrid Instruments. *Methods in Enzymology* 1990, *193*, 154-200.
[77] Peterman, S. M., Dufresne, C. P., Horning, S., The use of a hybrid linear trap/FT-ICR mass spectrometer for on-line high resolution/high mass accuracy bottom-up sequencing. *J Biomol Tech* 2005, *16*, 112-124.
[78] Gizzi, G., Hoogenboom, L. A. P., Von Holst, C., Rose, M., Anklam, E., Determination of dioxins (PCDDs/PCDFs) and PCBs in food and feed using the DR CALUX (R) bioassay: Results of an international validation study. *Food Additives and Contaminants* 2005, *22*, 472-481.
[79] Aebersold, R., Mann, M., Mass spectrometry-based proteomics. *Nature* 2003, *422*, 198-207.
[80] Bendall, S. C., Hughes, C., Campbell, J. L., Stewart, M. H., Pittock, P., Liu, S.*, et al.*, An enhanced mass spectrometry approach reveals human embryonic stem cell growth factors in culture. *Mol Cell Proteomics* 2009, *8*, 421-432.
[81] Fang, Y., Robinson, D. P., Foster, L. J., Quantitative analysis of proteome coverage and recovery rates for upstream fractionation methods in proteomics. *J Proteome Res* 2010, *9*, 1902-1912.
[82] Domon, B., Aebersold, R., Review - Mass spectrometry and protein analysis. *Science* 2006, *312*, 212-217.
[83] Hayes, R. N., Gross, M. L., Collision-Induced Dissociation. *Methods in Enzymology* 1990, *193*, 237-263.
[84] McLuckey, S. A., Goeringer, D. E., Glish, G. L., Collisional activation with random noise in ion trap mass spectrometry. *Anal Chem* 1992, *64*, 1455-1460.
[85] Morris, H. R., Paxton, T., Dell, A., Langhorne, J., Berg, M., Bordoli, R. S.*, et al.*, High sensitivity collisionally-activated decomposition tandem mass spectrometry on a novel quadrupole/orthogonal-acceleration time-of-flight mass spectrometer. *Rapid Commun Mass Spectrom* 1996, *10*, 889-896.
[86] Appella, E., Anderson, C. W., New prospects for proteomics--electron-capture (ECD) and electron-transfer dissociation (ETD) fragmentation techniques and combined fractional diagonal chromatography (COFRADIC). *FEBS J* 2007, *274*, 6255.
[87] Zubarev, R. A., Electron-capture dissociation tandem mass spectrometry. *Curr Opin Biotechnol* 2004, *15*, 12-16.
[88] Zubarev, R. A., Horn, D. M., Fridriksson, E. K., Kelleher, N. L., Kruger, N. A., Lewis, M. A.*, et al.*, Electron capture dissociation for structural characterization of multiply charged protein cations. *Anal Chem* 2000, *72*, 563-573.
[89] Swaney, D. L., McAlister, G. C., Coon, J. J., Decision tree-driven tandem mass spectrometry for shotgun proteomics. *Nat Methods* 2008, *5*, 959-964.
[90] Forner, F., Foster, L. J., Toppo, S., Mass spectrometry data analysis in the proteomics era. *Current Bioinformatics* 2007, *2*, 63-93.
[91] Johnson, R. S., Davis, M. T., Taylor, J. A., Patterson, S. D., Informatics for protein identification by mass spectrometry. *Methods* 2005, *35*, 223-236.
[92] Lam, H., Deutsch, E. W., Eddes, J. S., Eng, J. K., Stein, S. E., Aebersold, R., Building consensus spectral libraries for peptide identification in proteomics. *Nature Methods* 2008, *5*, 873-875.
[93] Xu, C., Ma, B., Software for computational peptide identification from MS-MS data. *Drug Discov Today* 2006, *11*, 595-600.
[94] Dancik, V., Addona, T. A., Clauser, K. R., Vath, J. E., Pevzner, P. A., De novo peptide sequencing via tandem mass spectrometry. *J Comput Biol* 1999, *6*, 327-342.

[95] Johnson, R. S., Taylor, J. A., Searching sequence databases via de novo peptide sequencing by tandem mass spectrometry. *Mol Biotechnol* 2002, *22*, 301-315.
[96] Taylor, J. A., Johnson, R. S., Sequence database searches via de novo peptide sequencing by tandem mass spectrometry. *Rapid Commun Mass Spectrom* 1997, *11*, 1067-1075.
[97] Taylor, J. A., Johnson, R. S., Implementation and uses of automated de novo peptide sequencing by tandem mass spectrometry. *Anal Chem* 2001, *73*, 2594-2604.
[98] Lu, B., Chen, T., A suboptimal algorithm for de novo peptide sequencing via tandem mass spectrometry. *J Comput Biol* 2003, *10*, 1-12.
[99] Samgina, T. Y., Artemenko, K. A., Gorshkov, V. A., Ogourtsov, S. V., Zubarev, R. A., Lebedev, A. T., De novo sequencing of peptides secreted by the skin glands of the Caucasian Green Frog Rana ridibunda. *Rapid Commun Mass Spectrom* 2008, *22*, 3517-3525.
[100] Standing, K. G., Peptide and protein de novo sequencing by mass spectrometry. *Curr Opin Struct Biol* 2003, *13*, 595-601.
[101] Xu, C., Ma, B., Complexity and scoring function of MS/MS peptide de novo sequencing. *Comput Syst Bioinformatics Conf* 2006, 361-369.
[102] Boutilier, K., Ross, M., Podtelejnikov, A. V., Orsi, C., Taylor, R., Taylor, P*., et al.*, Comparison of different search engines using validated MS/MS test datasets. *Analytica Chimica Acta* 2005, *534*, 11-20.
[103] Wedge, D. C., Krishna, R., Blackhurst, P., Siepen, J. A., Jones, A. R., Hubbard, S. J., FDRAnalysis: A Tool for the Integrated Analysis of Tandem Mass Spectrometry Identification Results from Multiple Search Engines. *Journal of Proteome Research* 2011, *10*, 2088-2094.
[104] Jones, A. R., Siepen, J. A., Hubbard, S. J., Paton, N. W., Improving sensitivity in proteome studies by analysis of false discovery rates for multiple search engines. *Proteomics* 2009, *9*, 1220-1229.
[105] Mueller, L. N., Brusniak, M. Y., Mani, D. R., Aebersold, R., An assessment of software solutions for the analysis of mass spectrometry based quantitative proteomics data. *Journal of Proteome Research* 2008, *7*, 51-61.
[106] Domon, B., Aebersold, R., Options and considerations when selecting a quantitative proteomics strategy. *Nature Biotechnology* 2010, *28*, 710-721.
[107] Ross, P. L., Huang, Y. L. N., Marchese, J. N., Williamson, B., Parker, K., Hattan, S*., et al.*, Multiplexed protein quantitation in Saccharomyces cerevisiae using amine-reactive isobaric tagging reagents. *Molecular & Cellular Proteomics* 2004, *3*, 1154-1169.
[108] Hsu, J. L., Huang, S. Y., Chow, N. H., Chen, S. H., Stable-isotope dimethyl labeling for quantitative proteomics. *Analytical Chemistry* 2003, *75*, 6843-6852.
[109] Boersema, P. J., Raijmakers, R., Lemeer, S., Mohammed, S., Heck, A. J. R., Multiplex peptide stable isotope dimethyl labeling for quantitative proteomics. *Nature Protocols* 2009, *4*, 484-494.
[110] Mann, M., Functional and quantitative proteomics using SILAC. *Nature Reviews Molecular Cell Biology* 2006, *7*, 952-958.
[111] Ong, S. E., Blagoev, B., Kratchmarova, I., Kristensen, D. B., Steen, H., Pandey, A*., et al.*, Stable isotope labeling by amino acids in cell culture, SILAC, as a simple and accurate approach to expression proteomics. *Molecular & Cellular Proteomics* 2002, *1*, 376-386.
[112] Krijgsveld, J., Ketting, R. F., Mahmoudi, T., Johansen, J., Artal-Sanz, M., Verrijzer, C. P*., et al.*, Metabolic labeling of C-elegans and D-melanogaster for quantitative proteomics. *Nature Biotechnology* 2003, *21*, 927-931.
[113] Larance, M., Bailly, A. P., Pourkarimi, E., Hay, R. T., Buchanan, G., Coulthurst, S*., et al.*, Stable-isotope labeling with amino acids in nematodes. *Nature Methods* 2011, *8*, 849-U114.
[114] Ludwig, T., J, A. T., Defined, feeder-independent medium for human embryonic stem cell culture. *Curr Protoc Stem Cell Biol* 2007, *Chapter 1*, Unit 1C 2.
[115] Ludwig, T. E., Bergendahl, V., Levenstein, M. E., Yu, J., Probasco, M. D., Thomson, J. A., Feeder-independent culture of human embryonic stem cells. *Nat Methods* 2006, *3*, 637-646.
[116] Hoffman, L. M., Carpenter, M. K., Characterization and culture of human embryonic stem cells. *Nat Biotechnol* 2005, *23*, 699-708.
[117] Ginis, I., Luo, Y. Q., Miura, T., Thies, S., Brandenberger, R., Gerecht-Nir, S*., et al.*, Differences between human and mouse embryonic stem cells. *Developmental Biology* 2004, *269*, 360-380.
[118] Stewart, M. H., Bendall, S. C., Bhatia, M., Deconstructing human embryonic stem cell cultures: niche regulation of self-renewal and pluripotency. *J Mol Med* 2008, *86*, 875-886.

[119] Richards, M., Tan, S., Fong, C. Y., Biswas, A., Chan, W. K., Bongso, A., Comparative evaluation of various human feeders for prolonged undifferentiated growth of human embryonic stem cells. *Stem Cells* 2003, *21*, 546-556.
[120] Meng, G. L., Liu, S. Y., Li, X. Y., Krawetz, R., Rancourt, D. E., Extracellular Matrix Isolated From Foreskin Fibroblasts Supports Long-Term Xeno-Free Human Embryonic Stem Cell Culture. *Stem Cells and Development* 2010, *19*, 547-556.
[121] Amit, M., Margulets, V., Segev, H., Shariki, K., Laevsky, I., Coleman, R*., et al.*, Human feeder layers for human embryonic stem cells. *Biology of Reproduction* 2003, *68*, 2150-2156.
[122] Chen, H. F., Chuang, C. Y., Shieh, Y. K., Chang, H. W., Ho, H. N., Kuo, H. C., Novel autogenic feeders derived from human embryonic stem cells (hESCs) support an undifferentiated status of hESCs in xeno-free culture conditions. *Human Reproduction* 2009, *24*, 1114-1125.
[123] Hovatta, O., Mikkola, M., Gertow, K., Stromberg, A. M., Inzunza, J., Hreinsson, J*., et al.*, A culture system using human foreskin fibroblasts as feeder cells allows production of human embryonic stem cells. *Human Reproduction* 2003, *18*, 1404-1409.
[124] Kibschull, M., Mileikovsky, M., Nagy, A., Lye, S. J., Human Embryonic Fibroblast Lines Provide Enhanced Support of Human Embryonic Stem Cells in Xeno-Free Culture Conditions. *Reproductive Sciences* 2009, *16*, 282a-282a.
[125] Xu, C., Inokuma, M. S., Denham, J., Golds, K., Kundu, P., Gold, J. D*., et al.*, Feeder-free growth of undifferentiated human embryonic stem cells. *Nat Biotechnol* 2001, *19*, 971-974.
[126] Kleinman, H. K., Martin, G. R., Matrigel: basement membrane matrix with biological activity. *Semin Cancer Biol* 2005, *15*, 378-386.
[127] Kleinman, H. K., McGarvey, M. L., Liotta, L. A., Robey, P. G., Tryggvason, K., Martin, G. R., Isolation and characterization of type IV procollagen, laminin, and heparan sulfate proteoglycan from the EHS sarcoma. *Biochemistry* 1982, *21*, 6188-6193.
[128] Vukicevic, S., Kleinman, H. K., Luyten, F. P., Roberts, A. B., Roche, N. S., Reddi, A. H., Identification of multiple active growth factors in basement membrane Matrigel suggests caution in interpretation of cellular activity related to extracellular matrix components. *Exp Cell Res* 1992, *202*, 1-8.
[129] Hakala, H., Rajala, K., Ojala, M., Panula, S., Areva, S., Kellomaki, M*., et al.*, Comparison of Biomaterials and Extracellular Matrices as a Culture Platform for Multiple, Independently Derived Human Embryonic Stem Cell Lines. *Tissue Eng Part A* 2009.
[130] Emonard, H., Grimaud, J. A., Nusgens, B., Lapiere, C. M., Foidart, J. M., Reconstituted basement-membrane matrix modulates fibroblast activities in vitro. *J Cell Physiol* 1987, *133*, 95-102.
[131] Hughes, C. S., Postovit, L. M., Lajoie, G. A., Matrigel: A complex protein mixture required for optimal growth of cell culture. *Proteomics* 2010, *10*, 1886-1890.
[132] Vukicevic, S., Somogyi, L., Martinovic, I., Zic, R., Kleinman, H. K., Marusic, M., Reconstituted Basement-Membrane (Matrigel) Promotes the Survival and Influences the Growth of Murine Tumors. *International Journal of Cancer* 1992, *50*, 791-795.
[133] Gerecht, S., Burdick, J. A., Ferreira, L. S., Townsend, S. A., Langer, R., Vunjak-Novakovic, G., Hyaluronic acid hydrogel for controlled self-renewal and differentiation of human embryonic stem cells. *Proc Natl Acad Sci U S A* 2007, *104*, 11298-11303.
[134] Braam, S. R., Zeinstra, L., Litjens, S., Ward-van Oostwaard, D., van den Brink, S., van Laake, L*., et al.*, Recombinant vitronectin is a functionally defined substrate that supports human embryonic stem cell self-renewal via alpha V beta 5 integrin. *Stem Cells* 2008, *26*, 2257-2265.
[135] Hakala, H., Rajala, K., Ojala, M., Panula, S., Areva, S., Kellomaki, M*., et al.*, Comparison of Biomaterials and Extracellular Matrices as a Culture Platform for Multiple, Independently Derived Human Embryonic Stem Cell Lines. *Tissue Engineering Part A* 2009, *15*, 1775-1785.
[136] Ludwig, T. E., Levenstein, M. E., Jones, J. M., Berggren, W. T., Mitchen, E. R., Frane, J. L*., et al.*, Derivation of human embryonic stem cells in defined conditions. *Nat Biotechnol* 2006, *24*, 185-187.
[137] Amit, M., Shariki, C., Margulets, V., Itskovitz-Eldor, J., Feeder layer- and serum-free culture of human embryonic stem cells. *Biology of Reproduction* 2004, *70*, 837-845.
[138] Jones, M. B., Chu, C. H., Pendleton, J. C., Betenbaugh, M. J., Shiloach, J., Baljinnyam, B*., et al.*, Proliferation and Pluripotency of Human Embryonic Stem Cells Maintained on Type I Collagen. *Stem Cells Dev* 2010.

[139] Manton, K. J., Richards, S., Van Lonkhuyzen, D., Cormack, L., Leavesley, D., Upton, Z., A chimeric vitronectin: igf-I protein supports feeder-cell-free and serum-free culture of human embryonic stem cells. *Stem Cells Dev* 2010, *19*, 1297-1305.
[140] Mei, Y., Saha, K., Bogatyrev, S. R., Yang, J., Hook, A. L., Kalcioglu, Z. I*., et al.*, Combinatorial development of biomaterials for clonal growth of human pluripotent stem cells. *Nat Mater* 2010, *9*, 768-778.
[141] Klim, J. R., Li, L. Y., Wrighton, P. J., Piekarczyk, M. S., Kiessling, L. L., A defined glycosaminoglycan-binding substratum for human pluripotent stem cells. *Nature Methods* 2010, *7*, 989-U972.
[142] Harb, N., Archer, T. K., Sato, N., The Rho-Rock-Myosin Signaling Axis Determines Cell-Cell Integrity of Self-Renewing Pluripotent Stem Cells. *Plos One* 2008, *3*, -.
[143] Miyazaki, T., Futaki, S., Hasegawa, K., Kawasaki, M., Sanzen, N., Hayashi, M*., et al.*, Recombinant human laminin isoforms can support the undifferentiated growth of human embryonic stem cells. *Biochemical and Biophysical Research Communications* 2008, *375*, 27-32.
[144] Vuoristo, S., Virtanen, I., Takkunen, M., Palgi, J., Kikkawa, Y., Rousselle, P*., et al.*, Laminin isoforms in human embryonic stem cells: synthesis, receptor usage and growth support. *Journal of Cellular and Molecular Medicine* 2009, *13*, 2622-2633.
[145] Derda, R., Li, L., Orner, B. P., Lewis, R. L., Thomson, J. A., Kiessling, L. L., Defined substrates for human embryonic stem cell growth identified from surface arrays. *ACS Chem Biol* 2007, *2*, 347-355.
[146] Brafman, D. A., Chang, C. W., Fernandez, A., Willert, K., Varghese, S., Chien, S., Long-term human pluripotent stem cell self-renewal on synthetic polymer surfaces. *Biomaterials* 2010, *31*, 9135-9144.
[147] Kolhar, P., Kotamraju, V. R., Hikita, S. T., Clegg, D. O., Ruoslahti, E., Synthetic surfaces for human embryonic stem cell culture. *J Biotechnol* 2010, *146*, 143-146.
[148] Melkoumian, Z., Weber, J. L., Weber, D. M., Fadeev, A. G., Zhou, Y., Dolley-Sonneville, P*., et al.*, Synthetic peptide-acrylate surfaces for long-term self-renewal and cardiomyocyte differentiation of human embryonic stem cells. *Nat Biotechnol* 2010, *28*, 606-610.
[149] Akopian, V., Andrews, P. W., Beil, S., Benvenisty, N., Brehm, J., Christie, M*., et al.*, Comparison of defined culture systems for feeder cell free propagation of human embryonic stem cells. *In Vitro Cellular & Developmental Biology-Animal* 2010, *46*, 247-258.
[150] Chen, G. K., Gulbranson, D. R., Hou, Z. G., Bolin, J. M., Ruotti, V., Probasco, M. D*., et al.*, Chemically defined conditions for human iPSC derivation and culture. *Nature Methods* 2011, *8*, 424-U476.
[151] Chin, A. C. P., Fong, W. J., Goh, L. T., Philp, R., Oh, S. K. W., Choo, A. B. H., Identification of proteins from feeder conditioned medium that support human embryonic stem cells. *Journal of Biotechnology* 2007, *130*, 320-328.
[152] Lim, J. W. E., Bodnar, A., Proteome analysis of conditioned medium from mouse embryonic fibroblast feeder layers which support the growth of human embryonic stem cells. *Proteomics* 2002, *2*, 1187-1203.
[153] Prowse, A. B. J., McQuade, L. R., Bryant, K. J., Marcal, H., Gray, P. P., Identification of potential pluripotency determinants for human embryonic stem cells following proteomic analysis of human and mouse fibroblast conditioned media. *Journal of Proteome Research* 2007, *6*, 3796-3807.
[154] Prowse, A. B. J., McQuade, L. R., Bryant, K. J., Van Dyk, D. D., Tuch, B. E., Gray, P. P., A proteome analysis of conditioned media from human neonatal fibroblasts used in the maintenance of human embryonic stem cells. *Proteomics* 2005, *5*, 978-989.
[155] Gonzalez, R., Jennings, L. L., Knuth, M., Orth, A. P., Klock, H. E., Ou, W*., et al.*, Screening the mammalian extracellular proteome for regulators of embryonic human stem cell pluripotency. *Proc Natl Acad Sci U S A* 2010, *107*, 3552-3557.
[156] Beattie, G. M., Lopez, A. D., Bucay, N., Hinton, A., Firpo, M. T., King, C. C*., et al.*, Activin A maintains pluripotency of human embryonic stem cells in the absence of feeder layers. *Stem Cells* 2005, *23*, 489-495.
[157] James, D., Levine, A. J., Besser, D., Hemmati-Brivanlou, A., TGFbeta/activin/nodal signaling is necessary for the maintenance of pluripotency in human embryonic stem cells. *Development* 2005, *132*, 1273-1282.
[158] Schofield, R., The relationship between the spleen colony-forming cell and the haemopoietic stem cell. *Blood Cells* 1978, *4*, 7-25.

[159] Li, L., Xie, T., Stem cell niche: structure and function. *Annu Rev Cell Dev Biol* 2005, *21*, 605-631.
[160] Spradling, A., Drummond-Barbosa, D., Kai, T., Stem cells find their niche. *Nature* 2001, *414*, 98-104.
[161] Davey, R. E., Zandstra, P. W., Spatial organization of embryonic stem cell responsiveness to autocrine gp130 ligands reveals an autoregulatory stem cell niche. *Stem Cells* 2006, *24*, 2538-2548.
[162] Stewart, M. H., Bosse, M., Chadwick, K., Menendez, P., Bendall, S. C., Bhatia, M., Clonal isolation of hESCs reveals heterogeneity within the pluripotent stem cell compartment. *Nature Methods* 2006, *3*, 807-815.
[163] Bendall, S. C., Stewart, M. H., Menendez, P., George, D., Vijayaragavan, K., Werbowetski-Ogilvie, T.*, et al.*, IGF and FGF cooperatively establish the regulatory stem cell niche of pluripotent human cells in vitro. *Nature* 2007, *448*, 1015-1021.
[164] Bendall, S. C., Hughes, C., Campbell, J. L., Stewart, M. H., Pittock, P., Liu, S.*, et al.*, An Enhanced Mass Spectrometry Approach Reveals Human Embryonic Stem Cell Growth Factors in Culture. *Molecular & Cellular Proteomics* 2009, *8*, 421-432.
[165] Hynes, R. O., The extracellular matrix: not just pretty fibrils. *Science* 2009, *326*, 1216-1219.
[166] Hendrix, M. J., Seftor, E. A., Seftor, R. E., Kasemeier-Kulesa, J., Kulesa, P. M., Postovit, L. M., Reprogramming metastatic tumour cells with embryonic microenvironments. *Nat Rev Cancer* 2007, *7*, 246-255.
[167] Postovit, L. M., Seftor, E. A., Seftor, R. E., Hendrix, M. J., A three-dimensional model to study the epigenetic effects induced by the microenvironment of human embryonic stem cells. *Stem Cells* 2006, *24*, 501-505.
[168] Postovit, L. M., Margaryan, N. V., Seftor, E. A., Kirschmann, D. A., Lipavsky, A., Wheaton, W. W.*, et al.*, Human embryonic stem cell microenvironment suppresses the tumorigenic phenotype of aggressive cancer cells. *Proc Natl Acad Sci U S A* 2008, *105*, 4329-4334.

Chapter 2

Development and Optimization of Growth Conditions for SILAC Experiments in Pluripotent Stem Cells

2.1 Introduction

Large scale identification of proteins using mass spectrometry (MS)-based proteomics has been made possible by recent advances in instrumentation, separation sciences, and bioinformatics [1]. However, the generation of increasingly long lists of proteins now confronts researchers with the more challenging problem of determining the biological significance of particular proteins. For this reason, quantitative proteomic strategies can now be used in order to extract more meaningful information from their datasets. By comparing multiple samples and different conditions *vs* controls, it is often possible to discern proteins that are altered in a given set of experimental or biological conditions from the thousands that are identified [2].

This chapter contains excerpts with permission from the following paper:

Bendall, S.C.*, Hughes, C.S.*, Stewart, M.H., Doble, B., Bhatia, M., Lajoie, G.A.. (2008) "Prevention of Amino Acid Conversion in SILAC Experiments with Embryonic Stem Cells". *Molecular and Cellular Proteomics*. 7:1587 – 1597

*Denotes equal author contribution

In MS-based proteomics, quantitative strategies typically involve the use of stable isotopic reagents to generate ‘heavy’ and ‘light’ samples, which retain their chemical identity and can then be differentiated and directly compared by MS analysis. While chemical labeling methods such as ICAT have demonstrated widespread applicability [1], metabolic incorporation strategies such as stable isotope labeling with amino acids in cell culture (SILAC) are becoming more common for cell types that can be grown for extensive periods of time *in vitro*. Though there are numerous advantages for using SILAC based methods, compared to chemical labeling, a major drawback is the unintended metabolic inter-conversion of isotopic amino acids in the labeling process, generating artifacts affecting the quantification. This is a particular problem with arginine which is a metabolic precursor for proline biosynthesis (Figure 2.1). In general, large scale SILAC experiments use both arginine and lysine to obtain labeling of all possible tryptic peptides thereby maximizing quantitative coverage of all potential peptides in a given experiment.

Several studies using SILAC have described the problematic conversion of isotopically labeled arginine to labeled proline in cells [3-7] (Figure 2.1) which results in an underestimation of the abundance of ‘heavy’ tryptic peptides containing proline in a relative quantification experiment. This is of particular concern since ~50% of all tryptic peptides between 700 and 6000 Da in the international protein index (IPI) human database contains at least one proline. Moreover, in a recent study it was reported that ~30-40% of all observable proline containing peptides exhibited some level of conversion from heavy arginine [7]. Besides acting to skew the relative abundance observed, conversion of ‘heavy’ arginine to ‘heavy’ proline also further complicates the

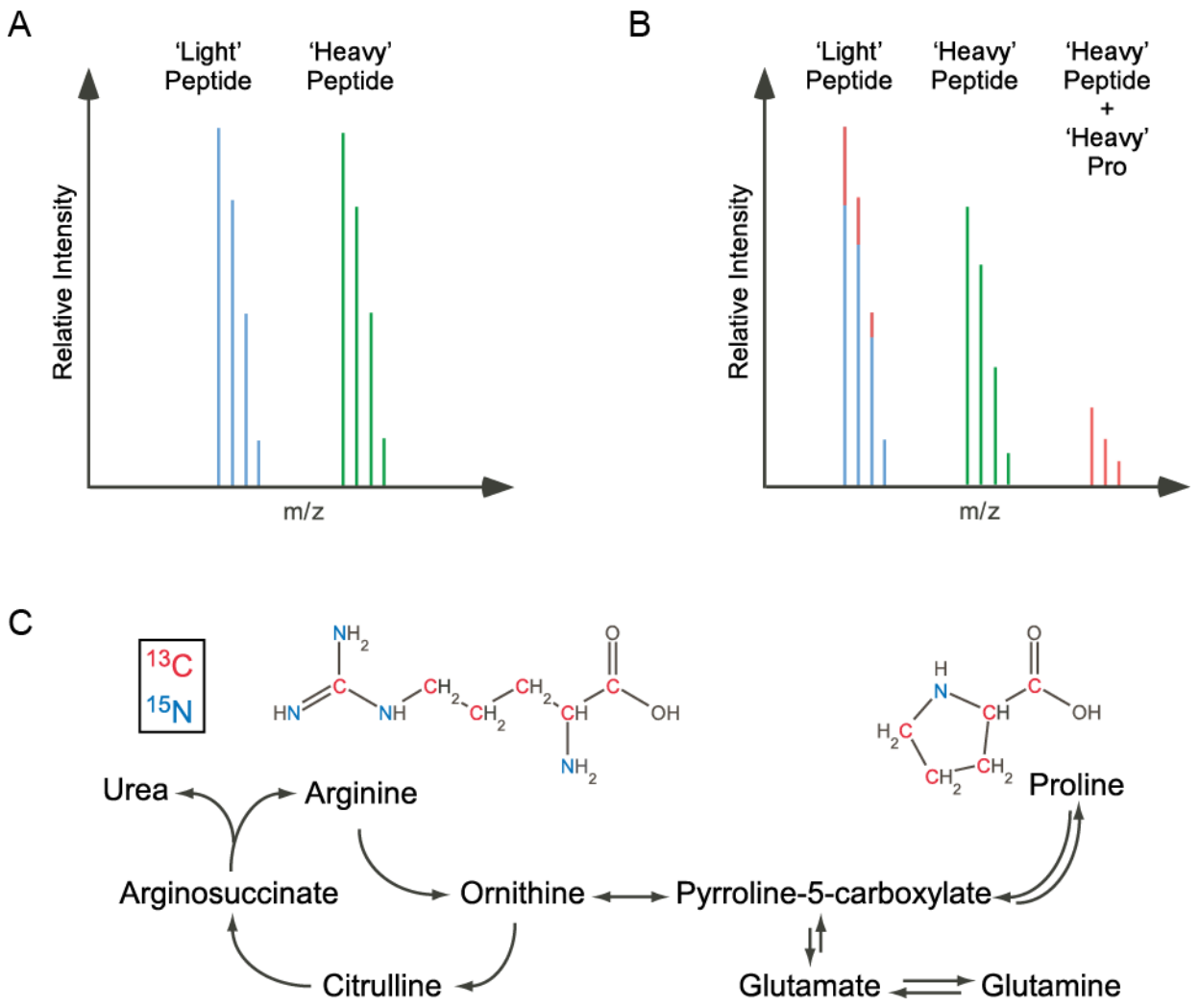

Figure 2.1. Metabolic conversion of isotope-coded arginine to proline in SILAC experiments. The unpredictable conversion of isotopic arginine to proline creates inaccuracy in SILAC based quantitative proteomic experiments. (A) A conceptual mass spectra of a non-proline containing peptide ion from a 1:1 mixture of 'light' and 'heavy' labeled samples. Here the expected 'light' and 'heavy' peptide ions have an equivalent signal. (B) A spectra from a proline containing peptide where arginine to proline conversion has occurred in the same 1:1 mixture. The resulting heavy proline peptide signal (red) has been subtracted from the expected 'heavy' peptide ion signal. (C) Metabolic pathway outlining the inter-conversion of arginine and proline. Isotope-coded arginine with carbon 13 (red) and nitrogen 15 (green) that when used as a synthetic precursor increases the expected mass of proline.

mass spectrometry data by increasing the number of peptide ion peaks. One proposed strategy to minimize this problem is the reduction of the arginine concentration in the SILAC media rendering it metabolically unfavorable as a precursor for proline synthesis [8]. While this does reduce the conversion, it does not prevent it completely [3]. The other is to avoid the use of arginine altogether or by removing the ability to perform arginine catabolism [3, 9, 10]. Finally, alternative corrections can be done mathematically, post-analysis, but these are inaccurate and do not solve the problem of increased peptide ion complexity [4, 11-14].

While reducing the concentration of available arginine in SILAC labeling media was a simple method for preventing its conversion to proline, this approach would be problematic for particular cells types like those with rapid cellular metabolism [15]. Moreover, certain sensitive cell types, such as human embryonic stem cells (hESCs) die or differentiate under restrictive metabolic conditions [7, 16]. To this end, Vanhoof et al. [7] sought to compensate for arginine to proline conversion in SILAC experiments by advocating the use of isotopically labeled arginine ($^{15}N_4$ Arg) in 'light' SILAC media as well as ($^{15}N_4$ $^{13}C_6$ Arg) in the 'heavy' media. With the assumption that arginine to proline conversion would be the same under both conditions, the monoisotopic peak of 'light' and 'heavy' proline containing peptide ions could be compared to correctly determine relative abundance, as both would be reduced proportionately. This method does provide a solution but it further complicates the procedure by generating additional converted proline peptide ions in the MS spectra and by adding the cost of expensive isotopic reagents. Also, there is no guarantee that the rate of arginine to proline conversion will be the same when comparing different cell types or treatments. Adding

to these difficulties is the fact that SILAC labeling of both hESCs [7] and ESCs from the mouse (mESC) [17] required the use of mouse embryonic fibroblast (MEF) feeder cells which precludes the attainment of high cell numbers necessary for large scale, SILAC-based proteomic applications [8, 18-21]. Faced with these challenges, we sought a simple solution, for arginine to proline conversion in SILAC experiments that would be compatible with a robust hESC culture protocol free of feeder cells.

In this chapter, we demonstrate that by supplementing SILAC media with standard L-proline, the conversion of isotope coded arginine to labeled proline can be prevented. In addition, when providing sufficient amounts of arginine, no back conversion from the increased proline supplement was observed. When proline supplementation of SILAC media was adapted to both mouse and human ESC culture reagents complete labeling with isotope-coded lysine and arginine can be routinely achieved using standard procedures in the absence of feeder cells without compromising the ESC phenotype. We then extend our approach to demonstrate the growth of hESC and hiPSC lines in SILAC conditions using fully-defined, serum-free growth medium.

2.2 Results

In mammalian cells, the metabolism of arginine and proline are related and each can serve as precursors for one another through slightly different, but related pathways (Figure 2.1 C, reviewed in [22]). In a related pathway, both glutamate and glutamine can be precursors for arginine biosynthesis and products of arginine metabolism (Figure 2.1 C). However, only artifacts of proline synthesis from isotopic arginine have been reported in SILAC experiments. This observation raised the question of availability of amino acids *in vitro* cell culture media, particularly in SILAC formulations, since previous *in vivo* mammalian studies have demonstrated that the inter-conversion of amino acids in this pathway (Figure 2.1 C) is primarily dependent on their bioavailability [23]. Since L-proline is a non-essential amino acid, its concentration in the two main basal media used in standard SILAC experiments, RPMI and DMEM, is only 20 and 0 mg/L, respectively. At the same time, the typical concentration of arginine, a metabolic precursor of proline (Figure 1B), is 200 and 84 mg/L, respectively. Based on this we surmised that the arginine to proline conversion artifacts in SILAC experiments were a direct result of the low or absent concentration of proline in standard SILAC labeling formulations.

2.2.1 - Proline availability effects on isotopic arginine conversion to proline. In standard DMEM based SILAC media, in the absence of proline supplement, cells readily convert isotopic arginine to proline, which is then incorporated into newly synthesized proteins. This conversion divides the MS signal of the ‘heavy’ proline containing peptide in a complex fashion, resulting in false relative abundance values when compared to an

equal amount of ‘light’ sample (Figure 2.1 A-B). To eliminate this artifact in arginine-based SILAC procedures, we investigated whether increased L-proline supplementation could prevent the conversion in a concentration dependent manner.

Equal amounts of cell lysates extracted from HeLa cells cultured in SILAC media ($^{13}C_6$ Arg) containing 0 – 800 mg/L proline were digested with trypsin and subjected to LC-MS/MS analysis. Detected proline conversion peptides were used to build a list of peptide candidates for quantification. By using +2 or +3 charge states, the selection of the peptide candidates was based on whether they were observed in all samples, the number of proline residues, the extent of conversion observed, and whether the sequence contained arginine. Based on the triplicate analysis of all lysates, a list of thirteen peptide candidates was chosen and quantified across the 0 – 800 mg/L proline concentrations.

Throughout the titration of L-proline in SILAC media signals of the converted proline containing peptides were monitored (Figure 2.2 A-B). In addition, the ratio of ‘heavy’ labeled Arg peptide to light peptide was measured in order to detect whether a decrease in the converted proline peptide signal resulted in a subsequent increase in the expected ‘heavy’ peptide (Figure 2.2 A-B). Within the set of peptide candidates proline conversion consumed an average of 28% of the monoisotopic signal of the ‘heavy’ arginine peptide in the 0 mg/L proline sample (standard SILAC media) [5]. As the proline concentration was increased to 50, 100, and 200mg/L the monoisotopic ‘heavy’ proline peak occupied 9%, 3%, and 2%, respectively. However, within this list of proline containing peptides no peaks corresponding to a converted proline could be

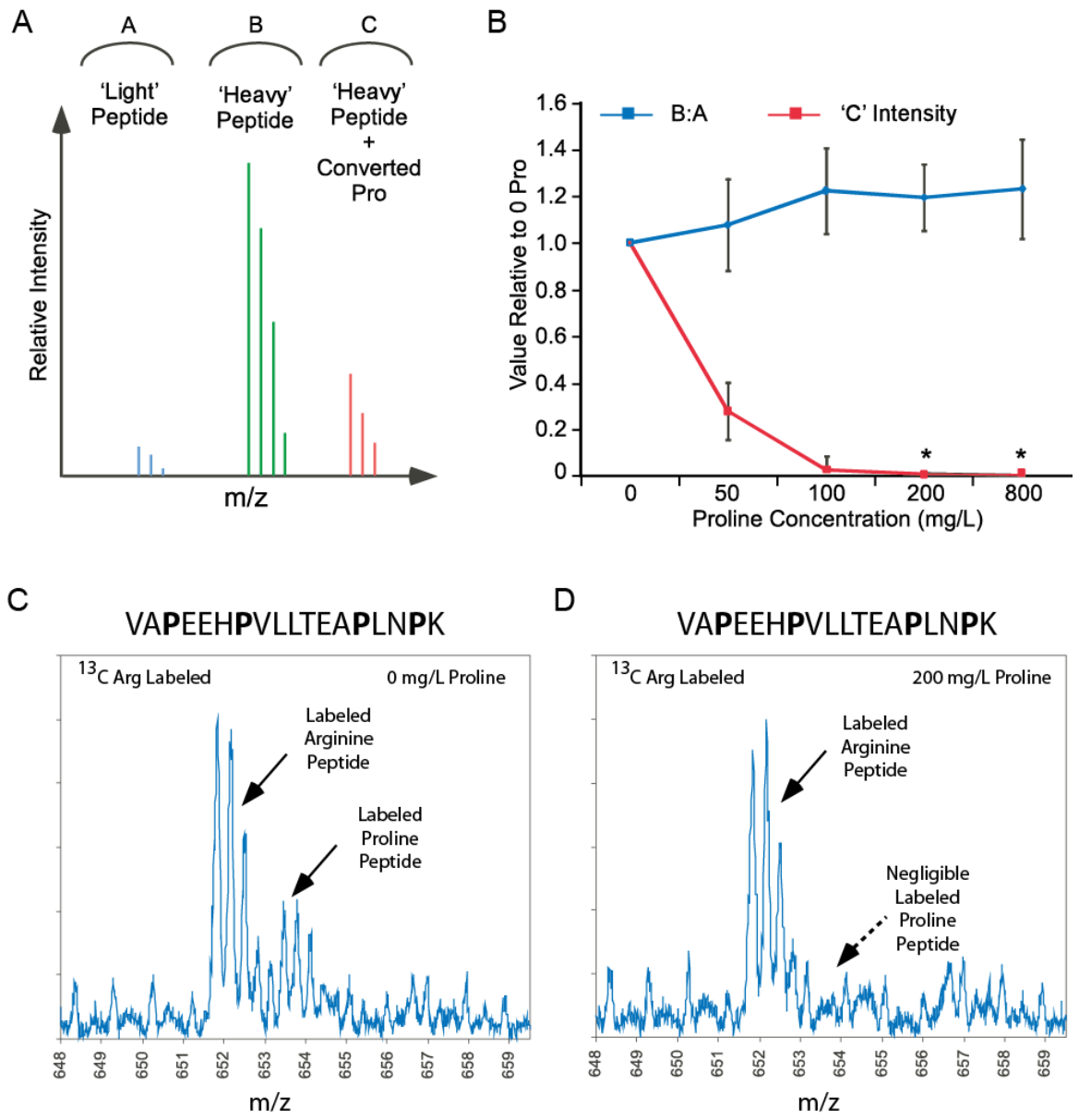

Figure 2.2. Titration of proline during SILAC labeling with isotope coded arginine. Candidate proline containing tryptic peptides were monitored in whole cell extracts in 13C6 arginine samples with 0-800 mg/L L-proline. (A) A conceptual mass spectra indicating the possible peptide ion peaks observed in the arginine labeling experiment. Both the ratio of labeled to unlabeled peptide as well as relative intensity of converted proline peptide ion were monitored in the experiment across 0 – 800 mg/L proline (B) where * indicates no converted proline peptide ions were detectable from background. (C) A mass spectrum from 0 mg/L proline sample representing the peptide VAPEEHPVLLTEAPLNPK at m/z 652 demonstrating a prevalent converted proline peak at +1.7 m/z from the expected peptide ion. (D) Mass spectrum from the 200 mg/L proline sample depicting the same peptide ion as in (C) and the converted proline ion is notably absent.

detected in the MS spectrum beyond 100 mg/L of proline. As such, the 2% of total signal seen at 200 mg/L of proline was a result of un-subtracted background in the MS spectrum where there was low signal-to-noise. Moreover, maximum relative signal of 'heavy' arginine labeled peptide (~20% increase vs 0 mg/L Pro) was seen at 200 mg/L and beyond (Figure 2.2 B). Consequently, even in some of the worst cases of proline conversion (Figure 2.2 C) no proline conversion could be observed in cells supplemented with 200 mg/L of proline or greater (Figure 2.2 D). Taken together, these data not only demonstrate that supplementation of standard SILAC media can eliminate the proline conversion, but also return the "lost signal" to the expected peak within the 'heavy' SILAC sample. Most surprisingly, this critical improvement in arginine-based SILAC methods can be achieved by supplementing cell culture media with as little as 200 mg/L of L-proline.

2.2.2 - Proline availability effects on isotopic arginine labeling. One concern with supplementing an arginine-based SILAC experiment with proline is that, by a similar biosynthetic mechanism (Figure 2.1 C), the excess proline might be a precursor for arginine synthesis thereby decreasing the efficiency of labeling by the isotope-coded arginine provided. While proline is known to be one of the main substrates in the formation of citrulline, a direct precursor for arginine biosynthesis, it has been demonstrated that this process is only favorable when there is a lack of available arginine [23, 24]. Moreover, to date, the presence of other citrulline precursors, such as glutamine in standard SILAC media, has had no reported detrimental effect on SILAC procedures.

To prevent back conversion of proline into arginine and to increase the media's compatibility with nutritionally sensitive cell types like ESCs [7], we re-supplemented the DMEM-based SILAC media with its standard complement of isotope-coded arginine (0.398 mM). This was in direct contrast to the reported reduction of the concentration of isotope-coded arginine in order to prevent its availability for conversion to proline [5, 8]. At the endpoint in the same proline titration experiments we monitored the 'heavy' arginine labeling efficiency by tracking the ratio of 'heavy' to 'light' peptides which contained arginine (Figure 2.3 A). To minimize proline conversion artifacts that would interfere with these calculations, we avoided peptides with proline in their sequence.

In comparison to 0 mg/L proline (standard SILAC media), the average relative peak area for the 50 – 800 mg/L proline samples exhibited only slight deviations, but overall remained unchanged (Figure 2.3 B). Larger deviations were only observed for peptides with lower signal-to-noise ratios and did not have a noticeable trend as a function of proline concentration. None of the arginine peptides examined in the 0 mg/L proline sample (Figure 2.3 C) or even in samples that were supplemented with 800 mg/L of proline (Figure 2.3 D) exhibited an increase in unlabeled 'light' peptide signal. These data provide evidence that our SILAC media formulation (standard arginine in combination with proline supplementation) is effective in minimizing arginine to proline conversion artifacts without compromising the efficiency of isotope-coded arginine labeling. Thus, in the cell types examined here, an arginine concentration of 0.398 mM, even in the presence of high exogenous proline (up to 800 mg/L), is sufficient to prevent observable proline to arginine back conversion that would interfere with SILAC labeling efficiency.

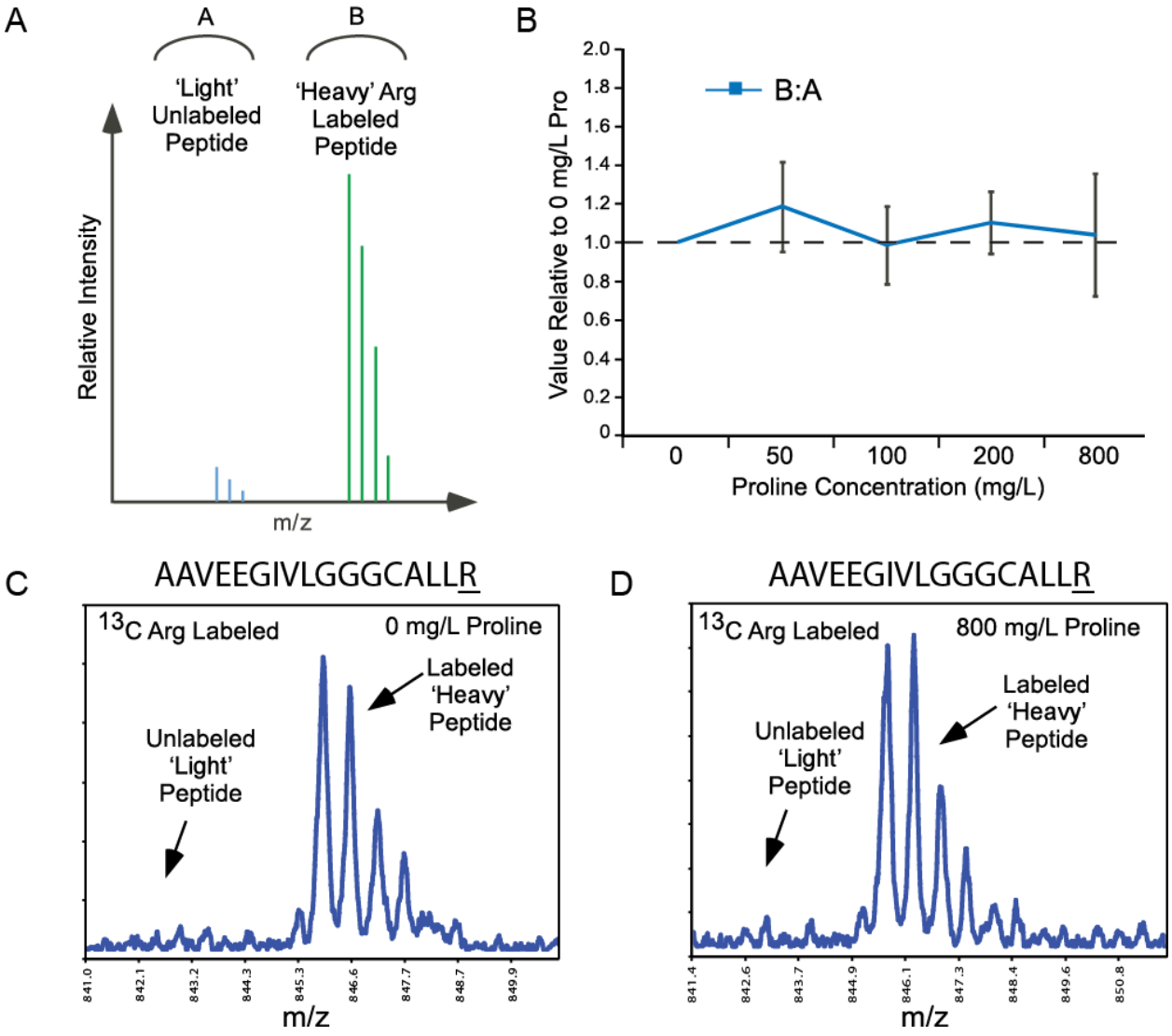

Figure 2.3. Isotope coded arginine labeling efficiency across the titration of proline. Candidate arginine containing tryptic peptides lacking proline were monitored in whole cell extracts in 13C6 arginine samples with 0-800 mg/L L-proline. (A) A conceptual mass spectra indicating the possible peptide ion peaks observed in the arginine labeling experiment. The peak area ratio between the 'heavy' and 'light' arginine monoisotopic peaks was monitored across the 0 - 800 mg/L proline samples and plotted relative to 0 mg/L proline (B). (C) A mass spectrum representing the peptide AAVEEGIVLGGGCALLR at m/z 845 from the 0mg/L proline sample. (D) Mass spectra of the same peptide ion in the 800 mg/L proline sample demonstrating no compromise in the isotope-coded arginine labeling efficiency or proline to arginine back-conversion. Isotopic amino acids are underlined.

2.2.3 - Adaptation of SILAC labeling to feeder-free hESC culture. In order to perform a wide variety of large-scale SILAC-based proteomic experiments with hESCs the ability to generate large numbers of labeled cells has to be achieved. It became clear that SILAC methods compatible with feeder-cell free culture systems would be necessary to attain these high cell numbers (reviewed in [16]). In an attempt to extend standard SILAC labeling procedures to feeder-free hESC culture we confirmed incompatibilities previously highlighted using a feeder-cell based culture system [7]. Using standard SILAC media with $^{13}C_6$ arginine and supplemented with 36 ng/mL basic fibroblast growth factor (bFGF) [25], hESC cultures achieved maximum levels of isotope-coded arginine incorporation after only 2 passages or after more than 12 days under SILAC culture conditions (Figure 2.4 A). By day 15 in SILAC media, hESCs had reached 96.5% average efficiency in isotope coded amino acid labeling. However, in the same period of time the hESCs rapidly differentiated as demonstrated by the loss of SSEA3 expression (Figure 2.4 A), a marker of pluripotent stem cells. We also observed the loss of defined hESC undifferentiated colony structure and tight cell morphology indicating the presence of differentiated cell types (Figure 2.4 B). Moreover, manual inspection of the MS data showed that the conversion of arginine to proline was exacerbated in these cells. While it was clear that arginine incorporation was complete in day 14 samples the proline converted peptide ions were prevalent (Figure 2.4 C). In some extreme cases, converted proline peptide ions consumed greater than 50% of the expected peptide ion signal (Figure 2.4 D). The instability of the hESC phenotype combined with the pronounced arginine to proline conversion artifacts indicated that the

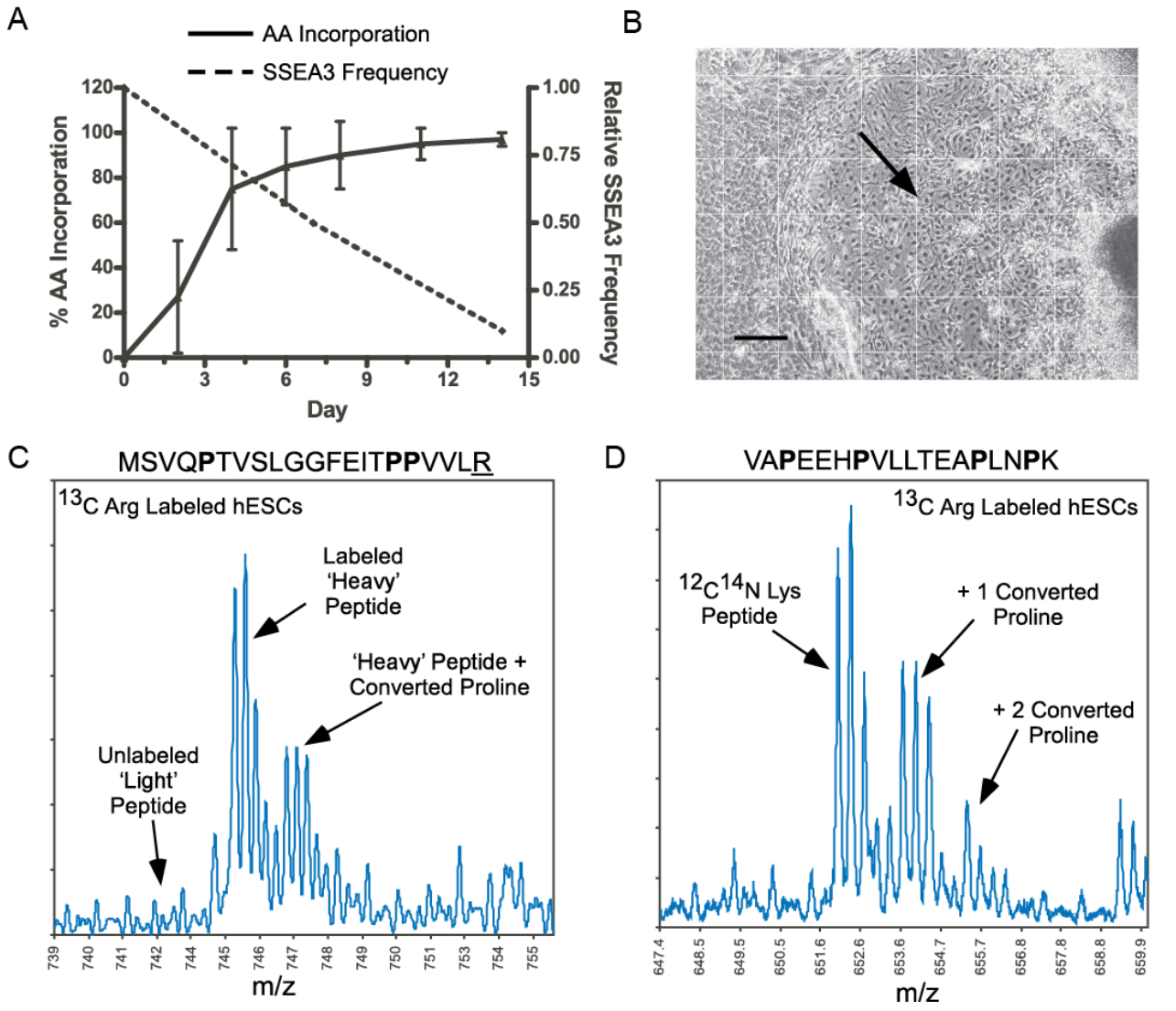

Figure 2.4. Labeling feeder cell free hESCs in standard SILAC media. hESCs culture on Matrigel™ were grown in standard SILAC media (13C6 Arg, dialyzed FBS, 0 mg/L proline) for two weeks. Arginine incorporation, conversion to proline, and hESC phenotype were monitored. (A) The relative SSEA3 frequency and percent heavy arginine incorporation over the SILAC labeling time-course. (B) Differentiated phenotype of hESC after 14 days in standard SILAC media as observed by light microscopy. Scale bars equal 250 µm. (C) A mass spectrum of heavy arginine peptide ion MSVQPTVSLGGFEITPPVVLR at 745 m/z. Indicated are the prominent converted proline peptide ion shifted +1.7 m/z, and the absence of the unlabeled 'light' arginine peptide ion corresponding to the high level of isotopic amino acid incorporation. (D) A mass spectrum of the peptide ion VAPEEHPVLLTEAPLNPK at 652 m/z. Indicated are the peptide ions shifted +1.7 m/z and +3.4 m/z corresponding to the incorporation of 1 and 2 converted 'heavy' proline and consuming more than half of the expected peptide ion intensity. Isotopic amino acids are underlined.

standard SILAC media formulation was not a suitable protocol to adapt to feeder-cell free hESC culture.

There are two main factors responsible for the incompatibility of standard SILAC media with hESC culture, the first being the dialyzed fetal bovine serum (FBS) and the second, the limited growth factor microenvironment (problems reviewed in [16]). To address these issues we revisited the original development of feeder-cell free hESC culture protocols [26]. Xu and co-workers formulated a DMEM based hESC media using a serum replacement reagent [27] that is now commercially available as knockout serum replacement (KOSR – Invitrogen). The hESC media was then pre-conditioned on MEF cell feeder layers to supply the appropriate complement of signaling molecules and growth factors to maintain hESC homeostasis. This method has since become the most widely adopted form of feeder-cell free hESC culture. Coincidently, the KOSR formulation contains no free lysine or arginine, making it compatible with most popular SILAC applications. Moreover, as we demonstrate to be important here, KOSR contributes 800 mg/L of proline when used at 20% (v/v) in hESC media [27].

A hESC SILAC media with 20% KOSR and ^{13}C ^{15}N arginine and lysine was formulated taking into account the SILAC compatibility of the media (see experimental methods). The hESC SILAC media was then pre-conditioned on irradiated MEFs according to previously established protocols [26]. The resulting media, when supplemented with 8 ng/mL of bFGF, allowed hESCs to incorporate the isotope coded amino acids at the same rate as observed with standard SILAC media where after 2 passages and more than 12 days in SILAC culture hESC had reached their maximum levels of incorporation

(Figure 2.5 A). Consistent with the preliminary proline titration data, there was no difficulty encountered in isotopic amino acid labeling since the cells were on average 96.1% labeled by day 14. Moreover, in the new media formulation the cells were now able to maintain SSEA3 expression (Figure 2.5 A) and continue to form tight, undifferentiated colony structures (Figure 2.5 B). Inspection of the MS spectra (Figure 2.5 C) of the hESC lysates labeled using the new formulation demonstrated the same level of isotopic amino acid incorporation as standard SILAC media when examining the same peptides (Figure 2.4 C). Additionally, for the same peptide there was no longer any arginine to proline conversion artifacts observed (Figure 2.5 C), even when examining peptides with the highest proportion of converted proline peptide ions (Figure 2.5 D vs 2.4 D). Consequently, when a 14 day SILAC labeled (^{13}C ^{15}N Arg and Lys) hESC extract was mixed 1:1 with a 'light' hESC lysate, equivalent levels of the expected 'light' and 'heavy' peptides are observed even in sequences most susceptible to proline conversion artifacts (Figure 2.5 D). These observations clearly demonstrate that combining KOSR as an alternative serum supplement with both a SILAC compatible hESC media formulation and pre-conditioning on feeder cells offers a reliable solution for large-scale hESC applications in quantitative proteomic without compromising data quality.

2.2.4 - SILAC procedures with feeder-free mESC cultures. Recently, a landmark analysis of mESCs using a SILAC approach was reported by Graumann *et al*. in which a total of 5111 proteins were identified [17]. However, this study was also routed in a feeder-cell based culture system which, by the authors own admission, contributed to contamination in the analysis. To circumvent this issue these authors performed a

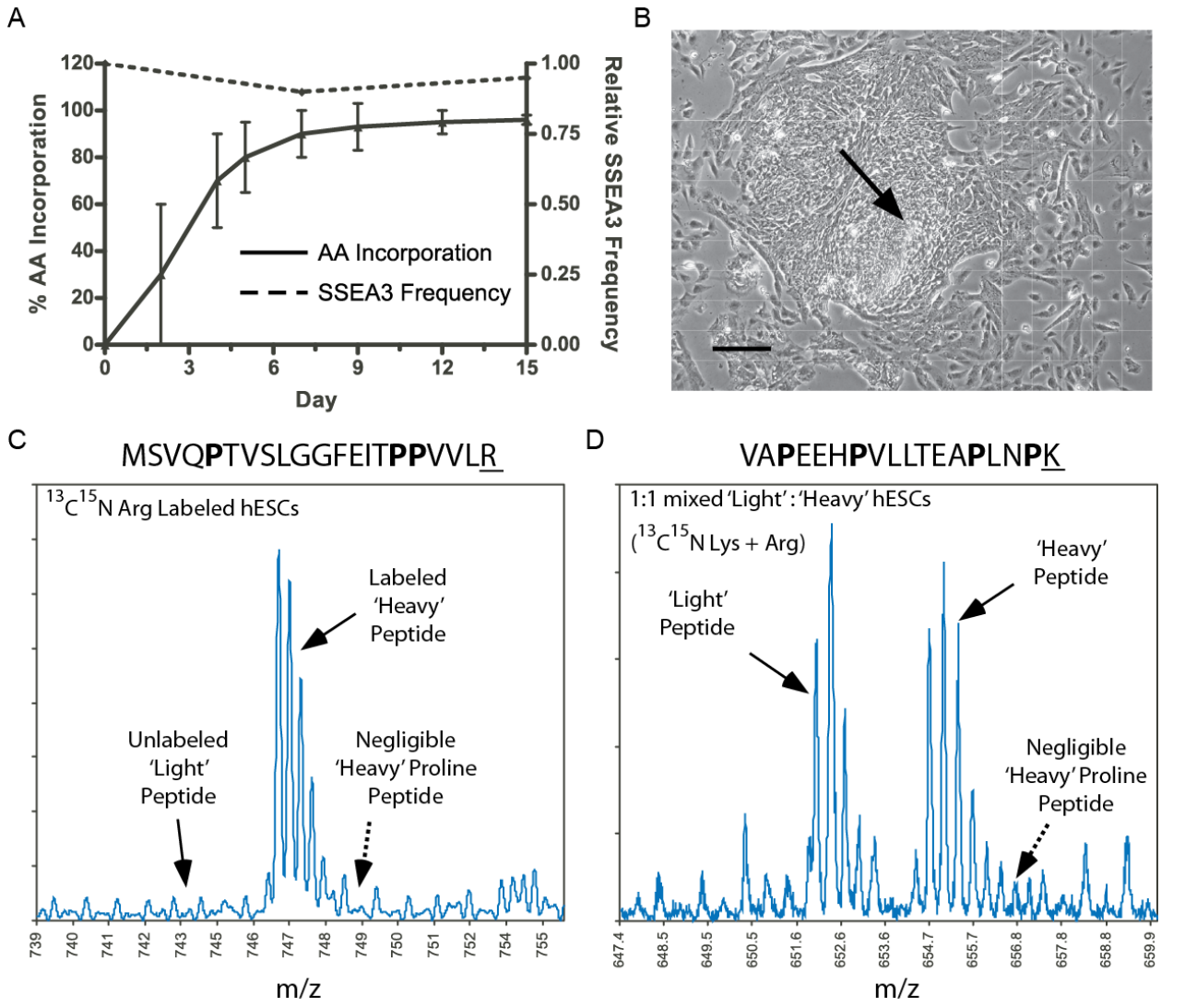

Figure 2.5. Labeling feeder cell free hESCs in conditioned SILAC media with KOSR. hESCs cultured on Matrigel™ were grown in MEF conditioned ESC optimized SILAC media (13C 15N Arg and Lys, 20% KOSR providing 800 mg/L L-proline) for two weeks. Amino acid incorporation, conversion of arginine to proline, and hESC phenotype were monitored. (A) The relative SSEA3 frequency and percent heavy amino acid incorporation over the SILAC labeling time-course. (B) Undifferentiated phenotype maintained by hESCs after more than 15 days in optimized SILAC media as observed by light microscopy. Scale bars equal 250 µm. (C) A mass spectrum of heavy arginine peptide ion MSVQPTVSLGGFEITPPVLR at ~747 m/z. Indicated are the absence of both a converted proline peptide ion and the unlabeled 'light' arginine peptide ion. The absent 'light' peptide ion at 743 m/z also indicates no back-conversion of proline to unlabeled arginine. (D) A mass spectrum of the 1:1 mixed labeled and unlabeled hESC lysates showing 'light' and 'heavy' peptide ion VAPEEHPVLLTEAPLNPK at ~652 m/z and 655 m/z. The prominent converted proline peptide ions are now almost undetectable and do not effect the observed 1:1 ratio. Isotopic amino acids are underlined.

cumbersome transition from feeder cell to feeder cell free culture during the labeling process. As these authors noted, the use of dialyzed FBS, prescribed in standard SILAC media [28], made feeder cell independent culture of mESCs difficult. Moreover, having to culture mESCs on feeder layers and/or transition those to feeder cell independent conditions could negatively impact both the scalability of this procedure and the integrity of the mESC phenotype. Because KOSR was originally designed and used as an alternative to FBS for the culture of mESCs [27] we hypothesize that the formulation that we successfully applied to hESCs could also be used in creating a protocol to perform SILAC on completely feeder-cell independent mESC cultures.

Therefore a mESC SILAC media containing 15% KOSR was formulated [27] and the media supplemented with 1000 U/mL of leukemia inhibitory factor (LIF) prior to addition to feeder cell free mESC cultures. After 4 passages in our mESC SILAC media the pluripotent culture morphology was indiscernible from those mESCs cultured under standard conditions (Figure 2.6 A-B). After the same period of time mESCs also achieved maximum incorporation of isotopic amino acids (^{13}C ^{15}N Arg and Lys) (Figure 2.6 C) with an average labeling of 96.3%. Moreover, visual inspection of SILAC labeled mESC MS spectra demonstrates similar results as observed with hESCs samples where there is no compromise with levels of isotopic arginine incorporation and no detectable incidence of proline conversion artifacts even in peptide ions with multiple proline residues in the sequence (Figure 2.6 D). In accordance with the observations in the hESC system, the application of a KOSR based SILAC media to a feeder-cell free mouse ESC culture, now provides a robust protocol for routine, large-scale quantitative proteomic experiments using SILAC in mESCs as well.

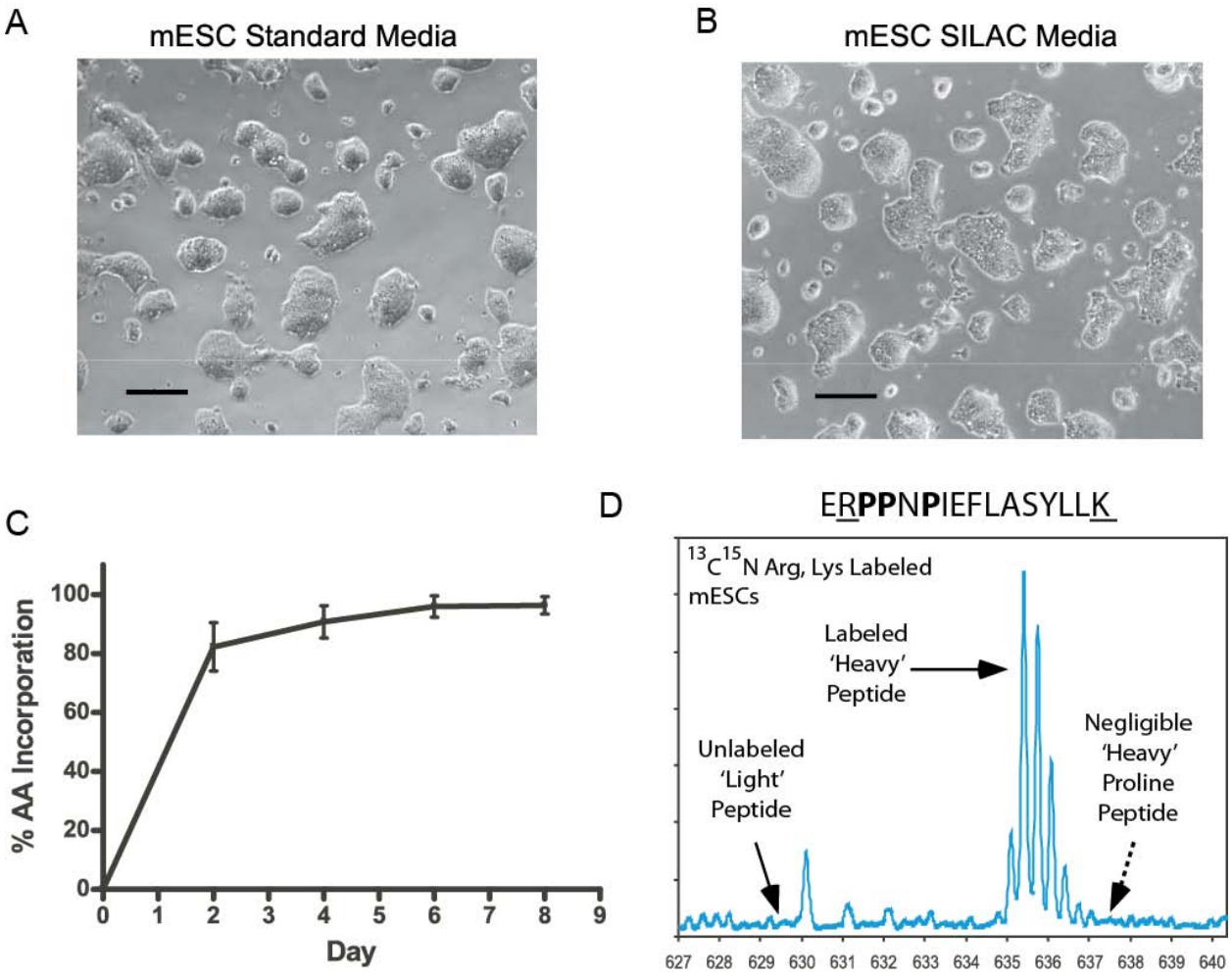

Figure 2.6. Labeling feeder cell free mESCs in conditioned SILAC media with KOSR. mESCs cultured on gelatin were grown in ESC optimized SILAC media (13C 15N Arg and Lys, 15% KOSR providing 600 mg/L L-proline) for 4 passages (8 days). Amino acid incorporation, conversion of arginine to proline, and mESC phenotype were monitored. The undifferentiated phenotype of mESCs grown under standard feeder cell free conditions (A) compared to those grown in optimized SILAC media for 8 days (B) as observed by light microscopy. Scale bars equal 250 µm. (C) The average heavy Lys and Arg incorporation over the SILAC labeling time-course. (D) A mass spectrum of peptide ERPPNPIEFLASYLLK at 635.6 m/z from mESCs in ESC optimized SILAC media. The 'heavy' Lys and Arg peptide ion is prominent while the unlabeled 'light' peptide or converted 'heavy' proline peptide ions are absent. The absent 'light' peptide ion at m/z 633 also indicates no back-conversion of proline to unlabeled arginine. Isotopic amino acids are underlined.

2.2.5 - SILAC of hESCs and hiPSCs in Defined Conditions. With the recent demonstration that somatic cells can be reprogrammed to generate pluripotent cells, a significant increase in the number of studies employing these induced pluripotent stem cells (iPSC) have been carried out [29]. The clinical potential of human iPSCs (hiPSC) necessitates the need for their culture in defined, xeno-free conditions. As such, a variety of formulations have recently become commercially available [30], many of which can be paired with xeno-free growth matrices. However, very few of these alternatives offer the tested stability and universality of MEF-CM combined with the basement matrix Matrigel™™.

Our previously discussed methods for performing SILAC in human and mouse ESCs utilizes an undefined KOSR-based medium. Since this medium requires pre-conditioning on MEF feeder layers, it is xenogenic and undefined in nature. Coupled with this is the potential for contamination with unlabeled amino acids as a result of conditioning. Although proteomic analyses have attempted to profile the MEF derived contribution to MEF-CM, the composition can vary significantly from batch to batch [31-33]. In order to perform SILAC in any cell system, the ability to control culture medium components is essential. Development of a defined culture medium amenable to SILAC experimentation in hESCs and hiPSCs would be a significant development for proteomics researchers.

Based on this, we have adapted a commercially available, fully-defined, serum-free medium formulation for performing SILAC in hESCs and hiPSCs [34]. After 10 passages in SILAC medium (>60 days), H9, CA1, and BJ-1D stem cell lines maintained

expression for Oct3/4 and Nanog as indicated by RT-PCR (Figure 2.7 A). All of the tested stem cell lines also retained Oct3/4 and SSEA4 marker expression as visualized using immunofluroescence (Figure 2.7 B). Marker expression was further validated using flow cytometry for SSEA4 and SSEA1 in all cell lines (Figure 2.7 C). After the induction of differentiation *in vitro* using embryoid body assays, all cell lines exhibited increased expression of markers characteristic of each of the three primary germ layers (Figure 2.7 D). Additionally, H9 and CA1 hESCs also retained the ability to differentiate *in vivo* as observed using a teratoma assay. Taken together, these data indicate that extended culture in StemPro-based SILAC medium is capable of maintaining hESC and hiPSC lines in an undifferentiated and pluripotent state.

To test the compatibility of the defined medium for SILAC experimentation, we monitored incorporation of isotopically labeled versions of arginine and lysine. Examining multiple peptides revealed that >96% incorporation can be achieved after just 7 days in defined medium supplemented with isotopically labeled arginine and lysine (Figure 2.8 A). By examining the amino acid composition of the defined culture medium we determined that there was no significant source of L-proline. When cells were grown in defined medium containing no exogenous L-proline, significant conversion from arginine can be observed (Figure 2.8 B). After the addition of 800mg/L of L-proline, there is no longer any signal observable for the isotopically labeled proline containing peptide (Figure 2.8 C). Analysis of 1:1 mixed light and heavy lysates reveals that the addition of L-proline in defined medium restores the previously skewed expected peptide abundance ratio (Figure 2.8 B-C). These observations validate our previous data for SILAC experiments performed in KOSR-based medium.

Figure 2.7. Labeling feeder cell free hESCs and hiPSCs in defined serum-free SILAC media. H9, CA1, and BJ-1D were maintained in StemPro SILAC medium with 13C, 15N Arg and Lys, as well as 800mg/L of L-Proline. Following 10 passages, each cell line was assayed for conventional markers of an undifferentiated state. (A) Each cell line maintained strong expression for the markers Oct3/4 and Nanog as determined by RT-PCR. Data is relative to specific matched cell line controls on Matrigel™ in MEF-CM. Error bars represent SD, n=3 (B) Immunocytochemistry data demonstrate expression of Oct3/4 and SSEA4 in all cultures. Scale bars indicate 250um. (C) Flow cytometry data for all cell lines assaying SSEA4 and SSEA1 expression, n=3. All lines maintained strong signal for SSEA4 with minimal SSEA1. Viability was determined using 7-AAD staining. Populations were gated based on 7-AAD exclusion. (D) Embryoid bodies were generated using cells grown in SILAC medium. Phase contrast images showing representative embryoid bodies for each cell line. Scale bars represent 250um. Graphs below show RT-PCR analysis for the markers of pluripotency (Oct3/4, Nanog), trophoblast (CDX2), ectoderm (NeuroD1, PAX6), endoderm (GATA6, GATA4, alpha-fetoprotein), mesoderm (T). Values are fold change relative to cell line specific undifferentiated controls. Error bars represent SD, n=2. RT-PCR assays in both (A) and (D) use RPLPO as a positive control. (E) In vivo analysis of pluripotency. Representative tissues from the three primary germ layers are displayed. Endoderm : gut epithelium (i), columnar epithelium (iv), Mesoderm: muscle tissue (ii, v), cartilage (iv), Ectoderm: neural epithelium (iii), neural-like tissue (vi). Arrows denote structures of interest. Scale bars represent 100um.

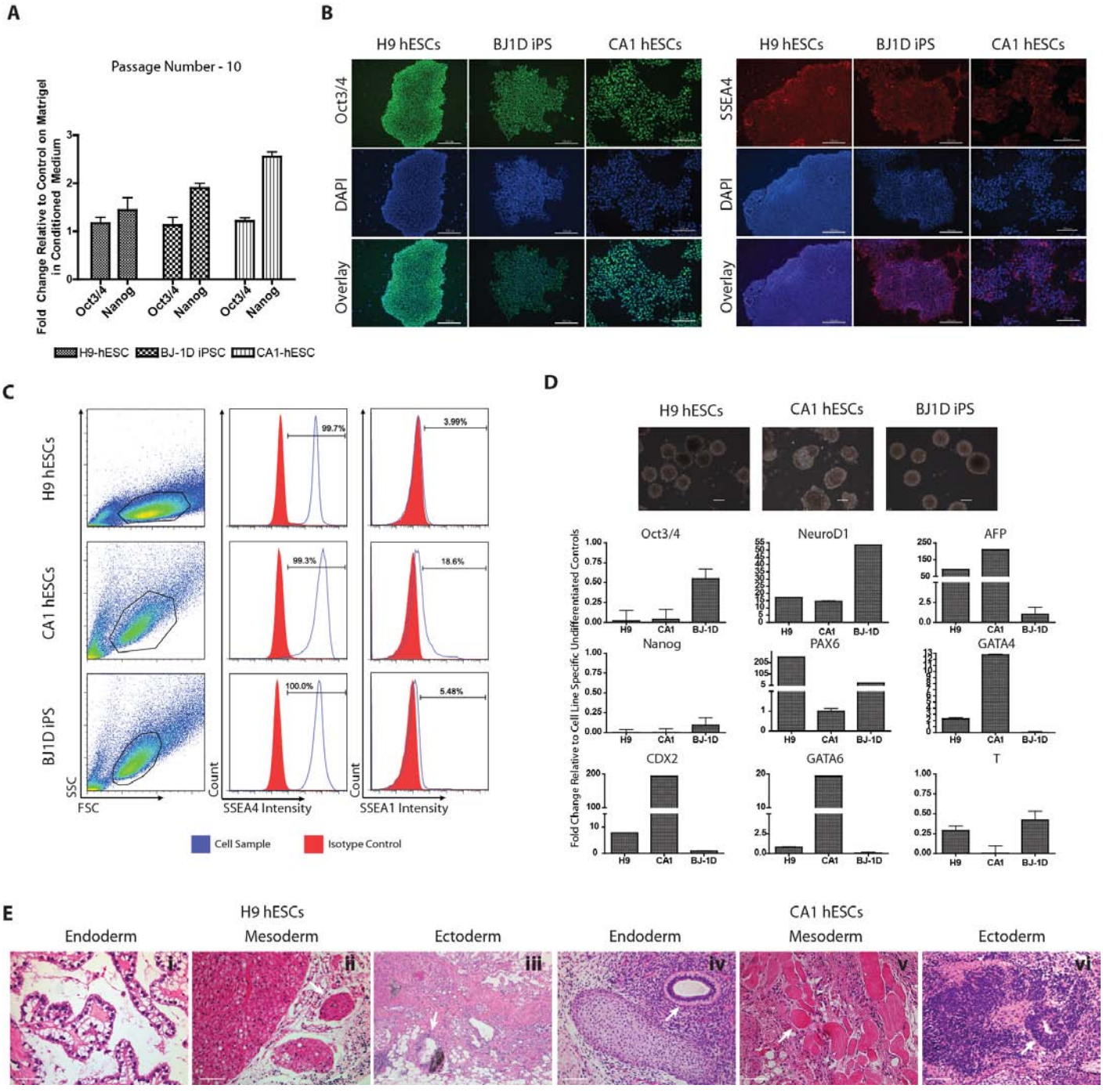
A
Passage Number - 10
Fold Change Relative to Control on Matrigel in Conditioned Medium
Oct3/4
Nanog
H9-hESC
BJ-1D iPSC
CA1-hESC
B
H9 hESCs
BJ1D iPS
CA1 hESCs
Oct3/4
DAPI
Overlay
SSEA4
C
H9 hESCs
CA1 hESCs
BJ1D iPS
99.7%
3.99%
99.3%
18.6%
100.0%
5.48%
SSC
FSC
Count
SSEA4 Intensity
SSEA1 Intensity
Cell Sample
Isotype Control
D
H9 hESCs
CA1 hESCs
BJ1D iPS
Oct3/4
NeuroD1
AFP
Nanog
PAX6
GATA4
CDX2
GATA6
T
Fold Change Relative to Cell Line Specific Undifferentiated Controls
H9
CA1
BJ-1D
E
H9 hESCs
CA1 hESCs
Endoderm
Mesoderm
Ectoderm
Endoderm
Mesoderm
Ectoderm
i
ii
iii
iv
v
vi

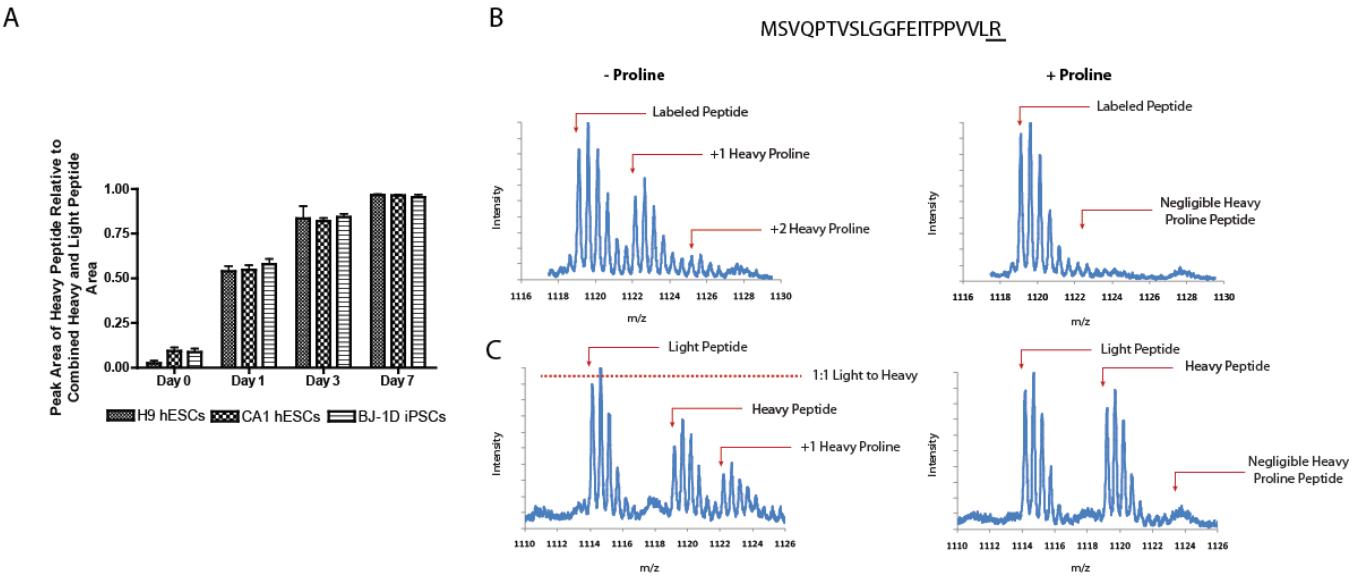

Figure 2.8. Efficient isotopic label incorporation achieved through the use of defined SILAC medium. hESCs and hiPSCs were grown for a period of 7 days in StemPro SILAC medium containing 13C, 15N arginine and lysine. (A) H9, CA1, and BJ-1D stem cells were harvested at 0,1,3, and 7 days following application of StemPro SILAC medium. Label incorporation was obtained by comparing peak areas for combined scans of light and heavy peptides. A total of 5 peptides were compared in each cell line. (B-C) H9 stem cells grown in the presence and absence of L-proline were tryptically digested and analyzed by MS. Analysis of the proline containing peptide MSVQPTVSLGGFEITPPVVLR revealed a significant heavy proline amino acid signal in the absence of exogenous L-proline. The resulting skew in expected peptide ratio from a 1:1 mixture of light and heavy cell lysate can be seen in (C). Following the addition of L-proline, negligible signal for the heavy proline containing peptide remains and the expected peptide ratio is restored in (C). Isotopically labeled amino acids are underlined.

2.3 Discussion

Most SILAC procedures take a reductionist approach in controlling amino acid content in cell culture to achieve the desired labeling outcome. These include the use of dialyzed FBS, reduced concentration or total removal of many amino acids (i.e. Arg and Pro), and overall culture conditions optimized using immortalized tissue culture. We believed these methodological aspects preclude the extension of SILAC procedures to ESCs and were at the heart of amino acid conversion artifacts seen using the general labeling procedure. In this chapter, we demonstrate that through supplementation of isotope-coded arginine based SILAC experiments with as little as 200 mg/L of L-proline, isotopic arginine to proline conversion artifacts can be virtually eliminated in a variety of cell types. In addition, using KOSR which provides 800 mg/L of L-proline at 20% as a serum supplement in lysine and arginine based SILAC experiments instead of dialyzed FBS creates a robust media formulation for completely feeder-cell free SILAC experiments using ESCs from both the mouse and the human. We also tested the compatibility of a fully-defined, serum-free medium for use in SILAC experiments with hESCs and hiPSCs. With this medium we were able to maintain all hESC and hiPSC lines tested for an extended period in an undifferentiated and pluripotent state. Moreover, with the addition of L-proline at a concentration of 800mg/L to the medium, we could successfully eliminate conversion from isotopically labeled arginine.

Based on the cellular pathways of proline and arginine metabolism, the addition of proline is an obvious solution to the conversion issue, however the concern has always been the potential back conversion to arginine which would interfere with isotope-coded

arginine labeling [8]. Some studies, such as the recent one using SILAC in mESCs stress that all reagents were prepared without proline for this very reason [17]. To our knowledge, no study to date has demonstrated that the presence of proline actually induces significant back conversion to arginine in a concentration dependent manner during a SILAC procedure. In fact, we demonstrate here that between 0 and 800 mg/L proline that there is no significant change detectable in the labeling of cells with isotope-coded arginine.

Proline is a preferred precursor for arginine biosynthesis in neonates *in vivo* just as arginine is for proline. However it has been clearly demonstrated in a number of studies that the *de novo* biosynthesis of either arginine or proline using the other as a precursor is most strongly influenced by their bioavailability [23, 24, 35]. In other words, if there is sufficient free proline present to maintain cellular homeostasis the endogenous production of proline will not be favored, regardless of the concentration of its available precursors. The same statement can be made in the opposite direction for arginine. With respect to energy and metabolism this observation makes sense as it would be the most efficient. Even though a diminished arginine concentration may be sufficient in certain cell types, it has been reported that this is not completely efficient at preventing proline conversion artifacts [3, 8]. Our study suggests that this was due to the absence of proline in the standard SILAC media formulation. While the inter-conversion of proline and arginine may still exist in cells labeled with isotope-coded arginine using our media formulation, we were unable to detect it with any level of significance. More importantly, our strategy of supplying additional or high concentrations of amino acids

appears to be more effective at eliminating the problem and makes our strategy the most applicable to biologically important *in vitro* cell types like embryonic stem cells.

This work however, is limited in the number of cell lines and peptides tested. Recent research from two groups has expanded this analysis to include a variety of cell lines and thousands of peptides [36, 37]. Comparing the log2 ratios of peptides and proteins from 293T cells harvested under conventional SILAC conditions or those where proline is supplemented, Lossner *et al.* observed a shift in the expected peptide ratio only in the absence of exogenous proline supplementation. Marcilla *et al.* were able to virtually abolish arginine conversion by supplementing with as little as 300 mg/L of proline [37]. They also observed that there was no back conversion to arginine after proline supplementation as has been suggested previously [38], further validating our results. Both of these studies indicated no negative effects on cell viability as a result of proline addition.

We have illustrated the ability to eliminate conversion of isotopically labeled arginine to proline when performing SILAC experiments in ESCs. Through the supplementation of as little as 200mg/L of L-proline, conversion can be eliminated to undetectable levels. We also demonstrated the growth and maintenance of hESC and hiPSC lines in fully defined SILAC medium. Since our publication other groups have demonstrated large-scale characterization of hESCs using our methods [39]. Although the ability to perform SILAC in defined conditions is a significant step for hESCs and hiPSCs, extension of this work to a xeno-free medium is desirable.

2.4 Experimental Methods

2.4.1 SILAC media formulations - All SILAC media formulations and labeling procedures were modified from previously described protocols [5, 28]. With the exception of the defined SILAC medium, all SILAC labeling experiments used embryonic stem cell qualified Dulbecco's Modified Eagle's Medium (DMEM – 4500mg/L glucose, with Na pyruvate, and no L-glutamine) that was custom ordered without lysine or arginine (Specialty Media – Millipore). Before use, media was re-supplemented with 2.5 mM L-glutamine (Invitrogen), 0.798 mM isotope-coded L-lysine ($^{13}C_6$ $^{15}N_2$), and 0.398 mM isotope-coded L-arginine (either $^{13}C_6$ or $^{13}C_6$ $^{15}N_4$). In the case of 'light' media, standard L-lysine and L-arginine were used. The DMEM for ESC cell culture was supplemented with 0.1 mM 2-mercaptoethanol, 1% non-essential amino acids (NEAA - Invitrogen), and 20% or 15% Knockout Serum Replacement (KOSR - Invitrogen) reagent for hESC or mESC culture, respectively. Note that ESC media with 1% NEAA will have 11.5 mg/L proline while KOSR at 20% and 15% (v/v) will contribute an additional 800 and 600 mg/L of L-proline, respectively [27]. For HeLa cell culture the DMEM was supplemented with 10% (v/v) dialyzed fetal bovine serum (FBS), 1% (v/v) penicillin-streptomycin (both Invitrogen), and 0 to 800 mg/L of L-proline (Sigma). All media were filter sterilized at 0.2 µM.

2.4.2 SILAC labeling of human and mouse ESCs and iPSCs - For SILAC labeling of both hESC, hiPSC, and mESC cultures measures were taken to remove all non-isotopic Arg and Lys from the system. All cells were washed with either PBS or DMEM lacking Arg and Lys prior to exposure to SILAC media. Any reagents requiring dilution with

DMEM were prepared in DMEM lacking Arg and Lys as well. hESC lines H1 and H9 [40] were maintained in feeder-free culture on 1:15 Matrigel™™ (BD Biosciences) coated plates. hESC SILAC media was supplemented with 4 ng/mL basic fibroblast growth factor (bFGF – Invitrogen) and pre-conditioned on irradiated mouse embryonic fibroblasts (MEFs) according to previously established protocols [26]. The MEF conditioned hESC SILAC media was further supplemented with 8 ng/ml bFGF prior to addition to hESC cultures and changed daily. Cells were passaged every 5-7 days through dissociation with 200 U/mL collagenase IV (Invitrogen). hESCs were cultured for two passages (> 12 days) in SILAC media to achieve maximum isotopic amino acid incorporation. Analysis of hESC culture integrity and expression of pluripotent cell surface markers was performed as previously described [41]. E14K mESC cultures from 129Ola mice were also maintained in the absence of feeder cells on 0.1%(v/v) gelatin (Sigma) coated plates as previously described [42]. mESC SILAC media was supplemented with 1000 units/ml leukemia inhibitory factor (LIF – ESGROW, Millipore) prior to addition to cultures. Cells were passaged 1:3 every 2 days through dissociation in 0.25% trypsin, 2.21 mM EDTA (Wisent). mESCs were cultured for 4 passages (> 8 days) in SILAC media to achieve maximum isotopic amino acid incorporation.

For SILAC experiments in defined medium, hESC (H9, CA1) and hiPSC (BJ-1D) cell lines were grown in feeder-free conditions on 1:30 Matrigel™™ (BD Biosciences. The CA1 hESC line used in all experiments was obtained from Dr. Cheryle Séguin of The University of Western Ontario [43, 44]. The hiPSC line BJ-1D was derived by reprogramming using retroviral transduction of BJ fibroblasts with the Yamanaka factors

essentially as we have previously described [45] and validated as pluripotent using in vitro and in vivo differentiation assays and expression profiling (unpublished results). Custom DMEM/F12-glutamax that contained no L-arginine or L-lysine was ordered from Invitrogen. SILAC medium was prepared using the StemPro hESC Media system with our custom DMEM/F12 (Invitrogen) according to manufacturer instructions. [$^{13}C_6$, $^{15}N_4$] – L-arginine and [$^{13}C_6$, $^{15}N_2$] – L-lysine (Cambridge Isotope Laboratories, Andover, MA) were supplemented into the SILAC medium at 71.42mg/L and 80mg/L respectively. Unlabeled L-proline was added to the SILAC medium at a final concentration of 800mg/L. Culture medium was changed daily and cells were passaged every 4-5 days by manual dissection and harvesting of colonies.

Embryoid bodies (EB) were generated using Aggrewell 400Ex plates (StemCell Technologies, Vancouver, Canada). Briefly, 2 x 10^6 hESCs were harvested enzymatically using Accutase (Invitrogen) from Matrigel™™ coated plates. Cells were reconstituted in Aggrewell medium supplemented with Rock inhibitor (Y-27632, Sigma-Aldrich, St. Louis, MO) at a final concentration of 10μM. After plating in Aggrewell dishes, EBs were grown for 48 hours at 37°C prior to transfer to ultra-low adherence tissue culture dishes (Corning, Lowell, MA). After 15 days of culture, EB RNA was harvested using Trizol extraction according to the manufacturer's instructions (Invitrogen). EBs were assayed for expression of CDX2, alpha-feto protein (AFP), GATA-6, GATA-4, Oct3/4, PAX-6, T-brachyury, Nanog, and Neurogenic differentiation 1 (NeuroD1) using TaqMan primer probe sets (Invitrogen). Assay information can be found in Appendix Table 1.15. All EB assays were performed in biological and technical duplicate for each cell line and condition.

2.4.3 Preparation and digestion of cell samples - To monitor isotopic amino acid incorporation and conversion trypsin digests were prepared from whole cell lysates for LC-MS analysis. Cell culture media was removed and cells were washed with PBS. Cells were then mechanically removed from the plate, lysed by dissociation in 8M urea and 50 mM ammonium bicarbonate, and frozen at -80°C. The protein content was determined by Bradford assay and, where indicated, 'light' and 'heavy' isotopic samples were mixed 1:1 based on total protein concentration prior to digestion. For trypsin digestion, samples were reduced with 10 mM DTT, alkylated with 30 mM iodoacetamide, diluted 1:4 with 50 mM NH_4CO_3 and treated with modified trypsin (1:25 enzyme/substrate ratio - Promega) at 37°C overnight. The resulting tryptic peptides were extracted using a 1-mL C_{18} solid phase extraction cartridge (Waters), eluted with 50% (v/v) ACN, 0.1% (v/v) formic acid (FA) to remove urea and salts and were re-concentrated in a vacuum centrifuge. Dried fractions were reconstituted in 10% FA for LC-MS/MS analysis.

2.4.4 Liquid chromatography tandem mass spectrometry (LC-MS/MS) analysis - Between 1.0 and 0.5 µg of each original sample was injected on a NanoAcquity UPLC (Waters) equipped with a 15cm x 75µm C18 reverse phase column employing a 90-minute LC gradient (5-40% ACN, 0.1% FA) and detected in a data-dependent acquisition (DDA) mode by tandem MS (Q-ToF Ultima - Waters). The MS was directed to use the following DDA parameters: survey scan range 400-1800 m/z, 1 s scan, 1-4 precursors selected based on charge state (+2, +3 and +4 ions). MS/MS fragmentation was then performed on the ions using the charge state collision energy profile function.

2.4.5 Analysis of isotopic amino acid labeling and conversion - Data analysis for all samples was performed in PEAKS 5.3 software (Bioinformatic Solutions Inc., Waterloo, Canada) [46, 47]. After import into PEAKS, MS/MS spectra from raw data files were refined using the following settings: merge spectra – true (100ppm mass tolerance, 60 second retention time tolerance), correct precursor mass – true, determine precursor charge state – true (minimum charge +2, maximum charge +5), spectral quality filter – true (0.65 threshold), centroid, deisotope, and deconvolute – true. Resulting MS/MS spectra were then *de novo* sequenced using the following parameters: parent monoisotopic mass tolerance – 100ppm, fragment monoisotopic mass tolerance – 0.15 daltons, enzyme specificity –Trypsin, fixed modifications – carbamidomethylation and +10 daltons on Arginine and +8 daltons on Lysine for SILAC, variable modifications – oxidized methionine. After *de novo* analysis, data were searched against the UniProt sequence database (Human taxonomy specified, 20236 total entries) using the following parameters: parent monoisotopic mass tolerance – 100ppm, fragment monoisotopic mass tolerance – 0.15 daltons, , enzyme specificity –Trypsin, fixed modifications – carbamidomethylation and +10 daltons on Arginine and +8 daltons on Lysine for SILAC, variable modifications – oxidized methionine, estimate false-discovery rate – true. Identified peptides were chosen randomly to be investigated manually using MassLynx 4.1. The peak area was determined by integration using the built-in algorithm in MassLynx 4.1 to output peak area values. Peak area of the monoisotopic ions were used for comparison and determination of quantitative ratios of peptide candidates.

2.4.6 Titration of proline - HeLa cells were passaged twice at a ratio of 1:8 in SILAC media containing the indicated amount of L-proline to ensure maximum incorporation of the isotopic arginine label (either $^{13}C_6$ or $^{13}C_6$ $^{15}N_4$ Arg). SILAC media was changed every 3 days, or as needed based on phenol red indicator. Whole cell lysates were digested and subject to LC-MS/MS in the initial sample analysis. Both potential and confirmed (by MS/MS) proline containing peptides resulting from the conversion of isotopic arginine were noted. All samples were then re-run in triplicate using the "include only" function to target previously detected/suspected proline containing peptides across all samples. The candidate list of proline containing peptides was then used to follow the conversion of arginine to proline over varying proline supplement concentrations. Peptides containing labeled proline derived from isotope-coded arginine were confirmed by MS/MS in the 0 and 50 mg/L proline samples. Thirteen proline converted peptides observed in the replicate analysis and confirmed by MS/MS were used to monitor isotopic arginine to proline conversion in these experiments. These were: VAPEEHPVLLTEAPINPK, LILPGELAK, PMFIVNTNVPR, NTGIICTIGPASR, MSVQPTVSLGGFEITPPVVLR, PPYTVVYFPVRGR, YSSLVPIEK, AVFPSLVGRPR, VAPEEHPVLLTEAPINPK, SSGPYGGGGQYFAKPR, QYPKVPR, LAVNMVPFPR, and SSRAGLQFPVGR.

To investigate the possible back conversion of proline to arginine, a similar process was repeated except the arginine containing peptide candidates did not have a proline in their sequence, so that proline conversion could not interfere with arginine incorporation calculations. Based on replicate analysis, those peptides used for arginine incorporation that were consistently observed and confirmed MS/MS were: STELLIR,

AGTGVDNVDLEAATR, VIGSGCNLDSAR, TIAQDYGVLKADEGISFR, GKVKVGVDGFGR, and GITINAAHVEYSTAAR.

2.4.7 SILAC Label Incorporation - In order to monitor isotope-coded amino acid incorporation and determine the optimum times for SILAC adaptation a list of both Lys and Arg containing candidate peptides for both human and mouse ESCs was generated. Incorporation was obtained by comparing peak areas from combined scans of light and heavy peptides. Those candidate peptides that were consistently identified by MS/MS across all samples during the labeling time course were: NLPQYVSNELLEEAFSVFGQVER, IHFPLATYAPVISAEK, SLQDIIAILGMDELSEEDKLTVSR, LISWYDNEFGYSNR, GVDEVTIVNILTNR, SSGPTSLFAVTVAPPGAR, ALMLQGVDLLADAVAVTMGPK, EVAAFAQFGSDLDAATQQLLSR, LLEDGEDFNLGDALDSSNSMQTIQK, EKPYFPIPEEYTFIQNVPLEDR, VGKDELFALEQSCAQVVLQAANER, GFGFVTYATVEEVDAAMNARPHK, VVLAYEPVWAIGTGK, and YPIEHGIITNWDDMEK for hESCs; and KATGPPVSELITK, ALLFVPR, GLFIIDDK, YQAVTATLEEK, ALMLQGVDLLADAVAVTMGPK, SGETEDTFIADLVVGLCTGQIK, MVNHFIAEFK, IGYPAPNFK, IAIYELLFK, ALYETELADARR, SLMDEVVKATSR, ERPPNPIEFLASYLLK, TKVHAELADVLTEAVVDSILAIR for mESCs.

For hESCs and hiPSCs grown in defined SILAC medium, label incorporation was monitored for 7 days after exposure to heavy medium. Incorporation was determined through examination of the following peptides: HQGVMVGMGQKDSYVGDEAQSKR, HLEINPDHPIVETLR, HVFGESDELIGQK, IHEGCEEPATHNALAK,

GVVDSEDIPLNLSR, FQSSHHPTDITSLDQYVER, SNYNFEKPFLWLAR, ISEQFTAMFR, VIHDNFGIVEGLMTTVHAITATQK, HSQFIGYPITLYLEKER, VILHLKEDQTEYLEERR, MTDQEAIQDLWQWRK.

2.4.8 Real-time PCR – RNA was purified using Trizol reagent according to the manufacturer's instructions (Invitrogen) or with the 5 Prime PerfectPure RNA Extraction Kit (5 Prime, Gaithersburg, MD). After NanoDrop quantification, 1µg of cDNA was synthesized using the High Capacity cDNA Reverse Transcription Kit with RNase inhibitor (Invitrogen). Real-time PCR was performed using the TaqMan® Universal PCR Master Mix (Invitrogen). Samples were incubated at 50°C for 2 minutes followed by 10 minutes at 95°C. Samples were then amplified at 95°C for 15 seconds followed by 1 minute at 58°C for 46 cycles. All samples were normalized to RPLPO as a positive control. All primers were obtained from Invitrogen and assay information can be found in Appendix Table 1.15. Each biological replicate was run in triplicate for every marker assayed. All reagents were used according to the manufacturer's instructions.

2.4.9 Immunofluorescence – After 10 passages in SILAC medium, H9, CA1, and BJ-1D cells were plated in 6-well dishes coated with Matrigel™™. After 4 days of culture, cells were rinsed and fixed with 4% para-formaldehyde containing 20 mM sucrose. Prior to staining, cells were blocked using the Dako Serum Free Protein Block solution (Dako, Cambridgeshire, UK). Oct-4 (clone 10H11.2), SSEA-4 (clone MC-813-70), and SSEA-1 (clone MC-480) primary antibodies were obtained from Millipore (Billerica, MA). Cells for Oct-4 labeling were permeabilized using a 0.1% Triton X-100 solution prior to blocking. Cells were labeled with primary antibodies for Oct-4 or SSEA-4 as

undifferentiated markers and SSEA-1 for differentiated cells all at concentrations concentrations of 2 µg/mL for 60 minutes at room temperature. Secondary Alexa-fluor 488 goat anti-mouse IgG and Alexa-fluor 568 goat anti-mouse IgM were obtained from Invitrogen (Carlsbad, CA). Secondary antibodies were probed at concentrations of 1 µg/mL for 60 minutes at room temperature. All products were used according to manufacturer's instructions.

2.4.10 Flow Cytometry – All reagents and probes for flow cytometry were obtained from eBiosciences (San Diego, CA) unless noted otherwise. Cells were enzymatically harvested using Accutase (Invitrogen) to obtain a single cell suspension. After centrifugation, cell pellets were resuspended in 5% FBS in PBS. Alexa-488 conjugated SSEA-4 and Alexa-647 conjugated SSEA1 were diluted into the cell mixture according to the manufacturer's instructions. Negative control samples contained respective isotype controls for the primary antibodies used. Solutions were incubated for 2 hours and analyzed using an Accuri C6 (BD Biosciences) flow cytometer after rinsing to remove unbound antibody. Populations were gated according to forward and side scatter patterns with filtering for viable cells using 7-aminoactinomycin D staining. Data were analyzed using FlowJo software (Tree Star, Ashland, OR).

2.4.11 Teratoma Formation and Histological Analysis – All animal protocols used here have been approved by the University of Western Ontario Council on Animal Care. Nude (Crl:NU-*Foxn1*^{nu}*;* Charles River) mice were injected in the flank subcutaneously with H9 or CA1 hESCs grown for >10 passages in StemPro SILAC medium. Prior to injection, hESCs were rinsed with PBS, trypsinized, and counted

using trypan blue exclusion. Approximately $1x10^6$ cells based on live cell counts were resuspended in a 50:50 DMEM:Matrigel™™ mixture totaling 100µL in volume. Injections were performed on each side of three separate mice for each treatment (n=3). Teratomas were allowed to form for 6 – 8 weeks. Teratomas were removed, fixed and embedded in paraffin. Sections were taken from three areas spaced evenly through the tissue and tissue types were defined with hematoxylin and eosin staining.

2.4.12 Statistical Analysis – Statistical analyses were performed using GraphPad Prism software. Results are expressed as SD or SEM as indicated in figure legends. Statistical significance was determined using unpaired Students T-tests. Differences were reported as follows: * $p < 0.05$, ** $p < 0.01$, *** $p < 0.001$.

2.5 References

[1] Aebersold, R., Mann, M., Mass spectrometry-based proteomics. *Nature* 2003, *422*, 198-207.
[2] Ong, S. E., Mann, M., Mass spectrometry-based proteomics turns quantitative. *Nat Chem Biol* 2005, *1*, 252-262.
[3] Hwang, S. I., Lundgren, D. H., Mayya, V., Rezaul, K., Cowan, A. E., Eng, J. K.*, et al.*, Systematic characterization of nuclear proteome during apoptosis: a quantitative proteomic study by differential extraction and stable isotope labeling. *Mol Cell Proteomics* 2006, *5*, 1131-1145.
[4] Ong, S. E., Kratchmarova, I., Mann, M., Properties of 13C-substituted arginine in stable isotope labeling by amino acids in cell culture (SILAC). *J Proteome Res* 2003, *2*, 173-181.
[5] Ong, S. E., Mann, M., A practical recipe for stable isotope labeling by amino acids in cell culture (SILAC). *Nat Protoc* 2006, *1*, 2650-2660.
[6] Schmidt, F., Strozynski, M., Salus, S. S., Nilsen, H., Thiede, B., Rapid determination of amino acid incorporation by stable isotope labeling with amino acids in cell culture (SILAC). *Rapid Commun Mass Spectrom* 2007, *21*, 3919-3926.
[7] Van Hoof, D., Pinkse, M. W., Oostwaard, D. W., Mummery, C. L., Heck, A. J., Krijgsveld, J., An experimental correction for arginine-to-proline conversion artifacts in SILAC-based quantitative proteomics. *Nat Methods* 2007, *4*, 677-678.
[8] Blagoev, B., Mann, M., Quantitative proteomics to study mitogen-activated protein kinases. *Methods* 2006, *40*, 243-250.
[9] Bicho, C. C., Alves, F. D., Chen, Z. A., Rappsilber, J., Sawin, K. E., A Genetic Engineering Solution to the "Arginine Conversion Problem" in Stable Isotope Labeling by Amino Acids in Cell Culture (SILAC). *Molecular & Cellular Proteomics* 2010, *9*, 1567-1577.
[10] Larance, M., Bailly, A. P., Pourkarimi, E., Hay, R. T., Buchanan, G., Coulthurst, S.*, et al.*, Stable-isotope labeling with amino acids in nematodes. *Nature Methods* 2011, *8*, 849-U114.
[11] Gruhler, A., Olsen, J. V., Mohammed, S., Mortensen, P., Faergeman, N. J., Mann, M.*, et al.*, Quantitative phosphoproteomics applied to the yeast pheromone signaling pathway. *Mol Cell Proteomics* 2005, *4*, 310-327.
[12] Park, S. K., Liao, L., Kim, J. Y., Yates, J. R., 3rd, A computational approach to correct arginine-to-proline conversion in quantitative proteomics. *Nat Methods* 2009, *6*, 184-185.
[13] Park, S. K., Venable, J. D., Xu, T., Yates, J. R., 3rd, A quantitative analysis software tool for mass spectrometry-based proteomics. *Nat Methods* 2008, *5*, 319-322.
[14] van Breukelen, B., van den Toorn, H. W., Drugan, M. M., Heck, A. J., StatQuant: a post-quantification analysis toolbox for improving quantitative mass spectrometry. *Bioinformatics* 2009, *25*, 1472-1473.
[15] Scott, L., Lamb, J., Smith, S., Wheatley, D. N., Single amino acid (arginine) deprivation: rapid and selective death of cultured transformed and malignant cells. *Br J Cancer* 2000, *83*, 800-810.
[16] Hoffman, L. M., Carpenter, M. K., Characterization and culture of human embryonic stem cells. *Nat Biotechnol* 2005, *23*, 699-708.
[17] Graumann, J., Hubner, N. C., Kim, J. B., Ko, K., Moser, M., Kumar, C.*, et al.*, SILAC-labeling and proteome quantitation of mouse embryonic stem cells to a depth of 5111 proteins. *Mol Cell Proteomics* 2007.
[18] Andersen, J. S., Lam, Y. W., Leung, A. K., Ong, S. E., Lyon, C. E., Lamond, A. I.*, et al.*, Nucleolar proteome dynamics. *Nature* 2005, *433*, 77-83.
[19] Ong, S. E., Mittler, G., Mann, M., Identifying and quantifying in vivo methylation sites by heavy methyl SILAC. *Nat Methods* 2004, *1*, 119-126.
[20] Selbach, M., Mann, M., Protein interaction screening by quantitative immunoprecipitation combined with knockdown (QUICK). *Nat Methods* 2006, *3*, 981-983.
[21] Yocum, A. K., Gratsch, T. E., Leff, N., Strahler, J. R., Hunter, C. L., Walker, A. K.*, et al.*, Coupled global and targeted proteomics of human embryonic stem cells during induced differentiation. *Mol Cell Proteomics* 2008.
[22] Morris, S. M., Jr., Enzymes of arginine metabolism. *J Nutr* 2004, *134*, 2743S-2747S; discussion 2765S-2767S.

[23] Urschel, K. L., Rafii, M., Pencharz, P. B., Ball, R. O., A multitracer stable isotope quantification of the effects of arginine intake on whole body arginine metabolism in neonatal piglets. *Am J Physiol Endocrinol Metab* 2007, *293*, E811-818.
[24] Urschel, K. L., Evans, A. R., Wilkinson, C. W., Pencharz, P. B., Ball, R. O., Parenterally fed neonatal piglets have a low rate of endogenous arginine synthesis from circulating proline. *J Nutr* 2007, *137*, 601-606.
[25] Wang, L., Li, L., Menendez, P., Cerdan, C., Bhatia, M., Human embryonic stem cells maintained in the absence of mouse embryonic fibroblasts or conditioned media are capable of hematopoietic development. *Blood* 2005, *105*, 4598-4603.
[26] Xu, C., Inokuma, M. S., Denham, J., Golds, K., Kundu, P., Gold, J. D.*, et al.*, Feeder-free growth of undifferentiated human embryonic stem cells. *Nat Biotechnol* 2001, *19*, 971-974.
[27] Price, P. J., Goldsborough, M. D., Tilkin, M. L., 1998, p. 28.
[28] Ong, S. E., Blagoev, B., Kratchmarova, I., Kristensen, D. B., Steen, H., Pandey, A.*, et al.*, Stable isotope labeling by amino acids in cell culture, SILAC, as a simple and accurate approach to expression proteomics. *Mol Cell Proteomics* 2002, *1*, 376-386.
[29] Takahashi, K., Tanabe, K., Ohnuki, M., Narita, M., Ichisaka, T., Tomoda, K.*, et al.*, Induction of pluripotent stem cells from adult human fibroblasts by defined factors. *Cell* 2007, *131*, 861-872.
[30] Akopian, V., Andrews, P. W., Beil, S., Benvenisty, N., Brehm, J., Christie, M.*, et al.*, Comparison of defined culture systems for feeder cell free propagation of human embryonic stem cells. *In Vitro Cellular & Developmental Biology-Animal* 2010, *46*, 247-258.
[31] Prowse, A. B. J., McQuade, L. R., Bryant, K. J., Marcal, H., Gray, P. P., Identification of potential pluripotency determinants for human embryonic stem cells following proteomic analysis of human and mouse fibroblast conditioned media. *Journal of Proteome Research* 2007, *6*, 3796-3807.
[32] Prowse, A. B. J., McQuade, L. R., Bryant, K. J., Van Dyk, D. D., Tuch, B. E., Gray, P. P., A proteome analysis of conditioned media from human neonatal fibroblasts used in the maintenance of human embryonic stem cells. *Proteomics* 2005, *5*, 978-989.
[33] Bendall, S. C., Hughes, C., Campbell, J. L., Stewart, M. H., Pittock, P., Liu, S.*, et al.*, An enhanced mass spectrometry approach reveals human embryonic stem cell growth factors in culture. *Mol Cell Proteomics* 2009, *8*, 421-432.
[34] Wang, L., Schulz, T. C., Sherrer, E. S., Dauphin, D. S., Shin, S., Nelson, A. M.*, et al.*, Self-renewal of human embryonic stem cells requires insulin-like growth factor-1 receptor and ERBB2 receptor signaling. *Blood* 2007, *110*, 4111-4119.
[35] Wilkinson, D. L., Bertolo, R. F., Brunton, J. A., Shoveller, A. K., Pencharz, P. B., Ball, R. O., Arginine synthesis is regulated by dietary arginine intake in the enterally fed neonatal piglet. *Am J Physiol Endocrinol Metab* 2004, *287*, E454-462.
[36] Lossner, C., Warnken, U., Pscherer, A., Schnolzer, M., Preventing arginine-to-proline conversion in a cell-line-independent manner during cell cultivation under stable isotope labeling by amino acids in cell culture (SILAC) conditions. *Analytical Biochemistry* 2011, *412*, 123-125.
[37] Marcilla, M., Alpizar, A., Paradela, A., Albar, J. P., A systematic approach to assess amino acid conversions in SILAC experiments. *Talanta* 2011, *84*, 430-436.
[38] Ong, S. E., Mann, M., Stable isotope labeling by amino acids in cell culture for quantitative proteomics. *Methods Mol Biol* 2007, *359*, 37-52.
[39] Rigbolt, K. T. G., Prokhorova, T. A., Akimov, V., Henningsen, J., Johansen, P. T., Kratchmarova, I.*, et al.*, System-Wide Temporal Characterization of the Proteome and Phosphoproteome of Human Embryonic Stem Cell Differentiation. *Science Signaling* 2011, *4*.
[40] Thomson, J. A., Itskovitz-Eldor, J., Shapiro, S. S., Waknitz, M. A., Swiergiel, J. J., Marshall, V. S.*, et al.*, Embryonic stem cell lines derived from human blastocysts. *Science* 1998, *282*, 1145-1147.
[41] Bendall, S. C., Stewart, M. H., Menendez, P., George, D., Vijayaragavan, K., Werbowetski-Ogilvie, T.*, et al.*, IGF and FGF cooperatively establish the regulatory stem cell niche of pluripotent human cells in vitro. *Nature* 2007, *448*, 1015-1021.
[42] Doble, B. W., Patel, S., Wood, G. A., Kockeritz, L. K., Woodgett, J. R., Functional redundancy of GSK-3alpha and GSK-3beta in Wnt/beta-catenin signaling shown by using an allelic series of embryonic stem cell lines. *Dev Cell* 2007, *12*, 957-971.
[43] Seguin, C. A., Draper, J. S., Nagy, A., Rossant, J., Establishment of endoderm progenitors by SOX transcription factor expression in human embryonic stem cells. *Cell Stem Cell* 2008, *3*, 182-195.

[44] Peerani, R., Rao, B. M., Bauwens, C., Yin, T., Wood, G. A., Nagy, A.*, et al.*, Niche-mediated control of human embryonic stem cell self-renewal and differentiation. *EMBO J* 2007, *26*, 4744-4755.
[45] Hotta, A., Cheung, A. Y., Farra, N., Garcha, K., Chang, W. Y., Pasceri, P.*, et al.*, EOS lentiviral vector selection system for human induced pluripotent stem cells. *Nat Protoc* 2009, *4*, 1828-1844.
[46] Ma, B., Zhang, K. Z., Hendrie, C., Liang, C. Z., Li, M., Doherty-Kirby, A.*, et al.*, PEAKS: powerful software for peptide de novo sequencing by tandem mass spectrometry. *Rapid Communications in Mass Spectrometry* 2003, *17*, 2337-2342.
[47] Zhang, J., Xin, L., Shan, B., Chen, W., Xie, M., Yuen, D.*, et al.*, PEAKS DB: De Novo Sequencing Assisted Database Search for Sensitive and Accurate Peptide Identification. *Mol Cell Proteomics* 2012, *11*, M111 010587.

Chapter 3

Proteomic Analysis of Complex Matrices used in Human Embryonic Stem Cell Culture

3.1 Introduction

The *in vivo* and *in vitro* extracellular matrix (ECM) is known to play an important role in numerous decisions that direct cell fate and behavior [1-4]. Typical ECM mixtures include combinations of laminins, collagens, glycoproteins, and proteoglycans [5, 6]. However, the constituents of the ECM differ greatly between tissue types. *In vitro*, the main function of the extracellular matrix is to support cell growth and maintenance. For example, the ECM provides physical support for cells whilst maintaining cellular polarization and tissue morphology. Moreover, the ECM is a reservoir for cell signals as it contains specific carbohydrates, proteins, nutrients and growth factors that can direct cellular processes and behavior. An example ECM component being laminin, which cells sense via integrin receptors. Such interactions between cells and laminin have been shown to affect a variety of biological functions, such as cell growth, morphology, differentiation, and migration in a cell-specific manner [7].

This chapter contains excerpts with permission from the following papers:

Hughes, C.S., Postovit, L.M., Lajoie, G.A.. (2010) “Matrigel: A Complex Protein Mixture Required for Optimal Growth of Cell Culture”. *Proteomics*. 10;9:1886 – 1890

Hughes, C.S., Radan, L., Betts, D., Postovit, L.M., Lajoie, G.A.. (2011) “Proteomic Analysis of Extracellular Matrices used in Stem Cell Culture”. *Proteomics*. 11;20:3983 – 3991

In vitro, protein matrices are commonly used when cell proliferation is not favorable on chemically treated tissue culture plastic. Depending on the cellular system of interest, these matrices can consist of a range of components. The most widely utilized example of this is the basement-membrane matrix commercialized as Matrigel™ [8, 9]. Matrigel™ is an assortment of extracellular matrix proteins that have been extracted from Englebreth-Holm-Swarm tumors in mice [8-10]. Matrigel™, which primarily consists of laminin, collagen IV, and enactin, is considered to be a reconstituted basement membrane preparation. Previous research studies have emphasized the need for caution when drawing conclusions based on changes in cellular activity when using Matrigel™ [11]. This recommendation was based on the detection of several growth factors in standard Matrigel™ through the use of immunoassays; these included bFGF, EGF, IGF-1, TGF-β, PDGF, and NGF [11]. Growth factor reduced (GFR) is a version of Matrigel™ that has been modified to reduce the abundance levels of these growth factors [11].

One important application of Matrigel™ is its use for the growth of human embryonic stem cells (hESC). In contrast to mouse ESC culture, hESCs cannot be maintained in an undifferentiated and pluripotent state on gelatin. Thus, Matrigel™ is conventionally used as a substitute for gelatin in feeder-free hESC culture. Unfortunately, the derivation of Matrigel™ from mouse tissue makes it undesirable for the growth of hESCs that can be potentially applied in therapeutic treatments [12, 13]. A variety of alternative ECM proteins or culture systems have been evaluated for their ability to support hESC proliferation [14-28]. In combination or individually, some of these promote the pluripotent growth of undifferentiated hESCs in 2D, 3D, and suspension

culture [16, 29]. Cell-derived matrices generated from human fibroblasts have also been shown to promote pluripotent hESC growth, but the supportive constituents of such preparations are largely unknown or proprietary [30-35]. While most of the previously noted matrices have been shown to support the maintenance of self-renewal and pluripotency in hESCs, none have proven as effective as Matrigel™ [36].

The lack of a defined xeno-free growth matrix remains a significant limitation for the potential extension of hESCs to therapeutic applications [17, 37, 38]. It would be of tremendous value if support proteins that enhance the *in vitro* culture of hESCs could be identified. The development of a defined matrix for hESC growth is currently limited by our understanding of the ECM proteins that regulate hESC attachment and proliferation. Although it has been the subject of a number of studies, there is still a lack of understanding of how ESCs interact with the surrounding ECM *in vitro* and *in vivo* [39-45]. Proteomic analysis of supportive matrices could help elucidate components that promote hESC growth, analogous to the characterization of conditioned medium from supportive fibroblast feeder layers for the identification of soluble regulatory cytokines [46-50].

A major obstacle that examination of these matrices presents is the significant challenge in proteomic analysis due to the complex nature of the samples. ECM mixtures typically consist of large amounts of high molecular weight protein and a variety of low abundance species. Identification of these low abundance proteins can only be obtained by extensive fractionation prior to liquid chromatography (LC) mass spectrometry (MS) analysis [51, 52]. The two most common methods used in

proteomics are fractionation with one dimensional SDS-PAGE at the protein level or, after digestion with trypsin, by ion exchange chromatography at the peptide level. These fractionation steps are typically followed by further separation on a reversed-phase column prior to MS analysis [53]. It has recently been shown that some fractionation protocols prior to LC-MS are in fact complementary [46, 54].

In this chapter we utilize a combination of fractionation and digestion protocols for the analysis of complex ECM samples to attempt to identify hESC supportive proteins. We show that Matrigel™ contains an array of proteins in addition to those known to be directly involved in the structural basis of the basement matrix. This is accomplished by utilizing an in-depth proteomic approach that employs ammonium sulfate precipitation and a dynamic iterative exclusion MS (IE-MS) strategy to detect low abundance components [46]. Using a combination of strong anion and cation exchange as well as SDS-PAGE methods [46, 55], we analyze CellStart, StemXVivo, BridgeECM, and HumanBME, four previously uncharacterized ECM matrices. We also analyze a matrix deposited by irradiated mouse embryonic feeder layers (MEF-CMTX) after maintenance on gelatin for 7 days. After MEF lysis, the remaining matrix has been shown to promote the undifferentiated growth of pluripotent hESCs [56]. By comparing the proteins identified from these samples, we identify fibronectin as a primary component of nearly all the matrix samples, suggesting its importance in the promotion of hESC maintenance and pluripotency. To validate this observation, H9 and CA1 hESCs were cultured in mTeSR1 medium on fibronectin as the sole matrix component.

3.2 Results

3.2.1 Fractionation of Matrigel. Matrigel™ is known to be highly enriched in laminin, collagen, and enactin. Previously published research that revealed the presence of multiple active growth factors in Matrigel™ was based upon detection using immunoassays that are not amenable to a more global analysis of protein composition [11]. Comprehensive analysis of Matrigel™ using MS-based proteomics could potentially reveal the presence of other growth factors and cytokines. The main protein components of Matrigel™, laminin (800,000 Da), collagen IV (540,000 Da), and enactin (158,000 Da) are all significantly larger than the average size of most protein growth factors (<~45,000Da). To facilitate identification of these low abundance factors, fractionation that depletes the abundant high molecular weight (MW) components of Matrigel™ is critical.

Using size exclusion chromatography (SEC) to fractionate Matrigel™ samples, we were unable to obtain effective separation. We observed a large peak early due to the more rapid elution of large proteins from both the standard (N-GFR) and GFR Matrigel™. SEC runs were repeated for 3 technical replicates and typically resulted in ~15 fractions dependent on the elution profile of the sample. Analysis of each SEC fraction with one dimensional SDS-PAGE (1D-SDS-Gel) resulted in gels with very poor resolution, and showed minute amounts of low molecular weight proteins, as determined by Coomassie blue staining. Nevertheless fractions resulting from SEC runs were digested in-solution with trypsin prior to analysis by LC-MS.

Due to the limited separation and loading capacity provided by 1D-SDS-Gels, and the poor resolution of SEC, we adapted a two step ammonium sulfate (AS) precipitation protocol to fractionate both N-GFR and GFR Matrigel™ (Figure 3.1). AS precipitation is not commonly used in proteomics, but has been used for the depletion of N-GFR Matrigel™ to generate the GFR variety [11]. The two step procedure utilized here precipitates protein from Matrigel™ at 15% and 90% AS (w/v). Treatment of Matrigel™ with 15% AS gave a precipitate that was further fractionated by SEC prior to in-solution trypsin digestion. The supernatants from the 15% AS step were further adjusted to 90% AS. The resulting pellets were reconstituted in 8M urea and separated on a 1D-SDS-Gel. These gels contained visible amounts of low molecular weight proteins after staining that were then digested with trypsin and subjected to IE-MS analysis.

3.2.2 LC-MS Analysis of Fractionated Matrigel. LC-MS analysis of the SEC fractions from N-GFR Matrigel™ resulted in identification of 1117 unique peptides. The same analysis on GFR Matrigel™ SEC fractions resulted in the identification of 1521 unique peptides (Figure 3.2 C). The overlap between the two datasets indicates (~20% common) significant differences between the two types of Matrigel™ based on unique peptide identifications. LC-MS analysis of the pellets from 90% AS precipitation after 1D-SDS-Gel fractionation resulted in the identification of 5465 unique peptides for N-GFR and 5080 from GFR (Figure 3.2 C). Combination of SEC and AS precipitation datasets resulted in an increase in the total number of unique peptide identifications to 5910 for N-GFR and 5604 for GFR Matrigel™. Of these peptides, only 457 were matched to laminin/enactin from N-GFR Matrigel™, and 681 from GFR.

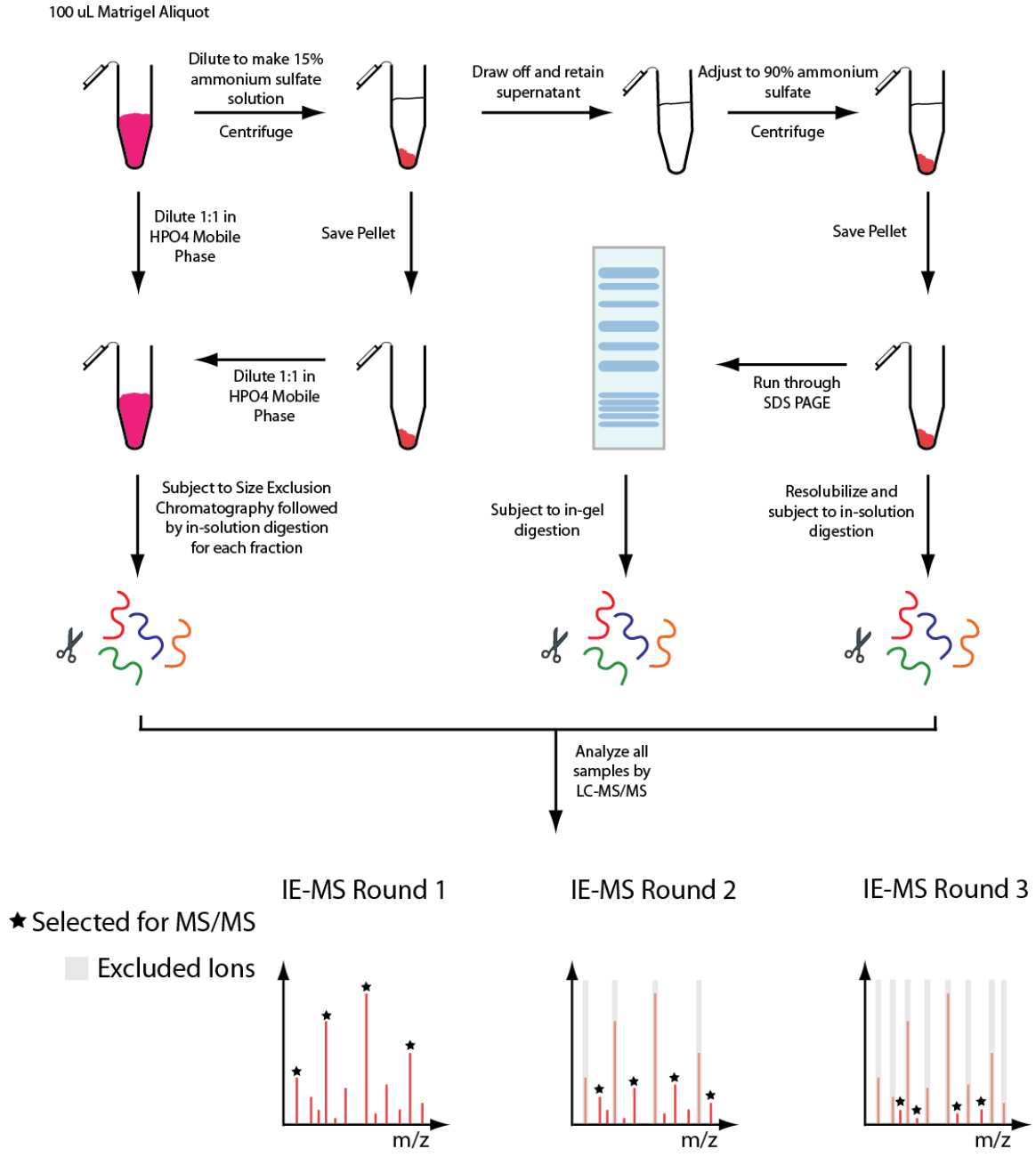

Figure 3.1. Schematic of experimental preparation of N-GFR and GFR Matrigel samples for proteomic analysis. Aliquots of Matrigel were subject to fractionation with SEC without prior precipitation using AS methods. The pellets of Matrigel aliquots that were precipitated with 15% AS were also subjected to SEC fractionation prior to in-solution digestion with trypsin and LC-MS analysis. The retained supernatent from 15% AS precipitation was further adjusted to 90% AS. Following centrifugation, the re-solubilized pellet was subject to in-solution digestion with trypsin or further fractionation using a 1D-SDS-Gel. All samples were analyzed using a combination of LC-MS and IE-MS approaches to maximize the depth of sample coverage.

Even with utilization of SEC and AS precipitation coupled with 1D-SDS-Gels, there was still a considerable dynamic range in each fraction to address. To address this, we employed IE analysis to facilitate identification of low-abundance peptide species in the MS as demonstrated previously [11]. IE-MS analysis of the SEC fractions resulted in an increase in the number of unique peptides identified in N-GFR and GFR Matrigel™ to 2588 and 3781 respectively after 4 exclusion rounds (Figure 3.2 B). Six rounds of IE-MS analysis of the fractions resulting from 1D-SDS-Gel separation of the reconstituted pellets from 90% AS precipitation resulted in an increase in unique peptides identified to 11955 and 10368 for N-GFR and GFR Matrigel™ respectively (Figure 3.2 B). Combination of the IE-MS datasets from the SEC and AS methods resulted in an increase in the total number of unique peptides identified to 13016 in N-GFR Matrigel™, corresponding to 1180 proteins (Appendix Table 1.1 – 1.2). Combination of the data for GFR Matrigel™ increased the total number of identifications to 12033 for peptides and 1007 for proteins. These values represent an approximate 2-fold increase in the number of proteins identified through the use of IE-MS with samples from all fractionation types (Figure 3.2 A).

Through the combination of the data from N-GFR and GFR Matrigel™, we can generate a comprehensive dataset. Combination of the SEC datasets from N-GFR and GFR Matrigel™ resulted in the identification 5288 peptides and 452 unique proteins (Figure 3.2 C). Combination of the AS precipitation data resulted in 16995 peptide and 1343 protein identifications (Figure 3.2 C). Of the peptide hits, 748 were assigned to laminin/enactin for samples from SEC fractionation and 1046 for the samples from AS precipitation. These results illustrate the utility of the AS precipitation protocol for the

A **Total Unique Peptide Identifications**

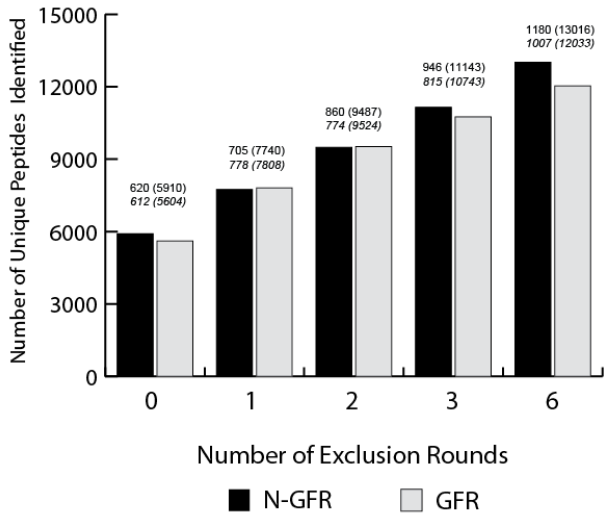

B **Laminin/Enactin Peptide Identifications**

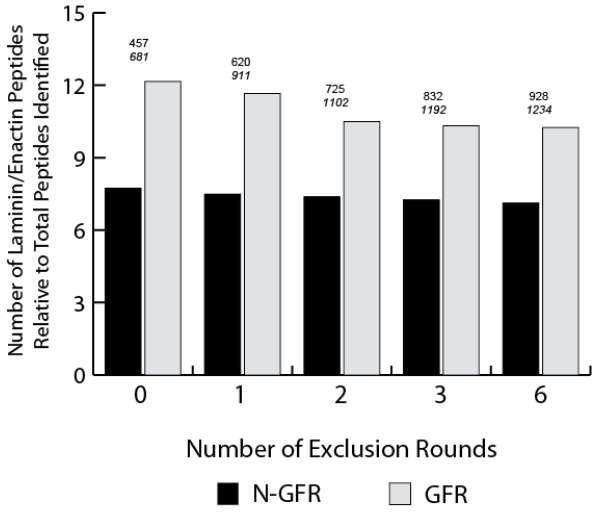

C **Total Unique Peptide Identifications**

	SEC		AS Precipitation		Combined	
	LC-MS	**IE-MS**	**LC-MS**	**IE-MS**	**LC-MS**	**IE-MS**
N-GFR	1117	2588	5465	11955	5910	13016
GFR	1521	3781	5080	10368	5604	12033
Combined	2184	5288	7835	16995	8529	19063

Figure 3.2. Iterative exclusion analysis of Matrigel samples. Samples of N-GFR and GFR Matrigel were fractionated using either SEC or AS precipitation coupled with 1D-SDS-Gel methods prior to IE-MS analysis. All LC-MS data files were searched using PEAKS 5.3 software as described in the Methods. (A) Total numbers of unique peptides identified in each round of IE-MS analysis. The number of peptide hits is given above each set of exclusion bars in the format protein# (peptide#) with N-GFR values in normal font and GFR in italics. Values represent total identifications following the combination of SEC and AS datasets. (B) Relative number of laminin/enactin peptides to the total number of identifications as assigned by PEAKS 5.3 across 6 exclusion rounds. As before, total numbers are found above with GFR in italics. (C) Lists the total numbers of peptide identifications found using conventional LC-MS analysis compared with IE-MS for SEC or AS fractionation of N-GFR and GFR Matrigel. LC-MS represents a single injection for each sample, whereas IE-MS represents multiple injections with exclusion lists applied during data acquisition.

depletion of high-MW components in comparison with SEC in order to facilitate the identification of other proteins in Matrigel™. Combining the data from all Matrigel™ batches and fractionation protocols, we identified a total of 19063 unique peptides and 1466 unique proteins from 280 LC-MS datafiles (Figure 3.3). Gene ontology analysis of the N-GFR and GFR Matrigel™ datasets revealed the presence of numerous intracellular proteins in both formulations (Figure 3.3). Taken together, these data indicate the significant complexity at the protein level for both N-GFR and GFR Matrigel™.

3.2.3 Comparative Analysis of N-GFR and GFR Matrigel. GFR is a variant of N-GFR Matrigel™ that has decreased levels of the growth factors and other low molecular weight proteins [11]. This is achieved using an AS precipitation protocol which we have adapted to facilitate analysis of all Matrigel™ samples tested in this study (Figure 3.4 A). Comparison of N-GFR and GFR Matrigel™ revealed that there are at least 721 proteins in common between the two preparations (Figure 3.4 B). N-GFR and GFR Matrigel™ yielded an additional 459 and 286 protein identifications specific to each dataset. Primary structural proteins common between the two types of Matrigel™ such as laminin, nidogen, and fibronectin were more abundant in GFR based on unique peptide number. In N-GFR proteins secondary to the main structural components of Matrigel™, such as SPARC and transferrin were more abundant. Interestingly, a variety of growth factors and their associated pathway members were identified in N-GFR that were not in GFR Matrigel™ (Figure 3.4 C).

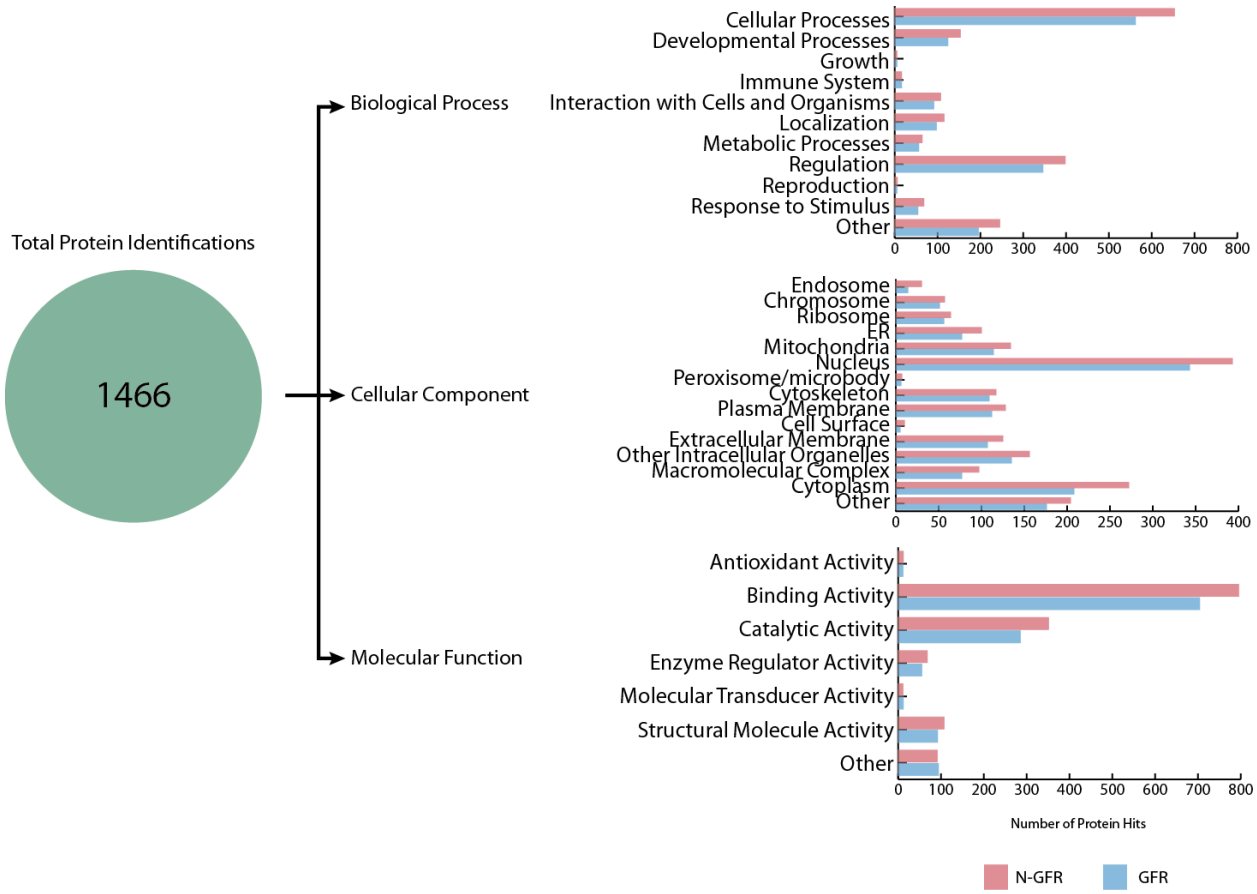

Figure 3.3. Comprehensive proteomics dataset from the analysis of N-GFR and GFR Matrigel. The number in the green circle on the left represents the total number of protein identifications obtained following the analysis of the combined N-GFR and GFR Matrigel datasets. Identifications were made using PEAKS 5.3 software. Protein identifiers from the list of N-GFR and GFR proteins were mapped to Gene Ontology terms using STRAP software. The three graphs represent Biological Process, Cellular Component, and Molecular Function ontology groupings. The number of mapped annotations for each term for N-GFR can be found in red and for GFR in blue. The wide range of terms that the identifiers mapped to indicates the complexity and range of cellular localizations present for the proteins found in either variety of Matrigel.

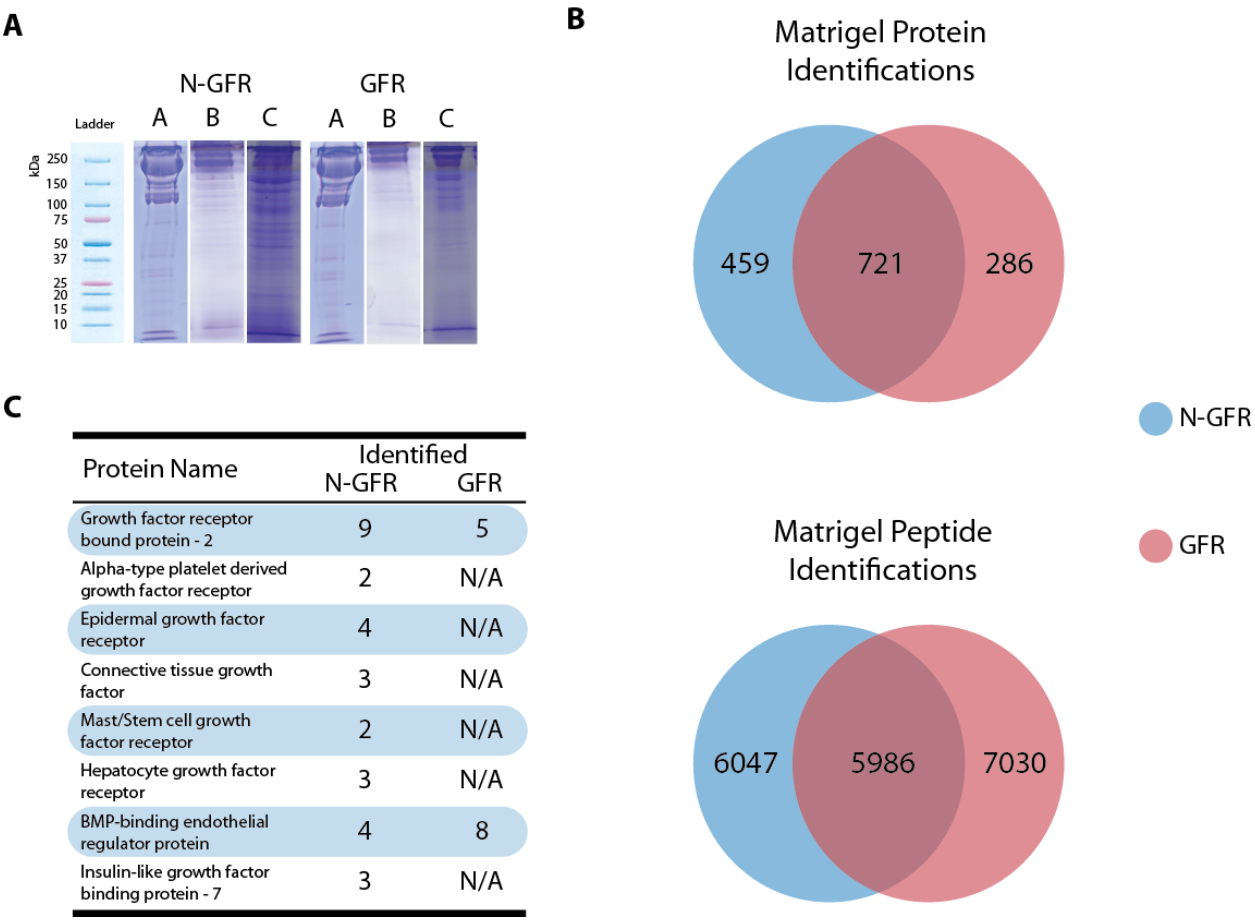

C

Protein Name	Identified N-GFR	GFR
Growth factor receptor bound protein - 2	9	5
Alpha-type platelet derived growth factor receptor	2	N/A
Epidermal growth factor receptor	4	N/A
Connective tissue growth factor	3	N/A
Mast/Stem cell growth factor receptor	2	N/A
Hepatocyte growth factor receptor	3	N/A
BMP-binding endothelial regulator protein	4	8
Insulin-like growth factor binding protein - 7	3	N/A

Figure 3.4. Comparative analysis of N-GFR and GFR Matrigel. (A) Representative lanes from N-GFR and GFR Matrigel samples that were subject to electrophoresis on 1D-SDS gels. Lane A is neat Matrigel directly as it comes from the manufacturer. Lane B is the pellet that remains after precipitation using a solution of 15% ammonium sulfate precipitation. Lane C is the supernatent after precipitation with 90% ammonium sulfate. Following AS precipitation, a significant increase in protein staining can be seen in the low-MW range in 1D-SDS-Gels of N-GFR and GFR Matrigel samples. (B) Venn diagram illustrating the number of protein and peptide identifications for N-GFR (blue) and GFR (red) Matrigel. Numbers represent total numbers of identifications from data generated by employing IE-MS analysis of Matrigel samples prepared using SEC and AS precipitation fractionation protocols. Data files were analyzed using PEAKS 5.3 software as discussed in the Methods. (C) Table of growth factor and associated binding proteins found in N-GFR or GFR Matrigel. Values in the N-GFR and GFR columns represent the number of unique peptide identifications in each matrix as determined by PEAKS 5.3 software. If the protein was not found, it is denoted by “N/A”.

3.2.4 Fractionation of Alternative hESC Supportive Matrices. Adaptation of the AS protocol to the analysis of the HumanBME proved straightforward due to the similar protein abundance profile it shares with Matrigel™. Fractionation of CellStart with the AS protocol proved difficult due to the increased abundance of high-MW protein in this matrix compared with Matrigel™. Due to the limited amount of material we could obtain for MEF-CMTX, BridgeECM, and StemXVivo matrices, we were unable to apply the AS protocol. The limited utility of the AS protocol for the analysis of these matrices highlights the primary shortcoming of this method: the requirement for a large amount of sample due to the high potential for protein loss during the procedure.

In order to overcome the dynamic range of abundance and detect low abundance proteins in these new matrices, we employed a combination of conventional proteomic fractionation and digestion techniques. By utilizing an in-solution digestion protocol coupled to fractionation on strong cation and anion exchange chromatography columns, we could overcome loading constraints caused by lane bleeding on 1D-SDS-Gels to facilitate detection of low-abundance proteins. However, 1D-SDS-Gel fractionation proved applicable to HumanBME, StemXVivo, BridgeECM, and MEF-CMTX, but could not be used for the CellStart matrix due to lane bleeding problems caused by the large abundance of high-MW proteins.

Optimization of the fractionation methods on a HeLa whole cell lysate revealed that numerous peptide identifications were isolated to a single method (Figure 3.5). We also observed that the number of unique peptides identified could be increased by employing IE-MS analysis as described previously [46]. Comparison of the peptides identified for

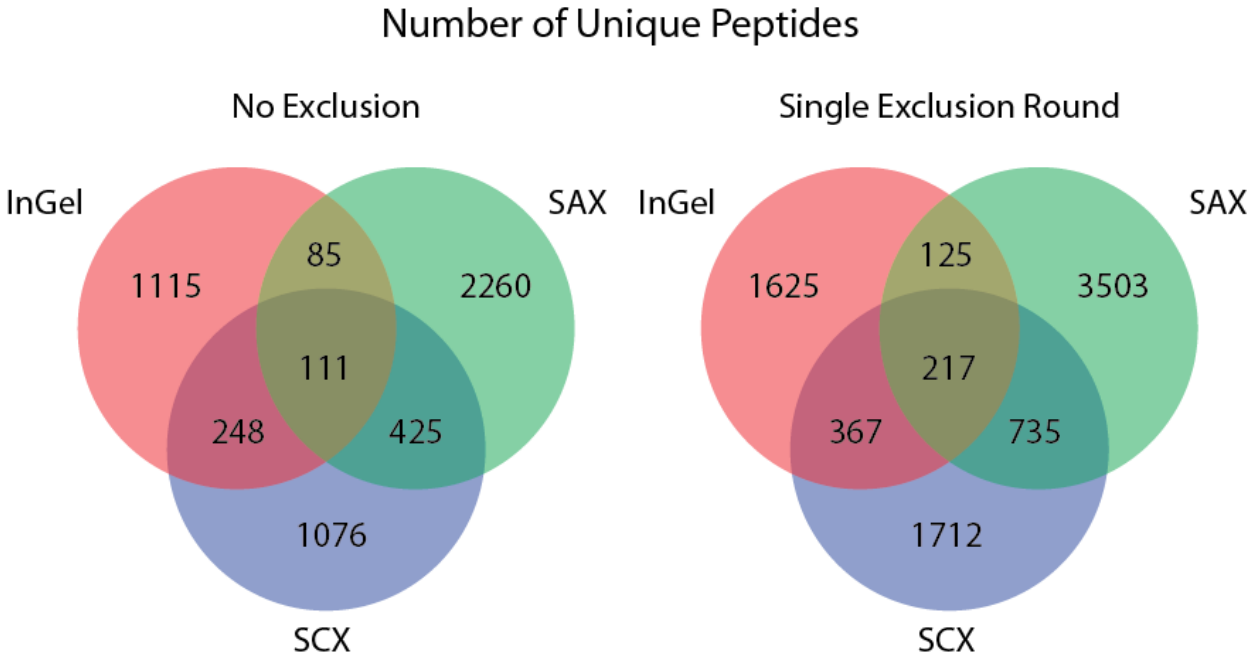

Figure 3.5. Comparison of methods used to fractionate a complex HeLa cell lysate. Following enzymatic digestion using trypsin with an in-solution protocol, samples were fractionated using SCX or SAX with a pH gradient elution. Alternatively, cell lysate was separated using a 1D-SDS-Gel and subsequently digested using trypsin with an in-gel protocol. Samples were analyzed by MS with (Single Exclusion Round) or without (No Exclusion) IE-MS. Numbers represent the number of unique peptides identified in the combined fractions for each sample following analysis in PEAKS 5.3 software. Score thresholds were set to ensure an FDR<1% in all datasets.

the three primary fractionation methods tested (SDS-PAGE, SCX, and SAX), revealed that there was only a 2.0% overlap prior to iterative exclusion, and 2.6% after IE-MS analysis (Figure 3.5). This indicates that the differences in identifications are a result of the fractionation methods, as IE analysis will limit changes due to under-sampling of ions in the MS. These results prompted us to employ a combination of in-solution digestion followed by SCX, SAX, or SDS-PAGE fractionation and analysis using IE-MS.

3.2.5 Analysis of Alternative hESC Supportive Matrices. Using SAX and SCX fractionation with pH elution, a total of 70 proteins were identified in the CellStart matrix (Figure 3.6, Appendix Table 1.3). From these LC-MS analyses, the two most abundant proteins were fibronectin and serum albumin, representing >60% of all unique peptide identifications. These two high abundance proteins were likely the cause of the difficulties in the 1D-SDS-Gel method, where increasing the gel load resulted in their overloading. The other proteins identified represented a mix of intra and extracellular proteins, the majority of which were identified in Matrigel™.

Fractionation of HumanBME with SAX, SCX, and SDS-PAGE methods yielded 208 protein identifications (Figure 3.6, Appendix Table 1.4). From the analysis we observed that HumanBME is primarily composed of fibronectin, nidogen-1, and alpha-2, gamma-1, and beta-2 laminin isoforms based on the number of unique peptides identified. Other proteins identified included vitronectin, biglycan, insulin-like growth factor – 2, transforming growth factor beta 2, and growth receptor bound protein 2 (Grb2). Comparing the composition of HumanBME with that of Matrigel™ based on protein identifiers indicates a significant similarity between the two matrices. Although the

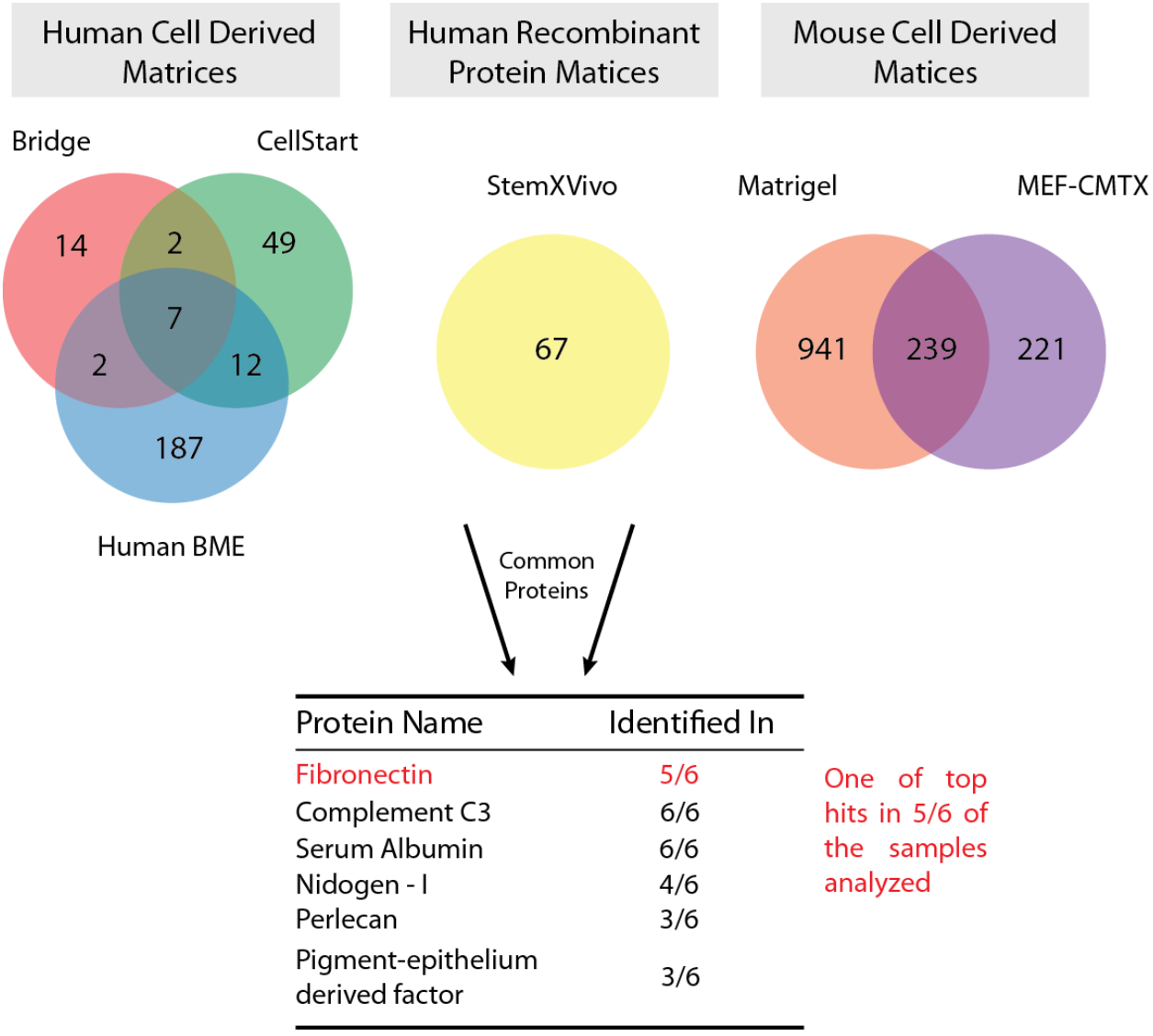

Protein Name	Identified In
Fibronectin	5/6
Complement C3	6/6
Serum Albumin	6/6
Nidogen - I	4/6
Perlecan	3/6
Pigment-epithelium derived factor	3/6

One of top hits in 5/6 of the samples analyzed

Figure 3.6. Comparison of the most abundant components of the ECM samples tested. Each sample was fractionated using either SCX or SAX chromatography, or 1D-SDS-Gel separation. Fractions were analyzed using IE-MS for a single exclusion round. Numbers in each circle represent the total number of protein identifications for the labeled matrix following the combination of data from all fractionation methods. Protein lists for CellStart, Human BME, StemXVivo, BridgeECM, and MEF-CMTX were generated and compared using PEAKS 5.3 software. Identification numbers include proteins that were matched with 2 unique peptides and had scores above the 1% FDR threshold. Six proteins commonly found at high abundances across the ECM samples are listed in the lower table. Of the proteins identified, fibronectin was an abundant component of 5 of the 6 matrices.

HumanBME dataset appears less complex based the total number of proteins identified when compared with Matrigel™, only a single exclusion round of IE-MS for was performed for the analysis.

Fractionation of StemXVivo with SCX, SAX, and SDS-PAGE methods resulted in a total of 67 unique proteins (Figure 3.6, Appendix Table 1.5). StemXVivo is primarily composed of nidogen-1 and vitronectin. These two proteins comprised >50% of the total unique peptides identified from analysis of StemXVivo. In addition to the primary components identified, a variety of other intra and extracellular proteins were also found, such as syndecan-2, multiple isoforms of actin, and pigment epithelium derived factor (PEDF). A search of unidentified spectra from the StemXVivo dataset against the entire UniProt database (not species restricted, Appendix Table 1.6) yielded numerous non-human peptides, such as 24 for bovine albumin. StemXVivo is marketed as a mixture of recombinant proteins, so the presence of non-human proteins is somewhat surprising.

After fractionation of the MEF-CMTX layer with SAX, SCX, and SDS-PAGE, a total of 460 proteins were identified (Figure 3.6, Appendix Table 1.7). As this matrix is generated through the lysis of mouse feeder cells, the increase in complexity as indicated by the number of proteins identified is not surprising. However, the primary constituents, fibronectin and perlecan, are both classified as extracellular based on gene ontology. The data for MEF-CMTX correlates well with a previous LC-MS analysis of a matrix generated through the lysis of human foreskin fibroblasts [30]. Although the analysis of matrix composition completed by Meng *et al.* was only to a minimal depth,

the majority of proteins identified in their matrices are present in MEF-CMTX based on comparison with our data.

Fractionation of the BridgeECM matrix with SAX, SCX, and SDS-PAGE resulted in 25 protein identifications (Figure 3.6, Appendix Table 1.8). BridgeECM matrix is primarily composed of albumin, comprising 45 of the total 142 identified unique peptides. The matrix also contained the fibronectin, retinol-binding protein 4, plasminogen activator inhibitor 1, and SPARC. Gene ontology analysis of the proteins found in BridgeECM and the other cell-derived ECMs indicates the presence of a range of cellular localization assignments, and a variety of non-ECM proteins (Figure 3.7).

3.2.6 hESC Growth on a Defined Fibronectin Surface. Of the ECM samples analyzed, CellStart, BridgeECM, and StemXVivo are marketed as products for the maintenance of hESCs [35, 56]. CellStart and BridgeECM are sold as humanized growth matrices, and StemXVivo as a defined recombinant protein mixture for hESC growth. We were able to maintain H9 hESCs that retained expression of Oct4 and Nanog on CellStart, StemXVivo, and MEF-CMTX matrices using mTeSR1 medium for a maximum of 5 passages (Figure 3.8 A). We were, however, unable to maintain H9 hESCs on BridgeECM or HumanBME matrices for >1 passage using mTeSR1. Despite the limited ability of these matrices to promote hESC growth with mTeSR1, we decided to investigate the viability of a defined matrix based upon the abundant components identified in the matrices analyzed.

Upon comparative examination of the matrix datasets, we observed that fibronectin is a primary component of the all of the cell-derived matrices (Figure 3.6). Based on

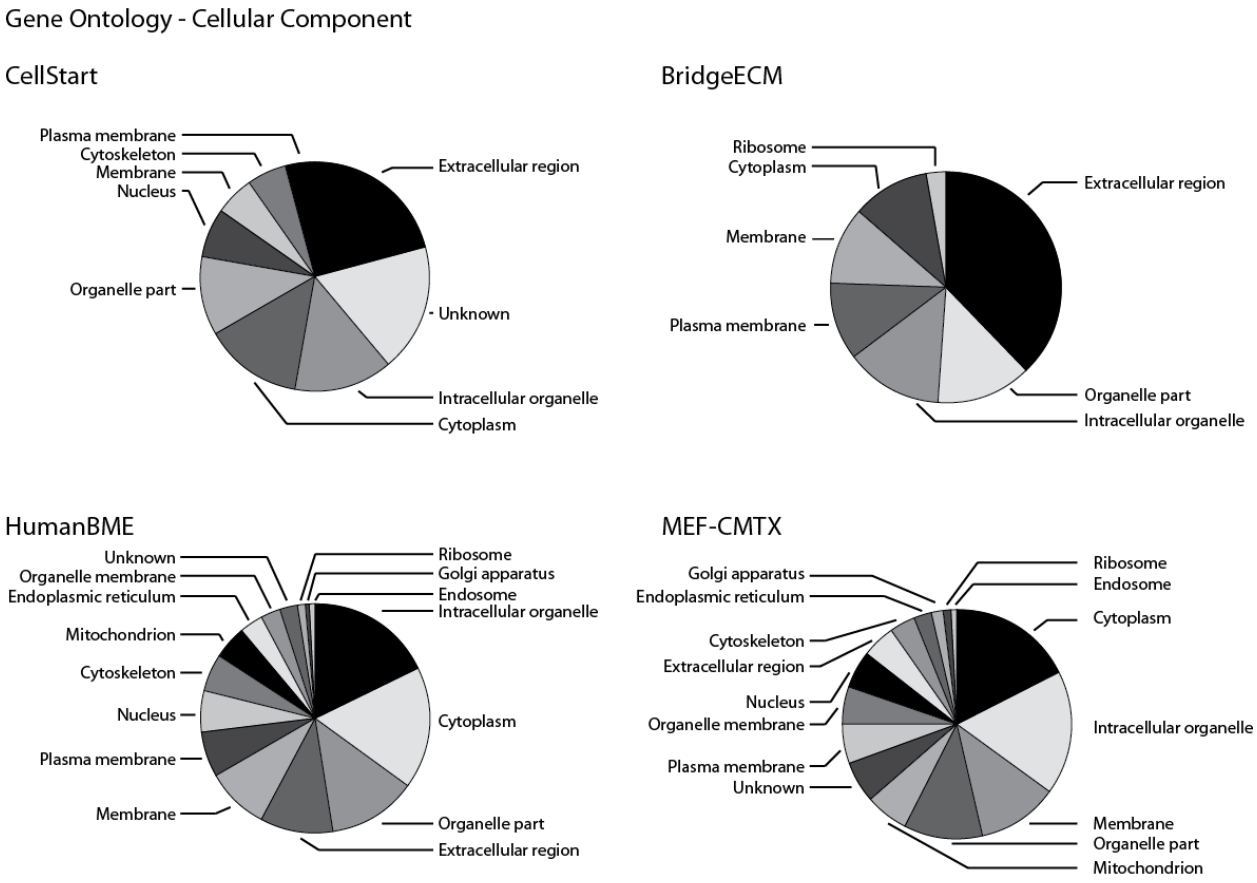

Figure 3.7. Gene ontology analysis of the cell-derived matrices tested. Analysis was done using Scaffold 3.0 software to search protein identifiers against the NCBI Entrez Gene knowledgebase. Protein identifiers were generated using IE-MS analysis of fractionated matrices. With the exception of BridgeECM, all of the matrices tested share similar cellular component profiles with Matrigel (Figure 3.3) and are composed of numerous intracellular proteins. Complete protein identification datasets can be found in the Appendix.

previous evidence that hESCs can be maintained on a combination of collagen IV, laminin, fibronectin, and vitronectin with TeSR1 [17] or on fibronectin alone with defined medium [18, 37], we evaluated a defined system that utilized a combination of fibronectin and mTeSR1. After 10 and 5 passages on fibronectin coated plates, H9 and CA1 hESCs retained typical colony morphology and strong staining for both Oct4 and SSEA-4 markers (Figure 3.8 C-D). For CA1 hESCs, cell growth was not as robust on fibronectin as with H9's, making it difficult to retain a stable culture free of differentiation and amenable to expansion. On other matrices, as well as fibronectin, H9 hESCs retained high levels of Oct4 and Nanog transcript as evidenced by RT-PCR data when compared with hESCs grown on Matrigel™ (Figure 3.8 A). Embryoid bodies generated from H9 cells displayed strong signal for markers of endoderm, ectoderm, and mesoderm lineages in comparison to undifferentiated hESCs grown on fibronectin (Figure 3.8 B). Taken together, these results indicate the ability of fibronectin to sustain H9 hESC self-renewal and pluripotency *in vitro*.

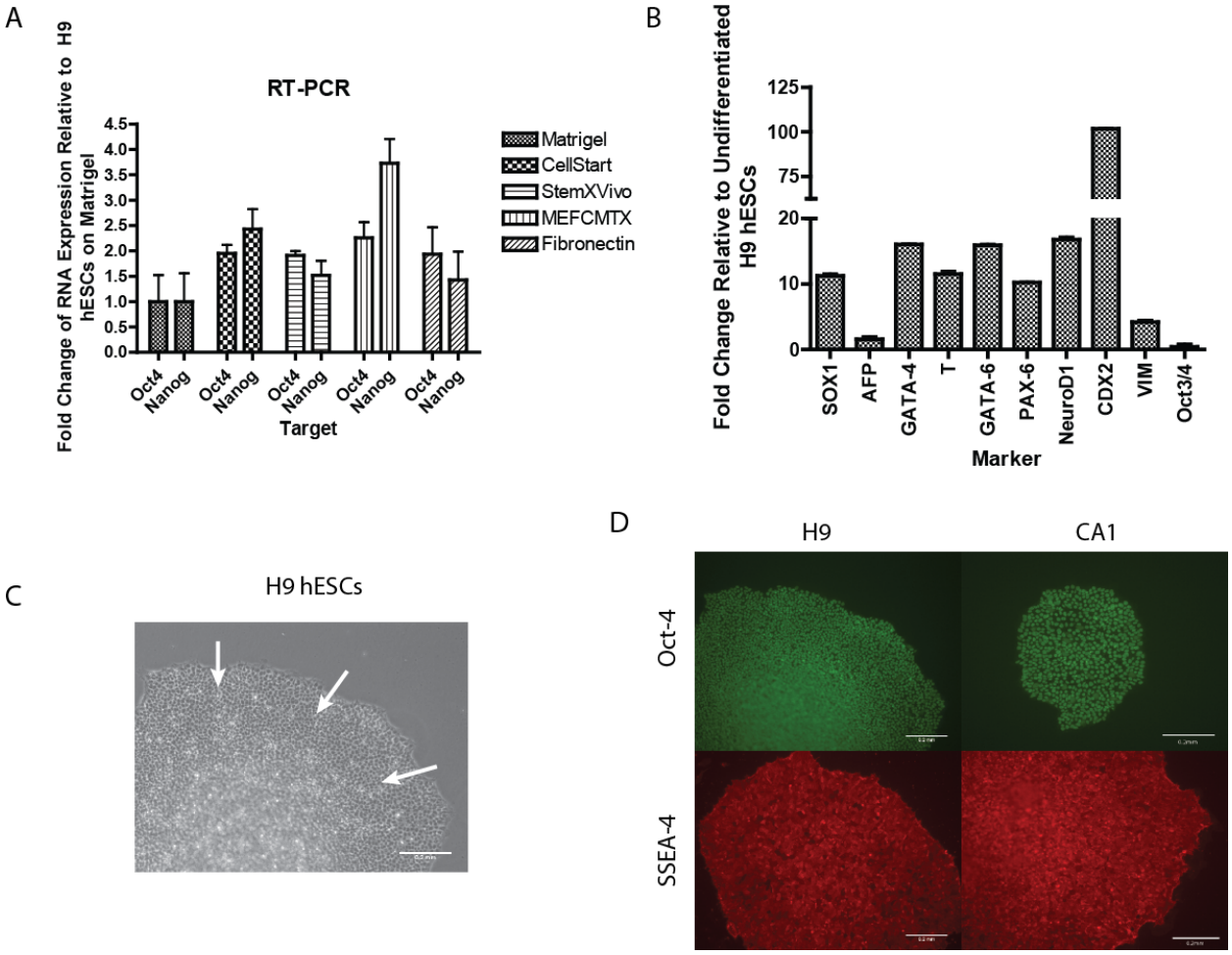

Figure 3.8. hESC growth characteristics on fibronectin. H9 and CA1 hESCs were grown on fibronectin for a period of 10 or 5 passages and analyzed for markers of an undifferentiated phenotype. (A) Shows fold change values for Oct4 and Nanog expression in H9 hESCs relative to those grown on Matrigel™ based on RT-PCR analysis. (B) RT-PCR data for embryoid body markers and the pluripotency marker Oct3/4. Values are shown as fold change for embryoid bodies relative to undifferentiated hESCs grown on fibronectin using GAPDH as a control. In both (A) and (B), error bars represent SD, n=3. (C) Phase contrast image illustrating colony morphology during growth on fibronectin coated plates for H9 hESCs. White arrows indicate areas for point of reference to observe undifferentiated cells. (D) Shows immunofluorescence pictures from H9 and CA1 hESCs grown on fibronectin coated plates for 10 or 5 passages respectively. Immunofluorescence was done directly in 24-well fibronectin coated dishes for the markers Oct3/4 and SSEA-4. Scale bars represent 0.2mm on all images.

3.3 Discussion

An often overlooked aspect in stem cell culture systems is the composition of the ECM. The primary matrix currently in use continues to be Matrigel™ in the absence of an acceptable alternative that is supportive of a wide range of hESC lines and media formulations. Exactly how Matrigel™ helps stem cells remain in an undifferentiated state remains poorly understood. With the rising demand for xeno-free hESC products, the development of a suitable defined growth matrix is of paramount importance. A contributing factor to the recent developments of defined culture media for hESC growth were data yielded from the analyses of conditioned medium from supportive feeder-cell layers [46-48, 50, 57]. Analogous to the analysis of conditioned medium, characterization of the components of cell-derived matrices could potentially aid in the development of defined surfaces for hESC culture. However, proteomic analysis of complex ECM mixtures is difficult due to the abundance profiles of the common constituents. Here, we demonstrate the development and optimization of methods for the fractionation and analysis of complex ECM mixtures to aid in the identification of hESC supportive matrix components.

In the analysis of Matrigel™, SEC fractionation proved to be of limited utility, even when used in combination with IE-MS. A significant number of the unique peptides identified were assigned to laminin/enactin, the primary components of Matrigel™. AS precipitation in combination with 1D-SDS-Gel fractionation facilitated the identification of a large number of peptides outside of those belonging to laminin and enactin. Gene ontology analysis of the Matrigel™ dataset indicates the presence of numerous cellular

proteins that were either cytoplasmic or nuclear in origin. This implies that although structurally important proteins such as laminin constitute the bulk of what is being extracted from the EHS sarcoma cells, there are also numerous intracellular proteins present. Depletion of low molecular weight components using AS precipitation to create GFR Matrigel™ results in the enrichment of laminin/enactin peptides in comparison to N-GFR. However, the lack of specificity for this method means that numerous other matrix components are lost, as shown through analysis of the supernatant obtained after 15% AS precipitation. This lack of reproducibility combined with limitations in the MS approach due to dynamic range constraints likely contributed to the identification of proteins apparently unique to GFR Matrigel™. As GFR is derived from N-GFR Matrigel™, the identification of proteins unique to GFR Matrigel™ is unexpected. Further proteomic analysis of Matrigel™ using the SAX and SCX methods utilized on the other matrices tested would potentially reconcile these differences by obtaining greater depth of coverage. However, differences between N-GFR and GFR are potentially derived from batch-to-batch variability of Matrigel™ that cannot be addressed in the proteomics approach.

As noted above, Matrigel™ was previously reported to contain specific growth factors [11]. With the optimized proteomics protocol used here we identified several growth and transcription factors such as Grb2 and connective tissue growth factor (CTGF). However, the growth and transcription factors represent only a small fraction of the proteins identified in the analysis of the matrix. We identified numerous proteins directly related to binding and signaling of growth factors. Other ECM proteins identified in this study, fibronectin [58], collagen type IV [59], follistatin [60], and thrombospondin [61],

have been proposed to interact with members TGF-β superfamily. The presumed functions of these interactions are to enhance activity and stability of these cytokines in culture. Examples of these ECM interactions have been found to be involved in a variety of pathways, such as fibronectin and vitronectin binding to hepatocyte growth factor receptors leading to enhanced cell migration [62]. Fibronectin type-III domains have also been shown to be involved with vascular endothelial growth factor (VEGF) signaling [63]. Similar interactions have also been demonstrated for a variety of other growth factors [64-67].

The in-depth proteomic analysis of Matrigel™ presented in this study reveals a complex and intricate mixture consisting of numerous structural, growth factors and their binding partners, as well as several other proteins of roles that are not clear in cell culture. We speculate that many of these of proteins play a role in the self-renewal of stem cells when cultured in the presence of Matrigel™. Our analysis of Matrigel™ revealed that it was primarily composed of laminin, collagen, enactin, and fibronectin. Of these, laminin, nidogen-1, and different collagen isoforms have all been shown to be beneficial for hESC maintenance [17, 23, 24, 68-71]. It is perhaps not surprising then that Matrigel™ is the gold standard for the maintenance of a wide array of hESC lines, as it contains most of the proteins shown to promote hESC growth when used individually. However, as a result of the significant depth of coverage we were able to obtain with the use of AS-IE-MS methods, this study also suggests that it will be challenging to replace Matrigel™ in a variety of cell culture and experimental assays due to its complexity.

To complement the Matrigel™ data and facilitate the identification of hESC supportive proteins, we sought to compare matrix components from a variety of cell-culture matrices. Employing a combination of SCX, SAX, and 1D-SDS-Gel approaches, we analyzed other cell-derived and commercial matrices used in hESC culture. Upon inspection of CellStart, StemXVivo, BridgeECM, HumanBME, MEF-CMTX, and Matrigel™ proteomic data, the complexity of these protein mixtures becomes apparent. Based on the number of proteins identified StemXVivo, BridgeECM, and CellStart are more defined matrices in comparison with HumanBME, MEF-CMTX, and Matrigel™. However, based on the proteomics data presented here, none of these matrices are fully defined. Although CellStart and StemXVivo are marketed as such, the number of proteins found indicates they are not as well defined as suggested by the manufacturers.

With the exception of StemXVivo, fibronectin was found to be highly abundant in all of the matrices analyzed. StemXVivo is manufactured as a recombinant protein mixture, and based on our analysis is primarily composed of vitronectin. Vitronectin has previously been shown to sustain hESC pluripotency and survival [15, 19]. This is highlighted in our study by the ability of StemXVivo to promote the growth of H9 hESCs that retain expression of markers indicative of an undifferentiated state (Figure 3.7 A). It has previously been shown that fibronectin and vitronectin both bind integrins that support hESC adhesion [15, 72]. Recent research into synthetic growth surfaces has revealed that integrin RGD and heparin binding peptides promote attachment and proliferation of hESCs [25-28, 73]. These studies suggest that integrin binding by the primary proteins present in ECM mixtures regulate attachment and proliferation.

Undifferentiated hESCs are known to express the fibronectin-specific integrin receptor $\alpha_5\beta_1$ [18], thus supporting the observation of fibronectin as an effective growth matrix. However, it is likely that other proteins detected in these matrices are also of importance for the growth of a wide range of hESC lines, such as is the case with culture on Matrigel™ or MEFs. This is highlighted by the identification of other proteins like serum albumin and PEDF in several of the matrices analyzed. FBS, of which serum albumin is a primary component, has previously been used as a growth matrix for hESCs [74]. Moreover, PEDF has recently been shown to be beneficial for the feeder-free maintenance of hESCs [75].

Here, we have illustrated the utility of employing different and complementary fractionation methods for the analysis of complex ECM samples in order to elucidate factors essential for hESC survival. Our proteomics analysis reveals the ubiquity of fibronectin in the majority of commonly available matrices. It is noteworthy that none of the matrices tested, including fibronectin, were able to promote and maintain the growth of hESCs with the same efficiency and stability of Matrigel™ when using mTeSR1 medium. H9 and CA1 hESCs differentiated and proliferated poorly after 15 and 5 passages on fibronectin respectively. This indicates that while a defined matrix consisting of a sole component, such as fibronectin is suitable for hESC growth, long-term maintenance and expansion requires a mixture of supportive components in the matrix, medium, or both. Revealing these components through characterization of hESC supportive matrices is a valuable tool for elucidating factors that can have a positive effect on the maintenance of pluripotency.

3.4 Methods

3.4.1 Cell culture and harvest – H9 (passage 26) and CA1 (passage 27) hESCs were maintained on hESC Qualified Geltrex (Invitrogen, Carlsbad, CA) before passage on to fibronectin coated plates (Millipore, Billerica, MA or BD Biosciences, Franklin Lake, NJ). H9 cells were obtained from WiCell (Wisconsin). The CA1 hESC line used in all experiments was obtained from Dr. Cheryle Séguin of The University of Western Ontario [76, 77]. For all fibronectin experiments conventional 6 well dishes were used. Geltrex, StemXVivo, and BridgeECM were used according to the manufacturer's instructions. CellStart was used as a 25X solution instead of the manufacturer recommended 50X. Cells were maintained in mTeSR1 medium (StemCell Technologies, Vancouver, Canada) on all matrices. Cells were passaged mechanically to minimize variability from enzymatic methods.

Embryoid bodies were generated using the RCCS-2SC 3D bioreactor (Synthecon, Houston, TX) with 2 x10 mL high aspect ratio vessels (HARV). Briefly, ~2 x 10^6 hESCs were harvested from fibronectin coated plates. The equivalent of ~1 x 10^6 hESCs were re-suspended in 8 mL of EB medium containing Knockout DMEM/F12, 20% KOSR (Invitrogen), 2 mM L-glutamine, 0.1 mM β-mercaptoethanol, and 1% non-essential amino acids. The remaining 2 mL was added using syringes to ensure the removal of air bubbles from the vessels. Vessels were left in a 37°C incubator with a rotation rate of 8 rpm. Once EBs had formed (typically after 3-4 days), they were transferred to ultra-low adherence cell culture dishes and grown for a period of 21 days. Cells were then harvested and assayed by RT-PCR for the differentiation markers CDX2, alpha-feto

protein (AFP), GATA-6, GATA-4, Sox-1, PAX-6, T-brachyury, Vimentin, and Neurogenic differentiation 1 (NeuroD1) using TaqMan primer probe sets (Appendix Table 1.15).

3.4.2 Extracellular matrix analysis – Human Cultrex basement membrane extract from Trevigen (Gaithersberg, MD), BridgeECM (GlobalStem, Rockville, MD), and CellStart matrix from Invitrogen (Carlsbad, CA) were assayed for protein content using a Bradford assay (data not shown). StemXVivo (R&D Systems, Minneapolis, MN) and BridgeECM were concentrated from their stock solutions using 3 kDa centrifugal filters and reconstituted in 8M Urea and 100mM ammonium bicarbonate (ABC). Lysed MEF matrix was generated by plating of 250,000 irradiated CF-1 cells in each well of a 6-well plate coated with 0.1% gelatin. After 7 days the cells were lysed using a 20 mM NH_4OH solution. MEF-matrix layers were harvested using a solution of 8 M urea and 100 mM ABC. All matrix samples were analyzed using in-solution digestion followed by fractionation on SCX and SAX columns with pH elution. All samples were also fractionated with 1D-SDS-PAGE and prepared with an in-gel digestion as described earlier. Each fractionation method was run using iterative exclusion as a single technical replicate for each matrix analyzed, for a total of 2 injections per sample.

3.4.3 Matrigel Preparation - Two separate lots of growth factor reduced Matrigel™ (A1105 & A3105, CAT# 356234, BD Biosciences, Mississauga, Canada), and one lot of standard Matrigel™ (A3873, CAT# 356230) were aliquoted into 100 µl fractions and stored at -80°C until use. The stock solution of Matrigel™ is at a concentration of ~10 mg/mL based on manufacturer specifications. Protein concentration was assessed with the Bradford assay.

3.4.4 Reduced Matrigel by Precipitation - Individual aliquots of standard and GFR Matrigel™ were precipitated using a 15% AS solution as described previously [11]. While the previous study employed a 20% AS solution, we found the 15% AS solution provided a precipitation that resulted in a greater removal of low molecular weight components as deduced from SDS gels analysis. Aliquots were diluted 1:1 using a 30% saturated AS solution to give a final concentration of 15%. Mixtures were left at 4°C for 60 minutes before centrifuging at 12000 g for 15 minutes. The supernatant was drawn into a new tube and brought to 90% AS saturation to precipitate any remaining protein. Solutions were centrifuged for 15 minutes at 12000g and the pellet was reconstituted in 100 mM NH_4CO_3. The reconstituted pellet was then subjected to an in-solution digestion with trypsin, or in-gel following 1D-SDS PAGE [46, 78].

3.4.5 Size Exclusion Chromatrography – 500 µg equivalents of Matrigel™ (as determined by the Bradford assay), as well as pellets from the 15% AS precipitation were run through an off-line size exclusion system. A BioSep-SEC-S2000 column (Phenomenex) fitted with a Security Guard pre-column (Phenomenex) with a phosphate buffer (BioShop Canada Inc.)(0.5 M, pH 7.0) mobile phase was used for separation. The sample was injected manually to an Agilent 1100 HPLC system (Agilent Technologies Inc.) system that provided flow (1 ml/min) as well as detection at 210 nm and 280 nm using a diode array detector.

3.4.6 In-solution trypsin digestion – Matrix samples were reduced with 10 mM dithiothreitol (DTT) for 60 minutes. Samples were then alkylated with 40 mM iodoacetamide (IAA) for 60 minutes. The reactions were quenched through the addition

of DTT and left to incubate for another 60 minutes. Samples were then diluted 1/6 in 50 mM ABC. Trypsin (Promega, Madison, WI) at a concentration of 1 µg enzyme to 25 µg of total protein was added to the mixtures and left to incubate for 24 hours at 37°C. The next day, digests were acidified using neat trifluoroacetic acid and desalted on C18 cartridges (CAT# 2001, Applied Separations, Lehigh Valley, PA). After elution with 50% acetonitrile, samples were evaporated using a SpeedVac. Prior to loading on an SCX column, dried samples were reconstituted in 0.5% formic acid at a pH of ~2. Samples for SAX analysis were reconstituted in 0.5% NaOH at a pH of ~12.

3.4.7 In-gel trypsin digestion – 40 µg of each matrix was diluted in Laemmli buffer. After heating, matrix samples were loaded in each of two lanes on a 12% SDS-Gel. The gel was stained with Coomassie blue and the gel lanes were divided into 12 fractions based on visual assessment of protein concentration. Gel cubes in each fraction were destained using 20% acetonitrile (ACN) in 1M ABC. Proteins were reduced using 10 mM DTT for 60 minutes, followed by alkylation with 100 mM IAA for 60 minutes. Digestion was carried out using trypsin at a 1/25 ratio overnight in a 37°C water bath. Fractions were extracted the next day using 10% formic acid, sonication, and a final ACN step. Each fraction was dried using a SpeedVac and reconstituted in 10% formic acid prior to injection on to the MS.

3.4.8 Column preparation – Columns were packed in 360 O.D. x 200 I.D. capillaries (PolyMicro Technologies, Phoenix, AZ) using a conventional pressure bomb (Next Advance, Averill Park, NY). Frits were prepared by mixing 75 µL of potassium silicate with 25 µL of formamide, vortexing for 1 minute and rapidly inserting and removing the

capillary end from the resulting mixture. Capillary frits were dried and hardened in a 100°C oven for 2 hours. Capillaries were then rinsed with forward and reverse flow of methanol using the pressure bomb at 200 psi. Prior to packing, capillaries were rinsed for 30 minutes with 0.5% formic acid for SCX and 0.5% NaOH for SAX columns. PolySULFOETHYL A SCX beads (5 µm, 300Å, CAT# PLBMSE0503) were purchased from PolyLC (Columbia, MD) and reconstituted in 10 mM citric acid. SAX beads were purchased from Varian Inc. (10 µm, 1000Å, CAT# PL1451-2102, Palo Alto, CA) and reconstituted in 10 mM NH_4OH. SCX and SAX columns were packed to a length of ~3 cm for all experiments. All packing was done at a pressure of 200 psi until the desired column length was obtained, then pressurized to 1000 psi to complete packing. Packed columns were rinsed with solvents for conditioning as recommended by the manufacturer.

3.4.9 Peptide Fractionation – Peptides were fractionated with SCX and SAX columns using a CapLC system (Waters, Milford, MA) with a flow rate of 2 µL/min. Mobile phase A was composed of 10mM citric acid at a pH of ~2.3, mobile phase B was pH 11.4 10 mM NH_4OH, and mobile phase C was 500 mM ammonium acetate. Mobile phases were all prepared fresh prior to fractionation to ensure the stability of pH from run to run. Fractionation with pH was carried out using a 120 minute gradient from pH 2 to 12 for SCX, and 12 to 2 for SAX. Salt fractionation was carried using the following steps:

0 mM, 7.5 mM, 15 mM, 30 mM, 45 mM, 60 mM, 75 mM, 90 mM, 105 mM, 120 mM, 150 mM, 300 mM, 500 mM ammonium acetate over 120 minutes. Each fraction was collected offline in a volume of 20 µL. Fractions were dried using a SpeedVac, and reconstituted in 10% formic acid prior to injection on the MS.

3.4.10 MS Data Acquisition – Fractions were injected and separated using a nanoAcquity system (Waters, Milford, MA) equipped with a 25 cm x 75 µm I.D. C18 column. Fractions were separated using a 1 to 40% ACN gradient over 90 minutes at a flow rate of 300 nL/min. MS analysis was done on a Q-ToF Ultima (Micromass/Waters) using data-dependent acquisition with selection of the four top precursor masses per survey scan. Survey scans were set at 1s, and MS/MS acquisition set at 1s or 6000 cps TIC cut-off. Exclusion lists were generated using in-house software that automatically adds 0.7amu to the precursor masses selected in previous runs and outputs a file also containing retention time information. Each fraction was analyzed for a single exclusion round (2 injections total), adjusting the injection volume dependent on signal intensity in the previous run. In analyses of Matrigel™, each fraction was injected a total of 7 times (6 exclusion rounds).

3.4.11 MS Data analysis – Data analysis for all matrices tested was performed in PEAKS 5.3 software (Bioinformatic Solutions Inc., Waterloo, Canada) [79, 80]. After import into PEAKS, MS/MS spectra from raw data files were refined using the following settings: merge spectra – true (100 ppm mass tolerance, 60 second retention time tolerance), correct precursor mass – true, determine precursor charge state – true (minimum charge +2, maximum charge +5), spectral quality filter – true (0.65 threshold), centroid, deisotope, and deconvolute – true. Resulting MS/MS spectra were then *de novo* sequenced using the following parameters: parent monoisotopic mass tolerance – 100ppm, fragment monoisotopic mass tolerance – 0.15 daltons, enzyme specificity – semi-Trypsin, fixed modifications – carbamidomethylation, variable modifications – N-terminal acetylation and oxidized methionine. After *de novo* analysis, data were

searched against the UniProt sequence database (Human taxonomy specified, 20236 total entries or Mouse taxonomy specified, 16376 total entries) using the following parameters: parent monoisotopic mass tolerance – 100 ppm, fragment monoisotopic mass tolerance – 0.15 daltons, enzyme specificity – semi-Trypsin, fixed modifications – carbamidomethylation, variable modifications – N-terminal acetylation and oxidized methionine, estimate false-discovery rate – true.

3.4.12 Protein identification – Resultant protein identification data from the database search were processed using PEAKS 5.3 software [81]. Identifications were filtered by assigned score to give a <1.0% false-discovery rate for peptide-spectral matches based on estimation from a decoy-fusion method of database search. Identified proteins were also required to be matched by >2 unique peptides. Proteins that contained similar peptides and could not be differentiated based on MS/MS analysis alone were grouped to satisfy the principles of parsimony. For all matrices analyzed, keratin hits were manually removed from the final datasets.

3.4.13 Real-time PCR – RNA was purified using Trizol reagent according to the manufacturer's instructions (Invitrogen) or with the 5 Prime PerfectPure RNA Extraction Kit (5 Prime, Gaithersburg, MD). After NanoDrop quantification, 1 µg of cDNA was synthesized using the High Capacity cDNA Reverse Transcription Kit with RNase inhibitor (Invitrogen). Real-time PCR was performed using the TaqMan® Universal PCR Master Mix (Invitrogen). Samples were incubated at 50°C for 2 minutes followed by 10 minutes at 95°C. Samples were then amplified at 95°C for 15 seconds followed by 1 minute at 58°C for 46 cycles. All samples were normalized to large ribosomal

protein RPLPO as a positive control. All primers were obtained from Invitrogen and assay information can be found in Appendix Table 1.15. Each biological replicate was run in triplicate for every marker assayed. All reagents were used according to the manufacturer's instructions.

3.4.14 Immunofluorescence – Passage 10 H9 and 5 CA1 hESCs grown on fibronectin were plated in wells of a 24-well dish coated with the same matrix. After 4 days of culture in mTeSR1 medium cells were rinsed and fixed with 4% para-formaldehyde containing 20 mM sucrose. Prior to staining, cells were blocked using the Dako Serum Free Protein Block solution (Dako, Cambridgeshire, UK). Oct-4 (clone 10H11.2), SSEA-4 (clone MC-813-70), and SSEA-1 (clone MC-480) primary antibodies were obtained from Millipore (Billerica, MA). Cells for Oct-4 labeling were permeabilized using a 0.1% Triton X-100 solution prior to blocking. Cells were labeled with primary antibodies for Oct-4 or SSEA-4 as undifferentiated markers and SSEA-1 for differentiated cells all at concentrations of 2 µg/mL for 60 minutes at room temperature. Secondary Alexa-fluor 488 goat anti-mouse IgG and Alexa-fluor 568 goat anti-mouse IgM were obtained from Invitrogen (Carlsbad, CA). Secondary antibodies were probed at concentrations of 1 µg/mL for 60 minutes at room temperature. All products were used according to manufacturer's instructions.

3.4 References

[1] Lin, C. Q., Bissell, M. J., Multi-faceted regulation of cell differentiation by extracellular matrix. *FASEB J* 1993, *7*, 737-743.
[2] Martin, G. R., Kleinman, H. K., Extracellular matrix proteins give new life to cell culture. *Hepatology* 1981, *1*, 264-266.
[3] Kleinman, H. K., Graf, J., Iwamoto, Y., Kitten, G. T., Ogle, R. C., Sasaki, M.*, et al.*, Role of basement membranes in cell differentiation. *Ann N Y Acad Sci* 1987, *513*, 134-145.
[4] Kleinman, H. K., Klebe, R. J., Martin, G. R., Role of collagenous matrices in the adhesion and growth of cells. *J Cell Biol* 1981, *88*, 473-485.
[5] Erickson, A. C., Couchman, J. R., Still more complexity in mammalian basement membranes. *J Histochem Cytochem* 2000, *48*, 1291-1306.
[6] Sawada, N., Tomomura, A., Sattler, C. A., Sattler, G. L., Kleinman, H. K., Pitot, H. C., Extracellular matrix components influence DNA synthesis of rat hepatocytes in primary culture. *Exp Cell Res* 1986, *167*, 458-470.
[7] Kleinman, H. K., Cannon, F. B., Laurie, G. W., Hassell, J. R., Aumailley, M., Terranova, V. P.*, et al.*, Biological activities of laminin. *J Cell Biochem* 1985, *27*, 317-325.
[8] Kleinman, H. K., Martin, G. R., Matrigel: basement membrane matrix with biological activity. *Semin Cancer Biol* 2005, *15*, 378-386.
[9] Kleinman, H. K., McGarvey, M. L., Liotta, L. A., Robey, P. G., Tryggvason, K., Martin, G. R., Isolation and characterization of type IV procollagen, laminin, and heparan sulfate proteoglycan from the EHS sarcoma. *Biochemistry* 1982, *21*, 6188-6193.
[10] Orkin, R. W., Gehron, P., McGoodwin, E. B., Martin, G. R., Valentine, T., Swarm, R., A murine tumor producing a matrix of basement membrane. *J Exp Med* 1977, *145*, 204-220.
[11] Vukicevic, S., Kleinman, H. K., Luyten, F. P., Roberts, A. B., Roche, N. S., Reddi, A. H., Identification of multiple active growth factors in basement membrane Matrigel suggests caution in interpretation of cellular activity related to extracellular matrix components. *Exp Cell Res* 1992, *202*, 1-8.
[12] Lei, T., Jacob, S., Ajil-Zaraa, I., Dubuisson, J. B., Irion, O., Jaconi, M.*, et al.*, Xeno-free derivation and culture of human embryonic stem cells: current status, problems and challenges. *Cell Research* 2007, *17*, 682-688.
[13] Skottman, H., Narkilahti, S., Hovatta, O., Challenges and approaches to the culture of pluripotent human embryonic stem cells. *Regen Med* 2007, *2*, 265-273.
[14] Gerecht, S., Burdick, J. A., Ferreira, L. S., Townsend, S. A., Langer, R., Vunjak-Novakovic, G., Hyaluronic acid hydrogel for controlled self-renewal and differentiation of human embryonic stem cells. *Proc Natl Acad Sci U S A* 2007, *104*, 11298-11303.
[15] Braam, S. R., Zeinstra, L., Litjens, S., Ward-van Oostwaard, D., van den Brink, S., van Laake, L.*, et al.*, Recombinant vitronectin is a functionally defined substrate that supports human embryonic stem cell self-renewal via alpha V beta 5 integrin. *Stem Cells* 2008, *26*, 2257-2265.
[16] Hakala, H., Rajala, K., Ojala, M., Panula, S., Areva, S., Kellomaki, M.*, et al.*, Comparison of Biomaterials and Extracellular Matrices as a Culture Platform for Multiple, Independently Derived Human Embryonic Stem Cell Lines. *Tissue Engineering Part A* 2009, *15*, 1775-1785.
[17] Ludwig, T. E., Levenstein, M. E., Jones, J. M., Berggren, W. T., Mitchen, E. R., Frane, J. L.*, et al.*, Derivation of human embryonic stem cells in defined conditions. *Nat Biotechnol* 2006, *24*, 185-187.
[18] Amit, M., Shariki, C., Margulets, V., Itskovitz-Eldor, J., Feeder layer- and serum-free culture of human embryonic stem cells. *Biology of Reproduction* 2004, *70*, 837-845.
[19] Manton, K. J., Richards, S., Van Lonkhuyzen, D., Cormack, L., Leavesley, D., Upton, Z., A chimeric vitronectin: igf-I protein supports feeder-cell-free and serum-free culture of human embryonic stem cells. *Stem Cells Dev* 2010, *19*, 1297-1305.
[20] Mei, Y., Saha, K., Bogatyrev, S. R., Yang, J., Hook, A. L., Kalcioglu, Z. I.*, et al.*, Combinatorial development of biomaterials for clonal growth of human pluripotent stem cells. *Nat Mater* 2010, *9*, 768-778.
[21] Klim, J. R., Li, L. Y., Wrighton, P. J., Piekarczyk, M. S., Kiessling, L. L., A defined glycosaminoglycan-binding substratum for human pluripotent stem cells. *Nature Methods* 2010, *7*, 989-U972.

[22] Harb, N., Archer, T. K., Sato, N., The Rho-Rock-Myosin Signaling Axis Determines Cell-Cell Integrity of Self-Renewing Pluripotent Stem Cells. *Plos One* 2008, *3*, -.
[23] Miyazaki, T., Futaki, S., Hasegawa, K., Kawasaki, M., Sanzen, N., Hayashi, M*., et al.*, Recombinant human laminin isoforms can support the undifferentiated growth of human embryonic stem cells. *Biochemical and Biophysical Research Communications* 2008, *375*, 27-32.
[24] Vuoristo, S., Virtanen, I., Takkunen, M., Palgi, J., Kikkawa, Y., Rousselle, P*., et al.*, Laminin isoforms in human embryonic stem cells: synthesis, receptor usage and growth support. *Journal of Cellular and Molecular Medicine* 2009, *13*, 2622-2633.
[25] Derda, R., Li, L., Orner, B. P., Lewis, R. L., Thomson, J. A., Kiessling, L. L., Defined substrates for human embryonic stem cell growth identified from surface arrays. *ACS Chem Biol* 2007, *2*, 347-355.
[26] Brafman, D. A., Chang, C. W., Fernandez, A., Willert, K., Varghese, S., Chien, S., Long-term human pluripotent stem cell self-renewal on synthetic polymer surfaces. *Biomaterials* 2010, *31*, 9135-9144.
[27] Kolhar, P., Kotamraju, V. R., Hikita, S. T., Clegg, D. O., Ruoslahti, E., Synthetic surfaces for human embryonic stem cell culture. *J Biotechnol* 2010, *146*, 143-146.
[28] Melkoumian, Z., Weber, J. L., Weber, D. M., Fadeev, A. G., Zhou, Y., Dolley-Sonneville, P*., et al.*, Synthetic peptide-acrylate surfaces for long-term self-renewal and cardiomyocyte differentiation of human embryonic stem cells. *Nat Biotechnol* 2010, *28*, 606-610.
[29] Steiner, D., Khaner, H., Cohen, M., Even-Ram, S., Gil, Y., Itsykson, P*., et al.*, Derivation, propagation and controlled differentiation of human embryonic stem cells in suspension. *Nat Biotechnol* 2010, *28*, 361-364.
[30] Meng, G. L., Liu, S. Y., Li, X. Y., Krawetz, R., Rancourt, D. E., Extracellular Matrix Isolated From Foreskin Fibroblasts Supports Long-Term Xeno-Free Human Embryonic Stem Cell Culture. *Stem Cells and Development* 2010, *19*, 547-556.
[31] Amit, M., Margulets, V., Segev, H., Shariki, K., Laevsky, I., Coleman, R*., et al.*, Human feeder layers for human embryonic stem cells. *Biology of Reproduction* 2003, *68*, 2150-2156.
[32] Chen, H. F., Chuang, C. Y., Shieh, Y. K., Chang, H. W., Ho, H. N., Kuo, H. C., Novel autogenic feeders derived from human embryonic stem cells (hESCs) support an undifferentiated status of hESCs in xeno-free culture conditions. *Human Reproduction* 2009, *24*, 1114-1125.
[33] Hovatta, O., Mikkola, M., Gertow, K., Stromberg, A. M., Inzunza, J., Hreinsson, J*., et al.*, A culture system using human foreskin fibroblasts as feeder cells allows production of human embryonic stem cells. *Human Reproduction* 2003, *18*, 1404-1409.
[34] Kibschull, M., Mileikovsky, M., Nagy, A., Lye, S. J., Human Embryonic Fibroblast Lines Provide Enhanced Support of Human Embryonic Stem Cells in Xeno-Free Culture Conditions. *Reproductive Sciences* 2009, *16*, 282a-282a.
[35] Swistowski, A., Peng, J., Han, Y., Swistowska, A. M., Rao, M. S., Zeng, X., Xeno-free defined conditions for culture of human embryonic stem cells, neural stem cells and dopaminergic neurons derived from them. *Plos One* 2009, *4*, e6233.
[36] Hakala, H., Rajala, K., Ojala, M., Panula, S., Areva, S., Kellomaki, M*., et al.*, Comparison of Biomaterials and Extracellular Matrices as a Culture Platform for Multiple, Independently Derived Human Embryonic Stem Cell Lines. *Tissue Eng Part A* 2009.
[37] Lu, J., Hou, R. H., Booth, C. J., Yang, S. H., Snyder, M., Defined culture conditions of human embryonic stem cells. *Proceedings of the National Academy of Sciences of the United States of America* 2006, *103*, 5688-5693.
[38] Mallon, B. S., Park, K. Y., Chen, K. G., Hamilton, R. S., McKay, R. D. G., Toward xeno-free culture of human embryonic stem cells. *International Journal of Biochemistry & Cell Biology* 2006, *38*, 1063-1075.
[39] Li, Q., Wang, J., Shahani, S., Sun, D. D., Sharma, B., Elisseeff, J. H*., et al.*, Biodegradable and photocrosslinkable polyphosphoester hydrogel. *Biomaterials* 2006, *27*, 1027-1034.
[40] Chen, S. S., Fitzgerald, W., Zimmerberg, J., Kleinman, H. K., Margolis, L., Cell-cell and cell-extracellular matrix interactions regulate embryonic stem cell differentiation. *Stem Cells* 2007, *25*, 553-561.
[41] Philp, D., Chen, S. S., Fitzgerald, W., Orenstein, J., Margolis, L., Kleinman, H. K., Complex extracellular matrices promote tissue-specific stem cell differentiation. *Stem Cells* 2005, *23*, 288-296.
[42] McCloskey, K. E., Gilroy, M. E., Nerem, R. M., Use of embryonic stem cell-derived endothelial cells as a cell source to generate vessel structures in vitro. *Tissue Engineering* 2005, *11*, 497-505.

[43] Kim, M. S., Hwang, N. S., Lee, J., Kim, T. K., Leong, K., Shamblott, M. J.*, et al.*, Musculoskeletal differentiation of cells derived from human embryonic germ cells. *Stem Cells* 2005, *23*, 113-123.
[44] Battista, S., Guarnieri, D., Borselli, C., Zeppetelli, S., Borzacchiello, A., Mayol, L.*, et al.*, The effect of matrix composition of 3D constructs on embryonic stem cell differentiation. *Biomaterials* 2005, *26*, 6194-6207.
[45] Baxter, M. A., Camarasa, M. V., Bates, N., Small, F., Murray, P., Edgar, D.*, et al.*, Analysis of the distinct functions of growth factors and tissue culture substrates necessary for the long-term self-renewal of human embryonic stem cell lines. *Stem Cell Res* 2009.
[46] Bendall, S. C., Hughes, C., Campbell, J. L., Stewart, M. H., Pittock, P., Liu, S.*, et al.*, An Enhanced Mass Spectrometry Approach Reveals Human Embryonic Stem Cell Growth Factors in Culture. *Molecular & Cellular Proteomics* 2009, *8*, 421-432.
[47] Prowse, A. B. J., McQuade, L. R., Bryant, K. J., Marcal, H., Gray, P. P., Identification of potential pluripotency determinants for human embryonic stem cells following proteomic analysis of human and mouse fibroblast conditioned media. *Journal of Proteome Research* 2007, *6*, 3796-3807.
[48] Prowse, A. B. J., McQuade, L. R., Bryant, K. J., Van Dyk, D. D., Tuch, B. E., Gray, P. P., A proteome analysis of conditioned media from human neonatal fibroblasts used in the maintenance of human embryonic stem cells. *Proteomics* 2005, *5*, 978-989.
[49] Lim, J. W. E., Bodnar, A., Proteome analysis of conditioned medium from mouse embryonic fibroblast feeder layers which support the growth of human embryonic stem cells. *Proteomics* 2002, *2*, 1187-1203.
[50] Chin, A. C. P., Fong, W. J., Goh, L. T., Philp, R., Oh, S. K. W., Choo, A. B. H., Identification of proteins from feeder conditioned medium that support human embryonic stem cells. *Journal of Biotechnology* 2007, *130*, 320-328.
[51] Faca, V., Pitteri, S. J., Newcomb, L., Glukhova, V., Phanstiel, D., Krasnoselsky, A.*, et al.*, Contribution of protein fractionation to depth of analysis of the serum and plasma proteomes. *J Proteome Res* 2007, *6*, 3558-3565.
[52] de Godoy, L. M., Olsen, J. V., de Souza, G. A., Li, G., Mortensen, P., Mann, M., Status of complete proteome analysis by mass spectrometry: SILAC labeled yeast as a model system. *Genome Biol* 2006, *7*, R50.
[53] Washburn, M. P., Wolters, D., Yates, J. R., 3rd, Large-scale analysis of the yeast proteome by multidimensional protein identification technology. *Nat Biotechnol* 2001, *19*, 242-247.
[54] Fang, Y., Robinson, D. P., Foster, L. J., Quantitative analysis of proteome coverage and recovery rates for upstream fractionation methods in proteomics. *J Proteome Res* 2010, *9*, 1902-1912.
[55] Wang, N., Li, L., Exploring the precursor ion exclusion feature of liquid chromatography-electrospray ionization quadrupole time-of-flight mass spectrometry for improving protein identification in shotgun proteome analysis. *Anal Chem* 2008, *80*, 4696-4710.
[56] Klimanskaya, I., Chung, Y., Meisner, L., Johnson, J., West, M. D., Lanza, R., Human embryonic stem cells derived without feeder cells. *Lancet* 2005, *365*, 1636-1641.
[57] Bendall, S. C., Stewart, M. H., Menendez, P., George, D., Vijayaragavan, K., Werbowetski-Ogilvie, T.*, et al.*, IGF and FGF cooperatively establish the regulatory stem cell niche of pluripotent human cells in vitro. *Nature* 2007, *448*, 1015-1021.
[58] Fava, R. A., McClure, D. B., Fibronectin-associated transforming growth factor. *J Cell Physiol* 1987, *131*, 184-189.
[59] Ruoslahti, E., Yamaguchi, Y., Hildebrand, A., Border, W. A., Extracellular matrix/growth factor interactions. *Cold Spring Harb Symp Quant Biol* 1992, *57*, 309-315.
[60] Nakamura, T., Sugino, K., Titani, K., Sugino, H., Follistatin, an activin-binding protein, associates with heparan sulfate chains of proteoglycans on follicular granulosa cells. *J Biol Chem* 1991, *266*, 19432-19437.
[61] Murphy-Ullrich, J. E., Schultz-Cherry, S., Hook, M., Transforming growth factor-beta complexes with thrombospondin. *Mol Biol Cell* 1992, *3*, 181-188.
[62] Rahman, S., Patel, Y., Murray, J., Patel, K. V., Sumathipala, R., Sobel, M.*, et al.*, Novel hepatocyte growth factor (HGF) binding domains on fibronectin and vitronectin coordinate a distinct and amplified Met-integrin induced signalling pathway in endothelial cells. *BMC Cell Biol* 2005, *6*, 8.
[63] Wijelath, E. S., Rahman, S., Namekata, M., Murray, J., Nishimura, T., Mostafavi-Pour, Z.*, et al.*, Heparin-II domain of fibronectin is a vascular endothelial growth factor-binding domain - Enhancement of

VEGF biological activity by a singular growth factor/matrix protein synergism. *Circulation Research* 2006, *99*, 853-860.
[64] Golombick, T., Dajee, D., Bezwoda, W. R., Extracellular matrix interactions. 2: Extracellular matrix structure is important for growth factor localization and function. *In Vitro Cell Dev Biol Anim* 1995, *31*, 396-403.
[65] Taipale, J., Keski-Oja, J., Growth factors in the extracellular matrix. *FASEB J* 1997, *11*, 51-59.
[66] Dinbergs, I. D., Brown, L., Edelman, E. R., Cellular response to transforming growth factor-beta1 and basic fibroblast growth factor depends on release kinetics and extracellular matrix interactions. *J Biol Chem* 1996, *271*, 29822-29829.
[67] Butzow, R., Fukushima, D., Twardzik, D. R., Ruoslahti, E., A 60-kD protein mediates the binding of transforming growth factor-beta to cell surface and extracellular matrix proteoglycans. *J Cell Biol* 1993, *122*, 721-727.
[68] Evseenko, D., Schenke-Layland, K., Dravid, G., Zhu, Y. H., Hao, Q. L., Scholes, J.*, et al.*, Identification of the Critical Extracellular Matrix Proteins that Promote Human Embryonic Stem Cell Assembly. *Stem Cells and Development* 2009, *18*, 919-927.
[69] Li, Y., Powell, S., Brunette, E., Lebkowski, J., Mandalam, R., Expansion of human embryonic stem cells in defined serum-free medium devoid of animal-derived products. *Biotechnology and Bioengineering* 2005, *91*, 688-698.
[70] Furue, M. K., Na, J., Jackson, J. P., Okamoto, T., Jones, M., Baker, D.*, et al.*, Heparin promotes the growth of human embryonic stem cells in a defined serum-free medium (vol 105, art no 13409, 2008). *Proceedings of the National Academy of Sciences of the United States of America* 2008, *105*, 18071-18071.
[71] Draper, J. S., Moore, H. D., Ruban, L. N., Gokhale, P. J., Andrews, P. W., Culture and characterization of human embryonic stem cells. *Stem Cells and Development* 2004, *13*, 325-336.
[72] Baxter, M. A., Camarasa, M. V., Bates, N., Small, F., Murray, P., Edgar, D.*, et al.*, Analysis of the distinct functions of growth factors and tissue culture substrates necessary for the long-term self-renewal of human embryonic stem cell lines. *Stem Cell Research* 2009, *3*, 28-38.
[73] Meng, Y., Eshghi, S., Li, Y. J., Schmidt, R., Schaffer, D. V., Healy, K. E., Characterization of integrin engagement during defined human embryonic stem cell culture. *FASEB J* 2010, *24*, 1056-1065.
[74] Vallier, L., Alexander, M., Pedersen, R. A., Activin/Nodal and FGF pathways cooperate to maintain pluripotency of human embryonic stem cells. *J Cell Sci* 2005, *118*, 4495-4509.
[75] Gonzalez, R., Jennings, L. L., Knuth, M., Orth, A. P., Klock, H. E., Ou, W.*, et al.*, Screening the mammalian extracellular proteome for regulators of embryonic human stem cell pluripotency. *Proc Natl Acad Sci U S A* 2010, *107*, 3552-3557.
[76] Seguin, C. A., Draper, J. S., Nagy, A., Rossant, J., Establishment of endoderm progenitors by SOX transcription factor expression in human embryonic stem cells. *Cell Stem Cell* 2008, *3*, 182-195.
[77] Peerani, R., Rao, B. M., Bauwens, C., Yin, T., Wood, G. A., Nagy, A.*, et al.*, Niche-mediated control of human embryonic stem cell self-renewal and differentiation. *EMBO J* 2007, *26*, 4744-4755.
[78] Shevchenko, A., Tomas, H., Havlis, J., Olsen, J. V., Mann, M., In-gel digestion for mass spectrometric characterization of proteins and proteomes. *Nat Protoc* 2006, *1*, 2856-2860.
[79] Ma, B., Zhang, K. Z., Hendrie, C., Liang, C. Z., Li, M., Doherty-Kirby, A.*, et al.*, PEAKS: powerful software for peptide de novo sequencing by tandem mass spectrometry. *Rapid Communications in Mass Spectrometry* 2003, *17*, 2337-2342.
[80] Zhang, J., Xin, L., Shan, B., Chen, W., Xie, M., Yuen, D.*, et al.*, PEAKS DB: De Novo sequencing assisted database search for sensitive and accurate peptide identification. *Mol Cell Proteomics*.
[81] Zhang, J., Xin, L., Shan, B., Chen, W., Xie, M., Yuen, D.*, et al.*, PEAKS DB: De Novo Sequencing Assisted Database Search for Sensitive and Accurate Peptide Identification. *Mol Cell Proteomics* 2012, *11*, M111 010587.

Chapter 4

Proteomic Analysis of the Human Embryonic Stem Cell Depositome

4.1 Introduction

The ECM is a complex network of structural proteins and glycosaminoglycans that function to support cells through the regulation of processes such as adhesion and growth factor signaling [1]. It is not surprising that the generation of a well-defined matrix supportive of these processes in the complex hESC microenvironment has been difficult. Although gelatin is sufficient for the maintenance of mESCs in the presence of specific growth factors, hESCs cannot be propagated in the same conditions. Currently, in the absence of a suitable alternative, Matrigel™ remains the matrix of choice for hESC culture *in vitro*. However, the complex nature of Matrigel™ has been demonstrated previously in this thesis (Chapter 3), and has been described by others who have revealed that it contains numerous growth factors and signaling proteins [2]. Although recent studies have revealed that a variety of defined matrices support the growth of hESCs, few of these can maintain a wide array of stem cell lines and as such are typically not used in place of Matrigel™ [3]. The universality of Matrigel™ indicates that current defined matrices are lacking in critical components required to generate a supportive hESC microenvironment.

This chapter contains excerpts from the following paper:

Hughes, C.S., Radan, L., Stanford, W., Postovit, L.M., Lajoie, G.A.. (2012) “Proteomics Analysis of the Human Embryonic Stem Cell Depositome”. (In Preparation)

Because of the challenge proteomic examination of the ECM presents, the majority of studies that have analyzed the hESC microenvironment have focused on support cells and paracrine signaling pathways. The desire to generate well-defined conditions for hESC culture *in vitro* has prompted these investigations into the factors critical for the maintenance of stem cells. Proteomic studies have focused on the analysis of media conditioned by hESC supportive feeder cell layers to elucidate pathways important for maintaining the balance between self-renewal and differentiation [4-9]. These analyses were important contributors to our current knowledge of how hESCs are regulated in the extracellular space by pathways in the soluble portion of the microenvironment. However, there is still a lack of information of how the ECM modulates hESC behavior *in vitro* through interactions with both the cells themselves and the soluble cytokines present in the extracellular milieu.

Given the common underlying plasticity of stem and cancer cells, recent studies have established the ability of embryonic microenvironments to alter the tumorigenic properties of cancer cells (reviewed in [10]). Building on these findings, it was later observed that metastatic melanoma cells could be 'reprogrammed' to a more benign melanocyte phenotype following exposure to a matrix microenvironment generated from hESCs [11]. Importantly, this effect was found to be dependent on the exposure of metastatic cells to the conditioned matrix, and was not observed after treatment with hESC conditioned medium. It was later found that the left-right determination (Lefty) proteins that were deposited in the matrix by hESCs were effectors of the cellular change observed in metastatic cells [12]. The Lefty proteins are antagonists of TGF-β signaling that act directly on Nodal protein. Differences in the methylation status and

microRNA profiles for genes and pathways directly related to Lefty/Nodal signaling in metastatic cells on conditioned matrix have recently been observed [13]. Subsequent work with conditioned matrix utilizing mESCs implicated the bone morphogenic protein (BMP) 4 antagonist Gremlin as a primary regulator of the observed changes in metastatic cells [14]. Collectively, these studies were all biased by a targeted analysis of potential effectors of metastatic cells. A comprehensive proteomic analysis of the matrix microenvironment could potentially reveal other factors involved in metastatic cell reprogramming. Furthermore, proteomic analysis of the conditioned matrix could reveal factors important in the regulation of hESC and human induced pluripotent stem cell (hiPSC) pluripotency by the microenvironment *in vitro*.

To this end, we have employed a mass spectrometry (MS)-based proteomics screen to identify proteins deposited by hESCs and hiPSCs grown on Matrigel™ *in vitro*. To investigate the hESC-derived matrix, we utilize a metabolic labeling technique known as stable isotope labeling with amino acids in cell culture (SILAC) [15]. SILAC facilitates the identification of hESC-derived proteins in the presence of significant background protein complexity from Matrigel™. Additionally, in order to minimize intracellular protein contamination in our analysis, we have developed methods that remove the requirement for cell lysis to generate CMTX. From proteomic analysis of H9, CA1, and BJ-1D pluripotent stem cell lines, we identify a total of 621, 1355, and 1350 unique proteins respectively. This work represents the first analysis of a stem cell conditioned matrix and resulted in the identification of at least one new microenvironmental contributor responsible for the regulation of hESCs and hiPSCs.

4.2 Results

4.2.1 Proteomic Analysis of Pluripotent Stem Cell Derived CMTX. To determine factors being deposited by hESCs during growth on Matrigel™, we employed a global MS-based proteomics approach to screen CMTX. Previous studies that have illustrated the effects of CMTX on metastatic cells have employed an NH_4OH cellular lysis protocol to remove hESCs from Matrigel™. Lysis of cells on the matrix could potentially confound our analysis by releasing high abundance intracellular proteins. To limit the potential for intracellular protein contamination in the CMTX resulting from lysis, we developed a protocol based on Matrigel™ de-polymerization to remove intact cells from the matrix. With this method, the vast majority of the hESCs that were removed remained intact and viable as indicated by 7-AAD staining in flow cytometry (Figure 4.1 B). Moreover, the removal of cell-lysis from the protocol permitted analysis of the undifferentiated state and differentiation capacity of the cells that deposited the matrix (Figure 4.1 A, C).

After cell removal and concentration of the CMTX solution, a combination of strong cation and anion exchange (SCX, SAX), and 1D-Gel methods was employed for fractionation of the complex ECM-like mixture with iterative exclusion MS analysis as discussed previously (Chapter 3). MS analysis of these samples illustrated the limited ability of our assay to determine hESC-derived proteins in our list of identifications (Figure 4.2 A – B). This limitation is directly the result of performing the CMTX experiments on Matrigel™. Since the mixture that gets analyzed by MS represents a mixture of hESC-derived and Matrigel™ proteins, identification specificity is reliant on non-homology between human and mouse proteins. However, by searching the

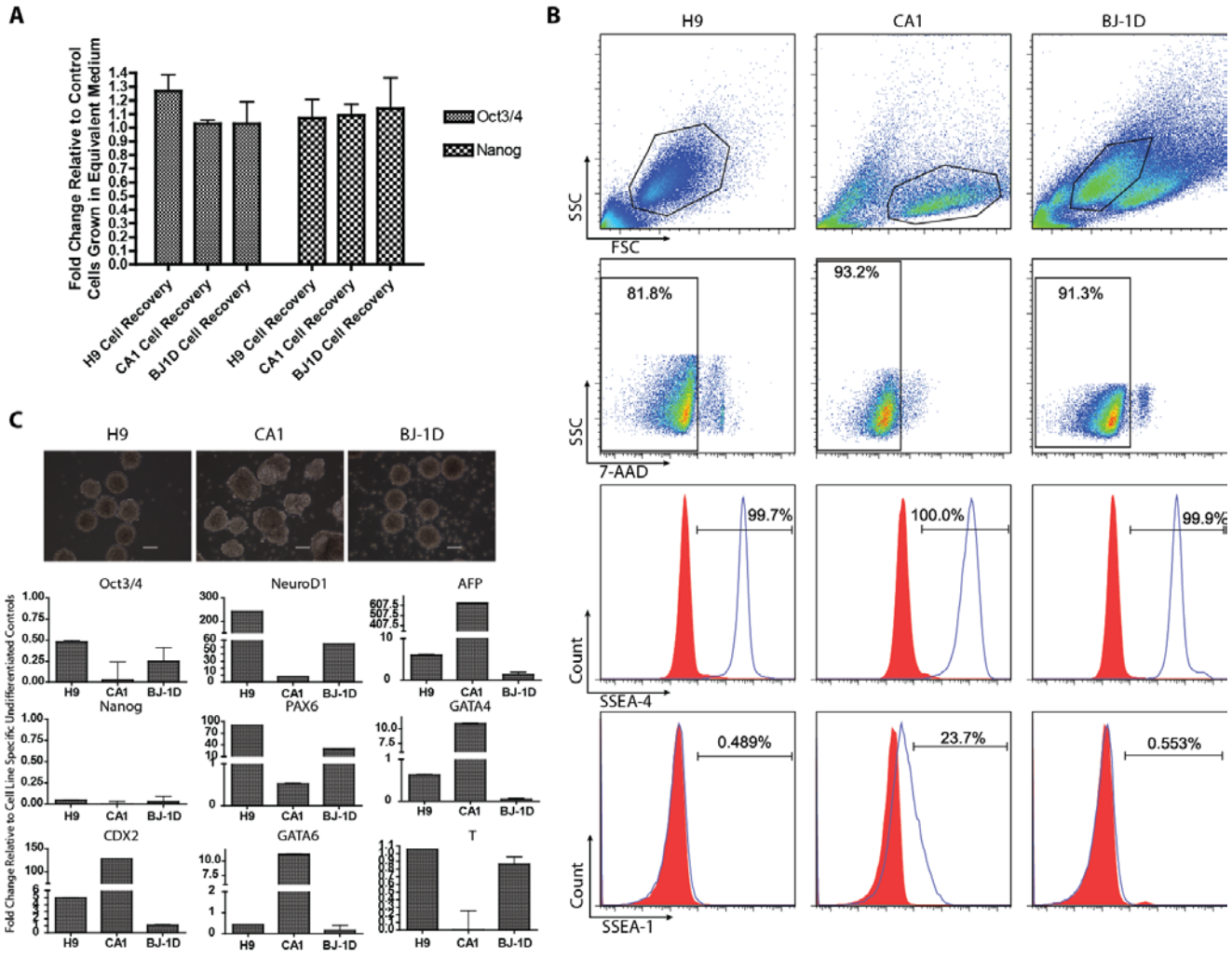

Figure 4.1. Cell viability and pluripotency during generation and harvest of CMTX. H9 and CA1 hESCs as well as BJ-1D iPSCs were used to generate CMTX. Following harvesting using our cell recovery method that eliminates cell lysis, remaining cells were assayed for viability and markers of pluripotency. (A) RT-PCR analysis of harvested cells for the markers Oct3/4 and Nanog. Values are relative to undifferentiated cells grown in feeder-free conditions not exposed to the CMTX harvesting methods. Error bars represent SD, n=3. (B) Flow cytometry analysis of cells harvested from CMTX. Cells were assayed for SSEA4 and SSEA1. Viability was determining using 7-AAD staining. (C) Cells harvested from CMTX were used to generate embryoid bodies. Following 14 days in culture, embryoid bodies were harvested and assayed for markers of pluripotency (Oct3/4, Nanog), trophoblast (CDX2), ectoderm (NeuroD1, PAX6), endoderm (GATA6, GATA4, alpha-fetoprotein), and mesoderm (T). Error bars represent SD, n=2. Values are fold change relative to undifferentiated cells. Phase contrast images of embryoid bodies are provided above. Scale bars represent 250um. In both (A) and (C), RPLPO is used as a positive control.

data set against a concatenated human and mouse sequence database, we observe that few proteins are identified as belonging to a single species (Figure 4.2 A - B). Many of the identified proteins have also been found in Matrigel™ in our previous proteomic analysis (Figure 4.2 A - B). Taken together, these complications severely limit the specificity and sensitivity of the proteomic analysis. To overcome these challenges, we employed a metabolic labeling approach known as SILAC that we have previously optimized for application in hESCs and hiPSCs (Chapter 2). Using this approach, hESCs and hiPSCs would be fully labeled with 'heavy' arginine and lysine prior to being plated for CMTX generation (Figure 4.3). In this approach, proteins that were deposited during CMTX generation will carry a heavy label and can be distinguished on the MS from Matrigel™ contaminants.

With this protocol, we analyzed CMTX from H9 and CA1 hESCs, as well as BJ-1D hiPSCs. MS analysis yielded a total of 621, 1355, and 1350 labeled proteins identified for H9, CA1, and BJ-1D cell lines respectively (Figure 4.4 A, Appendix Tables 1.9 - 1.11). Comparison of protein identifiers between the cell lines indicates a ~30% overlap between the three datasets (Figure 4.4 A). The gain in the number of proteins in the CA1 and BJ-1D stem cell lines is due to their decreased stability in the StemPro SILAC medium. We observed an increase in cell death and subsequent lysis during general growth of the CA1 and BJ-1D cell lines compared with H9 in StemPro SILAC medium resulting in the identification of additional intracellular proteins. Gene ontology analysis revealed that in the dataset corresponding to each cell line there are proteins representative of several cellular components present. This suggests that a variable

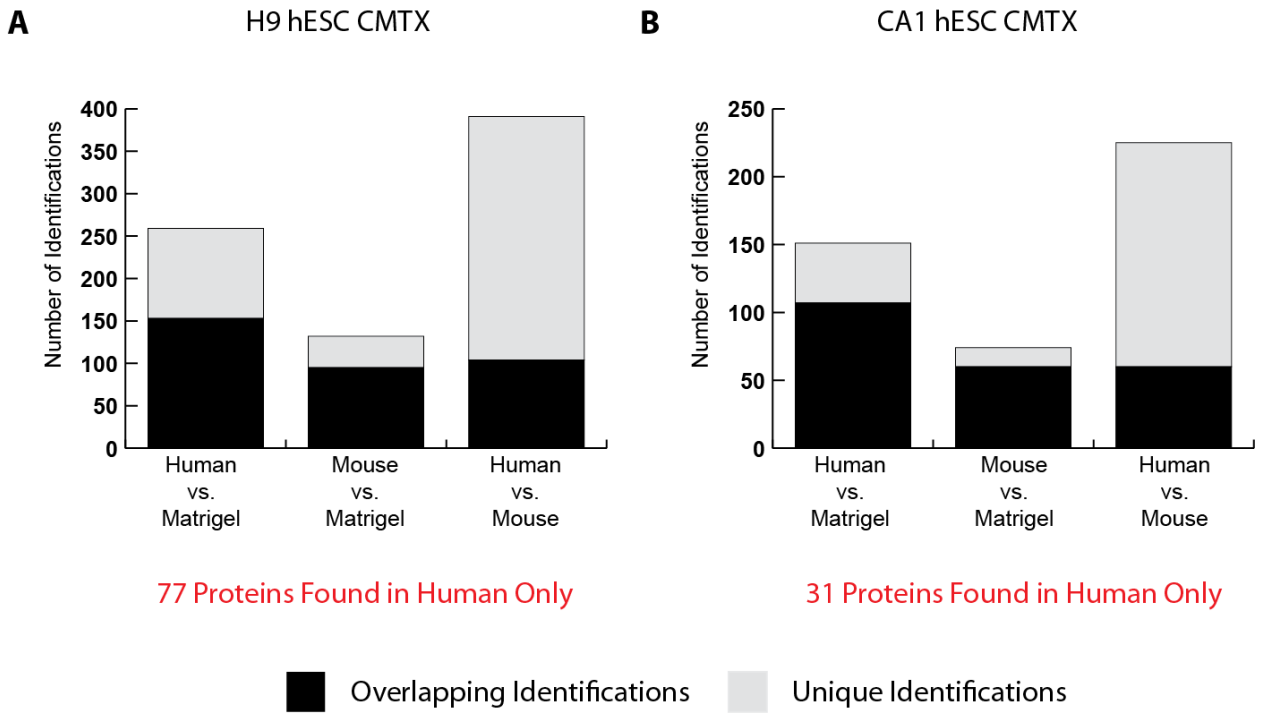

Figure 4.2. Proteomic analysis of unlabeled hESC derived CMTX. H9 (A) and CA1 (B) hESC CMTX generated using unlabeled cells was analyzed using an MS-based proteomics approach. Data were searched simultaneously against a concatenated database containing all Mouse and Human protein sequences available in UniProt. Human vs. Matrigel represents the overlap between proteins identified as Human derived in CMTX by PEAKS 5.3 compared with those found in Matrigel (Chapter 3). Mouse vs. Matrigel represents the overlap between proteins identified as Mouse derived in CMTX by PEAKS 5.3 compared with those found in Matrigel. Human vs. Mouse represents the overlap within the CMTX dataset between proteins specified as Human or Mouse derived by PEAKS 5.3. To facilitate inter-species comparisons, protein descriptions were used in all cases. Comparisons were done manually. Overlapping identifications are denoted by a solid black box, and those that are unique by a grey box. For both H9 and CA1 derived CMTX, n=1.

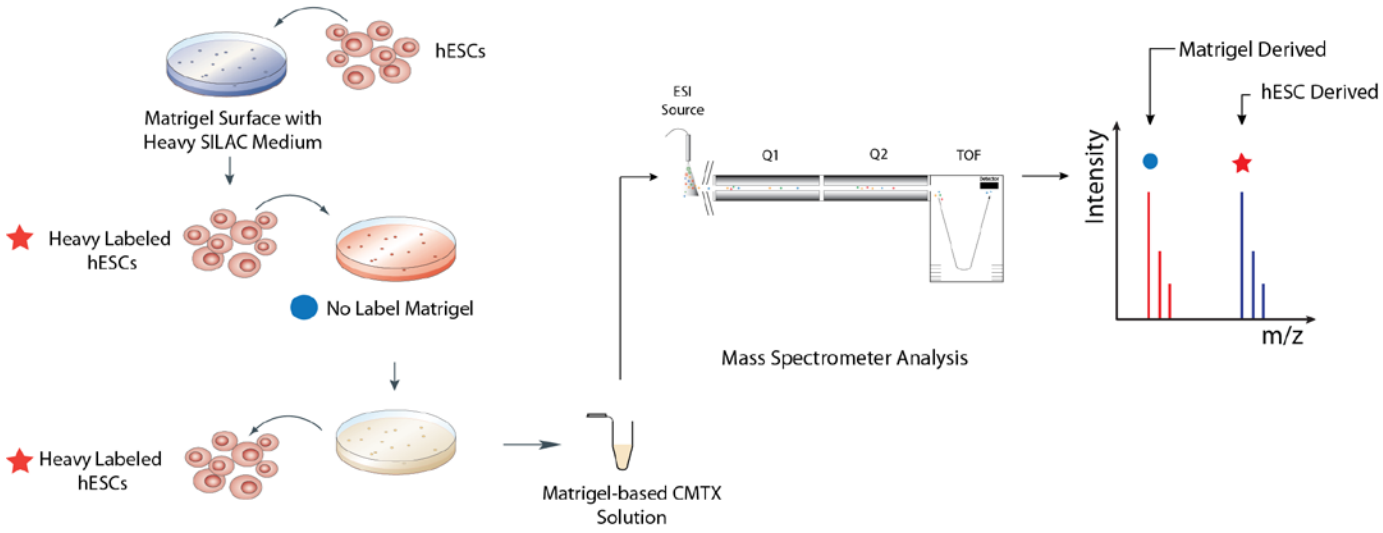

Figure 4.3. Proteomic analysis of CMTX from hESCs cultured in SILAC medium. H9 and CA1 hESCs, and BJ-1D iPSCs are grown in defined SILAC medium containing [$^{13}C_6$, $^{15}N_4$] - arginine and [$^{13}C_6$, $^{15}N_2$] - lysine optimized previously (Chapter 2). After culture for a sufficient amount of time to obtain complete labeling, cells are passaged to culture dishes pre-coated with Matrigel. After 4-5 days of culture on Matrigel in medium containing the heavy isotopic labels, cells are removed using a protocol that does not induce lysis of the cells (see Methods). The remaining conditioned matrix layer is rinsed and harvested. The conditioned matrix solution is then enzymatically digested and fractionated using protocols optimized previously (Chapter 3). Mass spectrometry analysis of the conditioned matrix generated using labeled hESCs permits identification of human proteins. Peptides derived from hESCs will carry an isotopic label and will display a resultant mass shift in the MS, whereas those previously present in Matrigel will not have this difference.

amount of cell lysis is occurring during growth or harvest of the CMTX for all the cell lines.

To limit the contaminants from cell lysis, the dataset was filtered using the “extracellular” and “cell surface” cellular component gene ontology terms. Filtering reduced the number of proteins identified in each dataset to 71, 100, and 95 labeled proteins for H9, CA1, and BJ-1D respectively (Figure 4.4 A, Appendix Tables 1.12 – 1.14). However, the data still contained numerous intracellular proteins (histones, mitochondrial, and cytoskeleton associated). This is primarily the result of the limited specificity of the gene ontology assignments. The overlap between the three individual CMTX datasets is ~35% based on protein identifiers after gene ontology filtering. However, coverage between biological replicates of the same cell line using the identical fractionation methods overlap a minimum of 71% across the samples in the experiment. The reproducibility between biological replicates from single stem cell lines illustrates the consistency of not only the proteomics method, but of the CMTX assay itself.

The hESC and hiPSC CMTX proteomics data indicate that numerous cell line specific factors were deposited based on comparisons between the protein lists. When comparing core ECM proteins, isoforms of fibronectin and laminins, and heparan sulfate proteoglycan linked proteins were present at similar abundance levels based on the number of unique peptides in CMTX from H9 and BJ-1D cell lines. However, BJ-1D CMTX was enriched in matrix remodeling factors, such as matrix metalloproteinase-14 and -15. On the other hand, CMTX derived from CA1 hESCs was found to contain multiple collagen and laminin isoforms not identified in the matrices from the other stem

cell lines. Low abundance factors such as soluble frizzled related protein (sFRP) 1 and 2, and Lefty A and B were identified in CMTX from all cell lines. Interestingly, connective tissue growth factor (CTGF) was identified in CMTX from both hESC lines, but not in that from BJ-1D hiPSCs. In addition, other low abundance factors such as Cerberus and fibroblast growth factor-15 were only identified in CA1 CMTX.

4.2.2 Secretome Analysis of the hESC Microenvironment. To further validate and enrich for candidates in the CMTX data, a comparison was performed with a previously published proteomics screen of the H9 hESC secretome obtained from the analysis of hESC conditioned medium [6]. We performed a re-analysis of the H9 hESC secretome raw dataset in the same software (PEAKS 5.3) used to process the CMTX data, to facilitate comparison and minimize variability from protein assignments or identifiers. Comparison with the H9 hESC secretome protein identifiers revealed a 73%, 55%, and 54% overlap between the unfiltered and 77%, 72%, and 68% for the filtered H9, CA1, and BJ-1D CMTX datasets (Figure 4.4 B). These data indicate that although there was a significant variability in the cellular localization of proteins in the unfiltered dataset, this distribution is not unexpected since proteins in the secretome and CMTX datasets share similar profiles. Comparison with the Matrigel™ dataset previously acquired (Chapter 3) revealed that 53%, 40%, and 40% of proteins for H9, CA1, and BJ-1D cell lines are identified in both matrices prior to filtering (Figure 4.4 C). Gene ontology filtered datasets share 62%, 55%, and 50% of proteins with Matrigel™ for H9, CA1, and BJ-1D cell lines. These data illustrate the necessity for SILAC when performing this analysis because many of the proteins found in the CMTX are also found in Matrigel™.

Furthermore, it highlights the ability of this methodology to enhance the sensitivity of our analysis by increasing the confidence in the identification of hESC-derived proteins.

4.2.3 Factors Identified in Stem Cell Derived CMTX. As mentioned previously, investigation of the CMTX dataset revealed the presence of numerous hESC and hiPSC regulatory proteins. In order to enrich for hESC and hiPSC derived proteins that are facilitating the maintenance of an undifferentiated state on CMTX, we opted to focus on only those classified as extracellular or cell surface by gene ontology. Not surprisingly, within this filtered dataset we find many core ECM proteins that are also present in Matrigel™ (Figure 4.5 A). The presence of hESC and hiPSC-derived labeled versions of these proteins indicates that the stem cells are generating a self-supporting matrix microenvironment *in vitro*. Further investigation of the filtered CMTX dataset revealed the presence of numerous factors with potential roles in hESC and hiPSC pluripotency (Figure 4.5 B). Other identified factors, such as hepatoma derived (HDGF) and connective tissue growth factor (CTGF) are of particular interest due to their relevance in cancer cell systems, as well as the known interactions of CTGF with the ECM [16-18]. Interestingly, after pathway analysis of the filtered datasets we observe a significant enrichment for molecules involved in cell motility as well as apoptosis or invasion of cancer cells (Figure 4.5 C).

Also of interest in the list of hESC proteins identified are the potential extracellular regulators of hESCs (Figure 4.5 B). The soluble frizzled related proteins (sFRP) 1 and 2 are inhibitors of canonical Wnt signaling [19]. Wnt signaling has been observed to

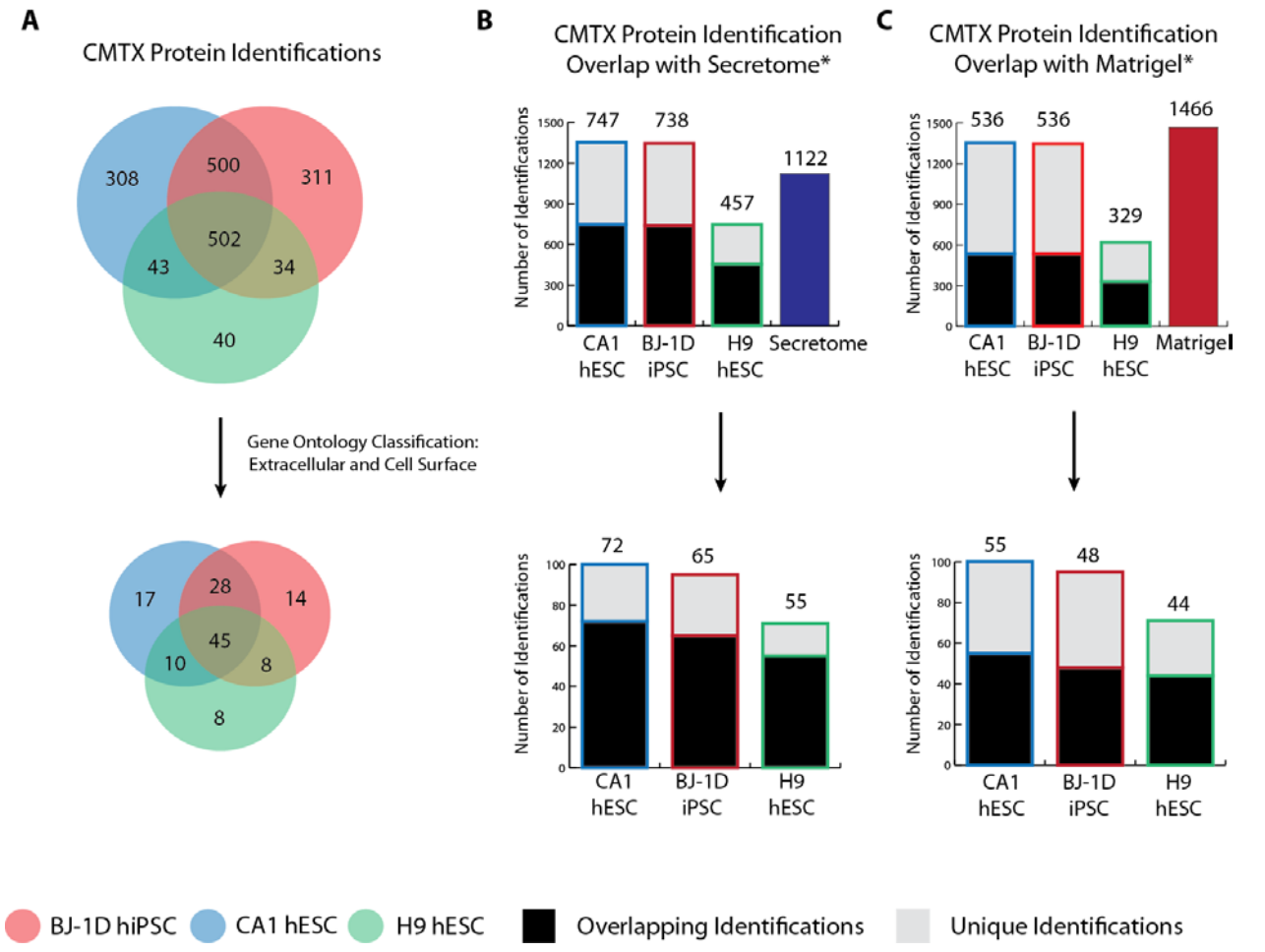

Figure 4.4. Proteomic analysis of SILAC hESC and hiPSC derived CMTX. (A) CMTX from H9 and CA1 hESCs, as well as BJ-1D hiPSCs was analyzed in biological triplicate using an MS-based proteomics protocol. Data files were analyzed using PEAKS 5.3 software. Numbers within the Venn diagrams represent the total number of protein identifications found in each matrix for the specific overlap. Data sets were also filtered using gene ontology classification for cellular component based on the terms "extracellular" and "cell surface". These values are represented in the lower diagram. (B) CMTX identifications were further compared with a secretome data set acquired through proteomic analysis of hESC conditioned medium. (C) Each data set was individually compared with that previously acquired for Matrigel (Chapter 3). Overlapping identifications are denoted by a black box, and unique identifications are found in grey. The total number of overlapping identifications can be found at the top of the bar in text. All comparisons were done manually based upon protein identifiers. In the case of Matrigel data, protein descriptions were used for comparison as identifiers are species specific. Gene ontology filtered data were compared against entire Matrigel or Secretome data sets. The rightmost bar in the top graphs of (B) and (C) represent total identifications found in Matrigel respectivelyand the Secretome. * - datasets can be found in reference 6 and Chapter 3.

A

Protein Name	# Unique Peptides		
	H9	CA1	BJ-1D
Fibronectin	7	7	8
Laminin (gamma-1)	9	3	3
Laminin (alpha-1)	9	3	3
Collagen-1 (alpha)	5	3	4
Titin	3	6	4
Perlecan	5	N/A	5
Fibulin - 1	18	5	12
Vinculin	46	51	88
Filamin-A	32	72	83

B

Protein Name	# Unique Peptides		
	H9	CA1	BJ-1D
Connective tissue growth factor	3	4	N/A
Hepatoma derived growth factor	3	3	4
Left-right determination protein - 1	3	N/A*	2
Left-right determination protein - 2	2	2	3
Soluble frizzled related protein - 1	5	N/A*	6
Soluble frizzled related protein - 2	2	2	N/A*
Cerberus	N/A	2	N/A*
Growth/differentiation factor - 15	N/A	4	N/A*

C

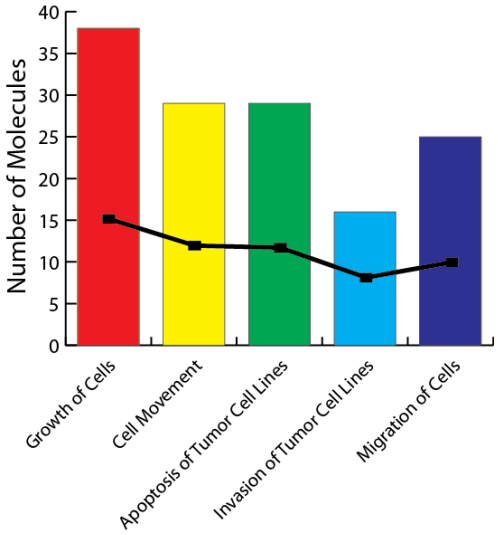

Figure 4.5. Proteins and pathways identified in CMTX from hESCs and hiPSCs. CMTX was analyzed using an IE-MS proteomics based approach. Proteins were identified using PEAKS 5.3 software. (A) Represents a subset of the core ECM proteins found in CMTX that were also identified in the previous proteomics analysis of Matrigel (Chapter 3). In the case of collagen, the top isoform was chosen. (B) Represents growth factors and proteins known to regulate core hESC pluripotency pathways found in CMTX. * - indicates when a protein was identified as a single peptide hit. Only proteins with 2 unique peptides are retained, such that these single peptide hits are lost in the final dataset. (C) Pathway analysis performed using Ingenuity Systems Software. The top biological functions identified in all three cell lines were related to cellular movement, growth, and death or invasion of tumor cell lines. Number of molecules denotes the number of candidate proteins identified as being involved with that function found in our dataset. Black boxes represent the -log(p-value) for the probability of identifying these pathways as being enriched in our dataset by chance.

contribute to the regulation of both mESCs and hESCs [20]. Extracellular antagonists of Activin/Nodal signaling, left-right determination factors (Lefty) A and B, are also found in the CMTX [21]. Since the Lefty proteins were previously implicated as being involved in the reprogramming of metastatic cells with CMTX, their identification provides additional validation of our proteomics approach [12]. We also identify Cerberus in the CMTX, a regulator of both TGF-β and bone morphogenic protein (BMP) signaling. Previous studies directed at the analysis of hESC-derived CMTX have focused on antagonism of the BMP pathway using Gremlin, a protein which shares significant overlap in functionality with Cerberus [14, 21]. The presence of these factors is not surprising since several have previously been identified in screens of MEF and hESC conditioned medium [6]. However, their identification in the CMTX indicates that the ECM is potentially playing a role in their activity.

4.3 Discussion

A thorough knowledge of the processes that control the maintenance of pluripotency or differentiation to lineage specific cell types will be critical as hESC research moves toward the clinic. Central to this goal is comprehensive characterization of the extracellular processes governing regulation of hESCs and hiPSCs in their niche. Proteomic analysis of conditioned medium has aided in the development of an understanding of signaling pathways present in the microenvironment. However, few studies have examined the direct interactions of hESCs with the matrix portion of the microenvironment. Utilizing cell culture and proteomics methods developed earlier, we report the characterization of matrices conditioned by hESCs as well as hiPSCs.

The presence of core ECM components in CMTX, such as isoforms of fibronectin, collagen, and laminin illustrates that hESCs and hiPSCs generate a self-supportive niche for attachment and proliferation. All three of these matrix proteins have been shown to promote the growth of hESCs when used as the sole growth support [3, 22-25]. These core proteins regulate critical cellular processes such as cell attachment through integrin binding. Integrin interactions are capable of mediating signal transduction responses similar to those triggered by soluble ligands [26, 27]. Therefore, hESCs potentially utilize these interactions to regulate a diverse array of cellular functions. The presence of these core ECM proteins in the matrix likely promotes these interactions, and explains why matrices that contain them in combination are better at facilitating hESC and hiPSC growth, such as is the case with Matrigel™ [3, 28].

The identification of multiple growth factors and their binding partners in CMTX highlights another potential function for these core fibrous ECM proteins in the matrix. The ECM has been proposed to contribute to the regulation of growth factor signaling in the microenvironment (reviewed in [1]). Central to this function is the presence of specialized domains designed to bind growth factors like VEGF, EGF, HGF, and PDGF on proteins such as fibronectin and laminin. Furthermore, fibronectin has been observed to contribute to TGF-β signaling through interaction with latent-TGF-β binding proteins [29, 30]. Binding between growth factors and these glycoproteins can also be mediated by interactions with heparan sulfate, a molecule that has been shown to regulate the self-renewal of hESCs [1, 31]. In addition to core ECM proteins, the CMTX also contains an array of binding proteins involved in pathways such as IGF, BMP, and EGF signaling. These binding partners can complement interactions with glycoproteins such as fibronectin. The result of these interactions potentially implicates the ECM in the direction of cellular processes through binding and sequestering of growth factors.

The importance of controlling the activity and concentration of growth factors present in the microenvironment is critical for maintenance of the hESC and hiPSC state. Three key pathways from which we identified regulatory proteins in the CMTX are Wnt, TGF-β through Activin/Nodal, and BMP signaling. The sFRP1 and sFRP2 proteins are thought to regulate canonical Wnt signaling through direct binding to the Wnt proteins, although their role in hESCs remains unclear (reviewed in [32]). Wnt signaling through the canonical pathway has been shown to be important in the maintenance of mESC and hESC self-renewal and pluripotency [20]. Lefty A and B are known to regulate TGF-β signaling through antagonism of the activating protein Nodal [33]. TGF-β activation

through Activin/Nodal signaling is one of the core pathways critical for the maintenance of self-renewal and pluripotency of hESCs [21]. The Lefty proteins were also identified in the original CMTX work involving metastatic cells as a potential regulator of the observed phenotype, acting through hESC-derived matrix deposition [12]. Inhibition of BMP mediated activation of TGFβ signaling also promotes the maintenance of hESC pluripotency. BMP activates SMAD1/5/8 mediated TGF-β pathways that have been implicated in the differentiation of hESCs [21]. Cerberus is an inhibitor of BMP mediated activation that acts through antagonism of BMP-4 [34, 35]. Interestingly, Cerberus has also been shown to inhibit Nodal as well as Wnt signaling pathways [35, 36].

The identification of sFRP1 and sFRP2 as well as the Lefty A and Lefty B proteins further validates the ability of our CMTX proteomic analysis to identify potential regulators of hESC fate. Aside from their activity in the regulation of core hESC pluripotency pathways, both sFRP and Lefty proteins are known to be matrix deposited [37, 38]. Taken together, the findings of this study highlight the ability of MS-based proteomics screening of CMTX to determine *in vitro* effectors of hESC control involving the ECM microenvironment.

4.4 Methods

4.4.1 Cell culture and harvest – H9 (passage 26) and CA1 (passage 20) hESCs, and BJ-1D (passage 65) iPSCs were maintained on CF-1 irradiated mouse embryonic fibroblast (MEF) feeder layers (GlobalStem, Rockville, MD) using media composed of knockout DMEM/F12, 20% knockout serum replacement, 1% non-essential amino acids, 2mM glutamine (CellGro, Manassas, VA), 0.1 mM 2-mercaptoethanol (Fisher, Toronto, ON), and 4 ng/mL of basic fibroblast growth factor. All media reagents were obtained from Invitrogen unless noted otherwise. H9 cells were obtained from WiCell (WISC, Wisconsin). The CA1 hESC line used in all experiments was obtained from Dr. Cheryle Séguin of The University of Western Ontario [39, 40]. The hiPSC line BJ-1D was derived by reprogramming using retroviral transduction of BJ fibroblasts with the Yamanaka factors essentially as we have previously described [41] and validated as pluripotent using in vitro and in vivo differentiation assays and expression profiling (unpublished results). Cells were passaged mechanically in all experiments and for general maintenance.

For SILAC experiments, hESC and hiPSC cell lines were grown in feeder-free conditions on Matrigel™ (BD Biosciences, Franklin Lake, NJ). Custom DMEM/F12-glutamax that contained no L-arginine or L-lysine was ordered from Invitrogen. SILAC medium was prepared using the StemPro hESC Media system with our custom DMEM/F12 (Invitrogen) according to manufacturer instructions. [$^{13}C_6$, $^{15}N_4$] – L-arginine and [$^{13}C_6$, $^{15}N_2$] – L-lysine (Cambridge Isotope Laboratories, Andover, MA) were

supplemented into the SILAC medium at 90mg/L and 92mg/L respectively. Unlabeled L-proline was added to the SILAC medium at a final concentration of 800 mg/L [42].

Embryoid bodies (EB) were generated using Aggrewell 400Ex plates (StemCell Technologies, Vancouver, Canada). Briefly, 2 x 10^6 hESCs were harvested enzymatically using Accutase (Invitrogen) from Matrigel™ coated plates. Cells were reconstituted in Aggrewell medium supplemented with Rock inhibitor (Y-27632, Sigma-Aldrich, St. Louis, MO) at a final concentration of 10 μM. After plating in Aggrewell dishes, EBs were grown for 48 hours at 37°C prior to transfer to ultra-low adherence tissue culture dishes (Corning, Lowell, MA). After 15 days of culture, EB RNA was harvested using Trizol extraction according to the manufacturer's instructions (Invitrogen). EBs were assayed for expression of CDX2, alpha-feto protein (AFP), GATA-6, GATA-4, Oct3/4, PAX-6, T-brachyury, Nanog, and Neurogenic differentiation 1 (NeuroD1) using TaqMan primer probe sets (Invitrogen). Details of this assay can be found in Appendix Table 1.15. All EB assays were performed in biological and technical duplicate for each cell line and each condition.

4.4.2 Generation and Harvest of Conditioned Matrix – H9, CA1, or BJ-1D stem cells were grown in feeder-free conditions on Matrigel™ in heavy-isotope containing SILAC medium for 7 days prior to passaging to plates for CMTX preparation. SILAC labeled stem cells were permitted to grow for a period of 5 days on Matrigel™ in SILAC medium for generation of CMTX. Wells were then rinsed thoroughly with PBS to ensure removal of medium components and cells removed from the Matrigel™ layer using Cell Recovery Solution according to the manufacturer's instructions (BD Biosciences). The

remaining CMTX layer was incubated in a solution containing 8 M urea, 100 mM ammonium bicarbonate (ABC), and 1 M NaCl for 24 hours at 4°C. After the removal of stem cells by spinning, the cell recovery solution was combined with the urea solution and concentrated using high-capacity C18 cartridges (Phenomenex, Torrance, CA). Eluted components were dried using a SpeedVac and reconstituted in 8 M urea with 100 mM ABC for analysis by 1D-SDS-PAGE, strong cation exchange (SCX), or strong anion exchange (SAX) fractionation. CMTX was analyzed in technical duplicate and biological triplicate for each cell line.

4.4.3 In-solution trypsin digestion – Matrix samples were reduced with 10 mM dithiothreitol (DTT) for 60 minutes. Samples were then alkylated with 40 mM iodoacetamide (IAA) for 60 minutes. The reactions were quenched through the addition of DTT and left to incubate for another 60 minutes. Samples were then diluted 1/6 in 50 mM ABC. Trypsin (Promega, Madison, WI) at a concentration of 1 ug enzyme to 25 µg of total protein was added to the mixtures and left to incubate for 24 hours at 37°C. The next day, digests were acidified using neat trifluoroacetic acid and desalted on C18 cartridges (Phenomenex, Torrance, CA). After elution with 50% acetonitrile, samples were evaporated using a SpeedVac. Dried samples were reconstituted in 0.5% formic acid at a pH of ~2 prior to loading on an SCX column. Samples for SAX analysis were reconstituted in 0.5% NaOH at a pH of ~12.

4.4.4 Column preparation – Columns were packed in 360 O.D. x 200 I.D. capillaries (PolyMicro Technologies, Phoenix, AZ) using a conventional pressure bomb (Next Advance, Averill Park, NY). Frits were prepared by mixing 75 µL of potassium silicate

with 25 µL of formamide, vortexing for 1 minute and rapidly inserting and removing the capillary end from the resulting mixture. Capillary frits were dried in a 100°C oven for 2 hours. Capillaries were then rinsed with forward and reverse flow of methanol using the pressure bomb at 200 psi. Prior to packing, capillaries were rinsed for 30 minutes with 0.5% formic acid or 0.5% NaOH for SCX and SAX respectively. PolySULFOETHYL A SCX beads (5 µM, 300Å, CAT# PLBMSE0503) were purchased from PolyLC (Columbia, MD) and reconstituted in 50% MeOH. SAX beads were purchased from Varian Inc. (10um, 1000Å, CAT# PL1451-2102, Palo Alto, CA) and used in the vendor supplied buffer. SCX and SAX columns were packed to a length of 3 cm for all experiments. All packing was done at a pressure of 200 psi until the desired column length was obtained, then pressurized to 1000 psi to complete packing. Packed columns were rinsed with solvents for conditioning as recommended by the manufacturer.

4.4.5 Peptide Fractionation – Peptides were fractionated off of SCX and SAX columns using a CapLC system (Waters, Milford, MA) with a flow rate of 2 µL/min. Mobile phase A was composed of 20 mM citric acid at a pH of ~2.3, mobile phase B was pH 11.4 20 mM NH_4OH. Mobile phases were all prepared fresh prior to fractionation to ensure the stability of pH from run to run. Fractionation with pH was carried out using a 120 minute gradient from pH 2 to 12 for SCX, and 12 to 2 for SAX. Each fraction was collected offline at a volume of 20 µL. Fractions were dried using a SpeedVac, and reconstituted in 10% formic acid prior to injection on the MS.

4.4.6 In-gel trypsin digestion – 60 µg of conditioned matrix was diluted in Laemmli buffer. Matrix samples were loaded in each of two lanes on a 10% SDS-Gel. After staining of the gel with Coomassie blue, gel lanes were divided into fractions based on visual assessment of protein concentration. Gel cubes in each fraction were destained using 20% acetonitrile (ACN) in 1 M ABC. Proteins were reduced using 10 mM DTT for 60 minutes, followed by alkylation with 100mM IAA for 60 minutes. Digestions were carried out using trypsin at a 1/25 ratio overnight in a 37°C water bath. Fractions were extracted the next day using 10% formic acid and ACN with sonication. Each fraction was dried using a SpeedVac and reconstituted in 10% formic acid prior to injection on the MS.

4.4.7 MS analysis – Fractions were injected and separated using a nanoAcquity system (Waters, Milford, MA) equipped with a 25 cm x 75 µm I.D. C18 column. Fractions were separated using a 1 to 40% ACN gradient over 150 minutes at a flow rate of 300 nL/min. MS analysis was done on a Q-ToF Ultima (Micromass/Waters) using data-dependent acquisition with selection of the four top precursor masses per survey scan. Survey scans were set at 1 s, and MS/MS acquisition set at 1 s or 8000 cps TIC cut-off. Exclusion lists were generated using in-house software that automatically adds 0.7 amu to the precursor masses selected in previous runs and outputs a file also containing retention time information. Each fraction was analyzed for a four exclusion rounds (5 injections total), adjusting the injection volume dependent on signal intensity in the MS survey scan.

4.4.8 Proteomic Data analysis – Data analysis for all samples was performed in PEAKS 5.3 software (Bioinformatics Solutions Inc., Waterloo, Canada) [43, 44]. After import into PEAKS, MS/MS spectra from raw data files were refined using the following settings: merge spectra – true (100 ppm mass tolerance, 60 second retention time tolerance), correct precursor mass – true, determine precursor charge state – true (minimum charge +2, maximum charge +5), spectral quality filter – true (0.65 threshold), centroid, deisotope, and deconvolute – true. Resulting MS/MS spectra were then *de novo* sequenced using the following parameters: parent monoisotopic mass tolerance – 100ppm, fragment monoisotopic mass tolerance – 0.15 daltons, enzyme specificity – semi-Trypsin, fixed modifications – carbamidomethylation and +10 daltons on Arginine and +8 daltons on Lysine for SILAC, variable modifications – N-terminal acetylation and oxidized methionine. After *de novo* analysis, data were searched against the UniProt sequence database (Human taxonomy specified, 20236 total entries) using the following parameters: parent monoisotopic mass tolerance – 100 ppm, fragment monoisotopic mass tolerance – 0.15 daltons, enzyme specificity – semi-Trypsin, fixed modifications – carbamidomethylation and +10 daltons on Arginine and +8 daltons on Lysine for SILAC, variable modifications – N-terminal acetylation and oxidized methionine, estimate false-discovery rate – true.

Resultant protein identification data from the database search were further processed using PEAKS 5.3 software. Proteins were filtered by assigned score to give a <1.0% false-discovery rate for peptide-spectral matches based on estimation from a decoy-fusion method of database search. Identified proteins were also required to be derived by >2 unique peptides. Proteins that contained similar peptides and could not be

differentiated based on MS/MS analysis alone were grouped to satisfy the principles of parsimony. For all matrices analyzed, keratin hits were manually removed from the final datasets. Gene ontology analysis was performed using STRAP software (CPC Tools).

4.4.9 Real-time PCR – RNA was purified using Trizol reagent according to the manufacturer's instructions (Invitrogen) with the following modification: precipitated RNA pellets in isopropanol were centrifuged for 60 minutes at 12000 g at room temperature. After NanoDrop quantification, 1 µg of cDNA was synthesized using the High Capacity cDNA Reverse Transcription Kit with RNase inhibitor (Invitrogen). Real-time PCR was performed using the TaqMan® Universal PCR Master Mix (Invitrogen). Samples were incubated at 50°C for 2 minutes followed by 10 minutes at 95°C. DNA was then amplified at 95°C for 15 seconds followed by 1 minute at 58°C for 46 cycles. All samples were normalized to the large ribosomal protein RPLPO as a positive control. All primers were obtained from Invitrogen and details of the assay can be found in Appendix Table 1.15. Each biological replicate was run in triplicate for every marker assayed. All reagents were used according to the manufacturer's instructions.

4.4.10 Flow Cytometry – All reagents and probes for flow cytometry were obtained from eBiosciences (San Diego, CA) unless noted otherwise. Cells were enzymatically harvested using Accutase (Invitrogen) to obtain a single cell suspension. After centrifugation, cell pellets were resuspended in 5% FBS in PBS. Alexa-488 conjugated SSEA-4 and Alexa-647 conjugated SSEA1 were diluted into the cell mixture according to the manufacturer's instructions. Negative control samples contained respective isotype controls for the primary antibodies used. Solutions were incubated for 2 hours

and analyzed using an Accuri C6 (BD Biosciences) flow cytometer after rinsing to remove unbound antibody. Populations were gated according to forward and side scatter patterns with filtering for viable cells using 7-aminoactinomycin D staining. Data was analyzed using FlowJo software (Tree Star, Ashland, OR).

4.5 References

[1] Hynes, R. O., The extracellular matrix: not just pretty fibrils. *Science* 2009, *326*, 1216-1219.
[2] Vukicevic, S., Kleinman, H. K., Luyten, F. P., Roberts, A. B., Roche, N. S., Reddi, A. H., Identification of Multiple Active Growth-Factors in Basement-Membrane Matrigel Suggests Caution in Interpretation of Cellular-Activity Related to Extracellular-Matrix Components. *Experimental Cell Research* 1992, *202*, 1-8.
[3] Hakala, H., Rajala, K., Ojala, M., Panula, S., Areva, S., Kellomaki, M.*, et al.*, Comparison of biomaterials and extracellular matrices as a culture platform for multiple, independently derived human embryonic stem cell lines. *Tissue Eng Part A* 2009, *15*, 1775-1785.
[4] Prowse, A. B. J., McQuade, L. R., Bryant, K. J., Marcal, H., Gray, P. P., Identification of potential pluripotency determinants for human embryonic stem cells following proteomic analysis of human and mouse fibroblast conditioned media. *Journal of Proteome Research* 2007, *6*, 3796-3807.
[5] Prowse, A. B. J., McQuade, L. R., Bryant, K. J., Van Dyk, D. D., Tuch, B. E., Gray, P. P., A proteome analysis of conditioned media from human neonatal fibroblasts used in the maintenance of human embryonic stem cells. *Proteomics* 2005, *5*, 978-989.
[6] Bendall, S. C., Hughes, C., Campbell, J. L., Stewart, M. H., Pittock, P., Liu, S.*, et al.*, An enhanced mass spectrometry approach reveals human embryonic stem cell growth factors in culture. *Mol Cell Proteomics* 2009, *8*, 421-432.
[7] Bendall, S. C., Stewart, M. H., Menendez, P., George, D., Vijayaragavan, K., Werbowetski-Ogilvie, T.*, et al.*, IGF and FGF cooperatively establish the regulatory stem cell niche of pluripotent human cells in vitro. *Nature* 2007, *448*, 1015-1021.
[8] Buhr, N., Carapito, C., Schaeffer, C., Hovasse, A., Van Dorsselaer, A., Viville, S., Proteome analysis of the culture environment supporting undifferentiated mouse embryonic stem and germ cell growth. *Electrophoresis* 2007, *28*, 1615-1623.
[9] Lim, J. W. E., Bodnar, A., Proteome analysis of conditioned medium from mouse embryonic fibroblast feeder layers which support the growth of human embryonic stem cells. *Proteomics* 2002, *2*, 1187-1203.
[10] Hendrix, M. J., Seftor, E. A., Seftor, R. E., Kasemeier-Kulesa, J., Kulesa, P. M., Postovit, L. M., Reprogramming metastatic tumour cells with embryonic microenvironments. *Nat Rev Cancer* 2007, *7*, 246-255.
[11] Postovit, L. M., Seftor, E. A., Seftor, R. E., Hendrix, M. J., A three-dimensional model to study the epigenetic effects induced by the microenvironment of human embryonic stem cells. *Stem Cells* 2006, *24*, 501-505.
[12] Postovit, L. M., Margaryan, N. V., Seftor, E. A., Kirschmann, D. A., Lipavsky, A., Wheaton, W. W.*, et al.*, Human embryonic stem cell microenvironment suppresses the tumorigenic phenotype of aggressive cancer cells. *Proc Natl Acad Sci U S A* 2008, *105*, 4329-4334.
[13] Costa, F. F., Seftor, E. A., Bischof, J. M., Kirschmann, D. A., Strizzi, L., Arndt, K.*, et al.*, Epigenetically reprogramming metastatic tumor cells with an embryonic microenvironment. *Epigenomics* 2009, *1*, 387-398.
[14] Kim, M. O., Kim, S. H., Oi, N., Lee, M. H., Yu, D. H., Kim, D. J.*, et al.*, Embryonic stem-cell-preconditioned microenvironment induces loss of cancer cell properties in human melanoma cells. *Pigment Cell Melanoma Res* 2011, *24*, 922-931.
[15] Ong, S. E., Blagoev, B., Kratchmarova, I., Kristensen, D. B., Steen, H., Pandey, A.*, et al.*, Stable isotope labeling by amino acids in cell culture, SILAC, as a simple and accurate approach to expression proteomics. *Mol Cell Proteomics* 2002, *1*, 376-386.
[16] Chu, C. Y., Chang, C. C., Prakash, E., Kuo, M. L., Connective tissue growth factor (CTGF) and cancer progression. *J Biomed Sci* 2008, *15*, 675-685.
[17] Everett, A. D., Bushweller, J., Hepatoma derived growth factor is a nuclear targeted mitogen. *Current Drug Targets* 2003, *4*, 367-371.
[18] Chen, C. C., Lau, L. F., Functions and mechanisms of action of CCN matricellular proteins. *Int J Biochem Cell Biol* 2009, *41*, 771-783.
[19] Galli, L. M., Barnes, T., Cheng, T., Acosta, L., Anglade, A., Willert, K.*, et al.*, Differential inhibition of Wnt-3a by Sfrp-1, Sfrp-2, and Sfrp-3. *Dev Dyn* 2006, *235*, 681-690.

[20] Sato, N., Meijer, L., Skaltsounis, L., Greengard, P., Brivanlou, A. H., Maintenance of pluripotency in human and mouse embryonic stem cells through activation of Wnt signaling by a pharmacological GSK-3-specific inhibitor. *Nat Med* 2004, *10*, 55-63.
[21] Vallier, L., Alexander, M., Pedersen, R. A., Activin/Nodal and FGF pathways cooperate to maintain pluripotency of human embryonic stem cells. *J Cell Sci* 2005, *118*, 4495-4509.
[22] Hughes, C. S., Radan, L., Betts, D., Postovit, L. M., Lajoie, G. A., Proteomic analysis of extracellular matrices used in stem cell culture. *Proteomics* 2011, *11*, 3983-3991.
[23] Miyazaki, T., Futaki, S., Hasegawa, K., Kawasaki, M., Sanzen, N., Hayashi, M.*, et al.*, Recombinant human laminin isoforms can support the undifferentiated growth of human embryonic stem cells. *Biochem Biophys Res Commun* 2008, *375*, 27-32.
[24] Baxter, M. A., Camarasa, M. V., Bates, N., Small, F., Murray, P., Edgar, D.*, et al.*, Analysis of the distinct functions of growth factors and tissue culture substrates necessary for the long-term self-renewal of human embryonic stem cell lines. *Stem Cell Res* 2009.
[25] Furue, M. K., Na, J., Jackson, J. P., Okamoto, T., Jones, M., Baker, D.*, et al.*, Heparin promotes the growth of human embryonic stem cells in a defined serum-free medium. *Proc Natl Acad Sci U S A* 2008, *105*, 13409-13414.
[26] Berrier, A. L., Yamada, K. M., Cell-matrix adhesion. *J Cell Physiol* 2007, *213*, 565-573.
[27] Legate, K. R., Wickstrom, S. A., Fassler, R., Genetic and cell biological analysis of integrin outside-in signaling. *Genes Dev* 2009, *23*, 397-418.
[28] Ludwig, T. E., Levenstein, M. E., Jones, J. M., Berggren, W. T., Mitchen, E. R., Frane, J. L.*, et al.*, Derivation of human embryonic stem cells in defined conditions. *Nat Biotechnol* 2006, *24*, 185-187.
[29] Munger, J. S., Sheppard, D., Cross Talk among TGF-beta Signaling Pathways, Integrins, and the Extracellular Matrix. *Cold Spring Harbor Perspectives in Biology* 2011, *3*.
[30] Ramirez, F., Rifkin, D. B., Extracellular microfibrils: contextual platforms for TGFbeta and BMP signaling. *Curr Opin Cell Biol* 2009, *21*, 616-622.
[31] Sasaki, N., Okishio, K., Ui-Tei, K., Saigo, K., Kinoshita-Toyoda, A., Toyoda, H.*, et al.*, Heparan sulfate regulates self-renewal and pluripotency of embryonic stem cells. *J Biol Chem* 2008, *283*, 3594-3606.
[32] Esteve, P., Bovolenta, P., The advantages and disadvantages of sfrp1 and sfrp2 expression in pathological events. *Tohoku J Exp Med* 2010, *221*, 11-17.
[33] Schier, A. F., Nodal signaling in vertebrate development. *Annu Rev Cell Dev Biol* 2003, *19*, 589-621.
[34] Belo, J. A., Bachiller, D., Agius, E., Kemp, C., Borges, A. C., Marques, S.*, et al.*, Cerberus-like is a secreted BMP and nodal antagonist not essential for mouse development. *Genesis* 2000, *26*, 265-270.
[35] Piccolo, S., Agius, E., Leyns, L., Bhattacharyya, S., Grunz, H., Bouwmeester, T.*, et al.*, The head inducer Cerberus is a multifunctional antagonist of Nodal, BMP and Wnt signals. *Nature* 1999, *397*, 707-710.
[36] Kawano, Y., Kypta, R., Secreted antagonists of the Wnt signalling pathway. *J Cell Sci* 2003, *116*, 2627-2634.
[37] Lee, J. L., Lin, C. T., Chueh, L. L., Chang, C. J., Autocrine/paracrine secreted Frizzled-related protein 2 induces cellular resistance to apoptosis: a possible mechanism of mammary tumorigenesis. *J Biol Chem* 2004, *279*, 14602-14609.
[38] Marjoram, L., Wright, C., Rapid differential transport of Nodal and Lefty on sulfated proteoglycan-rich extracellular matrix regulates left-right asymmetry in Xenopus. *Development* 2011, *138*, 475-485.
[39] Seguin, C. A., Draper, J. S., Nagy, A., Rossant, J., Establishment of endoderm progenitors by SOX transcription factor expression in human embryonic stem cells. *Cell Stem Cell* 2008, *3*, 182-195.
[40] Peerani, R., Rao, B. M., Bauwens, C., Yin, T., Wood, G. A., Nagy, A.*, et al.*, Niche-mediated control of human embryonic stem cell self-renewal and differentiation. *EMBO J* 2007, *26*, 4744-4755.
[41] Hotta, A., Cheung, A. Y., Farra, N., Garcha, K., Chang, W. Y., Pasceri, P.*, et al.*, EOS lentiviral vector selection system for human induced pluripotent stem cells. *Nat Protoc* 2009, *4*, 1828-1844.
[42] Bendall, S. C., Hughes, C., Stewart, M. H., Doble, B., Bhatia, M., Lajoie, G. A., Prevention of amino acid conversion in SILAC experiments with embryonic stem cells. *Mol Cell Proteomics* 2008, *7*, 1587-1597.
[43] Ma, B., Zhang, K. Z., Hendrie, C., Liang, C. Z., Li, M., Doherty-Kirby, A.*, et al.*, PEAKS: powerful software for peptide de novo sequencing by tandem mass spectrometry. *Rapid Communications in Mass Spectrometry* 2003, *17*, 2337-2342.

[44] Zhang, J., Xin, L., Shan, B., Chen, W., Xie, M., Yuen, D., *et al.*, PEAKS DB: De Novo Sequencing Assisted Database Search for Sensitive and Accurate Peptide Identification. *Mol Cell Proteomics* 2012, *11*, M111 010587.

Chapter 5

Functional Characterization of hESC-Derived CMTX

5.1 Introduction

The two defining characteristics of human embryonic stem cells (hESC), self-renewal and pluripotency, are maintained by a delicate balance of intracellular and extracellular signaling processes. Extracellular regulation is primarily the result of changes in the microenvironment surrounding the cells during growth *in vitro* or *in vivo*. hESCs interact with this 'niche' through support cells, extracellular matrix (ECM) components, and autocrine/paracrine signaling (reviewed in [1-3]). Modulation of any of these supportive elements individually or in combination has been used extensively to alter hESC behavior [1-3]. For example, exogenous growth factor supplementation is used to facilitate the maintenance of hESCs as well as to induce their differentiation. Moreover, recent studies have illustrated that hESC self-renewal and differentiation can be altered through modulation of the properties of the ECM using synthetic mimics, highlighting its importance in the microenvironment (reviewed in [4]).

This chapter contains excerpts from the following paper:

Hughes, C.S., Radan, L., Stanford, W., Betts, D., Postovit, L.M., Lajoie, G.A.. (2012) "Proteomics Analysis of the Human Embryonic Stem Cell Depositome". (In Preparation)

A number of proteomics studies have been conducted to determine factors secreted by feeder layers in an attempt to elucidate proteins and pathways essential for hESC survival [5-8]. Currently only one of these studies has identified members of the soluble frizzled related protein (sFRP) family [9]. As part of our proteomics investigation into the components of CMTX, we identified sFRP1 and 2 across multiple cell lines. The sFRP family of proteins has been shown to regulate canonical Wnt signaling through direct binding to the secreted Wnt cytokines [10]. Central to this role is the direct interaction of sFRP1 and sFRP2 with Wnt3a [11]. The Wnt family is a group of secreted glycoproteins consisting of 19 members that contain 22 - 24 conserved cysteine residues (reviewed in [12]). Wnt signaling plays a prominent role during development and its aberrant regulation plays a role in multiple disease phenotypes (reviewed in [13]).

In humans, the sFRP family is made up of 5 members, sFRP1 – 5 [14]. The sFRPs were originally discovered due to their shared sequence similarity with the frizzled receptors that are directly involved with Wnt signaling [15, 16]. This family now constitutes the largest group of Wnt antagonists [17]. Structurally, the sFRP proteins contain two distinctive domains, an N-terminal cysteine rich domain (CRD) and a C-terminal netrin-like domain [18]. The CRD contains ten conserved cysteine residues and shares a significant similarity with the extracellular domain of the frizzled receptors [19]. The C-terminal netrin domain is postulated to confer heparin binding properties [18, 20, 21]. The primary interest in the sFRPs however, stems from the properties of the N-terminal CRD, that because of the sequence homology with the frizzled receptors,

has been proposed to bind Wnt proteins. This ability to bind Wnt proteins has subsequently been verified and intensely studied since that time (reviewed in [17]).

The sFRP family of proteins have been shown to encompass a diverse profile of expression patterns and context dependent interactions in a variety of tissues and cellular systems (reviewed in [22]). However, although sFRPs family members are known to be important during embryonic development, very little is known about their role in the regulation of ESCs [22]. This is surprising when it is considered that Wnt signaling has been shown to be involved in the direct regulation of the pluripotent state of ESCs (reviewed in [23]). Furthermore, in a recent study comparing 59 different hESC lines a positive correlation between Nanog and sFRP2 gene expression was observed [24]. In addition, sFRP2 was identified as a potential target for Nanog in ChIP on CHIP analyses of hESCs [25]. Taken together, these findings indicate that sFRP family members are potentially playing a vital role in hESC pluripotency.

Here we investigate the ability of hESC conditioned matrix (CMTX) to enhance the maintenance of undifferentiated stem cells. To identify and characterize factors potentially responsible for this effect, we utilize the data generated in our proteomics screen of CMTX (Chapter 4) to validate the role of sFRP1 and sFRP2. A combination of techniques is used to characterize the role of the sFRP candidates in the regulation of hESC pluripotency *in vitro*. Additionally, utilizing a metastatic melanoma cell line we demonstrate the effects of exogenous supplementation of sFRP1 and sFRP2. This work represents the first investigation of the hESC and hiPSC matrix microenvironment.

5.2 Results

5.2.1 hESC Derived Matrix for the Maintenance of an Undifferentiated State. The ability of embryonic microenvironments to suppress the tumorigenic phenotype has been previously illustrated in a number of developmental and cellular systems (reviewed in [26]). However, a limited number of studies have focused on reprogramming stem cells with these same microenvironments. Analogous to metastatic cells, embryonic stem cells can direct cellular changes in response to cues from their microenvironment. With the recent observation that a hESC-derived matrix microenvironment could modulate the behavior of metastatic cells [27], we sought determine what effect exposure would have on the stem cell phenotype. To this end, we monitored changes in the gene and protein expression of hESCs grown on CMTX in the absence of exogenous growth factor supplementation. In this way, matrix dependent changes in hESC behavior could be monitored without interference from soluble factors present in MEF-CM.

After 4 days of culture in medium that contained no exogenous bFGF (embryoid body medium, EB medium), a decrease in Oct3/4 and Nanog gene and protein expression was observed for H9 hESCs grown on control Matrigel™ and CMTX. However, the reduction in expression was significantly smaller in H9 hESCs grown on CMTX when compared with control cells (Figure 5.1 A-B). A similar trend was observed when H9 hESCs were measured using flow cytometry for SSEA4 and SSEA1 fluorescence. H9 hESCs induced to differentiate on CMTX exhibited an increase in SSEA4 mean fluorescence intensity relative to SSEA1 when compared with control cells (Figure 5.1 C-D). When cultures were examined by immunofluorescence, pockets of SSEA1

Figure 5.1. hESC generated CMTX enhances the maintenance of an undifferentiated state in H9 cells when compared to those grown on Matrigel™. Matrigel™/CMTX was generated by growing H9 hESCs on Matrigel™ for 4 days. Following cell removal, fresh H9 hESCs were plated on the CMTX layers. Control Matrigel™ was generated by treating normal Matrigel™ with the cell removal procedure prior to the plating of fresh hESCs as discussed in the Methods. Cells in both conditions were fed with medium not containing bFGF for 4 days. Control samples are hESCs grown on normal Matrigel™ in MEF-CM. (A) RT-PCR data for H9 hESCs cultured on control Matrigel™ and Matrigel™/CMTX. Values represent fold change of Oct3/4 or Nanog expression relative to control hESCs cultured under standard conditions. RPLPO was used as an internal control for both samples. Error bars represent SEM, n=3. (B) Western blot for Oct3/4 and Nanog in H9 hESCs grown on CMTX. Actin is shown as a control. (C) Flow cytometry data for H9 hESCs grown on CMTX. For each sample, plot (i) shows SSEA4 fluorescence (blue) relative to a matched isotype control (solid red), (ii) shows SSEA1 fluorescence relative to isotype control, (iii) scatter plot with the gated cell population shown, (iv) scatter plot with the viable cell population gated. Percentages denote fraction of cells within the gates shown. (D) Results from flow cytometry analysis of H9 hESCs grown on CMTX for the markers SSEA4 and SSEA1. Values represent mean fluorescence intensity of SSEA4 relative to SSEA1 for Matrigel™ Control or Matrigel™/CMTX samples. Values are derived from the data in (C). Error bars represent SEM, n=3. (D) Immunocytochemistry for H9 hESCs grown on Control Matrigel™ or Matrigel™/CMTX. Cells were stained with Oct3/4, SSEA4, DAPI, and SSEA1. Scale bars represent 250um.

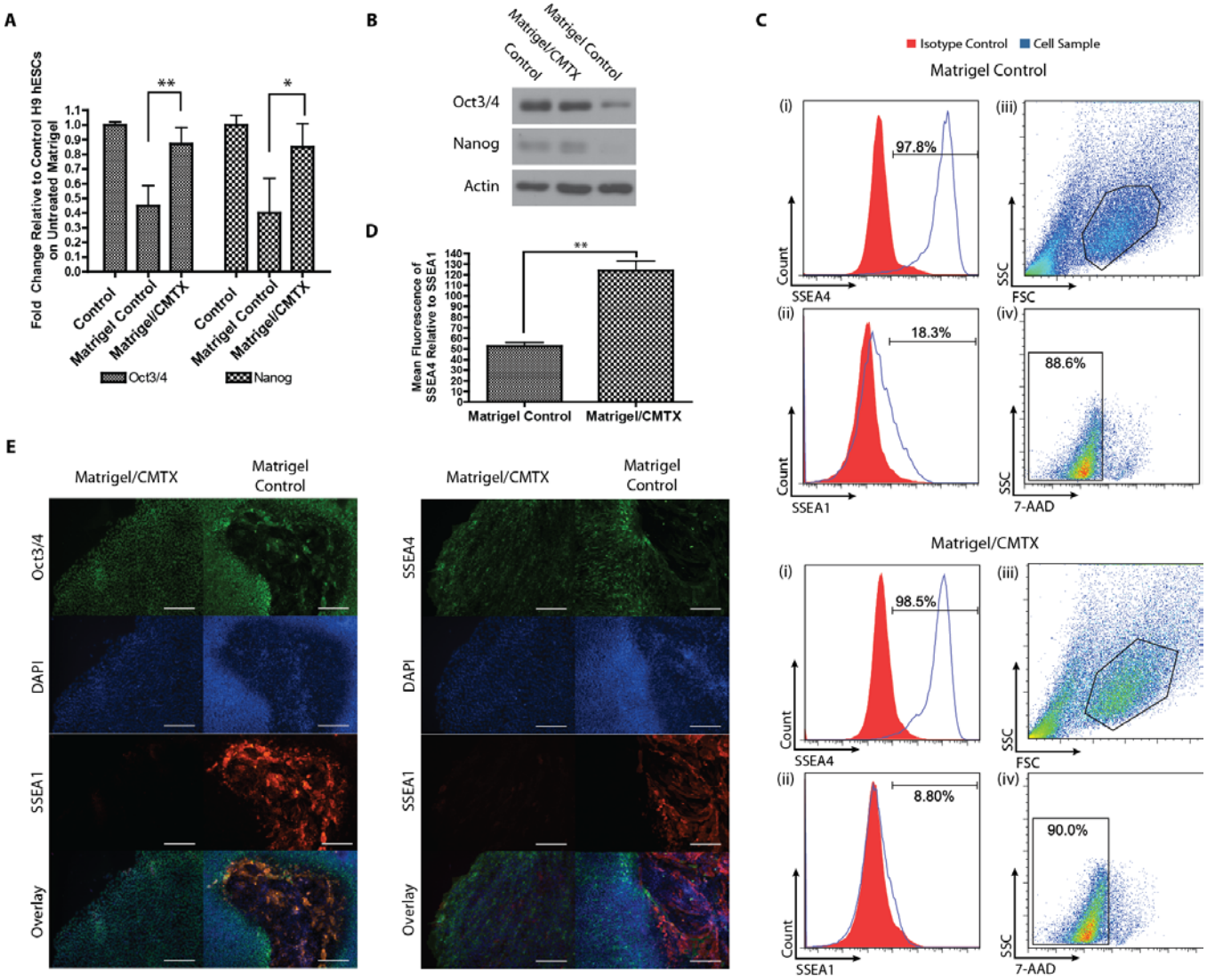
A
Fold Change Relative to Control H9 hESCs on Untreated Matrigel
Control
Matrigel Control
Matrigel/CMTX
Oct3/4
Nanog
B
Matrigel Control
Matrigel/CMTX
Control
Oct3/4
Nanog
Actin
C
Isotype Control
Cell Sample
Matrigel Control
97.8%
18.3%
88.6%
Matrigel/CMTX
98.5%
8.80%
90.0%
SSEA4
SSEA1
FSC
SSC
7-AAD
Count
D
Mean Fluorescence of SSEA4 Relative to SSEA1
Matrigel Control
Matrigel/CMTX
E
Matrigel/CMTX
Matrigel Control
Oct3/4
DAPI
SSEA1
Overlay
SSEA4

Figure 5.2. hESC generated CMTX enhances the maintenance of an undifferentiated state in CA1 cells when compared to those grown on Matrigel™. Matrigel™/CMTX was generated by growing CA1 hESCs on Matrigel™ for 4 days. Following cell removal, fresh CA1 hESCs were plated on the CMTX layers. Control Matrigel™ was generated by treating normal Matrigel™ with the cell removal procedure prior to the plating of fresh hESCs as discussed in the Methods. Cells in both conditions were fed with medium not containing bFGF for 4 days. Control samples are hESCs grown on normal Matrigel™ in MEF-CM. (A) RT-PCR data for CA1 hESCs cultured on control Matrigel™ and Matrigel™/CMTX. Values represent fold change of Oct3/4 or Nanog expression relative to control hESCs cultured under standard conditions. RPLPO was used as an internal control for both samples. Error bars represent SEM, n=3. (B) Western blot for Oct3/4 and Nanog in CA1 hESCs grown on CMTX. Actin is shown as a control. (C) Flow cytometry data for CA1 hESCs grown on CMTX. For each sample, plot (i) shows SSEA4 fluorescence (blue) relative to a matched isotype control (solid red), (ii) shows SSEA1 fluorescence relative to isotype control, (iii) scatter plot with the gated cell population shown, (iv) scatter plot with the viable cell population gated. Percentages denote fraction of cells within the gates shown. (D) Results from flow cytometry analysis of CA1 hESCs grown on CMTX for the markers SSEA4 and SSEA1. Values represent mean fluorescence intensity of SSEA4 relative to SSEA1 for Matrigel™ Control or Matrigel™/CMTX samples. Values are derived from the data in (C). Error bars represent SEM, n=3. (D) Immunocytochemistry for CA1 hESCs grown on Control Matrigel™ or Matrigel™/CMTX. Cells were stained with Oct3/4, SSEA4, DAPI, and SSEA1. Scale bars represent 250um.

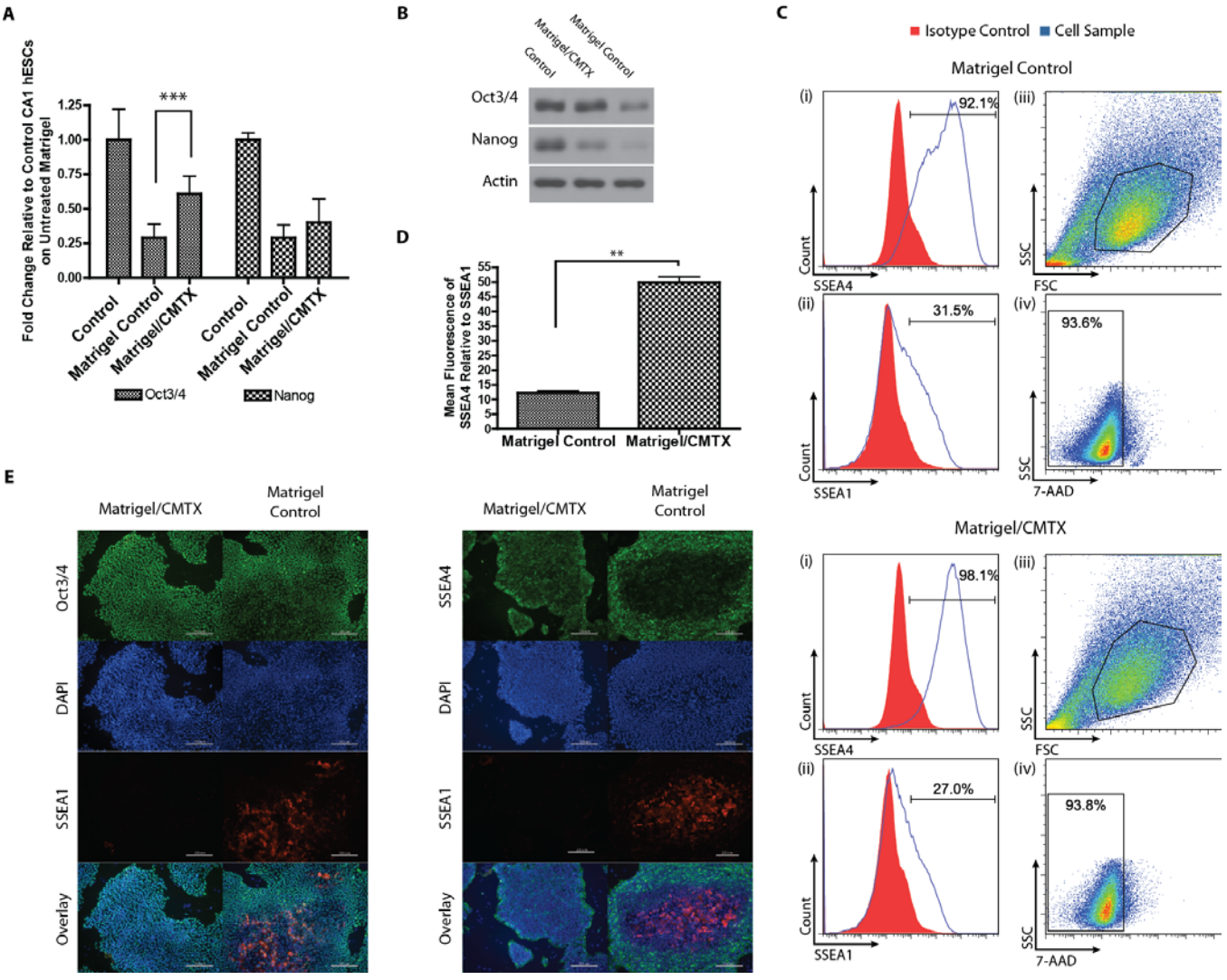
A
Fold Change Relative to Control CA1 hESCs on Untreated Matrigel
***
1.25
1.00
0.75
0.50
0.25
0.00
Control
Matrigel Control
Matrigel/CMTX
Control
Matrigel Control
Matrigel/CMTX
Oct3/4
Nanog
B
Control
Matrigel/CMTX
Matrigel Control
Oct3/4
Nanog
Actin
D
Mean Fluorescence of SSEA4 Relative to SSEA1
**
Matrigel Control
Matrigel/CMTX
C
Isotype Control
Cell Sample
Matrigel Control
(i)
92.1%
(iii)
Count
SSEA4
SSC
FSC
(ii)
31.5%
(iv)
93.6%
Count
SSEA1
SSC
7-AAD
Matrigel/CMTX
(i)
98.1%
(iii)
Count
SSEA4
SSC
FSC
(ii)
27.0%
(iv)
93.8%
Count
SSEA1
SSC
7-AAD
E
Matrigel/CMTX
Matrigel Control
Oct3/4
DAPI
SSEA1
Overlay
Matrigel/CMTX
Matrigel Control
SSEA4
DAPI
SSEA1
Overlay

positive cells could be observed in control cells, indicating differentiation (Figure 5.1 E). SSEA1 positive colonies were observed with a reduced frequency in cells cultured on CMTX. Subsequent analysis of a second hESC line, CA1, revealed similar trends (Figure 5.2 A-E). Taken together, these data indicate that CMTX promotes the preservation of an undifferentiated state and hESCs secrete factors into the matrix that are beneficial for their own maintenance.

5.2.2 Generation and Testing of an Artificial CMTX. To functionally validate the proteomics method for profiling the CMTX to identify hESC regulatory proteins, we investigated the roles of sFRP1, sFRP2, Lefty A, and Gremlin further. These proteins were selected on the basis of their suspected roles in hESC regulation as well as their previous implications in CMTX studies involving metastatic cells [27-29]. Moreover, these proteins were not identified in Matrigel™ itself, making their functional validation possible in a CMTX assay that utilizes this matrix without background interference. To determine the potential roles of these candidates in the CMTX, we repeated the hESC CMTX experiments utilizing two separate platforms for analysis.

We first sought to determine if supplementation of recombinant proteins to the matrix, in the absence of conditioning prior to hESC plating, could enhance the maintenance of an undifferentiated state. Recombinant versions of sFRP1 and sFRP2, Lefty A, and Gremlin were supplemented into Matrigel™ at a maximum concentration of 5μg/mL prior to gelation. To ensure maximal recombinant protein incorporation into the matrix, undiluted Matrigel™ was used in all assays to coat culture dishes. The Matrigel™™ layer was then treated with the lysis-free cell removal process (see Chapter 4) prior to

hESC plating to ensure reproducibility with the previous experiments. In H9 hESCs, supplementation with any of the selected proteins did not significantly enhance the expression of the markers of pluripotency Oct3/4 and Nanog (Figure 5.3 A). Alone or in combination, none of the proteins were able to fully replicate the effect observed on CMTX. Similar trends are seen in the CA1 hESC line, where individually or in combination, the matrix supplemented proteins are unable to promote maintenance of an undifferentiated state (Figure 5.3 C). In immunoblotting for Oct3/4 and Nanog we observe analogous changes in Oct3/4 and Nanog protein abundance in both H9 and CA1 hESCs (Figure 5.3 E). These data suggest that sFRP1, sFRP2, Gremlin, and Lefty A are unable to replicate the effects observed on hESC-derived CMTX. However, previous studies have shown that recombinant proteins are not as effective as their equivalent hESC-derived versions [27].

Antibody blocking experiments were performed to further investigate the potential role of the sFRP and Lefty proteins in the CMTX. CMTX was generated by growing H9 or CA1 hESCs on Matrigel™ as before. After cell removal, CMTX was treated with antibodies specific for sFRP1, sFRP2, or Lefty A candidates, individually or in combination, to generate a ‘knockdown’ CMTX. Unbound antibody was removed by washing and fresh hESCs were plated and grown in EB medium. In this way, sFRP or Lefty proteins that had been deposited in the CMTX during hESC growth would no longer be available for interaction with the newly plated cells. Monitoring changes in gene expression and protein abundance of Oct3/4 and Nanog revealed that none of the antibody treatments promoted a reduction in the maintenance of an undifferentiated state of H9 hESCs when compared with a secondary antibody control (Figure 5.3 B, F). Assay of the CA1

Figure 5.3. Characteristics of hESCs on recombinant and knockdown CMTX. Recombinant CMTX was generated by supplementing Matrigel™ with recombinant versions of sFRP1, sFRP2, Lefty, or Gremlin alone or in combination. Knockdown CMTX was made by incubating hESC-derived CMTX with antibodies specific for sFRP1, sFRP2, or Lefty A and Lefty B prior to plating of fresh hESCs. (A) Oct3/4 and Nanog expression in H9 hESCs grown on Recombinant CMTX as determined by RT-PCR. Values represent fold change relative to hESCs grown on Control Matrigel™ (treated with the cell removal process, but not supplemented with recombinant protein). Error bars indicate SD, n=3. (B) Oct3/4 and Nanog expression in H9 hESCs grown on Knockdown CMTX as determined by RT-PCR. Values represent fold change relative to hESCs grown on Matrigel™/CMTX (hESC-derived CMTX treated with the cell removal process, not treated with antibody). Error bars represent SD, n=3. Secondary denotes CMTX treated with a secondary antibody as a control (C) Oct3/4 and Nanog expression in CA1 hESCs on Recombinant CMTX . Error bars indicate SD, n=5. (D) CA1 hESCs on Knockdown CMTX. Error bars indicate SD, n=4. All RT-PCR experiments used RPLPO as an internal control for each sample. (E) Western blots for Oct3/4 and Nanog in H9 and CA1 hESCs grown on Recombinant CMTX. Actin is shown as a control. (F) Western blots for Oct3/4 and Nanog in H9 and CA1 hESCs grown on Knockdown CMTX. Actin is shown as a control.

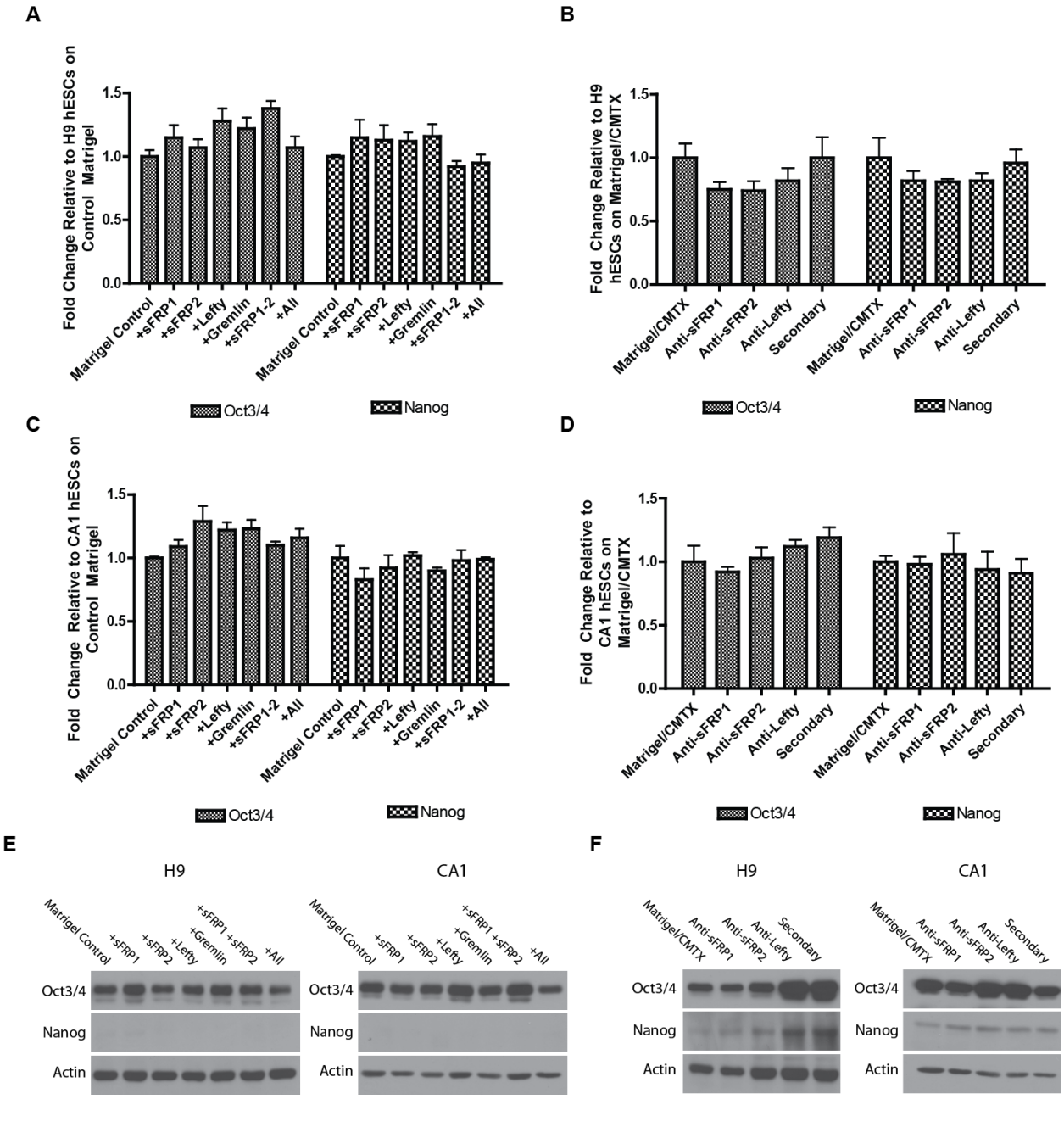
A
Fold Change Relative to H9 hESCs on Control Matrigel
1.5
1.0
0.5
0.0
Matrigel Control
+sFRP1
+sFRP2
+Lefty
+Gremlin
+sFRP1-2
+All
Oct3/4
Nanog
B
Fold Change Relative to H9 hESCs on Matrigel/CMTX
Matrigel/CMTX
Anti-sFRP1
Anti-sFRP2
Anti-Lefty
Secondary
C
Fold Change Relative to CA1 hESCs on Control Matrigel
D
Fold Change Relative to CA1 hESCs on Matrigel/CMTX
E
H9
CA1
+sFRP1 +sFRP2
Oct3/4
Nanog
Actin
F

hESC line revealed identical trends to the H9 cell line (Figure 5.3 D, F). Taken together, these experiments indicate that the sFRP and Lefty proteins do not solely modulate the state of hESCs on the CMTX. This suggests that there are other factors potentially acting to enhance undifferentiated hESC maintenance on CMTX. However, it is also possible that the antibodies utilized are potentially unable to block the function of the selected proteins, or are unable to bind if the target is localized in the matrix.

5.2.3 Roles of sFRP Proteins in hESC Pluripotency. Canonical Wnt signaling is a critical pathway with characterized roles during development as well as in ESCs themselves (reviewed in [12]). However, the regulation of hESC pluripotency through Wnt signaling is poorly understood, specifically how the pathway is controlled in the extracellular space. The sFRP family of proteins are known Wnt antagonists whose differential expression has been shown to have significant effects in a variety of cell types and pathological conditions (reviewed in [17]). Interactions between the sFRPs and hESCs and the resultant effects on self-renewal or differentiation are inadequately characterized. Given the importance of Wnt signaling in developmental processes, we chose to investigate the role of the sFRP1 and sFRP2 in the maintenance and regulation of hESC pluripotency.

To measure the effect of sFRP1 and sFRP2 on hESC behavior, we employed shRNA mediated knockdowns of each target gene. Initially we attempted to utilize the tetracycline inducible vector, pTRIPZ (Open Biosystems). An inducible system was chosen to permit generation of a homogenous population of undifferentiated cells should our shRNA promote differentiation. We successfully generated stable lines in

HEK293 cells and subsequently verified sFRP1 and sFRP2 knockdown. However, after production of stable H9 and CA1 hESC lines, we were unable to induce shRNA or reporter gene expression using doxycycline in any of the clones tested. Since the puromycin resistance and shRNA genes are on separate promoters, the effect we observe is potentially the result of promoter silencing, a common occurrence in hESCs [30]. To overcome this problem, we utilized a separate tetracycline inducible vector system known as pSUPERIOR. Along with the tetracycline repressor vector, pTetRnls, pSUPERIOR had previously been used to generate stable inducible Oct3/4 shRNA expressing cell lines [31]. However, although we were able to successfully generate stable H9 and CA1 lines, the cells grew poorly under dual-antibiotic selection and were prone to differentiation.

Because of these difficulties, we decided to employ a transient expression of our shRNAs in hESCs. Transient knockdown of gene expression in hESCs is challenging due to the poor efficiency of transfection of these cells. Using cationic lipid based transfection of H9 and CA1 hESCs we were able to achieve >60% efficiency based on GFP reporter expression (Figure 5.4 A-B). Expression of the shRNA constructs could be maintained by transfection on multiple days during experimentation as we did not observe a global reduction in viability as a result of the protocol (Figure 5.4 B). However, when examining colonies that contained small numbers of cells in conditions containing sFRP1 and sFRP2 shRNAs (<10 total cells), we observed a significant reduction in viability in both H9 and CA1 hESCs compared with controls (Figure 5.4 C). Using transient expression of our shRNA constructs, we were only able to obtain ~30% knockdown for both sFRP1 and sFRP2 based on gene expression in H9 and CA1

Figure 5.4. shRNA mediated knockdown of sFRP1 and sFRP2 expression. sFRP1 and sFRP2 expression were individually knocked down in H9 and CA1 hESCs using pSUPERIOR plasmid containing shRNA constructs against target transcripts. (A) Phase contrast and fluorescence images of H9 and CA1 hESC colonies transfected with pSUPERIOR plasmid expressing GFP and a scrambled shRNA control. Scale bars represent 250um. (B) Efficiency of transfection using flow cytometry detection of GFP positive cells after treatment. Smaller plots show viability using 7-AAD staining. N=2 for both cell lines. (C) Phase contrast images demonstrating the poor viability of small hESC colonies following transfection compared with scrambled control hESC lines. Scale bars represent 250um. (D) Knockdown of sFRP1 and sFRP2 expression in H9 and CA1 hESCs as measured by RT-PCR. Values are fold change relative to control samples transfected with a scrambled shRNA. Error bars depict SD, n=3. (E) Oct3/4 and Nanog expression in knockdown cells as determined by RT-PCR. Error bars show SD, n=3. For all RT-PCR experiments RPLPO is used as an internal sample control. (F) Immunoblot for Oct3/4, Nanog, sFRP1, and sFRP2 in knockdown and control H9 and CA1 hESCs. Actin is shown as a control for both cell lines.

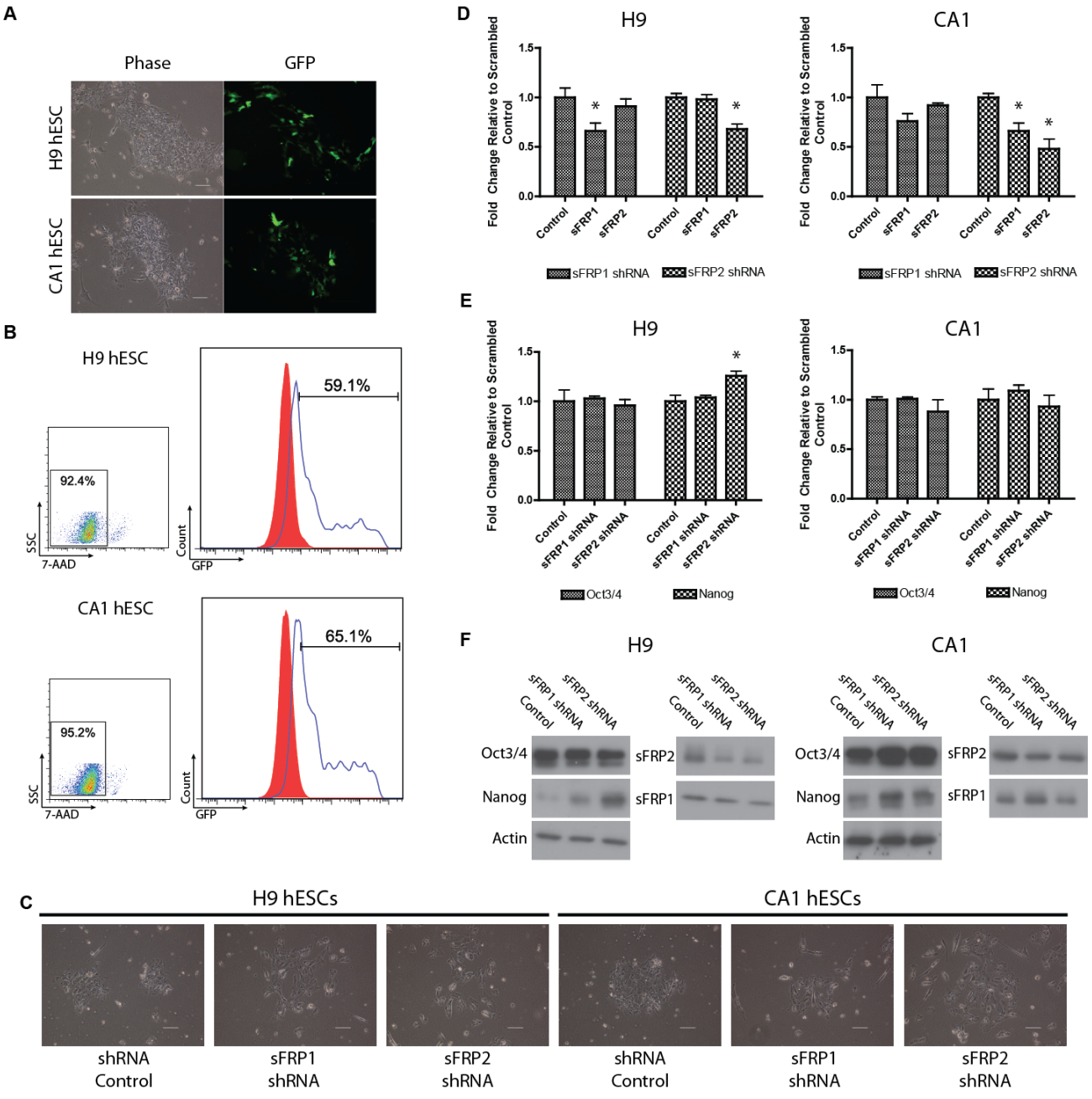
A
Phase
GFP
H9 hESC
CA1 hESC
B
H9 hESC
92.4%
59.1%
SSC
7-AAD
Count
GFP
CA1 hESC
95.2%
65.1%
D
H9
CA1
Fold Change Relative to Scrambled Control
Control
sFRP1
sFRP2
sFRP1 shRNA
sFRP2 shRNA
E
H9
CA1
Oct3/4
Nanog
F
H9
CA1
Oct3/4
Nanog
Actin
sFRP2
sFRP1
C
H9 hESCs
CA1 hESCs
shRNA Control
sFRP1 shRNA
sFRP2 shRNA

hESCs (Figure 5.4 D). To test the effects of these knockdowns on hESC behavior, H9 and CA1 cells were grown in MEF-CM for 4 days post-transfection. In hESCs containing sFRP1 or sFRP2 shRNA expressing plasmids grown in MEF-CM, we observed no significant change in Oct3/4 and Nanog at both the transcript and protein level (Figure 5.4 E-F). Taken together, these data suggest that sFRP1 and sFRP2 are unable, on their own, to modulate pluripotency marker expression in MEF-CM. However, the effectiveness of the shRNA treatment is potentially confounded by the limited extent of knockdown achieved.

Although we obtained a knockdown of gene expression for sFRP1 and 2 in the hESC lines tested, we observed that the protein level remained relatively unchanged compared with control cells (Figure 5.4 F). To effect sFRP signaling at the protein level, we utilized two separate small molecule inhibitors specific for sFRP1 (herein referred to as sFRP1 Inhibitor A and sFRP1 Inhibitor B) [32]. When H9 or CA1 hESCs grown in MEF-CM were supplemented with either inhibitor, we observed only minor alterations in Oct3/4 and Nanog expression that were not significant at the transcript level (Figure 5.5 A-B). Additionally, we observed no differences based on immunoblot data, indicating that the changes observed at the transcript level were not biologically significant (Figure 5.5 C). Taken together, these results suggest that inhibition of sFRP1 cannot, on its own, promote the changes in the expression of genes directly involved in the maintenance of the stem cell phenotype in MEF-CM.

To test whether inhibition of sFRP1 by small molecule inhibitors has an effect on the differentiation of hESCs, we supplemented multiple concentrations of either inhibitor in

Figure 5.5. hESCs in MEF-CM supplemented with sFRP1 inhibitors. H9 and CA1 hESCs were grown in MEF-CM that was supplemented with small molecule inhibitors of sFRP1. Oct3/4 and Nanog expression were assayed by RT-PCR following 4 days of culture in the presence of supplementation. (A) Fold change of Oct3/4 and Nanog expression relative to control for H9 and CA1 hESCs grown in MEF-CM supplemented with sFRP1 inhibitor A. (B) Fold change of Oct3/4 and Nanog expression relative to control for H9 and CA1 hESCs grown in MEF-CM supplemented with sFRP1 inhibitor B. Error bars represent SD, n=3. All RT-PCR experiments used RPLPO as an internal control. (C) Western blots depicting Oct3/4 and Nanog protein expression for H9 and CA1 hESCs grown in MEF-CM supplemented with sFRP1 inhibitors. Actin is shown as a control.

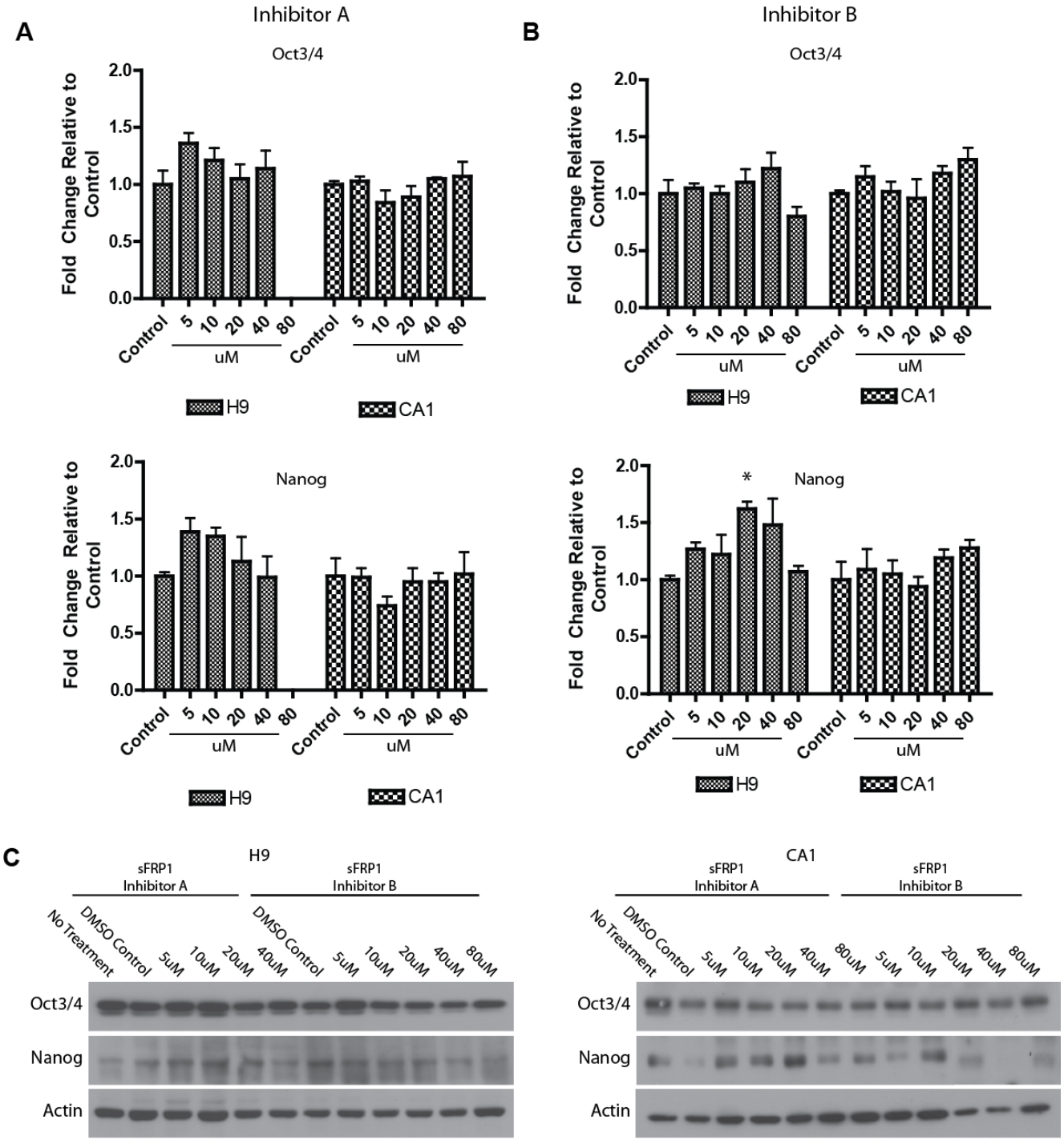
A
Inhibitor A
Oct3/4
Fold Change Relative to Control
2.0
1.5
1.0
0.5
0.0
Control
5
10
20
40
80
uM
H9
CA1
Nanog
B
Inhibitor B
*
C
H9
CA1
sFRP1 Inhibitor A
sFRP1 Inhibitor B
No Treatment
DMSO Control
5uM
10uM
20uM
40uM
80uM
Oct3/4
Nanog
Actin

EB medium. Similar to the observed effect in MEF-CM, neither sFRP1 inhibitor was able to alter the expression of Oct3/4 or Nanog in H9 or CA1 hESCs (Figure 5.6 A-B). Analogous to MEF-CM, no observable changes were seen in immunoblots for Oct3/4 and Nanog (Figure 5.6 C). However, due to the poor abundance of Nanog following differentiation based on immunoblots, correlation of gene expression and protein abundance data is challenging.

Since Wnt signaling is known to be involved in the induction of mesendoderm, we examined whether hESCs grown in EB medium supplemented with sFRP1 inhibitors would display an induction of this lineage type [33]. As indicators of mesendoderm, we monitored Goosecoid (GSC) [34] and Mix paired-like homeobox 1 (MIXL1) [35] expression. We observed a significant decrease in GSC expression and subsequent increase in MIXL1 in H9 hESCs grown in the presence of sFRP1 inhibitor A in EB medium (Figure 5.6 D). We observe a similar trend for H9 hESCs grown in the presence of sFRP1 inhibitor B; although significance is not reached in the case of MIXL1 (Figure 5.6 E). We observe no significant change in GSC or MIXL1 expression in CA1 hESCs grown in the presence of either sFRP1 inhibitor in EB medium (Figure 5.6 D).

In order to maximize the knockdown in sFRP1 and sFRP2 activity, we combined transient transfection of the hESCs with small molecule inhibition in both MEF-CM and EB medium. Similar to the previous results in MEF-CM and EB medium supplemented with either sFRP1 inhibitor, we observed no significant changes Oct3/4 in transcript or protein abundance in sFRP1 and sFRP2 shRNA expressing hESCs (Figure 5.7 A-D).

Figure 5.6. hESCs in embryoid body medium supplemented with sFRP1 inhibitors. H9 and CA1 hESCs were grown in EB medium that was supplemented with small molecule inhibitors of sFRP1. Oct3/4 and Nanog expression were assayed by RT-PCR following 4 days of culture in the presence of supplementation. (A) Fold change of Oct3/4 and Nanog expression relative to control for H9 and CA1 hESCs grown in EB medium supplemented with sFRP1 inhibitor A. (B) Fold change of Oct3/4 and Nanog expression relative to control for H9 and CA1 hESCs grown in EB medium supplemented with sFRP1 inhibitor B. Error bars represent SD, n=3. (C) Western blots depicting Oct3/4 and Nanog protein expression for H9 and CA1 hESCs grown in embryoid body medium supplemented with sFRP1 inhibitors. Actin is shown as a control. (D) Goosecoid and MIXL1 expression as indicators of mesendoderm induction for H9 and CA1 hESCs grown in the presence of sFRP1 inhibitor A. (E) Goosecoid and MIXL1 expression as indicators of mesendoderm induction for H9 and CA1 hESCs grown in the presence of sFRP1 inhibitor B. Significance was determined through comparison with embryoid body controls. Error bars represent SD, n=3. All RT-PCR experiments used RPLPO as an internal control.

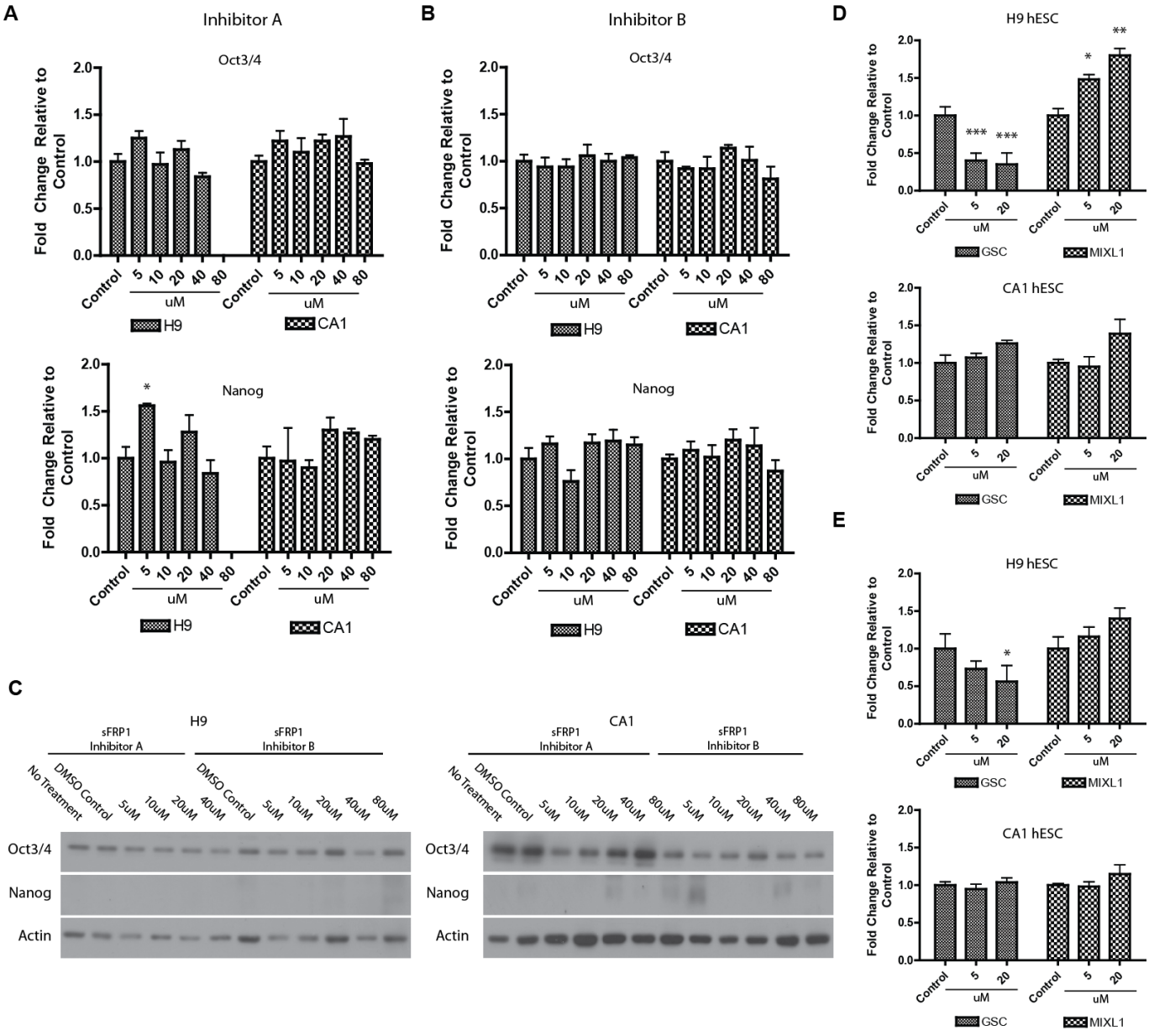
A
Inhibitor A
Oct3/4
Fold Change Relative to Control
Control
5 10 20 40 80
uM
H9
CA1
Nanog
*
B
Inhibitor B
C
H9
CA1
sFRP1 Inhibitor A
sFRP1 Inhibitor B
No Treatment
DMSO Control
5uM
10uM
20uM
40uM
80uM
Oct3/4
Nanog
Actin
D
H9 hESC
CA1 hESC
***
*
**
GSC
MIXL1
E

Examination of hESCs grown in EB medium supplemented with sFRP1 inhibitor A or B revealed significant increases in GSC and MIXL1 expression in the sFRP2 knockdown CA1 lines (Figure 5.7 G-J). No significant changes were observed in the H9 hESC line in the presence of either inhibitor (Figure 5.7 G-J). Taken together, these results suggest that modulation of sFRP using sFRP1 inhibitors or shRNA knockdowns are unable to direct changes in hESCs in MEF-CM.

To further examine the potential effects of sFRP1 and sFRP2 on hESCs, we supplemented recombinant versions of these proteins in MEF-CM and EB medium. Since the sFRP family is known to regulate Wnt signaling, and sFRP1 and sFRP2 act directly on Wnt3a, we decided to investigate what role this pathway plays in hESCs [11]. Direct supplementation of Wnt3a in either MEF-CM or EB medium proved beneficial for the maintenance of Oct3/4 and Nanog expression (Figure 5.8 A - C). Supplementation with Wnt3a in EB medium also induced the expression of GSC in H9 and CA1 hESCs (Figure 5.8 D). MIXL1 expression was also significantly upregulated in CA1 hESCs grown in the presence of Wnt3a (Figure 5.8 E).

When H9 and CA1 hESCs were supplemented with recombinant sFRP1, sFRP2, and Wnt3a in MEF-CM, we observed that no significant changes were present at both the transcript and protein level (Figure 5.9 A, C, E). However, in EB medium, we observed a significant increase in Nanog expression when sFRP1 or sFRP2 were supplemented in combination with Wnt3a (Figure 5.9 D, F). In CA1 hESCs, we also observed an increase in Oct3/4 expression in the presence of Wnt3a and sFRP1 or sFRP2 (Figure 5.9 B, F). Unfortunately, the low-abundance of Nanog in differentiated hESCs

Figure 5.7. hESCs with combined exposure to sFRP1 inhibitors and shRNA mediated knockdowns. H9 and CA1 hESCs transfected with shRNA expressing vectors against sFRP1, sFRP2, or scrambled control were grown in MEF-CM or embryoid body medium that was supplemented with small molecule inhibitors of sFRP1. Oct3/4 and Nanog expression were assayed by RT-PCR following 4 days of culture in the presence of supplementation. (A) Fold change of Oct3/4 and Nanog expression relative to control for H9 and CA1 hESCs grown in MEF-CM supplemented with sFRP1 inhibitor A. Error bars represent SD, n=3. (B) Fold change of Oct3/4 and Nanog expression relative to control for H9 and CA1 hESCs grown in embryoid body medium supplemented with sFRP1 inhibitor A. Error bars represent SD, n=3. (C) Fold change of Oct3/4 and Nanog expression relative to control for H9 and CA1 hESCs grown in MEF-CM supplemented with sFRP1 inhibitor B. Error bars represent SD, n=3. (D) Fold change of Oct3/4 and Nanog expression relative to control for H9 and CA1 hESCs grown in embryoid body medium supplemented with sFRP1 inhibitor B. Error bars represent SD, n=3. (E) Western blots for Oct3/4 and Nanog in H9 and CA1 hESCs transfected with shRNA expressing vectors grown in MEF-CM supplemented with sFRP1 inhibitors. Actin is shown as an internal control. (F) Western blots for Oct3/4 and Nanog in H9 and CA1 hESCs transfected with shRNA expressing vectors grown in embryoid body medium supplemented with sFRP1 inhibitors. Actin is shown as an internal control. (G-J) Fold change of Goosecoid and MIXL1 expression relative to control for H9 and CA1 hESCs grown in embryoid body medium supplemented with sFRP1 inhibitor A (G-H) or sFRP1 inhibitor B (I-J). Error bars represent SD, n=3. All RT-PCR experiments used RPLPO as an internal control.

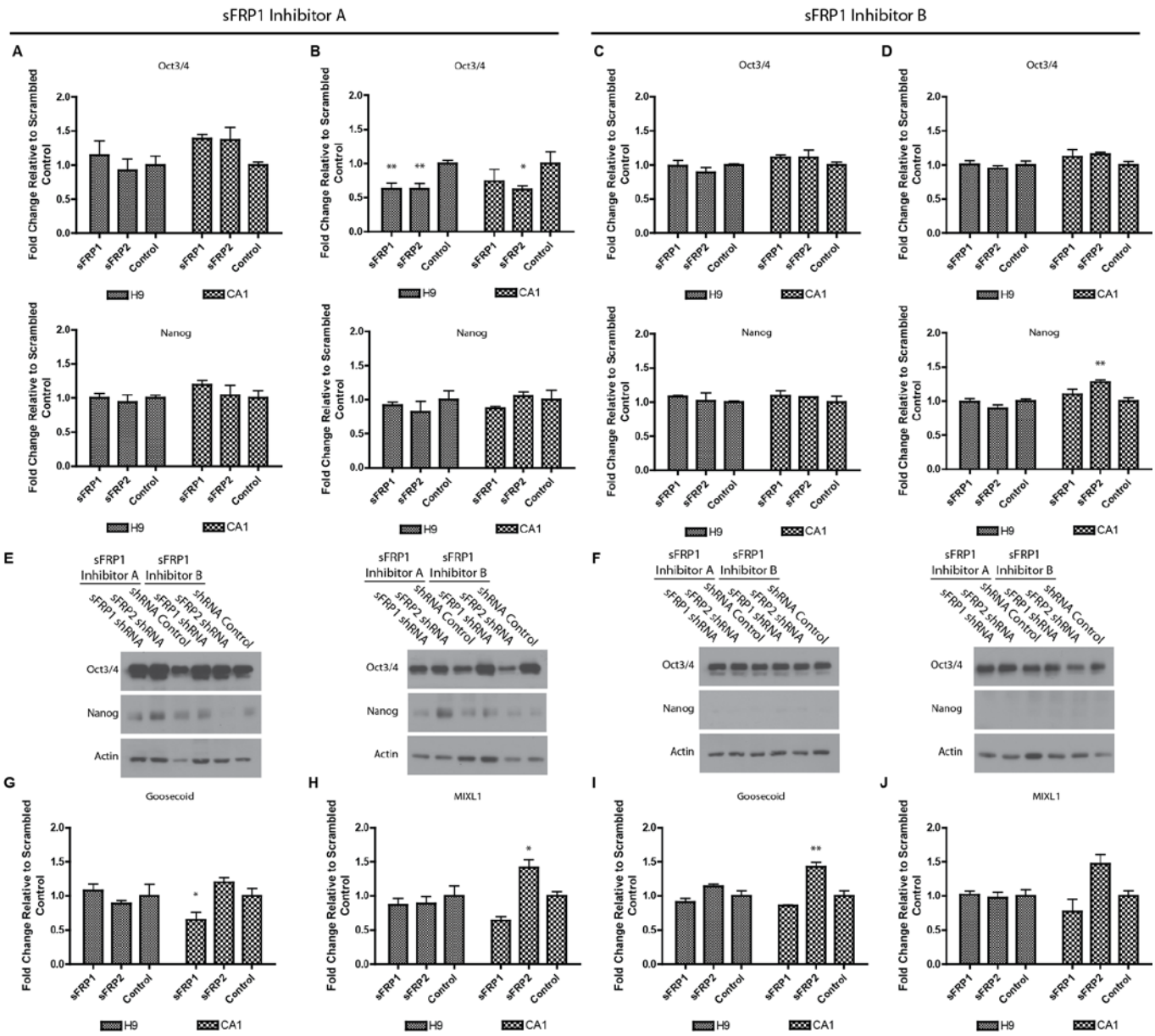
sFRP1 Inhibitor A
sFRP1 Inhibitor B
A
B
C
D
Oct3/4
Nanog
Fold Change Relative to Scrambled Control
sFRP1
sFRP2
Control
H9
CA1
E
F
sFRP1 Inhibitor A
sFRP1 Inhibitor B
sFRP1 shRNA
sFRP2 shRNA
shRNA Control
Oct3/4
Nanog
Actin
G
H
I
J
Goosecoid
MIXL1

Figure 5.8. hESCs in MEF-CM and embryoid body medium with recombinant Wnt3a supplementation. H9 and CA1 hESCs were grown in MEF-CM or embryoid body medium that was supplemented with recombinant Wnt3a. Oct3/4 and Nanog expression were assayed by RT-PCR following 4 days of culture in the presence of supplementation. (A) Fold change of Oct3/4 expression relative to control for H9 and CA1 hESCs grown in MEF-CM or EB medium supplemented with recombinant Wnt3a at 100ng/mL. Error bars represent SD, n=3. (B) Fold change of Nanog expression relative to control for H9 and CA1 hESCs grown in MEF-CM or EB medium supplemented with recombinant Wnt3a at 100ng/mL. Error bars represent SD, n=3. (C) Western blots for Oct3/4 and Nanog in H9 and CA1 hESCs grown in the presence or absence of 100 ng/mL of Wnt3a. Actin is shown as a control. (D) Fold change of Goosecoid expression relative to control for H9 and CA1 hESCs grown in embryoid body medium supplemented with recombinant Wnt3a, at 100ng/mL. Significance was determined through comparison with the appropriate EB medium control. Error bars represent SD, n=3. (E) Fold change of Goosecoid expression relative to control for H9 and CA1 hESCs grown in embryoid body medium supplemented with recombinant Wnt3a, at 100ng/mL. Significance was determined through comparison with the appropriate EB medium control. Error bars represent SD, n=3. All RT-PCR experiments use RPLPO as an internal control.

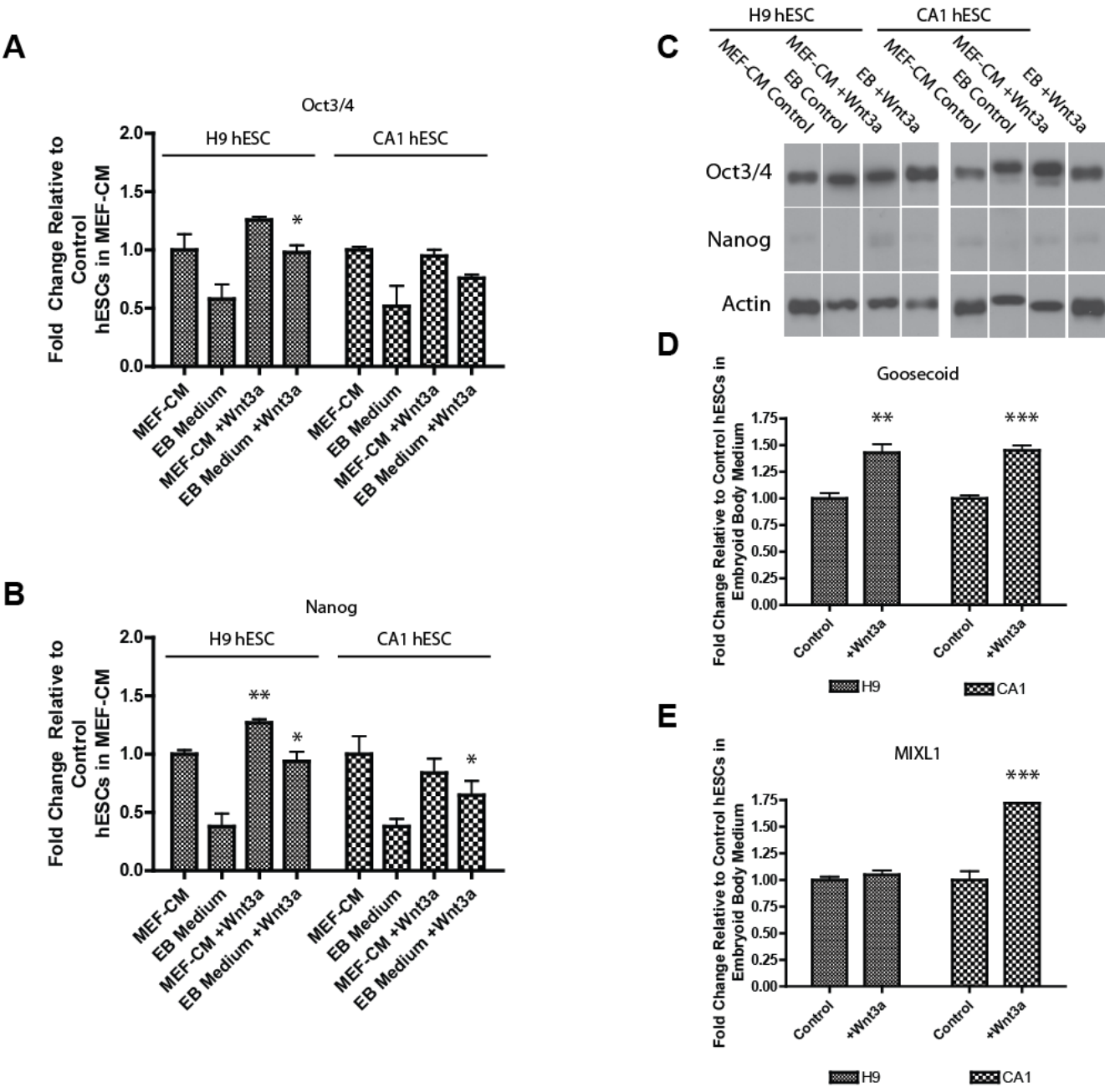
A
Oct3/4
H9 hESC
CA1 hESC
Fold Change Relative to Control hESCs in MEF-CM
2.0
1.5
1.0
0.5
0.0
*
MEF-CM
EB Medium
MEF-CM +Wnt3a
EB Medium +Wnt3a
B
Nanog
H9 hESC
CA1 hESC
Fold Change Relative to Control hESCs in MEF-CM
**
*
*
C
H9 hESC
CA1 hESC
MEF-CM Control
EB Control
MEF-CM +Wnt3a
EB +Wnt3a
Oct3/4
Nanog
Actin
D
Goosecoid
Fold Change Relative to Control hESCs in Embryoid Body Medium
1.75
1.50
1.25
1.00
0.75
0.50
0.25
0.00
**
***
Control
+Wnt3a
H9
CA1
E
MIXL1
Fold Change Relative to Control hESCs in Embryoid Body Medium
***
Control
+Wnt3a
H9
CA1

confounded the validation of gene expression results at the protein level (Figure 5.9 E-F). Examination of GSC expression revealed significant increases in H9 hESCs in the presence of Wnt3a and sFRP1 or sFRP2 (Figure 5.9 G). GSC could be reduced through the addition of sFRP1 and sFRP2 in CA1 hESCs (Figure 5.9 G). However, this reduction could be reversed through the addition of Wnt3a (Figure 5.9 G). In CA1 hESCs we also observed a significant induction in MIXL1 expression in the presence of Wnt3a, sFRP1, and sFRP2 (Figure 5.8 H). These data indicate that sFRP1 and sFRP2 proteins are able to act on hESCs during differentiation on their own or through interaction with Wnt3a dependent on the growth factor composition of the microenvironment.

5.2.4 Effect of sFRP Expression in Metastatic Melanoma Cells. sFRP1 and sFRP2 have multiple convergent and divergent roles in metastatic cell types (reviewed in [10]). To examine the effects of sFRP1 and sFRP2 expression we utilized a metastatic melanoma cell line (C8161) that was previously employed to demonstrate the reprogramming ability of hESC-derived CMTX [27, 36]. Expression of sFRP2 was found to be minimal in C8161 cells when compared with hESCs and HEK293 lines (Figure 5.10 A). Interestingly, sFRP1 expression was similar to H9 hESCs based on RT-PCR data (Figure 5.10 A). Since sFRP2 expression was found to be low, we transfected the C8161 cells with a vector containing the sFRP2 open-reading frame (ORF) under the control of a constitutive promoter. After 48 hours post-transfection, C8161s transfected with the sFRP2 ORF had a significant decrease in total cell number compared to control cells transfected with the same vector without the sFRP2 ORF (Figure 5.10 B). After selection with puromycin, no cells were able to form stable cell

lines from those transfected with the sFRP2 ORF, whereas numerous clones were derived from the control plate (Figure 5.10 B). However, validation of sFRP2 expression in C8161 cells was difficult due to the inability to harvest cellular RNA and protein as a result of cell death.

To further assess the effects of sFRP1 and sFRP2 on the C8161s we carried out an anchorage independent growth assay. C8161 cells that had been supplemented with 200 ng/mL of sFRP1 and sFRP2 for 4 and 7 days were seeded into soft-agar and permitted to form colonies for 14 days. Cells exposed to sFRP1 and sFRP2 had a significant increase in colony formation relative to control, whereas those exposed to sFRP2 had a significant decrease (Figure 5.10 C). Although the sFRP2 supplemented wells displayed colonies, they tended to be smaller than those found in the sFRP1 or control wells (Figure 5.10 D). Taken together, these data indicate divergent roles for sFRP1 and sFRP2 in metastatic C8161 cells.

Figure 5.9. hESCs in MEF-CM and embryoid body medium with recombinant protein supplementation. H9 and CA1 hESCs were grown in MEF-CM or embryoid body medium that was supplemented with recombinant versions of sFRP1, sFRP2, and Wnt3a. Oct3/4 and Nanog expression were assayed by RT-PCR following 4 days of culture in the presence of supplementation. (A) Fold change of Oct3/4 expression relative to control for H9 and CA1 hESCs grown in MEF-CM medium supplemented with recombinant sFRP1, sFRP2, and Wnt3a, each at 100ng/mL. (B) Fold change of Oct3/4 expression relative to control for H9 and CA1 hESCs grown in embryoid body medium supplemented with recombinant sFRP1, sFRP2, and Wnt3a, each at 100ng/mL. (C) Fold change of Nanog expression relative to control for H9 and CA1 hESCs grown in MEF-CM medium supplemented with recombinant sFRP1, sFRP2, and Wnt3a, each at 100ng/mL. (D) Fold change of Nanog expression relative to control for H9 and CA1 hESCs grown in embryoid body medium supplemented with recombinant sFRP1, sFRP2, and Wnt3a, each at 100ng/mL. Significance was determined through comparison with the appropriate MEF-CM or EB medium control. Error bars represent SD, n=3. (E-F) Western blots depicting Oct3/4 and Nanog protein expression for all experiments. Actin is shown as a control. (G-H) Goosecoid and MIXL1 expression as indicators of mesendoderm induction for H9 and CA1 hESCs grown in embryoid body medium supplemented with recombinant sFRP1, sFRP2, and Wnt3a, each at 100ng/mL. Significance was determined by comparison with MEF-CM and EB medium controls . All RT-PCR experiments use RPLPO as an internal control.

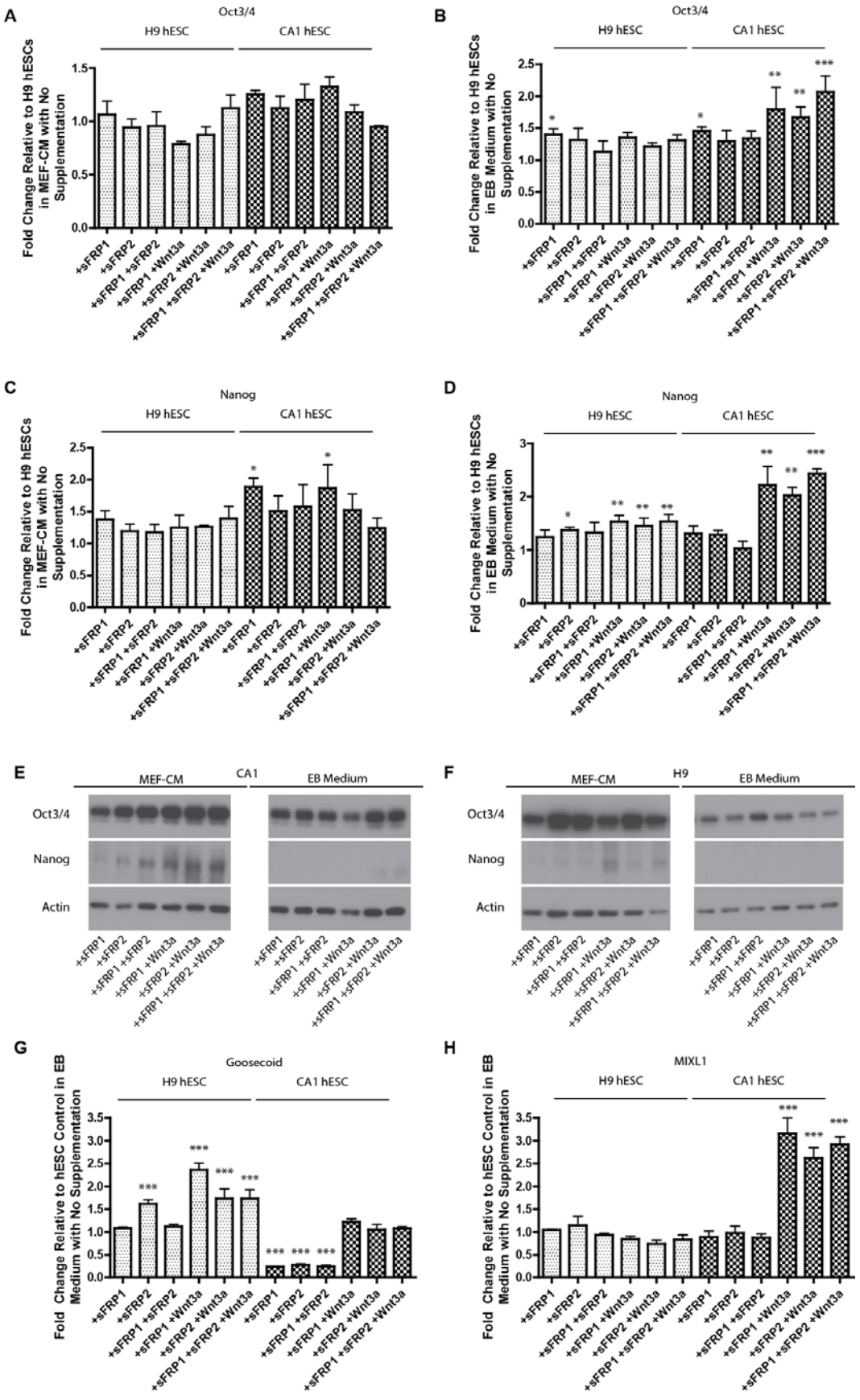
A
Oct3/4
H9 hESC
CA1 hESC
Fold Change Relative to H9 hESCs in MEF-CM with No Supplementation
B
Oct3/4
H9 hESC
CA1 hESC
Fold Change Relative to H9 hESCs in EB Medium with No Supplementation
C
Nanog
H9 hESC
CA1 hESC
Fold Change Relative to H9 hESCs in MEF-CM with No Supplementation
D
Nanog
H9 hESC
CA1 hESC
Fold Change Relative to H9 hESCs in EB Medium with No Supplementation
+sFRP1
+sFRP2
+sFRP1 +sFRP2
+sFRP1 +Wnt3a
+sFRP2 +Wnt3a
+sFRP1 +sFRP2 +Wnt3a
E
MEF-CM
CA1
EB Medium
Oct3/4
Nanog
Actin
F
MEF-CM
H9
EB Medium
Oct3/4
Nanog
Actin
G
Goosecoid
H9 hESC
CA1 hESC
Fold Change Relative to hESC Control in EB Medium with No Supplementation
H
MIXL1
H9 hESC
CA1 hESC
Fold Change Relative to hESC Control in EB Medium with No Supplementation

Figure 5.10. Metastatic melanoma cell line characteristics following sFRP1 and sFRP2 modulation. C8161 metastatic melanoma cells were grown in the presence or absence of recombinant sFRP1 and sFRP2 or transfected with the sFRP2 open-reading frame under the control of a constitutive promoter. (A) Expression of sFRP1 and sFRP2 in H9 and CA1 hESCs, HEK293, and C8161 cells as determined by RT-PCR. RT-PCR values are fold change relative to H9 hESCs using RPLPO as an internal control. Error bars represent SEM, n=2. (B) C8161 cells were transfected with either a vector containing the sFRP2 open-reading frame or with the same vector containing no insert. Cells were counted 48 hours post transfection and 7-days following the addition of puromycin to assess survival. Error bars represent SD, n=3. (C) C8161 cells grown in the presence or absence of 200 ng/mL of sFRP1 and sFRP2 for 4 or 7 days were tested for anchorage independent growth using a soft-agar assay. Pictures were taken after 7 days, colonies were allowed to form for a total of 14 days prior to counting. Error bars represent SD, n=3. Significance was determined relative to control for all treatments.

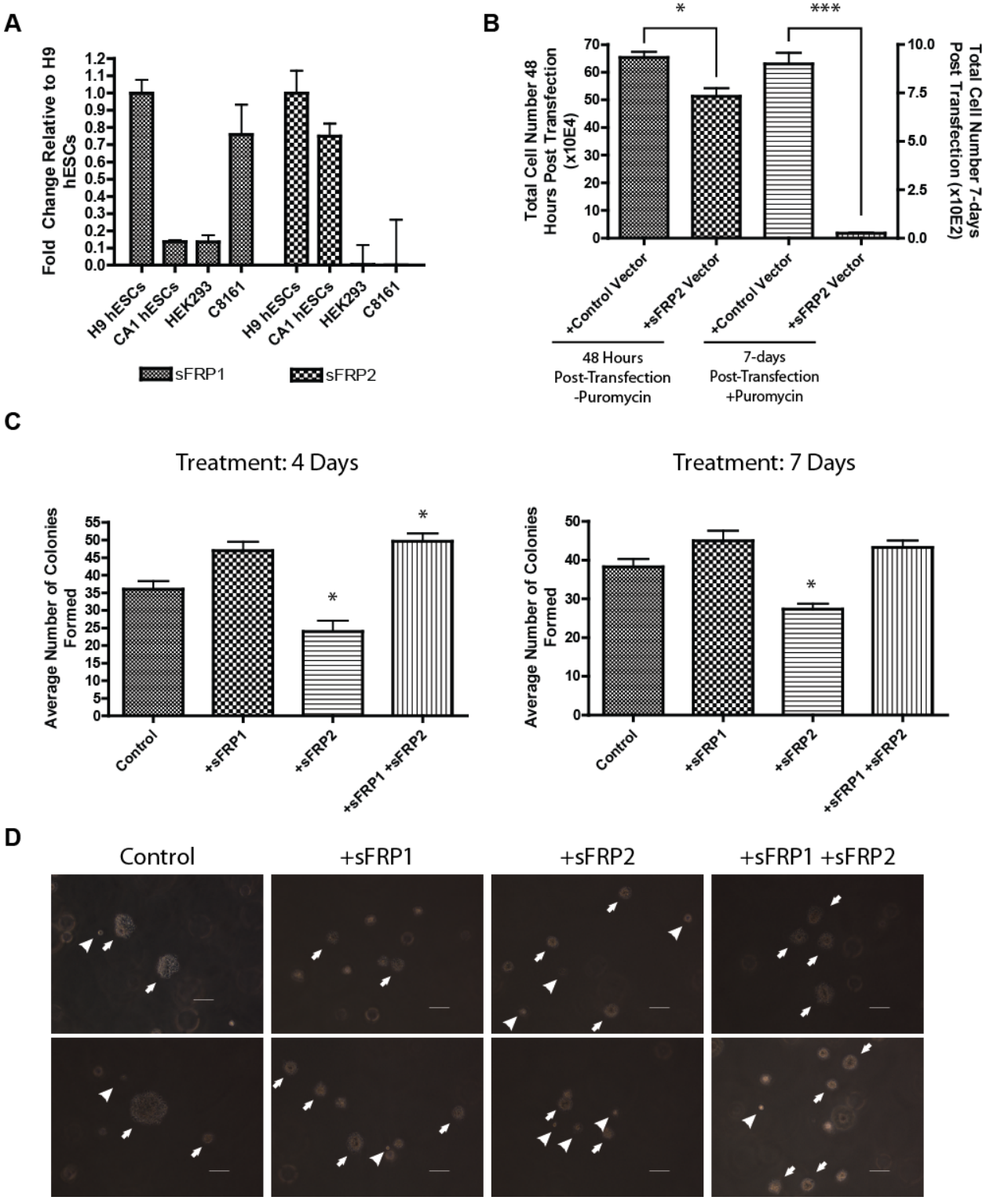
A
Fold Change Relative to H9 hESCs
1.2
1.1
1.0
0.9
0.8
0.7
0.6
0.5
0.4
0.3
0.2
0.1
0.0
H9 hESCs
CA1 hESCs
HEK293
C8161
H9 hESCs
CA1 hESCs
HEK293
C8161
sFRP1
sFRP2
B
*
***
Total Cell Number 48 Hours Post Transfection (x10E4)
70
60
50
40
30
20
10
0
Total Cell Number 7-days Post Transfection (x10E2)
10.0
7.5
5.0
2.5
0.0
+Control Vector
+sFRP2 Vector
+Control Vector
+sFRP2 Vector
48 Hours Post-Transfection -Puromycin
7-days Post-Transfection +Puromycin
C
Treatment: 4 Days
Average Number of Colonies Formed
55
50
45
40
35
30
25
20
15
10
5
0
*
*
Control
+sFRP1
+sFRP2
+sFRP1 +sFRP2
Treatment: 7 Days
Average Number of Colonies Formed
50
40
30
20
10
0
*
Control
+sFRP1
+sFRP2
+sFRP1 +sFRP2
D
Control
+sFRP1
+sFRP2
+sFRP1 +sFRP2

5.3 Discussion

The interactions between hESCs and their soluble microenvironment are essential for control over pathways related to self-renewal and differentiation. Cytokines involved in the regulation of these core pathways are often associated with other factors in the microenvironment that aid in the management of their activity or stability. Many of these co-factors can be bound to, or present in the ECM. As such, the study of the interactions between hESCs and the ECM represents a potentially rich source of information regarding regulation of core pluripotency pathways. Highlighting this is the recent observation that hESC-derived matrix microenvironments can reprogram metastatic melanoma cells [27, 36]. Bioactive factors deposited by hESCs during growth are able to direct cell-fate through activity in extracellular pathways within the microenvironment [27]. However, currently there are few studies that aim to investigate the interactions of hESCs with the ECM mediated by protein deposition in the extracellular space.

Based on our work, growth on CMTX in the absence of bFGF promotes the maintenance of an undifferentiated state in hESCs. This indicates that hESCs are depositing factors in the CMTX that serve to regulate the stem cell state. To investigate this finding further and to validate the ability of our MS-based proteomics screen to identify hESC regulatory factors in the matrix, we targeted sFRP1 and sFRP2 for functional analysis. sFRP1 and sFRP2 are thought to regulate canonical Wnt signaling through direct binding to the soluble Wnt cytokines or their cognate membrane receptors (reviewed in [23]). However, the role of sFRP1 and sFRP2 in hESCs remains

unclear. By utilizing a combination of methods, we analyzed the roles of these Wnt regulators in hESCs.

Using shRNA mediated inhibition of sFRP1 and 2 we observed no significant change in Oct3/4 and Nanog in MEF-CM. Similar trends can be observed in the sFRP1 inhibitor data, where neither inhibitor is able to direct a significant change in pluripotency marker expression at both the transcript and protein level. When shRNA mediated knockdown of expression sFRP1 or sFRP2 is combined with the sFRP1 inhibitors, we observe no significant change in Oct3/4 and Nanog expression at the transcript and protein level. Taken together, these findings indicate that sFRP1 and sFRP2 are not able to direct a significant change in hESCs grown in the complex growth factor microenvironment provided by MEF-CM. However, these findings are limited by the lack of positive control for the small molecule inhibitor due to the poor transfectability coupled with the low activity of the canonical Wnt pathway in hESCs.

To determine whether sFRP1 or sFRP2 were acting through Wnt signaling activated by Wnt3a, we investigated their effects when supplemented exogenously. Previous studies have demonstrated that Wnt signaling in ESCs functions in an ‘activation’ type model [37, 38]. In this model, Wnt signaling induced by Wnt3a promotes hESC survival and proliferation, but also differentiation to mesendoderm, dependent on the culture conditions. However, there is discordance in the literature regarding the activity of Wnt signaling in hESCs, where activation of canonical signaling through Wnt3a is believed to prevent differentiation, referred to as the ‘maintenance’ model [39]. Based on our observations Wnt3a functions in the ‘activation’ model to promote stem cell fate

determination. Supplementation of exogenous Wnt3a promotes hESC survival and proliferation, as well as differentiation dependent on the growth factor conditions. Addition of recombinant sFRP1 and sFRP2 in combination with Wnt3a were able to induce pluripotency marker expression, but only in EB medium in the absence of other exogenous growth factors. When supplemented into Matrigel™ matrix to generate an artificial CMTX, both sFRP1 and sFRP2 could not induce maintenance of an undifferentiated state of hESCs. These data suggest that sFRP1 and sFRP2 are not required for the maintenance of hESC pluripotency in the presence of other growth factors, such as in MEF-CM. However, based on the observation that sFRP1 and sFRP2 can regulate the expression of GSC and MIXL1, they are potentially acting to regulate Wnt induced formation of mesendoderm in differentiating hESCs.

These findings are in agreement with the current ‘activation’ type model suggested for Wnt regulation in hESCs and recent data regarding the cooperative action of the Wnt, FGF, and Activin/Nodal pathways [37]. Wnt activation in hESCs grown in the presence of a supportive growth factor environment can help promote survival and proliferation [39]. However, in MEF-CM Wnt signaling is not required for the maintenance of self-renewal or pluripotency, and cannot direct a cellular change in the presence of strong activation of the core stem cell Activin/Nodal and FGF signaling pathways [40]. In the absence of growth factor supplementation, activation of Wnt signaling promotes differentiation to mesendoderm, a process that can potentially be regulated by sFRP1 and sFRP2.

Due to the biphasic mode of activity for sFRPs as well as Wnt signaling, the ability of sFRP1 or sFRP2 to regulate hESC behavior is potentially dependent on the dynamic balance between the interacting partners [20, 41]. The recombinant protein concentrations tested in our assay may not have been optimal for sFRP activity in the presence of other Wnt regulatory proteins. Previous studies that have attempted to study the effects of sFRP supplementation on hESCs have required the use of non-physiological amounts of recombinant protein to observe a minor effect [42, 43]. The interactions between sFRP proteins and Wnt ligands may also require facilitation through binding with the ECM, as indicated by the identification of sFRP1 and sFRP2 in the CMTX. sFRP action is known to be regulated by heparin mediated binding to Wnt as well as to the ECM [20, 44]. These interacting factors may cooperate to promote hESC fate determination through regulation of Wnt ligand availability. In other cell types, the sFRP proteins have been reported to antagonize, but also augment canonical Wnt signaling [11, 45]. In the metastatic C8161 cell line we observed that sFRP1 promoted and sFRP2 inhibited their malignant potential based on colony formation in a soft-agar assay. In addition, overexpression of sFRP2 prompted a significant decrease in viable cell number. These findings are not surprising given the divergent roles for sFRP1 and sFRP2 in a variety of pathological conditions (reviewed in [17, 22]). However, based on the limited effects of sFRP1 and sFRP2 on hESC state, it is likely that other factors are combining to contribute to the dynamic regulation of the core pluripotency pathways *in vitro*.

5.4 Methods

5.4.1 Cell culture and harvest – H9 (passage 26) and CA1 (passage 20) hESCs were maintained on CF-1 irradiated mouse embryonic fibroblast (MEF) feeder layers (GlobalStem, Rockville, MD) using media composed of knockout DMEM/F12, 20% knockout serum replacement, 1% non-essential amino acids, 2 mM glutamine (CellGro, Manassas, VA), 0.1 mM 2-mercaptoethanol (Fisher, Toronto, ON), and 4 ng/mL of basic fibroblast growth factor. For feeder-free growth, conventional hESC medium that was conditioned on a layer of mouse embryonic fibroblast feeders (MEF-CM) was used with Matrigel™ (BD Biosciences, Franklin Lake, NJ) coated plates. Medium used for the induction of differentiation in CMTX experiments uses the same recipe as conventional hESC media for growth on MEF feeders as outlined above, minus basic FGF. All media reagents were obtained from Invitrogen unless noted otherwise. H9 cells were obtained from WiCell (WISC, Wisconsin). The CA1 hESC line used in all experiments was obtained from Dr. Cheryle Séguin of The University of Western Ontario [46, 47]. The hiPSC line BJ-1D was derived by reprogramming using retroviral transduction of BJ fibroblasts with the Yamanaka factors essentially as we have previously described [48] and validated as pluripotent using in vitro and in vivo differentiation assays and expression profiling (unpublished results). Cells were passaged mechanically in all experiments and for general maintenance.

Embryoid bodies (EB) were generated using Aggrewell 400Ex plates (StemCell Technologies, Vancouver, Canada). Briefly, 2 x 10^6 hESCs were harvested

enzymatically using Accutase (Invitrogen) from Matrigel™ coated plates. Cells were reconstituted in Aggrewell medium supplemented with Rock inhibitor (Y-27632, Sigma-Aldrich, St. Louis, MO) at a final concentration of 10 μM. After plating in Aggrewell dishes, EBs were grown for 48 hours at 37°C prior to transfer to ultra-low adherence tissue culture dishes (Corning, Lowell, MA). After 15 days of culture, EB RNA was harvested using Trizol extraction according to the manufacturer's instructions (Invitrogen). EBs were assayed for expression of CDX2, alpha-feto protein (AFP), GATA-6, GATA-4, Oct3/4, PAX-6, T-brachyury, Nanog, and Neurogenic differentiation 1 (NeuroD1) using TaqMan primer probe sets (Invitrogen). Assay information can be found in Appendix Table 1.15. All EB assays were performed in biological and technical duplicate for each cell line and condition.

5.4.2 sFRP Knockdown and Inhibition - sFRP2 and sFRP1 shRNA knockdown cell lines were generated using the pSUPERIOR.neo + GFP vector (Oligoengine, Seattle, USA). shRNA sequences were obtained using the shRNA design tool from Ambion. Oligos were designed to contain 5' XhoI and 3' HindIII restriction enzyme sites. All oligos were synthesized by Invitrogen unless otherwise noted. Oligos were ligated into pSUPERIOR.neo + GFP vector that was previously digested with XhoI and HindIII (New England Bioloabs, Ontario, Canada) and transformed into TOP10 chemically competent E. *coli* (Invitrogen). Transformed clones were selected based on ampicillin resistance and plasmid purified using a PureLink HiPure Midi-prep kit (Invitrogen). shRNA effectiveness was tested in HEK293 cells stably transfected with the pCAGTetRnls vector (Addgene.org). After transfection with pSUPERIOR, HEK293 cells were maintained in RPMI + 10% FBS containing 700 ng/mL puromycin and 700 μg/mL G418.

shRNA efficiency was determined after 4 days of induction using 1 µg/mL of doxycycline. Sequences for the shRNA constructs found to give the greatest decrease in specific gene expression were selected for use in hESCs. Selected shRNA sequences can be found in Appendix Table 1.16.

hESC lines were transiently transfected with GeneIn reagent (GlobalStem, Rockville, MD). H9 (p30) and CA1 (p22) hESCs were plated at ~80% confluence 24 hours prior to transfection. GeneIn reagents (1:1 mixing ratio) were combined with 4 µg of vector and supplemented into MEF-CM. hESCs were incubated in the media-transfection reagent mixture for 24 hours, followed by a second treatment for a further 24 hours. In cases where differentiation was induced, the second transfection was performed in hESC media –bFGF. Transfection efficiency was determined using flow cytometry based on detection of the GFP reported on the pSUPERIOR vector.

Inhibition of sFRP-1 was carried out using two separate small molecules obtained from Calbiochem (EMD Biosciences, Darmstadt, Germany) [32]. Inhibitors were supplemented at concentrations of 5, 10, 20, 40, and 80 µM in MEF-CM or medium that contained no bFGF. Controls were supplemented with the maximum amount of DMSO used in the experiments with inhibitors present. hESCs were grown in the presence of inhibitor for a period of 4 days during which medium was changed daily.

5.4.3 Generation of Conditioned Matrix – H9 or CA1 stem cells were grown in feeder-free conditions on Matrigel™ in MEF-CM. Stem cells were permitted to grow for a period of 5 days on Matrigel™ for generation of CMTX. Wells were then rinsed thoroughly with PBS to ensure removal of medium components and cells removed from

the Matrigel™ layer using Cell Recovery Solution according to the manufacturer's instructions (BD Biosciences). Fresh hESCs were plated on the after rinsing of the matrix layer. After 24h of culture, hESCs were induced to differentiate through feeding with conventional hESC media –bFGF. Control experiments were prepared using regular Matrigel™ that had not been conditioned but had been treated with the cell removal process.

In antibody blocking CMTX experiments, antibodies were obtained as follows: sFRP2 (Origene, Rockville, MD), sFRP1, Lefty 1, 2 (Epitomics, Burlingame, CA). Anti-rabbit IgG secondary antibody was used as a control. After cell removal from the conditioned Matrigel™, layers were rinsed with 1:1000 dilutions of manufacturer antibody stocks in 1% bovine albumin in PBS. Matrices were incubated for 2 hours at 37°C. After incubation, layers were rinsed multiple times with PBS prior to plating of fresh hESCs. In supplementation CMTX experiments, recombinant sFRP1, sFRP2, Lefty A or B, or Gremlin were added to Matrigel™ prior to polymerization at a concentration of 5 µg/mL. After incubation at 37°C for 1 hour, matrices were treated with the cell removal process and rinsed prior to playing of fresh hESCs. Recombinant sFRP1 & 2, Lefty A, and Gremlin proteins were obtained from R&D Systems (Minneapolis, MN). Recombinant Lefty B was obtained from Sigma (St. Louis, MO). In all cases, cells were fed daily with hESC media –bFGF for 3 days prior to harvest.

5.4.4 Metastatic Melanoma Cell Experimentation – C8161 cells (described in [49]) were cultured in RPMI containing 10% FBS (Invitrogen). In anchorage independent growth assays, C8161 cells were maintained in the presence or absence of 200ng/mL of

sFRP1 and sFRP2 for 4 – 7 days. At each time point, cells were harvested by trypsinization and counted. Soft-agar experiments were performed by resuspending 9,000 cells in a mixture of RPMI/10% FBS + 0.35% agarose. This mixture was plated onto a previously prepared layer of RPMI/10% FBS + 0.5% agarose in single well of a 6-well dish. Cells in soft-agar were fed every 3 days. Colonies were allowed to form for 14 days after plating. Colonies were counted after staining with 0.005% crystal violet in PBS. Soft-agar assays were performed in triplicate for each time point and condition tested.

C8161 transfections were carried out using GeneIn Reagent (GlobalStem). For each transfection, 2 µg of total DNA was diluted in 200 µL of OptiMEM with 3 µL of each GeneIn reagent. Approximately 10,000 C8161 cells were plated in a single well of a 6-well dish 24 hours prior to transfection. Cells were transfected with the pCMV-IRES-GFP-Puro (Origene, Rockville, MD) vector with or without the sFRP2 open reading frame (Origene). Transfection efficiency was monitored using GFP expression. Cells were selected using 700 ng/mL of puromycin 48 hours after transfection. Total viable cells were counted using typan blue exclusion 48 hours and 7-days post transfection. Experiments were repeated in triplicate for each treatment.

5.4.5 Real-time PCR – RNA was purified using Trizol reagent according to the manufacturer's instructions (Invitrogen) with the following modification: precipitated RNA pellets in isopropanol were centrifuged for 60 minutes at 12000 g at room temperature. After NanoDrop quantification, 1 µg of cDNA was synthesized using the High Capacity cDNA Reverse Transcription Kit with RNase inhibitor (Invitrogen). Real-time PCR was

performed using the TaqMan® Universal PCR Master Mix (Invitrogen). Samples were incubated at 50°C for 2 minutes followed by 10 minutes at 95°C. Samples were then amplified at 95°C for 15 seconds followed by 1 minute at 58°C for 46 cycles. All samples were normalized to the large ribosomal protein RPLPO as a positive control. All primers were obtained from Invitrogen and assay information can be found in Appendix Table 1.15. Each biological replicate was run in triplicate for every marker assayed. All reagents were used according to the manufacturer's instructions.

5.4.6 Immunofluorescence – Immunofluorescence was performed as described previously [50]. Briefly, cells were rinsed and fixed with 4% para-formaldehyde containing 20 mM sucrose. Fixed cells were permeabilized using 0.1% Triton-X100. Prior to staining, cells were blocked using the Dako Serum Free Protein Block solution (Dako, Cambridgeshire, UK). Oct-4 (clone 10H11.2), SSEA-4 (clone MC-813-70), and SSEA-1 (clone MC-480) primary antibodies were obtained from Millipore (Billerica, MA). Cells for Oct-4 labeling were permeabilized using a 0.1% Triton X-100 solution prior to blocking. Cells were labeled with primary antibodies for Oct-4 or SSEA-4 as undifferentiated markers and SSEA-1 for differentiated cells all at concentrations concentrations of 2 µg/mL for 60 minutes at room temperature. Secondary Alexa-fluor 488 goat anti-mouse IgG and Alexa-fluor 568 goat anti-mouse IgM were obtained from Invitrogen (Carlsbad, CA). Secondary antibodies were probed at concentrations of 1 µg/mL for 60 minutes at room temperature. All products were used according to manufacturer's instructions.

5.4.7 Flow Cytometry – All reagents and probes for flow cytometry were obtained from eBiosciences (San Diego, CA) unless noted otherwise. Cells were enzymatically harvested using Accutase (Invitrogen) to obtain a single cell suspension. After centrifugation, cell pellets were resuspended in 5% FBS in PBS. Alexa-488 conjugated SSEA-4 and Alexa-647 conjugated SSEA1 were diluted into the cell mixture according to the manufacturer's instructions. Negative control samples contained respective isotype controls for the primary antibodies used. Solutions were incubated for 2 hours and analyzed using an Accuri C6 (BD Biosciences) flow cytometer after rinsing to remove unbound antibody. Populations were gated according to forward and side scatter patterns with filtering for viable cells using 7-aminoactinomycin D staining. Data was analyzed using FlowJo software (Tree Star, Ashland, OR).

5.4.8 Immunoblotting – Harvested cell pellets were reconstituted in mammalian protein extraction reagent containing protease inhibitor cocktail (Thermo Fisher, Toronto, Canada). 20 µg of protein based on Bradford assay was run on an 8% SDS-Gel. Proteins were transferred to a PVDF membrane (Millipore) and incubated in 5% milk overnight at 4°C. After rinsing in TBS containing 0.1% Tween-20, membranes were incubated for 4 hours with primary antibodies. Oct3/4, Nanog, sFRP1, and sFRP2 antibodies were obtained from Epitomics (Burlingame, CA). β-Actin antibody was obtained from Santa Cruz Biotech (Santa Cruz, CA). After rinsing, membranes were incubated with specific HRP-conjugated secondary antibodies for 1 hour. Blots were developed using Pierce ECL reagent and CL-Xposure film (Thermo).

5.4.9 Statistical Analysis – Statistical analyses were performed using GraphPad Prism software. Results are expressed as SD or SEM as indicated in figure legends. Statistical significance was determined using one-way ANOVA with Tukey post-hoc analysis. When only two samples were being compared, unpaired Students T-tests were applied. Differences were reported as follows: * $p < 0.05$, ** $p < 0.01$, *** $p < 0.001$.

5.5 References

[1] Li, L., Xie, T., Stem cell niche: structure and function. *Annu Rev Cell Dev Biol* 2005, *21*, 605-631.
[2] Spradling, A., Drummond-Barbosa, D., Kai, T., Stem cells find their niche. *Nature* 2001, *414*, 98-104.
[3] Watt, F. M., Hogan, B. L. M., Out of Eden: Stem cells and their niches. *Science* 2000, *287*, 1427-1430.
[4] Dawson, E., Mapili, G., Erickson, K., Taqvi, S., Roy, K., Biomaterials for stem cell differentiation. *Adv Drug Deliv Rev* 2008, *60*, 215-228.
[5] Chin, A. C. P., Fong, W. J., Goh, L. T., Philp, R., Oh, S. K. W., Choo, A. B. H., Identification of proteins from feeder conditioned medium that support human embryonic stem cells. *Journal of Biotechnology* 2007, *130*, 320-328.
[6] Lim, J. W. E., Bodnar, A., Proteome analysis of conditioned medium from mouse embryonic fibroblast feeder layers which support the growth of human embryonic stem cells. *Proteomics* 2002, *2*, 1187-1203.
[7] Prowse, A. B. J., McQuade, L. R., Bryant, K. J., Marcal, H., Gray, P. P., Identification of potential pluripotency determinants for human embryonic stem cells following proteomic analysis of human and mouse fibroblast conditioned media. *Journal of Proteome Research* 2007, *6*, 3796-3807.
[8] Prowse, A. B. J., McQuade, L. R., Bryant, K. J., Van Dyk, D. D., Tuch, B. E., Gray, P. P., A proteome analysis of conditioned media from human neonatal fibroblasts used in the maintenance of human embryonic stem cells. *Proteomics* 2005, *5*, 978-989.
[9] Bendall, S. C., Hughes, C., Campbell, J. L., Stewart, M. H., Pittock, P., Liu, S*., et al.*, An enhanced mass spectrometry approach reveals human embryonic stem cell growth factors in culture. *Mol Cell Proteomics* 2009, *8*, 421-432.
[10] Kawano, Y., Kypta, R., Secreted antagonists of the Wnt signalling pathway. *J Cell Sci* 2003, *116*, 2627-2634.
[11] Galli, L. M., Barnes, T., Cheng, T., Acosta, L., Anglade, A., Willert, K*., et al.*, Differential inhibition of Wnt-3a by Sfrp-1, Sfrp-2, and Sfrp-3. *Dev Dyn* 2006, *235*, 681-690.
[12] MacDonald, B. T., Tamai, K., He, X., Wnt/beta-catenin signaling: components, mechanisms, and diseases. *Dev Cell* 2009, *17*, 9-26.
[13] Clevers, H., Wnt/beta-catenin signaling in development and disease. *Cell* 2006, *127*, 469-480.
[14] Jones, S. E., Jomary, C., Secreted Frizzled-related proteins: searching for relationships and patterns. *Bioessays* 2002, *24*, 811-820.
[15] Hoang, B., Moos, M., Jr., Vukicevic, S., Luyten, F. P., Primary structure and tissue distribution of FRZB, a novel protein related to Drosophila frizzled, suggest a role in skeletal morphogenesis. *J Biol Chem* 1996, *271*, 26131-26137.
[16] Leyns, L., Bouwmeester, T., Kim, S. H., Piccolo, S., DeRobertis, E. M., Frzb-1 is a secreted antagonist of Wnt signaling expressed in the Spemann organizer. *Cell* 1997, *88*, 747-756.
[17] Bovolenta, P., Esteve, P., Ruiz, J. M., Cisneros, E., Lopez-Rios, J., Beyond Wnt inhibition: new functions of secreted Frizzled-related proteins in development and disease. *J Cell Sci* 2008, *121*, 737-746.
[18] Chong, J. M., Uren, A., Rubin, J. S., Speicher, D. W., Disulfide bond assignments of secreted Frizzled-related protein-1 provide insights about Frizzled homology and netrin modules. *J Biol Chem* 2002, *277*, 5134-5144.
[19] Roszmusz, E., Patthy, A., Trexler, M., Patthy, L., Localization of disulfide bonds in the frizzled module of Ror1 receptor tyrosine kinase. *J Biol Chem* 2001, *276*, 18485-18490.
[20] Uren, A., Reichsman, F., Anest, V., Taylor, W. G., Muraiso, K., Bottaro, D. P*., et al.*, Secreted frizzled-related protein-1 binds directly to Wingless and is a biphasic modulator of Wnt signaling. *J Biol Chem* 2000, *275*, 4374-4382.
[21] Banyai, L., Patthy, L., The NTR module: domains of netrins, secreted frizzled related proteins, and type I procollagen C-proteinase enhancer protein are homologous with tissue inhibitors of metalloproteases. *Protein Sci* 1999, *8*, 1636-1642.
[22] Esteve, P., Bovolenta, P., The advantages and disadvantages of sfrp1 and sfrp2 expression in pathological events. *Tohoku J Exp Med* 2010, *221*, 11-17.
[23] Sokol, S. Y., Maintaining embryonic stem cell pluripotency with Wnt signaling. *Development* 2011, *138*, 4341-4350.

[24] Adewumi, O., Aflatoonian, B., Ahrlund-Richter, L., Amit, M., Andrews, P. W., Beighton, G.*, et al.*, Characterization of human embryonic stem cell lines by the International Stem Cell Initiative. *Nat Biotechnol* 2007, *25*, 803-816.
[25] Boyer, L. A., Lee, T. I., Cole, M. F., Johnstone, S. E., Levine, S. S., Zucker, J. P.*, et al.*, Core transcriptional regulatory circuitry in human embryonic stem cells. *Cell* 2005, *122*, 947-956.
[26] Hendrix, M. J., Seftor, E. A., Seftor, R. E., Kasemeier-Kulesa, J., Kulesa, P. M., Postovit, L. M., Reprogramming metastatic tumour cells with embryonic microenvironments. *Nat Rev Cancer* 2007, *7*, 246-255.
[27] Postovit, L. M., Margaryan, N. V., Seftor, E. A., Kirschmann, D. A., Lipavsky, A., Wheaton, W. W.*, et al.*, Human embryonic stem cell microenvironment suppresses the tumorigenic phenotype of aggressive cancer cells. *Proc Natl Acad Sci U S A* 2008, *105*, 4329-4334.
[28] Kim, M. O., Kim, S. H., Oi, N., Lee, M. H., Yu, D. H., Kim, D. J.*, et al.*, Embryonic stem-cell-preconditioned microenvironment induces loss of cancer cell properties in human melanoma cells. *Pigment Cell Melanoma Res* 2011, *24*, 922-931.
[29] Costa, F. F., Seftor, E. A., Bischof, J. M., Kirschmann, D. A., Strizzi, L., Arndt, K.*, et al.*, Epigenetically reprogramming metastatic tumor cells with an embryonic microenvironment. *Epigenomics* 2009, *1*, 387-398.
[30] Norrman, K., Fischer, Y., Bonnamy, B., Wolfhagen Sand, F., Ravassard, P., Semb, H., Quantitative comparison of constitutive promoters in human ES cells. *PLoS One* 2010, *5*, e12413.
[31] Zafarana, G., Avery, S. R., Avery, K., Moore, H. D., Andrews, P. W., Specific knockdown of OCT4 in human embryonic stem cells by inducible short hairpin RNA interference. *Stem Cells* 2009, *27*, 776-782.
[32] Gopalsamy, A., Shi, M., Stauffer, B., Bahat, R., Billiard, J., Ponce-de-Leon, H.*, et al.*, Identification of diarylsulfone sulfonamides as secreted frizzled related protein-1 (sFRP-1) inhibitors. *J Med Chem* 2008, *51*, 7670-7672.
[33] Bakre, M. M., Hoi, A., Mong, J. C., Koh, Y. Y., Wong, K. Y., Stanton, L. W., Generation of multipotential mesendodermal progenitors from mouse embryonic stem cells via sustained Wnt pathway activation. *J Biol Chem* 2007, *282*, 31703-31712.
[34] Tada, S., Era, T., Furusawa, C., Sakurai, H., Nishikawa, S., Kinoshita, M.*, et al.*, Characterization of mesendoderm: a diverging point of the definitive endoderm and mesoderm in embryonic stem cell differentiation culture. *Development* 2005, *132*, 4363-4374.
[35] Izumi, N., Era, T., Akimaru, H., Yasunaga, M., Nishikawa, S., Dissecting the molecular hierarchy for mesendoderm differentiation through a combination of embryonic stem cell culture and RNA interference. *Stem Cells* 2007, *25*, 1664-1674.
[36] Postovit, L. M., Seftor, E. A., Seftor, R. E., Hendrix, M. J., A three-dimensional model to study the epigenetic effects induced by the microenvironment of human embryonic stem cells. *Stem Cells* 2006, *24*, 501-505.
[37] Dravid, G., Ye, Z., Hammond, H., Chen, G., Pyle, A., Donovan, P.*, et al.*, Defining the role of Wnt/beta-catenin signaling in the survival, proliferation, and self-renewal of human embryonic stem cells. *Stem Cells* 2005, *23*, 1489-1501.
[38] Cai, L., Ye, Z., Zhou, B. Y., Mali, P., Zhou, C., Cheng, L., Promoting human embryonic stem cell renewal or differentiation by modulating Wnt signal and culture conditions. *Cell Res* 2007, *17*, 62-72.
[39] Sato, N., Meijer, L., Skaltsounis, L., Greengard, P., Brivanlou, A. H., Maintenance of pluripotency in human and mouse embryonic stem cells through activation of Wnt signaling by a pharmacological GSK-3-specific inhibitor. *Nat Med* 2004, *10*, 55-63.
[40] Singh, Amar M., Reynolds, D., Cliff, T., Ohtsuka, S., Mattheyses, Alexa L., Sun, Y.*, et al.*, Signaling Network Crosstalk in Human Pluripotent Cells: A Smad2/3-Regulated Switch that Controls the Balance between Self-Renewal and Differentiation. *Cell Stem Cell* 2012, *10*, 312-326.
[41] Naito, A. T., Shiojima, I., Akazawa, H., Hidaka, K., Morisaki, T., Kikuchi, A.*, et al.*, Developmental stage-specific biphasic roles of Wnt/beta-catenin signaling in cardiomyogenesis and hematopoiesis. *Proc Natl Acad Sci U S A* 2006, *103*, 19812-19817.
[42] Jones, M. B., Chu, C. H., Pendleton, J. C., Betenbaugh, M. J., Shiloach, J., Baljinnyam, B.*, et al.*, Proliferation and pluripotency of human embryonic stem cells maintained on type I collagen. *Stem Cells Dev* 2010, *19*, 1923-1935.

[43] Villa-Diaz, L. G., Pacut, C., Slawny, N. A., Ding, J., O'Shea, K. S., Smith, G. D., Analysis of the Factors that Limit the Ability of Feeder Cells to Maintain the Undifferentiated State of Human Embryonic Stem Cells. *Stem Cells and Development* 2009, *18*, 641-651.
[44] Lee, J. L., Lin, C. T., Chueh, L. L., Chang, C. J., Autocrine/paracrine secreted Frizzled-related protein 2 induces cellular resistance to apoptosis: a possible mechanism of mammary tumorigenesis. *J Biol Chem* 2004, *279*, 14602-14609.
[45] von Marschall, Z., Fisher, L. W., Secreted Frizzled-related protein-2 (sFRP2) augments canonical Wnt3a-induced signaling. *Biochem Biophys Res Commun* 2010, *400*, 299-304.
[46] Seguin, C. A., Draper, J. S., Nagy, A., Rossant, J., Establishment of endoderm progenitors by SOX transcription factor expression in human embryonic stem cells. *Cell Stem Cell* 2008, *3*, 182-195.
[47] Peerani, R., Rao, B. M., Bauwens, C., Yin, T., Wood, G. A., Nagy, A.*, et al.*, Niche-mediated control of human embryonic stem cell self-renewal and differentiation. *EMBO J* 2007, *26*, 4744-4755.
[48] Hotta, A., Cheung, A. Y., Farra, N., Garcha, K., Chang, W. Y., Pasceri, P.*, et al.*, EOS lentiviral vector selection system for human induced pluripotent stem cells. *Nat Protoc* 2009, *4*, 1828-1844.
[49] Welch, D. R., Bisi, J. E., Miller, B. E., Conaway, D., Seftor, E. A., Yohem, K. H.*, et al.*, Characterization of a highly invasive and spontaneously metastatic human malignant melanoma cell line. *Int J Cancer* 1991, *47*, 227-237.
[50] Hughes, C. S., Radan, L., Betts, D., Postovit, L. M., Lajoie, G. A., Proteomic analysis of extracellular matrices used in stem cell culture. *Proteomics* 2011, *11*, 3983-3991.

Chapter 6

Discussion

6.1 Summary of Accomplishments

It is clear that the microenvironment plays a critical role in the regulation of hESC fate. Central to the potential application of hESCs in therapeutic applications are advances in controlled methods for modulating the pluripotent state. Paramount for development is increasing our knowledge of the processes eliciting control in this dynamic environment. To obtain a complete understanding of the *in vitro* stem cell niche, analysis of soluble and ECM contributors to this environment is necessary. Due to the complex requirements for the *in vitro* maintenance of hESCs, direct analysis of the ECM presents a significant challenge. To this end, we have developed proteomic methodologies for the direct study of the ECM portion of the microenvironment (Chapters 2 – 3). Additionally, we have demonstrated the application of these methods to the analysis of this complex environment, and in doing so have elucidated novel factors involved in hESC regulation (Chapters 4-5).

This chapter contains excerpts from the following paper:

Hughes, C.S., Radan, L., Stanford, W., Betts, D., Postovit, L.M., Lajoie, G.. (2012) “Mass Spectrometry-Based Proteomics Analysis of the Matrix Microenvironment in Pluripotent Stem Cell Culture”. (In Preparation)

The complexity of Matrigel™ necessitates the use of quantitative proteomics techniques to study the ECM portion of the microenvironment. To this end, we have developed conditions for the application of the metabolic labeling approach, SILAC, to hESCs (Chapter 2). This new protocol eliminates conversion of isotopically labeled arginine amino acids to proline derivatives and represents a significant increase in simplicity and reduction in cost when compared with alternative methods for addressing this conversion. We also further extend our SILAC approach to a defined hESC media formulation. This defined alternative offers an attractive platform for the study of the microenvironment free of contaminating contributions from MEF feeder layers present in conditioned medium. Furthermore, the extension of this defined medium to the growth of hiPSCs presents new opportunities for the quantitative study of stem cell biology.

A secondary challenge for the analysis of the ECM portion of the microenvironment is the protein complexity of these matrices. MS-based proteomics studies consistently struggle to identify the low-abundance components of complex mixtures in the face of a large dynamic range of protein concentration. This is further complicated with ECM mixtures due to their propensity to polymerize when not chilled. Although our quantitative SILAC strategy would enable distinction between hESC and Matrigel derived proteins, the presence of candidates derived from both sources significantly increases the complexity of the CMTX solution. In order to facilitate the detection of low abundance hESC derived proteins, we have shown the benefits of using a combination of conventional proteomics techniques (Chapter 3). Upon application for the analysis of Matrigel and other cell-derived matrices, we successfully achieve significant depth of coverage in these complex samples. Furthermore, we illustrated the utility of analyzing

matrices used in stem cell culture for the elucidation of components critical for the maintenance of hESC pluripotency.

Finally, through application of the SILAC (Chapter 2) and ECM analysis methodologies (Chapter 3), we obtained a proteomic profile of a matrix layer preconditioned by hESCs (Chapter 4). We then reconcile proteomic datasets from the soluble and ECM portions of the microenvironment previously obtained. Investigation of the CMTX revealed that hESCs generate a self-sustaining niche rich in supportive factors found in Matrigel, as well as in conditioned medium. Functional validation of candidate factors illustrates the complexity of hESC-ECM interactions (Chapter 5). Taken together, these studies will aid in the development of tools for studying the complex interactions between hESCs and their microenvironment.

6.2 The hESC Niche and the ECM

One of the primary goals of research focused on the microenvironment is to elucidate all the processes involved in the control of hESC fate. The ability to control if a stem cell self-renews or differentiates is critical to the potential therapeutic application of hESCs. Parallel to this need is the ability to direct lineage specific differentiation to generate pure populations of tissue-specific cell types. Currently, hESC differentiation is directed through the use of cocktails of exogenously supplemented growth factors (reviewed in [1]). Depending on the desired cell type, multiple differing cocktails can be required dependent on the time point of the differentiation protocol [2]. Which factors are supplemented is conventionally determined through large screens of proteins involved in pathways that are known to be critical for the regulation of pluripotency. However,

many of these generated protocols struggle to produce pure populations of tissue-specific cell types. This shortcoming stems from an incomplete understanding of all of the processes contributing to hESC control within the *in vitro* microenvironment. As we have shown in this thesis, these processes can potentially be governed by interactions of hESCs or cytokines with the ECM.

6.2.1 Wnt Signaling in the Microenvironment

There are three primary pathways that are activated upon binding of Wnt ligands to their cognate receptors (For a review of Wnt signaling, see [3, 4]). The canonical pathway involves interaction of Wnt ligands at the cell surface with Frizzled (Fz)/low-density lipoprotein receptor-related protein (LRP) complexes. In the absence of Wnt, cytoplasmic β-catenin is associated with a complex containing Axin and Adenomatous Polyposis Coli (APC). This complex facilitates the phosphorylation of β-catenin by glycogen synthase kinase 3-β (GSK-3β) resulting in its subsequent degradation. Upon binding of Wnt ligands, phosphorylation of β-catenin is inhibited allowing it to translocate to the nucleus where it regulates gene expression through interaction with lymphoid enhancer factor (LEF)/T-cell factor (TCF) transcription factors.

In the extracellular space, Wnt proteins are relatively insoluble due to the presence of a palmitoyl lipid modification. This modification has been shown to be important for the secretion, activity, and solubility of Wnt proteins as well as for their interactions with binding partners [5]. In the extracellular space Wnt signaling is antagonized through interactions with a variety of inhibitors (reviewed in [6]). The two main groups are the soluble frizzled related proteins (sFRP) and the Dikkopf (Dkk) family. Dkk proteins are

believed to inhibit canonical Wnt signaling through interaction with the LRP receptors [6]. The sFRP family is thought to bind directly to the Wnt ligands themselves, leading to a diverse array of potential roles for these proteins other than antagonism. This is emphasized by the multiple divergent roles for the sFRP family members in a variety of pathological conditions (reviewed in [7, 8]).

In mouse ESCs, activation of the canonical Wnt pathway is understood to promote the maintenance of self-renewal and pluripotency (reviewed in [9]). In human ESCs, the picture is less clear, and contrasting roles for canonical Wnt signaling have been suggested [10, 11]. However, recent data has garnered support for a model of Wnt signaling activation that supports stem cell fate determination [12, 13]. Activation of canonical Wnt signaling enhances hESC growth and survival in an undifferentiated state, as well as their differentiation. However, aberrant regulation of the canonical pathway is thought to be involved in diseases such as cancer [3]. Therefore, control over the activity of Wnt ligands in the extracellular space is potentially critical for the proper maintenance of the ES cell phenotype.

From our analysis it remains unclear what role the sFRP proteins play in the regulation of Wnt signaling in the extracellular space and the resultant changes in hESC phenotype (Chapter 5). shRNA mediated knockdown of sFRP1 or 2 gene expression or direct inhibition of sFRP1 protein using a small molecule inhibitor results in no change in expression for Oct3/4 and Nanog, hallmarks of pluripotency. Based on our findings with direct supplementation of soluble recombinant Wnt3a, it is clear that Wnt3a promotes stem cell fate determination dependent on the growth factor microenvironment. sFRP1

and sFRP2 are unable to inhibit Wnt3a induced changes when supplemented in MEF-CM. These data are potentially confounded by the presence of numerous other Wnt regulatory proteins in both hESC conditioned medium [14] and in the CMTX (Chapter 4-5), such as Cerberus. The reduction of sFRP activity through small molecule inhibition or shRNA knockdown is potentially compensated for by these other regulatory proteins or increased activity of additional sFRP family members. The effects of direct supplementation of sFRP1 and sFRP2 are also potentially reduced in this way, where other proteins can restore the proper balance of Wnt activity. The complexity and cross-talk in signaling pathways present in the microenvironment suggests that a combination of factors act on hESCs. This is highlighted by the results of our proteomics screen where other antagonists of core pluripotency pathways were identified.

6.2.2 TGF-β Signaling in the Microenvironment

In the MS-based proteomics screen of CMTX we identified factors implicated in the regulation of TGF-β pathways, specifically Lefty 1 and 2 and Cerberus proteins (Chapter 4). The TGF-β superfamily of proteins consists of over 30 members, including Activins, Nodal, and bone morphogenic proteins (BMP). TGF-β family members are directly involved in processes such as cell growth and apoptosis. Furthermore, this family has been implicated as playing a prominent role during embryonic development in processes such as gastrulation and patterning (reviewed in [15]). TGF-β signaling primarily operates via transmission of extracellular signals through complexes of type-I (activin receptor-like kinases, e.g. ALK4, ALK7) and type-II (activin receptor IIB,

ActRIIB) transmembrane receptors and their associated co-factors (e.g. Cripto). These signals are translated to phosphorylation events in different complexes of Smad proteins that in turn regulate target gene expression in the nucleus (reviewed in [15]).

TGF-β signaling is mediated through interactions between soluble factors in the microenvironment. The Lefty proteins are extracellular antagonists of TGF-β signaling that act through inhibition of the embryonic morphogen Nodal [16]. Regulation of Nodal activity through inhibition by Lefty has been shown to be critical for proper development during embryogenesis [16]. In hESCs, activation of the Smad2/3 branch of the TGF-β pathway mediated by Nodal or Activin is known to be one of the core processes critical for the maintenance of self-renewal and pluripotency [17, 18]. Defined media such as E8 and the defined SILAC medium employed here contain exogenous Activin or Nodal to facilitate the maintenance of undifferentiated hESCs [19, 20]. Activin has also been found in MEF conditioned medium screened using MS-based proteomics [14, 21]. Inhibition of Lefty proteins has been shown to promote maintenance of undifferentiated hESCs; however, correct differentiation of these cells is impaired [22]. Interestingly however, inhibition of Nodal using Lefty does not induce differentiation of hESCs [18]. Moreover, induction of Lefty has been observed to be important for exit from the pluripotent state in embryoid body formation assays [23]. Taken together, these findings indicate that Lefty functions to maintain a balance of Nodal induced TGF-β initiation in hESCs.

Detection of Lefty isoforms in CMTX illustrates that hESCs are secreting factors to generate a matrix microenvironment designed to regulate extracellular signaling

involving soluble factors. Although the direct supplementation of recombinant Lefty was not able to enhance the maintenance of an undifferentiated state in hESCs induced to differentiate, regulation of Nodal signaling by Lefty in the microenvironment has previously been observed to be facilitated through interactions with the ECM [24]. In *Xenopus* embryos, the interaction of Lefty with ECM linked heparan sulfate proteoglycans has been observed to facilitate control over Nodal signaling [24]. The ECM enhances the stability, transport, and effective range of the Lefty and Nodal proteins [24]. These effects aid in the generation of morphogen gradients important for proper development. Similar processes in the microenvironment potentially contribute to maintenance of a 'primed' hESC state, wherein control over differentiation is enhanced by interactions between Lefty and Nodal facilitated by the ECM.

The ability of Lefty containing CMTX to enhance maintenance of an undifferentiated state is potentially acting through pathways alternative to Nodal induced TGF-β activation. The positive effects of Nodal signaling on hESCs are well established [17, 18]. However, exogenous supplementation with Lefty does not induce differentiation of hESCs [18]. Expression of Nodal and Lefty proteins are known to be rapidly decreased following the induction of differentiation [25]. The presence of Lefty in the CMTX and the absence of hESC derived Nodal following differentiation potentially confer an enhancement in the maintenance of undifferentiated cells through other TGF-β pathways. BMP signaling through Smad 1/5/8 is observed to be increased specifically in differentiated hESCs [25]. Moreover, BMP signaling induced by the extracellular cytokine BMP-4 is known to induce differentiation of hESCs, and its inhibition using antagonists such as Noggin to block differentiation [26, 27]. Lefty has been observed to

inhibit BMP-4 induced TGF-β activation by blocking the phosphorylation of Smad proteins in P19 embryonal carcinoma cells [28]. In our CMTX experiments, Lefty may be acting on BMP-4 induced TGF-β signaling and thereby inhibiting differentiation resulting from activation of this pathway. This is highlighted by the presence of other factors in the CMTX that inhibit Nodal/BMP signaling, such as Cerberus.

6.2.3 New View of the hESC Microenvironment

Using the assays presented here we observed the ability of the CMTX, containing regulators of the Wnt and TGF-β pathways, to alter the behavior of hESCs in the microenvironment. However, in our recombinant and antibody blocking CMTX experiments, both of these pathways were monitored individually and neither was able to fully recapitulate the positive effect observed for hESCs on CMTX. The microenvironment is considered to be an effector of cellular change acting through a dynamic balance resulting from an array of contributors. As such, it is likely that the core pathways we have investigated here function together in the CMTX to generate the observed effect. Indeed, multiple levels of cross-talk have been suggested amongst the FGF/TGF-β/Wnt pathways [13, 29]. In hESCs, the maintenance of self-renewal and pluripotency is controlled by the co-operative activity of these three core pathways. The addition of the ECM to this model adds an additional layer of complexity, wherein proteins bound to the matrix can act to regulate individual pathways, the effects of which are subsequently potentiated through cross-talk with others. Given the known roles of the ECM in the contribution to the generation of morphogen gradients in other

developmental systems, it is not hard to envision a similar activity regulating pluripotency in the hESC niche.

6.3 Development of ECM Environments for hESCs

The ECM is one of the core elements governing cellular changes in the microenvironment. Not only can the ECM regulate cell growth, attachment, and movement, but in hESC culture can affect processes such as differentiation. The beneficial effects of the ECM are further highlighted by the positive outcome observed when *in vivo* injections directed at teratoma formation are performed using hESCs diluted in Matrigel™ [30]. The proposed mechanism for the enhancement observed in the presence of Matrigel™ is related to the reduction of apoptosis through interactions with the ECM and the potential for Matrigel to induce growth factor stimulation [30]. The xenogenic nature of Matrigel inhibits its use with injections or otherwise in potential therapeutic strategies. Developing an understanding of the processes and factors regulated by the components of Matrigel, or other hESC supportive matrices will aid in the generation of xeno-free matrices for use *in vitro* or *in vivo*.

Using the techniques presented in this thesis, analysis of the diverse range of matrices available for hESC culture will assist in the development of ECM supports suitable for a wide range of hESCs. Using MS-based proteomics we demonstrate the utility of determining the composition of cell-derived and recombinant growth matrices used in hESC culture (Chapter 3). From these studies we were able to elucidate factors directly related to the enhancement of hESC growth in *in vitro* culture. Moreover, using the methods developed and optimized here to facilitate the analysis of hESC-derived

matrices, we were able to characterize a novel self-supportive matrix microenvironment generated by the stem cells during growth *in vitro*. The findings of these works will have a direct application towards obtaining a comprehensive understanding of hESC interactions within the microenvironment. Perhaps more importantly however, the information contained in this thesis can be used to aid in the development of biomaterials designed to mimic the ECM.

In recent years, as a direct result of the potential for the application of stem cells in therapeutic applications, numerous biomaterials have been tested for their viability for the maintenance of hESCs (reviewed in [31]). Natural materials such as collagen, hyaluronic acid, and alginate have all shown promise for the control of self-renewal or differentiation of stem cells [32-34]. Synthetic materials such as PLGA and PEG have also been utilized to control the properties of stem cells *in vitro* (reviewed in [35]). Pioneering work from the Langer group was one of the first studies to analyze hESC-ECM interactions on a large-scale using synthetic polymer based arrays [36, 37]. Utilizing different combinations of acrylate, diacrylate, dimethacrylate, and triacrylate monomers, they profile over 1700 ECM interactions in a single array. In recent years, nano-scale array platforms that utilize conventional DNA spotting technology have facilitated the analysis of a wide range of biomaterials for their effect on stem cell maintenance and differentiation [38-42]. The designs of polymers or bioactive materials to be screened are typically done in a discovery type fashion, or through mimicry of known cell-ECM interactions. Elucidating core ECM factors present in cell-derived matrices can potentially aid in directing these array-based screens. By focusing on

matrices known to be beneficial for stem cell maintenance, factors identified in our proteomics screen can be used to generate biomaterials tailored for hESCs.

Aside from the ability to regulate the activity of these matrices through modulation of properties such as stiffness, size, and shape, other physical modifications can be made to promote the desired experimental outcome [35]. The addition of bioactive growth factors directly to the polymerized matrix has been used to modulate the self-renewal and differentiation of hESCs [43, 44]. Controlling the availability of these growth factors can be regulated through the addition of compounds such as heparan sulfate to the matrix [35]. Based on the findings presented here, the presence of multiple soluble growth factor binding and regulatory proteins in the matrix can regulate the differentiation of stem cells. By determining the pathways that are potentially regulated by candidate proteins identified in the CMTX, our proteomic analyses can aid in the development of biomaterials that mimic the necessary binding or cytokine requirements. Furthermore, investigating components of hESC-derived matrix microenvironments as we have attempted to do here can be completed on defined matrices instead of Matrigel. The ability to control the deposition and release of bioactive growth factors from the matrix through the use of synthetic alternatives will permit direct validation of deposited factors. Together, these complementary studies would be beneficial for determining ECM-associated regulatory proteins that can be combined with biomaterials to control pathways related to self-renewal and differentiation.

6.4 Studying hESCs using Quantitative Proteomics

With the increase in research focused on ESCs, the number of developmentally related cell types that can be successfully cultured *in vitro* is rising. It is clear that comparison of pluripotent or multipotent progenitor cells with differentiated sub-types can provide valuable information on stem cell regulation. The application of high-throughput genomic technologies in these areas has already resulted in advancement in our understanding of stem cells. However, global screening using proteomics methods has lagged behind, partially due to the difficulty in achieving cell quantities amenable to these experiments. This is particularly difficult for hESCs due to their strict culture requirements.

Application of metabolic labeling approaches such as SILAC opens new avenues for performing comparative analyses of multipotent and differentiated cell types. Utilization of our SILAC protocol provides researchers with the tools necessary to acquire the quantities of cells required, in a reproducible fashion, for proteomics experiments. Currently there is only one other example of a defined hESC culture medium amenable to SILAC experimentation presented in the literature [45]. However, as the efficiency of methods for the *in vitro* culture of hESCs continues to increase, so too will the development of enhanced media for their culture. This is highlighted by recent work from the Thomson lab where they systematically tested individual medium components to assess their necessity for the maintenance of hESCs and hiPSCs [20]. They demonstrated that the SCs could be maintained for extended periods in media containing just eight ingredients, referred to as E8 (insulin, selenium, transferrin,

l-ascorbic acid, FGF2 and TGF-β (or Nodal) in DMEM/F12). E8 has the added benefit of being serum-free, offering an attractive platform for the analysis of conditioned media from hESCs grown in feeder-free conditions. As we have demonstrated here (Chapter 2), the adaption of chemically defined culture media such as E8 to SILAC experimentation can be achieved simply by modulating the amino acid composition, even for metabolically sensitive cell types such as hESCs.

Outside of direct comparisons of pluripotent and differentiated cell types, quantitative proteomics methods like SILAC offer many other attractive research avenues in the study of hESC biology. An emerging area where quantitative mass spectrometry approaches have a direct application is in the analysis of global protein turnover in hESCs. The metabolic incorporation of the SILAC label permits time-dependent analysis of protein synthesis and degradation rates, analogous to a pulse-chase style experiment [46]. Currently there are no examples of the direct analysis of protein turnover on a global scale in mouse or human ESCs. The most comprehensive proteomics studies of hESCs and hiPSCs to date have focused on measuring abundance snapshots [47]. Recent work from the Selbach lab has demonstrated the utility of measuring protein and mRNA degradation rates to obtain a picture of global cell regulation as a function of turnover [48].

It is not hard to envision the potential applications for SILAC derived turnover measurements in hESCs or their niches. Direct examination of the pathways that feed into the maintenance of homeostasis through modulation of the synthesis and degradation of proteins on a global scale can potentially clarify the mechanisms

governing pluripotency of hESCs and preservation of a state primed for differentiation. Furthermore, metabolic labeling with SILAC can be used to unlock the potential mechanisms that regulate the switch from a primed state to differentiation in stem cell populations. When coupled with established methods for measuring mRNA turnover [49], or high-resolution screens of global translation rates using ribosome density profiling [50], the potential acquisition of a global measurement of hESC control makes the application of SILAC protocols such as those developed here (Chapter 2) an attractive platform in stem cell research. Additionally, coupling these quantitative proteomics analysis platforms to investigation of hESC niches offers the opportunity to monitor temporal signaling patterns as indicated by differential protein levels in conditioned media or matrices.

6.5 Future Applications in Stem Cell Research

6.5.1 Niches from other stem cells

The hESC niche represents a dynamic environment that is critical for control over decisions concerning cell fate and its analysis is crucial for a complete understanding of pluripotency. However, the recent expansion of research involving adult stem cells (ASC) offers new opportunities for studies directed at investigation of the microenvironment. Furthermore, the rapid expansion of derived induced pluripotent stem (iPS) cells from a variety of tissue and disease types offers interesting new avenues for study of the microenvironment. The analysis of CMTX completed here (Chapter 4) was performed on a single iPS cell line. Our findings indicate significant similarity between the hESC and iPS cell derived matrices analyzed. However, due to

the distinct differences between iPS lines dependent on their derivation method or parental cell origin [51, 52] (reviewed in [53]), expansion of our analysis to include other lines is desirable.

The application of quantitative proteomic methodologies such as those developed here (Chapter 2) also offer interesting avenues for continuing exploratory studies in stem cell niches *in vitro*. The induction of pluripotency in iPS cells is known to take upwards of 30 days following transgene expression in culture [54]. Quantitative changes of protein turnover during reprogramming coupled with temporal examination of secreted factors in the niche would provide valuable insight into processes contributing to the induction of pluripotency. The assessment of expression patterns during reprogramming of candidate proteins identified in this thesis (Chapter 4) could reveal valuable information on factors such as the sFRP, Cerberus, and Lefty proteins. With the previous knowledge that these proteins function at the crossroads of the undifferentiated and differentiated state, their examination during reprogramming could reveal distinct expression patterns that contribute to pluripotency. Additionally, these trends can be compared to data generated in this and other studies of the microenvironment to characterize their correlation to known roles in hESCs.

6.5.2 Addressing heterogeneity in stem cell cultures

Two of the core components of the microenvironment are the ECM support and paracrine/autocrine signaling regulated by soluble factors. In the hESC niche this can be expanded to include accessory or support cells that contribute to processes involved with both of the previously mentioned core components. In two-dimensional adherent

cultures *in vitro* hESCs tend to grow as tight aggregates. hESCs are refractory to passaging or maintenance as single cells. Within these cell clusters, recent work has observed the ability of hESCs to generate colony specific niches that contain signaling gradients that effect core pluripotency pathways [55]. These findings suggest that a level of cellular heterogeneity exists within hESC cultures and even within specific colonies. The non-homogeneous nature of stem cell culture has been noted before in the literature [56-60]. This variability can be the result of differences in cell cycle progression as well as spontaneous differentiation. Even in a wholly undifferentiated population, differences in core pluripotency genes such as Nanog have been observed [61]. Considering the ability of the microenvironment to elicit changes in cell behavior, differences in hESC colony specific niches can potentially be a significant contributor to this heterogeneity. By collecting data that represents an average of a heterogeneous population, the potential sensitivity of the results is limited as changes represented in a sub-type of cells will be diluted. Therefore, developing methods directed at monitoring hESC characteristics at a single-cell level are critical for in-depth microenvironment analysis.

Recent developments in methods for single-cell monitoring of global processes such as transcription and translation offer new avenues for stem cell research (reviewed in [62, 63]). Furthermore, with the development of methods for high-throughput analysis of matrices using spotted arrays (see Section 5.3), single-cell analysis of the hESC niche is now potentially viable. As such, studies directed at single-cell analysis of behavior patterns in hESC niches have been presented [55]. The work presented here offers potential extensions for modeling of single-cells in hESC niches. Using factors

identified in our proteomic characterizations of matrices (Chapter 3 – 4) in combination with micropatterning techniques for generating ECM arrays, the activity of single cells within colonies in response to seeded gradients of deposited factors could be assayed. Arrays such as these can potentially reveal the specific regulatory mechanisms of factors identified in our analysis of CMTX, such as the sFRP and Lefty proteins. The expression of Lefty B has previously been observed to change dependent on hESC colony size, indicating the potentially dynamic nature of these inhibitors [55]. Furthermore, the established gradient signaling mechanisms of both the Wnt and Nodal pathways in development indicate that a similar process may be occurring *in vitro* in the hESC niche. The ability to perform directed screens based off of factors identified in our study coupled with high-resolution single-cell data acquisition offers an attractive platform for addressing key questions concerning the hESC microenvironment.

6.6 References

[1] Trounson, A., The production and directed differentiation of human embryonic stem cells. *Endocrine Reviews* 2006, *27*, 208-219.
[2] D'Amour, K. A., Bang, A. G., Eliazer, S., Kelly, O. G., Agulnick, A. D., Smart, N. G.*, et al.*, Production of pancreatic hormone-expressing endocrine cells from human embryonic stem cells. *Nat Biotechnol* 2006, *24*, 1392-1401.
[3] Clevers, H., Wnt/beta-catenin signaling in development and disease. *Cell* 2006, *127*, 469-480.
[4] MacDonald, B. T., Tamai, K., He, X., Wnt/beta-catenin signaling: components, mechanisms, and diseases. *Dev Cell* 2009, *17*, 9-26.
[5] Mulligan, K. A., Fuerer, C., Ching, W., Fish, M., Willert, K., Nusse, R., Secreted Wingless-interacting molecule (Swim) promotes long-range signaling by maintaining Wingless solubility. *Proc Natl Acad Sci U S A* 2011, *109*, 370-377.
[6] Kawano, Y., Kypta, R., Secreted antagonists of the Wnt signalling pathway. *J Cell Sci* 2003, *116*, 2627-2634.
[7] Bovolenta, P., Esteve, P., Ruiz, J. M., Cisneros, E., Lopez-Rios, J., Beyond Wnt inhibition: new functions of secreted Frizzled-related proteins in development and disease. *J Cell Sci* 2008, *121*, 737-746.
[8] Esteve, P., Bovolenta, P., The advantages and disadvantages of sfrp1 and sfrp2 expression in pathological events. *Tohoku J Exp Med* 2010, *221*, 11-17.
[9] Sokol, S. Y., Maintaining embryonic stem cell pluripotency with Wnt signaling. *Development* 2011, *138*, 4341-4350.
[10] Dravid, G., Ye, Z., Hammond, H., Chen, G., Pyle, A., Donovan, P.*, et al.*, Defining the role of Wnt/beta-catenin signaling in the survival, proliferation, and self-renewal of human embryonic stem cells. *Stem Cells* 2005, *23*, 1489-1501.
[11] Sato, N., Meijer, L., Skaltsounis, L., Greengard, P., Brivanlou, A. H., Maintenance of pluripotency in human and mouse embryonic stem cells through activation of Wnt signaling by a pharmacological GSK-3-specific inhibitor. *Nat Med* 2004, *10*, 55-63.
[12] Cai, L., Ye, Z., Zhou, B. Y., Mali, P., Zhou, C., Cheng, L., Promoting human embryonic stem cell renewal or differentiation by modulating Wnt signal and culture conditions. *Cell Res* 2007, *17*, 62-72.
[13] Singh, Amar M., Reynolds, D., Cliff, T., Ohtsuka, S., Mattheyses, Alexa L., Sun, Y.*, et al.*, Signaling Network Crosstalk in Human Pluripotent Cells: A Smad2/3-Regulated Switch that Controls the Balance between Self-Renewal and Differentiation. *Cell Stem Cell* 2012, *10*, 312-326.
[14] Bendall, S. C., Hughes, C., Campbell, J. L., Stewart, M. H., Pittock, P., Liu, S.*, et al.*, An enhanced mass spectrometry approach reveals human embryonic stem cell growth factors in culture. *Mol Cell Proteomics* 2009, *8*, 421-432.
[15] Wu, M. Y., Hill, C. S., Tgf-beta superfamily signaling in embryonic development and homeostasis. *Dev Cell* 2009, *16*, 329-343.
[16] Schier, A. F., Nodal signaling in vertebrate development. *Annu Rev Cell Dev Biol* 2003, *19*, 589-621.
[17] James, D., Levine, A. J., Besser, D., Hemmati-Brivanlou, A., TGF beta/activin/nodal signaling is necessary for the maintenance of pluripotency in human embryonic stem. *Development* 2005, *132*, 1273-1282.
[18] Vallier, L., Alexander, M., Pedersen, R. A., Activin/Nodal and FGF pathways cooperate to maintain pluripotency of human embryonic stem cells. *J Cell Sci* 2005, *118*, 4495-4509.
[19] Wang, L., Schulz, T. C., Sherrer, E. S., Dauphin, D. S., Shin, S., Nelson, A. M.*, et al.*, Self-renewal of human embryonic stem cells requires insulin-like growth factor-1 receptor and ERBB2 receptor signaling. *Blood* 2007, *110*, 4111-4119.
[20] Chen, G., Gulbranson, D. R., Hou, Z., Bolin, J. M., Ruotti, V., Probasco, M. D.*, et al.*, Chemically defined conditions for human iPSC derivation and culture. *Nat Methods* 2011, *8*, 424-429.
[21] Prowse, A. B. J., McQuade, L. R., Bryant, K. J., Marcal, H., Gray, P. P., Identification of potential pluripotency determinants for human embryonic stem cells following proteomic analysis of human and mouse fibroblast conditioned media. *Journal of Proteome Research* 2007, *6*, 3796-3807.

[22] Barroso-delJesus, A., Lucena-Aguilar, G., Sanchez, L., Ligero, G., Gutierrez-Aranda, I., Menendez, P., The Nodal inhibitor Lefty is negatively modulated by the microRNA miR-302 in human embryonic stem cells. *Faseb Journal* 2011, *25*, 1497-1508.
[23] Dvash, T., Sharon, N., Yanuka, O., Benvenisty, N., Molecular analysis of LEFTY-expressing cells in early human embryoid bodies. *Stem Cells* 2007, *25*, 465-472.
[24] Marjoram, L., Wright, C., Rapid differential transport of Nodal and Lefty on sulfated proteoglycan-rich extracellular matrix regulates left-right asymmetry in Xenopus. *Development* 2011, *138*, 475-485.
[25] Besser, D., Expression of nodal, lefty-a, and lefty-B in undifferentiated human embryonic stem cells requires activation of Smad2/3. *J Biol Chem* 2004, *279*, 45076-45084.
[26] Xu, R. H., Chen, X., Li, D. S., Li, R., Addicks, G. C., Glennon, C.*, et al.*, BMP4 initiates human embryonic stem cell differentiation to trophoblast. *Nat Biotechnol* 2002, *20*, 1261-1264.
[27] Xu, R. H., Peck, R. M., Li, D. S., Feng, X., Ludwig, T., Thomson, J. A., Basic FGF and suppression of BMP signaling sustain undifferentiated proliferation of human ES cells. *Nat Methods* 2005, *2*, 185-190.
[28] Ulloa, L., Tabibzadeh, S., Lefty inhibits receptor-regulated Smad phosphorylation induced by the activated transforming growth factor-beta receptor. *J Biol Chem* 2001, *276*, 21397-21404.
[29] Guo, X., Wang, X. F., Signaling cross-talk between TGF-beta/BMP and other pathways. *Cell Res* 2009, *19*, 71-88.
[30] Prokhorova, T. A., Harkness, L. M., Frandsen, U., Ditzel, N., Schroder, H. D., Burns, J. S.*, et al.*, Teratoma formation by human embryonic stem cells is site dependent and enhanced by the presence of Matrigel. *Stem Cells Dev* 2009, *18*, 47-54.
[31] Fu, R. H., Wang, Y. C., Liu, S. P., Huang, C. M., Kang, Y. H., Tsai, C. H.*, et al.*, Differentiation of stem cells: strategies for modifying surface biomaterials. *Cell Transplant* 2011, *20*, 37-47.
[32] Gerecht, S., Burdick, J. A., Ferreira, L. S., Townsend, S. A., Langer, R., Vunjak-Novakovic, G., Hyaluronic acid hydrogel for controlled self-renewal and differentiation of human embryonic stem cells. *Proc Natl Acad Sci U S A* 2007, *104*, 11298-11303.
[33] Gerecht-Nir, S., Cohen, S., Ziskind, A., Itskovitz-Eldor, J., Three-dimensional porous alginate scaffolds provide a conducive environment for generation of well-vascularized embryoid bodies from human embryonic stem cells. *Biotechnol Bioeng* 2004, *88*, 313-320.
[34] Baharvand, H., Hashemi, S. M., Kazemi Ashtiani, S., Farrokhi, A., Differentiation of human embryonic stem cells into hepatocytes in 2D and 3D culture systems in vitro. *Int J Dev Biol* 2006, *50*, 645-652.
[35] Dawson, E., Mapili, G., Erickson, K., Taqvi, S., Roy, K., Biomaterials for stem cell differentiation. *Adv Drug Deliv Rev* 2008, *60*, 215-228.
[36] Anderson, D. G., Levenberg, S., Langer, R., Nanoliter-scale synthesis of arrayed biomaterials and application to human embryonic stem cells. *Nat Biotechnol* 2004, *22*, 863-866.
[37] Levenberg, S., Huang, N. F., Lavik, E., Rogers, A. B., Itskovitz-Eldor, J., Langer, R., Differentiation of human embryonic stem cells on three-dimensional polymer scaffolds. *Proc Natl Acad Sci U S A* 2003, *100*, 12741-12746.
[38] Gobaa, S., Hoehnel, S., Roccio, M., Negro, A., Kobel, S., Lutolf, M. P., Artificial niche microarrays for probing single stem cell fate in high throughput. *Nat Methods* 2011, *8*, 949-955.
[39] Brafman, D. A., Shah, K. D., Fellner, T., Chien, S., Willert, K., Defining long-term maintenance conditions of human embryonic stem cells with arrayed cellular microenvironment technology. *Stem Cells Dev* 2009, *18*, 1141-1154.
[40] Soen, Y., Mori, A., Palmer, T. D., Brown, P. O., Exploring the regulation of human neural precursor cell differentiation using arrays of signaling microenvironments. *Mol Syst Biol* 2006, *2*, 37.
[41] Underhill, G. H., Bhatia, S. N., High-throughput analysis of signals regulating stem cell fate and function. *Curr Opin Chem Biol* 2007, *11*, 357-366.
[42] Flaim, C. J., Chien, S., Bhatia, S. N., An extracellular matrix microarray for probing cellular differentiation. *Nat Methods* 2005, *2*, 119-125.
[43] Jansen, J. A., Vehof, J. W., Ruhe, P. Q., Kroeze-Deutman, H., Kuboki, Y., Takita, H.*, et al.*, Growth factor-loaded scaffolds for bone engineering. *J Control Release* 2005, *101*, 127-136.
[44] Richardson, T. P., Peters, M. C., Ennett, A. B., Mooney, D. J., Polymeric system for dual growth factor delivery. *Nat Biotechnol* 2001, *19*, 1029-1034.
[45] Wang, S., Tian, R., Li, L., Figeys, D., Wang, L., An enhanced chemically defined SILAC culture system for quantitative proteomics study of human embryonic stem cells. *Proteomics* 2011, *11*, 4040-4046.

[46] Doherty, M. K., Hammond, D. E., Clague, M. J., Gaskell, S. J., Beynon, R. J., Turnover of the human proteome: determination of protein intracellular stability by dynamic SILAC. *J Proteome Res* 2009, *8*, 104-112.
[47] Phanstiel, D. H., Brumbaugh, J., Wenger, C. D., Tian, S., Probasco, M. D., Bailey, D. J.*, et al.*, Proteomic and phosphoproteomic comparison of human ES and iPS cells. *Nat Methods* 2011, *8*, 821-827.
[48] Schwanhausser, B., Busse, D., Li, N., Dittmar, G., Schuchhardt, J., Wolf, J.*, et al.*, Global quantification of mammalian gene expression control. *Nature* 2011, *473*, 337-342.
[49] Friedel, C. C., Dolken, L., Ruzsics, Z., Koszinowski, U. H., Zimmer, R., Conserved principles of mammalian transcriptional regulation revealed by RNA half-life. *Nucleic Acids Res* 2009, *37*, e115.
[50] Ingolia, N. T., Ghaemmaghami, S., Newman, J. R., Weissman, J. S., Genome-wide analysis in vivo of translation with nucleotide resolution using ribosome profiling. *Science* 2009, *324*, 218-223.
[51] Lister, R., Pelizzola, M., Kida, Y. S., Hawkins, R. D., Nery, J. R., Hon, G.*, et al.*, Hotspots of aberrant epigenomic reprogramming in human induced pluripotent stem cells. *Nature* 2011, *471*, 68-73.
[52] Polo, J. M., Liu, S., Figueroa, M. E., Kulalert, W., Eminli, S., Tan, K. Y.*, et al.*, Cell type of origin influences the molecular and functional properties of mouse induced pluripotent stem cells. *Nat Biotechnol* 2010, *28*, 848-855.
[53] Sullivan, G. J., Bai, Y., Fletcher, J., Wilmut, I., Induced pluripotent stem cells: epigenetic memories and practical implications. *Mol Hum Reprod* 2010, *16*, 880-885.
[54] Takahashi, K., Tanabe, K., Ohnuki, M., Narita, M., Ichisaka, T., Tomoda, K.*, et al.*, Induction of pluripotent stem cells from adult human fibroblasts by defined factors. *Cell* 2007, *131*, 861-872.
[55] Peerani, R., Rao, B. M., Bauwens, C., Yin, T., Wood, G. A., Nagy, A.*, et al.*, Niche-mediated control of human embryonic stem cell self-renewal and differentiation. *EMBO J* 2007, *26*, 4744-4755.
[56] Bauwens, C. L., Peerani, R., Niebruegge, S., Woodhouse, K. A., Kumacheva, E., Husain, M.*, et al.*, Control of human embryonic stem cell colony and aggregate size heterogeneity influences differentiation trajectories. *Stem Cells* 2008, *26*, 2300-2310.
[57] Gibbs, K. D., Jr., Gilbert, P. M., Sachs, K., Zhao, F., Blau, H. M., Weissman, I. L.*, et al.*, Single-cell phospho-specific flow cytometric analysis demonstrates biochemical and functional heterogeneity in human hematopoietic stem and progenitor compartments. *Blood* 2011, *117*, 4226-4233.
[58] Huang, S., Non-genetic heterogeneity of cells in development: more than just noise. *Development* 2009, *136*, 3853-3862.
[59] Morita, Y., Ema, H., Nakauchi, H., Heterogeneity and hierarchy within the most primitive hematopoietic stem cell compartment. *J Exp Med* 2010, *207*, 1173-1182.
[60] Schroeder, T., Hematopoietic stem cell heterogeneity: subtypes, not unpredictable behavior. *Cell Stem Cell* 2010, *6*, 203-207.
[61] Chambers, I., Silva, J., Colby, D., Nichols, J., Nijmeijer, B., Robertson, M.*, et al.*, Nanog safeguards pluripotency and mediates germline development. *Nature* 2007, *450*, 1230-1234.
[62] Rubakhin, S. S., Romanova, E. V., Nemes, P., Sweedler, J. V., Profiling metabolites and peptides in single cells. *Nat Methods* 2011, *8*, S20-29.
[63] Tang, F., Lao, K., Surani, M. A., Development and applications of single-cell transcriptome analysis. *Nat Methods* 2011, *8*, S6-11.

Appendix I

Supporting Datasets and Information for the Analysis of the Pluripotent Stem Cell Depositome

Table A1.1 N-GFR Matrigel Protein Identifications. List of all proteins identified in N-GFR Matrigel (non-growth factor reduced) with corresponding accession, description, PEAKS score, unique peptide numbers, and coverage (in %).

Accession	Description	Score	Coverage (%)	#Unique
P19137|LAMA1_MOUSE	Laminin subunit alpha-1 OS=M	548.72	73	299
P02469|LAMB1_MOUSE	Laminin subunit beta-1 OS=M	534.59	81	232
P10493|NID1_MOUSE	Nidogen-1 OS=Mus musculus	506.09	91	199
P02468|LAMC1_MOUSE	Laminin subunit gamma-1 OS	521.29	88	198
Q8VDD5|MYH9_MOUSE	Myosin-9 OS=Mus musculus (	445.87	74	117
Q05793|PGBM_MOUSE	Basement membrane-specific	426.69	56	115
P16546|SPTA2_MOUSE	Spectrin alpha chain, brain OS	399.37	77	113
P07724|ALBU_MOUSE	Serum albumin OS=Mus musc	394.86	93	79
P20029|GRP78_MOUSE	78 kDa glucose-regulated prot	418.33	86	78
P19324|SERPH_MOUSE	Serpin H1 OS=Mus musculus	385.85	87	77
P63038|CH60_MOUSE	60 kDa heat shock protein, mi	380.07	92	74
P01027|CO3_MOUSE	Complement C3 OS=Mus mus	330.22	67	67
P07214|SPRC_MOUSE	SPARC OS=Mus musculus G	395.48	80	66
P20152|VIME_MOUSE	Vimentin OS=Mus musculus (	390.87	96	66
P09103|PDIA1_MOUSE	Protein disulfide-isomerase OS	372.59	93	66
Q80X90|FLNB_MOUSE	Filamin-B OS=Mus musculus	322.12	52	59
Q62261|SPTB2_MOUSE	Spectrin beta chain, brain 1 O	307.59	61	59
Q9QXS1|PLEC_MOUSE	Plectin OS=Mus musculus GN	255.85	52	58
P63017|HSP7C_MOUSE	Heat shock cognate 71 kDa pr	415.5	89	56
Q3UQ28|PXDN_MOUSE	Peroxidasin homolog OS=Mus	364.3	72	56
Q01853|TERA_MOUSE	Transitional endoplasmic retic	333.88	72	55
P27773|PDIA3_MOUSE	Protein disulfide-isomerase A3	333.85	80	54
Q9JHU4|DYHC1_MOUSE	Cytoplasmic dynein 1 heavy ch	282.97	49	54
P14733|LMNB1_MOUSE	Lamin-B1 OS=Mus musculus	373.76	86	52
Q6P5E4|UGGG1_MOUSE	UDP-glucose:glycoprotein gluc	325.06	61	52
Q921I1|TRFE_MOUSE	Serotransferrin OS=Mus musc	335.58	78	50
Q9D0E1|HNRPM_MOUSE	Heterogeneous nuclear ribonu	305.06	83	50
Q61838|A2M_MOUSE	Alpha-2-macroglobulin OS=Mu	319.31	66	46
A2ARV4|LRP2_MOUSE	Low-density lipoprotein recept	253.95	51	46
P48678|LMNA_MOUSE	Prelamin-A/C OS=Mus muscu	311.51	74	45
P08113|ENPL_MOUSE	Endoplasmin OS=Mus muscu	284.57	64	44
Q8VIJ6|SFPQ_MOUSE	Splicing factor, proline- and gl	311.2	69	43
Q9R0B9|PLOD2_MOUSE	Procollagen-lysine,2-oxoglutar	302.4	71	43
Q64727|VINC_MOUSE	Vinculin OS=Mus musculus G	290.92	81	43
P38647|GRP75_MOUSE	Stress-70 protein, mitochondri	317.3	74	42
Q8K310|MATR3_MOUSE	Matrin-3 OS=Mus musculus G	310.31	65	40
Q61879|MYH10_MOUSE	Myosin-10 OS=Mus musculus	328.74	54	39
P26039|TLN1_MOUSE	Talin-1 OS=Mus musculus GN	216.74	48	39
Q8CGC7|SYEP_MOUSE	Bifunctional aminoacyl-tRNA s	283.42	51	38
P14211|CALR_MOUSE	Calreticulin OS=Mus musculus	300.3	91	37
P08003|PDIA4_MOUSE	Protein disulfide-isomerase A4	285.22	69	37
Q68FD5|CLH_MOUSE	Clathrin heavy chain 1 OS=Mu	244.47	51	37
P11276|FINC_MOUSE	Fibronectin OS=Mus musculus	298.28	37	36
P13020|GELS_MOUSE	Gelsolin OS=Mus musculus G	277.29	59	35
P16858|G3P_MOUSE	Glyceraldehyde-3-phosphate (	323.25	84	33
P62806|H4_MOUSE	Histone H4 OS=Mus musculus	247.47	82	33
Q922R8|PDIA6_MOUSE	Protein disulfide-isomerase A6	328.41	80	32
O08677|KNG1_MOUSE	Kininogen-1 OS=Mus musculu	310.69	53	32
P56480|ATPB_MOUSE	ATP synthase subunit beta, m	287.08	86	31
Q99PV0|PRP8_MOUSE	Pre-mRNA-processing-splicing	247.66	40	31
Q6PDQ2|CHD4_MOUSE	Chromodomain-helicase-DNA	241.84	43	31
P09405|NUCL_MOUSE	Nucleolin OS=Mus musculus (	266.11	69	30
P06909|CFAH_MOUSE	Complement factor H OS=Mus	263.83	41	30
P10126|EF1A1_MOUSE	Elongation factor 1-alpha 1 OS	252.38	71	29

P08032|SPTA1_MOUSE	Spectrin alpha chain, erythroc	249.83	39	29
O70133|DHX9_MOUSE	ATP-dependent RNA helicase	229.17	42	29
O88569|ROA2_MOUSE	Heterogeneous nuclear ribonu	297.94	78	28
Q8K0E8|FIBB_MOUSE	Fibrinogen beta chain OS=Mu	315.58	74	27
P08249|MDHM_MOUSE	Malate dehydrogenase, mitocl	307.82	77	27
Q8BTM8|FLNA_MOUSE	Filamin-A OS=Mus musculus	240.2	31	27
P17742|PPIA_MOUSE	Peptidyl-prolyl cis-trans isome	294.46	83	26
P52480|KPYM_MOUSE	Pyruvate kinase isozymes M1	254.26	59	26
Q8VCM7|FIBG_MOUSE	Fibrinogen gamma chain OS=	289.26	72	25
Q03265|ATPA_MOUSE	ATP synthase subunit alpha, r	280.6	75	25
P29341|PABP1_MOUSE	Polyadenylate-binding protein	265.8	59	25
Q91W90|TXND5_MOUSE	Thioredoxin domain-containin	276.26	78	24
O08795|GLU2B_MOUSE	Glucosidase 2 subunit beta OS	265.43	59	24
Q9D8E6|RL4_MOUSE	60S ribosomal protein L4 OS=	243.16	59	24
P29533|VCAM1_MOUSE	Vascular cell adhesion protein	228.91	54	24
P05202|AATM_MOUSE	Aspartate aminotransferase, r	223.94	67	24
Q99PL5|RRBP1_MOUSE	Ribosome-binding protein 1 O	202.39	28	24
P11499|HS90B_MOUSE	Heat shock protein HSP 90-be	294.42	69	23
O88322|NID2_MOUSE	Nidogen-2 OS=Mus musculus	271.23	40	23
P21614|VTDB_MOUSE	Vitamin D-binding protein OS=	257.96	67	22
Q9R0E2|PLOD1_MOUSE	Procollagen-lysine,2-oxoglutar	243.69	48	22
P39061|COIA1_MOUSE	Collagen alpha-1(XVIII) chain	228.75	34	22
Q61001|LAMA5_MOUSE	Laminin subunit alpha-5 OS=M	227.53	28	22
Q91W39|NCOA5_MOUSE	Nuclear receptor coactivator 5	216.62	47	22
P47911|RL6_MOUSE	60S ribosomal protein L6 OS=	215.87	67	22
P20108|PRDX3_MOUSE	Thioredoxin-dependent peroxi	273.48	86	21
Q8R326|PSPC1_MOUSE	Paraspeckle component 1 OS	223.02	53	21
Q9JKR6|HYOU1_MOUSE	Hypoxia up-regulated protein 1	219.62	50	21
P14206|RSSA_MOUSE	40S ribosomal protein SA OS=	272.53	71	20
Q01405|SC23A_MOUSE	Protein transport protein Sec2	270.64	62	20
Q9WTP6|KAD2_MOUSE	Adenylate kinase 2, mitochon	247.36	80	20
P01942|HBA_MOUSE	Hemoglobin subunit alpha OS	243.8	100	20
P61979|HNRPK_MOUSE	Heterogeneous nuclear ribonu	242.52	71	20
P58252|EF2_MOUSE	Elongation factor 2 OS=Mus m	241.7	45	20
Q9D8N0|EF1G_MOUSE	Elongation factor 1-gamma OS	227.23	62	20
Q00623|APOA1_MOUSE	Apolipoprotein A-I OS=Mus m	223.26	73	20
Q99K48|NONO_MOUSE	Non-POU domain-containing o	216.7	65	20
Q3U1J4|DDB1_MOUSE	DNA damage-binding protein	214.68	34	20
Q8BU30|SYIC_MOUSE	Isoleucyl-tRNA synthetase, cy	208.43	39	20
P62259|1433E_MOUSE	14-3-3 protein epsilon OS=Mu	279.64	87	19
P17225|PTBP1_MOUSE	Polypyrimidine tract-binding pr	273.25	71	19
P02088|HBB1_MOUSE	Hemoglobin subunit beta-1 OS	269.07	83	19
Q91X72|HEMO_MOUSE	Hemopexin OS=Mus musculu	242.73	60	19
Q8VDJ3|VIGLN_MOUSE	Vigilin OS=Mus musculus GN=	208	28	19
P57759|ERP29_MOUSE	Endoplasmic reticulum reside	244.39	68	18
Q9Z247|FKBP9_MOUSE	Peptidyl-prolyl cis-trans isome	230.77	51	18
Q9DC23|DJC10_MOUSE	DnaJ homolog subfamily C me	217.63	56	18
Q61595|KTN1_MOUSE	Kinectin OS=Mus musculus G	209.35	42	18
Q9EQK5|MVP_MOUSE	Major vault protein OS=Mus m	182.04	42	18
Q9CU62|SMC1A_MOUSE	Structural maintenance of chr	176.97	30	18
Q7TPR4|ACTN1_MOUSE	Alpha-actinin-1 OS=Mus musc	318.99	62	17
Q61292|LAMB2_MOUSE	Laminin subunit beta-2 OS=M	218.1	25	17
P62301|RS13_MOUSE	40S ribosomal protein S13 OS	209.86	44	17
P62908|RS3_MOUSE	40S ribosomal protein S3 OS=	191.2	70	17
P61982|1433G_MOUSE	14-3-3 protein gamma OS=Mu	270.33	96	16

Q61937|NPM_MOUSE	Nucleophosmin OS=Mus mus	224.16	63	16
Q9Z1Q9|SYVC_MOUSE	Valyl-tRNA synthetase OS=Mu	216.69	31	16
Q9CZU6|CISY_MOUSE	Citrate synthase, mitochondria	198.63	42	16
Q64433|CH10_MOUSE	10 kDa heat shock protein, mi	197.06	85	16
P25444|RS2_MOUSE	40S ribosomal protein S2 OS=	193.63	72	16
P29758|OAT_MOUSE	Ornithine aminotransferase, m	192.73	46	16
Q9WTM5|RUVB2_MOUSE	RuvB-like 2 OS=Mus musculu	164.84	51	16
A2ASS6|TITIN_MOUSE	Titin OS=Mus musculus GN=T	70.94	6	16
Q9Z2X1|HNRPF_MOUSE	Heterogeneous nuclear ribonu	249.84	70	15
P27659|RL3_MOUSE	60S ribosomal protein L3 OS=	237.73	63	15
P23780|BGAL_MOUSE	Beta-galactosidase OS=Mus r	229.32	45	15
Q9WV54|ASAH1_MOUSE	Acid ceramidase OS=Mus mu	224.05	46	15
P57776|EF1D_MOUSE	Elongation factor 1-delta OS=	223.25	76	15
Q8R3Q6|CCD58_MOUSE	Coiled-coil domain-containing	212.39	81	15
Q922B2|SYDC_MOUSE	Aspartyl-tRNA synthetase, cyt	207.71	50	15
O08810|U5S1_MOUSE	116 kDa U5 small nuclear ribo	205.25	31	15
O08749|DLDH_MOUSE	Dihydrolipoyl dehydrogenase,	204.92	62	15
P61358|RL27_MOUSE	60S ribosomal protein L27 OS	191.92	53	15
P53026|RL10A_MOUSE	60S ribosomal protein L10a O	188.98	43	15
Q9Z1Z0|USO1_MOUSE	General vesicular transport fa	100.33	43	15
O35643|AP1B1_MOUSE	AP-1 complex subunit beta-1 (	248.1	50	14
Q9D1M4|MCA3_MOUSE	Eukaryotic translation elongati	230.67	84	14
Q9DBG5|PLIN3_MOUSE	Perilipin-3 OS=Mus musculus	222.6	73	14
P62962|PROF1_MOUSE	Profilin-1 OS=Mus musculus (	222.4	86	14
P97496|SMRC1_MOUSE	SWI/SNF complex subunit SM	219.45	54	14
Q61207|SAP_MOUSE	Sulfated glycoprotein 1 OS=M	215.05	51	14
Q3UPH1|PRRC1_MOUSE	Protein PRRC1 OS=Mus mus	209.4	55	14
Q587J6|LITD1_MOUSE	LINE-1 type transposase dom	206.2	42	14
P40142|TKT_MOUSE	Transketolase OS=Mus musc	205.43	39	14
P62918|RL8_MOUSE	60S ribosomal protein L8 OS=	202.4	70	14
P62082|RS7_MOUSE	40S ribosomal protein S7 OS=	192.4	63	14
Q91VM5|RBMXL_MOUSE	Heterogeneous nuclear ribonu	184.22	51	14
P29699|FETUA_MOUSE	Alpha-2-HS-glycoprotein OS=	286.43	69	13
P62843|RS15_MOUSE	40S ribosomal protein S15 OS	240.01	82	13
P07901|HS90A_MOUSE	Heat shock protein HSP 90-al	230.89	57	13
Q3THW5|H2AV_MOUSE	Histone H2A.V OS=Mus musc	222.74	79	13
P12970|RL7A_MOUSE	60S ribosomal protein L7a OS	218.32	50	13
Q61576|FKB10_MOUSE	Peptidyl-prolyl cis-trans isome	211.94	50	13
Q99JR5|TINAL_MOUSE	Tubulointerstitial nephritis anti	211.76	47	13
P24369|PPIB_MOUSE	Peptidyl-prolyl cis-trans isome	207.16	63	13
Q9CYZ2|TPD54_MOUSE	Tumor protein D54 OS=Mus m	204.5	71	13
Q8BG05|ROA3_MOUSE	Heterogeneous nuclear ribonu	197.34	36	13
Q9DBJ1|PGAM1_MOUSE	Phosphoglycerate mutase 1 O	191.64	72	13
Q8BP92|RCN2_MOUSE	Reticulocalbin-2 OS=Mus mus	169.45	66	13
Q62376|RU17_MOUSE	U1 small nuclear ribonucleopr	169	31	13
P62270|RS18_MOUSE	40S ribosomal protein S18 OS	152.31	62	13
P63101|1433Z_MOUSE	14-3-3 protein zeta/delta OS=	278.83	85	12
Q9CQU0|TXD12_MOUSE	Thioredoxin domain-containin	237.42	85	12
Q9D1Q6|ERP44_MOUSE	Endoplasmic reticulum reside	227.11	72	12
P31001|DESM_MOUSE	Desmin OS=Mus musculus G	224.21	54	12
P62317|SMD2_MOUSE	Small nuclear ribonucleoprote	213.65	72	12
Q8BWT1|THIM_MOUSE	3-ketoacyl-CoA thiolase, mitoc	212.23	64	12
P18242|CATD_MOUSE	Cathepsin D OS=Mus musculu	198.86	54	12
Q3V1T4|P3H1_MOUSE	Prolyl 3-hydroxylase 1 OS=Mu	197.25	34	12
Q9CXW3|CYBP_MOUSE	Calcyclin-binding protein OS=	197.07	54	12

Q8BH97|RCN3_MOUSE	Reticulocalbin-3 OS=Mus mus	186.96	63	12
P62754|RS6_MOUSE	40S ribosomal protein S6 OS=	181.51	41	12
Q99JI4|PSMD6_MOUSE	26S proteasome non-ATPase	171.19	60	12
Q9CSN1|SNW1_MOUSE	SNW domain-containing prote	163.32	40	12
Q8BJ71|NUP93_MOUSE	Nuclear pore complex protein	160.84	57	12
P80316|TCPE_MOUSE	T-complex protein 1 subunit e	155.97	52	12
Q8BH61|F13A_MOUSE	Coagulation factor XIII A chair	142.51	22	12
P57780|ACTN4_MOUSE	Alpha-actinin-4 OS=Mus musc	261.83	52	11
P49312|ROA1_MOUSE	Heterogeneous nuclear ribonu	225.25	60	11
O35658|C1QBP_MOUSE	Complement component 1 Q s	225.2	64	11
O89086|RBM3_MOUSE	Putative RNA-binding protein 3	209.29	80	11
Q99020|ROAA_MOUSE	Heterogeneous nuclear ribonu	209.03	46	11
Q9EQH3|VPS35_MOUSE	Vacuolar protein sorting-assoc	195.32	37	11
P31230|AIMP1_MOUSE	Aminoacyl tRNA synthase com	191.2	59	11
Q9JKF1|IQGA1_MOUSE	Ras GTPase-activating-like pr	188.25	29	11
Q9WVA4|TAGL2_MOUSE	Transgelin-2 OS=Mus muscul	187.6	60	11
Q922Q8|LRC59_MOUSE	Leucine-rich repeat-containing	187.54	44	11
Q9Z2N8|ACL6A_MOUSE	Actin-like protein 6A OS=Mus	186.72	46	11
Q60716|P4HA2_MOUSE	Prolyl 4-hydroxylase subunit a	186.15	47	11
P97351|RS3A_MOUSE	40S ribosomal protein S3a OS	178.15	46	11
P06151|LDHA_MOUSE	L-lactate dehydrogenase A ch	177.41	40	11
Q9CPR4|RL17_MOUSE	60S ribosomal protein L17 OS	170.26	49	11
Q8C854|MYEF2_MOUSE	Myelin expression factor 2 OS	170.12	38	11
P20918|PLMN_MOUSE	Plasminogen OS=Mus muscu	167.79	28	11
Q9EPU0|RENT1_MOUSE	Regulator of nonsense transcr	164.61	26	11
P63085|MK01_MOUSE	Mitogen-activated protein kina	161.4	45	11
Q8BMS1|ECHA_MOUSE	Trifunctional enzyme subunit a	149.87	44	11
P32067|LA_MOUSE	Lupus La protein homolog OS	147.52	51	11
Q9QZQ1|AFAD_MOUSE	Afadin OS=Mus musculus GN	133.07	17	11
Q60902|EP15R_MOUSE	Epidermal growth factor recep	125.71	29	11
P26443|DHE3_MOUSE	Glutamate dehydrogenase 1,	118.4	31	11
P68254|1433T_MOUSE	14-3-3 protein theta OS=Mus	251.79	82	10
O35887|CALU_MOUSE	Calumenin OS=Mus musculus	217.5	82	10
P62307|RUXF_MOUSE	Small nuclear ribonucleprote	209.92	99	10
Q8VHX6|FLNC_MOUSE	Filamin-C OS=Mus musculus	188.92	25	10
Q8CG70|P3H3_MOUSE	Prolyl 3-hydroxylase 3 OS=Mu	187.37	39	10
O08547|SC22B_MOUSE	Vesicle-trafficking protein SEC	185.45	60	10
Q02257|PLAK_MOUSE	Junction plakoglobin OS=Mus	182.85	37	10
P62264|RS14_MOUSE	40S ribosomal protein S14 OS	182.34	72	10
Q9R0E1|PLOD3_MOUSE	Procollagen-lysine,2-oxoglutar	179.05	31	10
P16675|PPGB_MOUSE	Lysosomal protective protein C	176.42	24	10
P07356|ANXA2_MOUSE	Annexin A2 OS=Mus musculu	170.13	43	10
Q99KI0|ACON_MOUSE	Aconitate hydratase, mitochon	169.72	28	10
Q9Z204|HNRPC_MOUSE	Heterogeneous nuclear ribonu	169.56	36	10
P60122|RUVB1_MOUSE	RuvB-like 1 OS=Mus musculu	153.17	41	10
Q60864|STIP1_MOUSE	Stress-induced-phosphoprotei	151.8	29	10
P23249|MOV10_MOUSE	Putative helicase MOV-10 OS	149.84	19	10
P70699|LYAG_MOUSE	Lysosomal alpha-glucosidase	143.05	19	10
Q8BX10|PGAM5_MOUSE	Serine/threonine-protein phos	138.1	55	10
Q8R1Q8|DC1L1_MOUSE	Cytoplasmic dynein 1 light inte	137.93	41	10
P35700|PRDX1_MOUSE	Peroxiredoxin-1 OS=Mus mus	137.09	59	10
Q6PDM2|SRSF1_MOUSE	Serine/arginine-rich splicing fa	135.94	47	10
O08585|CLCA_MOUSE	Clathrin light chain A OS=Mus	127.56	22	10
Q8R4X3|RBM12_MOUSE	RNA-binding protein 12 OS=M	123.46	14	10
P62204|CALM_MOUSE	Calmodulin OS=Mus musculu	233.23	99	9

P62315|SMD1_MOUSE	Small nuclear ribonucleoprote	214.63	81	9
Q8R2Z5|VWA1_MOUSE	von Willebrand factor A domai	191.31	53	9
Q9CQ92|FIS1_MOUSE	Mitochondrial fission 1 protein	190.05	75	9
Q9CQF3|CPSF5_MOUSE	Cleavage and polyadenylation	189.59	62	9
P36552|HEM6_MOUSE	Coproporphyrinogen-III oxidas	185.7	47	9
P56959|FUS_MOUSE	RNA-binding protein FUS OS=	184.78	27	9
Q62167|DDX3X_MOUSE	ATP-dependent RNA helicase	182.47	46	9
Q9WTX5|SKP1_MOUSE	S-phase kinase-associated pr	178.41	66	9
P60335|PCBP1_MOUSE	Poly(rC)-binding protein 1 OS=	176.4	54	9
Q8R081|HNRPL_MOUSE	Heterogeneous nuclear ribonu	174.18	34	9
Q60715|P4HA1_MOUSE	Prolyl 4-hydroxylase subunit a	173.86	35	9
Q99KN9|EPN4_MOUSE	Clathrin interactor 1 OS=Mus	170.43	22	9
P47963|RL13_MOUSE	60S ribosomal protein L13 OS	169.23	44	9
P46412|GPX3_MOUSE	Glutathione peroxidase 3 OS=	169.14	41	9
Q9R0U0|SRS10_MOUSE	Serine/arginine-rich splicing fa	169	24	9
Q9WU78|PDC6I_MOUSE	Programmed cell death 6-inter	166.5	30	9
P99029|PRDX5_MOUSE	Peroxiredoxin-5, mitochondria	164.98	43	9
P48036|ANXA5_MOUSE	Annexin A5 OS=Mus musculu	162.59	50	9
Q61147|CERU_MOUSE	Ceruloplasmin OS=Mus musc	161.4	21	9
Q9CYR0|SSBP_MOUSE	Single-stranded DNA-binding	158.75	56	9
Q60749|KHDR1_MOUSE	KH domain-containing, RNA-b	157.57	53	9
Q60597|ODO1_MOUSE	2-oxoglutarate dehydrogenase	155	30	9
Q6ZQI3|MLEC_MOUSE	Malectin OS=Mus musculus G	153.92	42	9
Q8C0C7|SYFA_MOUSE	Phenylalanyl-tRNA synthetase	149.8	30	9
Q3U0V1|FUBP2_MOUSE	Far upstream element-binding	148.22	26	9
Q91YN9|BAG2_MOUSE	BAG family molecular chaperc	147.76	59	9
Q501J6|DDX17_MOUSE	Probable ATP-dependent RNA	147.43	26	9
Q7TMK9|HNRPQ_MOUSE	Heterogeneous nuclear ribonu	145.1	23	9
Q60631|GRB2_MOUSE	Growth factor receptor-bound	137.42	52	9
Q6NZJ6|IF4G1_MOUSE	Eukaryotic translation initiation	131.75	15	9
Q9Z110|P5CS_MOUSE	Delta-1-pyrroline-5-carboxylate	129.88	20	9
Q61656|DDX5_MOUSE	Probable ATP-dependent RNA	126.9	23	9
Q9R1C7|PR40A_MOUSE	Pre-mRNA-processing factor 4	120.39	15	9
P24270|CATA_MOUSE	Catalase OS=Mus musculus C	120.12	37	9
Q9Z0X1|AIFM1_MOUSE	Apoptosis-inducing factor 1, m	115.55	23	9
Q9Z1D1|EIF3G_MOUSE	Eukaryotic translation initiation	111.96	20	9
Q61696|HS71A_MOUSE	Heat shock 70 kDa protein 1A	273.85	61	8
Q01768|NDKB_MOUSE	Nucleoside diphosphate kinas	236.67	72	8
P07759|SPA3K_MOUSE	Serine protease inhibitor A3K	225.39	54	8
P15532|NDKA_MOUSE	Nucleoside diphosphate kinas	215.23	74	8
P61924|COPZ1_MOUSE	Coatomer subunit zeta-1 OS=	206.86	77	8
Q9CPT4|CS010_MOUSE	UPF0556 protein C19orf10 ho	199.77	49	8
Q60605|MYL6_MOUSE	Myosin light polypeptide 6 OS=	198.17	67	8
Q9D3D9|ATPD_MOUSE	ATP synthase subunit delta, m	196.56	64	8
P16045|LEG1_MOUSE	Galectin-1 OS=Mus musculus	193.94	77	8
Q8BL97|SRSF7_MOUSE	Serine/arginine-rich splicing fa	192.06	39	8
Q9DB20|ATPO_MOUSE	ATP synthase subunit O, mito	186.39	55	8
Q9JIQ3|DBLOH_MOUSE	Diablo homolog, mitochondria	179.04	58	8
Q9QXT0|CNPY2_MOUSE	Protein canopy homolog 2 OS	176.77	66	8
P17751|TPIS_MOUSE	Triosephosphate isomerase O	171.23	53	8
Q61584|FXR1_MOUSE	Fragile X mental retardation sy	170.2	36	8
Q9JHJ0|TMOD3_MOUSE	Tropomodulin-3 OS=Mus mus	169.13	45	8
Q3TCN2|PLBL2_MOUSE	Putative phospholipase B-like	168.8	30	8
P62983|RS27A_MOUSE	Ubiquitin-40S ribosomal protei	168.18	67	8
P63276|RS17_MOUSE	40S ribosomal protein S17 OS	167.5	50	8

Q08879|FBLN1_MOUSE	Fibulin-1 OS=Mus musculus C	159.57	35	8
Q61171|PRDX2_MOUSE	Peroxiredoxin-2 OS=Mus mus	157.72	63	8
P28656|NP1L1_MOUSE	Nucleosome assembly protein	156.32	42	8
Q9D2G2|ODO2_MOUSE	Dihydrolipoyllysine-residue su	150.86	34	8
P62858|RS28_MOUSE	40S ribosomal protein S28 OS	148.94	61	8
Q99PT1|GDIR1_MOUSE	Rho GDP-dissociation inhibito	148.52	41	8
P08228|SODC_MOUSE	Superoxide dismutase [Cu-Zn	144.71	44	8
Q06890|CLUS_MOUSE	Clusterin OS=Mus musculus C	143.09	33	8
P21107|TPM3_MOUSE	Tropomyosin alpha-3 chain OS	141.88	43	8
Q9D0I9|SYRC_MOUSE	Arginyl-tRNA synthetase, cyto	135.72	20	8
Q9D338|RM19_MOUSE	39S ribosomal protein L19, mi	135.71	37	8
P10605|CATB_MOUSE	Cathepsin B OS=Mus musculu	134.87	25	8
P70372|ELAV1_MOUSE	ELAV-like protein 1 OS=Mus m	134.43	31	8
Q9CX56|PSMD8_MOUSE	26S proteasome non-ATPase	131.98	42	8
Q61646|HPT_MOUSE	Haptoglobin OS=Mus musculu	131.2	38	8
P55302|AMRP_MOUSE	Alpha-2-macroglobulin recepto	130.45	24	8
Q8BGD9|IF4B_MOUSE	Eukaryotic translation initiation	127.26	31	8
O70493|SNX12_MOUSE	Sorting nexin-12 OS=Mus mus	120.16	53	8
P39447|ZO1_MOUSE	Tight junction protein ZO-1 OS	117.3	21	8
Q61464|ZN638_MOUSE	Zinc finger protein 638 OS=Mu	116.1	17	8
Q6ZWN5|RS9_MOUSE	40S ribosomal protein S9 OS=	114.88	41	8
Q6NV83|SR140_MOUSE	U2 snRNP-associated SURP	108.89	17	8
Q8CGK3|LONM_MOUSE	Lon protease homolog, mitoch	95.66	31	8
P17156|HSP72_MOUSE	Heat shock-related 70 kDa pro	297.25	50	7
Q00898|A1AT5_MOUSE	Alpha-1-antitrypsin 1-5 OS=Mu	244.08	56	7
Q9CQV8|1433B_MOUSE	14-3-3 protein beta/alpha OS=	231.61	80	7
Q03734|SPA3M_MOUSE	Serine protease inhibitor A3M	231.04	68	7
Q91WP6|SPA3N_MOUSE	Serine protease inhibitor A3N	210.64	50	7
P28665|MUG1_MOUSE	Murinoglobulin-1 OS=Mus mu	191.6	27	7
P63242|IF5A1_MOUSE	Eukaryotic translation initiation	183.7	60	7
P62830|RL23_MOUSE	60S ribosomal protein L23 OS	183.07	79	7
P21619|LMNB2_MOUSE	Lamin-B2 OS=Mus musculus	181.24	41	7
P29788|VTNC_MOUSE	Vitronectin OS=Mus musculus	179.24	35	7
Q9QUR7|PIN1_MOUSE	Peptidyl-prolyl cis-trans isome	177.79	75	7
P62996|TRA2B_MOUSE	Transformer-2 protein homolo	176.31	45	7
P58022|LOXL2_MOUSE	Lysyl oxidase homolog 2 OS=	173.8	38	7
Q62093|SRSF2_MOUSE	Serine/arginine-rich splicing fa	172.65	50	7
P83877|TXN4A_MOUSE	Thioredoxin-like protein 4A OS	171.32	77	7
Q9D0W5|PPIL1_MOUSE	Peptidyl-prolyl cis-trans isome	165.4	55	7
Q9Z2U0|PSA7_MOUSE	Proteasome subunit alpha typ	163.82	48	7
Q9CQR2|RS21_MOUSE	40S ribosomal protein S21 OS	159.77	66	7
P35564|CALX_MOUSE	Calnexin OS=Mus musculus C	159.57	34	7
Q9Z2U1|PSA5_MOUSE	Proteasome subunit alpha typ	158.72	56	7
P61458|PHS_MOUSE	Pterin-4-alpha-carbinolamine	157.62	58	7
Q9CQL1|MGNR_MOUSE	Protein mago nashi homolog 1	155.58	58	7
P61327|MGN_MOUSE	Protein mago nashi homolog C	155.58	58	7
P35980|RL18_MOUSE	60S ribosomal protein L18 OS	147.12	46	7
Q8R4R6|NUP53_MOUSE	Nucleoporin NUP53 OS=Mus	142.03	45	7
P70670|NACAM_MOUSE	Nascent polypeptide-associate	141.54	18	7
Q8VDM4|PSMD2_MOUSE	26S proteasome non-ATPase	139.68	36	7
P03975|IGEB_MOUSE	IgE-binding protein OS=Mus m	138.53	20	7
Q9CXI5|MANF_MOUSE	Mesencephalic astrocyte-deriv	138.06	51	7
P08905|LYZ2_MOUSE	Lysozyme C-2 OS=Mus musc	135.63	61	7
Q04447|KCRB_MOUSE	Creatine kinase B-type OS=M	134.76	40	7
O09061|PSB1_MOUSE	Proteasome subunit beta type	133.9	54	7

Q9D6Z1|NOP56_MOUSE	Nucleolar protein 56 OS=Mus	133.24	32	7
Q62189|SNRPA_MOUSE	U1 small nuclear ribonucleopr	130.42	32	7
P84089|ERH_MOUSE	Enhancer of rudimentary hom	129.86	38	7
Q9QZH3|PPIE_MOUSE	Peptidyl-prolyl cis-trans isome	129.57	49	7
Q6ZQ38|CAND1_MOUSE	Cullin-associated NEDD8-diss	126.99	22	7
P14148|RL7_MOUSE	60S ribosomal protein L7 OS=	118.82	27	7
P30416|FKBP4_MOUSE	Peptidyl-prolyl cis-trans isome	117.11	22	7
Q03173|ENAH_MOUSE	Protein enabled homolog OS=	116.98	15	7
P17427|AP2A2_MOUSE	AP-2 complex subunit alpha-2	116.16	21	7
Q91WJ8|FUBP1_MOUSE	Far upstream element-binding	114.06	17	7
Q9CZX8|RS19_MOUSE	40S ribosomal protein S19 OS	108.86	37	7
Q8R180|ERO1A_MOUSE	ERO1-like protein alpha OS=M	107.75	26	7
P09411|PGK1_MOUSE	Phosphoglycerate kinase 1 OS	105.87	34	7
Q3UPL0|SC31A_MOUSE	Protein transport protein Sec3	99.98	15	7
Q8BX70|VP13C_MOUSE	Vacuolar protein sorting-assoc	92.49	8	7
P22599|A1AT2_MOUSE	Alpha-1-antitrypsin 1-2 OS=Mu	267.66	71	6
Q9QZQ8|H2AY_MOUSE	Core histone macro-H2A.1 OS	202.82	47	6
P62305|RUXE_MOUSE	Small nuclear ribonucleoprote	191.04	77	6
P62897|CYC_MOUSE	Cytochrome c, somatic OS=M	189.27	63	6
Q6IRU2|TPM4_MOUSE	Tropomyosin alpha-4 chain OS	169.6	75	6
Q8CDN6|TXNL1_MOUSE	Thioredoxin-like protein 1 OS=	166.23	57	6
Q6PDG5|SMRC2_MOUSE	SWI/SNF complex subunit SM	160.75	36	6
Q7M6Y3|PICA_MOUSE	Phosphatidylinositol-binding cl	160.26	21	6
P40124|CAP1_MOUSE	Adenylyl cyclase-associated p	157.78	33	6
P16110|LEG3_MOUSE	Galectin-3 OS=Mus musculus	157.13	26	6
Q921F2|TADBP_MOUSE	TAR DNA-binding protein 43 O	155.04	28	6
Q9CXZ1|NDUS4_MOUSE	NADH dehydrogenase [ubiqui	154.95	51	6
Q9CWZ3|RBM8A_MOUSE	RNA-binding protein 8A OS=M	152.18	53	6
O55135|IF6_MOUSE	Eukaryotic translation initiation	151.91	34	6
P99028|QCR6_MOUSE	Cytochrome b-c1 complex sub	147.81	61	6
P11404|FABPH_MOUSE	Fatty acid-binding protein, hea	145.61	65	6
Q9D967|MGDP1_MOUSE	Magnesium-dependent phosp	139.1	54	6
P97807|FUMH_MOUSE	Fumarate hydratase, mitochon	138.43	31	6
P56391|CX6B1_MOUSE	Cytochrome c oxidase subunit	136.35	63	6
P28798|GRN_MOUSE	Granulins OS=Mus musculus	135.27	41	6
Q76MZ3|2AAA_MOUSE	Serine/threonine-protein phos	134.5	33	6
Q9D0F9|PGM1_MOUSE	Phosphoglucomutase-1 OS=M	130.29	30	6
Q9CVB6|ARPC2_MOUSE	Actin-related protein 2/3 comp	127.56	49	6
P47962|RL5_MOUSE	60S ribosomal protein L5 OS=	126.81	25	6
P06728|APOA4_MOUSE	Apolipoprotein A-IV OS=Mus m	125.6	32	6
Q68FL6|SYMC_MOUSE	Methionyl-tRNA synthetase, cy	125.23	35	6
Q6NVF9|CPSF6_MOUSE	Cleavage and polyadenylation	125.21	23	6
O55128|SAP18_MOUSE	Histone deacetylase complex	124.82	48	6
Q61704|ITIH3_MOUSE	Inter-alpha-trypsin inhibitor he	123.95	40	6
P47738|ALDH2_MOUSE	Aldehyde dehydrogenase, mit	122.02	19	6
Q8BND5|QSOX1_MOUSE	Sulfhydryl oxidase 1 OS=Mus	121.41	22	6
P62911|RL32_MOUSE	60S ribosomal protein L32 OS	119.51	45	6
O35206|COFA1_MOUSE	Collagen alpha-1(XV) chain O	118.93	12	6
Q9D620|RFIP1_MOUSE	Rab11 family-interacting prote	118.52	39	6
P14131|RS16_MOUSE	40S ribosomal protein S16 OS	115.94	42	6
P26369|U2AF2_MOUSE	Splicing factor U2AF 65 kDa s	113.64	18	6
Q6Y7W8|PERQ2_MOUSE	PERQ amino acid-rich with GY	113.33	11	6
P08226|APOE_MOUSE	Apolipoprotein E OS=Mus mu	110.83	43	6
P62702|RS4X_MOUSE	40S ribosomal protein S4, X is	107.6	37	6
P62751|RL23A_MOUSE	60S ribosomal protein L23a O	106.34	33	6

P97311|MCM6_MOUSE	DNA replication licensing factc	105.9	32	6
Q9CPP6|NDUA5_MOUSE	NADH dehydrogenase [ubiqui	102.93	60	6
Q8K297|GT251_MOUSE	Procollagen galactosyltransfer	102.73	24	6
O88477|IF2B1_MOUSE	Insulin-like growth factor 2 mR	102.59	27	6
Q9CQE1|NPS3A_MOUSE	Protein NipSnap homolog 3A (	99.65	31	6
Q91VA6|PDIP2_MOUSE	Polymerase delta-interacting p	97.93	30	6
Q8C8U0|LIPB1_MOUSE	Liprin-beta-1 OS=Mus muscul	97.25	38	6
Q08943|SSRP1_MOUSE	FACT complex subunit SSRP	95.91	18	6
Q8VEK3|HNRPU_MOUSE	Heterogeneous nuclear ribonu	94.26	13	6
P04186|CFAB_MOUSE	Complement factor B OS=Mus	93.37	19	6
Q99ME9|NOG1_MOUSE	Nucleolar GTP-binding protein	92.9	19	6
Q99K30|ES8L2_MOUSE	Epidermal growth factor recep	89.96	28	6
P17182|ENOA_MOUSE	Alpha-enolase OS=Mus musc	85.55	28	6
Q8VDP4|K1967_MOUSE	Protein KIAA1967 homolog OS	85.25	15	6
Q8C7E9|CSTFT_MOUSE	Cleavage stimulation factor su	81.11	31	6
O54724|PTRF_MOUSE	Polymerase I and transcript re	75.87	30	6
Q61830|MRC1_MOUSE	Macrophage mannose recepto	74.94	15	6
P27661|H2AX_MOUSE	Histone H2A.x OS=Mus musc	298.05	80	5
P68033|ACTC_MOUSE	Actin, alpha cardiac muscle 1	288.9	79	5
P99024|TBB5_MOUSE	Tubulin beta-5 chain OS=Mus	276.71	72	5
Q64475|H2B1B_MOUSE	Histone H2B type 1-B OS=Mu	230.53	69	5
Q6ZWY9|H2B1C_MOUSE	Histone H2B type 1-C/E/G OS	230.53	69	5
P10853|H2B1F_MOUSE	Histone H2B type 1-F/J/L OS=	230.53	69	5
Q64478|H2B1H_MOUSE	Histone H2B type 1-H OS=Mu	230.53	69	5
P10854|H2B1M_MOUSE	Histone H2B type 1-M OS=Mu	230.53	69	5
Q8CGP2|H2B1P_MOUSE	Histone H2B type 1-P OS=Mu	230.53	69	5
Q64525|H2B2B_MOUSE	Histone H2B type 2-B OS=Mu	230.53	69	5
O35737|HNRH1_MOUSE	Heterogeneous nuclear ribonu	209.95	45	5
P62960|YBOX1_MOUSE	Nuclease-sensitive element-bi	179.02	48	5
Q9EPJ9|ARFG1_MOUSE	ADP-ribosylation factor GTPas	157.19	43	5
Q99KR7|PPIF_MOUSE	Peptidyl-prolyl cis-trans isome	149.63	50	5
P23506|PIMT_MOUSE	Protein-L-isoaspartate(D-aspa	147.94	48	5
P01837|IGKC_MOUSE	Ig kappa chain C region OS=M	146.11	68	5
P01872|IGHM_MOUSE	Ig mu chain C region secreted	145.64	18	5
P01873|MUCM_MOUSE	Ig mu chain C region membra	145.64	17	5
P61089|UBE2N_MOUSE	Ubiquitin-conjugating enzyme	145.42	68	5
P62320|SMD3_MOUSE	Small nuclear ribonucleoprote	145.08	69	5
P62492|RB11A_MOUSE	Ras-related protein Rab-11A (	144.29	38	5
Q9WVA2|TIM8A_MOUSE	Mitochondrial import inner me	142.52	82	5
Q91WK2|EIF3H_MOUSE	Eukaryotic translation initiation	142.35	42	5
Q8K2C9|HACD3_MOUSE	3-hydroxyacyl-CoA dehydratas	142.17	27	5
Q923G2|RPAB3_MOUSE	DNA-directed RNA polymeras	141.08	47	5
Q62523|ZYX_MOUSE	Zyxin OS=Mus musculus GN=	139.77	33	5
Q6P5E6|GGA2_MOUSE	ADP-ribosylation factor-bindin	139.48	39	5
P62242|RS8_MOUSE	40S ribosomal protein S8 OS=	137.35	32	5
P23198|CBX3_MOUSE	Chromobox protein homolog 3	137.04	32	5
O88696|CLPP_MOUSE	Putative ATP-dependent Clp p	136.87	50	5
O70325|GPX41_MOUSE	Phospholipid hydroperoxide gl	131.66	32	5
Q9WV98|TIM9_MOUSE	Mitochondrial import inner me	131.61	74	5
Q8BKC5|IPO5_MOUSE	Importin-5 OS=Mus musculus	131.18	50	5
P14115|RL27A_MOUSE	60S ribosomal protein L27a O	130.47	39	5
Q9CYL5|GAPR1_MOUSE	Golgi-associated plant pathog	130.25	61	5
Q61990|PCBP2_MOUSE	Poly(rC)-binding protein 2 OS=	129.95	42	5
P80317|TCPZ_MOUSE	T-complex protein 1 subunit ze	129.84	38	5
P68037|UB2L3_MOUSE	Ubiquitin-conjugating enzyme	129.59	64	5

P98078|DAB2_MOUSE	Disabled homolog 2 OS=Mus	129.02	16	5
P18760|COF1_MOUSE	Cofilin-1 OS=Mus musculus G	128.27	57	5
P68510|1433F_MOUSE	14-3-3 protein eta OS=Mus m	127.7	63	5
Q9WV55|VAPA_MOUSE	Vesicle-associated membrane	127.6	46	5
P49722|PSA2_MOUSE	Proteasome subunit alpha typ	125.75	34	5
Q9QYJ0|DNJA2_MOUSE	DnaJ homolog subfamily A me	125.55	44	5
P84099|RL19_MOUSE	60S ribosomal protein L19 OS	124.59	26	5
Q61233|PLSL_MOUSE	Plastin-2 OS=Mus musculus G	124.26	26	5
Q3TXS7|PSMD1_MOUSE	26S proteasome non-ATPase	123.94	21	5
P14824|ANXA6_MOUSE	Annexin A6 OS=Mus musculu	123.83	23	5
Q6DFW4|NOP58_MOUSE	Nucleolar protein 58 OS=Mus	123.27	38	5
Q8K2B3|DHSA_MOUSE	Succinate dehydrogenase [ub	121.47	28	5
P52196|THTR_MOUSE	Thiosulfate sulfurtransferase G	120.95	31	5
Q61545|EWS_MOUSE	RNA-binding protein EWS OS	120.79	20	5
Q9CQF9|PCYOX_MOUSE	Prenylcysteine oxidase OS=M	120.7	30	5
Q60668|HNRPD_MOUSE	Heterogeneous nuclear ribonu	120.36	32	5
Q8C0E2|VP26B_MOUSE	Vacuolar protein sorting-assoc	119.49	38	5
Q9CZM2|RL15_MOUSE	60S ribosomal protein L15 OS	119.27	36	5
Q8BP40|PPA6_MOUSE	Lysophosphatidic acid phosph	119.24	29	5
Q8QZT1|THIL_MOUSE	Acetyl-CoA acetyltransferase,	117.51	25	5
Q6GU68|ISLR_MOUSE	Immunoglobulin superfamily c	117	25	5
Q61166|MARE1_MOUSE	Microtubule-associated protein	116.89	35	5
P68040|GBLP_MOUSE	Guanine nucleotide-binding pr	116.23	32	5
Q8CG71|P3H2_MOUSE	Prolyl 3-hydroxylase 2 OS=Mu	116.03	25	5
P80314|TCPB_MOUSE	T-complex protein 1 subunit b	114.83	21	5
Q99KJ8|DCTN2_MOUSE	Dynactin subunit 2 OS=Mus m	110.29	21	5
Q02819|NUCB1_MOUSE	Nucleobindin-1 OS=Mus musc	110.19	28	5
Q9JJI8|RL38_MOUSE	60S ribosomal protein L38 OS	109.1	37	5
Q8BIQ5|CSTF2_MOUSE	Cleavage stimulation factor su	108.24	39	5
P01868|IGHG1_MOUSE	Ig gamma-1 chain C region se	107.77	23	5
P01869|IGH1M_MOUSE	Ig gamma-1 chain C region, m	107.77	19	5
Q9D6R2|IDH3A_MOUSE	Isocitrate dehydrogenase [NA	106.01	31	5
P01864|GCAB_MOUSE	Ig gamma-2A chain C region s	105.64	25	5
Q9DBH5|LMAN2_MOUSE	Vesicular integral-membrane p	105.5	16	5
P60843|IF4A1_MOUSE	Eukaryotic initiation factor 4A-	104.88	39	5
P60867|RS20_MOUSE	40S ribosomal protein S20 OS	103.56	36	5
Q9CXF4|TBC15_MOUSE	TBC1 domain family member	103.27	20	5
Q05117|PPA5_MOUSE	Tartrate-resistant acid phosph	102.8	25	5
Q8K2C7|OS9_MOUSE	Protein OS-9 OS=Mus muscu	101.23	21	5
Q61768|KINH_MOUSE	Kinesin-1 heavy chain OS=Mu	101.04	18	5
Q9CR09|UFC1_MOUSE	Ubiquitin-fold modifier-conjuga	100.86	29	5
P53994|RAB2A_MOUSE	Ras-related protein Rab-2A O	100.6	35	5
Q9CQA3|DHSB_MOUSE	Succinate dehydrogenase [ub	98.53	48	5
Q8BTV2|CPSF7_MOUSE	Cleavage and polyadenylation	95.34	25	5
Q9CQE8|CN166_MOUSE	UPF0568 protein C14orf166 h	94.34	43	5
Q9DCW4|ETFB_MOUSE	Electron transfer flavoprotein s	93.52	24	5
P26516|PSD7_MOUSE	26S proteasome non-ATPase	92.26	29	5
O35593|PSDE_MOUSE	26S proteasome non-ATPase	91.81	35	5
P14685|PSMD3_MOUSE	26S proteasome non-ATPase	89.43	17	5
P28653|PGS1_MOUSE	Biglycan OS=Mus musculus G	89.11	18	5
Q921X9|PDIA5_MOUSE	Protein disulfide-isomerase A5	89.11	25	5
P09671|SODM_MOUSE	Superoxide dismutase [Mn], m	88.39	43	5
Q9D1M0|SEC13_MOUSE	Protein SEC13 homolog OS=M	86.18	47	5
Q5XJY5|COPD_MOUSE	Coatomer subunit delta OS=M	84.37	20	5
Q8CGF7|TCRG1_MOUSE	Transcription elongation regul	83.91	11	5

P62281|RS11_MOUSE	40S ribosomal protein S11 OS	81.73	22	5
P15508|SPTB1_MOUSE	Spectrin beta chain, erythrocy	80.59	12	5
P12023|A4_MOUSE	Amyloid beta A4 protein OS=M	62.12	18	5
Q80UW8|RPAB1_MOUSE	DNA-directed RNA polymeras	61.88	40	5
O88685|PRS6A_MOUSE	26S protease regulatory subu	57.92	25	5
A2AAJ9|OBSCN_MOUSE	Obscurin OS=Mus musculus (	26.01	4	5
Q8BFZ3|ACTBL_MOUSE	Beta-actin-like protein 2 OS=M	267.16	65	4
O08638|MYH11_MOUSE	Myosin-11 OS=Mus musculus	214.94	29	4
Q3THE2|ML12B_MOUSE	Myosin regulatory light chain 1	192.28	77	4
P85094|ISC2A_MOUSE	Isochorismatase domain-conta	179.06	63	4
Q6URW6|MYH14_MOUSE	Myosin-14 OS=Mus musculus	171.93	23	4
Q9QZM0|UBQL2_MOUSE	Ubiquilin-2 OS=Mus musculus	160.23	18	4
O08807|PRDX4_MOUSE	Peroxiredoxin-4 OS=Mus mus	153.87	40	4
P84078|ARF1_MOUSE	ADP-ribosylation factor 1 OS=	152.99	58	4
P61205|ARF3_MOUSE	ADP-ribosylation factor 3 OS=	152.99	58	4
Q64213|SF01_MOUSE	Splicing factor 1 OS=Mus mus	145.58	13	4
Q08369|GATA4_MOUSE	Transcription factor GATA-4 O	144.96	18	4
Q9DB15|RM12_MOUSE	39S ribosomal protein L12, mi	141.47	66	4
P84104|SRSF3_MOUSE	Serine/arginine-rich splicing fa	139.23	36	4
P09542|MYL3_MOUSE	Myosin light chain 3 OS=Mus	137.71	36	4
P62748|HPCL1_MOUSE	Hippocalcin-like protein 1 OS=	137.1	52	4
Q9D1B9|RM28_MOUSE	39S ribosomal protein L28, mi	133.83	48	4
Q9QUM9|PSA6_MOUSE	Proteasome subunit alpha typ	131.26	21	4
P99027|RLA2_MOUSE	60S acidic ribosomal protein P	130.62	63	4
Q80UM7|MOGS_MOUSE	Mannosyl-oligosaccharide glu	130.11	22	4
Q9DBR0|AKAP8_MOUSE	A-kinase anchor protein 8 OS=	129.59	34	4
O70251|EF1B_MOUSE	Elongation factor 1-beta OS=M	129.02	32	4
Q64010|CRK_MOUSE	Adapter molecule crk OS=Mus	128.1	26	4
Q9DBG6|RPN2_MOUSE	Dolichyl-diphosphooligosaccha	125.84	18	4
Q3UZ39|LRRF1_MOUSE	Leucine-rich repeat flightless-i	124.96	19	4
P62075|TIM13_MOUSE	Mitochondrial import inner me	124.46	54	4
Q99LT0|DPY30_MOUSE	Protein dpy-30 homolog OS=M	123.87	83	4
Q9R099|TBL2_MOUSE	Transducin beta-like protein 2	123.17	18	4
Q3V1L4|5NTC_MOUSE	Cytosolic purine 5'-nucleotidas	123.14	18	4
Q9Z2D8|MBD3_MOUSE	Methyl-CpG-binding domain p	122.12	30	4
P43274|H14_MOUSE	Histone H1.4 OS=Mus muscu	119.7	37	4
P63323|RS12_MOUSE	40S ribosomal protein S12 OS	118.78	36	4
P59708|PM14_MOUSE	Pre-mRNA branch site protein	117.18	44	4
O55029|COPB2_MOUSE	Coatomer subunit beta' OS=M	116.91	18	4
Q9CYD3|CRTAP_MOUSE	Cartilage-associated protein C	116.23	31	4
Q9WVK4|EHD1_MOUSE	EH domain-containing protein	115.68	17	4
P62309|RUXG_MOUSE	Small nuclear ribonucleoprote	115.17	83	4
P30412|PPIC_MOUSE	Peptidyl-prolyl cis-trans isome	114.97	34	4
P97371|PSME1_MOUSE	Proteasome activator complex	114.85	29	4
O09167|RL21_MOUSE	60S ribosomal protein L21 OS	112.76	38	4
Q9CZU3|SK2L2_MOUSE	Superkiller viralicidic activity 2	112.67	22	4
Q8CIE6|COPA_MOUSE	Coatomer subunit alpha OS=M	111.18	16	4
O35900|LSM2_MOUSE	U6 snRNA-associated Sm-like	111.13	62	4
P62267|RS23_MOUSE	40S ribosomal protein S23 OS	111.05	64	4
Q8QZY1|EIF3L_MOUSE	Eukaryotic translation initiation	110.88	15	4
Q7TPV4|MBB1A_MOUSE	Myb-binding protein 1A OS=M	110.37	19	4
P45878|FKBP2_MOUSE	Peptidyl-prolyl cis-trans isome	109.14	68	4
P14869|RLA0_MOUSE	60S acidic ribosomal protein P	109.08	24	4
P97493|THIOM_MOUSE	Thioredoxin, mitochondrial OS	108.77	51	4
Q9DAR7|DCPS_MOUSE	Scavenger mRNA-decapping	108.34	43	4

P51410|RL9_MOUSE	60S ribosomal protein L9 OS=	108.33	37	4
Q5SUC9|SCO1_MOUSE	Protein SCO1 homolog, mitoc	107.84	37	4
Q9ERK4|XPO2_MOUSE	Exportin-2 OS=Mus musculus	106.79	18	4
Q99JB2|STML2_MOUSE	Stomatin-like protein 2 OS=Mu	106.55	33	4
Q99P88|NU155_MOUSE	Nuclear pore complex protein	106.13	25	4
O88653|LTOR3_MOUSE	Ragulator complex protein LA	105.85	50	4
P08122|CO4A2_MOUSE	Collagen alpha-2(IV) chain OS	104.41	11	4
Q9Z0R4|ITSN1_MOUSE	Intersectin-1 OS=Mus muscul	104.23	13	4
Q9CR57|RL14_MOUSE	60S ribosomal protein L14 OS	104.03	27	4
Q9QX47|SON_MOUSE	Protein SON OS=Mus muscul	103.93	13	4
Q8R1B4|EIF3C_MOUSE	Eukaryotic translation initiation	103.41	18	4
P05064|ALDOA_MOUSE	Fructose-bisphosphate aldolas	103.26	21	4
Q9DAW9|CNN3_MOUSE	Calponin-3 OS=Mus musculus	103.23	25	4
Q6ZWY3|RS27L_MOUSE	40S ribosomal protein S27-like	102.88	39	4
Q9JJH1|RNAS4_MOUSE	Ribonuclease 4 OS=Mus mus	102.87	36	4
B2RY56|RBM25_MOUSE	RNA-binding protein 25 OS=M	102.76	16	4
P46938|YAP1_MOUSE	Yorkie homolog OS=Mus mus	102.71	37	4
Q8BP67|RL24_MOUSE	60S ribosomal protein L24 OS	102.26	19	4
P25206|MCM3_MOUSE	DNA replication licensing facto	100.52	17	4
P70318|TIAR_MOUSE	Nucleolysin TIAR OS=Mus mu	99.09	26	4
Q61733|RT31_MOUSE	28S ribosomal protein S31, m	97.62	19	4
Q9WTP7|KAD3_MOUSE	GTP:AMP phosphotransferase	96.96	33	4
Q9WUK2|IF4H_MOUSE	Eukaryotic translation initiation	95.49	22	4
P81117|NUCB2_MOUSE	Nucleobindin-2 OS=Mus musc	93.85	27	4
Q3UQN2|FCHO2_MOUSE	FCH domain only protein 2 OS	93.43	8	4
P61759|PFD3_MOUSE	Prefoldin subunit 3 OS=Mus m	93.36	24	4
Q6ZQL4|WDR43_MOUSE	WD repeat-containing protein	93.31	15	4
Q9QXC1|FETUB_MOUSE	Fetuin-B OS=Mus musculus G	92.2	26	4
O54962|BAF_MOUSE	Barrier-to-autointegration facto	91.84	51	4
Q9R1P0|PSA4_MOUSE	Proteasome subunit alpha typ	91.52	28	4
Q9R0N0|GALK1_MOUSE	Galactokinase OS=Mus musc	90.6	20	4
O08788|DCTN1_MOUSE	Dynactin subunit 1 OS=Mus m	90.59	24	4
P62073|TIM10_MOUSE	Mitochondrial import inner me	88.1	50	4
Q8VE22|RT23_MOUSE	28S ribosomal protein S23, m	87.88	47	4
P62869|ELOB_MOUSE	Transcription elongation factor	87.83	34	4
Q8BG32|PSD11_MOUSE	26S proteasome non-ATPase	86.82	25	4
P18572|BASI_MOUSE	Basigin OS=Mus musculus GI	86.81	15	4
Q07813|BAX_MOUSE	Apoptosis regulator BAX OS=	86.37	28	4
Q8BI84|MIA3_MOUSE	Melanoma inhibitory activity pr	85.77	15	4
Q8CJ69|BMPER_MOUSE	BMP-binding endothelial regul	85.61	8	4
Q9JII6|AK1A1_MOUSE	Alcohol dehydrogenase [NADI	83.12	17	4
Q9D2M8|UB2V2_MOUSE	Ubiquitin-conjugating enzyme	82.5	30	4
Q9CZY3|UB2V1_MOUSE	Ubiquitin-conjugating enzyme	82.5	24	4
P63158|HMGB1_MOUSE	High mobility group protein B1	82.49	30	4
Q9QZD9|EIF3I_MOUSE	Eukaryotic translation initiation	81.23	15	4
Q8BHN3|GANAB_MOUSE	Neutral alpha-glucosidase AB	80.52	17	4
Q01279|EGFR_MOUSE	Epidermal growth factor recep	80.35	8	4
P0C6F1|DYH2_MOUSE	Dynein heavy chain 2, axonem	79.82	5	4
Q64012|RALY_MOUSE	RNA-binding protein Raly OS=	79.36	24	4
P51150|RAB7A_MOUSE	Ras-related protein Rab-7a OS	78.31	27	4
Q9Z1Y4|TRIP6_MOUSE	Thyroid receptor-interacting pr	78.28	18	4
P54728|RD23B_MOUSE	UV excision repair protein RA	76.89	16	4
P62852|RS25_MOUSE	40S ribosomal protein S25 OS	74.95	36	4
Q6NWW9|FND3B_MOUSE	Fibronectin type III domain-co	74.33	7	4
P45376|ALDR_MOUSE	Aldose reductase OS=Mus mu	74.17	17	4

Q921M3|SF3B3_MOUSE	Splicing factor 3B subunit 3 O	73.92	10	4
Q99LC5|ETFA_MOUSE	Electron transfer flavoprotein s	70.88	19	4
P23116|EIF3A_MOUSE	Eukaryotic translation initiation	69.55	12	4
P62245|RS15A_MOUSE	40S ribosomal protein S15a O	69.42	32	4
Q8BMF4|ODP2_MOUSE	Dihydrolipoyllysine-residue ac	69.37	15	4
Q8VHN8|SDOS_MOUSE	Protein syndesmos OS=Mus r	68.74	32	4
Q60675|LAMA2_MOUSE	Laminin subunit alpha-2 OS=M	67.04	13	4
Q91VD9|NDUS1_MOUSE	NADH-ubiquinone oxidoreduc	65.74	15	4
Q9Z0R6|ITSN2_MOUSE	Intersectin-2 OS=Mus muscul	54.58	14	4
Q6NS46|RRP5_MOUSE	Protein RRP5 homolog OS=M	53.84	7	4
Q91YU8|SSF1_MOUSE	Suppressor of SWI4 1 homolo	51.26	20	4
Q91ZX7|LRP1_MOUSE	Prolow-density lipoprotein rece	49.22	6	4
Q62407|SPEG_MOUSE	Striated muscle-specific serine	43.9	4	4
Q6GSS7|H2A2A_MOUSE	Histone H2A type 2-A OS=Mu	299.33	88	3
P16627|HS71L_MOUSE	Heat shock 70 kDa protein 1-l	245.91	63	3
P84228|H32_MOUSE	Histone H3.2 OS=Mus muscu	225.13	78	3
Q60972|RBBP4_MOUSE	Histone-binding protein RBBP	181.84	37	3
O08583|THOC4_MOUSE	THO complex subunit 4 OS=M	177.44	55	3
Q9R0B6|LAMC3_MOUSE	Laminin subunit gamma-3 OS	157.72	12	3
Q8VEA4|MIA40_MOUSE	Mitochondrial intermembrane	147.38	32	3
Q61029|LAP2B_MOUSE	Lamina-associated polypeptid	141.23	28	3
Q9DBG9|TX1B3_MOUSE	Tax1-binding protein 3 OS=Mu	127.96	47	3
P61971|NTF2_MOUSE	Nuclear transport factor 2 OS=	124.44	57	3
Q8VDM6|HNRL1_MOUSE	Heterogeneous nuclear ribonu	122.56	29	3
Q60973|RBBP7_MOUSE	Histone-binding protein RBBP	121.86	28	3
Q8BFY9|TNPO1_MOUSE	Transportin-1 OS=Mus muscu	121.11	35	3
P24452|CAPG_MOUSE	Macrophage-capping protein G	116.32	21	3
P70296|PEBP1_MOUSE	Phosphatidylethanolamine-bin	115.57	33	3
Q5SFM8|RBM27_MOUSE	RNA-binding protein 27 OS=M	114.99	14	3
Q99P27|PG12B_MOUSE	Group XIIB secretory phospho	114.95	42	3
P05201|AATC_MOUSE	Aspartate aminotransferase, c	112.61	17	3
O88630|GOSR1_MOUSE	Golgi SNAP receptor complex	112.52	26	3
Q9DCJ5|NDUA8_MOUSE	NADH dehydrogenase [ubiqui	111.93	23	3
Q91ZW3|SMCA5_MOUSE	SWI/SNF-related matrix-asso	110.71	20	3
Q9CXW4|RL11_MOUSE	60S ribosomal protein L11 OS	109.24	20	3
Q99KE1|MAOM_MOUSE	NAD-dependent malic enzyme	109.22	18	3
P24472|GSTA4_MOUSE	Glutathione S-transferase A4	108.91	30	3
Q6ZWV7|RL35_MOUSE	60S ribosomal protein L35 OS	108.47	22	3
Q9EQU5|SET_MOUSE	Protein SET OS=Mus musculu	108.04	22	3
Q61581|IBP7_MOUSE	Insulin-like growth factor-bindi	107.86	31	3
Q9D7V9|NAAA_MOUSE	N-acylethanolamine-hydrolyzin	106.78	16	3
P51660|DHB4_MOUSE	Peroxisomal multifunctional en	106.33	11	3
O55057|PDE6D_MOUSE	Retinal rod rhodopsin-sensitive	106.28	29	3
P12787|COX5A_MOUSE	Cytochrome c oxidase subunit	105.87	70	3
Q61247|A2AP_MOUSE	Alpha-2-antiplasmin OS=Mus	105.7	15	3
Q920A5|RISC_MOUSE	Retinoid-inducible serine carbo	105.45	13	3
P62849|RS24_MOUSE	40S ribosomal protein S24 OS	105.44	29	3
P12265|BGLR_MOUSE	Beta-glucuronidase OS=Mus m	103.8	9	3
P29391|FRIL1_MOUSE	Ferritin light chain 1 OS=Mus	103.19	31	3
Q08093|CNN2_MOUSE	Calponin-2 OS=Mus musculus	103.04	21	3
Q91VC3|IF4A3_MOUSE	Eukaryotic initiation factor 4A-	102.5	27	3
P70168|IMB1_MOUSE	Importin subunit beta-1 OS=M	102.1	9	3
P11438|LAMP1_MOUSE	Lysosome-associated membra	101.69	27	3
P35979|RL12_MOUSE	60S ribosomal protein L12 OS	101.62	42	3
Q9CY16|RT28_MOUSE	28S ribosomal protein S28, m	100.73	29	3

Q80UY2|KCMF1_MOUSE	E3 ubiquitin-protein ligase KC	99.9	16	3
Q9ES28|ARHG7_MOUSE	Rho guanine nucleotide excha	99.82	13	3
P97429|ANXA4_MOUSE	Annexin A4 OS=Mus musculu	99.76	29	3
Q3TKT4|SMCA4_MOUSE	Transcription activator BRG1 (	99.26	8	3
Q8VH51|RBM39_MOUSE	RNA-binding protein 39 OS=M	98.83	16	3
Q61823|PDCD4_MOUSE	Programmed cell death protei	98.32	23	3
Q8BGS0|MAK16_MOUSE	Protein MAK16 homolog OS=	98.24	24	3
P08074|CBR2_MOUSE	Carbonyl reductase [NADPH]	97.51	26	3
Q61703|ITIH2_MOUSE	Inter-alpha-trypsin inhibitor he	97.11	15	3
Q9D8U8|SNX5_MOUSE	Sorting nexin-5 OS=Mus musc	96.46	18	3
P63028|TCTP_MOUSE	Translationally-controlled tumo	95.69	28	3
P63325|RS10_MOUSE	40S ribosomal protein S10 OS	95.03	31	3
Q9Z0H3|SNF5_MOUSE	SWI/SNF-related matrix-assoc	94.48	21	3
P00920|CAH2_MOUSE	Carbonic anhydrase 2 OS=Mu	92.49	16	3
Q9CR68|UCRI_MOUSE	Cytochrome b-c1 complex sub	92.31	35	3
Q9CPX7|RT16_MOUSE	28S ribosomal protein S16, m	92.02	29	3
P97390|VPS45_MOUSE	Vacuolar protein sorting-assoc	91.87	12	3
Q922Y1|UBXN1_MOUSE	UBX domain-containing protei	91.79	26	3
Q6ZQ88|KDM1A_MOUSE	Lysine-specific histone demet	90.79	7	3
P24547|IMDH2_MOUSE	Inosine-5'-monophosphate de	90.54	18	3
Q9R0X4|ACOT9_MOUSE	Acyl-coenzyme A thioesterase	90.19	24	3
P29416|HEXA_MOUSE	Beta-hexosaminidase subunit	90.14	18	3
Q8BYK6|YTHD3_MOUSE	YTH domain family protein 3 (	89.41	16	3
Q9R1P3|PSB2_MOUSE	Proteasome subunit beta type	89.33	28	3
P99026|PSB4_MOUSE	Proteasome subunit beta type	89.03	26	3
P46467|VPS4B_MOUSE	Vacuolar protein sorting-assoc	88.96	20	3
P62821|RAB1A_MOUSE	Ras-related protein Rab-1A O	88.86	38	3
Q60649|CLPB_MOUSE	Caseinolytic peptidase B prote	88.36	10	3
Q6ZPY7|KDM3B_MOUSE	Lysine-specific demethylase 3	87.93	12	3
P07146|TRY2_MOUSE	Anionic trypsin-2 OS=Mus mu	87.92	19	3
Q7TN75|PEG10_MOUSE	Retrotransposon-derived prote	87.76	17	3
P04117|FABP4_MOUSE	Fatty acid-binding protein, adi	87.65	27	3
Q9QYS9|QKI_MOUSE	Protein quaking OS=Mus mus	87.43	29	3
P19536|COX5B_MOUSE	Cytochrome c oxidase subunit	87.3	30	3
Q8VE88|F1142_MOUSE	Protein FAM114A2 OS=Mus r	87	35	3
Q9Z0P5|TWF2_MOUSE	Twinfilin-2 OS=Mus musculus	86.77	10	3
Q9CQ40|RM49_MOUSE	39S ribosomal protein L49, mi	86.41	22	3
Q9EQS3|MYCBP_MOUSE	C-Myc-binding protein OS=Mu	86.21	58	3
P42932|TCPQ_MOUSE	T-complex protein 1 subunit th	86.11	18	3
Q921G8|GCP2_MOUSE	Gamma-tubulin complex comp	86.02	26	3
Q8R010|AIMP2_MOUSE	Aminoacyl tRNA synthase con	85.74	26	3
Q06138|CAB39_MOUSE	Calcium-binding protein 39 OS	84.6	12	3
Q922V4|PLRG1_MOUSE	Pleiotropic regulator 1 OS=Mu	83.77	8	3
Q9D0F3|LMAN1_MOUSE	Protein ERGIC-53 OS=Mus m	83.65	10	3
Q9CPV4|GLOD4_MOUSE	Glyoxalase domain-containing	83.52	22	3
Q64511|TOP2B_MOUSE	DNA topoisomerase 2-beta OS	82.94	6	3
P46935|NEDD4_MOUSE	E3 ubiquitin-protein ligase NE	82.54	20	3
Q3U7R1|ESYT1_MOUSE	Extended synaptotagmin-1 OS	82.33	12	3
Q9JMA1|UBP14_MOUSE	Ubiquitin carboxyl-terminal hyd	82.27	16	3
Q69ZA1|CDK13_MOUSE	Cyclin-dependent kinase 13 O	82.26	11	3
Q3U9G9|LBR_MOUSE	Lamin-B receptor OS=Mus mu	82.19	10	3
O88544|CSN4_MOUSE	COP9 signalosome complex s	82.02	31	3
Q3UKC1|TAXB1_MOUSE	Tax1-binding protein 1 homolo	81.85	22	3
A2AGT5|CKAP5_MOUSE	Cytoskeleton-associated prote	80.73	11	3
Q9DBY8|NVL_MOUSE	Nuclear valosin-containing pro	80.32	10	3

Q9DBG7|SRPR_MOUSE	Signal recognition particle rec	79.88	10	3
Q8VC70|RBMS2_MOUSE	RNA-binding motif, single-stra	78.67	30	3
Q921F4|HNRLL_MOUSE	Heterogeneous nuclear ribonu	78.49	13	3
P01029|CO4B_MOUSE	Complement C4-B OS=Mus m	77.2	10	3
Q9CZ44|NSF1C_MOUSE	NSFL1 cofactor p47 OS=Mus	76.88	12	3
P61961|UFM1_MOUSE	Ubiquitin-fold modifier 1 OS=M	75.89	69	3
P41105|RL28_MOUSE	60S ribosomal protein L28 OS	75.18	29	3
Q6ZWV3|RL10_MOUSE	60S ribosomal protein L10 OS	75.07	19	3
O55023|IMPA1_MOUSE	Inositol monophosphatase 1 C	75.02	28	3
Q9D1K7|CT027_MOUSE	UPF0687 protein C20orf27 ho	74.68	25	3
P62827|RAN_MOUSE	GTP-binding nuclear protein R	74.63	17	3
Q7TQH0|ATX2L_MOUSE	Ataxin-2-like protein OS=Mus	74.44	8	3
Q9QXV1|CBX8_MOUSE	Chromobox protein homolog 8	74.42	9	3
Q80WJ7|LYRIC_MOUSE	Protein LYRIC OS=Mus musc	74.26	24	3
Q3V4B5|COMD6_MOUSE	COMM domain-containing pro	73.82	47	3
Q9CQP2|TPPC2_MOUSE	Trafficking protein particle con	73.21	35	3
Q99J99|THTM_MOUSE	3-mercaptopyruvate sulfurtran	73.12	14	3
P62900|RL31_MOUSE	60S ribosomal protein L31 OS	72.65	40	3
P59325|IF5_MOUSE	Eukaryotic translation initiation	72.42	12	3
P61965|WDR5_MOUSE	WD repeat-containing protein	71.65	16	3
Q8BX22|SALL4_MOUSE	Sal-like protein 4 OS=Mus mu	71.53	11	3
O88508|DNM3A_MOUSE	DNA (cytosine-5)-methyltransf	71.08	7	3
Q6PB66|LPPRC_MOUSE	Leucine-rich PPR motif-contai	70.76	6	3
Q9CR00|PSMD9_MOUSE	26S proteasome non-ATPase	70.41	22	3
Q9CR21|ACPM_MOUSE	Acyl carrier protein, mitochond	70.38	14	3
Q6PGN1|F132B_MOUSE	Protein FAM132B OS=Mus m	69.87	9	3
Q8BL66|EEA1_MOUSE	Early endosome antigen 1 OS	69.47	8	3
Q9Z1N2|ORC1_MOUSE	Origin recognition complex su	68.93	9	3
Q8C5Q4|GRSF1_MOUSE	G-rich sequence factor 1 OS=	68.88	20	3
Q61263|SOAT1_MOUSE	Sterol O-acyltransferase 1 OS	68.41	43	3
Q9R087|GPC6_MOUSE	Glypican-6 OS=Mus musculus	67.47	21	3
P63168|DYL1_MOUSE	Dynein light chain 1, cytoplasm	67.42	48	3
Q80U93|NU214_MOUSE	Nuclear pore complex protein	67.23	10	3
Q9WUU7|CATZ_MOUSE	Cathepsin Z OS=Mus musculu	65.2	25	3
Q9CZG9|PDZ11_MOUSE	PDZ domain-containing protei	64.59	65	3
O35604|NPC1_MOUSE	Niemann-Pick C1 protein OS=	64.28	8	3
P11983|TCPA_MOUSE	T-complex protein 1 subunit a	63.34	13	3
Q9Z1N5|DX39B_MOUSE	Spliceosome RNA helicase DC	62.3	16	3
Q9D6J6|NDUV2_MOUSE	NADH dehydrogenase [ubiqui	61.76	24	3
Q80W00|PP1RA_MOUSE	Serine/threonine-protein phos	60.53	17	3
P80318|TCPG_MOUSE	T-complex protein 1 subunit g	59.81	38	3
P54775|PRS6B_MOUSE	26S protease regulatory subu	59.62	8	3
Q9CQM9|GLRX3_MOUSE	Glutaredoxin-3 OS=Mus musc	59.13	16	3
P14901|HMOX1_MOUSE	Heme oxygenase 1 OS=Mus m	58.37	19	3
Q8BMJ2|SYLC_MOUSE	Leucyl-tRNA synthetase, cyto	58	8	3
P29268|CTGF_MOUSE	Connective tissue growth fact	57.19	13	3
Q6P5F9|XPO1_MOUSE	Exportin-1 OS=Mus musculus	57.04	7	3
Q9CR98|F136A_MOUSE	Protein FAM136A OS=Mus m	56.87	25	3
Q9DCD5|TJAP1_MOUSE	Tight junction-associated prot	54.46	5	3
P83940|ELOC_MOUSE	Transcription elongation factor	53.8	44	3
Q9JJ28|FLII_MOUSE	Protein flightless-1 homolog O	53.33	10	3
Q63870|CO7A1_MOUSE	Collagen alpha-1(VII) chain O	48.67	11	3
Q80T85|DCAF5_MOUSE	DDB1- and CUL4-associated	47.52	10	3
P70336|ROCK2_MOUSE	Rho-associated protein kinase	47.44	7	3
Q99KW3|TARA_MOUSE	TRIO and F-actin-binding prot	43.34	8	3

P16056|MET_MOUSE	Hepatocyte growth factor rece	42.77	9	3
Q6QIY3|SCNAA_MOUSE	Sodium channel protein type 1	41.52	6	3
Q9CW03|SMC3_MOUSE	Structural maintenance of chr	40.92	12	3
Q8BJ37|TYDP1_MOUSE	Tyrosyl-DNA phosphodiestera	40.08	12	3
Q6ZWQ0|SYNE2_MOUSE	Nesprin-2 OS=Mus musculus	37.4	7	3
O88700|BLM_MOUSE	Bloom syndrome protein hom	36.33	8	3
Q6NZC7|S23IP_MOUSE	SEC23-interacting protein OS	34.81	6	3
Q6PDK2|MLL2_MOUSE	Histone-lysine N-methyltransfe	34.74	3	3
A2A7S8|K1522_MOUSE	Uncharacterized protein KIAA	34	7	3
Q9QXZ0|MACF1_MOUSE	Microtubule-actin cross-linking	33.73	4	3
Q924A2|CIC_MOUSE	Protein capicua homolog OS=	33.17	4	3
Q99PJ1|PCD15_MOUSE	Protocadherin-15 OS=Mus mu	32.93	5	3
Q6R5N8|TLR13_MOUSE	Toll-like receptor 13 OS=Mus	32.86	13	3
Q9CXA2|PRCM_MOUSE	Probable proline racemase OS	30.3	8	3
B2RX88|CSPP1_MOUSE	Centrosome and spindle pole	30.26	8	3
Q6PGL7|FAM21_MOUSE	WASH complex subunit FAM2	30.03	8	3
Q8BLN6|UNC80_MOUSE	Protein unc-80 homolog OS=M	29.79	8	3
B9EKI3|TMF1_MOUSE	TATA element modulatory fac	29.2	7	3
A2AAE1|K1109_MOUSE	Uncharacterized protein KIAA	27.33	7	3
Q766D5|B4GN4_MOUSE	N-acetyl-beta-glucosaminyl-gly	26.91	9	3
Q3UHU5|K0802_MOUSE	Uncharacterized protein KIAA(	26.9	4	3
Q80TY5|VP13B_MOUSE	Vacuolar protein sorting-assoc	26.69	4	3
Q6GQT6|SCAP_MOUSE	Sterol regulatory element-bind	26.49	9	3
Q9R244|TRPC2_MOUSE	Short transient receptor poten	25.77	8	3
A2ARZ3|FSIP2_MOUSE	Fibrous sheath-interacting pro	25.37	5	3
O88491|NSD1_MOUSE	Histone-lysine N-methyltransfe	24.67	4	3
Q4VK74|IL28A_MOUSE	Interleukin-28A OS=Mus musc	24.52	13	3
Q8CGK6|IL28B_MOUSE	Interleukin-28B OS=Mus musc	24.52	13	3
P06800|PTPRC_MOUSE	Receptor-type tyrosine-protein	21.91	7	3
P63260|ACTG_MOUSE	Actin, cytoplasmic 2 OS=Mus	354.61	86	2
Q64522|H2A2B_MOUSE	Histone H2A type 2-B OS=Mu	301.18	90	2
P07758|A1AT1_MOUSE	Alpha-1-antitrypsin 1-1 OS=M	257.13	61	2
P68372|TBB2C_MOUSE	Tubulin beta-2C chain OS=Mu	256.34	65	2
Q7TMM9|TBB2A_MOUSE	Tubulin beta-2A chain OS=Mu	245.26	60	2
Q9CWF2|TBB2B_MOUSE	Tubulin beta-2B chain OS=Mu	245.26	60	2
Q64524|H2B2E_MOUSE	Histone H2B type 2-E OS=Mu	212.55	72	2
Q922F4|TBB6_MOUSE	Tubulin beta-6 chain OS=Mus	210.98	45	2
P70333|HNRH2_MOUSE	Heterogeneous nuclear ribonu	178.13	29	2
Q9CQ19|MYL9_MOUSE	Myosin regulatory light polype	176.32	81	2
P63163|RSMN_MOUSE	Small nuclear ribonucleprote	165.88	50	2
Q9JKB3|DBPA_MOUSE	DNA-binding protein A OS=Mu	149.05	29	2
P26040|EZRI_MOUSE	Ezrin OS=Mus musculus GN=	133.84	17	2
P35550|FBRL_MOUSE	rRNA 2'-O-methyltransferase	131.03	30	2
P26043|RADI_MOUSE	Radixin OS=Mus musculus G	130.02	22	2
Q6PFR5|TRA2A_MOUSE	Transformer-2 protein homolo	125.44	26	2
Q6P1F6|2ABA_MOUSE	Serine/threonine-protein phos	122.58	30	2
P35278|RAB5C_MOUSE	Ras-related protein Rab-5C O	121.99	25	2
Q62241|RU1C_MOUSE	U1 small nuclear ribonucleopr	118.52	40	2
P01644|KV5AB_MOUSE	Ig kappa chain V-V region HP	117.47	47	2
P26041|MOES_MOUSE	Moesin OS=Mus musculus GN	115.89	25	2
P97461|RS5_MOUSE	40S ribosomal protein S5 OS=	111.9	50	2
P97290|IC1_MOUSE	Plasma protease C1 inhibitor (	110.09	15	2
Q60590|A1AG1_MOUSE	Alpha-1-acid glycoprotein 1 OS	109.67	38	2
Q9CQN1|TRAP1_MOUSE	Heat shock protein 75 kDa, m	106.44	15	2
Q9R1P1|PSB3_MOUSE	Proteasome subunit beta type	101.53	27	2

Q921H8|THIKA_MOUSE	3-ketoacyl-CoA thiolase A, pe	101.43	25	2
Q99JX3|GORS2_MOUSE	Golgi reassembly-stacking pro	100.57	17	2
Q62426|CYTB_MOUSE	Cystatin-B OS=Mus musculus	100.39	33	2
Q9ESB3|HRG_MOUSE	Histidine-rich glycoprotein OS	97.47	10	2
Q9CS42|PRPS2_MOUSE	Ribose-phosphate pyrophosph	97.36	25	2
P26883|FKB1A_MOUSE	Peptidyl-prolyl cis-trans isome	97.14	25	2
Q9ET22|DPP2_MOUSE	Dipeptidyl peptidase 2 OS=Mu	96.81	14	2
Q9ES46|PARVB_MOUSE	Beta-parvin OS=Mus musculu	96.59	11	2
Q9JJV2|PROF2_MOUSE	Profilin-2 OS=Mus musculus G	96.56	32	2
P97379|G3BP2_MOUSE	Ras GTPase-activating protein	95.87	15	2
Q9DCH4|EIF3F_MOUSE	Eukaryotic translation initiation	95.71	16	2
Q5I1X5|IASPP_MOUSE	RelA-associated inhibitor OS=	93.77	17	2
Q9DCD6|GBRAP_MOUSE	Gamma-aminobutyric acid rec	93.28	32	2
P47955|RLA1_MOUSE	60S acidic ribosomal protein P	92.16	42	2
P10639|THIO_MOUSE	Thioredoxin OS=Mus musculu	91.4	21	2
O88968|TCO2_MOUSE	Transcobalamin-2 OS=Mus m	91.23	12	2
P70663|SPRL1_MOUSE	SPARC-like protein 1 OS=Mus	90.96	10	2
Q8BHD7|ROD1_MOUSE	Regulator of differentiation 1 O	90.78	21	2
Q61510|TRI25_MOUSE	E3 ubiquitin/ISG15 ligase TRI	89.97	12	2
Q9Z1B5|MD2L1_MOUSE	Mitotic spindle assembly chec	89.56	24	2
Q8CI43|MYL6B_MOUSE	Myosin light chain 6B OS=Mus	88.95	25	2
O35744|CH3L3_MOUSE	Chitinase-3-like protein 3 OS=	88.68	18	2
Q8BRG8|TM209_MOUSE	Transmembrane protein 209 O	88.01	12	2
Q04857|CO6A1_MOUSE	Collagen alpha-1(VI) chain OS	86.6	8	2
Q7TPD3|ROBO2_MOUSE	Roundabout homolog 2 OS=M	86.24	9	2
P26618|PGFRA_MOUSE	Alpha-type platelet-derived gro	86.16	20	2
P62196|PRS8_MOUSE	26S protease regulatory subu	85.38	16	2
P04919|B3AT_MOUSE	Band 3 anion transport protein	85.3	9	2
Q6NZN0|RBM26_MOUSE	RNA-binding protein 26 OS=M	84.87	10	2
Q64324|STXB2_MOUSE	Syntaxin-binding protein 2 OS	84.53	12	2
Q8K183|PDXK_MOUSE	Pyridoxal kinase OS=Mus mus	83.89	14	2
Q6ZWM4|NAA38_MOUSE	N-alpha-acetyltransferase 38,	83.77	34	2
Q9WVJ2|PSD13_MOUSE	26S proteasome non-ATPase	83.47	18	2
P60824|CIRBP_MOUSE	Cold-inducible RNA-binding pr	83.03	36	2
Q9CQT2|RBM7_MOUSE	RNA-binding protein 7 OS=Mu	83.02	14	2
P97360|ETV6_MOUSE	Transcription factor ETV6 OS	82.86	12	2
Q8BSQ9|PB1_MOUSE	Protein polybromo-1 OS=Mus	82.61	9	2
P67984|RL22_MOUSE	60S ribosomal protein L22 OS	82.26	20	2
P22892|AP1G1_MOUSE	AP-1 complex subunit gamma	82.25	15	2
P62855|RS26_MOUSE	40S ribosomal protein S26 OS	82.11	39	2
Q6A065|CE170_MOUSE	Centrosomal protein of 170 kD	82.04	8	2
Q91YD3|DCP1A_MOUSE	mRNA-decapping enzyme 1A	80.74	9	2
P51885|LUM_MOUSE	Lumican OS=Mus musculus G	80.71	24	2
Q9CSU0|RPR1B_MOUSE	Regulation of nuclear pre-mRI	80.64	15	2
O35114|SCRB2_MOUSE	Lysosome membrane protein	80.59	9	2
Q8BKG3|PTK7_MOUSE	Inactive tyrosine-protein kinas	80.26	10	2
P97425|ECP2_MOUSE	Eosinophil cationic protein 2 O	80.11	38	2
Q9Z1Z2|STRAP_MOUSE	Serine-threonine kinase recep	80.08	24	2
Q9Z175|LOXL3_MOUSE	Lysyl oxidase homolog 3 OS=	79.56	4	2
Q69ZQ2|ISY1_MOUSE	Pre-mRNA-splicing factor ISY	78.99	19	2
Q9Z0M5|LICH_MOUSE	Lysosomal acid lipase/cholest	78.41	29	2
Q6A4J8|UBP7_MOUSE	Ubiquitin carboxyl-terminal hy	78.11	7	2
P02463|CO4A1_MOUSE	Collagen alpha-1(IV) chain OS	77.9	9	2
P10649|GSTM1_MOUSE	Glutathione S-transferase Mu	77.56	19	2
Q80W21|GSTM7_MOUSE	Glutathione S-transferase Mu	77.56	32	2

P15626|GSTM2_MOUSE	Glutathione S-transferase Mu	77.56	18	2
Q8CHU3|EPN2_MOUSE	Epsin-2 OS=Mus musculus G	77.46	10	2
P97855|G3BP1_MOUSE	Ras GTPase-activating protei	77.44	16	2
Q8K221|ARFP2_MOUSE	Arfaptin-2 OS=Mus musculus	77.15	24	2
O35841|API5_MOUSE	Apoptosis inhibitor 5 OS=Mus	76.97	14	2
P01887|B2MG_MOUSE	Beta-2-microglobulin OS=Mus	76.51	29	2
Q3UIA2|RHG17_MOUSE	Rho GTPase-activating protei	76.47	11	2
P17047|LAMP2_MOUSE	Lysosome-associated membra	76.26	10	2
Q9DCT8|CRIP2_MOUSE	Cysteine-rich protein 2 OS=M	76.03	35	2
O35207|CDKA1_MOUSE	Cyclin-dependent kinase 2-as	75.84	20	2
P54823|DDX6_MOUSE	Probable ATP-dependent RNA	75.65	13	2
A2ASQ1|AGRIN_MOUSE	Agrin OS=Mus musculus GN=	75.62	8	2
O08709|PRDX6_MOUSE	Peroxiredoxin-6 OS=Mus mus	75.59	14	2
P26231|CTNA1_MOUSE	Catenin alpha-1 OS=Mus mus	75.57	15	2
Q9QZ23|NFU1_MOUSE	NFU1 iron-sulfur cluster scaff	75.47	16	2
Q920B9|SP16H_MOUSE	FACT complex subunit SPT16	75.44	11	2
Q9WU28|PFD5_MOUSE	Prefoldin subunit 5 OS=Mus m	75.37	29	2
Q69ZW3|EHBP1_MOUSE	EH domain-binding protein 1 O	75.32	4	2
Q60692|PSB6_MOUSE	Proteasome subunit beta type	74.74	16	2
Q91VR2|ATPG_MOUSE	ATP synthase subunit gamma	74.65	25	2
Q9Z2Y8|PROSC_MOUSE	Proline synthase co-transcribe	74.53	19	2
Q60737|CSK21_MOUSE	Casein kinase II subunit alpha	74.48	17	2
Q9QUI0|RHOA_MOUSE	Transforming protein RhoA OS	74.2	20	2
O55234|PSB5_MOUSE	Proteasome subunit beta type	74.17	16	2
Q9D8C6|MED11_MOUSE	Mediator of RNA polymerase I	74.11	23	2
Q01730|RSU1_MOUSE	Ras suppressor protein 1 OS=	73.76	24	2
P10518|HEM2_MOUSE	Delta-aminolevulinic acid dehy	73.27	13	2
O08740|RPB11_MOUSE	DNA-directed RNA polymeras	73.26	47	2
Q99KV1|DJB11_MOUSE	DnaJ homolog subfamily B me	73.11	19	2
Q78HU3|F125A_MOUSE	Multivesicular body subunit 12	73.1	15	2
Q9D8W5|PSD12_MOUSE	26S proteasome non-ATPase	73.01	13	2
P06745|G6PI_MOUSE	Glucose-6-phosphate isomera	72.55	10	2
Q62419|SH3G1_MOUSE	Endophilin-A2 OS=Mus muscu	72.42	30	2
Q3UPF5|ZCCHV_MOUSE	Zinc finger CCCH-type antivira	72.3	12	2
P35441|TSP1_MOUSE	Thrombospondin-1 OS=Mus m	71.94	13	2
O70435|PSA3_MOUSE	Proteasome subunit alpha typ	71.91	14	2
Q91VY9|ZN622_MOUSE	Zinc finger protein 622 OS=Mu	71.75	12	2
Q9JJY4|DDX20_MOUSE	Probable ATP-dependent RNA	71.52	22	2
Q91ZA3|PCCA_MOUSE	Propionyl-CoA carboxylase alp	71.5	11	2
Q9JHW2|NIT2_MOUSE	Omega-amidase NIT2 OS=Mu	70.81	18	2
P06683|CO9_MOUSE	Complement component C9 O	70.71	13	2
P21460|CYTC_MOUSE	Cystatin-C OS=Mus musculus	70.4	20	2
Q6ZQ58|LARP1_MOUSE	La-related protein 1 OS=Mus	70.39	10	2
Q9CQ75|NDUA2_MOUSE	NADH dehydrogenase [ubiqui	70.08	24	2
O35459|ECH1_MOUSE	Delta(3,5)-Delta(2,4)-dienoyl-C	69.16	18	2
Q9JII5|DAZP1_MOUSE	DAZ-associated protein 1 OS=	68.92	15	2
Q8VDT9|RM50_MOUSE	39S ribosomal protein L50, mi	68.59	44	2
P47941|CRKL_MOUSE	Crk-like protein OS=Mus mus	68.58	15	2
Q5RKR3|ISLR2_MOUSE	Immunoglobulin superfamily c	68.47	16	2
Q9D883|U2AF1_MOUSE	Splicing factor U2AF 35 kDa s	68.36	32	2
Q9ESP1|SDF2L_MOUSE	Stromal cell-derived factor 2-li	67.99	24	2
Q923D2|BLVRB_MOUSE	Flavin reductase OS=Mus mu	67.58	18	2
Q8BX90|FND3A_MOUSE	Fibronectin type-III domain-co	67.34	8	2
Q8BIW1|PRUNE_MOUSE	Protein prune homolog OS=M	67.18	7	2
Q9Z2I0|LETM1_MOUSE	LETM1 and EF-hand domain-	67	9	2

Q9ERE7|MESD_MOUSE	LDLR chaperone MESD OS=M	66.71	17	2
Q9CPY7|AMPL_MOUSE	Cytosol aminopeptidase OS=M	65.46	16	2
P13634|CAH1_MOUSE	Carbonic anhydrase 1 OS=Mu	65.02	8	2
Q9R1P4|PSA1_MOUSE	Proteasome subunit alpha typ	64.79	24	2
Q91Z31|PTBP2_MOUSE	Polypyrimidine tract-binding pr	64.7	18	2
P53996|CNBP_MOUSE	Cellular nucleic acid-binding p	64.63	13	2
P10107|ANXA1_MOUSE	Annexin A1 OS=Mus musculu	64.25	11	2
P80313|TCPH_MOUSE	T-complex protein 1 subunit e	64.06	9	2
P19157|GSTP1_MOUSE	Glutathione S-transferase P 1	63.76	15	2
Q923D4|SF3B5_MOUSE	Splicing factor 3B subunit 5 O	63.72	33	2
Q9DCT2|NDUS3_MOUSE	NADH dehydrogenase [ubiqui	63.55	26	2
Q8CCS6|PABP2_MOUSE	Polyadenylate-binding protein	63.08	11	2
P39054|DYN2_MOUSE	Dynamin-2 OS=Mus musculus	63.07	8	2
Q80X50|UBP2L_MOUSE	Ubiquitin-associated protein 2	62.83	12	2
O88531|PPT1_MOUSE	Palmitoyl-protein thioesterase	62.02	8	2
Q9CWP6|MSPD2_MOUSE	Motile sperm domain-containi	61.36	8	2
Q9R0L7|AKP8L_MOUSE	A-kinase anchor protein 8-like	60.88	6	2
Q9DBT5|AMPD2_MOUSE	AMP deaminase 2 OS=Mus m	60.77	13	2
Q91W69|EPN3_MOUSE	Epsin-3 OS=Mus musculus G	60.37	5	2
P19253|RL13A_MOUSE	60S ribosomal protein L13a O	60.35	19	2
O35857|TIM44_MOUSE	Mitochondrial import inner me	60.22	12	2
Q6ZWX6|IF2A_MOUSE	Eukaryotic translation initiation	60.12	9	2
O35166|GOSR2_MOUSE	Golgi SNAP receptor complex	60.01	24	2
O55013|TPPC3_MOUSE	Trafficking protein particle com	59.05	14	2
P70335|ROCK1_MOUSE	Rho-associated protein kinase	59	8	2
O70439|STX7_MOUSE	Syntaxin-7 OS=Mus musculus	58.91	21	2
Q91YW3|DNJC3_MOUSE	DnaJ homolog subfamily C m	58.85	6	2
Q9Z108|STAU1_MOUSE	Double-stranded RNA-binding	58.73	5	2
Q9JLV6|PNKP_MOUSE	Bifunctional polynucleotide ph	58.49	10	2
P47757|CAPZB_MOUSE	F-actin-capping protein subun	57.36	25	2
Q9WTR2|M3K6_MOUSE	Mitogen-activated protein kina	57.36	3	2
Q62296|TEAD4_MOUSE	Transcriptional enhancer facto	57.16	12	2
Q8C170|MYO9A_MOUSE	Myosin-IXa OS=Mus musculu	57.04	4	2
P19096|FAS_MOUSE	Fatty acid synthase OS=Mus m	56.94	6	2
Q9CXY6|ILF2_MOUSE	Interleukin enhancer-binding f	56.84	11	2
Q7TQ95|LNP_MOUSE	Protein lunapark OS=Mus mus	56.79	14	2
Q8CCK0|H2AW_MOUSE	Core histone macro-H2A.2 OS	56.69	20	2
Q8QZY9|SF3B4_MOUSE	Splicing factor 3B subunit 4 O	56.55	17	2
Q61702|ITIH1_MOUSE	Inter-alpha-trypsin inhibitor he	56.44	7	2
P63037|DNJA1_MOUSE	DnaJ homolog subfamily A me	56.28	18	2
P80315|TCPD_MOUSE	T-complex protein 1 subunit d	56	11	2
P15306|TRBM_MOUSE	Thrombomodulin OS=Mus mu	55.83	12	2
Q8CGR5|KLK14_MOUSE	Kallikrein-14 OS=Mus muscul	55.64	13	2
P61211|ARL1_MOUSE	ADP-ribosylation factor-like pr	55.52	9	2
O70400|PDLI1_MOUSE	PDZ and LIM domain protein 1	55.42	24	2
P56565|S10A1_MOUSE	Protein S100-A1 OS=Mus mu	55.32	38	2
Q9CYI4|LUC7L_MOUSE	Putative RNA-binding protein	55.29	9	2
Q61598|GDIB_MOUSE	Rab GDP dissociation inhibito	55.15	12	2
P35951|LDLR_MOUSE	Low-density lipoprotein recept	55.07	9	2
Q9Z0J0|NPC2_MOUSE	Epididymal secretory protein E	55.07	12	2
P19221|THRB_MOUSE	Prothrombin OS=Mus muscul	54.98	8	2
Q8R3C6|RBM19_MOUSE	Probable RNA-binding protein	54.96	11	2
P62889|RL30_MOUSE	60S ribosomal protein L30 OS	54.55	16	2
Q7TT37|ELP1_MOUSE	Elongator complex protein 1 O	54.52	8	2
P34022|RANG_MOUSE	Ran-specific GTPase-activatin	54.33	29	2

Q9Z2L6|MINP1_MOUSE	Multiple inositol polyphosphate	53.85	11	2
Q9D945|LLPH_MOUSE	Protein LLP homolog OS=Mus	53.66	37	2
P70460|VASP_MOUSE	Vasodilator-stimulated phosph	53.54	23	2
Q8K1J6|TRNT1_MOUSE	CCA tRNA nucleotidyltransfera	53.46	18	2
P47753|CAZA1_MOUSE	F-actin-capping protein subun	52.82	10	2
Q00PI9|HNRL2_MOUSE	Heterogeneous nuclear ribonu	52.71	7	2
Q8CH25|SLTM_MOUSE	SAFB-like transcription modul	52.65	6	2
Q8BRF7|SCFD1_MOUSE	Sec1 family domain-containing	52.61	14	2
P23953|ESTN_MOUSE	Liver carboxylesterase N OS=	52.28	6	2
Q9CPW4|ARPC5_MOUSE	Actin-related protein 2/3 comp	52.22	21	2
Q569Z6|TR150_MOUSE	Thyroid hormone receptor-ass	52.02	4	2
Q148V7|K1468_MOUSE	LisH domain and HEAT repea	51.88	15	2
Q91VZ6|SMAP1_MOUSE	Stromal membrane-associated	51.54	13	2
Q9EPU4|CPSF1_MOUSE	Cleavage and polyadenylation	51.23	3	2
P32921|SYWC_MOUSE	Tryptophanyl-tRNA synthetase	51.1	11	2
Q62318|TIF1B_MOUSE	Transcription intermediary fac	50.94	8	2
Q8BL99|DOP1_MOUSE	Protein dopey-1 OS=Mus mus	50.82	5	2
P21126|UBL4A_MOUSE	Ubiquitin-like protein 4A OS=M	50.79	27	2
Q8K4M5|COMD1_MOUSE	COMM domain-containing pro	50.73	16	2
O08715|AKAP1_MOUSE	A-kinase anchor protein 1, mit	50.43	5	2
O88543|CSN3_MOUSE	COP9 signalosome complex s	50.16	19	2
Q9WTQ5|AKA12_MOUSE	A-kinase anchor protein 12 OS	49.83	8	2
O88958|GNPI1_MOUSE	Glucosamine-6-phosphate iso	49.58	21	2
P09528|FRIH_MOUSE	Ferritin heavy chain OS=Mus	48.67	12	2
Q9CWK8|SNX2_MOUSE	Sorting nexin-2 OS=Mus musc	48.6	13	2
Q9ERU9|RBP2_MOUSE	E3 SUMO-protein ligase RanB	47.93	5	2
Q07456|AMBP_MOUSE	Protein AMBP OS=Mus muscu	46.96	6	2
P05532|KIT_MOUSE	Mast/stem cell growth factor re	46.9	8	2
Q9D5V5|CUL5_MOUSE	Cullin-5 OS=Mus musculus G	46.6	13	2
Q8BNJ6|NETO2_MOUSE	Neuropilin and tolloid-like prote	46.6	10	2
Q6P3D0|NUD16_MOUSE	U8 snoRNA-decapping enzym	46.36	16	2
Q6ZWR6|SYNE1_MOUSE	Nesprin-1 OS=Mus musculus	46.01	4	2
Q8CG48|SMC2_MOUSE	Structural maintenance of chro	45.84	6	2
Q8BMK4|CKAP4_MOUSE	Cytoskeleton-associated prote	45.28	16	2
Q6PE15|ABHDA_MOUSE	Abhydrolase domain-containin	44.99	17	2
O70591|PFD2_MOUSE	Prefoldin subunit 2 OS=Mus m	44.78	27	2
Q8VHK9|DHX36_MOUSE	Probable ATP-dependent RNA	44.73	5	2
P70288|HDAC2_MOUSE	Histone deacetylase 2 OS=Mu	44.49	13	2
O09106|HDAC1_MOUSE	Histone deacetylase 1 OS=Mu	44.49	8	2
Q8BTS4|NUP54_MOUSE	Nuclear pore complex protein	44.27	10	2
Q05D44|IF2P_MOUSE	Eukaryotic translation initiation	43.78	11	2
Q9D1R9|RL34_MOUSE	60S ribosomal protein L34 OS	43.66	15	2
P47964|RL36_MOUSE	60S ribosomal protein L36 OS	42.33	12	2
Q61329|ZFHX3_MOUSE	Zinc finger homeobox protein	41.92	5	2
Q99LI8|HGS_MOUSE	Hepatocyte growth factor-regu	41.86	11	2
Q9CPN8|IF2B3_MOUSE	Insulin-like growth factor 2 mR	41.86	7	2
Q91YT0|NDUV1_MOUSE	NADH dehydrogenase [ubiqui	41.39	9	2
Q8R311|CTGE5_MOUSE	Cutaneous T-cell lymphoma-a	41.3	6	2
Q61599|GDIR2_MOUSE	Rho GDP-dissociation inhibito	40.99	16	2
Q8BYC4|GPR20_MOUSE	G-protein coupled receptor 20	40.87	13	2
Q99MY8|ASH1L_MOUSE	Probable histone-lysine N-met	39.28	5	2
Q9Z1P6|NDUA7_MOUSE	NADH dehydrogenase [ubiqui	38.74	34	2
Q62504|MINT_MOUSE	Msx2-interacting protein OS=M	38.6	6	2
Q91Z58|CF132_MOUSE	Uncharacterized protein C6orf	38.28	5	2
Q60952|CP250_MOUSE	Centrosome-associated protei	38.05	5	2

Q9JKP5|MBNL1_MOUSE	Muscleblind-like protein 1 OS=	37.89	5	2
Q8C181|MBNL2_MOUSE	Muscleblind-like protein 2 OS=	37.89	5	2
Q9CX34|SUGT1_MOUSE	Suppressor of G2 allele of SK	37.85	8	2
Q8JZM7|CDC73_MOUSE	Parafibromin OS=Mus muscu	37.15	4	2
Q80TC6|ZSWM5_MOUSE	Zinc finger SWIM domain-con	37	6	2
Q9QYC0|ADDA_MOUSE	Alpha-adducin OS=Mus musc	36.46	5	2
Q8BPY9|FIGL1_MOUSE	Fidgetin-like protein 1 OS=Mu	35.84	6	2
Q8R105|VP37C_MOUSE	Vacuolar protein sorting-assoc	35.71	25	2
Q14AX6|CDK12_MOUSE	Cyclin-dependent kinase 12 O	35.38	4	2
Q6ZQA0|NBEL2_MOUSE	Neurobeachin-like protein 2 O	34.98	3	2
P11369|POL2_MOUSE	Retrovirus-related Pol polypro	34.9	5	2
Q8BH31|MFSD8_MOUSE	Major facilitator superfamily do	34.85	5	2
Q04750|TOP1_MOUSE	DNA topoisomerase 1 OS=Mu	34.45	11	2
Q571H0|NPA1P_MOUSE	Nucleolar pre-ribosomal-assoc	34.37	4	2
Q9JK83|PAR6B_MOUSE	Partitioning defective 6 homol	34.28	17	2
Q91ZI0|CELR3_MOUSE	Cadherin EGF LAG seven-pas	33.62	6	2
Q61390|TCPW_MOUSE	T-complex protein 1 subunit z	33.6	24	2
Q8BGQ7|SYAC_MOUSE	Alanyl-tRNA synthetase, cytop	33.42	8	2
Q69ZH9|RHG23_MOUSE	Rho GTPase-activating protei	33.16	3	2
P49718|MCM5_MOUSE	DNA replication licensing fact	33.11	6	2
Q69ZN7|MYOF_MOUSE	Myoferlin OS=Mus musculus	32.75	6	2
Q9WTS6|TEN3_MOUSE	Teneurin-3 OS=Mus musculus	32.67	4	2
P98200|AT8A2_MOUSE	Probable phospholipid-transp	32.61	9	2
O35071|KIF1C_MOUSE	Kinesin-like protein KIF1C OS	32.57	8	2
Q8BLX7|COGA1_MOUSE	Collagen alpha-1(XVI) chain C	32.23	7	2
P48725|PCNT_MOUSE	Pericentrin OS=Mus musculus	32.23	5	2
Q61245|COBA1_MOUSE	Collagen alpha-1(XI) chain OS	31.75	6	2
Q9QZ09|PHTF1_MOUSE	Putative homeodomain transc	31.6	15	2
Q8CH77|NAV1_MOUSE	Neuron navigator 1 OS=Mus r	31.46	6	2
O35161|CELR1_MOUSE	Cadherin EGF LAG seven-pas	31.22	7	2
Q5QNQ9|CORA1_MOUSE	Collagen alpha-1(XXVII) chain	31.2	5	2
Q30D77|COOA1_MOUSE	Collagen alpha-1(XXIV) chain	30.6	8	2
Q9Z1X4|ILF3_MOUSE	Interleukin enhancer-binding f	30.52	3	2
Q3URV1|BROMI_MOUSE	Protein broad-minded OS=Mu	30.52	6	2
Q9Z2U2|ZN292_MOUSE	Zinc finger protein 292 OS=Mu	30.51	2	2
Q3V1M1|IGS10_MOUSE	Immunoglobulin superfamily m	30.43	7	2
Q9ERR7|SEP15_MOUSE	15 kDa selenoprotein OS=Mus	30.42	23	2
Q8VCW8|ACSF2_MOUSE	Acyl-CoA synthetase family m	30.34	9	2
Q8BGA5|KRR1_MOUSE	KRR1 small subunit processo	30.25	8	2
Q8BWT5|DIP2A_MOUSE	Disco-interacting protein 2 hor	30.17	4	2
Q9JHI4|S13A1_MOUSE	Solute carrier family 13 memb	29.98	15	2
P17710|HXK1_MOUSE	Hexokinase-1 OS=Mus muscu	29.84	5	2
Q80YF9|RHG33_MOUSE	Rho GTPase-activating protei	29.76	5	2
Q6AW69|CGNL1_MOUSE	Cingulin-like protein 1 OS=Mu	29.54	8	2
Q91WC3|ACSL6_MOUSE	Long-chain-fatty-acid--CoA lig	29.1	11	2
Q0GGX2|ZN541_MOUSE	Zinc finger protein 541 OS=Mu	29.07	9	2
P14873|MAP1B_MOUSE	Microtubule-associated protei	29.05	3	2
Q91XQ0|DYH8_MOUSE	Dynein heavy chain 8, axonem	28.88	2	2
Q811P8|RHG32_MOUSE	Rho GTPase-activating protei	28.64	2	2
Q8BRB7|MYST4_MOUSE	Histone acetyltransferase MYS	28.53	4	2
Q5SSE9|ABCAD_MOUSE	ATP-binding cassette sub-fam	28.36	4	2
Q3UNW5|TF2L1_MOUSE	Transcription factor CP2-like p	28.33	9	2
Q9JLN9|MTOR_MOUSE	Serine/threonine-protein kinas	28.02	5	2
Q8C8R3|ANK2_MOUSE	Ankyrin-2 OS=Mus musculus	27.89	5	2
Q69ZR2|HECD1_MOUSE	E3 ubiquitin-protein ligase HE	27.85	6	2

Q8CGE9|RGS12_MOUSE	Regulator of G-protein signalir	27.55	8	2
Q8BN57|CC033_MOUSE	Uncharacterized protein C3orf	27.51	17	2
Q80YV3|TRRAP_MOUSE	Transformation/transcription d	27.46	7	2
Q61941|NNTM_MOUSE	NAD(P) transhydrogenase, mi	27.45	16	2
Q91YD6|VILL_MOUSE	Villin-like protein OS=Mus mus	27.43	5	2
P11881|ITPR1_MOUSE	Inositol 1,4,5-trisphosphate re	27.36	7	2
Q3UHK3|GREB1_MOUSE	Protein GREB1 OS=Mus mus	27.29	7	2
Q80WE4|KI20B_MOUSE	Kinesin-like protein KIF20B OS	27.16	3	2
P58749|TM6S1_MOUSE	Transmembrane 6 superfamily	27.15	12	2
Q812E0|CPEB2_MOUSE	Cytoplasmic polyadenylation e	27	11	2
Q571C7|BDP1_MOUSE	Transcription factor TFIIIB cor	26.97	4	2
P54276|MSH6_MOUSE	DNA mismatch repair protein	26.93	7	2
P14719|ILRL1_MOUSE	Interleukin-1 receptor-like 1 O	26.87	6	2
Q60584|FBXW2_MOUSE	F-box/WD repeat-containing p	26.72	9	2
Q0VF58|COJA1_MOUSE	Collagen alpha-1(XIX) chain C	26.52	4	2
Q61290|CAC1E_MOUSE	Voltage-dependent R-type cal	26.47	4	2
P53995|APC1_MOUSE	Anaphase-promoting complex	26.44	6	2
Q9JHJ3|NCUG1_MOUSE	Lysosomal protein NCU-G1 O	26.39	11	2
Q8R554|OTU7A_MOUSE	OTU domain-containing protei	26.36	6	2
P31938|MP2K1_MOUSE	Dual specificity mitogen-activa	26.34	18	2
O88737|BSN_MOUSE	Protein bassoon OS=Mus mus	26.32	6	2
P70227|ITPR3_MOUSE	Inositol 1,4,5-trisphosphate re	26.31	3	2
Q45VK7|DYHC2_MOUSE	Cytoplasmic dynein 2 heavy c	26.3	7	2
Q3U108|ARI5A_MOUSE	AT-rich interactive domain-cor	25.88	3	2
Q3UVY5|CN135_MOUSE	Pecanex-like protein C14orf13	25.81	4	2
Q9R016|BIR1E_MOUSE	Baculoviral IAP repeat-contain	25.69	6	2
Q8JZM8|MUC4_MOUSE	Mucin-4 OS=Mus musculus G	25.62	5	2
A2RSQ0|DEN5B_MOUSE	DENN domain-containing prot	25.55	12	2
Q9Z351|KCNQ2_MOUSE	Potassium voltage-gated char	25.49	5	2
Q9ESK9|RBCC1_MOUSE	RB1-inducible coiled-coil prote	25.35	5	2
Q9CW46|RAVR1_MOUSE	Ribonucleoprotein PTB-bindin	25.22	10	2
Q9JMG7|HDGR3_MOUSE	Hepatoma-derived growth fact	25.17	6	2
Q8C0P7|ZN451_MOUSE	Zinc finger protein 451 OS=Mu	25.05	8	2
Q9QYT7|PIGQ_MOUSE	Phosphatidylinositol N-acetylg	24.96	12	2
Q68FH0|PKP4_MOUSE	Plakophilin-4 OS=Mus muscul	24.79	5	2
Q8CG73|FTM_MOUSE	Protein fantom OS=Mus musc	24.77	6	2
Q8BLG0|PHF20_MOUSE	PHD finger protein 20 OS=Mu	24.69	6	2
C4P6S0|SHTAP_MOUSE	Sperm head and tail associate	24.58	2	2
Q69ZC8|K1704_MOUSE	Uncharacterized protein KIAA	24.49	12	2
Q8CJ27|ASPM_MOUSE	Abnormal spindle-like microce	24.17	5	2
O70481|UBR1_MOUSE	E3 ubiquitin-protein ligase UB	24.17	5	2
P35546|RET_MOUSE	Proto-oncogene tyrosine-prote	23.92	3	2
P16283|B3A3_MOUSE	Anion exchange protein 3 OS=	23.68	3	2
Q2EY15|PRTG_MOUSE	Protogenin OS=Mus musculus	23.6	2	2
Q80VM7|ANR24_MOUSE	Ankyrin repeat domain-contain	23.57	11	2
Q4QRL3|CC88B_MOUSE	Coiled-coil domain-containing	23.41	8	2
A2APU8|CI14B_MOUSE	Transmembrane protein C9orf	23.41	7	2
Q9WU42|NCOR2_MOUSE	Nuclear receptor corepressor	23.33	6	2
Q3UH53|SDK1_MOUSE	Protein sidekick-1 OS=Mus m	23.02	5	2
Q91V27|MELPH_MOUSE	Melanophilin OS=Mus muscul	21.77	9	2
Q69ZX6|MOR2A_MOUSE	MORC family CW-type zinc fin	21.43	5	2
Q9Z0J4|NOS1_MOUSE	Nitric oxide synthase, brain OS	21.29	7	2
Q6PAJ1|BCR_MOUSE	Breakpoint cluster region prote	21.12	6	2
Q9Z0E1|CB065_MOUSE	Uncharacterized protein C2orf	20.12	3	2
Q69ZU6|THS7A_MOUSE	Thrombospondin type-1 doma	20.03	6	2

Table A1.2 GFR Matrigel Protein Identifications. List of all proteins identified in GFR Matrigel (growth factor reduced) with corresponding accession, description, PEAKS score, unique peptide numbers, and coverage (in %).

Accession	Description	Score	Coverage (%)	#Unique
P19137|LAMA1_MOUSE	Laminin subunit alpha-1 OS=Mu	628.63	84	416
P10493|NID1_MOUSE	Nidogen-1 OS=Mus musculus G	578.16	94	306
P02469|LAMB1_MOUSE	Laminin subunit beta-1 OS=Mus	567.28	80	267
P02468|LAMC1_MOUSE	Laminin subunit gamma-1 OS=M	569.94	87	245
Q05793|PGBM_MOUSE	Basement membrane-specific he	501.41	67	159
Q8VDD5|MYH9_MOUSE	Myosin-9 OS=Mus musculus GN	450.04	81	108
P16546|SPTA2_MOUSE	Spectrin alpha chain, brain OS=M	368.54	76	103
P20152|VIME_MOUSE	Vimentin OS=Mus musculus GN	420.08	97	90
Q9QXS1|PLEC_MOUSE	Plectin OS=Mus musculus GN=P	289.16	66	79
P01027|CO3_MOUSE	Complement C3 OS=Mus muscu	345.76	72	78
Q9JHU4|DYHC1_MOUSE	Cytoplasmic dynein 1 heavy chai	295.63	60	76
P19324|SERPH_MOUSE	Serpin H1 OS=Mus musculus GI	392.76	87	73
P63038|CH60_MOUSE	60 kDa heat shock protein, mitoc	377.09	91	67
P20029|GRP78_MOUSE	78 kDa glucose-regulated protein	393.79	80	66
Q3UQ28|PXDN_MOUSE	Peroxidasin homolog OS=Mus m	366.86	71	63
Q62261|SPTB2_MOUSE	Spectrin beta chain, brain 1 OS=	292.18	64	58
P14733|LMNB1_MOUSE	Lamin-B1 OS=Mus musculus GN	381.83	92	55
P07724|ALBU_MOUSE	Serum albumin OS=Mus muscul	381.35	88	55
Q8VIJ6|SFPQ_MOUSE	Splicing factor, proline- and gluta	342.28	75	55
Q9D0E1|HNRPM_MOUSE	Heterogeneous nuclear ribonucle	315.82	88	53
P63017|HSP7C_MOUSE	Heat shock cognate 71 kDa prot	408.96	92	49
P09103|PDIA1_MOUSE	Protein disulfide-isomerase OS=	337.38	93	49
Q80X90|FLNB_MOUSE	Filamin-B OS=Mus musculus GN	279.12	52	49
P48678|LMNA_MOUSE	Prelamin-A/C OS=Mus musculus	314.07	83	46
Q01853|TERA_MOUSE	Transitional endoplasmic reticulu	315.18	67	44
O88322|NID2_MOUSE	Nidogen-2 OS=Mus musculus G	312.75	57	44
Q68FD5|CLH_MOUSE	Clathrin heavy chain 1 OS=Mus	268.36	67	43
Q61879|MYH10_MOUSE	Myosin-10 OS=Mus musculus G	326.98	66	41
Q8K310|MATR3_MOUSE	Matrin-3 OS=Mus musculus GN=	312.04	67	40
Q8CGC7|SYEP_MOUSE	Bifunctional aminoacyl-tRNA syn	307.57	70	40
P29341|PABP1_MOUSE	Polyadenylate-binding protein 1 (	304.55	71	40
P26039|TLN1_MOUSE	Talin-1 OS=Mus musculus GN=T	259.38	56	40
Q64727|VINC_MOUSE	Vinculin OS=Mus musculus GN=	253.67	67	38
Q8K0E8|FIBB_MOUSE	Fibrinogen beta chain OS=Mus m	294.75	72	37
P16858|G3P_MOUSE	Glyceraldehyde-3-phosphate del	332.58	87	36
P38647|GRP75_MOUSE	Stress-70 protein, mitochondrial	285.7	78	36
O88569|ROA2_MOUSE	Heterogeneous nuclear ribonucle	330.65	69	35
P11276|FINC_MOUSE	Fibronectin OS=Mus musculus G	250.45	36	35
Q03265|ATPA_MOUSE	ATP synthase subunit alpha, mit	292.18	80	32
Q61001|LAMA5_MOUSE	Laminin subunit alpha-5 OS=Mu	263.25	38	32
Q9D8E6|RL4_MOUSE	60S ribosomal protein L4 OS=Mu	259.07	69	32
P56480|ATPB_MOUSE	ATP synthase subunit beta, mito	311.5	79	31
P27773|PDIA3_MOUSE	Protein disulfide-isomerase A3 O	254.3	68	30
Q921I1|TRFE_MOUSE	Serotransferrin OS=Mus muscul	259.15	54	29
Q99K48|NONO_MOUSE	Non-POU domain-containing oct	248.34	73	28
Q61595|KTN1_MOUSE	Kinectin OS=Mus musculus GN=	225.51	51	28
O08677|KNG1_MOUSE	Kininogen-1 OS=Mus musculus	321.8	58	27
Q8BTM8|FLNA_MOUSE	Filamin-A OS=Mus musculus GN	214.25	31	27
Q8VCM7|FIBG_MOUSE	Fibrinogen gamma chain OS=Mu	305.52	62	26
Q922R8|PDIA6_MOUSE	Protein disulfide-isomerase A6 O	289.63	89	26
P14211|CALR_MOUSE	Calreticulin OS=Mus musculus G	283.76	84	26
P08249|MDHM_MOUSE	Malate dehydrogenase, mitochon	274.69	81	26
P08032|SPTA1_MOUSE	Spectrin alpha chain, erythrocyte	227.32	45	25
A2ASS6|TITIN_MOUSE	Titin OS=Mus musculus GN=Ttn	79.26	8	25

Q61838|A2M_MOUSE	Alpha-2-macroglobulin OS=Mus	237.43	39	24
Q9EQK5|MVP_MOUSE	Major vault protein OS=Mus mus	234.07	65	24
P58252|EF2_MOUSE	Elongation factor 2 OS=Mus mus	210.56	45	24
P52480|KPYM_MOUSE	Pyruvate kinase isozymes M1/M	263.15	73	23
Q9R0B9|PLOD2_MOUSE	Procollagen-lysine,2-oxoglutarat	225.37	52	23
Q9CSN1|SNW1_MOUSE	SNW domain-containing protein	223.7	74	23
P08113|ENPL_MOUSE	Endoplasmin OS=Mus musculus	210.35	44	23
P07214|SPRC_MOUSE	SPARC OS=Mus musculus GN=	328.36	86	22
P61979|HNRPK_MOUSE	Heterogeneous nuclear ribonucl	275.26	78	22
Q6P5E4|UGGG1_MOUSE	UDP-glucose:glycoprotein glucos	245.58	46	22
Q8R326|PSPC1_MOUSE	Paraspeckle component 1 OS=M	237.26	72	22
O70133|DHX9_MOUSE	ATP-dependent RNA helicase A	231.54	39	22
Q9Z1Q9|SYVC_MOUSE	Valyl-tRNA synthetase OS=Mus	229.3	50	22
Q9R0E2|PLOD1_MOUSE	Procollagen-lysine,2-oxoglutarat	220.66	47	22
Q60902|EP15R_MOUSE	Epidermal growth factor recepto	204.53	57	22
P11499|HS90B_MOUSE	Heat shock protein HSP 90-beta	287.33	77	21
Q01405|SC23A_MOUSE	Protein transport protein Sec23A	253.94	51	21
P06909|CFAH_MOUSE	Complement factor H OS=Mus m	239.29	42	21
Q61576|FKB10_MOUSE	Peptidyl-prolyl cis-trans isomeras	231.43	70	21
Q8BU30|SYIC_MOUSE	Isoleucyl-tRNA synthetase, cytop	226.03	53	21
Q9DC23|DJC10_MOUSE	DnaJ homolog subfamily C mem	216.46	43	21
P57776|EF1D_MOUSE	Elongation factor 1-delta OS=Mu	245.75	59	20
P12970|RL7A_MOUSE	60S ribosomal protein L7a OS=M	234.46	65	20
P10126|EF1A1_MOUSE	Elongation factor 1-alpha 1 OS=I	230.27	64	20
P62908|RS3_MOUSE	40S ribosomal protein S3 OS=M	227.08	74	20
P28665|MUG1_MOUSE	Murinoglobulin-1 OS=Mus muscu	225.66	42	20
O08810|U5S1_MOUSE	116 kDa U5 small nuclear ribonu	215.23	50	20
Q99PV0|PRP8_MOUSE	Pre-mRNA-processing-splicing fa	205.05	44	20
Q80U93|NU214_MOUSE	Nuclear pore complex protein Nu	202.82	37	20
P25444|RS2_MOUSE	40S ribosomal protein S2 OS=M	248.19	74	19
P27659|RL3_MOUSE	60S ribosomal protein L3 OS=Mu	243.55	75	19
Q8BG05|ROA3_MOUSE	Heterogeneous nuclear ribonucl	239.4	56	19
P21614|VTDB_MOUSE	Vitamin D-binding protein OS=M	219.5	80	19
Q91X72|HEMO_MOUSE	Hemopexin OS=Mus musculus G	214.76	47	19
P47911|RL6_MOUSE	60S ribosomal protein L6 OS=Mu	213.42	63	19
P62806|H4_MOUSE	Histone H4 OS=Mus musculus G	211.8	89	19
Q8BMS1|ECHA_MOUSE	Trifunctional enzyme subunit alp	176.45	57	19
P17742|PPIA_MOUSE	Peptidyl-prolyl cis-trans isomeras	262.45	87	18
Q91W90|TXND5_MOUSE	Thioredoxin domain-containing p	243.31	72	18
Q60716|P4HA2_MOUSE	Prolyl 4-hydroxylase subunit alph	235.78	74	18
Q9Z247|FKBP9_MOUSE	Peptidyl-prolyl cis-trans isomeras	230.13	59	18
O08795|GLU2B_MOUSE	Glucosidase 2 subunit beta OS=	212.02	42	18
Q7TQH0|ATX2L_MOUSE	Ataxin-2-like protein OS=Mus mu	183.98	33	18
P56959|FUS_MOUSE	RNA-binding protein FUS OS=M	217.44	44	17
P06151|LDHA_MOUSE	L-lactate dehydrogenase A chain	214.78	58	17
Q3V1T4|P3H1_MOUSE	Prolyl 3-hydroxylase 1 OS=Mus m	202.57	41	17
Q60749|KHDR1_MOUSE	KH domain-containing, RNA-bind	167.03	64	17
Q99P88|NU155_MOUSE	Nuclear pore complex protein Nu	144.18	51	17
O35643|AP1B1_MOUSE	AP-1 complex subunit beta-1 OS	251.4	56	16
P14206|RSSA_MOUSE	40S ribosomal protein SA OS=M	236.01	65	16
P17225|PTBP1_MOUSE	Polypyrimidine tract-binding prote	233.6	69	16
P21619|LMNB2_MOUSE	Lamin-B2 OS=Mus musculus GN	226.76	68	16
P80316|TCPE_MOUSE	T-complex protein 1 subunit epsi	212.14	72	16
Q06890|CLUS_MOUSE	Clusterin OS=Mus musculus GN	208.92	61	16
Q60715|P4HA1_MOUSE	Prolyl 4-hydroxylase subunit alph	202.55	48	16

Q91VM5|RBMXL_MOUSE	Heterogeneous nuclear ribonucle	191.2	49	16
P62918|RL8_MOUSE	60S ribosomal protein L8 OS=Mu	187.04	45	16
Q8R0W0|EPIPL_MOUSE	Epiplakin OS=Mus musculus GN	138.44	22	16
P29699|FETUA_MOUSE	Alpha-2-HS-glycoprotein OS=Mu	254.26	78	15
Q9Z2X1|HNRPF_MOUSE	Heterogeneous nuclear ribonucle	246.37	73	15
Q99JR5|TINAL_MOUSE	Tubulointerstitial nephritis antige	221.83	49	15
Q61292|LAMB2_MOUSE	Laminin subunit beta-2 OS=Mus	199.43	33	15
P97496|SMRC1_MOUSE	SWI/SNF complex subunit SMAF	199	54	15
P53026|RL10A_MOUSE	60S ribosomal protein L10a OS=	197.71	50	15
Q3U0V1|FUBP2_MOUSE	Far upstream element-binding pr	196.1	40	15
Q9EPU0|RENT1_MOUSE	Regulator of nonsense transcript	194.67	50	15
Q99020|ROAA_MOUSE	Heterogeneous nuclear ribonucle	194.01	53	15
Q00623|APOA1_MOUSE	Apolipoprotein A-I OS=Mus mus	189.43	80	15
Q9Z110|P5CS_MOUSE	Delta-1-pyrroline-5-carboxylate s	184.08	42	15
Q8BMJ2|SYLC_MOUSE	Leucyl-tRNA synthetase, cytopla	168.22	35	15
P19096|FAS_MOUSE	Fatty acid synthase OS=Mus mu	143.77	33	15
P98078|DAB2_MOUSE	Disabled homolog 2 OS=Mus mu	236.55	36	14
P31001|DESM_MOUSE	Desmin OS=Mus musculus GN=	235.27	63	14
P57759|ERP29_MOUSE	Endoplasmic reticulum resident p	221.56	70	14
Q9WV54|ASAH1_MOUSE	Acid ceramidase OS=Mus musc	221.17	61	14
P39061|COIA1_MOUSE	Collagen alpha-1(XVIII) chain OS	199.06	32	14
Q9WU78|PDC6I_MOUSE	Programmed cell death 6-interac	198.76	35	14
P62301|RS13_MOUSE	40S ribosomal protein S13 OS=M	197.1	54	14
Q9D0I9|SYRC_MOUSE	Arginyl-tRNA synthetase, cytopla	187.49	60	14
Q68FL6|SYMC_MOUSE	Methionyl-tRNA synthetase, cyto	184.53	54	14
Q8K2B3|DHSA_MOUSE	Succinate dehydrogenase [ubiqu	184.26	53	14
P24270|CATA_MOUSE	Catalase OS=Mus musculus GN	179.58	44	14
Q3TXS7|PSMD1_MOUSE	26S proteasome non-ATPase re	178.57	55	14
P09405|NUCL_MOUSE	Nucleolin OS=Mus musculus GN	176.22	62	14
P02088|HBB1_MOUSE	Hemoglobin subunit beta-1 OS=I	221.35	88	13
Q9DB20|ATPO_MOUSE	ATP synthase subunit O, mitoch	215.62	78	13
Q08879|FBLN1_MOUSE	Fibulin-1 OS=Mus musculus GN	209.08	50	13
P61358|RL27_MOUSE	60S ribosomal protein L27 OS=M	196.06	59	13
P42567|EPS15_MOUSE	Epidermal growth factor receptor	185.33	48	13
Q9JKR6|HYOU1_MOUSE	Hypoxia up-regulated protein 1 O	179.9	43	13
Q8BH97|RCN3_MOUSE	Reticulocalbin-3 OS=Mus muscu	172.07	54	13
Q8BHN3|GANAB_MOUSE	Neutral alpha-glucosidase AB OS	167.31	56	13
Q9R0E1|PLOD3_MOUSE	Procollagen-lysine,2-oxoglutarate	160.58	42	13
Q99PL5|RRBP1_MOUSE	Ribosome-binding protein 1 OS=	157.4	19	13
P62270|RS18_MOUSE	40S ribosomal protein S18 OS=M	157.37	65	13
Q8K297|GT251_MOUSE	Procollagen galactosyltransferas	144.08	55	13
P49312|ROA1_MOUSE	Heterogeneous nuclear ribonucle	238.04	68	12
P62843|RS15_MOUSE	40S ribosomal protein S15 OS=M	233.43	83	12
Q8CG70|P3H3_MOUSE	Prolyl 3-hydroxylase 3 OS=Mus m	191.34	51	12
Q8R081|HNRPL_MOUSE	Heterogeneous nuclear ribonucle	188.9	38	12
Q8C0E2|VP26B_MOUSE	Vacuolar protein sorting-associat	184.32	63	12
Q501J6|DDX17_MOUSE	Probable ATP-dependent RNA h	166.08	31	12
Q9D8N0|EF1G_MOUSE	Elongation factor 1-gamma OS=	162.74	43	12
Q61545|EWS_MOUSE	RNA-binding protein EWS OS=M	162.55	32	12
P63085|MK01_MOUSE	Mitogen-activated protein kinase	162.49	58	12
O35887|CALU_MOUSE	Calumenin OS=Mus musculus G	161.42	57	12
P10605|CATB_MOUSE	Cathepsin B OS=Mus musculus	147	38	12
Q8BH61|F13A_MOUSE	Coagulation factor XIII A chain O	127.1	24	12
P07901|HS90A_MOUSE	Heat shock protein HSP 90-alpha	244.17	53	11
P62259|1433E_MOUSE	14-3-3 protein epsilon OS=Mus m	224.63	87	11

Q9CQU0|TXD12_MOUSE	Thioredoxin domain-containing p	204.43	78	11
P31230|AIMP1_MOUSE	Aminoacyl tRNA synthase compl	195.67	57	11
Q3UPH1|PRRC1_MOUSE	Protein PRRC1 OS=Mus muscul	191.79	45	11
Q9CPR4|RL17_MOUSE	60S ribosomal protein L17 OS=M	185.15	61	11
Q91W39|NCOA5_MOUSE	Nuclear receptor coactivator 5 O	170.94	51	11
Q9Z204|HNRPC_MOUSE	Heterogeneous nuclear ribonucle	169.11	48	11
Q64433|CH10_MOUSE	10 kDa heat shock protein, mitoc	167.21	74	11
P97461|RS5_MOUSE	40S ribosomal protein S5 OS=M	158.99	80	11
Q8CIE6|COPA_MOUSE	Coatomer subunit alpha OS=Mus	158.19	44	11
Q7TPV4|MBB1A_MOUSE	Myb-binding protein 1A OS=Mus	153.13	42	11
P80313|TCPH_MOUSE	T-complex protein 1 subunit eta (	142.58	47	11
Q9Z1Z0|USO1_MOUSE	General vesicular transport facto	104.98	49	11
P63101|1433Z_MOUSE	14-3-3 protein zeta/delta OS=Mu	238.87	73	10
Q60605|MYL6_MOUSE	Myosin light polypeptide 6 OS=M	201.05	88	10
P01942|HBA_MOUSE	Hemoglobin subunit alpha OS=M	197.41	92	10
Q8BP92|RCN2_MOUSE	Reticulocalbin-2 OS=Mus muscu	190.72	67	10
P13020|GELS_MOUSE	Gelsolin OS=Mus musculus GN=	187.12	40	10
P62830|RL23_MOUSE	60S ribosomal protein L23 OS=M	185.19	74	10
P62317|SMD2_MOUSE	Small nuclear ribonucleoprotein	184.64	72	10
Q3THW5|H2AV_MOUSE	Histone H2A.V OS=Mus musculu	184.51	90	10
P0C0S6|H2AZ_MOUSE	Histone H2A.Z OS=Mus musculu	184.51	84	10
Q76MZ3|2AAA_MOUSE	Serine/threonine-protein phospha	168.96	71	10
P09411|PGK1_MOUSE	Phosphoglycerate kinase 1 OS=	168.15	48	10
Q64478|H2B1H_MOUSE	Histone H2B type 1-H OS=Mus r	165.46	59	10
Q64525|H2B2B_MOUSE	Histone H2B type 2-B OS=Mus r	165.46	60	10
Q64475|H2B1B_MOUSE	Histone H2B type 1-B OS=Mus r	165.46	54	10
Q6ZWY9|H2B1C_MOUSE	Histone H2B type 1-C/E/G OS=M	165.46	54	10
P10853|H2B1F_MOUSE	Histone H2B type 1-F/J/L OS=Mu	165.46	54	10
Q8CGP1|H2B1K_MOUSE	Histone H2B type 1-K OS=Mus r	165.46	54	10
P10854|H2B1M_MOUSE	Histone H2B type 1-M OS=Mus r	165.46	54	10
Q9WTM5|RUVB2_MOUSE	RuvB-like 2 OS=Mus musculus (	163.48	37	10
Q9CQF3|CPSF5_MOUSE	Cleavage and polyadenylation sp	162.33	72	10
P29533|VCAM1_MOUSE	Vascular cell adhesion protein 1	147.87	26	10
P40142|TKT_MOUSE	Transketolase OS=Mus musculu	147.23	41	10
Q8BFY9|TNPO1_MOUSE	Transportin-1 OS=Mus musculus	145.26	51	10
Q8C854|MYEF2_MOUSE	Myelin expression factor 2 OS=M	140.81	29	10
Q9D6R2|IDH3A_MOUSE	Isocitrate dehydrogenase [NAD]	140.48	36	10
Q3UPL0|SC31A_MOUSE	Protein transport protein Sec31A	136.87	18	10
Q9CU62|SMC1A_MOUSE	Structural maintenance of chrom	131.66	19	10
Q91VD9|NDUS1_MOUSE	NADH-ubiquinone oxidoreductas	130.52	30	10
A2AN08|UBR4_MOUSE	E3 ubiquitin-protein ligase UBR4	130.21	14	10
O08788|DCTN1_MOUSE	Dynactin subunit 1 OS=Mus mus	123.77	28	10
P39447|ZO1_MOUSE	Tight junction protein ZO-1 OS=M	122.52	12	10
Q7TPR4|ACTN1_MOUSE	Alpha-actinin-1 OS=Mus muscul	231.84	61	9
P62962|PROF1_MOUSE	Profilin-1 OS=Mus musculus GN	213.75	98	9
P61982|1433G_MOUSE	14-3-3 protein gamma OS=Mus	205.68	68	9
Q8R2Z5|VWA1_MOUSE	von Willebrand factor A domain-	190.66	45	9
P16045|LEG1_MOUSE	Galectin-1 OS=Mus musculus G	186.91	84	9
P63276|RS17_MOUSE	40S ribosomal protein S17 OS=M	185.97	70	9
P17182|ENOA_MOUSE	Alpha-enolase OS=Mus musculu	182.71	71	9
Q8R4R6|NUP53_MOUSE	Nucleoporin NUP53 OS=Mus mu	182.35	63	9
P62754|RS6_MOUSE	40S ribosomal protein S6 OS=M	174.7	40	9
Q922Q8|LRC59_MOUSE	Leucine-rich repeat-containing p	173.54	34	9
Q8BJ71|NUP93_MOUSE	Nuclear pore complex protein Nu	173.53	60	9
P17751|TPIS_MOUSE	Triosephosphate isomerase OS=	172.68	57	9

Q91VA6|PDIP2_MOUSE	Polymerase delta-interacting pro	170.25	53	9
P35980|RL18_MOUSE	60S ribosomal protein L18 OS=M	169.27	45	9
Q8BWT1|THIM_MOUSE	3-ketoacyl-CoA thiolase, mitocho	162.73	50	9
P47963|RL13_MOUSE	60S ribosomal protein L13 OS=M	162.64	50	9
Q8R3Q6|CCD58_MOUSE	Coiled-coil domain-containing pr	161.95	77	9
P80314|TCPB_MOUSE	T-complex protein 1 subunit beta	161.92	49	9
P09542|MYL3_MOUSE	Myosin light chain 3 OS=Mus mu	160.79	77	9
Q61937|NPM_MOUSE	Nucleophosmin OS=Mus muscu	155.24	52	9
P35564|CALX_MOUSE	Calnexin OS=Mus musculus GN	153.24	34	9
P62264|RS14_MOUSE	40S ribosomal protein S14 OS=M	142.15	68	9
P08003|PDIA4_MOUSE	Protein disulfide-isomerase A4 O	141.22	32	9
P60122|RUVB1_MOUSE	RuvB-like 1 OS=Mus musculus G	138.76	43	9
P80318|TCPG_MOUSE	T-complex protein 1 subunit gam	138.39	39	9
P42932|TCPQ_MOUSE	T-complex protein 1 subunit thet	136.09	20	9
Q6P5F9|XPO1_MOUSE	Exportin-1 OS=Mus musculus G	134.69	21	9
P80315|TCPD_MOUSE	T-complex protein 1 subunit delt	130.63	66	9
Q60864|STIP1_MOUSE	Stress-induced-phosphoprotein 1	127.75	38	9
P14148|RL7_MOUSE	60S ribosomal protein L7 OS=Mu	127.72	54	9
P97807|FUMH_MOUSE	Fumarate hydratase, mitochondr	127.56	31	9
Q6Y7W8|PERQ2_MOUSE	PERQ amino acid-rich with GYF	120.16	19	9
P15508|SPTB1_MOUSE	Spectrin beta chain, erythrocyte	117.5	25	9
A2ASQ1|AGRIN_MOUSE	Agrin OS=Mus musculus GN=Ag	95.72	15	9
Q9QZQ1|AFAD_MOUSE	Afadin OS=Mus musculus GN=M	95.68	12	9
P07759|SPA3K_MOUSE	Serine protease inhibitor A3K OS	232.17	69	8
Q921F2|TADBP_MOUSE	TAR DNA-binding protein 43 OS	184.85	33	8
Q8BMF4|ODP2_MOUSE	Dihydrolipoyllysine-residue acety	181.28	23	8
Q64213|SF01_MOUSE	Splicing factor 1 OS=Mus muscu	177.48	38	8
P56391|CX6B1_MOUSE	Cytochrome c oxidase subunit 6I	164.45	76	8
Q61584|FXR1_MOUSE	Fragile X mental retardation syn	162.87	33	8
P47941|CRKL_MOUSE	Crk-like protein OS=Mus muscul	162.46	38	8
Q9D1M0|SEC13_MOUSE	Protein SEC13 homolog OS=Mu	162.4	53	8
Q9D1Q6|ERP44_MOUSE	Endoplasmic reticulum resident p	157.31	52	8
Q91WJ8|FUBP1_MOUSE	Far upstream element-binding pr	156.44	22	8
Q8CJ69|BMPER_MOUSE	BMP-binding endothelial regulato	149.26	26	8
Q61656|DDX5_MOUSE	Probable ATP-dependent RNA h	147.46	28	8
P03975|IGEB_MOUSE	IgE-binding protein OS=Mus mus	145.94	22	8
P54775|PRS6B_MOUSE	26S protease regulatory subunit	145.91	61	8
Q9QZD9|EIF3I_MOUSE	Eukaryotic translation initiation fa	145.41	58	8
P62858|RS28_MOUSE	40S ribosomal protein S28 OS=M	144.16	61	8
Q99MD9|NASP_MOUSE	Nuclear autoantigenic sperm pro	141.9	38	8
P62082|RS7_MOUSE	40S ribosomal protein S7 OS=Mu	136.64	44	8
P84089|ERH_MOUSE	Enhancer of rudimentary homolo	136.12	62	8
Q02819|NUCB1_MOUSE	Nucleobindin-1 OS=Mus muscul	135.8	36	8
Q9CYR0|SSBP_MOUSE	Single-stranded DNA-binding pro	135.27	55	8
Q8QZT1|THIL_MOUSE	Acetyl-CoA acetyltransferase, mi	134.28	35	8
P58022|LOXL2_MOUSE	Lysyl oxidase homolog 2 OS=Mu	130.35	32	8
P62702|RS4X_MOUSE	40S ribosomal protein S4, X isof	128.4	42	8
Q80X50|UBP2L_MOUSE	Ubiquitin-associated protein 2-lik	120.98	12	8
Q9Z0R4|ITSN1_MOUSE	Intersectin-1 OS=Mus musculus	113.86	21	8
Q9QXZ0|MACF1_MOUSE	Microtubule-actin cross-linking fa	87.91	10	8
P70670|NACAM_MOUSE	Nascent polypeptide-associated	74.36	15	8
Q8BFZ3|ACTBL_MOUSE	Beta-actin-like protein 2 OS=Mus	245.03	90	7
Q3THE2|ML12B_MOUSE	Myosin regulatory light chain 12B	219.34	86	7
P57780|ACTN4_MOUSE	Alpha-actinin-4 OS=Mus muscul	207.71	43	7
O35658|C1QBP_MOUSE	Complement component 1 Q sub	194.88	49	7

P20108|PRDX3_MOUSE	Thioredoxin-dependent peroxide	192.15	66	7
Q9CYZ2|TPD54_MOUSE	Tumor protein D54 OS=Mus mus	187.91	71	7
P62204|CALM_MOUSE	Calmodulin OS=Mus musculus G	181	92	7
P29788|VTNC_MOUSE	Vitronectin OS=Mus musculus G	172.36	40	7
Q8BL97|SRSF7_MOUSE	Serine/arginine-rich splicing factc	160.71	52	7
P62242|RS8_MOUSE	40S ribosomal protein S8 OS=M	160.65	37	7
P14115|RL27A_MOUSE	60S ribosomal protein L27a OS=	158.67	59	7
Q9R0U0|SRS10_MOUSE	Serine/arginine-rich splicing factc	154.71	50	7
Q8R1Q8|DC1L1_MOUSE	Cytoplasmic dynein 1 light interm	154.07	32	7
Q9D0W5|PPIL1_MOUSE	Peptidyl-prolyl cis-trans isomeras	146.53	52	7
Q9D1M4|MCA3_MOUSE	Eukaryotic translation elongation	145.93	81	7
P46412|GPX3_MOUSE	Glutathione peroxidase 3 OS=Mu	139.92	46	7
Q61207|SAP_MOUSE	Sulfated glycoprotein 1 OS=Mus	137.18	24	7
Q9CPT4|CS010_MOUSE	UPF0556 protein C19orf10 homc	136.72	66	7
Q9JKF1|IQGA1_MOUSE	Ras GTPase-activating-like prote	134.51	29	7
P97351|RS3A_MOUSE	40S ribosomal protein S3a OS=M	131.15	35	7
P47962|RL5_MOUSE	60S ribosomal protein L5 OS=Mu	129.5	35	7
Q922B2|SYDC_MOUSE	Aspartyl-tRNA synthetase, cytop	126.34	19	7
O08585|CLCA_MOUSE	Clathrin light chain A OS=Mus m	125.67	28	7
P14131|RS16_MOUSE	40S ribosomal protein S16 OS=M	124.48	49	7
P20918|PLMN_MOUSE	Plasminogen OS=Mus musculus	122.47	29	7
Q9WVK4|EHD1_MOUSE	EH domain-containing protein 1	121.32	47	7
Q60597|ODO1_MOUSE	2-oxoglutarate dehydrogenase, r	120.05	22	7
Q9CQN1|TRAP1_MOUSE	Heat shock protein 75 kDa, mitoc	117.9	57	7
P23116|EIF3A_MOUSE	Eukaryotic translation initiation fa	117.34	19	7
P61965|WDR5_MOUSE	WD repeat-containing protein 5 (	115.35	41	7
P68040|GBLP_MOUSE	Guanine nucleotide-binding prote	108.25	35	7
Q8VDP4|K1967_MOUSE	Protein KIAA1967 homolog OS=	86.8	12	7
Q9R1C7|PR40A_MOUSE	Pre-mRNA-processing factor 40	84.49	16	7
A2ARV4|LRP2_MOUSE	Low-density lipoprotein receptor-	83.4	14	7
P68033|ACTC_MOUSE	Actin, alpha cardiac muscle 1 OS	297.4	82	6
P68254|1433T_MOUSE	14-3-3 protein theta OS=Mus mu	191.19	67	6
Q61029|LAP2B_MOUSE	Lamina-associated polypeptide 2	167.55	32	6
Q9CQR2|RS21_MOUSE	40S ribosomal protein S21 OS=M	163.47	63	6
Q62523|ZYX_MOUSE	Zyxin OS=Mus musculus GN=Zy	156.93	32	6
O89086|RBM3_MOUSE	Putative RNA-binding protein 3 (	156.82	84	6
O08583|THOC4_MOUSE	THO complex subunit 4 OS=Mus	156.48	52	6
Q9DB15|RM12_MOUSE	39S ribosomal protein L12, mitoc	150.59	58	6
P16110|LEG3_MOUSE	Galectin-3 OS=Mus musculus G	146.21	25	6
Q6IRU2|TPM4_MOUSE	Tropomyosin alpha-4 chain OS=	145.92	72	6
P24369|PPIB_MOUSE	Peptidyl-prolyl cis-trans isomeras	142.75	61	6
P18760|COF1_MOUSE	Cofilin-1 OS=Mus musculus GN=	140.58	44	6
O70251|EF1B_MOUSE	Elongation factor 1-beta OS=Mu	139.33	33	6
P84099|RL19_MOUSE	60S ribosomal protein L19 OS=M	131.61	37	6
P47738|ALDH2_MOUSE	Aldehyde dehydrogenase, mitocl	130.38	23	6
Q8VDM4|PSMD2_MOUSE	26S proteasome non-ATPase re	130.05	47	6
P62996|TRA2B_MOUSE	Transformer-2 protein homolog b	129.59	36	6
Q9CZU3|SK2L2_MOUSE	Superkiller viralicidic activity 2-lik	128.24	36	6
P60335|PCBP1_MOUSE	Poly(rC)-binding protein 1 OS=M	126.85	41	6
Q9QZM0|UBQL2_MOUSE	Ubiquilin-2 OS=Mus musculus G	125.92	19	6
Q9CZM2|RL15_MOUSE	60S ribosomal protein L15 OS=M	125.6	43	6
P18242|CATD_MOUSE	Cathepsin D OS=Mus musculus	124.75	36	6
P19536|COX5B_MOUSE	Cytochrome c oxidase subunit 5I	124.52	81	6
P35700|PRDX1_MOUSE	Peroxiredoxin-1 OS=Mus muscu	122.67	52	6
P26443|DHE3_MOUSE	Glutamate dehydrogenase 1, mit	122.19	18	6

B2RY56|RBM25_MOUSE	RNA-binding protein 25 OS=Mus	121.82	16	6
Q9R0N0|GALK1_MOUSE	Galactokinase OS=Mus musculu	119.87	32	6
Q9DBG5|PLIN3_MOUSE	Perilipin-3 OS=Mus musculus GI	117.38	29	6
P08228|SODC_MOUSE	Superoxide dismutase [Cu-Zn] C	116.16	44	6
Q9CYA6|ZCHC8_MOUSE	Zinc finger CCHC domain-contai	116.06	28	6
P02463|CO4A1_MOUSE	Collagen alpha-1(IV) chain OS=M	113.52	25	6
Q9WVA4|TAGL2_MOUSE	Transgelin-2 OS=Mus musculus	112.12	48	6
Q8K2C9|HACD3_MOUSE	3-hydroxyacyl-CoA dehydratase	112.08	47	6
Q8R1B4|EIF3C_MOUSE	Eukaryotic translation initiation fa	105.56	16	6
Q8BX22|SALL4_MOUSE	Sal-like protein 4 OS=Mus musc	100.89	18	6
Q61646|HPT_MOUSE	Haptoglobin OS=Mus musculus	100.85	36	6
P36552|HEM6_MOUSE	Coproporphyrinogen-III oxidase,	100.71	26	6
Q60675|LAMA2_MOUSE	Laminin subunit alpha-2 OS=Mus	99.81	21	6
Q99KI0|ACON_MOUSE	Aconitate hydratase, mitochondri	97.86	21	6
Q8CGK3|LONM_MOUSE	Lon protease homolog, mitochon	97.43	24	6
Q6ZWN5|RS9_MOUSE	40S ribosomal protein S9 OS=M	79.64	34	6
Q6PDK2|MLL2_MOUSE	Histone-lysine N-methyltransfera	38.25	9	6
P99024|TBB5_MOUSE	Tubulin beta-5 chain OS=Mus m	308.45	75	5
P22599|A1AT2_MOUSE	Alpha-1-antitrypsin 1-2 OS=Mus	197.39	51	5
Q01768|NDKB_MOUSE	Nucleoside diphosphate kinase B	184.91	79	5
Q9CQV8|1433B_MOUSE	14-3-3 protein beta/alpha OS=M	174.06	65	5
Q9DBG3|AP2B1_MOUSE	AP-2 complex subunit beta OS=	173.99	30	5
Q9CQ92|FIS1_MOUSE	Mitochondrial fission 1 protein O	159.79	67	5
P62315|SMD1_MOUSE	Small nuclear ribonucleoprotein	154.51	50	5
Q9QZQ8|H2AY_MOUSE	Core histone macro-H2A.1 OS=M	151.84	51	5
Q61171|PRDX2_MOUSE	Peroxiredoxin-2 OS=Mus muscu	147.28	55	5
Q8BIQ5|CSTF2_MOUSE	Cleavage stimulation factor subu	145.22	40	5
Q9QYJ0|DNJA2_MOUSE	DnaJ homolog subfamily A mem	144.03	48	5
P62983|RS27A_MOUSE	Ubiquitin-40S ribosomal protein S	142.44	51	5
Q9Z2D8|MBD3_MOUSE	Methyl-CpG-binding domain prot	140.79	49	5
Q61147|CERU_MOUSE	Ceruloplasmin OS=Mus musculu	135.87	20	5
Q6PDG5|SMRC2_MOUSE	SWI/SNF complex subunit SMAR	135.55	35	5
Q99KV1|DJB11_MOUSE	DnaJ homolog subfamily B mem	130.5	43	5
P07356|ANXA2_MOUSE	Annexin A2 OS=Mus musculus (	129.89	42	5
Q8BKC5|IPO5_MOUSE	Importin-5 OS=Mus musculus G	126.81	36	5
P28798|GRN_MOUSE	Granulins OS=Mus musculus GN	126.15	27	5
Q5SFM8|RBM27_MOUSE	RNA-binding protein 27 OS=Mus	125.54	30	5
O35206|COFA1_MOUSE	Collagen alpha-1(XV) chain OS=	125.53	14	5
Q8VEK3|HNRPU_MOUSE	Heterogeneous nuclear ribonucle	124.81	23	5
Q9WTP6|KAD2_MOUSE	Adenylate kinase 2, mitochondria	122.92	46	5
P59708|PM14_MOUSE	Pre-mRNA branch site protein p1	122.52	42	5
P63323|RS12_MOUSE	40S ribosomal protein S12 OS=M	121.74	39	5
Q9DCJ5|NDUA8_MOUSE	NADH dehydrogenase [ubiquino	119.56	49	5
P70372|ELAV1_MOUSE	ELAV-like protein 1 OS=Mus mu	119.23	37	5
P70168|IMB1_MOUSE	Importin subunit beta-1 OS=Mus	117.19	28	5
P16675|PPGB_MOUSE	Lysosomal protective protein OS	115.23	15	5
Q91VC3|IF4A3_MOUSE	Eukaryotic initiation factor 4A-III	114.73	30	5
Q9CPP6|NDUA5_MOUSE	NADH dehydrogenase [ubiquino	113.59	59	5
P23780|BGAL_MOUSE	Beta-galactosidase OS=Mus mu	112.54	23	5
Q8BTV2|CPSF7_MOUSE	Cleavage and polyadenylation sp	112.13	28	5
Q9QUR7|PIN1_MOUSE	Peptidyl-prolyl cis-trans isomeras	112.03	57	5
Q5XJY5|COPD_MOUSE	Coatomer subunit delta OS=Mus	110.78	30	5
Q99JB2|STML2_MOUSE	Stomatin-like protein 2 OS=Mus	107.75	58	5
P63163|RSMN_MOUSE	Small nuclear ribonucleoprotein-	106.13	53	5
P27048|RSMB_MOUSE	Small nuclear ribonucleoprotein-	106.13	42	5

P35979|RL12_MOUSE	60S ribosomal protein L12 OS=M	104.43	39	5
P61161|ARP2_MOUSE	Actin-related protein 2 OS=Mus	104.22	45	5
Q6ZQ38|CAND1_MOUSE	Cullin-associated NEDD8-dissoc	102.51	23	5
Q80YR5|SAFB2_MOUSE	Scaffold attachment factor B2 O	101.78	10	5
P41105|RL28_MOUSE	60S ribosomal protein L28 OS=M	101.76	30	5
Q61164|CTCF_MOUSE	Transcriptional repressor CTCF	101.23	31	5
Q6NVF9|CPSF6_MOUSE	Cleavage and polyadenylation sp	98.57	18	5
Q60631|GRB2_MOUSE	Growth factor receptor-bound pr	97.96	30	5
P81117|NUCB2_MOUSE	Nucleobindin-2 OS=Mus muscul	97.27	35	5
P01887|B2MG_MOUSE	Beta-2-microglobulin OS=Mus m	96.82	40	5
Q6NZJ6|IF4G1_MOUSE	Eukaryotic translation initiation fa	94.61	9	5
P07146|TRY2_MOUSE	Anionic trypsin-2 OS=Mus musc	93.95	33	5
P17427|AP2A2_MOUSE	AP-2 complex subunit alpha-2 O	93.87	18	5
Q62318|TIF1B_MOUSE	Transcription intermediary factor	93.2	19	5
Q8BX70|VP13C_MOUSE	Vacuolar protein sorting-associat	91.94	8	5
Q99KN9|EPN4_MOUSE	Clathrin interactor 1 OS=Mus mu	91.69	21	5
Q9DCH4|EIF3F_MOUSE	Eukaryotic translation initiation fa	90.42	34	5
P26369|U2AF2_MOUSE	Splicing factor U2AF 65 kDa sub	89.38	24	5
Q921M4|GOGA2_MOUSE	Golgin subfamily A member 2 OS	88.85	18	5
Q9JIF7|COPB_MOUSE	Coatomer subunit beta OS=Mus	79.81	17	5
Q9EQH3|VPS35_MOUSE	Vacuolar protein sorting-associat	77.21	19	5
Q60865|CAPR1_MOUSE	Caprin-1 OS=Mus musculus GN	76.84	15	5
P62281|RS11_MOUSE	40S ribosomal protein S11 OS=M	75.98	34	5
Q8BYA0|TBCD_MOUSE	Tubulin-specific chaperone D OS	75.81	30	5
P62192|PRS4_MOUSE	26S protease regulatory subunit	72.86	18	5
Q91ZU6|DYST_MOUSE	Dystonin OS=Mus musculus GN	59.7	6	5
B2RX14|TUT4_MOUSE	Terminal uridylyltransferase 4 OS	47.93	9	5
Q8BYK6|YTHD3_MOUSE	YTH domain family protein 3 OS	47.63	13	5
P27661|H2AX_MOUSE	Histone H2A.x OS=Mus musculu	244.51	77	4
Q61696|HS71A_MOUSE	Heat shock 70 kDa protein 1A O	225.55	69	4
P17879|HS71B_MOUSE	Heat shock 70 kDa protein 1B O	225.55	70	4
O08638|MYH11_MOUSE	Myosin-11 OS=Mus musculus G	193.41	35	4
Q00898|A1AT5_MOUSE	Alpha-1-antitrypsin 1-5 OS=Mus	187.58	40	4
Q62167|DDX3X_MOUSE	ATP-dependent RNA helicase D	185.97	62	4
Q02257|PLAK_MOUSE	Junction plakoglobin OS=Mus m	141.54	40	4
Q99JX3|GORS2_MOUSE	Golgi reassembly-stacking protei	131.66	36	4
Q9D6Z1|NOP56_MOUSE	Nucleolar protein 56 OS=Mus mu	131.47	23	4
Q9WTX5|SKP1_MOUSE	S-phase kinase-associated prote	127.34	28	4
Q9Z175|LOXL3_MOUSE	Lysyl oxidase homolog 3 OS=Mu	126.2	14	4
Q9D3D9|ATPD_MOUSE	ATP synthase subunit delta, mito	125.78	64	4
Q9CX56|PSMD8_MOUSE	26S proteasome non-ATPase re	123.85	31	4
Q9CQT2|RBM7_MOUSE	RNA-binding protein 7 OS=Mus	123.77	42	4
Q99LC5|ETFA_MOUSE	Electron transfer flavoprotein sub	122.83	39	4
Q8CG71|P3H2_MOUSE	Prolyl 3-hydroxylase 2 OS=Mus	122.13	27	4
P62307|RUXF_MOUSE	Small nuclear ribonucleoprotein	121.18	60	4
P08122|CO4A2_MOUSE	Collagen alpha-2(IV) chain OS=M	119.75	18	4
P01837|IGKC_MOUSE	Ig kappa chain C region OS=Mus	118.81	42	4
O55029|COPB2_MOUSE	Coatomer subunit beta' OS=Mus	118.73	29	4
Q8VDJ3|VIGLN_MOUSE	Vigilin OS=Mus musculus GN=H	118.34	16	4
Q61704|ITIH3_MOUSE	Inter-alpha-trypsin inhibitor heav	117.12	16	4
Q9EPJ9|ARFG1_MOUSE	ADP-ribosylation factor GTPase-	115.62	21	4
Q9EPU4|CPSF1_MOUSE	Cleavage and polyadenylation sp	115.05	21	4
Q8VHX6|FLNC_MOUSE	Filamin-C OS=Mus musculus GN	114.76	10	4
O88968|TCO2_MOUSE	Transcobalamin-2 OS=Mus mus	114.39	36	4
P32261|ANT3_MOUSE	Antithrombin-III OS=Mus muscul	112.82	37	4

P62897|CYC_MOUSE	Cytochrome c, somatic OS=Mus	112.2	47	4
Q9D0F9|PGM1_MOUSE	Phosphoglucomutase-1 OS=Mus	111.21	20	4
P80317|TCPZ_MOUSE	T-complex protein 1 subunit zeta	111.11	21	4
Q9JHJ0|TMOD3_MOUSE	Tropomodulin-3 OS=Mus muscu	109.41	32	4
P51410|RL9_MOUSE	60S ribosomal protein L9 OS=Mu	109.2	47	4
O08749|DLDH_MOUSE	Dihydrolipoyl dehydrogenase, mi	108.8	29	4
Q9JLV5|CUL3_MOUSE	Cullin-3 OS=Mus musculus GN=	108.1	20	4
Q08369|GATA4_MOUSE	Transcription factor GATA-4 OS=	107.3	35	4
Q8C0C7|SYFA_MOUSE	Phenylalanyl-tRNA synthetase al	107.25	30	4
Q8BX10|PGAM5_MOUSE	Serine/threonine-protein phospha	106.16	22	4
Q9D1B9|RM28_MOUSE	39S ribosomal protein L28, mitoc	106.04	39	4
Q9CR57|RL14_MOUSE	60S ribosomal protein L14 OS=M	105.64	28	4
P40124|CAP1_MOUSE	Adenylyl cyclase-associated prot	105.1	19	4
Q6NZN0|RBM26_MOUSE	RNA-binding protein 26 OS=Mus	103.31	13	4
Q3U7R1|ESYT1_MOUSE	Extended synaptotagmin-1 OS=M	102.59	30	4
O09167|RL21_MOUSE	60S ribosomal protein L21 OS=M	101.91	41	4
P01864|GCAB_MOUSE	Ig gamma-2A chain C region sec	99.17	35	4
P97927|LAMA4_MOUSE	Laminin subunit alpha-4 OS=Mus	99.06	12	4
P60867|RS20_MOUSE	40S ribosomal protein S20 OS=M	98.94	29	4
P61924|COPZ1_MOUSE	Coatomer subunit zeta-1 OS=Mu	98.59	52	4
Q8BTS4|NUP54_MOUSE	Nuclear pore complex protein Nu	96.43	18	4
Q9DBJ1|PGAM1_MOUSE	Phosphoglycerate mutase 1 OS=	94.45	19	4
P05064|ALDOA_MOUSE	Fructose-bisphosphate aldolase	94.27	21	4
Q04447|KCRB_MOUSE	Creatine kinase B-type OS=Mus	93.86	22	4
P62855|RS26_MOUSE	40S ribosomal protein S26 OS=M	93.07	32	4
P21107|TPM3_MOUSE	Tropomyosin alpha-3 chain OS=	93.01	23	4
Q9CQL1|MGNR_MOUSE	Protein mago nashi homolog 1-r	92.09	64	4
P61327|MGN_MOUSE	Protein mago nashi homolog OS	92.09	64	4
Q00PI9|HNRL2_MOUSE	Heterogeneous nuclear ribonucle	91.8	23	4
Q91WK2|EIF3H_MOUSE	Eukaryotic translation initiation fa	91.09	27	4
Q8C5Q4|GRSF1_MOUSE	G-rich sequence factor 1 OS=Mu	90.98	22	4
P61458|PHS_MOUSE	Pterin-4-alpha-carbinolamine del	90.06	44	4
Q9Z2W0|DNPEP_MOUSE	Aspartyl aminopeptidase OS=Mu	89.81	23	4
Q9WVG6|CARM1_MOUSE	Histone-arginine methyltransfera	89.1	17	4
P99029|PRDX5_MOUSE	Peroxiredoxin-5, mitochondrial C	87.21	24	4
Q62093|SRSF2_MOUSE	Serine/arginine-rich splicing facto	85.94	32	4
Q6PDQ2|CHD4_MOUSE	Chromodomain-helicase-DNA-bi	85.9	13	4
P62267|RS23_MOUSE	40S ribosomal protein S23 OS=M	84.59	51	4
Q6ZQI3|MLEC_MOUSE	Malectin OS=Mus musculus GN=	84.3	36	4
Q9Z1D1|EIF3G_MOUSE	Eukaryotic translation initiation fa	84.07	10	4
Q07417|ACADS_MOUSE	Short-chain specific acyl-CoA de	83.73	17	4
Q8BH74|NU107_MOUSE	Nuclear pore complex protein Nu	83.48	20	4
Q6NV83|SR140_MOUSE	U2 snRNP-associated SURP mo	81.53	15	4
Q9CWE0|FA54B_MOUSE	Protein FAM54B OS=Mus muscu	80.94	27	4
P01898|HA10_MOUSE	H-2 class I histocompatibility anti	80.38	20	4
Q9JJF3|NO66_MOUSE	Lysine-specific demethylase NO	80.04	15	4
Q62189|SNRPA_MOUSE	U1 small nuclear ribonucleprote	79.57	18	4
Q8BGQ7|SYAC_MOUSE	Alanyl-tRNA synthetase, cytoplas	79.19	11	4
P11404|FABPH_MOUSE	Fatty acid-binding protein, heart	77.86	41	4
P28656|NP1L1_MOUSE	Nucleosome assembly protein 1-	77.2	17	4
Q8R4X3|RBM12_MOUSE	RNA-binding protein 12 OS=Mus	77.13	14	4
P19253|RL13A_MOUSE	60S ribosomal protein L13a OS=	76.89	25	4
O88685|PRS6A_MOUSE	26S protease regulatory subunit	72.54	26	4
P30416|FKBP4_MOUSE	Peptidyl-prolyl cis-trans isomeras	71.67	18	4
Q61464|ZN638_MOUSE	Zinc finger protein 638 OS=Mus	66.84	9	4

P62852|RS25_MOUSE	40S ribosomal protein S25 OS=M	65.93	42	4
Q9D0F3|LMAN1_MOUSE	Protein ERGIC-53 OS=Mus mus	63.66	7	4
Q9CW46|RAVR1_MOUSE	Ribonucleoprotein PTB-binding 1	53.82	20	4
Q8BTI8|SRRM2_MOUSE	Serine/arginine repetitive matrix	53.64	6	4
A2AAJ9|OBSCN_MOUSE	Obscurin OS=Mus musculus GN	49.59	7	4
Q6NZC7|S23IP_MOUSE	SEC23-interacting protein OS=M	47.32	13	4
Q63870|CO7A1_MOUSE	Collagen alpha-1(VII) chain OS=	45.39	13	4
Q8BKX6|SMG1_MOUSE	Serine/threonine-protein kinase S	43.86	6	4
Q69Z38|PEAK1_MOUSE	Pseudopodium-enriched atypical	42.38	4	4
Q8BLN6|UNC80_MOUSE	Protein unc-80 homolog OS=Mus	33.16	11	4
P68372|TBB2C_MOUSE	Tubulin beta-2C chain OS=Mus m	293.24	76	3
P17156|HSP72_MOUSE	Heat shock-related 70 kDa prote	274.47	53	3
Q922F4|TBB6_MOUSE	Tubulin beta-6 chain OS=Mus m	243.61	68	3
Q8R1M2|H2AJ_MOUSE	Histone H2A.J OS=Mus musculu	232.45	76	3
Q03734|SPA3M_MOUSE	Serine protease inhibitor A3M OS	224.13	62	3
P16627|HS71L_MOUSE	Heat shock 70 kDa protein 1-like	209.77	54	3
Q9R0B6|LAMC3_MOUSE	Laminin subunit gamma-3 OS=M	201.59	23	3
Q91WP6|SPA3N_MOUSE	Serine protease inhibitor A3N OS	176.74	47	3
P70333|HNRH2_MOUSE	Heterogeneous nuclear ribonucle	176.34	32	3
Q8R010|AIMP2_MOUSE	Aminoacyl tRNA synthase compl	142.86	48	3
Q61033|LAP2A_MOUSE	Lamina-associated polypeptide 2	142.83	28	3
P15532|NDKA_MOUSE	Nucleoside diphosphate kinase A	140.62	61	3
P84228|H32_MOUSE	Histone H3.2 OS=Mus musculus	140.31	81	3
O08807|PRDX4_MOUSE	Peroxiredoxin-4 OS=Mus muscu	127.14	37	3
Q923G2|RPAB3_MOUSE	DNA-directed RNA polymerases	124.51	37	3
Q6DFW4|NOP58_MOUSE	Nucleolar protein 58 OS=Mus mu	122.6	34	3
Q9WV55|VAPA_MOUSE	Vesicle-associated membrane pr	122.18	29	3
P62196|PRS8_MOUSE	26S protease regulatory subunit	115.88	33	3
P84104|SRSF3_MOUSE	Serine/arginine-rich splicing facto	114.67	33	3
Q7M6Y3|PICA_MOUSE	Phosphatidylinositol-binding clath	114.26	22	3
Q9QXT0|CNPY2_MOUSE	Protein canopy homolog 2 OS=M	113.92	26	3
P12787|COX5A_MOUSE	Cytochrome c oxidase subunit 5A	113.87	66	3
Q9CR68|UCRI_MOUSE	Cytochrome b-c1 complex subun	109.02	41	3
Q9JJI8|RL38_MOUSE	60S ribosomal protein L38 OS=M	108.21	57	3
P62320|SMD3_MOUSE	Small nuclear ribonucleoprotein S	105.51	36	3
Q8K4L0|DDX54_MOUSE	ATP-dependent RNA helicase DD	105.45	18	3
P99028|QCR6_MOUSE	Cytochrome b-c1 complex subun	105.09	66	3
Q99JX4|EIF3M_MOUSE	Eukaryotic translation initiation fa	104.91	45	3
Q921H8|THIKA_MOUSE	3-ketoacyl-CoA thiolase A, perox	104.91	11	3
Q9DCT8|CRIP2_MOUSE	Cysteine-rich protein 2 OS=Mus	104.25	24	3
P63242|IF5A1_MOUSE	Eukaryotic translation initiation fa	103.75	69	3
Q69ZA1|CDK13_MOUSE	Cyclin-dependent kinase 13 OS=	103.51	12	3
P62821|RAB1A_MOUSE	Ras-related protein Rab-1A OS=	101.93	37	3
P46938|YAP1_MOUSE	Yorkie homolog OS=Mus muscu	101.48	26	3
P62075|TIM13_MOUSE	Mitochondrial import inner memb	101.22	57	3
Q8BP67|RL24_MOUSE	60S ribosomal protein L24 OS=M	100.87	26	3
Q3TCN2|PLBL2_MOUSE	Putative phospholipase B-like 2 O	100.78	22	3
Q8VDM6|HNRL1_MOUSE	Heterogeneous nuclear ribonucle	99.82	25	3
Q6ZWV7|RL35_MOUSE	60S ribosomal protein L35 OS=M	98.56	27	3
Q9QX47|SON_MOUSE	Protein SON OS=Mus musculus	97.42	17	3
Q9R0L7|AKP8L_MOUSE	A-kinase anchor protein 8-like OS	96.95	30	3
P23198|CBX3_MOUSE	Chromobox protein homolog 3 OS	96.8	32	3
O88630|GOSR1_MOUSE	Golgi SNAP receptor complex m	96.36	14	3
Q3UIA2|RHG17_MOUSE	Rho GTPase-activating protein 17	95.21	27	3
P70318|TIAR_MOUSE	Nucleolysin TIAR OS=Mus musc	93.44	10	3

Q9ESB3|HRG_MOUSE	Histidine-rich glycoprotein OS=M	93.38	23	3
Q9CYD3|CRTAP_MOUSE	Cartilage-associated protein OS=	93.18	16	3
P46935|NEDD4_MOUSE	E3 ubiquitin-protein ligase NEDD	93.03	19	3
Q9DC61|MPPA_MOUSE	Mitochondrial-processing peptida	92.32	26	3
Q9R0I7|YLPM1_MOUSE	YLP motif-containing protein 1 O	91.61	13	3
P56399|UBP5_MOUSE	Ubiquitin carboxyl-terminal hydro	91.43	31	3
P26231|CTNA1_MOUSE	Catenin alpha-1 OS=Mus muscu	90.91	22	3
O88477|IF2B1_MOUSE	Insulin-like growth factor 2 mRNA	90.65	16	3
Q9CYL5|GAPR1_MOUSE	Golgi-associated plant pathogen	90.52	34	3
Q8VC70|RBMS2_MOUSE	RNA-binding motif, single-strand	90.27	23	3
P62849|RS24_MOUSE	40S ribosomal protein S24 OS=M	90.26	44	3
P05202|AATM_MOUSE	Aspartate aminotransferase, mito	89.84	17	3
P68510|1433F_MOUSE	14-3-3 protein eta OS=Mus mus	89.59	51	3
P62827|RAN_MOUSE	GTP-binding nuclear protein Ran	88.18	17	3
P04186|CFAB_MOUSE	Complement factor B OS=Mus m	88.15	9	3
P70335|ROCK1_MOUSE	Rho-associated protein kinase 1	87.37	9	3
Q64010|CRK_MOUSE	Adapter molecule crk OS=Mus m	87.25	26	3
Q9D824|FIP1_MOUSE	Pre-mRNA 3'-end-processing fac	86.98	13	3
Q64737|PUR2_MOUSE	Trifunctional purine biosynthetic	86.81	14	3
P62309|RUXG_MOUSE	Small nuclear ribonucleoprotein	86.46	33	3
P30412|PPIC_MOUSE	Peptidyl-prolyl cis-trans isomeras	86.31	34	3
Q9DCT2|NDUS3_MOUSE	NADH dehydrogenase [ubiquino	86.01	25	3
Q9CZ13|QCR1_MOUSE	Cytochrome b-c1 complex subun	85.07	18	3
Q63850|NUP62_MOUSE	Nuclear pore glycoprotein p62 O	85	11	3
Q8R0F3|SUMF1_MOUSE	Sulfatase-modifying factor 1 OS=	84.76	10	3
Q7TSC1|PRC2A_MOUSE	Protein PRRC2A OS=Mus musc	84.41	12	3
P62960|YBOX1_MOUSE	Nuclease-sensitive element-bind	84.26	29	3
Q9JJH1|RNAS4_MOUSE	Ribonuclease 4 OS=Mus muscu	83.51	57	3
Q02053|UBA1_MOUSE	Ubiquitin-like modifier-activating	82.99	18	3
Q99KJ8|DCTN2_MOUSE	Dynactin subunit 2 OS=Mus mus	82.91	16	3
Q8QZY1|EIF3L_MOUSE	Eukaryotic translation initiation fa	82.54	15	3
O08547|SC22B_MOUSE	Vesicle-trafficking protein SEC22	81.07	20	3
Q9CXF4|TBC15_MOUSE	TBC1 domain family member 15	80.43	11	3
Q99JI4|PSMD6_MOUSE	26S proteasome non-ATPase re	78.02	34	3
P25206|MCM3_MOUSE	DNA replication licensing factor M	77.85	12	3
Q3U2P1|SC24A_MOUSE	Protein transport protein Sec24A	76.92	10	3
Q9Z2I8|SUCB2_MOUSE	Succinyl-CoA ligase [GDP-formi	76.36	15	3
Q8BSQ9|PB1_MOUSE	Protein polybromo-1 OS=Mus mu	76.31	11	3
Q9JJY4|DDX20_MOUSE	Probable ATP-dependent RNA h	76.04	10	3
Q99PU8|DHX30_MOUSE	Putative ATP-dependent RNA he	75.5	14	3
Q61753|SERA_MOUSE	D-3-phosphoglycerate dehydroge	75.46	8	3
P21126|UBL4A_MOUSE	Ubiquitin-like protein 4A OS=Mus	75.08	29	3
Q6ZWV3|RL10_MOUSE	60S ribosomal protein L10 OS=M	75.02	22	3
Q8C7E9|CSTFT_MOUSE	Cleavage stimulation factor subu	74.97	56	3
P14685|PSMD3_MOUSE	26S proteasome non-ATPase re	74.42	17	3
O54774|AP3D1_MOUSE	AP-3 complex subunit delta-1 OS	74.23	11	3
Q9CZX8|RS19_MOUSE	40S ribosomal protein S19 OS=M	73.41	19	3
Q6ZQH8|NU188_MOUSE	Nucleoporin NUP188 homolog O	72.13	8	3
Q8K0V4|CNOT3_MOUSE	CCR4-NOT transcription comple	72.11	9	3
Q9D8W5|PSD12_MOUSE	26S proteasome non-ATPase re	71.65	22	3
Q9D6J6|NDUV2_MOUSE	NADH dehydrogenase [ubiquino	69.31	21	3
Q8CGR5|KLK14_MOUSE	Kallikrein-14 OS=Mus musculus	68.68	19	3
Q922D8|C1TC_MOUSE	C-1-tetrahydrofolate synthase, cy	68.32	6	3
Q8BJZ4|RT35_MOUSE	28S ribosomal protein S35, mito	67.61	25	3
Q9CQA3|DHSB_MOUSE	Succinate dehydrogenase [ubiqu	67.39	22	3

Q9ERU9|RBP2_MOUSE	E3 SUMO-protein ligase RanBP2	66.14	5	3
Q80W00|PP1RA_MOUSE	Serine/threonine-protein phospha	65.76	20	3
Q3UQN2|FCHO2_MOUSE	FCH domain only protein 2 OS=M	65.28	8	3
P46735|MYO1B_MOUSE	Myosin-Ib OS=Mus musculus GN	64.08	16	3
P62869|ELOB_MOUSE	Transcription elongation factor B	63.71	25	3
Q61768|KINH_MOUSE	Kinesin-1 heavy chain OS=Mus m	62.2	14	3
Q05186|RCN1_MOUSE	Reticulocalbin-1 OS=Mus muscu	61.69	17	3
P62911|RL32_MOUSE	60S ribosomal protein L32 OS=M	61.32	33	3
Q921G8|GCP2_MOUSE	Gamma-tubulin complex compor	59.65	8	3
Q60737|CSK21_MOUSE	Casein kinase II subunit alpha O	58.98	25	3
Q62425|NDUA4_MOUSE	NADH dehydrogenase [ubiquinor	58.48	52	3
P08226|APOE_MOUSE	Apolipoprotein E OS=Mus muscu	56.71	14	3
Q7TMK9|HNRPQ_MOUSE	Heterogeneous nuclear ribonucle	55.71	10	3
Q8JZQ9|EIF3B_MOUSE	Eukaryotic translation initiation fa	54.55	9	3
Q8R180|ERO1A_MOUSE	ERO1-like protein alpha OS=Mus	54.17	9	3
P70336|ROCK2_MOUSE	Rho-associated protein kinase 2	53.06	22	3
Q8BHP7|OLM2A_MOUSE	Olfactomedin-like protein 2A OS	52.24	5	3
Q80YT7|MYOME_MOUSE	Myomegalin OS=Mus musculus	50.3	6	3
P39054|DYN2_MOUSE	Dynamin-2 OS=Mus musculus G	48.76	16	3
Q921G7|ETFD_MOUSE	Electron transfer flavoprotein-ubi	45.85	15	3
Q8R4U0|STAB2_MOUSE	Stabilin-2 OS=Mus musculus GN	44.73	5	3
Q6PE13|PRRT3_MOUSE	Proline-rich transmembrane prot	44.01	16	3
Q2UY11|COSA1_MOUSE	Collagen alpha-1(XXVIII) chain C	43.61	6	3
Q6ZWR6|SYNE1_MOUSE	Nesprin-1 OS=Mus musculus GN	41.9	7	3
Q8C0S4|TT21A_MOUSE	Tetratricopeptide repeat protein 2	41.45	10	3
P58871|TB182_MOUSE	182 kDa tankyrase-1-binding pro	40.05	7	3
Q9DBT5|AMPD2_MOUSE	AMP deaminase 2 OS=Mus mus	38.76	4	3
Q8BRH4|MLL3_MOUSE	Histone-lysine N-methyltransfera	38.58	3	3
Q9WU60|ATRN_MOUSE	Attractin OS=Mus musculus GN=	37.9	4	3
O88700|BLM_MOUSE	Bloom syndrome protein homolo	36.94	7	3
Q8CC88|K0564_MOUSE	Uncharacterized protein KIAA05	36.03	7	3
Q99KW3|TARA_MOUSE	TRIO and F-actin-binding protein	35.79	5	3
Q60750|EPHA1_MOUSE	Ephrin type-A receptor 1 OS=Mu	35.56	7	3
P14404|EVI1_MOUSE	MDS1 and EVI1 complex locus p	35.51	5	3
Q8R3Y8|I2BP1_MOUSE	Interferon regulatory factor 2-bin	35.49	14	3
A2A884|ZEP3_MOUSE	Transcription factor HIVEP3 OS=	35.11	4	3
O88799|ZAN_MOUSE	Zonadhesin OS=Mus musculus	34.79	6	3
Q64331|MYO6_MOUSE	Myosin-VI OS=Mus musculus GN	33.61	13	3
Q70FJ1|AKAP9_MOUSE	A-kinase anchor protein 9 OS=M	32.52	8	3
O88935|SYN1_MOUSE	Synapsin-1 OS=Mus musculus C	31.79	6	3
Q3TLH4|PRC2C_MOUSE	Protein PRRC2C OS=Mus musc	31.21	4	3
Q80TL7|MON2_MOUSE	Protein MON2 homolog OS=Mus	30.86	6	3
Q8BUV3|GEPH_MOUSE	Gephyrin OS=Mus musculus GN	30.01	12	3
Q9WTS5|TEN2_MOUSE	Teneurin-2 OS=Mus musculus G	29.3	10	3
Q8CIQ7|DOCK3_MOUSE	Dedicator of cytokinesis protein 3	29.23	9	3
Q62059|CSPG2_MOUSE	Versican core protein OS=Mus m	29.06	2	3
Q99MZ6|MYO7B_MOUSE	Myosin-VIIb OS=Mus musculus	28.57	15	3
A2AJ76|HMCN2_MOUSE	Hemicentin-2 OS=Mus musculus	27.44	3	3
Q9Z0W3|NU160_MOUSE	Nuclear pore complex protein Nu	27.33	14	3
Q6ZQ93|UBP34_MOUSE	Ubiquitin carboxyl-terminal hydro	26.94	7	3
Q8C115|PKHH2_MOUSE	Pleckstrin homology domain-con	25.61	8	3
O88737|BSN_MOUSE	Protein bassoon OS=Mus muscu	24.57	7	3
Q8R4Y4|STAB1_MOUSE	Stabilin-1 OS=Mus musculus GN	24.53	7	3
P63260|ACTG_MOUSE	Actin, cytoplasmic 2 OS=Mus mu	320.19	81	2
Q64523|H2A2C_MOUSE	Histone H2A type 2-C OS=Mus m	225.53	81	2

Q6GSS7|H2A2A_MOUSE	Histone H2A type 2-A OS=Mus r	225.53	75	2
O35737|HNRH1_MOUSE	Heterogeneous nuclear ribonucle	200.41	36	2
P68368|TBA4A_MOUSE	Tubulin alpha-4A chain OS=Mus	200.31	69	2
Q6URW6|MYH14_MOUSE	Myosin-14 OS=Mus musculus G	167.87	32	2
P84084|ARF5_MOUSE	ADP-ribosylation factor 5 OS=Mu	151.3	48	2
Q5SX39|MYH4_MOUSE	Myosin-4 OS=Mus musculus GN	141.44	23	2
P61205|ARF3_MOUSE	ADP-ribosylation factor 3 OS=Mu	140.45	60	2
P84078|ARF1_MOUSE	ADP-ribosylation factor 1 OS=Mu	140.45	56	2
P61750|ARF4_MOUSE	ADP-ribosylation factor 4 OS=Mu	139.9	46	2
Q91Z83|MYH7_MOUSE	Myosin-7 OS=Mus musculus GN	126.27	19	2
Q62241|RU1C_MOUSE	U1 small nuclear ribonucleoprote	120.71	33	2
P13541|MYH3_MOUSE	Myosin-3 OS=Mus musculus GN	119.13	16	2
Q9CZU6|CISY_MOUSE	Citrate synthase, mitochondrial C	111.29	36	2
Q99LT0|DPY30_MOUSE	Protein dpy-30 homolog OS=Mus	110.44	45	2
Q60668|HNRPD_MOUSE	Heterogeneous nuclear ribonucle	110.12	17	2
P26040|EZRI_MOUSE	Ezrin OS=Mus musculus GN=Ez	108.86	11	2
Q9ES28|ARHG7_MOUSE	Rho guanine nucleotide exchang	103.72	18	2
Q9DBR0|AKAP8_MOUSE	A-kinase anchor protein 8 OS=M	102.68	30	2
P21550|ENOB_MOUSE	Beta-enolase OS=Mus musculus	102.22	42	2
Q71LX4|TLN2_MOUSE	Talin-2 OS=Mus musculus GN=T	101.27	15	2
O35593|PSDE_MOUSE	26S proteasome non-ATPase re	98.43	30	2
Q9JIQ3|DBLOH_MOUSE	Diablo homolog, mitochondrial O	97.61	22	2
Q9CXW3|CYBP_MOUSE	Calcyclin-binding protein OS=Mu	97.32	24	2
P01644|KV5AB_MOUSE	Ig kappa chain V-V region HP R1	96.08	51	2
P01645|KV5AC_MOUSE	Ig kappa chain V-V region HP 93	96.08	51	2
Q8BGS0|MAK16_MOUSE	Protein MAK16 homolog OS=Mu	95.36	27	2
P26043|RADI_MOUSE	Radixin OS=Mus musculus GN=	95.27	16	2
P17183|ENOG_MOUSE	Gamma-enolase OS=Mus musc	94.51	49	2
Q60710|SAMH1_MOUSE	SAM domain and HD domain-co	93.34	23	2
Q6P1F6|2ABA_MOUSE	Serine/threonine-protein phospha	93.13	33	2
Q9CWZ3|RBM8A_MOUSE	RNA-binding protein 8A OS=Mus	92.05	26	2
Q8R105|VP37C_MOUSE	Vacuolar protein sorting-associat	91.68	24	2
P51660|DHB4_MOUSE	Peroxisomal multifunctional enzy	90.69	7	2
O70325|GPX41_MOUSE	Phospholipid hydroperoxide gluta	89.86	19	2
P35922|FMR1_MOUSE	Fragile X mental retardation prot	89.72	19	2
Q91VR2|ATPG_MOUSE	ATP synthase subunit gamma, m	89.66	13	2
Q9CXW4|RL11_MOUSE	60S ribosomal protein L11 OS=M	89.42	17	2
P10639|THIO_MOUSE	Thioredoxin OS=Mus musculus (	88.05	47	2
Q8VDV3|R3GEF_MOUSE	Guanine nucleotide exchange fa	87.69	21	2
Q9CQF9|PCYOX_MOUSE	Prenylcysteine oxidase OS=Mus	86.94	19	2
Q8BGD9|IF4B_MOUSE	Eukaryotic translation initiation fa	86.82	20	2
P61971|NTF2_MOUSE	Nuclear transport factor 2 OS=M	86.8	32	2
P48962|ADT1_MOUSE	ADP/ATP translocase 1 OS=Mus	86.62	29	2
Q9QZH3|PPIE_MOUSE	Peptidyl-prolyl cis-trans isomeras	86.47	26	2
Q61733|RT31_MOUSE	28S ribosomal protein S31, mito	86.07	18	2
P67778|PHB_MOUSE	Prohibitin OS=Mus musculus GN	85.99	31	2
Q80UY2|KCMF1_MOUSE	E3 ubiquitin-protein ligase KCMF	85.6	34	2
Q9R099|TBL2_MOUSE	Transducin beta-like protein 2 OS	85.11	31	2
Q9DCX2|ATP5H_MOUSE	ATP synthase subunit d, mitocho	84.95	15	2
Q91YD3|DCP1A_MOUSE	mRNA-decapping enzyme 1A OS	84.92	6	2
Q6ZWX6|IF2A_MOUSE	Eukaryotic translation initiation fa	83.58	13	2
Q8R0G9|NU133_MOUSE	Nuclear pore complex protein Nu	83.05	12	2
Q9JJV2|PROF2_MOUSE	Profilin-2 OS=Mus musculus GN	82.6	28	2
P63325|RS10_MOUSE	40S ribosomal protein S10 OS=M	82.56	10	2
Q9ERK4|XPO2_MOUSE	Exportin-2 OS=Mus musculus G	82.54	17	2

Q9D620|RFIP1_MOUSE	Rab11 family-interacting protein	82.51	26	2
P54071|IDHP_MOUSE	Isocitrate dehydrogenase [NADP	81.51	8	2
P97371|PSME1_MOUSE	Proteasome activator complex s	81.37	27	2
P11983|TCPA_MOUSE	T-complex protein 1 subunit alph	81.29	15	2
Q5SUF2|LC7L3_MOUSE	Luc7-like protein 3 OS=Mus mus	80.99	13	2
P61963|DCAF7_MOUSE	DDB1- and CUL4-associated fac	80.62	31	2
P61211|ARL1_MOUSE	ADP-ribosylation factor-like prote	80.03	27	2
Q9R1Z8|VINEX_MOUSE	Vinexin OS=Mus musculus GN=	80.02	14	2
P26516|PSD7_MOUSE	26S proteasome non-ATPase re	79.54	14	2
Q9DBG9|TX1B3_MOUSE	Tax1-binding protein 3 OS=Mus	78.73	43	2
P26883|FKB1A_MOUSE	Peptidyl-prolyl cis-trans isomeras	78.72	34	2
Q61990|PCBP2_MOUSE	Poly(rC)-binding protein 2 OS=M	78.55	22	2
Q9CY57|FOP_MOUSE	Friend of PRMT1 protein OS=Mu	77.41	25	2
Q8C8U0|LIPB1_MOUSE	Liprin-beta-1 OS=Mus musculus	77.35	10	2
P62835|RAP1A_MOUSE	Ras-related protein Rap-1A OS=	77.17	13	2
Q99JI6|RAP1B_MOUSE	Ras-related protein Rap-1b OS=	77.17	13	2
Q99LF4|RTCB_MOUSE	tRNA-splicing ligase RtcB homol	77.06	12	2
Q9CXI5|MANF_MOUSE	Mesencephalic astrocyte-derived	76.98	13	2
P63168|DYL1_MOUSE	Dynein light chain 1, cytoplasmic	76.6	35	2
Q8C5L3|CNOT2_MOUSE	CCR4-NOT transcription comple	75.71	13	2
P01868|IGHG1_MOUSE	Ig gamma-1 chain C region secr	75.09	19	2
P01869|IGH1M_MOUSE	Ig gamma-1 chain C region, mer	75.09	16	2
Q80UM7|MOGS_MOUSE	Mannosyl-oligosaccharide glucos	74.72	8	2
P14901|HMOX1_MOUSE	Heme oxygenase 1 OS=Mus mu	74.63	40	2
P42227|STAT3_MOUSE	Signal transducer and activator o	74.54	19	2
Q9Z0H3|SNF5_MOUSE	SWI/SNF-related matrix-associa	74.19	15	2
P70365|NCOA1_MOUSE	Nuclear receptor coactivator 1 O	73.53	15	2
P47955|RLA1_MOUSE	60S acidic ribosomal protein P1	72.92	37	2
P99027|RLA2_MOUSE	60S acidic ribosomal protein P2	72.78	30	2
Q9Z0X1|AIFM1_MOUSE	Apoptosis-inducing factor 1, mito	72.22	10	2
P63037|DNJA1_MOUSE	DnaJ homolog subfamily A mem	71.92	38	2
Q7TQC7|GPTC2_MOUSE	G patch domain-containing prote	71.08	11	2
Q8R0S2|IQEC1_MOUSE	IQ motif and SEC7 domain-conta	70.66	12	2
O35207|CDKA1_MOUSE	Cyclin-dependent kinase 2-assoc	70.32	20	2
P43274|H14_MOUSE	Histone H1.4 OS=Mus musculus	70.04	22	2
Q9QXC1|FETUB_MOUSE	Fetuin-B OS=Mus musculus GN=	69.89	11	2
P70663|SPRL1_MOUSE	SPARC-like protein 1 OS=Mus m	69.73	4	2
Q8R0J7|VP37B_MOUSE	Vacuolar protein sorting-associat	69.64	22	2
Q91VC4|PLVAP_MOUSE	Plasmalemma vesicle-associated	69.64	14	2
Q9QZE5|COPG_MOUSE	Coatomer subunit gamma OS=M	69.47	15	2
Q80UW2|FBX2_MOUSE	F-box only protein 2 OS=Mus mu	69.44	14	2
Q9Z1Y4|TRIP6_MOUSE	Thyroid receptor-interacting prote	68.81	14	2
Q9D554|SF3A3_MOUSE	Splicing factor 3A subunit 3 OS=	68.44	12	2
P49717|MCM4_MOUSE	DNA replication licensing factor M	68.17	10	2
P62334|PRS10_MOUSE	26S protease regulatory subunit	67.7	23	2
Q99PT1|GDIR1_MOUSE	Rho GDP-dissociation inhibitor 1	67.44	18	2
Q04857|CO6A1_MOUSE	Collagen alpha-1(VI) chain OS=M	67.17	7	2
Q3TKT4|SMCA4_MOUSE	Transcription activator BRG1 OS	65.58	11	2
Q9DCW4|ETFB_MOUSE	Electron transfer flavoprotein sub	65.47	9	2
P28653|PGS1_MOUSE	Biglycan OS=Mus musculus GN=	65.22	8	2
P97360|ETV6_MOUSE	Transcription factor ETV6 OS=M	65.13	6	2
Q9DCT5|SDF2_MOUSE	Stromal cell-derived factor 2 OS=	64.76	18	2
Q99NG0|ARIP4_MOUSE	Helicase ARIP4 OS=Mus muscu	64.35	4	2
Q91YN9|BAG2_MOUSE	BAG family molecular chaperone	64.27	29	2
Q8BMP6|GCP60_MOUSE	Golgi resident protein GCP60 OS	64.12	13	2

Q99K28|ARFG2_MOUSE	ADP-ribosylation factor GTPase-	63.52	6	2
P67984|RL22_MOUSE	60S ribosomal protein L22 OS=M	63.41	19	2
P83877|TXN4A_MOUSE	Thioredoxin-like protein 4A OS=I	62.35	26	2
Q78YZ6|SCOC_MOUSE	Short coiled-coil protein OS=Mus	62.26	30	2
Q9JII5|DAZP1_MOUSE	DAZ-associated protein 1 OS=M	62.03	19	2
P28658|ATX10_MOUSE	Ataxin-10 OS=Mus musculus GN	62	6	2
P16125|LDHB_MOUSE	L-lactate dehydrogenase B chain	61.36	24	2
Q9CT10|RANB3_MOUSE	Ran-binding protein 3 OS=Mus m	61.25	4	2
Q921N6|DDX27_MOUSE	Probable ATP-dependent RNA h	61.05	7	2
Q62376|RU17_MOUSE	U1 small nuclear ribonucleprote	60.8	13	2
Q3UJB9|EDC4_MOUSE	Enhancer of mRNA-decapping p	60.77	11	2
Q8BFR5|EFTU_MOUSE	Elongation factor Tu, mitochondr	60.42	18	2
Q8JZN5|ACAD9_MOUSE	Acyl-CoA dehydrogenase family	58.91	18	2
P62748|HPCL1_MOUSE	Hippocalcin-like protein 1 OS=M	57.74	17	2
P26638|SYSC_MOUSE	Seryl-tRNA synthetase, cytoplasi	57.45	18	2
Q06335|APLP2_MOUSE	Amyloid-like protein 2 OS=Mus m	57.27	11	2
Q925F2|ESAM_MOUSE	Endothelial cell-selective adhesio	56.91	12	2
P01872|IGHM_MOUSE	Ig mu chain C region secreted fo	56.77	6	2
P01873|MUCM_MOUSE	Ig mu chain C region membrane	56.77	6	2
Q920Q4|VPS16_MOUSE	Vacuolar protein sorting-associat	56.71	6	2
P97452|BOP1_MOUSE	Ribosome biogenesis protein BO	56.65	12	2
Q9CXY6|ILF2_MOUSE	Interleukin enhancer-binding fact	56.64	11	2
Q3TW96|UAP1L_MOUSE	UDP-N-acetylhexosamine pyropl	56.56	12	2
Q8R317|UBQL1_MOUSE	Ubiquilin-1 OS=Mus musculus G	56.49	22	2
P53995|APC1_MOUSE	Anaphase-promoting complex su	55.99	6	2
Q64012|RALY_MOUSE	RNA-binding protein Raly OS=M	55.47	7	2
Q8CCS6|PABP2_MOUSE	Polyadenylate-binding protein 2 (	55.34	11	2
P34884|MIF_MOUSE	Macrophage migration inhibitory	55.3	28	2
O54941|SMCE1_MOUSE	SWI/SNF-related matrix-associa	55.22	8	2
P29758|OAT_MOUSE	Ornithine aminotransferase, mito	54.74	7	2
P18572|BASI_MOUSE	Basigin OS=Mus musculus GN=	54.49	12	2
Q99KR7|PPIF_MOUSE	Peptidyl-prolyl cis-trans isomeras	54.09	16	2
Q8BI84|MIA3_MOUSE	Melanoma inhibitory activity prote	53.97	4	2
Q99N92|RM27_MOUSE	39S ribosomal protein L27, mitoc	53.9	17	2
P62814|VATB2_MOUSE	V-type proton ATPase subunit B,	53.54	13	2
P40646|SOX7_MOUSE	Transcription factor SOX-7 OS=I	53.49	17	2
P60766|CDC42_MOUSE	Cell division control protein 42 ho	53.08	10	2
O35286|DHX15_MOUSE	Putative pre-mRNA-splicing factc	52.9	8	2
Q99K30|ES8L2_MOUSE	Epidermal growth factor receptor	52.7	14	2
Q9CW03|SMC3_MOUSE	Structural maintenance of chrom	52.28	6	2
O35864|CSN5_MOUSE	COP9 signalosome complex sub	52.05	20	2
Q60972|RBBP4_MOUSE	Histone-binding protein RBBP4 (	51.91	13	2
P01867|IGG2B_MOUSE	Ig gamma-2B chain C region OS	51.91	6	2
Q8BGA5|KRR1_MOUSE	KRR1 small subunit processome	51.9	16	2
Q64324|STXB2_MOUSE	Syntaxin-binding protein 2 OS=M	51.85	17	2
Q8BMK4|CKAP4_MOUSE	Cytoskeleton-associated protein	51.81	7	2
P46471|PRS7_MOUSE	26S protease regulatory subunit	51.55	13	2
Q9WUU7|CATZ_MOUSE	Cathepsin Z OS=Mus musculus	51.49	12	2
Q3UPH7|ARH40_MOUSE	Rho guanine nucleotide exchang	50.93	11	2
Q8BYC4|GPR20_MOUSE	G-protein coupled receptor 20 O	50.69	19	2
O35218|CPSF2_MOUSE	Cleavage and polyadenylation sp	50.31	18	2
Q8BPM0|DAAM1_MOUSE	Disheveled-associated activator	50.02	11	2
Q8VCW8|ACSF2_MOUSE	Acyl-CoA synthetase family mem	49.9	15	2
Q9WUM5|SUCA_MOUSE	Succinyl-CoA ligase [GDP-formi	49.64	12	2
Q9WTR2|M3K6_MOUSE	Mitogen-activated protein kinase	49.27	6	2

Q6A0A9|F120A_MOUSE	Constitutive coactivator of PPAR	49.24	5	2
Q8C0T5|SI1L1_MOUSE	Signal-induced proliferation-assc	49.08	7	2
Q9D1A2|CNDP2_MOUSE	Cytosolic non-specific dipeptidas	48.79	12	2
O55201|SPT5H_MOUSE	Transcription elongation factor S	48.38	12	2
Q921M3|SF3B3_MOUSE	Splicing factor 3B subunit 3 OS=	47.94	8	2
Q8CDN6|TXNL1_MOUSE	Thioredoxin-like protein 1 OS=M	47.36	28	2
Q8VHN7|GPR98_MOUSE	G-protein coupled receptor 98 O	47.22	3	2
P37889|FBLN2_MOUSE	Fibulin-2 OS=Mus musculus GN	47.03	8	2
Q8CGF7|TCRG1_MOUSE	Transcription elongation regulato	46.76	8	2
Q61510|TRI25_MOUSE	E3 ubiquitin/ISG15 ligase TRIM2	46.03	6	2
Q8VD65|PI3R4_MOUSE	Phosphoinositide 3-kinase regula	45.7	9	2
Q8CH18|CCAR1_MOUSE	Cell division cycle and apoptosis	45.46	3	2
Q6A4J8|UBP7_MOUSE	Ubiquitin carboxyl-terminal hydro	45.28	13	2
Q9CXZ1|NDUS4_MOUSE	NADH dehydrogenase [ubiquinor	45.15	19	2
P24547|IMDH2_MOUSE	Inosine-5'-monophosphate dehyd	44.07	10	2
Q9EP97|SENP3_MOUSE	Sentrin-specific protease 3 OS=M	43.8	8	2
O88783|FA5_MOUSE	Coagulation factor V OS=Mus m	43.75	5	2
Q8K4Z5|SF3A1_MOUSE	Splicing factor 3A subunit 1 OS=	43.58	5	2
O55057|PDE6D_MOUSE	Retinal rod rhodopsin-sensitive c	43.32	21	2
O88543|CSN3_MOUSE	COP9 signalosome complex sub	43.24	16	2
Q9WTQ5|AKA12_MOUSE	A-kinase anchor protein 12 OS=I	43.17	3	2
Q8VE97|SRSF4_MOUSE	Serine/arginine-rich splicing factc	42.77	10	2
O35465|FKBP8_MOUSE	Peptidyl-prolyl cis-trans isomeras	42.75	14	2
Q8C419|GP158_MOUSE	Probable G-protein coupled rece	42.71	10	2
P97379|G3BP2_MOUSE	Ras GTPase-activating protein-b	42.53	9	2
Q61425|HCDH_MOUSE	Hydroxyacyl-coenzyme A dehydr	42.22	20	2
Q9Z0R6|ITSN2_MOUSE	Intersectin-2 OS=Mus musculus	42.1	10	2
Q8C9B9|DIDO1_MOUSE	Death-inducer obliterator 1 OS=M	41.39	5	2
Q8BU51|BPIL3_MOUSE	Bactericidal/permeability-increas	40.62	14	2
P97479|MYO7A_MOUSE	Myosin-VIIa OS=Mus musculus (	39.51	9	2
Q91YT0|NDUV1_MOUSE	NADH dehydrogenase [ubiquinor	39.51	14	2
Q08943|SSRP1_MOUSE	FACT complex subunit SSRP1 O	38.94	14	2
A2AAE1|K1109_MOUSE	Uncharacterized protein KIAA11(	38.91	6	2
P70390|SHOX2_MOUSE	Short stature homeobox protein 2	38.86	8	2
O88444|ADCY1_MOUSE	Adenylate cyclase type 1 OS=Mu	38.61	12	2
P48725|PCNT_MOUSE	Pericentrin OS=Mus musculus G	38.53	11	2
Q9D7N3|RT09_MOUSE	28S ribosomal protein S9, mitoch	38.32	13	2
Q64430|ATP7A_MOUSE	Copper-transporting ATPase 1 O	38.3	11	2
Q99PP2|ZN318_MOUSE	Zinc finger protein 318 (Fragmer	37.87	5	2
P84091|AP2M1_MOUSE	AP-2 complex subunit mu OS=M	37.8	14	2
Q8CGN4|BCOR_MOUSE	BCL-6 corepressor OS=Mus mus	37.77	4	2
Q9DC33|HM20A_MOUSE	High mobility group protein 20A (	37.72	10	2
P97384|ANX11_MOUSE	Annexin A11 OS=Mus musculus	37.56	4	2
P11531|DMD_MOUSE	Dystrophin OS=Mus musculus G	37.56	9	2
Q5SF07|IF2B2_MOUSE	Insulin-like growth factor 2 mRNA	37.18	12	2
Q01320|TOP2A_MOUSE	DNA topoisomerase 2-alpha OS	37.16	8	2
P08121|CO3A1_MOUSE	Collagen alpha-1(III) chain OS=M	37.05	9	2
Q69ZU6|THS7A_MOUSE	Thrombospondin type-1 domain-	36.94	6	2
Q9QZ09|PHTF1_MOUSE	Putative homeodomain transcrip	36.62	7	2
P52734|FGD1_MOUSE	FYVE, RhoGEF and PH domain-	36.61	4	2
Q91YW3|DNJC3_MOUSE	DnaJ homolog subfamily C mem	36.34	4	2
Q8CFE4|SCYL2_MOUSE	SCY1-like protein 2 OS=Mus mu	36.23	6	2
Q4QY64|ATAD5_MOUSE	ATPase family AAA domain-cont	35.76	7	2
Q8R0L9|TADA3_MOUSE	Transcriptional adapter 3 OS=Mu	35.73	14	2
O35954|PITM1_MOUSE	Membrane-associated phosphat	35.43	11	2

Q6PGN1|F132B_MOUSE	Protein FAM132B OS=Mus mus	35.41	8	2
Q9Z329|ITPR2_MOUSE	Inositol 1,4,5-trisphosphate rece	35.37	10	2
P54320|ELN_MOUSE	Elastin OS=Mus musculus GN=E	35.17	20	2
Q9Z108|STAU1_MOUSE	Double-stranded RNA-binding pr	34.73	23	2
O88491|NSD1_MOUSE	Histone-lysine N-methyltransfera	34.66	9	2
Q3UFQ8|LR16B_MOUSE	Leucine-rich repeat-containing p	34.6	8	2
Q6PHB0|I20RA_MOUSE	Interleukin-20 receptor subunit a	34.47	4	2
Q9DCC4|P5CR3_MOUSE	Pyrroline-5-carboxylate reductas	34.09	15	2
O54724|PTRF_MOUSE	Polymerase I and transcript relea	33.88	8	2
O88705|HCN3_MOUSE	Potassium/sodium hyperpolariza	33.88	11	2
Q61290|CAC1E_MOUSE	Voltage-dependent R-type calciu	33.64	7	2
Q6ZQ88|KDM1A_MOUSE	Lysine-specific histone demethyl	33.6	11	2
Q61702|ITIH1_MOUSE	Inter-alpha-trypsin inhibitor heav	33.31	8	2
Q6P4S8|INT1_MOUSE	Integrator complex subunit 1 OS	33.25	8	2
Q8BN57|CC033_MOUSE	Uncharacterized protein C3orf33	33.07	11	2
Q3UHK3|GREB1_MOUSE	Protein GREB1 OS=Mus muscul	33.07	5	2
Q91VR5|DDX1_MOUSE	ATP-dependent RNA helicase D	32.87	15	2
Q6ZWQ0|SYNE2_MOUSE	Nesprin-2 OS=Mus musculus GN	32.74	8	2
O35071|KIF1C_MOUSE	Kinesin-like protein KIF1C OS=M	32.69	12	2
Q922B9|SSFA2_MOUSE	Sperm-specific antigen 2 homolo	32.01	9	2
A8C756|THADA_MOUSE	Thyroid adenoma-associated pro	31.65	6	2
P0C5E4|PTPRQ_MOUSE	Phosphotidylinositol phosphatase	31.6	4	2
Q5DTT2|PSD1_MOUSE	PH and SEC7 domain-containing	31.4	8	2
Q6QIY3|SCNAA_MOUSE	Sodium channel protein type 10	31.28	8	2
Q0VGM9|RTEL1_MOUSE	Regulator of telomere elongation	31.22	5	2
Q8CH25|SLTM_MOUSE	SAFB-like transcription modulato	31.21	3	2
P55012|S12A2_MOUSE	Solute carrier family 12 member	31.03	10	2
Q8BXR5|NALCN_MOUSE	Sodium leak channel non-selecti	30.84	7	2
A1L3T7|FA65C_MOUSE	Protein FAM65C OS=Mus musc	30.82	9	2
Q8VE73|CUL7_MOUSE	Cullin-7 OS=Mus musculus GN=	30.65	7	2
Q8C0P7|ZN451_MOUSE	Zinc finger protein 451 OS=Mus	30.59	8	2
Q2EG98|PK1L3_MOUSE	Polycystic kidney disease protein	30.59	7	2
P13705|MSH3_MOUSE	DNA mismatch repair protein Ms	30.41	7	2
Q3URY6|ARMC2_MOUSE	Armadillo repeat-containing prote	30.02	11	2
P46737|BRCC3_MOUSE	Lys-63-specific deubiquitinase B	29.91	9	2
P97311|MCM6_MOUSE	DNA replication licensing factor M	29.82	11	2
Q8C267|SETB2_MOUSE	Histone-lysine N-methyltransfera	29.53	7	2
A7L9Z8|AT2C2_MOUSE	Calcium-transporting ATPase typ	29.51	10	2
Q4G0F8|UBN1_MOUSE	Ubinuclein-1 OS=Mus musculus	29.46	9	2
A2BH40|ARI1A_MOUSE	AT-rich interactive domain-conta	29.41	6	2
Q80WQ9|ZBED4_MOUSE	Zinc finger BED domain-containi	29.14	11	2
Q9JJN0|POLH_MOUSE	DNA polymerase eta OS=Mus m	29.05	9	2
P49582|ACHA7_MOUSE	Neuronal acetylcholine receptor	28.31	3	2
Q8C0R9|YG015_MOUSE	Leucine-rich repeat and death do	28.02	8	2
Q8JZR4|EAA5_MOUSE	Excitatory amino acid transporte	27.86	13	2
Q80TS3|LPHN3_MOUSE	Latrophilin-3 OS=Mus musculus	27.7	4	2
Q61037|TSC2_MOUSE	Tuberin OS=Mus musculus GN=	27.63	8	2
Q14BI7|TDRD9_MOUSE	Putative ATP-dependent RNA he	27.57	10	2
P04187|GRAB_MOUSE	Granzyme B(G,H) OS=Mus mus	27.37	20	2
Q91YU6|LZTS2_MOUSE	Leucine zipper putative tumor su	27.34	11	2
Q01815|CAC1C_MOUSE	Voltage-dependent L-type calciu	27.26	13	2
Q8C120|SH3R3_MOUSE	SH3 domain-containing RING fin	27.05	5	2
Q09XV5|CHD8_MOUSE	Chromodomain-helicase-DNA-bi	27.02	9	2
P59997|KDM2A_MOUSE	Lysine-specific demethylase 2A	27.01	8	2
P55937|GOGA3_MOUSE	Golgin subfamily A member 3 OS	27	8	2

Q8BG67|EFR3A_MOUSE	Protein EFR3 homolog A OS=Mu	26.89	11	2
Q6R5N8|TLR13_MOUSE	Toll-like receptor 13 OS=Mus mu	26.88	7	2
Q9QZS7|NPHN_MOUSE	Nephrin OS=Mus musculus GN=	26.87	5	2
P48356|LEPR_MOUSE	Leptin receptor OS=Mus muscul	26.62	8	2
Q9WV34|MPP2_MOUSE	MAGUK p55 subfamily member	26.62	4	2
Q6P1C6|LRIG3_MOUSE	Leucine-rich repeats and immun	26.43	7	2
P11247|PERM_MOUSE	Myeloperoxidase OS=Mus musc	26.16	14	2
Q61493|DPOLZ_MOUSE	DNA polymerase zeta catalytic s	26.14	8	2
A2ARZ3|FSIP2_MOUSE	Fibrous sheath-interacting protei	26.03	5	2
P97714|ADA1D_MOUSE	Alpha-1D adrenergic receptor OS	26.02	9	2
Q9D415|DLGP1_MOUSE	Disks large-associated protein 1	25.97	6	2
Q6IQX7|CHSS2_MOUSE	Chondroitin sulfate synthase 2 O	25.97	9	2
P57080|UBP25_MOUSE	Ubiquitin carboxyl-terminal hydro	25.95	7	2
Q8CHY3|DYM_MOUSE	Dymeclin OS=Mus musculus GN	25.91	7	2
B2RQE8|RHG42_MOUSE	Rho GTPase-activating protein 4	25.9	6	2
Q9D168|INT12_MOUSE	Integrator complex subunit 12 OS	25.79	10	2
P51557|STAR_MOUSE	Steroidogenic acute regulatory p	25.79	13	2
Q9D2K4|IQCH_MOUSE	IQ domain-containing protein H (	25.76	6	2
Q7TSH4|CP110_MOUSE	Centrosomal protein CP110 OS=	25.63	2	2
Q9Z1S0|BUB1B_MOUSE	Mitotic checkpoint serine/threoni	25.45	8	2
Q9QXL2|KI21A_MOUSE	Kinesin-like protein KIF21A OS=	25.35	9	2
Q9QXL1|KI21B_MOUSE	Kinesin-like protein KIF21B OS=	25.33	5	2
Q921C3|BRWD1_MOUSE	Bromodomain and WD repeat-co	25.28	4	2
P58742|AAAS_MOUSE	Aladin OS=Mus musculus GN=A	25.27	8	2
Q3TEI4|CO039_MOUSE	Uncharacterized protein C15orf3	25.22	10	2
Q7TSH7|KCNF1_MOUSE	Potassium voltage-gated channe	24.92	13	2
Q3ZT31|SNX25_MOUSE	Sorting nexin-25 OS=Mus muscu	24.89	13	2
Q8CJ12|GPR64_MOUSE	G-protein coupled receptor 64 O	24.82	6	2
Q6PIX5|RHDF1_MOUSE	Inactive rhomboid protein 1 OS=	24.8	13	2
Q9QXH4|ITAX_MOUSE	Integrin alpha-X OS=Mus muscu	24.77	10	2
Q8K0L0|ASB2_MOUSE	Ankyrin repeat and SOCS box pr	24.35	3	2
Q80T85|DCAF5_MOUSE	DDB1- and CUL4-associated fac	24.16	6	2
P70327|TBX6_MOUSE	T-box transcription factor TBX6 (	24.04	9	2
Q60603|KCNH1_MOUSE	Potassium voltage-gated channe	24	4	2
Q62388|ATM_MOUSE	Serine-protein kinase ATM OS=M	23.89	10	2
Q9JHW4|SELB_MOUSE	Selenocysteine-specific elongatio	23.85	17	2
Q6PR54|RIF1_MOUSE	Telomere-associated protein RIF	23.75	7	2
P59808|SASH1_MOUSE	SAM and SH3 domain-containing	23.72	6	2
P0CW70|D19L2_MOUSE	Protein dpy-19 homolog 2 OS=M	23.51	13	2
Q8C8R3|ANK2_MOUSE	Ankyrin-2 OS=Mus musculus GN	23.41	6	2
P53349|M3K1_MOUSE	Mitogen-activated protein kinase	23.32	5	2
Q9R155|S26A4_MOUSE	Pendrin OS=Mus musculus GN=	23.04	8	2
Q00519|XDH_MOUSE	Xanthine dehydrogenase/oxidase	22.92	7	2
C8YR32|LOXH1_MOUSE	Lipoxygenase homology domain-	22.87	5	2
P97303|BACH2_MOUSE	Transcription regulator protein BA	22.77	3	2
Q8BNJ2|ATS4_MOUSE	A disintegrin and metalloproteina	22.72	5	2
A7M7C7|SKOR2_MOUSE	SKI family transcriptional corepre	21.59	4	2
O88196|TTC3_MOUSE	E3 ubiquitin-protein ligase TTC3	21.07	6	2
Q8CI32|BAG5_MOUSE	BAG family molecular chaperone	20.8	11	2

Table A1.3 Cell Start Protein Identifications. List of all proteins identified in Cell Start growth matrix with corresponding accession, description, PEAKS score, unique peptide numbers, and coverage (in %).

Accession	Description	Score	Coverage (%)	#Unique
P02768|ALBU_HUMAN	Serum albumin OS=Homo sapiens GN=A	740.91	92	508
P02751|FINC_HUMAN	Fibronectin OS=Homo sapiens GN=FN1 F	590.06	67	213
P01023|A2MG_HUMAN	Alpha-2-macroglobulin OS=Homo sapiens	355.02	44	37
P02790|HEMO_HUMAN	Hemopexin OS=Homo sapiens GN=HPX	379.25	68	34
P43652|AFAM_HUMAN	Afamin OS=Homo sapiens GN=AFM PE=	308.01	62	25
P00738|HPT_HUMAN	Haptoglobin OS=Homo sapiens GN=HP F	398.12	67	23
P02675|FIBB_HUMAN	Fibrinogen beta chain OS=Homo sapiens	300.96	64	22
P02671|FIBA_HUMAN	Fibrinogen alpha chain OS=Homo sapiens	239.94	35	18
P02679|FIBG_HUMAN	Fibrinogen gamma chain OS=Homo sapie	253.11	53	17
P02765|FETUA_HUMAN	Alpha-2-HS-glycoprotein OS=Homo sapie	253.45	62	16
P02749|APOH_HUMAN	Beta-2-glycoprotein 1 OS=Homo sapiens	250.57	59	13
P04217|A1BG_HUMAN	Alpha-1B-glycoprotein OS=Homo sapiens	246.04	39	12
P02652|APOA2_HUMAN	Apolipoprotein A-II OS=Homo sapiens GN	234.22	73	10
P02766|TTHY_HUMAN	Transthyretin OS=Homo sapiens GN=TTR	225.45	68	10
P08253|MMP2_HUMAN	72 kDa type IV collagenase OS=Homo sa	197.89	32	8
Q96PD5|PGRP2_HUMAN	N-acetylmuramoyl-L-alanine amidase OS=	179.89	27	6
P01871|IGHM_HUMAN	Ig mu chain C region OS=Homo sapiens (	169.57	36	6
P01834|IGKC_HUMAN	Ig kappa chain C region OS=Homo sapien	189.08	78	5
P10909|CLUS_HUMAN	Clusterin OS=Homo sapiens GN=CLU PE	180.73	35	5
Q8WZ42|TITIN_HUMAN	Titin OS=Homo sapiens GN=TTN PE=1 S	50.51	2	5
P01876|IGHA1_HUMAN	Ig alpha-1 chain C region OS=Homo sapie	151.25	22	4
P69905|HBA_HUMAN	Hemoglobin subunit alpha OS=Homo sap	138.46	49	4
P02760|AMBP_HUMAN	Protein AMBP OS=Homo sapiens GN=AM	112.1	18	4
P00450|CERU_HUMAN	Ceruloplasmin OS=Homo sapiens GN=CP	103.12	8	4
P68871|HBB_HUMAN	Hemoglobin subunit beta OS=Homo sapie	176.25	48	3
P01860|IGHG3_HUMAN	Ig gamma-3 chain C region OS=Homo sa	166.83	34	3
P01024|CO3_HUMAN	Complement C3 OS=Homo sapiens GN=(	146.6	19	3
P35030|TRY3_HUMAN	Trypsin-3 OS=Homo sapiens GN=PRSS3	145.59	13	3
P0CG05|LAC2_HUMAN	Ig lambda-2 chain C regions OS=Homo sa	136.88	68	3
P0CG06|LAC3_HUMAN	Ig lambda-3 chain C regions OS=Homo sa	136.88	68	3
B9A064|IGLL5_HUMAN	Immunoglobulin lambda-like polypeptide 5	136.88	28	3
P0CG04|LAC1_HUMAN	Ig lambda-1 chain C regions OS=Homo sa	136.88	42	3
P05155|IC1_HUMAN	Plasma protease C1 inhibitor OS=Homo s	129.22	19	3
P0C0L4|CO4A_HUMAN	Complement C4-A OS=Homo sapiens GN	113.65	23	3
P0C0L5|CO4B_HUMAN	Complement C4-B OS=Homo sapiens GN	113.65	23	3
P02763|A1AG1_HUMAN	Alpha-1-acid glycoprotein 1 OS=Homo sa	110.28	46	3
P02647|APOA1_HUMAN	Apolipoprotein A-I OS=Homo sapiens GN	88.02	12	3
P02771|FETA_HUMAN	Alpha-fetoprotein OS=Homo sapiens GN=	69.2	4	3
P35556|FBN2_HUMAN	Fibrillin-2 OS=Homo sapiens GN=FBN2 P	45.74	5	3
Q2PPJ7|RGPA2_HUMAN	Ral GTPase-activating protein subunit alp	38.22	2	3
P20929|NEBU_HUMAN	Nebulin OS=Homo sapiens GN=NEB PE=	37.95	3	3
O15018|PDZD2_HUMAN	PDZ domain-containing protein 2 OS=Hor	32.88	3	3
P07477|TRY1_HUMAN	Trypsin-1 OS=Homo sapiens GN=PRSS1	143.81	26	2
Q16610|ECM1_HUMAN	Extracellular matrix protein 1 OS=Homo s	103.56	35	2
P02774|VTDB_HUMAN	Vitamin D-binding protein OS=Homo sapi	83.32	31	2
O14647|CHD2_HUMAN	Chromodomain-helicase-DNA-binding pro	43.46	4	2
Q9UNH5|CC14A_HUMAN	Dual specificity protein phosphatase CDC	43.19	6	2
Q9Y6W5|WASF2_HUMAN	Wiskott-Aldrich syndrome protein family m	38.65	2	2
P24821|TENA_HUMAN	Tenascin OS=Homo sapiens GN=TNC PE	36.58	3	2
Q3L8U1|CHD9_HUMAN	Chromodomain-helicase-DNA-binding pro	35.78	2	2
Q96KC8|DNJC1_HUMAN	DnaJ homolog subfamily C member 1 OS	35.29	12	2
Q95IE3|2B1C_HUMAN	HLA class II histocompatibility antigen, DR	32.1	10	2
P01911|2B1F_HUMAN	HLA class II histocompatibility antigen, DR	32.1	8	2
Q29974|2B1G_HUMAN	HLA class II histocompatibility antigen, DR	32.1	8	2

P04229|2B11_HUMAN	HLA class II histocompatibility antigen, DF	32.1	5	2
P01912|2B13_HUMAN	HLA class II histocompatibility antigen, DF	32.1	5	2
P20039|2B1B_HUMAN	HLA class II histocompatibility antigen, DF	32.1	5	2
Q5Y7A7|2B1D_HUMAN	HLA class II histocompatibility antigen, DF	32.1	5	2
Q9GIY3|2B1E_HUMAN	HLA class II histocompatibility antigen, DF	32.1	5	2
Q30154|DRB5_HUMAN	HLA class II histocompatibility antigen, DF	32.1	5	2
Q14517|FAT1_HUMAN	Protocadherin Fat 1 OS=Homo sapiens G	31.9	3	2
Q9Y4H2|IRS2_HUMAN	Insulin receptor substrate 2 OS=Homo sa	30.26	5	2
Q7L4P6|BEND5_HUMAN	BEN domain-containing protein 5 OS=Hor	30.07	8	2
O15083|ERC2_HUMAN	ERC protein 2 OS=Homo sapiens GN=ER	29.66	3	2
Q07075|AMPE_HUMAN	Glutamyl aminopeptidase OS=Homo sapi	29.26	3	2
O00555|CAC1A_HUMAN	Voltage-dependent P/Q-type calcium char	29.06	3	2
Q07869|PPARA_HUMAN	Peroxisome proliferator-activated recepto	28.92	2	2
Q15262|PTPRK_HUMAN	Receptor-type tyrosine-protein phosphata	28.88	5	2
Q96T88|UHRF1_HUMAN	E3 ubiquitin-protein ligase UHRF1 OS=Ho	28.46	3	2
Q2M329|CCD96_HUMAN	Coiled-coil domain-containing protein 96 C	27.76	3	2

Table A1.4 Human BME Protein Identifications. List of all proteins identified in Human BME growth matrix with corresponding accession, description, PEAKS score, unique peptide numbers, and coverage (in %).

Accession	Description	Score	Coverage (%)	#Unique
P02751|FINC_HUMAN	Fibronectin OS=Homo sapiens G	341.22	45	102
P24043|LAMA2_HUMAN	Laminin subunit alpha-2 OS=Hor	304.77	30	66
P55268|LAMB2_HUMAN	Laminin subunit beta-2 OS=Hom	283.73	35	46
Q05707|COEA1_HUMAN	Collagen alpha-1(XIV) chain OS=	264.19	41	46
P01023|A2MG_HUMAN	Alpha-2-macroglobulin OS=Hom	289	38	45
P11047|LAMC1_HUMAN	Laminin subunit gamma-1 OS=H	279.33	39	43
P98160|PGBM_HUMAN	Basement membrane-specific he	258.87	19	42
P08670|VIME_HUMAN	Vimentin OS=Homo sapiens GN	258.73	73	37
O15230|LAMA5_HUMAN	Laminin subunit alpha-5 OS=Hor	253.7	16	34
P07942|LAMB1_HUMAN	Laminin subunit beta-1 OS=Hom	238.75	24	27
P14543|NID1_HUMAN	Nidogen-1 OS=Homo sapiens G	237.82	30	27
P12111|CO6A3_HUMAN	Collagen alpha-3(VI) chain OS=H	226.55	19	27
Q16363|LAMA4_HUMAN	Laminin subunit alpha-4 OS=Hor	224.5	27	25
P01024|CO3_HUMAN	Complement C3 OS=Homo sapi	205.4	23	24
P11021|GRP78_HUMAN	78 kDa glucose-regulated protein	235.26	46	23
P14625|ENPL_HUMAN	Endoplasmin OS=Homo sapiens	215.43	38	22
O43707|ACTN4_HUMAN	Alpha-actinin-4 OS=Homo sapie	281.68	56	21
P02545|LMNA_HUMAN	Prelamin-A/C OS=Homo sapiens	213.42	47	21
P02768|ALBU_HUMAN	Serum albumin OS=Homo sapie	200.8	42	21
P12814|ACTN1_HUMAN	Alpha-actinin-1 OS=Homo sapie	269.31	58	20
P07237|PDIA1_HUMAN	Protein disulfide-isomerase OS=	206.6	45	19
Q13813|SPTA2_HUMAN	Spectrin alpha chain, brain OS=H	186.17	21	17
P02671|FIBA_HUMAN	Fibrinogen alpha chain OS=Hom	172.58	26	16
P23142|FBLN1_HUMAN	Fibulin-1 OS=Homo sapiens GN	200.91	25	15
Q15084|PDIA6_HUMAN	Protein disulfide-isomerase A6 C	197.7	42	15
P18206|VINC_HUMAN	Vinculin OS=Homo sapiens GN=	183.25	27	14
O75369|FLNB_HUMAN	Filamin-B OS=Homo sapiens GN	175.11	14	14
P02675|FIBB_HUMAN	Fibrinogen beta chain OS=Homo	169.47	42	14
P01243|CSH_HUMAN	Chorionic somatomammotropin	222.66	69	13
P11277|SPTB1_HUMAN	Spectrin beta chain, erythrocyte	181.32	19	13
P04083|ANXA1_HUMAN	Annexin A1 OS=Homo sapiens G	178.26	42	13
P08603|CFAH_HUMAN	Complement factor H OS=Homo	177.55	19	13
P10809|CH60_HUMAN	60 kDa heat shock protein, mitoc	176.8	45	13
P32119|PRDX2_HUMAN	Peroxiredoxin-2 OS=Homo sapie	183.65	38	12
P07355|ANXA2_HUMAN	Annexin A2 OS=Homo sapiens G	177.18	44	12
P02679|FIBG_HUMAN	Fibrinogen gamma chain OS=Ho	189.08	38	11
P30101|PDIA3_HUMAN	Protein disulfide-isomerase A3 C	155.47	33	11
Q15582|BGH3_HUMAN	Transforming growth factor-beta	154.17	36	11
P69905|HBA_HUMAN	Hemoglobin subunit alpha OS=H	180.04	64	10
P06576|ATPB_HUMAN	ATP synthase subunit beta, mito	174.82	34	10
P49748|ACADV_HUMAN	Very long-chain specific acyl-CoA	174.26	26	10
P21980|TGM2_HUMAN	Protein-glutamine gamma-glutan	161.7	24	10
P35579|MYH9_HUMAN	Myosin-9 OS=Homo sapiens GN	158.65	15	10
Q03252|LMNB2_HUMAN	Lamin-B2 OS=Homo sapiens GN	155.23	25	10
P51884|LUM_HUMAN	Lumican OS=Homo sapiens GN	140.59	34	10
P50454|SERPH_HUMAN	Serpin H1 OS=Homo sapiens GI	180.83	33	9
P21333|FLNA_HUMAN	Filamin-A OS=Homo sapiens GN	154.91	13	9
Q14112|NID2_HUMAN	Nidogen-2 OS=Homo sapiens G	146.91	12	9
P39059|COFA1_HUMAN	Collagen alpha-1(XV) chain OS=	163.68	18	8
Q9Y6N6|LAMC3_HUMAN	Laminin subunit gamma-3 OS=H	158.79	17	8
P14314|GLU2B_HUMAN	Glucosidase 2 subunit beta OS=	148.61	31	8
P60660|MYL6_HUMAN	Myosin light polypeptide 6 OS=H	145.14	75	8
P20700|LMNB1_HUMAN	Lamin-B1 OS=Homo sapiens GN	144.74	26	8
P55072|TERA_HUMAN	Transitional endoplasmic reticulu	142.86	15	8

P10909|CLUS_HUMAN	Clusterin OS=Homo sapiens GN	137.86	25	8
P38646|GRP75_HUMAN	Stress-70 protein, mitochondrial	145.13	27	7
P36957|ODO2_HUMAN	Dihydrolipoyllysine-residue succi	135.47	22	7
P00747|PLMN_HUMAN	Plasminogen OS=Homo sapiens	133.52	10	7
P02549|SPTA1_HUMAN	Spectrin alpha chain, erythrocyte	131.8	8	7
P30048|PRDX3_HUMAN	Thioredoxin-dependent peroxide	121.33	29	7
P00488|F13A_HUMAN	Coagulation factor XIII A chain O	116.64	18	7
P01857|IGHG1_HUMAN	Ig gamma-1 chain C region OS=	186.51	53	6
P11142|HSP7C_HUMAN	Heat shock cognate 71 kDa prot	184	28	6
P68871|HBB_HUMAN	Hemoglobin subunit beta OS=Ho	167.04	48	6
P04792|HSPB1_HUMAN	Heat shock protein beta-1 OS=H	151.58	36	6
P20774|MIME_HUMAN	Mimecan OS=Homo sapiens GN	135.79	34	6
P08758|ANXA5_HUMAN	Annexin A5 OS=Homo sapiens O	132.3	23	6
P21810|PGS1_HUMAN	Biglycan OS=Homo sapiens GN=	132.24	22	6
P62805|H4_HUMAN	Histone H4 OS=Homo sapiens O	130.91	41	6
P62937|PPIA_HUMAN	Peptidyl-prolyl cis-trans isomeras	129.29	42	6
P02647|APOA1_HUMAN	Apolipoprotein A-I OS=Homo sa	127.95	25	6
P04004|VTNC_HUMAN	Vitronectin OS=Homo sapiens G	127.76	16	6
P07585|PGS2_HUMAN	Decorin OS=Homo sapiens GN=	124	16	6
P00367|DHE3_HUMAN	Glutamate dehydrogenase 1, mit	122.42	21	6
P06396|GELS_HUMAN	Gelsolin OS=Homo sapiens GN=	119.73	13	6
Q12805|FBLN3_HUMAN	EGF-containing fibulin-like extra	116.62	19	6
P63104|1433Z_HUMAN	14-3-3 protein zeta/delta OS=Ho	116.55	47	6
P63267|ACTH_HUMAN	Actin, gamma-enteric smooth mu	194.38	40	5
P62736|ACTA_HUMAN	Actin, aortic smooth muscle OS=	194.38	40	5
P68032|ACTC_HUMAN	Actin, alpha cardiac muscle 1 OS	194.38	40	5
P68133|ACTS_HUMAN	Actin, alpha skeletal muscle OS=	194.38	40	5
Q9NYU2|UGGG1_HUMAN	UDP-glucose:glycoprotein glucos	135.54	7	5
P39060|COIA1_HUMAN	Collagen alpha-1(XVIII) chain OS	130.82	12	5
P51888|PRELP_HUMAN	Prolargin OS=Homo sapiens GN	127.01	14	5
P17661|DESM_HUMAN	Desmin OS=Homo sapiens GN=	126.75	25	5
P80303|NUCB2_HUMAN	Nucleobindin-2 OS=Homo sapie	124.47	28	5
P09211|GSTP1_HUMAN	Glutathione S-transferase P OS=	120.59	33	5
P25705|ATPA_HUMAN	ATP synthase subunit alpha, mit	114.16	18	5
P02748|CO9_HUMAN	Complement component C9 OS=	106.89	13	5
P0C0L4|CO4A_HUMAN	Complement C4-A OS=Homo sa	102.47	7	5
P0C0L5|CO4B_HUMAN	Complement C4-B OS=Homo sa	102.47	7	5
P35749|MYH11_HUMAN	Myosin-11 OS=Homo sapiens G	102.39	8	5
Q9NR28|DBLOH_HUMAN	Diablo homolog, mitochondrial O	101.43	24	5
P35555|FBN1_HUMAN	Fibrillin-1 OS=Homo sapiens GN	97.14	4	5
P07954|FUMH_HUMAN	Fumarate hydratase, mitochondr	89.86	17	5
Q01082|SPTB2_HUMAN	Spectrin beta chain, brain 1 OS=	87.78	6	5
P02765|FETUA_HUMAN	Alpha-2-HS-glycoprotein OS=Ho	80.75	25	5
P08238|HS90B_HUMAN	Heat shock protein HSP 90-beta	140.06	19	4
P40926|MDHM_HUMAN	Malate dehydrogenase, mitochon	132.99	30	4
Q06830|PRDX1_HUMAN	Peroxiredoxin-1 OS=Homo sapie	121.31	29	4
P24534|EF1B_HUMAN	Elongation factor 1-beta OS=Hon	119.55	30	4
Q13162|PRDX4_HUMAN	Peroxiredoxin-4 OS=Homo sapie	116.87	21	4
P13667|PDIA4_HUMAN	Protein disulfide-isomerase A4 O	110.55	11	4
Q14257|RCN2_HUMAN	Reticulocalbin-2 OS=Homo sapie	108.08	25	4
Q96HE7|ERO1A_HUMAN	ERO1-like protein alpha OS=Hon	106.34	13	4
P07737|PROF1_HUMAN	Profilin-1 OS=Homo sapiens GN	102.52	45	4
Q9BS26|ERP44_HUMAN	Endoplasmic reticulum resident p	97.38	14	4
Q9UBS4|DJB11_HUMAN	DnaJ homolog subfamily B mem	96.49	14	4
Q9UIJ7|KAD3_HUMAN	GTP:AMP phosphotransferase, m	93.16	21	4

Q07954|LRP1_HUMAN	Prolow-density lipoprotein recept	90.68	3	4
Q15008|PSMD6_HUMAN	26S proteasome non-ATPase re	87.94	14	4
P30041|PRDX6_HUMAN	Peroxiredoxin-6 OS=Homo sapie	85.61	29	4
P00450|CERU_HUMAN	Ceruloplasmin OS=Homo sapien	83.68	8	4
P30044|PRDX5_HUMAN	Peroxiredoxin-5, mitochondrial C	82.93	28	4
P24821|TENA_HUMAN	Tenascin OS=Homo sapiens GN	54.92	6	4
Q8IZT6|ASPM_HUMAN	Abnormal spindle-like microceph	44.64	5	4
P54652|HSP72_HUMAN	Heat shock-related 70 kDa prote	162.58	23	3
Q00887|PSG9_HUMAN	Pregnancy-specific beta-1-glycor	162.56	24	3
P34931|HS71L_HUMAN	Heat shock 70 kDa protein 1-like	129.92	20	3
P04040|CATA_HUMAN	Catalase OS=Homo sapiens GN	112.92	21	3
P62258|1433E_HUMAN	14-3-3 protein epsilon OS=Homo	108.22	16	3
P61604|CH10_HUMAN	10 kDa heat shock protein, mitoc	108.04	35	3
P01834|IGKC_HUMAN	Ig kappa chain C region OS=Hor	106.98	56	3
Q08380|LG3BP_HUMAN	Galectin-3-binding protein OS=H	100.86	8	3
P07437|TBB5_HUMAN	Tubulin beta chain OS=Homo sa	93.94	9	3
P09525|ANXA4_HUMAN	Annexin A4 OS=Homo sapiens C	92.2	15	3
Q9Y490|TLN1_HUMAN	Talin-1 OS=Homo sapiens GN=T	90.4	2	3
Q09666|AHNK_HUMAN	Neuroblast differentiation-associ	89.83	3	3
Q9BQE3|TBA1C_HUMAN	Tubulin alpha-1C chain OS=Hom	88	9	3
P35232|PHB_HUMAN	Prohibitin OS=Homo sapiens GN	85.74	15	3
P09382|LEG1_HUMAN	Galectin-1 OS=Homo sapiens G	85.61	30	3
P27797|CALR_HUMAN	Calreticulin OS=Homo sapiens C	83.22	19	3
P68104|EF1A1_HUMAN	Elongation factor 1-alpha 1 OS=	81.94	13	3
Q5VTE0|EF1A3_HUMAN	Putative elongation factor 1-alph	81.94	13	3
Q12874|SF3A3_HUMAN	Splicing factor 3A subunit 3 OS=	81.59	12	3
P04406|G3P_HUMAN	Glyceraldehyde-3-phosphate del	78.53	16	3
P31942|HNRH3_HUMAN	Heterogeneous nuclear ribonucle	77.15	12	3
Q10567|AP1B1_HUMAN	AP-1 complex subunit beta-1 OS	77.02	9	3
P20936|RASA1_HUMAN	Ras GTPase-activating protein 1	76.73	5	3
P01031|CO5_HUMAN	Complement C5 OS=Homo sapi	74.8	5	3
P54819|KAD2_HUMAN	Adenylate kinase 2, mitochondria	72.1	26	3
P07910|HNRPC_HUMAN	Heterogeneous nuclear ribonucle	71.44	23	3
Q13561|DCTN2_HUMAN	Dynactin subunit 2 OS=Homo sa	68.74	13	3
Q01518|CAP1_HUMAN	Adenylyl cyclase-associated prot	67.94	9	3
P60709|ACTB_HUMAN	Actin, cytoplasmic 1 OS=Homo s	216.5	44	2
P63261|ACTG_HUMAN	Actin, cytoplasmic 2 OS=Homo s	214.32	44	2
P01860|IGHG3_HUMAN	Ig gamma-3 chain C region OS=	175.52	51	2
P69892|HBG2_HUMAN	Hemoglobin subunit gamma-2 O	173.02	61	2
P69891|HBG1_HUMAN	Hemoglobin subunit gamma-1 O	170.8	61	2
P11465|PSG2_HUMAN	Pregnancy-specific beta-1-glycor	137.96	21	2
P07900|HS90A_HUMAN	Heat shock protein HSP 90-alph	131.12	23	2
P25815|S100P_HUMAN	Protein S100-P OS=Homo sapie	91.58	39	2
P63220|RS21_HUMAN	40S ribosomal protein S21 OS=H	90.01	30	2
P04206|KV307_HUMAN	Ig kappa chain V-III region GOL	89.85	45	2
P01620|KV302_HUMAN	Ig kappa chain V-III region SIE C	89.85	31	2
P01622|KV304_HUMAN	Ig kappa chain V-III region Ti OS	89.85	31	2
P01623|KV305_HUMAN	Ig kappa chain V-III region WOL	89.85	31	2
P18135|KV312_HUMAN	Ig kappa chain V-III region HAH	89.85	26	2
P18136|KV313_HUMAN	Ig kappa chain V-III region HIC C	89.85	26	2
P15311|EZRI_HUMAN	Ezrin OS=Homo sapiens GN=EZ	88.03	9	2
P23396|RS3_HUMAN	40S ribosomal protein S3 OS=H	85.87	11	2
P01019|ANGT_HUMAN	Angiotensinogen OS=Homo sap	85.07	12	2
P42126|ECI1_HUMAN	Enoyl-CoA delta isomerase 1, m	83.5	15	2
P01009|A1AT_HUMAN	Alpha-1-antitrypsin OS=Homo sa	82	9	2

P98095|FBLN2_HUMAN	Fibulin-2 OS=Homo sapiens GN	80.14	2	2
P01593|KV101_HUMAN	Ig kappa chain V-I region AG OS	79.95	31	2
P31949|S10AB_HUMAN	Protein S100-A11 OS=Homo sa	78.4	34	2
P62993|GRB2_HUMAN	Growth factor receptor-bound pr	76.56	11	2
Q6NZI2|PTRF_HUMAN	Polymerase I and transcript relea	76.06	10	2
P01617|KV204_HUMAN	Ig kappa chain V-II region TEW	75.38	29	2
P06309|KV205_HUMAN	Ig kappa chain V-II region GM60	75.38	19	2
P23528|COF1_HUMAN	Cofilin-1 OS=Homo sapiens GN=	75.06	14	2
Q15149|PLEC_HUMAN	Plectin OS=Homo sapiens GN=P	72.18	7	2
P01766|HV305_HUMAN	Ig heavy chain V-III region BRO	71.59	25	2
P51659|DHB4_HUMAN	Peroxisomal multifunctional enzy	69.47	6	2
P19404|NDUV2_HUMAN	NADH dehydrogenase [ubiquino	68.9	9	2
P30049|ATPD_HUMAN	ATP synthase subunit delta, mito	68.54	14	2
P05160|F13B_HUMAN	Coagulation factor XIII B chain O	68.43	4	2
Q13219|PAPP1_HUMAN	Pappalysin-1 OS=Homo sapiens	67.72	3	2
Q04837|SSBP_HUMAN	Single-stranded DNA-binding pro	65.41	18	2
P46109|CRKL_HUMAN	Crk-like protein OS=Homo sapie	65.25	11	2
P01042|KNG1_HUMAN	Kininogen-1 OS=Homo sapiens	64.19	3	2
Q08830|FGL1_HUMAN	Fibrinogen-like protein 1 OS=Ho	64.04	11	2
P07339|CATD_HUMAN	Cathepsin D OS=Homo sapiens	63.2	6	2
Q8IVN8|RPESP_HUMAN	RPE-spondin OS=Homo sapiens	62.23	9	2
P04843|RPN1_HUMAN	Dolichyl-diphosphooligosaccharid	61.45	4	2
Q16787|LAMA3_HUMAN	Laminin subunit alpha-3 OS=Hor	61.2	2	2
O43852|CALU_HUMAN	Calumenin OS=Homo sapiens G	58.94	17	2
Q15293|RCN1_HUMAN	Reticulocalbin-1 OS=Homo sapie	57.79	8	2
P30040|ERP29_HUMAN	Endoplasmic reticulum resident	57.42	21	2
P11940|PABP1_HUMAN	Polyadenylate-binding protein 1	52.1	5	2
Q9H361|PABP3_HUMAN	Polyadenylate-binding protein 3	52.1	6	2
P78371|TCPB_HUMAN	T-complex protein 1 subunit beta	49.77	9	2
P10412|H14_HUMAN	Histone H1.4 OS=Homo sapiens	46.66	13	2
Q14571|ITPR2_HUMAN	Inositol 1,4,5-trisphosphate rece	35.19	1	2
Q9P2P6|STAR9_HUMAN	StAR-related lipid transfer protei	31.91	2	2
Q9P2D1|CHD7_HUMAN	Chromodomain-helicase-DNA-bi	31.53	1	2
Q7Z2Z1|TICRR_HUMAN	Treslin OS=Homo sapiens GN=T	30.44	2	2
Q5TZA2|CROCC_HUMAN	Rootletin OS=Homo sapiens GN	30.02	4	2
Q03001|DYST_HUMAN	Dystonin OS=Homo sapiens GN	29.73	2	2
Q9P2F8|SI1L2_HUMAN	Signal-induced proliferation-asso	29.63	3	2
Q8WZ42|TITIN_HUMAN	Titin OS=Homo sapiens GN=TT	29.6	2	2
Q4LDE5|SVEP1_HUMAN	Sushi, von Willebrand factor type	28.41	1	2
Q8IVF2|AHNK2_HUMAN	Protein AHNAK2 OS=Homo sap	26.15	1	2
Q9NW75|GPTC2_HUMAN	G patch domain-containing prote	25.7	12	2
P07478|TRY2_HUMAN	Trypsin-2 OS=Homo sapiens GN	25.63	10	2
Q8IVL0|NAV3_HUMAN	Neuron navigator 3 OS=Homo s	25.51	2	2
Q9NU22|MDN1_HUMAN	Midasin OS=Homo sapiens GN=	24.63	2	2

Table A1.5 StemXVivo Protein Identifications. List of all proteins identified in StemXVivo growth matrix with corresponding accession, description, PEAKS score, unique peptide numbers, and coverage (in %).

Accession	Description	Score	Coverage (%)	#Unique
P04004|VTNC_HUMAN	Vitronectin OS=Homo sapiens GN	388.02	71	115
P14543|NID1_HUMAN	Nidogen-1 OS=Homo sapiens GN	412.42	53	109
P34741|SDC2_HUMAN	Syndecan-2 OS=Homo sapiens GI	239.36	43	22
P11142|HSP7C_HUMAN	Heat shock cognate 71 kDa protei	219.5	32	11
P02768|ALBU_HUMAN	Serum albumin OS=Homo sapiens	176.5	13	11
P26641|EF1G_HUMAN	Elongation factor 1-gamma OS=Ho	176.44	33	8
P34932|HSP74_HUMAN	Heat shock 70 kDa protein 4 OS=H	187.57	19	7
O94985|CSTN1_HUMAN	Calsyntenin-1 OS=Homo sapiens (	129.26	10	6
P01024|CO3_HUMAN	Complement C3 OS=Homo sapien	141.05	11	5
P07900|HS90A_HUMAN	Heat shock protein HSP 90-alpha (	196.22	24	4
P63261|ACTG_HUMAN	Actin, cytoplasmic 2 OS=Homo sa	146.59	30	4
P60709|ACTB_HUMAN	Actin, cytoplasmic 1 OS=Homo sa	146.59	27	4
P14618|KPYM_HUMAN	Pyruvate kinase isozymes M1/M2 (	140.5	21	4
P01023|A2MG_HUMAN	Alpha-2-macroglobulin OS=Homo	133.62	12	4
P23142|FBLN1_HUMAN	Fibulin-1 OS=Homo sapiens GN=F	118.99	6	4
P04083|ANXA1_HUMAN	Annexin A1 OS=Homo sapiens GN	118.41	11	4
P08238|HS90B_HUMAN	Heat shock protein HSP 90-beta O	199.68	28	3
Q9BQE3|TBA1C_HUMAN	Tubulin alpha-1C chain OS=Homo	121.93	20	3
P68363|TBA1B_HUMAN	Tubulin alpha-1B chain OS=Homo	121.93	20	3
P23396|RS3_HUMAN	40S ribosomal protein S3 OS=Hon	119.7	20	3
Q5VTE0|EF1A3_HUMAN	Putative elongation factor 1-alpha-	109.9	15	3
P68104|EF1A1_HUMAN	Elongation factor 1-alpha 1 OS=Ho	109.9	11	3
P00450|CERU_HUMAN	Ceruloplasmin OS=Homo sapiens	100.07	6	3
Q16543|CDC37_HUMAN	Hsp90 co-chaperone Cdc37 OS=H	90.9	19	3
P0C0L4|CO4A_HUMAN	Complement C4-A OS=Homo sapi	77.95	5	3
P0C0L5|CO4B_HUMAN	Complement C4-B OS=Homo sapi	77.95	5	3
Q9Y623|MYH4_HUMAN	Myosin-4 OS=Homo sapiens GN=I	67.15	4	3
P08865|RSSA_HUMAN	40S ribosomal protein SA OS=Hon	112.46	10	2
P19823|ITIH2_HUMAN	Inter-alpha-trypsin inhibitor heavy c	102.91	7	2
P67809|YBOX1_HUMAN	Nuclease-sensitive element-bindin	101.59	20	2
P02656|APOC3_HUMAN	Apolipoprotein C-III OS=Homo sap	98.62	16	2
P62263|RS14_HUMAN	40S ribosomal protein S14 OS=Ho	98.35	16	2
P02647|APOA1_HUMAN	Apolipoprotein A-I OS=Homo sapie	96.73	21	2
P01031|CO5_HUMAN	Complement C5 OS=Homo sapien	95.88	4	2
Q66LE6|2ABD_HUMAN	Serine/threonine-protein phosphata	94.37	9	2
P63151|2ABA_HUMAN	Serine/threonine-protein phosphata	94.37	11	2
P33778|H2B1B_HUMAN	Histone H2B type 1-B OS=Homo s	94.29	19	2
P62807|H2B1C_HUMAN	Histone H2B type 1-C/E/F/G/I OS=	94.29	19	2
P58876|H2B1D_HUMAN	Histone H2B type 1-D OS=Homo s	94.29	19	2
Q93079|H2B1H_HUMAN	Histone H2B type 1-H OS=Homo s	94.29	19	2
P06899|H2B1J_HUMAN	Histone H2B type 1-J OS=Homo sa	94.29	19	2
O60814|H2B1K_HUMAN	Histone H2B type 1-K OS=Homo s	94.29	19	2
Q99880|H2B1L_HUMAN	Histone H2B type 1-L OS=Homo s	94.29	19	2
Q99879|H2B1M_HUMAN	Histone H2B type 1-M OS=Homo s	94.29	19	2
Q99877|H2B1N_HUMAN	Histone H2B type 1-N OS=Homo s	94.29	19	2
P23527|H2B1O_HUMAN	Histone H2B type 1-O OS=Homo s	94.29	19	2
Q16778|H2B2E_HUMAN	Histone H2B type 2-E OS=Homo s	94.29	19	2
Q5QNW6|H2B2F_HUMAN	Histone H2B type 2-F OS=Homo s	94.29	19	2
Q8N257|H2B3B_HUMAN	Histone H2B type 3-B OS=Homo s	94.29	19	2
P57053|H2BFS_HUMAN	Histone H2B type F-S OS=Homo s	94.29	19	2
P53621|COPA_HUMAN	Coatomer subunit alpha OS=Homo	91.65	6	2
P36955|PEDF_HUMAN	Pigment epithelium-derived factor (	89.1	6	2
P60842|IF4A1_HUMAN	Eukaryotic initiation factor 4A-I OS	83.3	7	2
P53396|ACLY_HUMAN	ATP-citrate synthase OS=Homo sa	82.41	6	2

P31749|AKT1_HUMAN	RAC-alpha serine/threonine-protei	82.32	12	2
P68871|HBB_HUMAN	Hemoglobin subunit beta OS=Hom	78.59	25	2
P55072|TERA_HUMAN	Transitional endoplasmic reticulum	76.98	4	2
P46782|RS5_HUMAN	40S ribosomal protein S5 OS=Hom	76.59	11	2
O00506|STK25_HUMAN	Serine/threonine-protein kinase 25	75.38	9	2
P78371|TCPB_HUMAN	T-complex protein 1 subunit beta O	74.84	8	2
P05388|RLA0_HUMAN	60S acidic ribosomal protein P0 OS	74.81	15	2
Q8NHW5|RLA0L_HUMAN	60S acidic ribosomal protein P0-lik	74.81	11	2
P62269|RS18_HUMAN	40S ribosomal protein S18 OS=Ho	69.34	20	2
P62826|RAN_HUMAN	GTP-binding nuclear protein Ran O	68.52	27	2
P81605|DCD_HUMAN	Dermcidin OS=Homo sapiens GN=	59.42	13	2
O15169|AXIN1_HUMAN	Axin-1 OS=Homo sapiens GN=AX	47.22	3	2
P05546|HEP2_HUMAN	Heparin cofactor 2 OS=Homo sapi	37.09	4	2

Table A1.6 StemXVivo Protein Identifications (not species restricted). List of all proteins identified in StemXVivo growth matrix when searched against the entire UniProt database (not species restricted) with corresponding accession, description, PEAKS score, unique peptide numbers, and coverage (in %).

Accession	Description	Score	Coverage (%)	#Unique
Q7SIH1|A2MG_BOVIN	Alpha-2-macroglobulin OS=Bos tau	291.83	37	41
P15497|APOA1_BOVIN	Apolipoprotein A-I OS=Bos taurus G	286.69	75	32
Q2UVX4|CO3_BOVIN	Complement C3 OS=Bos taurus GN	253.94	33	29
P02769|ALBU_BOVIN	Serum albumin OS=Bos taurus GN=	297.68	67	22
P50448|F12AI_BOVIN	Factor XIIa inhibitor OS=Bos taurus	203.22	39	16
P02081|HBBF_BOVIN	Hemoglobin fetal subunit beta OS=B	201.32	66	14
P33433|HRG_BOVIN	Histidine-rich glycoprotein (Fragmer	196.95	28	10
Q3T052|ITIH4_BOVIN	Inter-alpha-trypsin inhibitor heavy ch	177.34	17	8
Q32PJ2|APOA4_BOVIN	Apolipoprotein A-IV OS=Bos taurus	136.8	28	8
P01030|CO4_BOVIN	Complement C4 (Fragments) OS=B	172.36	16	7
P80109|PHLD_BOVIN	Phosphatidylinositol-glycan-specific	141.5	10	6
P17697|CLUS_BOVIN	Clusterin OS=Bos taurus GN=CLU	122.97	15	6
Q32KY0|APOD_BOVIN	Apolipoprotein D OS=Bos taurus GN	110.26	27	6
P34955|A1AT_BOVIN	Alpha-1-antiproteinase OS=Bos tau	151.74	23	5
P56652|ITIH3_BOVIN	Inter-alpha-trypsin inhibitor heavy ch	123.99	9	5
P12763|FETUA_BOVIN	Alpha-2-HS-glycoprotein OS=Bos ta	148.64	25	4
P01044|KNG1_BOVIN	Kininogen-1 OS=Bos taurus GN=KN	176.7	21	3
Q3MHN5|VTDB_BOVIN	Vitamin D-binding protein OS=Bos t	103.11	12	3
P01045|KNG2_BOVIN	Kininogen-2 OS=Bos taurus GN=KN	170.41	19	2
Q3SZ57|FETA_BOVIN	Alpha-fetoprotein OS=Bos taurus G	116.63	8	2
P00735|THRB_BOVIN	Prothrombin OS=Bos taurus GN=F2	98.14	7	2
Q29443|TRFE_BOVIN	Serotransferrin OS=Bos taurus GN=	90.11	5	2
P81644|APOA2_BOVIN	Apolipoprotein A-II OS=Bos taurus (	80.49	26	2
Q32PF2|ACLY_BOVIN	ATP-citrate synthase OS=Bos tauru	77.96	7	2
Q3MHN2|CO9_BOVIN	Complement component C9 OS=Bo	71.57	6	2
Q03247|APOE_BOVIN	Apolipoprotein E OS=Bos taurus GN	57.34	8	2

Table A1.7 MEF-CMTX Protein Identifications. List of all proteins identified in MEF-CMTX (mouse embryonic fibroblast conditioned matrix) with corresponding accession, description, PEAKS score, unique peptide numbers, and coverage (in %).

Accession	Description	Score	Coverage (%)	#Unique
P11276|FINC_MOUSE	Fibronectin OS=Mus musculus GN	581.48	74	357
Q05793|PGBM_MOUSE	Basement membrane-specific hep	439.44	49	109
P37889|FBLN2_MOUSE	Fibulin-2 OS=Mus musculus GN=F	355.86	44	53
Q61554|FBN1_MOUSE	Fibrillin-1 OS=Mus musculus GN=F	365.34	34	51
P20152|VIME_MOUSE	Vimentin OS=Mus musculus GN=V	360.59	79	51
P35441|TSP1_MOUSE	Thrombospondin-1 OS=Mus musc	349.48	54	45
Q8VDD5|MYH9_MOUSE	Myosin-9 OS=Mus musculus GN=M	350.89	51	38
P56480|ATPB_MOUSE	ATP synthase subunit beta, mitoch	314.42	75	28
P11087|CO1A1_MOUSE	Collagen alpha-1(I) chain OS=Mus	282.08	47	26
Q60847|COCA1_MOUSE	Collagen alpha-1(XII) chain OS=Mu	253.63	28	26
P16858|G3P_MOUSE	Glyceraldehyde-3-phosphate dehyd	319.04	72	24
P19324|SERPH_MOUSE	Serpin H1 OS=Mus musculus GN=	295.98	75	24
Q80YX1|TENA_MOUSE	Tenascin OS=Mus musculus GN=T	307.73	27	22
P08113|ENPL_MOUSE	Endoplasmin OS=Mus musculus G	275.18	49	21
P48036|ANXA5_MOUSE	Annexin A5 OS=Mus musculus GN	246.52	45	20
P27773|PDIA3_MOUSE	Protein disulfide-isomerase A3 OS	240.13	59	20
P48678|LMNA_MOUSE	Prelamin-A/C OS=Mus musculus G	202.89	41	19
P08249|MDHM_MOUSE	Malate dehydrogenase, mitochond	277.85	64	18
P20029|GRP78_MOUSE	78 kDa glucose-regulated protein G	258.38	48	18
Q60932|VDAC1_MOUSE	Voltage-dependent anion-selective	245.44	61	18
P09103|PDIA1_MOUSE	Protein disulfide-isomerase OS=Mu	242.36	55	18
P62806|H4_MOUSE	Histone H4 OS=Mus musculus GN	214.42	54	18
Q99K41|EMIL1_MOUSE	EMILIN-1 OS=Mus musculus GN=	267.68	48	17
P10107|ANXA1_MOUSE	Annexin A1 OS=Mus musculus GN	248.47	62	17
Q68FD5|CLH_MOUSE	Clathrin heavy chain 1 OS=Mus mu	215.3	36	17
Q61879|MYH10_MOUSE	Myosin-10 OS=Mus musculus GN=	276.25	42	16
P07356|ANXA2_MOUSE	Annexin A2 OS=Mus musculus GN	267.91	65	16
P10126|EF1A1_MOUSE	Elongation factor 1-alpha 1 OS=Mu	231.29	49	16
Q9JHU4|DYHC1_MOUSE	Cytoplasmic dynein 1 heavy chain	198.4	26	16
P01027|CO3_MOUSE	Complement C3 OS=Mus musculu	191.3	29	16
Q99LC5|ETFA_MOUSE	Electron transfer flavoprotein subu	254.74	57	15
P67778|PHB_MOUSE	Prohibitin OS=Mus musculus GN=P	243.64	79	15
Q99JR5|TINAL_MOUSE	Tubulointerstitial nephritis antigen-l	242	47	15
P17742|PPIA_MOUSE	Peptidyl-prolyl cis-trans isomerase	233.89	59	15
P19783|COX41_MOUSE	Cytochrome c oxidase subunit 4 is	227.74	47	15
Q01149|CO1A2_MOUSE	Collagen alpha-2(I) chain OS=Mus	223.78	39	15
Q8BTM8|FLNA_MOUSE	Filamin-A OS=Mus musculus GN=	203.11	22	15
O35129|PHB2_MOUSE	Prohibitin-2 OS=Mus musculus GN	224.33	67	14
Q9WTI7|MYO1C_MOUSE	Myosin-Ic OS=Mus musculus GN=	210.49	41	14
P52480|KPYM_MOUSE	Pyruvate kinase isozymes M1/M2 O	188.48	56	14
Q9QXS1|PLEC_MOUSE	Plectin OS=Mus musculus GN=Ple	172.22	25	14
O88322|NID2_MOUSE	Nidogen-2 OS=Mus musculus GN=	248.24	20	13
Q9DCN2|NB5R3_MOUSE	NADH-cytochrome b5 reductase 3	245.19	52	13
Q9DBJ1|PGAM1_MOUSE	Phosphoglycerate mutase 1 OS=M	227.39	68	13
Q9DCX2|ATP5H_MOUSE	ATP synthase subunit d, mitochon	224.83	76	13
P07724|ALBU_MOUSE	Serum albumin OS=Mus musculus	188.34	34	13
Q03265|ATPA_MOUSE	ATP synthase subunit alpha, mitoc	247.63	56	12
P22777|PAI1_MOUSE	Plasminogen activator inhibitor 1 O	233.08	64	12
Q8BMK4|CKAP4_MOUSE	Cytoskeleton-associated protein 4	227.44	45	12
P06151|LDHA_MOUSE	L-lactate dehydrogenase A chain G	222.32	49	12
P09055|ITB1_MOUSE	Integrin beta-1 OS=Mus musculus	221.29	30	12
O88207|CO5A1_MOUSE	Collagen alpha-1(V) chain OS=Mus	184.56	35	12
P37804|TAGL_MOUSE	Transgelin OS=Mus musculus GN=	181.07	76	12
P63038|CH60_MOUSE	60 kDa heat shock protein, mitoch	243.31	53	11

P51655|GPC4_MOUSE	Glypican-4 OS=Mus musculus GN=	218.62	40	11
P17182|ENOA_MOUSE	Alpha-enolase OS=Mus musculus	207.07	59	11
P26039|TLN1_MOUSE	Talin-1 OS=Mus musculus GN=Tln	198.41	30	11
P17751|TPIS_MOUSE	Triosephosphate isomerase OS=M	196.62	53	11
Q8CG19|LTBP1_MOUSE	Latent-transforming growth factor b	185.33	17	11
Q8BMS1|ECHA_MOUSE	Trifunctional enzyme subunit alpha	212.35	39	10
P35564|CALX_MOUSE	Calnexin OS=Mus musculus GN=C	205.29	42	10
Q80X90|FLNB_MOUSE	Filamin-B OS=Mus musculus GN=	180.59	24	10
P35700|PRDX1_MOUSE	Peroxiredoxin-1 OS=Mus musculus	142.73	57	10
P01942|HBA_MOUSE	Hemoglobin subunit alpha OS=Mus	127.01	70	10
Q9D6X6|PRS23_MOUSE	Serine protease 23 OS=Mus musc	228.51	41	9
P16045|LEG1_MOUSE	Galectin-1 OS=Mus musculus GN=	200.58	65	9
Q61703|ITIH2_MOUSE	Inter-alpha-trypsin inhibitor heavy c	193.6	22	9
P14069|S10A6_MOUSE	Protein S100-A6 OS=Mus musculu	184.59	75	9
P38647|GRP75_MOUSE	Stress-70 protein, mitochondrial OS	173.67	33	9
Q9D1D4|TMEDA_MOUSE	Transmembrane emp24 domain-co	163.9	34	9
P63017|HSP7C_MOUSE	Heat shock cognate 71 kDa protein	216.39	36	8
P62962|PROF1_MOUSE	Profilin-1 OS=Mus musculus GN=P	184.52	64	8
P58252|EF2_MOUSE	Elongation factor 2 OS=Mus musc	179.44	31	8
O08756|HCD2_MOUSE	3-hydroxyacyl-CoA dehydrogenase	174.7	52	8
P49817|CAV1_MOUSE	Caveolin-1 OS=Mus musculus GN=	173.56	56	8
P42208|SEPT2_MOUSE	Septin-2 OS=Mus musculus GN=S	173.24	43	8
P99029|PRDX5_MOUSE	Peroxiredoxin-5, mitochondrial OS=	168.5	51	8
P05064|ALDOA_MOUSE	Fructose-bisphosphate aldolase A	160.07	38	8
P08121|CO3A1_MOUSE	Collagen alpha-1(III) chain OS=Mu	159.6	20	8
P24369|PPIB_MOUSE	Peptidyl-prolyl cis-trans isomerase	156.06	61	8
P32261|ANT3_MOUSE	Antithrombin-III OS=Mus musculus	155.97	40	8
Q60605|MYL6_MOUSE	Myosin light polypeptide 6 OS=Mus	197.87	74	7
P61982|1433G_MOUSE	14-3-3 protein gamma OS=Mus mu	197.21	48	7
P48962|ADT1_MOUSE	ADP/ATP translocase 1 OS=Mus m	195.35	53	7
P63101|1433Z_MOUSE	14-3-3 protein zeta/delta OS=Mus	187.73	45	7
P62259|1433E_MOUSE	14-3-3 protein epsilon OS=Mus mu	186.09	49	7
Q02257|PLAK_MOUSE	Junction plakoglobin OS=Mus mus	182.94	36	7
Q9DB77|QCR2_MOUSE	Cytochrome b-c1 complex subunit	181.77	34	7
Q62009|POSTN_MOUSE	Periostin OS=Mus musculus GN=P	169.26	33	7
Q9DBG6|RPN2_MOUSE	Dolichyl-diphosphooligosaccharide	167.93	18	7
Q99P72|RTN4_MOUSE	Reticulon-4 OS=Mus musculus GN	162.74	12	7
Q3V1M1|IGS10_MOUSE	Immunoglobulin superfamily memb	160.41	22	7
Q64433|CH10_MOUSE	10 kDa heat shock protein, mitocho	158.56	53	7
P14211|CALR_MOUSE	Calreticulin OS=Mus musculus GN	156.64	41	7
P47738|ALDH2_MOUSE	Aldehyde dehydrogenase, mitocho	152.71	28	7
Q9CPT4|CS010_MOUSE	UPF0556 protein C19orf10 homolo	151.83	50	7
P01831|THY1_MOUSE	Thy-1 membrane glycoprotein OS=	150.21	32	7
P30999|CTND1_MOUSE	Catenin delta-1 OS=Mus musculus	132.85	34	7
Q00623|APOA1_MOUSE	Apolipoprotein A-I OS=Mus muscu	111.33	14	7
P29699|FETUA_MOUSE	Alpha-2-HS-glycoprotein OS=Mus	93.03	12	7
P99024|TBB5_MOUSE	Tubulin beta-5 chain OS=Mus mus	300.34	70	6
Q922R8|PDIA6_MOUSE	Protein disulfide-isomerase A6 OS	177.82	28	6
P14206|RSSA_MOUSE	40S ribosomal protein SA OS=Mus	172.96	37	6
O54724|PTRF_MOUSE	Polymerase I and transcript release	165.27	41	6
Q9CQ60|6PGL_MOUSE	6-phosphogluconolactonase OS=M	163.4	58	6
Q9D6R2|IDH3A_MOUSE	Isocitrate dehydrogenase [NAD] su	162.7	32	6
P16546|SPTA2_MOUSE	Spectrin alpha chain, brain OS=Mu	154.23	30	6
Q64523|H2A2C_MOUSE	Histone H2A type 2-C OS=Mus mu	153.48	63	6
Q6GSS7|H2A2A_MOUSE	Histone H2A type 2-A OS=Mus mu	153.48	62	6

P18760|COF1_MOUSE	Cofilin-1 OS=Mus musculus GN=C	149.72	51	6
P19221|THRB_MOUSE	Prothrombin OS=Mus musculus GI	142.61	23	6
Q3U7R1|ESYT1_MOUSE	Extended synaptotagmin-1 OS=Mu	142.07	21	6
Q99JB2|STML2_MOUSE	Stomatin-like protein 2 OS=Mus m	140.46	36	6
P51150|RAB7A_MOUSE	Ras-related protein Rab-7a OS=Mu	140.24	36	6
Q61704|ITIH3_MOUSE	Inter-alpha-trypsin inhibitor heavy c	134.96	7	6
Q6GQT1|A2MP_MOUSE	Alpha-2-macroglobulin-P OS=Mus	133.24	10	6
Q9R0Q3|TMED2_MOUSE	Transmembrane emp24 domain-co	120.8	43	6
Q9Z0G4|WISP2_MOUSE	WNT1-inducible-signaling pathway	95.85	14	6
Q7TPR4|ACTN1_MOUSE	Alpha-actinin-1 OS=Mus musculus	209.95	29	5
Q9CPQ3|TOM22_MOUSE	Mitochondrial import receptor subu	162.06	73	5
Q64449|MRC2_MOUSE	C-type mannose receptor 2 OS=Mu	161.05	28	5
P97429|ANXA4_MOUSE	Annexin A4 OS=Mus musculus GN	160.41	25	5
Q9D051|ODPB_MOUSE	Pyruvate dehydrogenase E1 compo	158.08	31	5
Q6IRU2|TPM4_MOUSE	Tropomyosin alpha-4 chain OS=Mu	152.53	35	5
Q9WV54|ASAH1_MOUSE	Acid ceramidase OS=Mus musculu	151.8	36	5
Q9CQQ7|AT5F1_MOUSE	ATP synthase subunit b, mitochond	151.39	42	5
Q9CPQ8|ATP5L_MOUSE	ATP synthase subunit g, mitochond	148.8	43	5
Q9DB20|ATPO_MOUSE	ATP synthase subunit O, mitochon	145.36	55	5
Q9DCS9|NDUBA_MOUSE	NADH dehydrogenase [ubiquinone	144.59	40	5
Q91V41|RAB14_MOUSE	Ras-related protein Rab-14 OS=Mu	144.13	34	5
P63242|IF5A1_MOUSE	Eukaryotic translation initiation fact	141.88	52	5
Q8QZT1|THIL_MOUSE	Acetyl-CoA acetyltransferase, mito	139.92	25	5
P12787|COX5A_MOUSE	Cytochrome c oxidase subunit 5A,	137.05	52	5
Q9R0Y5|KAD1_MOUSE	Adenylate kinase isoenzyme 1 OS=	134.64	50	5
P62908|RS3_MOUSE	40S ribosomal protein S3 OS=Mus	134.44	25	5
P08207|S10AA_MOUSE	Protein S100-A10 OS=Mus muscu	132.92	49	5
P16460|ASSY_MOUSE	Argininosuccinate synthase OS=M	132.88	32	5
P62492|RB11A_MOUSE	Ras-related protein Rab-11A OS=M	132.84	26	5
P46638|RB11B_MOUSE	Ras-related protein Rab-11B OS=M	132.84	26	5
P57776|EF1D_MOUSE	Elongation factor 1-delta OS=Mus	132.4	20	5
P14602|HSPB1_MOUSE	Heat shock protein beta-1 OS=Mus	131.71	58	5
Q9DCW4|ETFB_MOUSE	Electron transfer flavoprotein subu	130.32	26	5
P29758|OAT_MOUSE	Ornithine aminotransferase, mitoch	127.65	28	5
Q08879|FBLN1_MOUSE	Fibulin-1 OS=Mus musculus GN=F	126.94	7	5
P57759|ERP29_MOUSE	Endoplasmic reticulum resident pro	126.22	30	5
Q3THE2|ML12B_MOUSE	Myosin regulatory light chain 12B C	123.64	31	5
O08807|PRDX4_MOUSE	Peroxiredoxin-4 OS=Mus musculus	120.68	36	5
P56395|CYB5_MOUSE	Cytochrome b5 OS=Mus musculus	114.04	25	5
Q02248|CTNB1_MOUSE	Catenin beta-1 OS=Mus musculus	113.49	17	5
O08709|PRDX6_MOUSE	Peroxiredoxin-6 OS=Mus musculus	113.38	33	5
P01029|CO4B_MOUSE	Complement C4-B OS=Mus muscu	109.12	23	5
P11688|ITA5_MOUSE	Integrin alpha-5 OS=Mus musculus	108.93	5	5
Q8VDP6|CDIPT_MOUSE	CDP-diacylglycerol--inositol 3-phos	107.11	26	5
P62301|RS13_MOUSE	40S ribosomal protein S13 OS=Mu	101.37	32	5
Q922F4|TBB6_MOUSE	Tubulin beta-6 chain OS=Mus mus	247.93	55	4
P57780|ACTN4_MOUSE	Alpha-actinin-4 OS=Mus musculus	193	30	4
O08638|MYH11_MOUSE	Myosin-11 OS=Mus musculus GN=	182.1	37	4
P97298|PEDF_MOUSE	Pigment epithelium-derived factor (	161.86	29	4
P00405|COX2_MOUSE	Cytochrome c oxidase subunit 2 O	160.13	33	4
P05202|AATM_MOUSE	Aspartate aminotransferase, mitoc	157.02	47	4
Q9R001|ATS5_MOUSE	A disintegrin and metalloproteinase	155.55	22	4
P68254|1433T_MOUSE	14-3-3 protein theta OS=Mus musc	153.89	38	4
Q64727|VINC_MOUSE	Vinculin OS=Mus musculus GN=V	148.88	39	4
Q9JKR6|HYOU1_MOUSE	Hypoxia up-regulated protein 1 OS	147.92	24	4

P09411|PGK1_MOUSE	Phosphoglycerate kinase 1 OS=Mu	146.68	35	4
P53994|RAB2A_MOUSE	Ras-related protein Rab-2A OS=M	145.57	42	4
Q9WVA4|TAGL2_MOUSE	Transgelin-2 OS=Mus musculus G	145.29	31	4
Q62186|SSRD_MOUSE	Translocon-associated protein sub	142.72	45	4
P34884|MIF_MOUSE	Macrophage migration inhibitory fa	141.34	46	4
Q6URW6|MYH14_MOUSE	Myosin-14 OS=Mus musculus GN=	141.17	24	4
O35639|ANXA3_MOUSE	Annexin A3 OS=Mus musculus GN	138.36	36	4
Q8CGP2|H2B1P_MOUSE	Histone H2B type 1-P OS=Mus mu	136.6	46	4
Q64475|H2B1B_MOUSE	Histone H2B type 1-B OS=Mus mu	136.6	37	4
Q6ZWY9|H2B1C_MOUSE	Histone H2B type 1-C/E/G OS=Mu	136.6	37	4
P10853|H2B1F_MOUSE	Histone H2B type 1-F/J/L OS=Mus	136.6	37	4
Q64478|H2B1H_MOUSE	Histone H2B type 1-H OS=Mus mu	136.6	37	4
Q8CGP1|H2B1K_MOUSE	Histone H2B type 1-K OS=Mus mu	136.6	37	4
P10854|H2B1M_MOUSE	Histone H2B type 1-M OS=Mus mu	136.6	37	4
Q64525|H2B2B_MOUSE	Histone H2B type 2-B OS=Mus mu	136.6	37	4
P07214|SPRC_MOUSE	SPARC OS=Mus musculus GN=Sp	135.04	24	4
P43406|ITAV_MOUSE	Integrin alpha-V OS=Mus musculus	132.86	14	4
Q61171|PRDX2_MOUSE	Peroxiredoxin-2 OS=Mus musculus	129.18	27	4
Q64310|SURF4_MOUSE	Surfeit locus protein 4 OS=Mus mu	127.56	22	4
Q9DBL1|ACDSB_MOUSE	Short/branched chain specific acyl-	127.15	47	4
Q9DCT2|NDUS3_MOUSE	NADH dehydrogenase [ubiquinone	125.81	13	4
Q9CXE7|TMED5_MOUSE	Transmembrane emp24 domain-co	124.12	21	4
O08992|SDCB1_MOUSE	Syntenin-1 OS=Mus musculus GN=	124.04	27	4
P97315|CSRP1_MOUSE	Cysteine and glycine-rich protein 1	123.53	46	4
P14148|RL7_MOUSE	60S ribosomal protein L7 OS=Mus	117.96	31	4
Q9D6U8|F162A_MOUSE	Protein FAM162A OS=Mus muscu	117.11	51	4
P0CG50|UBC_MOUSE	Polyubiquitin-C OS=Mus musculus	115.44	22	4
P0CG49|UBB_MOUSE	Polyubiquitin-B OS=Mus musculus	115.44	40	4
P62983|RS27A_MOUSE	Ubiquitin-40S ribosomal protein S2	115.44	37	4
P62984|RL40_MOUSE	Ubiquitin-60S ribosomal protein L4	115.44	27	4
Q99JI6|RAP1B_MOUSE	Ras-related protein Rap-1b OS=Mu	114.9	34	4
P62835|RAP1A_MOUSE	Ras-related protein Rap-1A OS=M	114.9	26	4
O54962|BAF_MOUSE	Barrier-to-autointegration factor OS	111.12	55	4
P10605|CATB_MOUSE	Cathepsin B OS=Mus musculus GI	111.07	30	4
Q9D2G2|ODO2_MOUSE	Dihydrolipoyllysine-residue succiny	110.35	35	4
Q9CZU6|CISY_MOUSE	Citrate synthase, mitochondrial OS	108.32	21	4
Q8BH95|ECHM_MOUSE	Enoyl-CoA hydratase, mitochondria	106.09	20	4
Q9WTP7|KAD3_MOUSE	GTP:AMP phosphotransferase, mi	105.03	21	4
P15532|NDKA_MOUSE	Nucleoside diphosphate kinase A (	104.98	43	4
Q9CQ92|FIS1_MOUSE	Mitochondrial fission 1 protein OS=	103.52	39	4
P56135|ATPK_MOUSE	ATP synthase subunit f, mitochond	103.42	36	4
O88783|FA5_MOUSE	Coagulation factor V OS=Mus mus	102.44	10	4
Q60715|P4HA1_MOUSE	Prolyl 4-hydroxylase subunit alpha-	101.08	16	4
Q9CRB9|CHCH3_MOUSE	Coiled-coil-helix-coiled-coil-helix do	99.03	33	4
Q9R0P5|DEST_MOUSE	Destrin OS=Mus musculus GN=Ds	97.52	29	4
Q99PT1|GDIR1_MOUSE	Rho GDP-dissociation inhibitor 1 O	93.01	28	4
Q7TMF3|NDUAC_MOUSE	NADH dehydrogenase [ubiquinone	88.86	28	4
Q07235|GDN_MOUSE	Glia-derived nexin OS=Mus muscu	86.54	22	4
O09131|GSTO1_MOUSE	Glutathione S-transferase omega-1	74.84	26	4
P51863|VA0D1_MOUSE	V-type proton ATPase subunit d 1 (	72.57	13	4
Q8BFZ3|ACTBL_MOUSE	Beta-actin-like protein 2 OS=Mus m	276.89	69	3
P62874|GBB1_MOUSE	Guanine nucleotide-binding protein	174.49	34	3
Q9CQV8|1433B_MOUSE	14-3-3 protein beta/alpha OS=Mus	155.48	30	3
P62821|RAB1A_MOUSE	Ras-related protein Rab-1A OS=M	146.8	59	3
P84084|ARF5_MOUSE	ADP-ribosylation factor 5 OS=Mus	146.56	71	3

Q9JKF1|IQGA1_MOUSE	Ras GTPase-activating-like protein	135.47	23	3
P19157|GSTP1_MOUSE	Glutathione S-transferase P 1 OS=	134.43	38	3
P10493|NID1_MOUSE	Nidogen-1 OS=Mus musculus GN=	132.54	19	3
P50543|S10AB_MOUSE	Protein S100-A11 OS=Mus muscu	131.95	78	3
Q60930|VDAC2_MOUSE	Voltage-dependent anion-selective	130.73	18	3
Q8VDN2|AT1A1_MOUSE	Sodium/potassium-transporting AT	128.81	28	3
P62880|GBB2_MOUSE	Guanine nucleotide-binding protein	127.98	29	3
Q08093|CNN2_MOUSE	Calponin-2 OS=Mus musculus GN	126.29	18	3
P68510|1433F_MOUSE	14-3-3 protein eta OS=Mus muscu	123.73	53	3
P61620|S61A1_MOUSE	Protein transport protein Sec61 sub	122.41	23	3
Q9CYN9|RENR_MOUSE	Renin receptor OS=Mus musculus	121.99	19	3
Q8BMF4|ODP2_MOUSE	Dihydrolipoyllysine-residue acetyltra	119.27	15	3
Q9CXD9|LRC17_MOUSE	Leucine-rich repeat-containing prot	118.67	19	3
Q9WVJ2|PSD13_MOUSE	26S proteasome non-ATPase regu	117.63	32	3
Q8VEM8|MPCP_MOUSE	Phosphate carrier protein, mitocho	117.42	21	3
P19096|FAS_MOUSE	Fatty acid synthase OS=Mus musc	116.59	10	3
O54734|OST48_MOUSE	Dolichyl-diphosphooligosaccharide	116.1	13	3
P27090|TGFB2_MOUSE	Transforming growth factor beta-2	115.87	14	3
P61027|RAB10_MOUSE	Ras-related protein Rab-10 OS=Mu	115.87	32	3
P17225|PTBP1_MOUSE	Polypyrimidine tract-binding protein	114.52	17	3
P25444|RS2_MOUSE	40S ribosomal protein S2 OS=Mus	114.32	18	3
Q01730|RSU1_MOUSE	Ras suppressor protein 1 OS=Mus	114.21	43	3
P10833|RRAS_MOUSE	Ras-related protein R-Ras OS=Mu	113.73	30	3
P70168|IMB1_MOUSE	Importin subunit beta-1 OS=Mus m	113.34	14	3
Q0GNC1|INF2_MOUSE	Inverted formin-2 OS=Mus musculu	112.8	15	3
Q9R087|GPC6_MOUSE	Glypican-6 OS=Mus musculus GN=	112.77	24	3
Q9CQ22|LTOR1_MOUSE	Ragulator complex protein LAMTO	111.96	35	3
P60867|RS20_MOUSE	40S ribosomal protein S20 OS=Mu	111.21	23	3
Q923D2|BLVRB_MOUSE	Flavin reductase OS=Mus musculu	110.61	23	3
P47911|RL6_MOUSE	60S ribosomal protein L6 OS=Mus	110.19	25	3
Q9Z1Q5|CLIC1_MOUSE	Chloride intracellular channel prote	109.84	36	3
P20108|PRDX3_MOUSE	Thioredoxin-dependent peroxide re	109.36	20	3
P19536|COX5B_MOUSE	Cytochrome c oxidase subunit 5B,	109.24	30	3
P15626|GSTM2_MOUSE	Glutathione S-transferase Mu 2 OS	108.99	43	3
P63323|RS12_MOUSE	40S ribosomal protein S12 OS=Mu	108.86	41	3
Q91YQ5|RPN1_MOUSE	Dolichyl-diphosphooligosaccharide	108.44	16	3
Q61469|LPP1_MOUSE	Lipid phosphate phosphohydrolase	107.49	25	3
P14869|RLA0_MOUSE	60S acidic ribosomal protein P0 OS	107.32	21	3
Q9WU78|PDC6I_MOUSE	Programmed cell death 6-interactin	106.72	24	3
P99028|QCR6_MOUSE	Cytochrome b-c1 complex subunit	106.2	63	3
P63024|VAMP3_MOUSE	Vesicle-associated membrane prot	106.02	46	3
P28653|PGS1_MOUSE	Biglycan OS=Mus musculus GN=B	105.83	27	3
Q8BH04|PCKGM_MOUSE	Phosphoenolpyruvate carboxykinas	104.74	19	3
P35279|RAB6A_MOUSE	Ras-related protein Rab-6A OS=M	104.23	39	3
P35762|CD81_MOUSE	CD81 antigen OS=Mus musculus (	104.22	29	3
Q62465|VAT1_MOUSE	Synaptic vesicle membrane protein	103.84	15	3
Q8R2G6|CCD80_MOUSE	Coiled-coil domain-containing prote	103.31	10	3
Q9CQH3|NDUB5_MOUSE	NADH dehydrogenase [ubiquinone	102.14	15	3
P30412|PPIC_MOUSE	Peptidyl-prolyl cis-trans isomerase	101.39	19	3
P14131|RS16_MOUSE	40S ribosomal protein S16 OS=Mu	99.66	27	3
P60843|IF4A1_MOUSE	Eukaryotic initiation factor 4A-I OS=	99.53	18	3
P62827|RAN_MOUSE	GTP-binding nuclear protein Ran (	98.85	16	3
P62270|RS18_MOUSE	40S ribosomal protein S18 OS=Mu	98.16	30	3
P09671|SODM_MOUSE	Superoxide dismutase [Mn], mitoch	96.59	21	3
P62264|RS14_MOUSE	40S ribosomal protein S14 OS=Mu	95.11	17	3

O70456|1433S_MOUSE	14-3-3 protein sigma OS=Mus mus	94.96	19	3
P62082|RS7_MOUSE	40S ribosomal protein S7 OS=Mus	94.49	26	3
P21614|VTDB_MOUSE	Vitamin D-binding protein OS=Mus	92.81	21	3
P80317|TCPZ_MOUSE	T-complex protein 1 subunit zeta O	92.62	16	3
Q9DAW9|CNN3_MOUSE	Calponin-3 OS=Mus musculus GN	91.81	23	3
P62702|RS4X_MOUSE	40S ribosomal protein S4, X isofor	91.05	15	3
P07091|S10A4_MOUSE	Protein S100-A4 OS=Mus musculu	91.04	26	3
O55143|AT2A2_MOUSE	Sarcoplasmic/endoplasmic reticulu	89.83	12	3
Q8K3J1|NDUS8_MOUSE	NADH dehydrogenase [ubiquinone	88.76	15	3
Q9EP69|SAC1_MOUSE	Phosphatidylinositide phosphatase	88.42	10	3
Q9R0P3|ESTD_MOUSE	S-formylglutathione hydrolase OS=	85.32	19	3
P61622|ITA11_MOUSE	Integrin alpha-11 OS=Mus musculu	85.14	14	3
Q9ERS2|NDUAD_MOUSE	NADH dehydrogenase [ubiquinone	84.05	21	3
Q06185|ATP5I_MOUSE	ATP synthase subunit e, mitochon	82.61	42	3
Q9QXS6|DREB_MOUSE	Drebrin OS=Mus musculus GN=Db	81.93	10	3
Q9CQS8|SC61B_MOUSE	Protein transport protein Sec61 sub	80.5	38	3
P97449|AMPN_MOUSE	Aminopeptidase N OS=Mus muscu	80.24	6	3
Q8R5J9|PRAF3_MOUSE	PRA1 family protein 3 OS=Mus mu	78.42	16	3
Q9QUI0|RHOA_MOUSE	Transforming protein RhoA OS=Mu	78.31	33	3
Q99KF1|TMED9_MOUSE	Transmembrane emp24 domain-co	77.07	16	3
Q8R2Q8|BST2_MOUSE	Bone marrow stromal antigen 2 OS	74.79	12	3
P08228|SODC_MOUSE	Superoxide dismutase [Cu-Zn] OS=	74.13	21	3
Q6PHZ2|KCC2D_MOUSE	Calcium/calmodulin-dependent pro	72.44	14	3
Q9CQW9|IFM3_MOUSE	Interferon-induced transmembrane	70.3	9	3
Q791V5|MTCH2_MOUSE	Mitochondrial carrier homolog 2 OS	62	17	3
Q07456|AMBP_MOUSE	Protein AMBP OS=Mus musculus (	57.51	6	3
Q8BFZ9|ERLN2_MOUSE	Erlin-2 OS=Mus musculus GN=Erli	55.84	21	3
Q61838|A2M_MOUSE	Alpha-2-macroglobulin OS=Mus m	53.7	20	3
P48722|HS74L_MOUSE	Heat shock 70 kDa protein 4L OS=	45.77	5	3
A2ASS6|TITIN_MOUSE	Titin OS=Mus musculus GN=Ttn P	40.13	3	3
P63260|ACTG_MOUSE	Actin, cytoplasmic 2 OS=Mus musc	363.12	92	2
P62737|ACTA_MOUSE	Actin, aortic smooth muscle OS=M	315.47	81	2
P63268|ACTH_MOUSE	Actin, gamma-enteric smooth mus	315.47	81	2
Q7TMM9|TBB2A_MOUSE	Tubulin beta-2A chain OS=Mus mu	280.71	63	2
P02088|HBB1_MOUSE	Hemoglobin subunit beta-1 OS=Mu	177.89	50	2
P61750|ARF4_MOUSE	ADP-ribosylation factor 4 OS=Mus	165.61	57	2
P51881|ADT2_MOUSE	ADP/ATP translocase 2 OS=Mus m	163.06	35	2
P61205|ARF3_MOUSE	ADP-ribosylation factor 3 OS=Mus	155.84	65	2
P84078|ARF1_MOUSE	ADP-ribosylation factor 1 OS=Mus	155.84	60	2
P21107|TPM3_MOUSE	Tropomyosin alpha-3 chain OS=Mu	148.08	33	2
P58771|TPM1_MOUSE	Tropomyosin alpha-1 chain OS=Mu	146.22	36	2
P08752|GNAI2_MOUSE	Guanine nucleotide-binding protein	136.24	33	2
P02104|HBE_MOUSE	Hemoglobin subunit epsilon-Y2 OS	133.34	27	2
P84244|H33_MOUSE	Histone H3.3 OS=Mus musculus G	130.48	54	2
Q03350|TSP2_MOUSE	Thrombospondin-2 OS=Mus musc	128.66	23	2
P35278|RAB5C_MOUSE	Ras-related protein Rab-5C OS=M	126.58	35	2
Q9D1G1|RAB1B_MOUSE	Ras-related protein Rab-1B OS=M	122.28	49	2
O35459|ECH1_MOUSE	Delta(3,5)-Delta(2,4)-dienoyl-CoA i	119.25	23	2
Q91V61|SFXN3_MOUSE	Sideroflexin-3 OS=Mus musculus (	117.24	45	2
P61021|RAB5B_MOUSE	Ras-related protein Rab-5B OS=M	114.26	22	2
Q01853|TERA_MOUSE	Transitional endoplasmic reticulum	112.67	19	2
Q9JK53|PRELP_MOUSE	Prolargin OS=Mus musculus GN=P	111.9	14	2
Q60931|VDAC3_MOUSE	Voltage-dependent anion-selective	109.35	22	2
Q8BMD8|SCMC1_MOUSE	Calcium-binding mitochondrial carr	105.08	16	2
P85094|ISC2A_MOUSE	Isochorismatase domain-containing	104.94	31	2

Q6ZQI3|MLEC_MOUSE	Malectin OS=Mus musculus GN=M	103.42	22	2
P62830|RL23_MOUSE	60S ribosomal protein L23 OS=Mu	102.63	34	2
P39876|TIMP3_MOUSE	Metalloproteinase inhibitor 3 OS=M	102.58	11	2
Q9CQM2|ERD22_MOUSE	ER lumen protein retaining recepto	101.35	15	2
P68040|GBLP_MOUSE	Guanine nucleotide-binding protein	101.13	20	2
P62196|PRS8_MOUSE	26S protease regulatory subunit 8 (	100.68	29	2
Q9CQ65|MTAP_MOUSE	S-methyl-5'-thioadenosine phospho	98.09	13	2
Q9CQN1|TRAP1_MOUSE	Heat shock protein 75 kDa, mitoch	97.72	10	2
Q9DB05|SNAA_MOUSE	Alpha-soluble NSF attachment pro	97.66	14	2
O70251|EF1B_MOUSE	Elongation factor 1-beta OS=Mus r	97.03	16	2
Q78IK2|USMG5_MOUSE	Up-regulated during skeletal muscl	96.61	43	2
O08547|SC22B_MOUSE	Vesicle-trafficking protein SEC22b	96.39	26	2
Q9DCJ5|NDUA8_MOUSE	NADH dehydrogenase [ubiquinone	96.35	40	2
Q9CYR0|SSBP_MOUSE	Single-stranded DNA-binding prote	95.48	18	2
O35640|ANXA8_MOUSE	Annexin A8 OS=Mus musculus GN	95.41	18	2
O88456|CPNS1_MOUSE	Calpain small subunit 1 OS=Mus m	94.89	30	2
O35682|MYADM_MOUSE	Myeloid-associated differentiation r	94.64	10	2
Q9CR62|M2OM_MOUSE	Mitochondrial 2-oxoglutarate/malat	94.6	11	2
P58022|LOXL2_MOUSE	Lysyl oxidase homolog 2 OS=Mus	94.52	6	2
Q9CY50|SSRA_MOUSE	Translocon-associated protein sub	93.99	20	2
Q9CXI5|MANF_MOUSE	Mesencephalic astrocyte-derived n	93.77	36	2
Q62425|NDUA4_MOUSE	NADH dehydrogenase [ubiquinone	93.05	27	2
Q9R118|HTRA1_MOUSE	Serine protease HTRA1 OS=Mus r	93.04	9	2
Q61937|NPM_MOUSE	Nucleophosmin OS=Mus musculus	92.11	32	2
P09535|IGF2_MOUSE	Insulin-like growth factor II OS=Mu	91.89	23	2
Q9CYL5|GAPR1_MOUSE	Golgi-associated plant pathogenes	91.45	17	2
P27659|RL3_MOUSE	60S ribosomal protein L3 OS=Mus	90.38	14	2
Q9D8E6|RL4_MOUSE	60S ribosomal protein L4 OS=Mus	89.83	15	2
Q9QXT0|CNPY2_MOUSE	Protein canopy homolog 2 OS=Mu	88.9	23	2
P13020|GELS_MOUSE	Gelsolin OS=Mus musculus GN=G	88.48	18	2
P17710|HXK1_MOUSE	Hexokinase-1 OS=Mus musculus (	88.14	6	2
Q8K482|EMIL2_MOUSE	EMILIN-2 OS=Mus musculus GN=	86.29	8	2
Q9D0S9|HINT2_MOUSE	Histidine triad nucleotide-binding p	86.18	31	2
P62245|RS15A_MOUSE	40S ribosomal protein S15a OS=M	86.18	34	2
P51174|ACADL_MOUSE	Long-chain specific acyl-CoA dehy	85.46	21	2
P62849|RS24_MOUSE	40S ribosomal protein S24 OS=Mu	84.93	20	2
Q99KV1|DJB11_MOUSE	DnaJ homolog subfamily B membe	84.65	11	2
P62843|RS15_MOUSE	40S ribosomal protein S15 OS=Mu	83.57	15	2
Q91VR2|ATPG_MOUSE	ATP synthase subunit gamma, mit	83.44	7	2
P06745|G6PI_MOUSE	Glucose-6-phosphate isomerase O	83.39	9	2
Q8BIJ6|SYIM_MOUSE	Isoleucyl-tRNA synthetase, mitoch	82.88	10	2
P67984|RL22_MOUSE	60S ribosomal protein L22 OS=Mu	82.75	27	2
P97807|FUMH_MOUSE	Fumarate hydratase, mitochondria	82.72	26	2
P36536|SAR1A_MOUSE	GTP-binding protein SAR1a OS=M	82.69	16	2
Q9CQE8|CN166_MOUSE	UPF0568 protein C14orf166 homo	82.45	19	2
Q8BG05|ROA3_MOUSE	Heterogeneous nuclear ribonucleo	81.66	10	2
Q9CQA3|DHSB_MOUSE	Succinate dehydrogenase [ubiquin	80.72	9	2
P61804|DAD1_MOUSE	Dolichyl-diphosphooligosaccharide	80.15	19	2
Q9CQZ6|NDUB3_MOUSE	NADH dehydrogenase [ubiquinone	80.01	27	2
Q99KI0|ACON_MOUSE	Aconitate hydratase, mitochondrial	79.04	10	2
Q921X9|PDIA5_MOUSE	Protein disulfide-isomerase A5 OS	78.78	16	2
Q64133|AOFA_MOUSE	Amine oxidase [flavin-containing] A	78.48	10	2
Q99L13|3HIDH_MOUSE	3-hydroxyisobutyrate dehydrogena	77.24	9	2
Q9CR68|UCRI_MOUSE	Cytochrome b-c1 complex subunit	77.2	24	2
P29391|FRIL1_MOUSE	Ferritin light chain 1 OS=Mus musc	76.87	21	2

Q9CXW4|RL11_MOUSE	60S ribosomal protein L11 OS=Mu	76.66	15	2
Q9D8N0|EF1G_MOUSE	Elongation factor 1-gamma OS=Mu	76.14	11	2
Q9JM76|ARPC3_MOUSE	Actin-related protein 2/3 complex s	75.8	13	2
Q9CPP6|NDUA5_MOUSE	NADH dehydrogenase [ubiquinone	75.54	25	2
Q9CQR4|ACO13_MOUSE	Acyl-coenzyme A thioesterase 13 O	75.28	43	2
P10404|ENV1_MOUSE	MLV-related proviral Env polyprote	75.22	11	2
P11370|ENV2_MOUSE	Retrovirus-related Env polyprotein	75.22	2	2
P61022|CHP1_MOUSE	Calcium-binding protein p22 OS=M	75.13	11	2
Q61207|SAP_MOUSE	Sulfated glycoprotein 1 OS=Mus m	74.74	10	2
O88569|ROA2_MOUSE	Heterogeneous nuclear ribonucleo	74.13	20	2
Q61702|ITIH1_MOUSE	Inter-alpha-trypsin inhibitor heavy c	73.75	4	2
Q9Z2I9|SUCB1_MOUSE	Succinyl-CoA ligase [ADP-forming]	72.79	12	2
P28301|LYOX_MOUSE	Protein-lysine 6-oxidase OS=Mus r	72.7	8	2
P46935|NEDD4_MOUSE	E3 ubiquitin-protein ligase NEDD4	72.13	9	2
Q8K4L4|POF1B_MOUSE	Protein POF1B OS=Mus musculus	70.24	5	2
P23927|CRYAB_MOUSE	Alpha-crystallin B chain OS=Mus m	70.2	18	2
Q8BKG3|PTK7_MOUSE	Inactive tyrosine-protein kinase 7 O	68.51	5	2
Q9DAS9|GBG12_MOUSE	Guanine nucleotide-binding protein	67.59	22	2
Q61425|HCDH_MOUSE	Hydroxyacyl-coenzyme A dehydrog	67.29	14	2
P63085|MK01_MOUSE	Mitogen-activated protein kinase 1	66.66	20	2
Q63844|MK03_MOUSE	Mitogen-activated protein kinase 3	66.66	10	2
Q2PZL6|FAT4_MOUSE	Protocadherin Fat 4 OS=Mus musc	65.7	4	2
O09111|NDUBB_MOUSE	NADH dehydrogenase [ubiquinone	65.07	13	2
Q8R2Y8|PTH2_MOUSE	Peptidyl-tRNA hydrolase 2, mitoch	64.81	20	2
Q60692|PSB6_MOUSE	Proteasome subunit beta type-6 OS	64.69	9	2
P63001|RAC1_MOUSE	Ras-related C3 botulinum toxin sub	64.06	20	2
Q9CZY3|UB2V1_MOUSE	Ubiquitin-conjugating enzyme E2 v	63.86	35	2
Q9CPR4|RL17_MOUSE	60S ribosomal protein L17 OS=Mu	63.81	9	2
Q9CZD3|SYG_MOUSE	Glycyl-tRNA synthetase OS=Mus m	63.72	6	2
Q3UIU2|NDUB6_MOUSE	NADH dehydrogenase [ubiquinone	63.65	13	2
Q9CZW5|TOM70_MOUSE	Mitochondrial import receptor subu	63.56	11	2
P12032|TIMP1_MOUSE	Metalloproteinase inhibitor 1 OS=M	63.55	11	2
Q9JHR7|IDE_MOUSE	Insulin-degrading enzyme OS=Mus	63.22	6	2
Q920A5|RISC_MOUSE	Retinoid-inducible serine carboxyp	62.58	11	2
P55002|MFAP2_MOUSE	Microfibrillar-associated protein 2 O	61.8	9	2
P08905|LYZ2_MOUSE	Lysozyme C-2 OS=Mus musculus	61.51	16	2
Q9D1M7|FKB11_MOUSE	Peptidyl-prolyl cis-trans isomerase	61.33	10	2
Q9QUM9|PSA6_MOUSE	Proteasome subunit alpha type-6 O	60.75	14	2
P47754|CAZA2_MOUSE	F-actin-capping protein subunit alp	59.89	13	2
P59999|ARPC4_MOUSE	Actin-related protein 2/3 complex s	59.63	18	2
P00493|HPRT_MOUSE	Hypoxanthine-guanine phosphoribo	59.29	17	2
Q99M71|EPDR1_MOUSE	Mammalian ependymin-related pro	58.98	9	2
Q61941|NNTM_MOUSE	NAD(P) transhydrogenase, mitoch	54.41	4	2
Q9CZ13|QCR1_MOUSE	Cytochrome b-c1 complex subunit	53.81	7	2
Q07813|BAX_MOUSE	Apoptosis regulator BAX OS=Mus	52.34	12	2
O08999|LTBP2_MOUSE	Latent-transforming growth factor b	50.49	4	2
Q9QZE5|COPG_MOUSE	Coatomer subunit gamma OS=Mus	50.39	6	2
O35166|GOSR2_MOUSE	Golgi SNAP receptor complex mem	44.67	13	2
Q04857|CO6A1_MOUSE	Collagen alpha-1(VI) chain OS=Mu	44.59	6	2
Q52KG5|KI26A_MOUSE	Kinesin-like protein KIF26A OS=Mu	43.45	4	2
P62331|ARF6_MOUSE	ADP-ribosylation factor 6 OS=Mus	40.97	21	2
Q62315|JARD2_MOUSE	Protein Jumonji OS=Mus musculus	40.51	3	2
Q6GQT0|CC14A_MOUSE	Dual specificity protein phosphatas	39.51	2	2
Q5GIG6|TNI3K_MOUSE	Serine/threonine-protein kinase TN	38.89	4	2
P80315|TCPD_MOUSE	T-complex protein 1 subunit delta O	38.75	10	2

Q9CQE1|NPS3A_MOUSE	Protein NipSnap homolog 3A OS=I	37.78	17	2
P28741|KIF3A_MOUSE	Kinesin-like protein KIF3A OS=Mus	37.2	9	2
Q8BQM9|MD12L_MOUSE	Mediator of RNA polymerase II tran	36.65	3	2
Q8R0P8|ABHD8_MOUSE	Abhydrolase domain-containing pro	36.05	5	2
Q99LP6|GRPE1_MOUSE	GrpE protein homolog 1, mitochon	35.76	9	2
Q9ET54|PALLD_MOUSE	Palladin OS=Mus musculus GN=P	35.55	4	2
P26041|MOES_MOUSE	Moesin OS=Mus musculus GN=Ms	34.74	7	2
Q9QYX7|PCLO_MOUSE	Protein piccolo OS=Mus musculus	32.29	4	2
Q3V0M2|LRC36_MOUSE	Leucine-rich repeat-containing prot	32.25	3	2
P49025|CTRO_MOUSE	Citron Rho-interacting kinase OS=I	31.72	3	2
P97433|RGNEF_MOUSE	Rho-guanine nucleotide exchange	31.29	3	2
Q8BV57|SRCRL_MOUSE	Scavenger receptor cysteine-rich d	30.76	2	2
Q9JKY5|HIP1R_MOUSE	Huntingtin-interacting protein 1-rela	30.61	3	2
Q8BXR9|OSBL6_MOUSE	Oxysterol-binding protein-related p	30.55	2	2
P58545|BTBD3_MOUSE	BTB/POZ domain-containing prote	29.84	3	2
Q6A026|PDS5A_MOUSE	Sister chromatid cohesion protein F	29.42	4	2
A2AAJ9|OBSCN_MOUSE	Obscurin OS=Mus musculus GN=O	29	2	2
Q7TN37|TRPM4_MOUSE	Transient receptor potential cation	29	5	2
Q99MZ6|MYO7B_MOUSE	Myosin-VIIb OS=Mus musculus GN	28.07	9	2
Q9D0K0|TBCD7_MOUSE	TBC1 domain family member 7 OS	27.8	4	2
Q8K4G1|LTBP4_MOUSE	Latent-transforming growth factor b	27.49	2	2

Table A1.8 Bridge ECM Protein Identifications. List of all proteins identified in Bridge ECM with corresponding accession, description, PEAKS score, unique peptide numbers, and coverage (in %).

Accession	Description	Score	Coverage (%)	#Unique
P02768|ALBU_HUMAN	Serum albumin OS=Homo sapiens (	380.41	61	45
P01308|INS_HUMAN	Insulin OS=Homo sapiens GN=INS	246.91	55	11
P01008|ANT3_HUMAN	Antithrombin-III OS=Homo sapiens (	203.89	42	10
P02753|RET4_HUMAN	Retinol-binding protein 4 OS=Homo	242.54	42	7
P02774|VTDB_HUMAN	Vitamin D-binding protein OS=Homo	240.19	40	7
P02647|APOA1_HUMAN	Apolipoprotein A-I OS=Homo sapien	186.29	39	4
Q16270|IBP7_HUMAN	Insulin-like growth factor-binding pro	158.22	38	4
P05121|PAI1_HUMAN	Plasminogen activator inhibitor 1 OS	156.04	33	4
P02751|FINC_HUMAN	Fibronectin OS=Homo sapiens GN=	154.81	14	4
Q15582|BGH3_HUMAN	Transforming growth factor-beta-ind	153.91	27	4
P61769|B2MG_HUMAN	Beta-2-microglobulin OS=Homo sap	139.26	59	4
P09486|SPRC_HUMAN	SPARC OS=Homo sapiens GN=SP/	180.39	41	3
P01024|CO3_HUMAN	Complement C3 OS=Homo sapiens	162.77	16	3
P69905|HBA_HUMAN	Hemoglobin subunit alpha OS=Hom	159.17	53	3
P06727|APOA4_HUMAN	Apolipoprotein A-IV OS=Homo sapie	151.78	20	3
P08697|A2AP_HUMAN	Alpha-2-antiplasmin OS=Homo sapi	145.85	21	3
P02656|APOC3_HUMAN	Apolipoprotein C-III OS=Homo sapie	138.57	25	3
Q15063|POSTN_HUMAN	Periostin OS=Homo sapiens GN=PC	127.09	23	3
P01861|IGHG4_HUMAN	Ig gamma-4 chain C region OS=Hor	105.87	25	3
P01859|IGHG2_HUMAN	Ig gamma-2 chain C region OS=Hor	105.87	27	3
P01857|IGHG1_HUMAN	Ig gamma-1 chain C region OS=Hor	105.87	28	3
P0C0L4|CO4A_HUMAN	Complement C4-A OS=Homo sapie	126.79	17	2
P0C0L5|CO4B_HUMAN	Complement C4-B OS=Homo sapie	126.79	17	2
P05546|HEP2_HUMAN	Heparin cofactor 2 OS=Homo sapier	95.37	2	2
Q9UNH5|CC14A_HUMAN	Dual specificity protein phosphatase	44.58	8	2

Table A1.9 H9 hESC CMTX Protein Identifications. List of all proteins identified in CMTX from H9 hESCs with corresponding accession, description, PEAKS score, unique peptide numbers, and coverage (in %).

Accession	Description	Score	Coverage (%)	#Unique
P18206|VINC_HUMAN	Vinculin OS=Homo sapiens GN=VCL PE	336.02	71	46
P49327|FAS_HUMAN	Fatty acid synthase OS=Homo sapiens G	335.58	49	39
P55072|TERA_HUMAN	Transitional endoplasmic reticulum ATPa	309.23	62	34
P04406|G3P_HUMAN	Glyceraldehyde-3-phosphate dehydroger	363.29	78	32
Q13813|SPTA2_HUMAN	Spectrin alpha chain, brain OS=Homo sa	310.79	58	32
P21333|FLNA_HUMAN	Filamin-A OS=Homo sapiens GN=FLNA	302.94	40	32
P02649|APOE_HUMAN	Apolipoprotein E OS=Homo sapiens GN=	308.11	90	28
P62258|1433E_HUMAN	14-3-3 protein epsilon OS=Homo sapien	320.22	72	26
P35579|MYH9_HUMAN	Myosin-9 OS=Homo sapiens GN=MYH9	300.44	56	25
P14625|ENPL_HUMAN	Endoplasmin OS=Homo sapiens GN=HS	284.56	64	24
P13639|EF2_HUMAN	Elongation factor 2 OS=Homo sapiens G	274.58	61	24
P53396|ACLY_HUMAN	ATP-citrate synthase OS=Homo sapiens	293.82	59	23
P07900|HS90A_HUMAN	Heat shock protein HSP 90-alpha OS=H	389.97	83	22
P07195|LDHB_HUMAN	L-lactate dehydrogenase B chain OS=Ho	303.38	72	21
P08670|VIME_HUMAN	Vimentin OS=Homo sapiens GN=VIM PE	265.5	66	21
P14618|KPYM_HUMAN	Pyruvate kinase isozymes M1/M2 OS=H	290.21	81	20
P04075|ALDOA_HUMAN	Fructose-bisphosphate aldolase A OS=H	262.37	69	20
P08238|HS90B_HUMAN	Heat shock protein HSP 90-beta OS=Ho	413.63	89	19
O75874|IDHC_HUMAN	Isocitrate dehydrogenase [NADP] cytopla	321.85	75	19
P30041|PRDX6_HUMAN	Peroxiredoxin-6 OS=Homo sapiens GN=	245.25	76	19
P63104|1433Z_HUMAN	14-3-3 protein zeta/delta OS=Homo sapi	304.18	84	18
P00338|LDHA_HUMAN	L-lactate dehydrogenase A chain OS=Ho	289.55	58	18
P13010|XRCC5_HUMAN	X-ray repair cross-complementing protei	251.16	66	18
P23142|FBLN1_HUMAN	Fibulin-1 OS=Homo sapiens GN=FBLN1	246.74	42	18
P62805|H4_HUMAN	Histone H4 OS=Homo sapiens GN=HIST	236.13	58	18
P68104|EF1A1_HUMAN	Elongation factor 1-alpha 1 OS=Homo sa	301.38	64	17
Q5VTE0|EF1A3_HUMAN	Putative elongation factor 1-alpha-like 3	301.38	62	17
P50454|SERPH_HUMAN	Serpin H1 OS=Homo sapiens GN=SERP	284.9	79	17
P07355|ANXA2_HUMAN	Annexin A2 OS=Homo sapiens GN=ANX	282.38	75	17
P06733|ENOA_HUMAN	Alpha-enolase OS=Homo sapiens GN=E	271.08	71	17
P08758|ANXA5_HUMAN	Annexin A5 OS=Homo sapiens GN=ANX	267.87	71	17
Q9HB71|CYBP_HUMAN	Calcyclin-binding protein OS=Homo sapi	247.66	80	17
P35580|MYH10_HUMAN	Myosin-10 OS=Homo sapiens GN=MYH	291.87	55	16
P62195|PRS8_HUMAN	26S protease regulatory subunit 8 OS=H	268.24	71	16
P29401|TKT_HUMAN	Transketolase OS=Homo sapiens GN=T	267.48	58	16
Q01995|TAGL_HUMAN	Transgelin OS=Homo sapiens GN=TAG	255.39	91	16
O75369|FLNB_HUMAN	Filamin-B OS=Homo sapiens GN=FLNB	249.62	37	16
P61247|RS3A_HUMAN	40S ribosomal protein S3a OS=Homo sa	247.05	65	16
P12956|XRCC6_HUMAN	X-ray repair cross-complementing protei	241.39	58	16
Q99623|PHB2_HUMAN	Prohibitin-2 OS=Homo sapiens GN=PHB	236.99	66	16
P63261|ACTG_HUMAN	Actin, cytoplasmic 2 OS=Homo sapiens	411.37	89	15
P12814|ACTN1_HUMAN	Alpha-actinin-1 OS=Homo sapiens GN=A	288.91	71	15
P19338|NUCL_HUMAN	Nucleolin OS=Homo sapiens GN=NCL P	283.04	74	15
P22314|UBA1_HUMAN	Ubiquitin-like modifier-activating enzyme	275.66	50	15
P11021|GRP78_HUMAN	78 kDa glucose-regulated protein OS=H	263.96	54	15
P05455|LA_HUMAN	Lupus La protein OS=Homo sapiens GN	262.72	65	14
Q01105|SET_HUMAN	Protein SET OS=Homo sapiens GN=SET	253.98	53	14
P49321|NASP_HUMAN	Nuclear autoantigenic sperm protein OS	238.83	57	14
P31939|PUR9_HUMAN	Bifunctional purine biosynthesis protein P	227.41	52	14
Q92626|PXDN_HUMAN	Peroxidasin homolog OS=Homo sapiens	224.22	34	14
P46777|RL5_HUMAN	60S ribosomal protein L5 OS=Homo sap	216.48	56	14
P60174|TPIS_HUMAN	Triosephosphate isomerase OS=Homo s	247.24	68	13
P62424|RL7A_HUMAN	60S ribosomal protein L7a OS=Homo sa	245.96	73	13
P28074|PSB5_HUMAN	Proteasome subunit beta type-5 OS=Hor	239.92	48	13

P62937|PPIA_HUMAN	Peptidyl-prolyl cis-trans isomerase A OS=	238.61	74	13
P23396|RS3_HUMAN	40S ribosomal protein S3 OS=Homo sap	214.29	71	13
Q14697|GANAB_HUMAN	Neutral alpha-glucosidase AB OS=Homo	194.72	37	13
P29692|EF1D_HUMAN	Elongation factor 1-delta OS=Homo sapi	191.68	63	13
P11142|HSP7C_HUMAN	Heat shock cognate 71 kDa protein OS=	285.01	63	12
P12268|IMDH2_HUMAN	Inosine-5'-monophosphate dehydrogena	248.93	62	12
P15311|EZRI_HUMAN	Ezrin OS=Homo sapiens GN=EZR PE=1	242.92	65	12
Q15008|PSMD6_HUMAN	26S proteasome non-ATPase regulatory	225.22	59	12
P62906|RL10A_HUMAN	60S ribosomal protein L10a OS=Homo s	220.28	51	12
Q01518|CAP1_HUMAN	Adenylyl cyclase-associated protein 1 OS	219.12	64	12
P10909|CLUS_HUMAN	Clusterin OS=Homo sapiens GN=CLU P	218.1	47	12
P26599|PTBP1_HUMAN	Polypyrimidine tract-binding protein 1 OS	211.9	45	12
P78371|TCPB_HUMAN	T-complex protein 1 subunit beta OS=Ho	206.5	63	12
P50990|TCPQ_HUMAN	T-complex protein 1 subunit theta OS=H	197.99	61	12
P62269|RS18_HUMAN	40S ribosomal protein S18 OS=Homo sa	180.58	65	12
Q9BWD1|THIC_HUMAN	Acetyl-CoA acetyltransferase, cytosolic C	171.83	57	12
O14818|PSA7_HUMAN	Proteasome subunit alpha type-7 OS=Ho	283.39	78	11
P51665|PSD7_HUMAN	26S proteasome non-ATPase regulatory	262.72	63	11
P34932|HSP74_HUMAN	Heat shock 70 kDa protein 4 OS=Homo	258.03	61	11
P05067|A4_HUMAN	Amyloid beta A4 protein OS=Homo sapie	245.23	42	11
P06748|NPM_HUMAN	Nucleophosmin OS=Homo sapiens GN=	244.29	58	11
Q9BT78|CSN4_HUMAN	COP9 signalosome complex subunit 4 O	228.48	65	11
Q15019|SEPT2_HUMAN	Septin-2 OS=Homo sapiens GN=SEPT2	227.76	68	11
P62277|RS13_HUMAN	40S ribosomal protein S13 OS=Homo sa	210.38	60	11
O00231|PSD11_HUMAN	26S proteasome non-ATPase regulatory	208.69	45	11
P33993|MCM7_HUMAN	DNA replication licensing factor MCM7 C	197.51	53	11
Q14152|EIF3A_HUMAN	Eukaryotic translation initiation factor 3 s	193.07	29	11
P31948|STIP1_HUMAN	Stress-induced-phosphoprotein 1 OS=Ho	189.36	47	11
Q01082|SPTB2_HUMAN	Spectrin beta chain, brain 1 OS=Homo s	187.11	24	11
P30101|PDIA3_HUMAN	Protein disulfide-isomerase A3 OS=Hom	187.11	44	11
O43175|SERA_HUMAN	D-3-phosphoglycerate dehydrogenase O	226.38	46	10
P08865|RSSA_HUMAN	40S ribosomal protein SA OS=Homo sap	217.03	50	10
P62333|PRS10_HUMAN	26S protease regulatory subunit 10B OS	204.95	63	10
P35998|PRS7_HUMAN	26S protease regulatory subunit 7 OS=H	193.65	49	10
P52209|6PGD_HUMAN	6-phosphogluconate dehydrogenase, de	183.14	45	10
P05388|RLA0_HUMAN	60S acidic ribosomal protein P0 OS=Hor	177.82	48	10
P49368|TCPG_HUMAN	T-complex protein 1 subunit gamma OS=	158.53	31	10
P61254|RL26_HUMAN	60S ribosomal protein L26 OS=Homo sa	145.76	63	10
P07437|TBB5_HUMAN	Tubulin beta chain OS=Homo sapiens G	349.97	77	9
P09211|GSTP1_HUMAN	Glutathione S-transferase P OS=Homo s	238.92	68	9
P27348|1433T_HUMAN	14-3-3 protein theta OS=Homo sapiens C	231.58	77	9
P61978|HNRPK_HUMAN	Heterogeneous nuclear ribonucleoprotei	228.4	68	9
Q04917|1433F_HUMAN	14-3-3 protein eta OS=Homo sapiens GN	220.77	63	9
Q9Y490|TLN1_HUMAN	Talin-1 OS=Homo sapiens GN=TLN1 PE	212.9	47	9
P04792|HSPB1_HUMAN	Heat shock protein beta-1 OS=Homo sa	205.19	68	9
P62826|RAN_HUMAN	GTP-binding nuclear protein Ran OS=Ho	205.06	54	9
Q9H9Z2|LN28A_HUMAN	Protein lin-28 homolog A OS=Homo sapi	202.17	54	9
Q08431|MFGM_HUMAN	Lactadherin OS=Homo sapiens GN=MFG	201.22	32	9
P11047|LAMC1_HUMAN	Laminin subunit gamma-1 OS=Homo sa	190.38	26	9
P17980|PRS6A_HUMAN	26S protease regulatory subunit 6A OS=	180.2	57	9
P25391|LAMA1_HUMAN	Laminin subunit alpha-1 OS=Homo sapie	175.98	19	9
P26641|EF1G_HUMAN	Elongation factor 1-gamma OS=Homo sa	157.43	36	9
P61160|ARP2_HUMAN	Actin-related protein 2 OS=Homo sapien	154.07	43	9
Q9Y617|SERC_HUMAN	Phosphoserine aminotransferase OS=Ho	129.68	38	9
O43707|ACTN4_HUMAN	Alpha-actinin-4 OS=Homo sapiens GN=A	286.21	68	8

P67936|TPM4_HUMAN	Tropomyosin alpha-4 chain OS=Homo s	271.24	69	8
P25787|PSA2_HUMAN	Proteasome subunit alpha type-2 OS=H	233.19	60	8
P31946|1433B_HUMAN	14-3-3 protein beta/alpha OS=Homo sap	228.19	62	8
P07737|PROF1_HUMAN	Profilin-1 OS=Homo sapiens GN=PFN1	220.45	69	8
P22626|ROA2_HUMAN	Heterogeneous nuclear ribonucleoprotei	207.89	56	8
Q92598|HS105_HUMAN	Heat shock protein 105 kDa OS=Homo s	207.71	44	8
P60900|PSA6_HUMAN	Proteasome subunit alpha type-6 OS=H	202.72	53	8
Q9Y224|CN166_HUMAN	UPF0568 protein C14orf166 OS=Homo s	197.1	45	8
P62314|SMD1_HUMAN	Small nuclear ribonucleoprotein Sm D1	188.31	65	8
Q9Y265|RUVB1_HUMAN	RuvB-like 1 OS=Homo sapiens GN=RU	188.12	62	8
Q9Y4L1|HYOU1_HUMAN	Hypoxia up-regulated protein 1 OS=Hom	185.61	39	8
Q9Y266|NUDC_HUMAN	Nuclear migration protein nudC OS=Hom	180.71	58	8
P20618|PSB1_HUMAN	Proteasome subunit beta type-1 OS=Ho	178.86	51	8
Q9P289|MST4_HUMAN	Serine/threonine-protein kinase MST4 O	172.08	30	8
P07942|LAMB1_HUMAN	Laminin subunit beta-1 OS=Homo sapie	163.14	32	8
P62249|RS16_HUMAN	40S ribosomal protein S16 OS=Homo sa	162	46	8
Q12906|ILF3_HUMAN	Interleukin enhancer-binding factor 3 OS	158.13	32	8
P40227|TCPZ_HUMAN	T-complex protein 1 subunit zeta OS=H	157.28	40	8
Q15907|RB11B_HUMAN	Ras-related protein Rab-11B OS=Homo	134.75	48	8
Q99613|EIF3C_HUMAN	Eukaryotic translation initiation factor 3 s	106.16	16	8
Q00610|CLH1_HUMAN	Clathrin heavy chain 1 OS=Homo sapien	262.2	47	7
P12277|KCRB_HUMAN	Creatine kinase B-type OS=Homo sapie	228.22	54	7
P32119|PRDX2_HUMAN	Peroxiredoxin-2 OS=Homo sapiens GN=	197.38	69	7
Q15084|PDIA6_HUMAN	Protein disulfide-isomerase A6 OS=Hom	193.64	44	7
P22234|PUR6_HUMAN	Multifunctional protein ADE2 OS=Homo	190.82	46	7
P43686|PRS6B_HUMAN	26S protease regulatory subunit 6B OS=	189.68	56	7
P23246|SFPQ_HUMAN	Splicing factor, proline- and glutamine-ric	188.3	44	7
P26038|MOES_HUMAN	Moesin OS=Homo sapiens GN=MSN PE	187.8	51	7
O60664|PLIN3_HUMAN	Perilipin-3 OS=Homo sapiens GN=PLIN3	185.14	41	7
O43809|CPSF5_HUMAN	Cleavage and polyadenylation specificity	179.4	46	7
P25789|PSA4_HUMAN	Proteasome subunit alpha type-4 OS=H	173.83	42	7
Q9UKK9|NUDT5_HUMAN	ADP-sugar pyrophosphatase OS=Homo	169.15	35	7
Q7KZF4|SND1_HUMAN	Staphylococcal nuclease domain-contain	168.24	35	7
P37837|TALDO_HUMAN	Transaldolase OS=Homo sapiens GN=T	160.44	39	7
P14543|NID1_HUMAN	Nidogen-1 OS=Homo sapiens GN=NID1	159.74	40	7
P11940|PABP1_HUMAN	Polyadenylate-binding protein 1 OS=Hom	158.35	42	7
Q02790|FKBP4_HUMAN	Peptidyl-prolyl cis-trans isomerase FKBP	157.52	34	7
P62081|RS7_HUMAN	40S ribosomal protein S7 OS=Homo sap	157.04	39	7
P09661|RU2A_HUMAN	U2 small nuclear ribonucleoprotein A' OS	156.58	28	7
P02751|FINC_HUMAN	Fibronectin OS=Homo sapiens GN=FN1	155.38	19	7
P39019|RS19_HUMAN	40S ribosomal protein S19 OS=Homo sa	150.74	68	7
Q99832|TCPH_HUMAN	T-complex protein 1 subunit eta OS=Hom	149.16	45	7
Q9Y230|RUVB2_HUMAN	RuvB-like 2 OS=Homo sapiens GN=RU	146.97	29	7
Q9Y3I0|RTCB_HUMAN	tRNA-splicing ligase RtcB homolog OS=	143.49	34	7
P25786|PSA1_HUMAN	Proteasome subunit alpha type-1 OS=H	141.46	35	7
P54577|SYYC_HUMAN	Tyrosyl-tRNA synthetase, cytoplasmic O	141.08	46	7
O15144|ARPC2_HUMAN	Actin-related protein 2/3 complex subunit	139.1	40	7
P09486|SPRC_HUMAN	SPARC OS=Homo sapiens GN=SPARC	135.89	24	7
P06753|TPM3_HUMAN	Tropomyosin alpha-3 chain OS=Homo s	293.76	60	6
P07910|HNRPC_HUMAN	Heterogeneous nuclear ribonucleoprotei	214.86	53	6
P61981|1433G_HUMAN	14-3-3 protein gamma OS=Homo sapien	213.26	63	6
P28066|PSA5_HUMAN	Proteasome subunit alpha type-5 OS=H	207.13	60	6
P02792|FRIL_HUMAN	Ferritin light chain OS=Homo sapiens GN	203.6	51	6
Q13162|PRDX4_HUMAN	Peroxiredoxin-4 OS=Homo sapiens GN=	199.84	52	6
Q96KP4|CNDP2_HUMAN	Cytosolic non-specific dipeptidase OS=H	195.71	58	6

P00558|PGK1_HUMAN	Phosphoglycerate kinase 1 OS=Homo sa	192.74	61	6
P35241|RADI_HUMAN	Radixin OS=Homo sapiens GN=RDX PE	188.72	44	6
P09972|ALDOC_HUMAN	Fructose-bisphosphate aldolase C OS=H	188.17	62	6
P62701|RS4X_HUMAN	40S ribosomal protein S4, X isoform OS=	187.43	51	6
P48643|TCPE_HUMAN	T-complex protein 1 subunit epsilon OS=	183.95	72	6
P25398|RS12_HUMAN	40S ribosomal protein S12 OS=Homo sa	182.76	80	6
O00299|CLIC1_HUMAN	Chloride intracellular channel protein 1 O	179.56	51	6
Q99598|TSNAX_HUMAN	Translin-associated protein X OS=Homo	178.92	57	6
P50991|TCPD_HUMAN	T-complex protein 1 subunit delta OS=H	177.82	49	6
P67809|YBOX1_HUMAN	Nuclease-sensitive element-binding prote	176.18	38	6
Q06830|PRDX1_HUMAN	Peroxiredoxin-1 OS=Homo sapiens GN=	175.86	54	6
Q16851|UGPA_HUMAN	UTP--glucose-1-phosphate uridylyltransf	173.41	43	6
Q99536|VAT1_HUMAN	Synaptic vesicle membrane protein VAT-	172.83	66	6
P62750|RL23A_HUMAN	60S ribosomal protein L23a OS=Homo s	170.76	50	6
P49720|PSB3_HUMAN	Proteasome subunit beta type-3 OS=Hor	169.9	67	6
P23528|COF1_HUMAN	Cofilin-1 OS=Homo sapiens GN=CFL1 P	166.71	57	6
Q96IZ0|PAWR_HUMAN	PRKC apoptosis WT1 regulator protein C	164.92	46	6
P25205|MCM3_HUMAN	DNA replication licensing factor MCM3 C	163.19	32	6
P62888|RL30_HUMAN	60S ribosomal protein L30 OS=Homo sa	161.64	66	6
Q13561|DCTN2_HUMAN	Dynactin subunit 2 OS=Homo sapiens G	160.54	46	6
P08708|RS17_HUMAN	40S ribosomal protein S17 OS=Homo sa	158.26	65	6
P13797|PLST_HUMAN	Plastin-3 OS=Homo sapiens GN=PLS3 P	158.08	34	6
P10809|CH60_HUMAN	60 kDa heat shock protein, mitochondria	158	56	6
P61604|CH10_HUMAN	10 kDa heat shock protein, mitochondria	157.8	76	6
P37802|TAGL2_HUMAN	Transgelin-2 OS=Homo sapiens GN=TA	154.49	46	6
P46940|IQGA1_HUMAN	Ras GTPase-activating-like protein IQGA	153.32	36	6
P62987|RL40_HUMAN	Ubiquitin-60S ribosomal protein L40 OS=	151.42	73	6
P0CG48|UBC_HUMAN	Polyubiquitin-C OS=Homo sapiens GN=U	151.42	44	6
P62979|RS27A_HUMAN	Ubiquitin-40S ribosomal protein S27a OS	151.42	50	6
P0CG47|UBB_HUMAN	Polyubiquitin-B OS=Homo sapiens GN=U	151.42	82	6
P11586|C1TC_HUMAN	C-1-tetrahydrofolate synthase, cytoplasm	150.42	36	6
P62263|RS14_HUMAN	40S ribosomal protein S14 OS=Homo sa	146.9	46	6
Q9Y295|DRG1_HUMAN	Developmentally-regulated GTP-binding	146.21	40	6
Q9P2J5|SYLC_HUMAN	Leucyl-tRNA synthetase, cytoplasmic OS	144.85	31	6
P27816|MAP4_HUMAN	Microtubule-associated protein 4 OS=Ho	139.1	35	6
P52788|SPSY_HUMAN	Spermine synthase OS=Homo sapiens G	133.44	36	6
P62851|RS25_HUMAN	40S ribosomal protein S25 OS=Homo sa	133.38	39	6
Q92945|FUBP2_HUMAN	Far upstream element-binding protein 2 (	132.08	31	6
Q14204|DYHC1_HUMAN	Cytoplasmic dynein 1 heavy chain 1 OS=	131.3	16	6
P14314|GLU2B_HUMAN	Glucosidase 2 subunit beta OS=Homo s	131.01	23	6
P17987|TCPA_HUMAN	T-complex protein 1 subunit alpha OS=H	124.66	35	6
P84243|H33_HUMAN	Histone H3.3 OS=Homo sapiens GN=H3	118.62	47	6
P68431|H31_HUMAN	Histone H3.1 OS=Homo sapiens GN=HI	118.62	50	6
Q71DI3|H32_HUMAN	Histone H3.2 OS=Homo sapiens GN=HI	118.62	50	6
Q16695|H31T_HUMAN	Histone H3.1t OS=Homo sapiens GN=H	118.62	50	6
P18077|RL35A_HUMAN	60S ribosomal protein L35a OS=Homo s	105.88	44	6
P09493|TPM1_HUMAN	Tropomyosin alpha-1 chain OS=Homo s	288.32	69	5
P09651|ROA1_HUMAN	Heterogeneous nuclear ribonucleoprotei	278.47	57	5
P18669|PGAM1_HUMAN	Phosphoglycerate mutase 1 OS=Homo s	245.89	85	5
P60842|IF4A1_HUMAN	Eukaryotic initiation factor 4A-I OS=Hom	216.02	60	5
P50395|GDIB_HUMAN	Rab GDP dissociation inhibitor beta OS=	209.42	58	5
O60506|HNRPQ_HUMAN	Heterogeneous nuclear ribonucleoprotei	197.27	41	5
Q16181|SEPT7_HUMAN	Septin-7 OS=Homo sapiens GN=SEPT7	185.8	60	5
P09429|HMGB1_HUMAN	High mobility group protein B1 OS=Hom	172.39	46	5
P61289|PSME3_HUMAN	Proteasome activator complex subunit 3	172.33	56	5

P06744|G6PI_HUMAN	Glucose-6-phosphate isomerase OS=Ho	166.32	31	5
P51149|RAB7A_HUMAN	Ras-related protein Rab-7a OS=Homo s	164.95	35	5
P55209|NP1L1_HUMAN	Nucleosome assembly protein 1-like 1 O	163.61	35	5
Q13263|TIF1B_HUMAN	Transcription intermediary factor 1-beta	163.39	27	5
P08133|ANXA6_HUMAN	Annexin A6 OS=Homo sapiens GN=ANX	159.78	38	5
Q8NC51|PAIRB_HUMAN	Plasminogen activator inhibitor 1 RNA-bi	158.06	53	5
P23526|SAHH_HUMAN	Adenosylhomocysteinase OS=Homo sap	157.63	40	5
P08195|4F2_HUMAN	4F2 cell-surface antigen heavy chain OS	157.23	28	5
P61353|RL27_HUMAN	60S ribosomal protein L27 OS=Homo sa	156.91	68	5
P02794|FRIH_HUMAN	Ferritin heavy chain OS=Homo sapiens	155.21	45	5
P09874|PARP1_HUMAN	Poly [ADP-ribose] polymerase 1 OS=Hor	153.6	24	5
P37108|SRP14_HUMAN	Signal recognition particle 14 kDa protein	153.37	71	5
Q7L2H7|EIF3M_HUMAN	Eukaryotic translation initiation factor 3 s	153.35	35	5
Q8N474|SFRP1_HUMAN	Secreted frizzled-related protein 1 OS=H	152.97	46	5
Q14566|MCM6_HUMAN	DNA replication licensing factor MCM6 O	152.81	35	5
Q15717|ELAV1_HUMAN	ELAV-like protein 1 OS=Homo sapiens	152.1	33	5
P39060|COIA1_HUMAN	Collagen alpha-1(XVIII) chain OS=Homo	151.31	31	5
P17174|AATC_HUMAN	Aspartate aminotransferase, cytoplasmic	149.96	37	5
O75347|TBCA_HUMAN	Tubulin-specific chaperone A OS=Homo	149.6	69	5
P30050|RL12_HUMAN	60S ribosomal protein L12 OS=Homo sa	149.08	46	5
P62316|SMD2_HUMAN	Small nuclear ribonucleoprotein Sm D2	149.08	61	5
P50502|F10A1_HUMAN	Hsc70-interacting protein OS=Homo sap	148.29	48	5
P63244|GBLP_HUMAN	Guanine nucleotide-binding protein subu	145.32	30	5
P15880|RS2_HUMAN	40S ribosomal protein S2 OS=Homo sap	144.24	40	5
P43487|RANG_HUMAN	Ran-specific GTPase-activating protein	143.31	33	5
P63162|RSMN_HUMAN	Small nuclear ribonucleoprotein-associat	141.93	45	5
P14678|RSMB_HUMAN	Small nuclear ribonucleoprotein-associat	141.93	40	5
Q9Y2Z0|SUGT1_HUMAN	Suppressor of G2 allele of SKP1 homolo	139.32	30	5
P16949|STMN1_HUMAN	Stathmin OS=Homo sapiens GN=STMN	139.17	38	5
P49721|PSB2_HUMAN	Proteasome subunit beta type-2 OS=Hor	136.22	38	5
Q15691|MARE1_HUMAN	Microtubule-associated protein RP/EB fa	136.04	26	5
P78417|GSTO1_HUMAN	Glutathione S-transferase omega-1 OS=	133.58	33	5
P62244|RS15A_HUMAN	40S ribosomal protein S15a OS=Homo s	132.41	48	5
P61758|PFD3_HUMAN	Prefoldin subunit 3 OS=Homo sapiens G	132.03	52	5
O43399|TPD54_HUMAN	Tumor protein D54 OS=Homo sapiens G	131.62	50	5
P46926|GNPI1_HUMAN	Glucosamine-6-phosphate isomerase 1	130.85	39	5
P00491|PNPH_HUMAN	Purine nucleoside phosphorylase OS=Ho	129.66	35	5
Q05682|CALD1_HUMAN	Caldesmon OS=Homo sapiens GN=CAL	129.12	23	5
P50914|RL14_HUMAN	60S ribosomal protein L14 OS=Homo sa	128.61	50	5
P35232|PHB_HUMAN	Prohibitin OS=Homo sapiens GN=PHB P	126.96	45	5
Q02878|RL6_HUMAN	60S ribosomal protein L6 OS=Homo sap	124.55	44	5
P59998|ARPC4_HUMAN	Actin-related protein 2/3 complex subunit	122.31	31	5
P14868|SYDC_HUMAN	Aspartyl-tRNA synthetase, cytoplasmic	121.1	19	5
Q9P2E9|RRBP1_HUMAN	Ribosome-binding protein 1 OS=Homo s	120.34	17	5
P98160|PGBM_HUMAN	Basement membrane-specific heparan s	118.87	9	5
P49736|MCM2_HUMAN	DNA replication licensing factor MCM2	118.52	28	5
P13667|PDIA4_HUMAN	Protein disulfide-isomerase A4 OS=Hom	118.29	21	5
Q8N163|K1967_HUMAN	Protein KIAA1967 OS=Homo sapiens GN	117.88	27	5
O43242|PSMD3_HUMAN	26S proteasome non-ATPase regulatory	116.46	30	5
P82979|SARNP_HUMAN	SAP domain-containing ribonucleoprotein	112.71	42	5
P62899|RL31_HUMAN	60S ribosomal protein L31 OS=Homo sa	110.06	49	5
P30044|PRDX5_HUMAN	Peroxiredoxin-5, mitochondrial OS=Hom	105.91	49	5
P46781|RS9_HUMAN	40S ribosomal protein S9 OS=Homo sap	105.12	45	5
Q14914|PTGR1_HUMAN	Prostaglandin reductase 1 OS=Homo sa	102	17	5
Q9UHD8|SEPT9_HUMAN	Septin-9 OS=Homo sapiens GN=SEPT9	96.07	12	5

Q9BYT8|NEUL_HUMAN	Neurolysin, mitochondrial OS=Homo sap	89.07	16	5
Q562R1|ACTBL_HUMAN	Beta-actin-like protein 2 OS=Homo sapie	283.36	65	4
P15531|NDKA_HUMAN	Nucleoside diphosphate kinase A OS=H	209.18	81	4
P84077|ARF1_HUMAN	ADP-ribosylation factor 1 OS=Homo sap	198.78	68	4
P61204|ARF3_HUMAN	ADP-ribosylation factor 3 OS=Homo sap	198.78	67	4
P61158|ARP3_HUMAN	Actin-related protein 3 OS=Homo sapien	186.94	55	4
A6NL28|TPM3L_HUMAN	Putative tropomyosin alpha-3 chain-like p	177.37	30	4
P06493|CDK1_HUMAN	Cyclin-dependent kinase 1 OS=Homo sa	176.85	45	4
P62917|RL8_HUMAN	60S ribosomal protein L8 OS=Homo sap	163.71	49	4
P98095|FBLN2_HUMAN	Fibulin-2 OS=Homo sapiens GN=FBLN2	161.78	22	4
Q9NTK5|OLA1_HUMAN	Obg-like ATPase 1 OS=Homo sapiens G	160.13	39	4
P05198|IF2A_HUMAN	Eukaryotic translation initiation factor 2 s	158.5	55	4
P14324|FPPS_HUMAN	Farnesyl pyrophosphate synthase OS=H	156.36	43	4
P46778|RL21_HUMAN	60S ribosomal protein L21 OS=Homo sa	155.43	37	4
Q12904|AIMP1_HUMAN	Aminoacyl tRNA synthase complex-intera	154.01	35	4
P54687|BCAT1_HUMAN	Branched-chain-amino-acid aminotransfe	148.58	35	4
Q13310|PABP4_HUMAN	Polyadenylate-binding protein 4 OS=Hom	148.03	38	4
Q15365|PCBP1_HUMAN	Poly(rC)-binding protein 1 OS=Homo sap	147.77	42	4
P62841|RS15_HUMAN	40S ribosomal protein S15 OS=Homo sa	146.2	57	4
Q96FW1|OTUB1_HUMAN	Ubiquitin thioesterase OTUB1 OS=Homo	145.27	56	4
P62191|PRS4_HUMAN	26S protease regulatory subunit 4 OS=H	144.04	49	4
P40925|MDHC_HUMAN	Malate dehydrogenase, cytoplasmic OS=	143.7	36	4
P18621|RL17_HUMAN	60S ribosomal protein L17 OS=Homo sa	142.87	36	4
P46783|RS10_HUMAN	40S ribosomal protein S10 OS=Homo sa	140.61	65	4
P62847|RS24_HUMAN	40S ribosomal protein S24 OS=Homo sa	139.36	47	4
P62158|CALM_HUMAN	Calmodulin OS=Homo sapiens GN=CAL	139.12	42	4
P07339|CATD_HUMAN	Cathepsin D OS=Homo sapiens GN=CT	138.13	35	4
Q9UHV9|PFD2_HUMAN	Prefoldin subunit 2 OS=Homo sapiens G	137.32	49	4
P12429|ANXA3_HUMAN	Annexin A3 OS=Homo sapiens GN=ANX	136.03	25	4
P40926|MDHM_HUMAN	Malate dehydrogenase, mitochondrial OS	134.76	52	4
Q14974|IMB1_HUMAN	Importin subunit beta-1 OS=Homo sapie	133.4	21	4
O00487|PSDE_HUMAN	26S proteasome non-ATPase regulatory	132	59	4
P16401|H15_HUMAN	Histone H1.5 OS=Homo sapiens GN=HI	130.92	55	4
Q15366|PCBP2_HUMAN	Poly(rC)-binding protein 2 OS=Homo sap	129.35	30	4
P62913|RL11_HUMAN	60S ribosomal protein L11 OS=Homo sa	126.26	26	4
P33991|MCM4_HUMAN	DNA replication licensing factor MCM4 C	124.89	21	4
Q86VP6|CAND1_HUMAN	Cullin-associated NEDD8-dissociated pro	122.03	21	4
Q01581|HMCS1_HUMAN	Hydroxymethylglutaryl-CoA synthase, cyt	120.32	39	4
P00492|HPRT_HUMAN	Hypoxanthine-guanine phosphoribosyltra	119.62	31	4
Q15631|TSN_HUMAN	Translin OS=Homo sapiens GN=TSN PE	119.35	37	4
P23381|SYWC_HUMAN	Tryptophanyl-tRNA synthetase, cytoplasm	119.1	26	4
Q71UI9|H2AV_HUMAN	Histone H2A.V OS=Homo sapiens GN=H	118.48	40	4
O75821|EIF3G_HUMAN	Eukaryotic translation initiation factor 3 s	118.24	30	4
O15145|ARPC3_HUMAN	Actin-related protein 2/3 complex subunit	118.05	26	4
O14974|MYPT1_HUMAN	Protein phosphatase 1 regulatory subuni	117.1	32	4
P25788|PSA3_HUMAN	Proteasome subunit alpha type-3 OS=Ho	116.52	20	4
P39023|RL3_HUMAN	60S ribosomal protein L3 OS=Homo sap	115.31	24	4
P27797|CALR_HUMAN	Calreticulin OS=Homo sapiens GN=CAL	114.84	24	4
P22102|PUR2_HUMAN	Trifunctional purine biosynthetic protein a	114.26	37	4
P26373|RL13_HUMAN	60S ribosomal protein L13 OS=Homo sa	109.44	27	4
Q7L5N1|CSN6_HUMAN	COP9 signalosome complex subunit 6 O	108.68	25	4
O76003|GLRX3_HUMAN	Glutaredoxin-3 OS=Homo sapiens GN=G	107.36	59	4
Q09666|AHNK_HUMAN	Neuroblast differentiation-associated pro	107.34	12	4
P49755|TMEDA_HUMAN	Transmembrane emp24 domain-contain	106.72	28	4
P24539|AT5F1_HUMAN	ATP synthase subunit b, mitochondrial O	103.2	26	4

Q16643|DREB_HUMAN	Drebrin OS=Homo sapiens GN=DBN1 P	102.08	22	4
O43324|MCA3_HUMAN	Eukaryotic translation elongation factor 1	100.42	66	4
P13798|ACPH_HUMAN	Acylamino-acid-releasing enzyme OS=H	99.27	9	4
Q9NZL4|HPBP1_HUMAN	Hsp70-binding protein 1 OS=Homo sapie	89.62	36	4
Q16555|DPYL2_HUMAN	Dihydropyrimidinase-related protein 2 OS	87.34	21	4
Q9Y376|CAB39_HUMAN	Calcium-binding protein 39 OS=Homo sa	70.45	25	4
Q13509|TBB3_HUMAN	Tubulin beta-3 chain OS=Homo sapiens	299.53	62	3
P62807|H2B1C_HUMAN	Histone H2B type 1-C/E/F/G/I OS=Homo	219.86	70	3
O60814|H2B1K_HUMAN	Histone H2B type 1-K OS=Homo sapiens	219.86	70	3
P05141|ADT2_HUMAN	ADP/ATP translocase 2 OS=Homo sapie	179.31	58	3
Q9NZI8|IF2B1_HUMAN	Insulin-like growth factor 2 mRNA-bindin	170.99	45	3
O75610|LFTY1_HUMAN	Left-right determination factor 1 OS=Hon	170.03	45	3
Q13765|NACA_HUMAN	Nascent polypeptide-associated complex	165.46	37	3
P60660|MYL6_HUMAN	Myosin light polypeptide 6 OS=Homo sap	159.68	56	3
P61163|ACTZ_HUMAN	Alpha-centractin OS=Homo sapiens GN=	156.76	51	3
O43390|HNRPR_HUMAN	Heterogeneous nuclear ribonucleoprotein	156.46	38	3
O14744|ANM5_HUMAN	Protein arginine N-methyltransferase 5 O	146.45	37	3
P04216|THY1_HUMAN	Thy-1 membrane glycoprotein OS=Homo	143.96	50	3
Q13126|MTAP_HUMAN	S-methyl-5'-thioadenosine phosphorylase	133.09	47	3
P46782|RS5_HUMAN	40S ribosomal protein S5 OS=Homo sap	130.54	50	3
Q07020|RL18_HUMAN	60S ribosomal protein L18 OS=Homo sa	130.02	40	3
Q14444|CAPR1_HUMAN	Caprin-1 OS=Homo sapiens GN=CAPRI	127.48	26	3
Q06323|PSME1_HUMAN	Proteasome activator complex subunit 1	126.52	42	3
Q07021|C1QBP_HUMAN	Complement component 1 Q subcompor	126.18	25	3
Q15056|IF4H_HUMAN	Eukaryotic translation initiation factor 4H	125.33	34	3
P49903|SPS1_HUMAN	Selenide, water dikinase 1 OS=Homo sa	123.68	30	3
P52907|CAZA1_HUMAN	F-actin-capping protein subunit alpha-1 C	123.21	22	3
Q15417|CNN3_HUMAN	Calponin-3 OS=Homo sapiens GN=CNN	122.16	28	3
P62873|GBB1_HUMAN	Guanine nucleotide-binding protein G(I)/C	121.55	19	3
P60866|RS20_HUMAN	40S ribosomal protein S20 OS=Homo sa	121.54	37	3
P51858|HDGF_HUMAN	Hepatoma-derived growth factor OS=Ho	120.58	45	3
P39687|AN32A_HUMAN	Acidic leucine-rich nuclear phosphoprote	119.87	42	3
P30086|PEBP1_HUMAN	Phosphatidylethanolamine-binding protei	117.71	26	3
Q9UL46|PSME2_HUMAN	Proteasome activator complex subunit 2	117.63	54	3
P31153|METK2_HUMAN	S-adenosylmethionine synthase isoform	116.44	37	3
P16422|EPCAM_HUMAN	Epithelial cell adhesion molecule OS=Ho	116.32	42	3
P30040|ERP29_HUMAN	Endoplasmic reticulum resident protein 2	114.65	35	3
P38159|HNRPG_HUMAN	Heterogeneous nuclear ribonucleoprotein	113.99	37	3
O43776|SYNC_HUMAN	Asparaginyl-tRNA synthetase, cytoplasm	113.91	17	3
O15372|EIF3H_HUMAN	Eukaryotic translation initiation factor 3 s	113.73	34	3
P55060|XPO2_HUMAN	Exportin-2 OS=Homo sapiens GN=CSE1	113.11	28	3
P07741|APT_HUMAN	Adenine phosphoribosyltransferase OS=	112.81	26	3
P68400|CSK21_HUMAN	Casein kinase II subunit alpha OS=Homo	112.49	23	3
P07814|SYEP_HUMAN	Bifunctional aminoacyl-tRNA synthetase	111.68	17	3
P61088|UBE2N_HUMAN	Ubiquitin-conjugating enzyme E2 N OS=	111.56	36	3
O75487|GPC4_HUMAN	Glypican-4 OS=Homo sapiens GN=GPC	108.65	22	3
Q9NYL9|TMOD3_HUMAN	Tropomodulin-3 OS=Homo sapiens GN=	105.91	36	3
Q96AE4|FUBP1_HUMAN	Far upstream element-binding protein 1 (	105.87	27	3
Q13868|EXOS2_HUMAN	Exosome complex component RRP4 OS	105.36	31	3
P23352|KALM_HUMAN	Anosmin-1 OS=Homo sapiens GN=KAL1	104.99	23	3
P28072|PSB6_HUMAN	Proteasome subunit beta type-6 OS=Hor	104.25	13	3
P07093|GDN_HUMAN	Glia-derived nexin OS=Homo sapiens GI	103.16	30	3
Q9BUL8|PDC10_HUMAN	Programmed cell death protein 10 OS=H	103.14	30	3
Q9Y262|EIF3L_HUMAN	Eukaryotic translation initiation factor 3 s	102.46	23	3
Q9NVA2|SEP11_HUMAN	Septin-11 OS=Homo sapiens GN=SEPT	101.76	16	3

Q99439|CNN2_HUMAN	Calponin-2 OS=Homo sapiens GN=CNN	101.4	35	3
Q86V81|THOC4_HUMAN	THO complex subunit 4 OS=Homo sapie	100.47	20	3
P19367|HXK1_HUMAN	Hexokinase-1 OS=Homo sapiens GN=H	99.53	25	3
O43143|DHX15_HUMAN	Putative pre-mRNA-splicing factor ATP-d	98.45	16	3
Q9NZL9|MAT2B_HUMAN	Methionine adenosyltransferase 2 subun	96.34	20	3
Q15785|TOM34_HUMAN	Mitochondrial import receptor subunit TO	95.81	30	3
O15347|HMGB3_HUMAN	High mobility group protein B3 OS=Homo	94.94	30	3
P35613|BASI_HUMAN	Basigin OS=Homo sapiens GN=BSG PE	94.46	21	3
O60701|UGDH_HUMAN	UDP-glucose 6-dehydrogenase OS=Hon	94.26	15	3
P36404|ARL2_HUMAN	ADP-ribosylation factor-like protein 2 OS	94.05	18	3
Q13283|G3BP1_HUMAN	Ras GTPase-activating protein-binding p	93.52	30	3
P62280|RS11_HUMAN	40S ribosomal protein S11 OS=Homo sa	92.73	26	3
P49588|SYAC_HUMAN	Alanyl-tRNA synthetase, cytoplasmic OS	92.24	23	3
Q92820|GGH_HUMAN	Gamma-glutamyl hydrolase OS=Homo s	91.51	14	3
P54709|AT1B3_HUMAN	Sodium/potassium-transporting ATPase	90.93	13	3
P52272|HNRPM_HUMAN	Heterogeneous nuclear ribonucleoprotein	90.72	29	3
P39656|OST48_HUMAN	Dolichyl-diphosphooligosaccharide--prote	90.22	12	3
P29279|CTGF_HUMAN	Connective tissue growth factor OS=Hon	89.8	26	3
O43852|CALU_HUMAN	Calumenin OS=Homo sapiens GN=CALU	89.45	34	3
Q8WZ42|TITIN_HUMAN	Titin OS=Homo sapiens GN=TTN PE=1	88.5	10	3
Q9UNM6|PSD13_HUMAN	26S proteasome non-ATPase regulatory	87.85	29	3
P26640|SYVC_HUMAN	Valyl-tRNA synthetase OS=Homo sapien	87.67	6	3
Q8WUD1|RAB2B_HUMAN	Ras-related protein Rab-2B OS=Homo s	86.44	37	3
P12109|CO6A1_HUMAN	Collagen alpha-1(VI) chain OS=Homo sa	86.44	11	3
P11717|MPRI_HUMAN	Cation-independent mannose-6-phospha	85.96	10	3
O00625|PIR_HUMAN	Pirin OS=Homo sapiens GN=PIR PE=1 S	85.62	11	3
O15067|PUR4_HUMAN	Phosphoribosylformylglycinamidine synth	85.19	14	3
P00505|AATM_HUMAN	Aspartate aminotransferase, mitochondri	84.18	24	3
P48556|PSMD8_HUMAN	26S proteasome non-ATPase regulatory	83.86	19	3
P28070|PSB4_HUMAN	Proteasome subunit beta type-4 OS=Hor	81.96	20	3
P30566|PUR8_HUMAN	Adenylosuccinate lyase OS=Homo sapie	81.94	14	3
P55786|PSA_HUMAN	Puromycin-sensitive aminopeptidase OS	81.73	17	3
O00232|PSD12_HUMAN	26S proteasome non-ATPase regulatory	80.72	28	3
Q00688|FKBP3_HUMAN	Peptidyl-prolyl cis-trans isomerase FKBP	78.08	20	3
Q16543|CDC37_HUMAN	Hsp90 co-chaperone Cdc37 OS=Homo s	77.65	12	3
Q01469|FABP5_HUMAN	Fatty acid-binding protein, epidermal OS	77.1	30	3
Q15233|NONO_HUMAN	Non-POU domain-containing octamer-bi	76.95	20	3
O43237|DC1L2_HUMAN	Cytoplasmic dynein 1 light intermediate c	76.74	15	3
Q13838|DX39B_HUMAN	Spliceosome RNA helicase DDX39B OS	76.23	14	3
O00148|DX39A_HUMAN	ATP-dependent RNA helicase DDX39A O	76.23	12	3
O75822|EIF3J_HUMAN	Eukaryotic translation initiation factor 3 s	74.95	27	3
P60953|CDC42_HUMAN	Cell division control protein 42 homolog O	74.69	16	3
O00303|EIF3F_HUMAN	Eukaryotic translation initiation factor 3 s	73.8	21	3
P13984|T2FB_HUMAN	General transcription factor IIF subunit 2	73.22	21	3
P33992|MCM5_HUMAN	DNA replication licensing factor MCM5 O	71.25	19	3
Q92769|HDAC2_HUMAN	Histone deacetylase 2 OS=Homo sapien	70.35	17	3
P12270|TPR_HUMAN	Nucleoprotein TPR OS=Homo sapiens G	69.44	11	3
A6NDG6|PGP_HUMAN	Phosphoglycolate phosphatase OS=Hon	64.58	13	3
Q7Z4W1|DCXR_HUMAN	L-xylulose reductase OS=Homo sapiens	63.74	18	3
Q58FF7|H90B3_HUMAN	Putative heat shock protein HSP 90-beta	351.09	74	2
Q9BYX7|ACTBM_HUMAN	Putative beta-actin-like protein 3 OS=Hor	242.61	54	2
P19105|ML12A_HUMAN	Myosin regulatory light chain 12A OS=Ho	184.34	72	2
O14950|ML12B_HUMAN	Myosin regulatory light chain 12B OS=Ho	184.34	72	2
O00292|LFTY2_HUMAN	Left-right determination factor 2 OS=Hon	176.3	53	2
P63241|IF5A1_HUMAN	Eukaryotic translation initiation factor 5A-	163.75	50	2

P13929|ENOB_HUMAN	Beta-enolase OS=Homo sapiens GN=EN	157.2	53	2
P21796|VDAC1_HUMAN	Voltage-dependent anion-selective chan	146.33	35	2
P20042|IF2B_HUMAN	Eukaryotic translation initiation factor 2 s	138.9	61	2
A6NK07|IF2BL_HUMAN	Eukaryotic translation initiation factor 2 s	138.9	54	2
P60983|GMFB_HUMAN	Glia maturation factor beta OS=Homo sa	132.25	51	2
P62136|PP1A_HUMAN	Serine/threonine-protein phosphatase PF	123.53	30	2
P50453|SPB9_HUMAN	Serpin B9 OS=Homo sapiens GN=SERF	123.16	28	2
Q13200|PSMD2_HUMAN	26S proteasome non-ATPase regulatory	122.62	29	2
P62829|RL23_HUMAN	60S ribosomal protein L23 OS=Homo sa	120.57	59	2
P60891|PRPS1_HUMAN	Ribose-phosphate pyrophosphokinase 1	120.08	43	2
P68402|PA1B2_HUMAN	Platelet-activating factor acetylhydrolase	119.43	46	2
P20290|BTF3_HUMAN	Transcription factor BTF3 OS=Homo sap	119.35	50	2
P61026|RAB10_HUMAN	Ras-related protein Rab-10 OS=Homo s	119.09	32	2
Q9Y3B4|PM14_HUMAN	Pre-mRNA branch site protein p14 OS=H	116.79	29	2
P35268|RL22_HUMAN	60S ribosomal protein L22 OS=Homo sa	116.54	27	2
O43765|SGTA_HUMAN	Small glutamine-rich tetratricopeptide rep	115.19	22	2
Q92688|AN32B_HUMAN	Acidic leucine-rich nuclear phosphoprote	114.51	26	2
Q5VYJ4|RUEL1_HUMAN	Putative small nuclear ribonucleoprotein	113.85	48	2
P62304|RUXE_HUMAN	Small nuclear ribonucleoprotein E OS=H	113.85	48	2
P62241|RS8_HUMAN	40S ribosomal protein S8 OS=Homo sap	112.85	33	2
Q99729|ROAA_HUMAN	Heterogeneous nuclear ribonucleoprotein	112.38	22	2
P20339|RAB5A_HUMAN	Ras-related protein Rab-5A OS=Homo s	110.79	32	2
P25705|ATPA_HUMAN	ATP synthase subunit alpha, mitochondr	110.15	42	2
P31943|HNRH1_HUMAN	Heterogeneous nuclear ribonucleoprotein	109.47	21	2
P24534|EF1B_HUMAN	Elongation factor 1-beta OS=Homo sapie	107.85	31	2
Q12905|ILF2_HUMAN	Interleukin enhancer-binding factor 2 OS	107.42	21	2
Q92522|H1X_HUMAN	Histone H1x OS=Homo sapiens GN=H1	106.49	34	2
P30048|PRDX3_HUMAN	Thioredoxin-dependent peroxide reducta	106.1	32	2
Q14103|HNRPD_HUMAN	Heterogeneous nuclear ribonucleoprotein	104.99	19	2
Q15046|SYK_HUMAN	Lysyl-tRNA synthetase OS=Homo sapier	103.8	19	2
O00151|PDLI1_HUMAN	PDZ and LIM domain protein 1 OS=Hom	103.42	39	2
P61020|RAB5B_HUMAN	Ras-related protein Rab-5B OS=Homo s	103.21	33	2
O00264|PGRC1_HUMAN	Membrane-associated progesterone rece	102.86	26	2
O15116|LSM1_HUMAN	U6 snRNA-associated Sm-like protein LS	101.19	25	2
P06576|ATPB_HUMAN	ATP synthase subunit beta, mitochondria	100.8	33	2
Q9UBT2|SAE2_HUMAN	SUMO-activating enzyme subunit 2 OS=	100.15	15	2
P55327|TPD52_HUMAN	Tumor protein D52 OS=Homo sapiens G	99.57	21	2
Q07866|KLC1_HUMAN	Kinesin light chain 1 OS=Homo sapiens (	99.17	19	2
Q04760|LGUL_HUMAN	Lactoylglutathione lyase OS=Homo sapie	98.72	23	2
P53367|ARFP1_HUMAN	Arfaptin-1 OS=Homo sapiens GN=ARFIP	98.07	26	2
O15212|PFD6_HUMAN	Prefoldin subunit 6 OS=Homo sapiens G	97.95	43	2
P09936|UCHL1_HUMAN	Ubiquitin carboxyl-terminal hydrolase iso	97.81	19	2
Q99873|ANM1_HUMAN	Protein arginine N-methyltransferase 1 O	97.08	16	2
P41091|IF2G_HUMAN	Eukaryotic translation initiation factor 2 s	97.06	22	2
Q2VIR3|IF2GL_HUMAN	Eukaryotic translation initiation factor 2 s	97.06	17	2
P13861|KAP2_HUMAN	cAMP-dependent protein kinase type II-a	95.1	23	2
P51571|SSRD_HUMAN	Translocon-associated protein subunit de	94.78	39	2
P21741|MK_HUMAN	Midkine OS=Homo sapiens GN=MDK PE	94.22	34	2
Q96CT7|CC124_HUMAN	Coiled-coil domain-containing protein 124	93.73	21	2
Q13576|IQGA2_HUMAN	Ras GTPase-activating-like protein IQGA	92.82	12	2
Q92890|UFD1_HUMAN	Ubiquitin fusion degradation protein 1 ho	92.65	27	2
Q9BZZ5|API5_HUMAN	Apoptosis inhibitor 5 OS=Homo sapiens	92.58	16	2
O95433|AHSA1_HUMAN	Activator of 90 kDa heat shock protein AT	92.26	36	2
Q15818|NPTX1_HUMAN	Neuronal pentraxin-1 OS=Homo sapiens	91.91	18	2
O15355|PPM1G_HUMAN	Protein phosphatase 1G OS=Homo sapi	91.32	14	2

P23284|PPIB_HUMAN	Peptidyl-prolyl cis-trans isomerase B OS=	91.23	50	2
P48047|ATPO_HUMAN	ATP synthase subunit O, mitochondrial O	90.81	57	2
Q00341|VIGLN_HUMAN	Vigilin OS=Homo sapiens GN=HDLBP P	90.4	18	2
Q99426|TBCB_HUMAN	Tubulin-folding cofactor B OS=Homo sap	90.35	34	2
O14745|NHRF1_HUMAN	Na(+)/H(+) exchange regulatory cofactor	89.18	20	2
P53621|COPA_HUMAN	Coatomer subunit alpha OS=Homo sapie	89	13	2
Q8WVM8|SCFD1_HUMAN	Sec1 family domain-containing protein 1	88.71	9	2
Q93009|UBP7_HUMAN	Ubiquitin carboxyl-terminal hydrolase 7 O	87.4	11	2
P19784|CSK22_HUMAN	Casein kinase II subunit alpha' OS=Hom	87	21	2
P52565|GDIR1_HUMAN	Rho GDP-dissociation inhibitor 1 OS=Ho	86.8	23	2
P25325|THTM_HUMAN	3-mercaptopyruvate sulfurtransferase OS	86.75	23	2
P48444|COPD_HUMAN	Coatomer subunit delta OS=Homo sapie	86.37	17	2
P31350|RIR2_HUMAN	Ribonucleoside-diphosphate reductase s	86.12	18	2
P47756|CAPZB_HUMAN	F-actin-capping protein subunit beta OS=	85.76	25	2
P47914|RL29_HUMAN	60S ribosomal protein L29 OS=Homo sa	85.69	28	2
Q96HF1|SFRP2_HUMAN	Secreted frizzled-related protein 2 OS=H	85.64	18	2
P46776|RL27A_HUMAN	60S ribosomal protein L27a OS=Homo s	85.06	45	2
P83731|RL24_HUMAN	60S ribosomal protein L24 OS=Homo sa	84.82	43	2
P46109|CRKL_HUMAN	Crk-like protein OS=Homo sapiens GN=(	84.45	10	2
Q13347|EIF3I_HUMAN	Eukaryotic translation initiation factor 3 s	84.43	36	2
Q13557|KCC2D_HUMAN	Calcium/calmodulin-dependent protein k	84.24	22	2
Q93008|USP9X_HUMAN	Probable ubiquitin carboxyl-terminal hydr	83.52	6	2
P31689|DNJA1_HUMAN	DnaJ homolog subfamily A member 1 OS	83.1	17	2
P62753|RS6_HUMAN	40S ribosomal protein S6 OS=Homo sap	83.1	20	2
O75477|ERLN1_HUMAN	Erlin-1 OS=Homo sapiens GN=ERLIN1 P	83.03	21	2
P48681|NEST_HUMAN	Nestin OS=Homo sapiens GN=NES PE=	82.69	7	2
Q15293|RCN1_HUMAN	Reticulocalbin-1 OS=Homo sapiens GN=	82.52	15	2
Q08211|DHX9_HUMAN	ATP-dependent RNA helicase A OS=Ho	82.38	12	2
P61201|CSN2_HUMAN	COP9 signalosome complex subunit 2 O	82.3	30	2
P07237|PDIA1_HUMAN	Protein disulfide-isomerase OS=Homo s	82.12	23	2
Q99460|PSMD1_HUMAN	26S proteasome non-ATPase regulatory	81.85	15	2
P23921|RIR1_HUMAN	Ribonucleoside-diphosphate reductase la	81.2	12	2
P20700|LMNB1_HUMAN	Lamin-B1 OS=Homo sapiens GN=LMNB	81.12	16	2
Q9NR31|SAR1A_HUMAN	GTP-binding protein SAR1a OS=Homo s	81.06	31	2
Q9Y4Z0|LSM4_HUMAN	U6 snRNA-associated Sm-like protein LS	80.17	24	2
Q9UKM9|RALY_HUMAN	RNA-binding protein Raly OS=Homo sap	80.15	23	2
Q13442|HAP28_HUMAN	28 kDa heat- and acid-stable phosphopr	79.27	18	2
P54578|UBP14_HUMAN	Ubiquitin carboxyl-terminal hydrolase 14	77.51	12	2
P10155|RO60_HUMAN	60 kDa SS-A/Ro ribonucleoprotein OS=H	77.36	14	2
P62318|SMD3_HUMAN	Small nuclear ribonucleoprotein Sm D3 O	77.19	30	2
P05937|CALB1_HUMAN	Calbindin OS=Homo sapiens GN=CALB	76.96	30	2
P31949|S10AB_HUMAN	Protein S100-A11 OS=Homo sapiens GN	76.5	66	2
P83916|CBX1_HUMAN	Chromobox protein homolog 1 OS=Hom	76.14	18	2
O60925|PFD1_HUMAN	Prefoldin subunit 1 OS=Homo sapiens G	76.11	17	2
P62857|RS28_HUMAN	40S ribosomal protein S28 OS=Homo sa	76.11	64	2
Q9BPX5|ARP5L_HUMAN	Actin-related protein 2/3 complex subunit	75.98	46	2
Q53GQ0|DHB12_HUMAN	Estradiol 17-beta-dehydrogenase 12 OS	75.89	26	2
P63220|RS21_HUMAN	40S ribosomal protein S21 OS=Homo sa	75.76	23	2
Q14166|TTL12_HUMAN	Tubulin--tyrosine ligase-like protein 12 O	75.74	12	2
P18065|IBP2_HUMAN	Insulin-like growth factor-binding protein	75.65	26	2
O14776|TCRG1_HUMAN	Transcription elongation regulator 1 OS=	75.28	11	2
P30419|NMT1_HUMAN	Glycylpeptide N-tetradecanoyltransferase	74.95	13	2
Q04837|SSBP_HUMAN	Single-stranded DNA-binding protein, mi	74.91	40	2
P61803|DAD1_HUMAN	Dolichyl-diphosphooligosaccharide--prote	74.36	19	2
P35606|COPB2_HUMAN	Coatomer subunit beta' OS=Homo sapie	73.93	9	2

Q71UM5|RS27L_HUMAN	40S ribosomal protein S27-like OS=Hom	73.48	25	2
P42677|RS27_HUMAN	40S ribosomal protein S27 OS=Homo sa	73.48	25	2
P09012|SNRPA_HUMAN	U1 small nuclear ribonucleoprotein A OS	72.57	17	2
Q9H9Q2|CSN7B_HUMAN	COP9 signalosome complex subunit 7b (	72.26	18	2
P51572|BAP31_HUMAN	B-cell receptor-associated protein 31 OS	72.21	26	2
Q9NR45|SIAS_HUMAN	Sialic acid synthase OS=Homo sapiens (	71.88	22	2
P14174|MIF_HUMAN	Macrophage migration inhibitory factor O	71.14	21	2
P35249|RFC4_HUMAN	Replication factor C subunit 4 OS=Homo	71.04	19	2
Q09028|RBBP4_HUMAN	Histone-binding protein RBBP4 OS=Hom	70.9	13	2
P54136|SYRC_HUMAN	Arginyl-tRNA synthetase, cytoplasmic OS	70.83	10	2
O75531|BAF_HUMAN	Barrier-to-autointegration factor OS=Hom	70.71	35	2
Q9UNZ2|NSF1C_HUMAN	NSFL1 cofactor p47 OS=Homo sapiens	69.71	19	2
Q96SM3|CPXM1_HUMAN	Probable carboxypeptidase X1 OS=Hom	69.31	18	2
Q9Y5K8|VATD_HUMAN	V-type proton ATPase subunit D OS=Ho	69.29	32	2
Q14257|RCN2_HUMAN	Reticulocalbin-2 OS=Homo sapiens GN=	68.29	21	2
O00410|IPO5_HUMAN	Importin-5 OS=Homo sapiens GN=IPO5	68.23	13	2
O95218|ZRAB2_HUMAN	Zinc finger Ran-binding domain-containir	67.78	14	2
P08243|ASNS_HUMAN	Asparagine synthetase [glutamine-hydrol	67.46	10	2
P12830|CADH1_HUMAN	Cadherin-1 OS=Homo sapiens GN=CDH	67.27	10	2
P18124|RL7_HUMAN	60S ribosomal protein L7 OS=Homo sap	67.2	16	2
P12081|SYHC_HUMAN	Histidyl-tRNA synthetase, cytoplasmic OS	66.96	18	2
Q07157|ZO1_HUMAN	Tight junction protein ZO-1 OS=Homo sa	66.86	11	2
P36578|RL4_HUMAN	60S ribosomal protein L4 OS=Homo sap	66.42	19	2
P29762|RABP1_HUMAN	Cellular retinoic acid-binding protein 1 OS	65.26	28	2
Q9UBW8|CSN7A_HUMAN	COP9 signalosome complex subunit 7a (	65.1	29	2
Q96K17|BT3L4_HUMAN	Transcription factor BTF3 homolog 4 OS	65.06	22	2
Q92896|GSLG1_HUMAN	Golgi apparatus protein 1 OS=Homo sap	64.9	11	2
Q9BVK6|TMED9_HUMAN	Transmembrane emp24 domain-contain	64.33	17	2
Q96S86|HPLN3_HUMAN	Hyaluronan and proteoglycan link protein	63.53	27	2
P35221|CTNA1_HUMAN	Catenin alpha-1 OS=Homo sapiens GN=	63.32	7	2
Q15758|AAAT_HUMAN	Neutral amino acid transporter B(0) OS=	61.89	14	2
Q14980|NUMA1_HUMAN	Nuclear mitotic apparatus protein 1 OS=I	61.85	11	2
Q13098|CSN1_HUMAN	COP9 signalosome complex subunit 1 O	61.49	9	2
Q96QK1|VPS35_HUMAN	Vacuolar protein sorting-associated prote	60.93	20	2
P04843|RPN1_HUMAN	Dolichyl-diphosphooligosaccharide--prote	60.23	13	2
Q9Y5K5|UCHL5_HUMAN	Ubiquitin carboxyl-terminal hydrolase iso	60.2	15	2
Q92922|SMRC1_HUMAN	SWI/SNF complex subunit SMARCC1 O	58.63	13	2
Q9Y624|JAM1_HUMAN	Junctional adhesion molecule A OS=Hor	58.15	14	2
Q92841|DDX17_HUMAN	Probable ATP-dependent RNA helicase	58.1	17	2
P17844|DDX5_HUMAN	Probable ATP-dependent RNA helicase	58.1	16	2
Q9Y5K6|CD2AP_HUMAN	CD2-associated protein OS=Homo sapie	58.01	12	2
Q13243|SRSF5_HUMAN	Serine/arginine-rich splicing factor 5 OS=	57.91	18	2
P20810|ICAL_HUMAN	Calpastatin OS=Homo sapiens GN=CAS	57.44	12	2
P46060|RAGP1_HUMAN	Ran GTPase-activating protein 1 OS=Ho	56.23	11	2
P19623|SPEE_HUMAN	Spermidine synthase OS=Homo sapiens	55.93	17	2
Q99614|TTC1_HUMAN	Tetratricopeptide repeat protein 1 OS=H	55.64	21	2
P09960|LKHA4_HUMAN	Leukotriene A-4 hydrolase OS=Homo sa	55.24	6	2
P62861|RS30_HUMAN	40S ribosomal protein S30 OS=Homo sa	54.98	34	2
Q96PK2|MACF4_HUMAN	Microtubule-actin cross-linking factor 1, i	52.81	11	2
P10768|ESTD_HUMAN	S-formylglutathione hydrolase OS=Homo	52.37	10	2
P07203|GPX1_HUMAN	Glutathione peroxidase 1 OS=Homo sap	52.1	12	2
Q96P16|RPR1A_HUMAN	Regulation of nuclear pre-mRNA domain	51.91	20	2
Q9BVC6|TM109_HUMAN	Transmembrane protein 109 OS=Homo	51.87	39	2
Q9UPG8|PLAL2_HUMAN	Zinc finger protein PLAGL2 OS=Homo s	51.33	10	2
Q99615|DNJC7_HUMAN	DnaJ homolog subfamily C member 7 OS	50.77	10	2

O94985|CSTN1_HUMAN	Calsyntenin-1 OS=Homo sapiens GN=C	50.13	6	2
Q9H4M9|EHD1_HUMAN	EH domain-containing protein 1 OS=Hor	49.9	16	2
P11413|G6PD_HUMAN	Glucose-6-phosphate 1-dehydrogenase	49	22	2
Q9H0I2|CP048_HUMAN	Uncharacterized protein C16orf48 OS=H	46.14	22	2
P06756|ITAV_HUMAN	Integrin alpha-V OS=Homo sapiens GN=	45.34	7	2
O15078|CE290_HUMAN	Centrosomal protein of 290 kDa OS=Hor	45.23	13	2
P02768|ALBU_HUMAN	Serum albumin OS=Homo sapiens GN=A	44.59	24	2
Q13043|STK4_HUMAN	Serine/threonine-protein kinase 4 OS=Ho	44.22	21	2
P40763|STAT3_HUMAN	Signal transducer and activator of transc	43.51	5	2
Q8NE01|CNNM3_HUMAN	Metal transporter CNNM3 OS=Homo sap	42.32	21	2
P45974|UBP5_HUMAN	Ubiquitin carboxyl-terminal hydrolase 5 O	41.68	9	2
P49454|CENPF_HUMAN	Centromere protein F OS=Homo sapiens	41.67	10	2
Q08752|PPID_HUMAN	Peptidyl-prolyl cis-trans isomerase D OS	41.04	16	2
P10586|PTPRF_HUMAN	Receptor-type tyrosine-protein phosphata	39.02	8	2
Q9BXP5|SRRT_HUMAN	Serrate RNA effector molecule homolog	38.84	16	2
P63000|RAC1_HUMAN	Ras-related C3 botulinum toxin substrate	37.18	17	2
Q7L4E1|FA73B_HUMAN	Protein FAM73B OS=Homo sapiens GN=	36.38	15	2

Table A1.10 CA1 hESC CMTX Protein Identifications. List of all proteins identified in CMTX from CA1 hESCs with corresponding accession, description, PEAKS score, unique peptide numbers, and coverage (in %).

Accession	Description	Score	Coverage (%)	#Unique
P21333|FLNA_HUMAN	Filamin-A OS=Homo sapiens GN=FLNA	348.93	55	72
P49327|FAS_HUMAN	Fatty acid synthase OS=Homo sapiens	346.52	58	67
Q13813|SPTA2_HUMAN	Spectrin alpha chain, brain OS=Homo s	328.54	61	63
O75369|FLNB_HUMAN	Filamin-B OS=Homo sapiens GN=FLNB	333.1	56	55
P13639|EF2_HUMAN	Elongation factor 2 OS=Homo sapiens (	340.62	73	53
P04406|G3P_HUMAN	Glyceraldehyde-3-phosphate dehydroge	333.99	91	52
P18206|VINC_HUMAN	Vinculin OS=Homo sapiens GN=VCL P	329.26	76	51
P29401|TKT_HUMAN	Transketolase OS=Homo sapiens GN=T	331.75	78	46
P14618|KPYM_HUMAN	Pyruvate kinase isozymes M1/M2 OS=H	332.22	90	44
Q01995|TAGL_HUMAN	Transgelin OS=Homo sapiens GN=TAG	307.02	95	41
P35580|MYH10_HUMAN	Myosin-10 OS=Homo sapiens GN=MYH	306.82	57	38
Q01082|SPTB2_HUMAN	Spectrin beta chain, brain 1 OS=Homo	296.14	61	38
P30041|PRDX6_HUMAN	Peroxiredoxin-6 OS=Homo sapiens GN	292.67	93	38
P06733|ENOA_HUMAN	Alpha-enolase OS=Homo sapiens GN=	301.35	88	37
P55072|TERA_HUMAN	Transitional endoplasmic reticulum ATP	275.21	62	36
P35579|MYH9_HUMAN	Myosin-9 OS=Homo sapiens GN=MYH9	314.85	63	35
P04075|ALDOA_HUMAN	Fructose-bisphosphate aldolase A OS=	311.67	82	33
P07355|ANXA2_HUMAN	Annexin A2 OS=Homo sapiens GN=AN	303.45	91	33
P68104|EF1A1_HUMAN	Elongation factor 1-alpha 1 OS=Homo s	315.8	76	32
P62258|1433E_HUMAN	14-3-3 protein epsilon OS=Homo sapie	302.7	87	32
Q06830|PRDX1_HUMAN	Peroxiredoxin-1 OS=Homo sapiens GN	299.56	88	31
P53396|ACLY_HUMAN	ATP-citrate synthase OS=Homo sapien	270.95	69	31
O75874|IDHC_HUMAN	Isocitrate dehydrogenase [NADP] cytop	294.86	76	30
P07195|LDHB_HUMAN	L-lactate dehydrogenase B chain OS=H	292.67	73	30
P60174|TPIS_HUMAN	Triosephosphate isomerase OS=Homo	279.5	96	30
P08758|ANXA5_HUMAN	Annexin A5 OS=Homo sapiens GN=AN	271.34	70	30
P12814|ACTN1_HUMAN	Alpha-actinin-1 OS=Homo sapiens GN=	315.82	71	28
P63104|1433Z_HUMAN	14-3-3 protein zeta/delta OS=Homo sap	308.88	83	27
P11142|HSP7C_HUMAN	Heat shock cognate 71 kDa protein OS	282.81	66	27
P07737|PROF1_HUMAN	Profilin-1 OS=Homo sapiens GN=PFN1	273.18	97	26
P62805|H4_HUMAN	Histone H4 OS=Homo sapiens GN=HIS	261.7	63	26
Q14315|FLNC_HUMAN	Filamin-C OS=Homo sapiens GN=FLNC	259.7	42	26
P10809|CH60_HUMAN	60 kDa heat shock protein, mitochondri	257.33	75	26
P50454|SERPH_HUMAN	Serpin H1 OS=Homo sapiens GN=SER	284.13	73	25
P00338|LDHA_HUMAN	L-lactate dehydrogenase A chain OS=H	282.93	81	25
P07900|HS90A_HUMAN	Heat shock protein HSP 90-alpha OS=H	321.76	60	24
O43707|ACTN4_HUMAN	Alpha-actinin-4 OS=Homo sapiens GN=	316.9	69	24
P23528|COF1_HUMAN	Cofilin-1 OS=Homo sapiens GN=CFL1	282.49	93	24
P05455|LA_HUMAN	Lupus La protein OS=Homo sapiens GN	262.62	72	24
P31939|PUR9_HUMAN	Bifunctional purine biosynthesis protein	254.56	72	24
P67936|TPM4_HUMAN	Tropomyosin alpha-4 chain OS=Homo s	319.2	95	23
P62937|PPIA_HUMAN	Peptidyl-prolyl cis-trans isomerase A OS	254.93	93	23
P61247|RS3A_HUMAN	40S ribosomal protein S3a OS=Homo s	240.82	77	23
P50990|TCPQ_HUMAN	T-complex protein 1 subunit theta OS=H	229.91	58	23
P02794|FRIH_HUMAN	Ferritin heavy chain OS=Homo sapiens	221.88	77	23
Q9Y490|TLN1_HUMAN	Talin-1 OS=Homo sapiens GN=TLN1 P	215.08	50	23
Q14914|PTGR1_HUMAN	Prostaglandin reductase 1 OS=Homo s	261.73	69	22
P37802|TAGL2_HUMAN	Transgelin-2 OS=Homo sapiens GN=TA	245.46	97	22
P14625|ENPL_HUMAN	Endoplasmin OS=Homo sapiens GN=H	241.99	47	22
P02649|APOE_HUMAN	Apolipoprotein E OS=Homo sapiens GN	240.53	71	22
Q9Y617|SERC_HUMAN	Phosphoserine aminotransferase OS=H	222.4	67	22
P27348|1433T_HUMAN	14-3-3 protein theta OS=Homo sapiens	300.35	76	21
P09211|GSTP1_HUMAN	Glutathione S-transferase P OS=Homo	279.58	92	21
Q04917|1433F_HUMAN	14-3-3 protein eta OS=Homo sapiens G	273.6	77	21
P12956|XRCC6_HUMAN	X-ray repair cross-complementing prote	251.79	61	21

P08133|ANXA6_HUMAN	Annexin A6 OS=Homo sapiens GN=AN	238.21	55	21
P30101|PDIA3_HUMAN	Protein disulfide-isomerase A3 OS=Hor	229.71	60	21
P09651|ROA1_HUMAN	Heterogeneous nuclear ribonucleoprote	268.74	90	20
P22314|UBA1_HUMAN	Ubiquitin-like modifier-activating enzyme	253.05	57	20
P23396|RS3_HUMAN	40S ribosomal protein S3 OS=Homo sa	251.58	85	20
P26038|MOES_HUMAN	Moesin OS=Homo sapiens GN=MSN P	231.03	52	20
P39019|RS19_HUMAN	40S ribosomal protein S19 OS=Homo s	213.37	81	20
P18669|PGAM1_HUMAN	Phosphoglycerate mutase 1 OS=Homo	291.45	94	19
Q00610|CLH1_HUMAN	Clathrin heavy chain 1 OS=Homo sapie	262.75	47	19
P52209|6PGD_HUMAN	6-phosphogluconate dehydrogenase, d	252.13	74	19
P25398|RS12_HUMAN	40S ribosomal protein S12 OS=Homo s	250.95	92	19
P08670|VIME_HUMAN	Vimentin OS=Homo sapiens GN=VIM P	247.55	59	19
P13010|XRCC5_HUMAN	X-ray repair cross-complementing prote	247.19	66	19
P06576|ATPB_HUMAN	ATP synthase subunit beta, mitochondr	246.2	72	19
Q99832|TCPH_HUMAN	T-complex protein 1 subunit eta OS=Ho	241.03	68	19
P48643|TCPE_HUMAN	T-complex protein 1 subunit epsilon OS	239.83	79	19
Q01469|FABP5_HUMAN	Fatty acid-binding protein, epidermal OS	260.11	90	18
P04083|ANXA1_HUMAN	Annexin A1 OS=Homo sapiens GN=AN	248.02	68	18
P02792|FRIL_HUMAN	Ferritin light chain OS=Homo sapiens G	247.82	73	18
P78371|TCPB_HUMAN	T-complex protein 1 subunit beta OS=H	239.24	67	18
P00558|PGK1_HUMAN	Phosphoglycerate kinase 1 OS=Homo s	236.01	73	18
P37837|TALDO_HUMAN	Transaldolase OS=Homo sapiens GN=	234.66	59	18
P22234|PUR6_HUMAN	Multifunctional protein ADE2 OS=Homo	233.69	64	18
O00231|PSD11_HUMAN	26S proteasome non-ATPase regulator	226.15	67	18
P62333|PRS10_HUMAN	26S protease regulatory subunit 10B OS	217.59	62	18
P49368|TCPG_HUMAN	T-complex protein 1 subunit gamma OS	214.46	57	18
Q14152|EIF3A_HUMAN	Eukaryotic translation initiation factor 3	209.47	34	18
P84243|H33_HUMAN	Histone H3.3 OS=Homo sapiens GN=H	175.68	66	18
P63241|IF5A1_HUMAN	Eukaryotic translation initiation factor 5A	255.86	87	17
P40926|MDHM_HUMAN	Malate dehydrogenase, mitochondrial O	252.14	77	17
P15311|EZRI_HUMAN	Ezrin OS=Homo sapiens GN=EZR PE=	245.75	62	17
O00299|CLIC1_HUMAN	Chloride intracellular channel protein 1	242.59	92	17
P34932|HSP74_HUMAN	Heat shock 70 kDa protein 4 OS=Homo	240.68	44	17
P46777|RL5_HUMAN	60S ribosomal protein L5 OS=Homo sa	239.17	61	17
P62195|PRS8_HUMAN	26S protease regulatory subunit 8 OS=	238.18	66	17
P11021|GRP78_HUMAN	78 kDa glucose-regulated protein OS=H	236.37	54	17
P62826|RAN_HUMAN	GTP-binding nuclear protein Ran OS=H	236	68	17
P46940|IQGA1_HUMAN	Ras GTPase-activating-like protein IQG	226.51	50	17
P11586|C1TC_HUMAN	C-1-tetrahydrofolate synthase, cytoplas	222.32	50	17
Q9P2E9|RRBP1_HUMAN	Ribosome-binding protein 1 OS=Homo	203.88	25	17
P62081|RS7_HUMAN	40S ribosomal protein S7 OS=Homo sa	201.56	65	17
P62269|RS18_HUMAN	40S ribosomal protein S18 OS=Homo s	194.93	70	17
P50395|GDIB_HUMAN	Rab GDP dissociation inhibitor beta OS	276.43	74	16
P61981|1433G_HUMAN	14-3-3 protein gamma OS=Homo sapie	258.46	86	16
P19338|NUCL_HUMAN	Nucleolin OS=Homo sapiens GN=NCL	252	64	16
P51665|PSD7_HUMAN	26S proteasome non-ATPase regulator	244.25	69	16
P09936|UCHL1_HUMAN	Ubiquitin carboxyl-terminal hydrolase is	239.85	83	16
P62424|RL7A_HUMAN	60S ribosomal protein L7a OS=Homo s	234.48	62	16
P09874|PARP1_HUMAN	Poly [ADP-ribose] polymerase 1 OS=Ho	232.46	43	16
P32119|PRDX2_HUMAN	Peroxiredoxin-2 OS=Homo sapiens GN	231.95	57	16
P25705|ATPA_HUMAN	ATP synthase subunit alpha, mitochond	231.84	71	16
P28074|PSB5_HUMAN	Proteasome subunit beta type-5 OS=Ho	230.33	59	16
O00410|IPO5_HUMAN	Importin-5 OS=Homo sapiens GN=IPO5	225.82	44	16
Q99497|PARK7_HUMAN	Protein DJ-1 OS=Homo sapiens GN=PA	225.33	84	16
P04792|HSPB1_HUMAN	Heat shock protein beta-1 OS=Homo sa	224.97	68	16
P31948|STIP1_HUMAN	Stress-induced-phosphoprotein 1 OS=H	224.9	47	16

Q96KP4|CNDP2_HUMAN	Cytosolic non-specific dipeptidase OS=	216.01	45	16
P35232|PHB_HUMAN	Prohibitin OS=Homo sapiens GN=PHB	215.51	82	16
P61604|CH10_HUMAN	10 kDa heat shock protein, mitochondri	200.28	83	16
P12277|KCRB_HUMAN	Creatine kinase B-type OS=Homo sapie	231.14	69	15
P61978|HNRPK_HUMAN	Heterogeneous nuclear ribonucleprote	230.93	58	15
Q9Y224|CN166_HUMAN	UPF0568 protein C14orf166 OS=Homo	227.23	89	15
P20618|PSB1_HUMAN	Proteasome subunit beta type-1 OS=H	226.83	73	15
O60664|PLIN3_HUMAN	Perilipin-3 OS=Homo sapiens GN=PLIN	225.59	69	15
P63244|GBLP_HUMAN	Guanine nucleotide-binding protein sub	225.36	67	15
P35998|PRS7_HUMAN	26S protease regulatory subunit 7 OS=	221.78	59	15
P12429|ANXA3_HUMAN	Annexin A3 OS=Homo sapiens GN=AN	220.33	71	15
P06744|G6PI_HUMAN	Glucose-6-phosphate isomerase OS=H	219.01	44	15
P07910|HNRPC_HUMAN	Heterogeneous nuclear ribonucleprote	210.07	58	15
P62316|SMD2_HUMAN	Small nuclear ribonucleoprotein Sm D2	204.96	69	15
Q9Y230|RUVB2_HUMAN	RuvB-like 2 OS=Homo sapiens GN=RU	199.09	41	15
P08238|HS90B_HUMAN	Heat shock protein HSP 90-beta OS=H	322.53	65	14
P31946|1433B_HUMAN	14-3-3 protein beta/alpha OS=Homo sa	273.43	78	14
P22626|ROA2_HUMAN	Heterogeneous nuclear ribonucleprote	245.9	60	14
O43175|SERA_HUMAN	D-3-phosphoglycerate dehydrogenase	239.46	69	14
Q9HB71|CYBP_HUMAN	Calcyclin-binding protein OS=Homo sap	236.91	71	14
P06748|NPM_HUMAN	Nucleophosmin OS=Homo sapiens GN=	223.88	69	14
P23246|SFPQ_HUMAN	Splicing factor, proline- and glutamine-r	206.38	47	14
P60900|PSA6_HUMAN	Proteasome subunit alpha type-6 OS=H	205.63	56	14
Q04760|LGUL_HUMAN	Lactoylglutathione lyase OS=Homo sap	200.5	55	14
P52272|HNRPM_HUMAN	Heterogeneous nuclear ribonucleprote	199.66	69	14
P30044|PRDX5_HUMAN	Peroxiredoxin-5, mitochondrial OS=Hor	198.85	79	14
Q01518|CAP1_HUMAN	Adenylyl cyclase-associated protein 1 C	197.81	63	14
P62263|RS14_HUMAN	40S ribosomal protein S14 OS=Homo s	197.37	56	14
Q7KZF4|SND1_HUMAN	Staphylococcal nuclease domain-conta	195.29	38	14
P62280|RS11_HUMAN	40S ribosomal protein S11 OS=Homo s	193.73	63	14
P46781|RS9_HUMAN	40S ribosomal protein S9 OS=Homo sa	174.48	42	14
P00441|SODC_HUMAN	Superoxide dismutase [Cu-Zn] OS=Hor	238.57	94	13
P26641|EF1G_HUMAN	Elongation factor 1-gamma OS=Homo s	218.09	45	13
P40227|TCPZ_HUMAN	T-complex protein 1 subunit zeta OS=H	216.61	51	13
O75347|TBCA_HUMAN	Tubulin-specific chaperone A OS=Hom	214.46	80	13
Q9H9Z2|LN28A_HUMAN	Protein lin-28 homolog A OS=Homo sa	212.11	61	13
P25789|PSA4_HUMAN	Proteasome subunit alpha type-4 OS=H	211.26	61	13
Q15631|TSN_HUMAN	Translin OS=Homo sapiens GN=TSN P	210.85	49	13
P62906|RL10A_HUMAN	60S ribosomal protein L10a OS=Homo	208.71	41	13
Q01581|HMCS1_HUMAN	Hydroxymethylglutaryl-CoA synthase, c	207.81	58	13
P13796|PLSL_HUMAN	Plastin-2 OS=Homo sapiens GN=LCP1	205.66	48	13
P54577|SYYC_HUMAN	Tyrosyl-tRNA synthetase, cytoplasmic	203.19	55	13
O15067|PUR4_HUMAN	Phosphoribosylformylglycinamidine syn	203.17	36	13
Q14019|COTL1_HUMAN	Coactosin-like protein OS=Homo sapie	195.2	61	13
P58107|EPIPL_HUMAN	Epiplakin OS=Homo sapiens GN=EPPK	162.59	25	13
O14818|PSA7_HUMAN	Proteasome subunit alpha type-7 OS=H	250.18	88	12
P09972|ALDOC_HUMAN	Fructose-bisphosphate aldolase C OS=	244.1	74	12
P50453|SPB9_HUMAN	Serpin B9 OS=Homo sapiens GN=SER	224.88	58	12
O75531|BAF_HUMAN	Barrier-to-autointegration factor OS=Ho	218.95	76	12
A8MW06|TMSL3_HUMAN	Thymosin beta-4-like protein 3 OS=Hon	213.97	89	12
P62328|TYB4_HUMAN	Thymosin beta-4 OS=Homo sapiens GN	213.97	89	12
P62277|RS13_HUMAN	40S ribosomal protein S13 OS=Homo s	210.57	61	12
Q9UL46|PSME2_HUMAN	Proteasome activator complex subunit 2	205.93	79	12
Q15008|PSMD6_HUMAN	26S proteasome non-ATPase regulator	201.47	41	12
Q99623|PHB2_HUMAN	Prohibitin-2 OS=Homo sapiens GN=PH	200.27	56	12
Q15056|IF4H_HUMAN	Eukaryotic translation initiation factor 4H	199.77	86	12

Q05682|CALD1_HUMAN	Caldesmon OS=Homo sapiens GN=CA	199.43	38	12
P23284|PPIB_HUMAN	Peptidyl-prolyl cis-trans isomerase B OS	197.78	58	12
P29692|EF1D_HUMAN	Elongation factor 1-delta OS=Homo sap	197.36	46	12
P49321|NASP_HUMAN	Nuclear autoantigenic sperm protein OS	196.07	45	12
P78417|GSTO1_HUMAN	Glutathione S-transferase omega-1 OS	195.01	44	12
Q13200|PSMD2_HUMAN	26S proteasome non-ATPase regulator	188.9	53	12
P17980|PRS6A_HUMAN	26S protease regulatory subunit 6A OS	182.86	53	12
O15144|ARPC2_HUMAN	Actin-related protein 2/3 complex subur	181.92	52	12
P61353|RL27_HUMAN	60S ribosomal protein L27 OS=Homo s	180.7	60	12
Q02878|RL6_HUMAN	60S ribosomal protein L6 OS=Homo sa	172.46	38	12
Q15907|RB11B_HUMAN	Ras-related protein Rab-11B OS=Homo	172.3	68	12
P42704|LPPRC_HUMAN	Leucine-rich PPR motif-containing prote	141.1	30	12
P30153|2AAA_HUMAN	Serine/threonine-protein phosphatase 2	249.96	67	11
P07741|APT_HUMAN	Adenine phosphoribosyltransferase OS	220.09	90	11
Q15084|PDIA6_HUMAN	Protein disulfide-isomerase A6 OS=Hor	218.87	67	11
P05387|RLA2_HUMAN	60S acidic ribosomal protein P2 OS=Ho	205.56	83	11
P28066|PSA5_HUMAN	Proteasome subunit alpha type-5 OS=H	204.62	72	11
P62158|CALM_HUMAN	Calmodulin OS=Homo sapiens GN=CA	201.81	59	11
P30086|PEBP1_HUMAN	Phosphatidylethanolamine-binding prote	201.55	68	11
Q92598|HS105_HUMAN	Heat shock protein 105 kDa OS=Homo	197.04	34	11
P40925|MDHC_HUMAN	Malate dehydrogenase, cytoplasmic OS	196.66	57	11
Q15691|MARE1_HUMAN	Microtubule-associated protein RP/EB f	196.23	44	11
P25786|PSA1_HUMAN	Proteasome subunit alpha type-1 OS=H	190.99	65	11
P17174|AATC_HUMAN	Aspartate aminotransferase, cytoplasmi	190.75	49	11
P43487|RANG_HUMAN	Ran-specific GTPase-activating protein	189.74	64	11
Q9BWD1|THIC_HUMAN	Acetyl-CoA acetyltransferase, cytosolic	186.62	61	11
P26639|SYTC_HUMAN	Threonyl-tRNA synthetase, cytoplasmic	183.97	41	11
Q04837|SSBP_HUMAN	Single-stranded DNA-binding protein, m	179.68	72	11
P46782|RS5_HUMAN	40S ribosomal protein S5 OS=Homo sa	179.5	57	11
P48681|NEST_HUMAN	Nestin OS=Homo sapiens GN=NES PE	178.4	18	11
P18621|RL17_HUMAN	60S ribosomal protein L17 OS=Homo s	174.85	61	11
P07093|GDN_HUMAN	Glia-derived nexin OS=Homo sapiens G	174.5	52	11
P60903|S10AA_HUMAN	Protein S100-A10 OS=Homo sapiens G	173.03	80	11
P18124|RL7_HUMAN	60S ribosomal protein L7 OS=Homo sa	172.34	59	11
P62760|VISL1_HUMAN	Visinin-like protein 1 OS=Homo sapiens	171.01	69	11
O15145|ARPC3_HUMAN	Actin-related protein 2/3 complex subur	163	49	11
P07814|SYEP_HUMAN	Bifunctional aminoacyl-tRNA synthetase	161.29	23	11
P09493|TPM1_HUMAN	Tropomyosin alpha-1 chain OS=Homo s	304.36	90	10
P06753|TPM3_HUMAN	Tropomyosin alpha-3 chain OS=Homo s	299.42	81	10
P31947|1433S_HUMAN	14-3-3 protein sigma OS=Homo sapiens	222.04	87	10
P62701|RS4X_HUMAN	40S ribosomal protein S4, X isoform OS	221.74	68	10
Q96FW1|OTUB1_HUMAN	Ubiquitin thioesterase OTUB1 OS=Hom	214.87	47	10
Q9Y696|CLIC4_HUMAN	Chloride intracellular channel protein 4 (	211.06	76	10
Q9NZI8|IF2B1_HUMAN	Insulin-like growth factor 2 mRNA-bindi	203.41	43	10
P63220|RS21_HUMAN	40S ribosomal protein S21 OS=Homo s	202.13	71	10
Q13907|IDI1_HUMAN	Isopentenyl-diphosphate Delta-isomera	201.96	59	10
O95336|6PGL_HUMAN	6-phosphogluconolactonase OS=Homo	201.05	77	10
P27695|APEX1_HUMAN	DNA-(apurinic or apyrimidinic site) lyase	200.37	61	10
P30084|ECHM_HUMAN	Enoyl-CoA hydratase, mitochondrial OS	199.04	68	10
Q7L2H7|EIF3M_HUMAN	Eukaryotic translation initiation factor 3	198.27	71	10
P26599|PTBP1_HUMAN	Polypyrimidine tract-binding protein 1 O	197.36	54	10
Q16851|UGPA_HUMAN	UTP--glucose-1-phosphate uridylyltrans	196.5	38	10
Q9Y265|RUVB1_HUMAN	RuvB-like 1 OS=Homo sapiens GN=RU	191.5	54	10
P62829|RL23_HUMAN	60S ribosomal protein L23 OS=Homo s	191.41	69	10
P30040|ERP29_HUMAN	Endoplasmic reticulum resident protein	190.48	56	10
P22102|PUR2_HUMAN	Trifunctional purine biosynthetic protein	189.59	42	10

P22061|PIMT_HUMAN	Protein-L-isoaspartate(D-aspartate) O-r	188.54	70	10
P50991|TCPD_HUMAN	T-complex protein 1 subunit delta OS=H	188.22	42	10
P24539|AT5F1_HUMAN	ATP synthase subunit b, mitochondrial (	187.12	48	10
O00151|PDLI1_HUMAN	PDZ and LIM domain protein 1 OS=Hor	184.55	42	10
O43242|PSMD3_HUMAN	26S proteasome non-ATPase regulator	181.74	44	10
P48047|ATPO_HUMAN	ATP synthase subunit O, mitochondrial	181.19	72	10
P15559|NQO1_HUMAN	NAD(P)H dehydrogenase [quinone] 1 O	177.1	56	10
P62249|RS16_HUMAN	40S ribosomal protein S16 OS=Homo s	174.88	66	10
Q00839|HNRPU_HUMAN	Heterogeneous nuclear ribonucleoprote	174.67	28	10
P51149|RAB7A_HUMAN	Ras-related protein Rab-7a OS=Homo s	174.17	56	10
Q14697|GANAB_HUMAN	Neutral alpha-glucosidase AB OS=Hom	174	28	10
Q07020|RL18_HUMAN	60S ribosomal protein L18 OS=Homo s	172.96	48	10
P62750|RL23A_HUMAN	60S ribosomal protein L23a OS=Homo	172.53	61	10
P63173|RL38_HUMAN	60S ribosomal protein L38 OS=Homo s	168.34	61	10
P53634|CATC_HUMAN	Dipeptidyl peptidase 1 OS=Homo sapie	165.77	31	10
P07237|PDIA1_HUMAN	Protein disulfide-isomerase OS=Homo s	165.08	39	10
P49755|TMEDA_HUMAN	Transmembrane emp24 domain-contair	164.65	48	10
P27816|MAP4_HUMAN	Microtubule-associated protein 4 OS=H	162.42	27	10
P17987|TCPA_HUMAN	T-complex protein 1 subunit alpha OS=	160.58	48	10
P26373|RL13_HUMAN	60S ribosomal protein L13 OS=Homo s	144.94	37	10
Q9GZZ1|NAA50_HUMAN	N-alpha-acetyltransferase 50, NatE cata	132.28	55	10
P12829|MYL4_HUMAN	Myosin light chain 4 OS=Homo sapiens	209.03	63	9
P09429|HMGB1_HUMAN	High mobility group protein B1 OS=Hom	205.41	61	9
P13797|PLST_HUMAN	Plastin-3 OS=Homo sapiens GN=PLS3	201.43	57	9
P49588|SYAC_HUMAN	Alanyl-tRNA synthetase, cytoplasmic O	197.17	52	9
P12268|IMDH2_HUMAN	Inosine-5'-monophosphate dehydrogen	194.48	37	9
P16401|H15_HUMAN	Histone H1.5 OS=Homo sapiens GN=H	193.64	58	9
P15880|RS2_HUMAN	40S ribosomal protein S2 OS=Homo sa	188.02	65	9
P09960|LKHA4_HUMAN	Leukotriene A-4 hydrolase OS=Homo s	186.75	46	9
P47756|CAPZB_HUMAN	F-actin-capping protein subunit beta OS	185.32	64	9
P00491|PNPH_HUMAN	Purine nucleoside phosphorylase OS=H	185.17	48	9
P14324|FPPS_HUMAN	Farnesyl pyrophosphate synthase OS=H	183.31	48	9
Q9UNM6|PSD13_HUMAN	26S proteasome non-ATPase regulator	182.21	55	9
P49720|PSB3_HUMAN	Proteasome subunit beta type-3 OS=Ho	181.6	64	9
P12004|PCNA_HUMAN	Proliferating cell nuclear antigen OS=Ho	180.66	59	9
P09382|LEG1_HUMAN	Galectin-1 OS=Homo sapiens GN=LGA	177.62	74	9
Q15404|RSU1_HUMAN	Ras suppressor protein 1 OS=Homo sa	174.31	68	9
P07108|ACBP_HUMAN	Acyl-CoA-binding protein OS=Homo sa	173.46	85	9
P38646|GRP75_HUMAN	Stress-70 protein, mitochondrial OS=Ho	171.62	31	9
Q99536|VAT1_HUMAN	Synaptic vesicle membrane protein VAT	170.64	52	9
P43686|PRS6B_HUMAN	26S protease regulatory subunit 6B OS	169.89	27	9
P62244|RS15A_HUMAN	40S ribosomal protein S15a OS=Homo	167.74	76	9
P09661|RU2A_HUMAN	U2 small nuclear ribonucleoprotein A' O	166.35	54	9
P14678|RSMB_HUMAN	Small nuclear ribonucleoprotein-associa	165.31	71	9
P63162|RSMN_HUMAN	Small nuclear ribonucleoprotein-associa	165.31	58	9
P60866|RS20_HUMAN	40S ribosomal protein S20 OS=Homo s	164.06	54	9
Q9Y295|DRG1_HUMAN	Developmentally-regulated GTP-binding	155.66	48	9
Q5T7N2|LITD1_HUMAN	LINE-1 type transposase domain-contai	154.94	32	9
P00505|AATM_HUMAN	Aspartate aminotransferase, mitochond	153.16	33	9
Q8N163|K1967_HUMAN	Protein KIAA1967 OS=Homo sapiens G	150.4	22	9
P41250|SYG_HUMAN	Glycyl-tRNA synthetase OS=Homo sapi	147.43	20	9
P18077|RL35A_HUMAN	60S ribosomal protein L35a OS=Homo	133.07	30	9
P60842|IF4A1_HUMAN	Eukaryotic initiation factor 4A-I OS=Hor	226.95	48	8
A6NL28|TPM3L_HUMAN	Putative tropomyosin alpha-3 chain-like	208.17	50	8
P61758|PFD3_HUMAN	Prefoldin subunit 3 OS=Homo sapiens (	199.6	68	8
Q01105|SET_HUMAN	Protein SET OS=Homo sapiens GN=SE	195.99	62	8

P54819|KAD2_HUMAN	Adenylate kinase 2, mitochondrial OS=H	185.35	69	8
P08865|RSSA_HUMAN	40S ribosomal protein SA OS=Homo sa	182.55	38	8
Q13185|CBX3_HUMAN	Chromobox protein homolog 3 OS=Hon	182.55	55	8
P60983|GMFB_HUMAN	Glia maturation factor beta OS=Homo s	180.6	61	8
P49903|SPS1_HUMAN	Selenide, water dikinase 1 OS=Homo s	180.22	53	8
P06493|CDK1_HUMAN	Cyclin-dependent kinase 1 OS=Homo s	179.88	62	8
P46783|RS10_HUMAN	40S ribosomal protein S10 OS=Homo s	179.6	57	8
P60981|DEST_HUMAN	Destrin OS=Homo sapiens GN=DSTN P	179.56	53	8
Q9Y3I0|RTCB_HUMAN	tRNA-splicing ligase RtcB homolog OS=	178.44	61	8
P31949|S10AB_HUMAN	Protein S100-A11 OS=Homo sapiens G	177.92	90	8
Q08J23|NSUN2_HUMAN	tRNA (cytosine(34)-C(5))-methyltransfe	177.48	41	8
Q99714|HCD2_HUMAN	3-hydroxyacyl-CoA dehydrogenase type	174.35	54	8
O43809|CPSF5_HUMAN	Cleavage and polyadenylation specificit	173.5	61	8
P61289|PSME3_HUMAN	Proteasome activator complex subunit 3	172.4	56	8
P16152|CBR1_HUMAN	Carbonyl reductase [NADPH] 1 OS=Ho	170.91	57	8
P62888|RL30_HUMAN	60S ribosomal protein L30 OS=Homo s	170.01	73	8
P60953|CDC42_HUMAN	Cell division control protein 42 homolog	169.87	53	8
Q13838|DX39B_HUMAN	Spliceosome RNA helicase DDX39B OS	168.78	32	8
Q14566|MCM6_HUMAN	DNA replication licensing factor MCM6 (	168.26	18	8
P62241|RS8_HUMAN	40S ribosomal protein S8 OS=Homo sa	166.8	57	8
P14550|AK1A1_HUMAN	Alcohol dehydrogenase [NADP+] OS=H	166.66	44	8
Q9NR30|DDX21_HUMAN	Nucleolar RNA helicase 2 OS=Homo sa	165.94	33	8
P61158|ARP3_HUMAN	Actin-related protein 3 OS=Homo sapie	165.63	31	8
P35268|RL22_HUMAN	60S ribosomal protein L22 OS=Homo s	164.76	71	8
O60701|UGDH_HUMAN	UDP-glucose 6-dehydrogenase OS=Ho	164.38	26	8
P25788|PSA3_HUMAN	Proteasome subunit alpha type-3 OS=H	164.07	49	8
O43765|SGTA_HUMAN	Small glutamine-rich tetratricopeptide re	163.55	43	8
P10909|CLUS_HUMAN	Clusterin OS=Homo sapiens GN=CLU P	161.11	26	8
Q9BT78|CSN4_HUMAN	COP9 signalosome complex subunit 4 (	161	44	8
Q15233|NONO_HUMAN	Non-POU domain-containing octamer-b	159.68	58	8
P30048|PRDX3_HUMAN	Thioredoxin-dependent peroxide reduct	158.44	42	8
P16949|STMN1_HUMAN	Stathmin OS=Homo sapiens GN=STMN	158.27	46	8
Q09666|AHNK_HUMAN	Neuroblast differentiation-associated pr	156.33	19	8
P35573|GDE_HUMAN	Glycogen debranching enzyme OS=Hor	155.97	22	8
Q9H9Q2|CSN7B_HUMAN	COP9 signalosome complex subunit 7b	155.47	46	8
Q9Y266|NUDC_HUMAN	Nuclear migration protein nudC OS=Ho	154.8	39	8
Q9P2J5|SYLC_HUMAN	Leucyl-tRNA synthetase, cytoplasmic O	154.16	25	8
P06454|PTMA_HUMAN	Prothymosin alpha OS=Homo sapiens (	153.41	62	8
P14868|SYDC_HUMAN	Aspartyl-tRNA synthetase, cytoplasmic	150.83	26	8
Q16181|SEPT7_HUMAN	Septin-7 OS=Homo sapiens GN=SEPT	149.87	45	8
Q07955|SRSF1_HUMAN	Serine/arginine-rich splicing factor 1 OS	147.48	47	8
P82979|SARNP_HUMAN	SAP domain-containing ribonucleoprote	146.35	57	8
P49721|PSB2_HUMAN	Proteasome subunit beta type-2 OS=Ho	145.15	36	8
Q9P258|RCC2_HUMAN	Protein RCC2 OS=Homo sapiens GN=R	140.96	34	8
P62851|RS25_HUMAN	40S ribosomal protein S25 OS=Homo s	138.86	38	8
Q15019|SEPT2_HUMAN	Septin-2 OS=Homo sapiens GN=SEPT	138.5	29	8
Q9UBE0|SAE1_HUMAN	SUMO-activating enzyme subunit 1 OS=	129.01	39	8
Q15075|EEA1_HUMAN	Early endosome antigen 1 OS=Homo s	118.81	15	8
P07437|TBB5_HUMAN	Tubulin beta chain OS=Homo sapiens (	336.6	82	7
P22392|NDKB_HUMAN	Nucleoside diphosphate kinase B OS=H	246.77	92	7
P84077|ARF1_HUMAN	ADP-ribosylation factor 1 OS=Homo sa	211.12	85	7
P61204|ARF3_HUMAN	ADP-ribosylation factor 3 OS=Homo sa	211.12	80	7
Q16555|DPYL2_HUMAN	Dihydropyrimidinase-related protein 2 O	197.25	55	7
P55209|NP1L1_HUMAN	Nucleosome assembly protein 1-like 1 (	196.55	34	7
P25787|PSA2_HUMAN	Proteasome subunit alpha type-2 OS=H	193.66	47	7
P60660|MYL6_HUMAN	Myosin light polypeptide 6 OS=Homo sa	188.78	68	7

P23526|SAHH_HUMAN	Adenosylhomocysteinase OS=Homo sa	185.35	45	7
Q99439|CNN2_HUMAN	Calponin-2 OS=Homo sapiens GN=CN	184.61	47	7
Q15181|IPYR_HUMAN	Inorganic pyrophosphatase OS=Homo	181.03	55	7
P02751|FINC_HUMAN	Fibronectin OS=Homo sapiens GN=FN	180.55	15	7
P30050|RL12_HUMAN	60S ribosomal protein L12 OS=Homo s	178.97	61	7
Q14195|DPYL3_HUMAN	Dihydropyrimidinase-related protein 3 O	178.97	41	7
Q12906|ILF3_HUMAN	Interleukin enhancer-binding factor 3 O	178.57	40	7
P07602|SAP_HUMAN	Proactivator polypeptide OS=Homo sap	174.69	49	7
P36405|ARL3_HUMAN	ADP-ribosylation factor-like protein 3 O	174.54	77	7
P27797|CALR_HUMAN	Calreticulin OS=Homo sapiens GN=CA	174.41	33	7
P52907|CAZA1_HUMAN	F-actin-capping protein subunit alpha-1	173.63	42	7
P45974|UBP5_HUMAN	Ubiquitin carboxyl-terminal hydrolase 5	173.14	24	7
P68036|UB2L3_HUMAN	Ubiquitin-conjugating enzyme E2 L3 OS	172.83	68	7
Q92499|DDX1_HUMAN	ATP-dependent RNA helicase DDX1 O	171.05	35	7
Q15942|ZYX_HUMAN	Zyxin OS=Homo sapiens GN=ZYX PE=	170.75	29	7
Q71UI9|H2AV_HUMAN	Histone H2A.V OS=Homo sapiens GN=	168.63	56	7
P0C0S5|H2AZ_HUMAN	Histone H2A.Z OS=Homo sapiens GN=	168.63	56	7
P62753|RS6_HUMAN	40S ribosomal protein S6 OS=Homo sa	168.53	34	7
P53999|TCP4_HUMAN	Activated RNA polymerase II transcripti	168.38	51	7
Q13126|MTAP_HUMAN	S-methyl-5'-thioadenosine phosphorylas	167.58	48	7
P61106|RAB14_HUMAN	Ras-related protein Rab-14 OS=Homo	166.8	52	7
P20290|BTF3_HUMAN	Transcription factor BTF3 OS=Homo sa	166.72	66	7
Q9Y2B0|CNPY2_HUMAN	Protein canopy homolog 2 OS=Homo s	166.64	60	7
P37108|SRP14_HUMAN	Signal recognition particle 14 kDa prote	166.3	43	7
P50502|F10A1_HUMAN	Hsc70-interacting protein OS=Homo sa	165.92	33	7
P05067|A4_HUMAN	Amyloid beta A4 protein OS=Homo sap	165.88	26	7
P33176|KINH_HUMAN	Kinesin-1 heavy chain OS=Homo sapie	164.98	43	7
Q9H4A6|GOLP3_HUMAN	Golgi phosphoprotein 3 OS=Homo sapi	164.79	39	7
Q92626|PXDN_HUMAN	Peroxidasin homolog OS=Homo sapien	164.48	19	7
Q12904|AIMP1_HUMAN	Aminoacyl tRNA synthase complex-inte	164.32	38	7
Q9Y3F4|STRAP_HUMAN	Serine-threonine kinase receptor-assoc	163.17	37	7
P62841|RS15_HUMAN	40S ribosomal protein S15 OS=Homo s	161.77	51	7
P24534|EF1B_HUMAN	Elongation factor 1-beta OS=Homo sap	161.67	39	7
Q13263|TIF1B_HUMAN	Transcription intermediary factor 1-beta	159.97	28	7
P61019|RAB2A_HUMAN	Ras-related protein Rab-2A OS=Homo	159.04	41	7
P63279|UBC9_HUMAN	SUMO-conjugating enzyme UBC9 OS=	158.47	32	7
Q15843|NEDD8_HUMAN	NEDD8 OS=Homo sapiens GN=NEDD8	157.58	62	7
P61088|UBE2N_HUMAN	Ubiquitin-conjugating enzyme E2 N OS=	156.94	68	7
Q02790|FKBP4_HUMAN	Peptidyl-prolyl cis-trans isomerase FKB	156.86	31	7
P46926|GNPI1_HUMAN	Glucosamine-6-phosphate isomerase 1	156.83	42	7
Q9HC38|GLOD4_HUMAN	Glyoxalase domain-containing protein 4	156.2	36	7
P30046|DOPD_HUMAN	D-dopachrome decarboxylase OS=Hom	155.11	56	7
Q9Y2Z0|SUGT1_HUMAN	Suppressor of G2 allele of SKP1 homol	154.77	47	7
Q13557|KCC2D_HUMAN	Calcium/calmodulin-dependent protein	154.3	42	7
Q9H3K6|BOLA2_HUMAN	BolA-like protein 2 OS=Homo sapiens	153.94	72	7
Q08211|DHX9_HUMAN	ATP-dependent RNA helicase A OS=H	153.93	17	7
Q02543|RL18A_HUMAN	60S ribosomal protein L18a OS=Homo	153.88	47	7
P08708|RS17_HUMAN	40S ribosomal protein S17 OS=Homo s	153.64	76	7
O00232|PSD12_HUMAN	26S proteasome non-ATPase regulator	153.09	39	7
P59998|ARPC4_HUMAN	Actin-related protein 2/3 complex subur	152.93	62	7
O75489|NDUS3_HUMAN	NADH dehydrogenase [ubiquinone] iron	152.91	50	7
P43243|MATR3_HUMAN	Matrin-3 OS=Homo sapiens GN=MATR	152.12	29	7
P32969|RL9_HUMAN	60S ribosomal protein L9 OS=Homo sa	151.38	58	7
P46778|RL21_HUMAN	60S ribosomal protein L21 OS=Homo s	151.07	40	7
P05937|CALB1_HUMAN	Calbindin OS=Homo sapiens GN=CALB	150.86	45	7
Q15149|PLEC_HUMAN	Plectin OS=Homo sapiens GN=PLEC P	149.19	18	7

Q5VYK3|ECM29_HUMAN	Proteasome-associated protein ECM29	149.05	37	7
Q9BYT8|NEUL_HUMAN	Neurolysin, mitochondrial OS=Homo sa	148.81	24	7
Q9NZL4|HPBP1_HUMAN	Hsp70-binding protein 1 OS=Homo sap	148.69	33	7
Q16658|FSCN1_HUMAN	Fascin OS=Homo sapiens GN=FSCN1	148.66	32	7
P55145|MANF_HUMAN	Mesencephalic astrocyte-derived neuro	148.56	54	7
P36578|RL4_HUMAN	60S ribosomal protein L4 OS=Homo sa	146.26	23	7
P62633|CNBP_HUMAN	Cellular nucleic acid-binding protein OS	146.06	53	7
Q13283|G3BP1_HUMAN	Ras GTPase-activating protein-binding	145.21	27	7
P55769|NH2L1_HUMAN	NHP2-like protein 1 OS=Homo sapiens	144.72	41	7
P61081|UBC12_HUMAN	NEDD8-conjugating enzyme Ubc12 OS	144.21	44	7
P62857|RS28_HUMAN	40S ribosomal protein S28 OS=Homo s	143.07	57	7
P63000|RAC1_HUMAN	Ras-related C3 botulinum toxin substrat	142.95	35	7
Q86VP6|CAND1_HUMAN	Cullin-associated NEDD8-dissociated p	141.54	17	7
Q9NP97|DLRB1_HUMAN	Dynein light chain roadblock-type 1 OS=	139.12	91	7
Q92616|GCN1L_HUMAN	Translational activator GCN1 OS=Homo	138.81	17	7
P27635|RL10_HUMAN	60S ribosomal protein L10 OS=Homo s	138.37	31	7
P25205|MCM3_HUMAN	DNA replication licensing factor MCM3 (	137.11	38	7
Q15370|ELOB_HUMAN	Transcription elongation factor B polype	136.92	49	7
P48556|PSMD8_HUMAN	26S proteasome non-ATPase regulator	129.8	35	7
O75947|ATP5H_HUMAN	ATP synthase subunit d, mitochondrial (	125.39	55	7
P52701|MSH6_HUMAN	DNA mismatch repair protein Msh6 OS=	125.36	15	7
O43324|MCA3_HUMAN	Eukaryotic translation elongation factor	117.5	40	7
Q9BXJ9|NAA15_HUMAN	N-alpha-acetyltransferase 15, NatA aux	117.3	13	7
P12270|TPR_HUMAN	Nucleoprotein TPR OS=Homo sapiens	117	12	7
P62136|PP1A_HUMAN	Serine/threonine-protein phosphatase F	243.73	62	6
Q9BUF5|TBB6_HUMAN	Tubulin beta-6 chain OS=Homo sapiens	236.14	78	6
P15531|NDKA_HUMAN	Nucleoside diphosphate kinase A OS=H	234.26	72	6
Q06323|PSME1_HUMAN	Proteasome activator complex subunit 1	180.47	65	6
P21291|CSRP1_HUMAN	Cysteine and glycine-rich protein 1 OS=	177.09	65	6
Q15121|PEA15_HUMAN	Astrocytic phosphoprotein PEA-15 OS=	173.78	88	6
P36404|ARL2_HUMAN	ADP-ribosylation factor-like protein 2 OS	172.92	53	6
P52292|IMA2_HUMAN	Importin subunit alpha-2 OS=Homo sap	172.76	37	6
P21796|VDAC1_HUMAN	Voltage-dependent anion-selective cha	168.48	43	6
Q9Y333|LSM2_HUMAN	U6 snRNA-associated Sm-like protein L	168.45	86	6
O60610|DIAP1_HUMAN	Protein diaphanous homolog 1 OS=Hor	168.43	26	6
Q99598|TSNAX_HUMAN	Translin-associated protein X OS=Homo	167.99	57	6
Q9Y262|EIF3L_HUMAN	Eukaryotic translation initiation factor 3	167.96	35	6
Q96FQ6|S10AG_HUMAN	Protein S100-A16 OS=Homo sapiens G	165.62	56	6
P04632|CPNS1_HUMAN	Calpain small subunit 1 OS=Homo sapi	164.99	63	6
Q14103|HNRPD_HUMAN	Heterogeneous nuclear ribonucleoprote	164.86	45	6
Q15365|PCBP1_HUMAN	Poly(rC)-binding protein 1 OS=Homo sa	164.63	64	6
P20700|LMNB1_HUMAN	Lamin-B1 OS=Homo sapiens GN=LMN	163.92	33	6
P35221|CTNA1_HUMAN	Catenin alpha-1 OS=Homo sapiens GN	162.63	41	6
Q9UBQ7|GRHPR_HUMAN	Glyoxylate reductase/hydroxypyruvate r	162.59	41	6
P13073|COX41_HUMAN	Cytochrome c oxidase subunit 4 isoform	161.11	62	6
P63313|TYB10_HUMAN	Thymosin beta-10 OS=Homo sapiens G	159.97	82	6
Q99471|PFD5_HUMAN	Prefoldin subunit 5 OS=Homo sapiens (	155.84	60	6
Q16643|DREB_HUMAN	Drebrin OS=Homo sapiens GN=DBN1 I	155.38	24	6
Q9Y3B8|ORN_HUMAN	Oligoribonuclease, mitochondrial OS=H	155.01	45	6
P62913|RL11_HUMAN	60S ribosomal protein L11 OS=Homo s	154.16	30	6
Q9UKK9|NUDT5_HUMAN	ADP-sugar pyrophosphatase OS=Homo	151.76	36	6
Q8WW12|PCNP_HUMAN	PEST proteolytic signal-containing nucl	151.72	57	6
P29762|RABP1_HUMAN	Cellular retinoic acid-binding protein 1 O	150.66	53	6
P84103|SRSF3_HUMAN	Serine/arginine-rich splicing factor 3 OS	150.21	46	6
O14737|PDCD5_HUMAN	Programmed cell death protein 5 OS=H	148.72	51	6
P33993|MCM7_HUMAN	DNA replication licensing factor MCM7 (	148.56	30	6

P11177|ODPB_HUMAN	Pyruvate dehydrogenase E1 componen	147.9	45	6
P05388|RLA0_HUMAN	60S acidic ribosomal protein P0 OS=Ho	147.46	30	6
Q9NTK5|OLA1_HUMAN	Obg-like ATPase 1 OS=Homo sapiens (	147.09	32	6
P50552|VASP_HUMAN	Vasodilator-stimulated phosphoprotein (	145.35	46	6
P49736|MCM2_HUMAN	DNA replication licensing factor MCM2 (	145.31	36	6
P62917|RL8_HUMAN	60S ribosomal protein L8 OS=Homo sa	144.43	38	6
P13667|PDIA4_HUMAN	Protein disulfide-isomerase A4 OS=Hor	143.85	16	6
Q9Y4L1|HYOU1_HUMAN	Hypoxia up-regulated protein 1 OS=Hor	143.53	25	6
Q12765|SCRN1_HUMAN	Secernin-1 OS=Homo sapiens GN=SCI	143.3	26	6
P00492|HPRT_HUMAN	Hypoxanthine-guanine phosphoribosyltr	143.03	31	6
Q9Y5K6|CD2AP_HUMAN	CD2-associated protein OS=Homo sapi	142.91	23	6
O00244|ATOX1_HUMAN	Copper transport protein ATOX1 OS=H	142.36	78	6
P13693|TCTP_HUMAN	Translationally-controlled tumor protein	141.86	40	6
O14579|COPE_HUMAN	Coatomer subunit epsilon OS=Homo sa	140.79	39	6
P49915|GUAA_HUMAN	GMP synthase [glutamine-hydrolyzing] (	140.65	31	6
O15372|EIF3H_HUMAN	Eukaryotic translation initiation factor 3	140.43	38	6
P02545|LMNA_HUMAN	Prelamin-A/C OS=Homo sapiens GN=L	139.03	22	6
O15347|HMGB3_HUMAN	High mobility group protein B3 OS=Hom	138.78	36	6
P49773|HINT1_HUMAN	Histidine triad nucleotide-binding protei	138.55	44	6
P47985|UCRI_HUMAN	Cytochrome b-c1 complex subunit Ries	138.07	50	6
P50914|RL14_HUMAN	60S ribosomal protein L14 OS=Homo s	137.31	41	6
P33991|MCM4_HUMAN	DNA replication licensing factor MCM4 (	136.27	29	6
Q92945|FUBP2_HUMAN	Far upstream element-binding protein 2	136.11	21	6
P62899|RL31_HUMAN	60S ribosomal protein L31 OS=Homo s	134.45	49	6
O75223|GGCT_HUMAN	Gamma-glutamylcyclotransferase OS=H	134.27	70	6
P54578|UBP14_HUMAN	Ubiquitin carboxyl-terminal hydrolase 14	134.27	27	6
P07686|HEXB_HUMAN	Beta-hexosaminidase subunit beta OS=	133.34	21	6
P07942|LAMB1_HUMAN	Laminin subunit beta-1 OS=Homo sapie	132.97	23	6
P24666|PPAC_HUMAN	Low molecular weight phosphotyrosine	132.04	51	6
P54136|SYRC_HUMAN	Arginyl-tRNA synthetase, cytoplasmic C	131.23	21	6
P07339|CATD_HUMAN	Cathepsin D OS=Homo sapiens GN=CT	129.38	24	6
P09525|ANXA4_HUMAN	Annexin A4 OS=Homo sapiens GN=AN	127.84	40	6
Q93009|UBP7_HUMAN	Ubiquitin carboxyl-terminal hydrolase 7	127.06	15	6
P27144|KAD4_HUMAN	Adenylate kinase isoenzyme 4, mitocho	126.67	32	6
O95671|ASML_HUMAN	N-acetylserotonin O-methyltransferase-	126.58	32	6
O76003|GLRX3_HUMAN	Glutaredoxin-3 OS=Homo sapiens GN=	126.53	43	6
P20674|COX5A_HUMAN	Cytochrome c oxidase subunit 5A, mito	126.09	43	6
P09669|COX6C_HUMAN	Cytochrome c oxidase subunit 6C OS=H	124.52	61	6
Q14204|DYHC1_HUMAN	Cytoplasmic dynein 1 heavy chain 1 OS	124.05	17	6
Q6PKG0|LARP1_HUMAN	La-related protein 1 OS=Homo sapiens	123.34	17	6
Q9NUP9|LIN7C_HUMAN	Protein lin-7 homolog C OS=Homo sapi	122.09	44	6
P46779|RL28_HUMAN	60S ribosomal protein L28 OS=Homo s	121.53	42	6
A0MZ66|SHOT1_HUMAN	Shootin-1 OS=Homo sapiens GN=KIAA	119.09	16	6
P46821|MAP1B_HUMAN	Microtubule-associated protein 1B OS=	117.05	12	6
P62312|LSM6_HUMAN	U6 snRNA-associated Sm-like protein L	112.24	46	6
P14174|MIF_HUMAN	Macrophage migration inhibitory factor (	107.42	21	6
Q14978|NOLC1_HUMAN	Nucleolar and coiled-body phosphoprot	99.59	20	6
O43491|E41L2_HUMAN	Band 4.1-like protein 2 OS=Homo sapie	97.88	13	6
Q8WZ42|TITIN_HUMAN	Titin OS=Homo sapiens GN=TTN PE=1	73.43	6	6
Q9H0U4|RAB1B_HUMAN	Ras-related protein Rab-1B OS=Homo	192.63	70	5
Q13765|NACA_HUMAN	Nascent polypeptide-associated comple	181.13	45	5
Q13310|PABP4_HUMAN	Polyadenylate-binding protein 4 OS=Ho	178.55	39	5
O60506|HNRPQ_HUMAN	Heterogeneous nuclear ribonucleprote	176.7	37	5
Q92841|DDX17_HUMAN	Probable ATP-dependent RNA helicase	175.85	36	5
Q99733|NP1L4_HUMAN	Nucleosome assembly protein 1-like 4 (	162.28	31	5
P83916|CBX1_HUMAN	Chromobox protein homolog 1 OS=Hon	160.03	36	5

O43399|TPD54_HUMAN	Tumor protein D54 OS=Homo sapiens (	158.98	63	5
P13804|ETFA_HUMAN	Electron transfer flavoprotein subunit al	158.63	42	5
P46060|RAGP1_HUMAN	Ran GTPase-activating protein 1 OS=H	158.3	59	5
O00429|DNM1L_HUMAN	Dynamin-1-like protein OS=Homo sapie	156.28	41	5
Q9Y5L4|TIM13_HUMAN	Mitochondrial import inner membrane tr	156	79	5
P22087|FBRL_HUMAN	rRNA 2'-O-methyltransferase fibrillarin (	155.35	45	5
Q9BUT1|BDH2_HUMAN	3-hydroxybutyrate dehydrogenase type	154.27	50	5
Q15185|TEBP_HUMAN	Prostaglandin E synthase 3 OS=Homo	153.53	63	5
O75348|VATG1_HUMAN	V-type proton ATPase subunit G 1 OS=	152.94	43	5
P62314|SMD1_HUMAN	Small nuclear ribonucleoprotein Sm D1	150.93	54	5
P36969|GPX4_HUMAN	Phospholipid hydroperoxide glutathione	150.71	42	5
P61970|NTF2_HUMAN	Nuclear transport factor 2 OS=Homo sa	150.68	81	5
P61160|ARP2_HUMAN	Actin-related protein 2 OS=Homo sapie	150.56	37	5
P52565|GDIR1_HUMAN	Rho GDP-dissociation inhibitor 1 OS=H	148.99	41	5
Q14444|CAPR1_HUMAN	Caprin-1 OS=Homo sapiens GN=CAPR	148.85	24	5
P28072|PSB6_HUMAN	Proteasome subunit beta type-6 OS=Ho	148.75	60	5
P05198|IF2A_HUMAN	Eukaryotic translation initiation factor 2	148.23	40	5
P17096|HMGA1_HUMAN	High mobility group protein HMG-I/HMG	146.09	71	5
Q15785|TOM34_HUMAN	Mitochondrial import receptor subunit T(	144.63	38	5
P55327|TPD52_HUMAN	Tumor protein D52 OS=Homo sapiens (	143.28	45	5
A6NDG6|PGP_HUMAN	Phosphoglycolate phosphatase OS=Ho	143.21	51	5
P43246|MSH2_HUMAN	DNA mismatch repair protein Msh2 OS=	142.84	23	5
P54920|SNAA_HUMAN	Alpha-soluble NSF attachment protein (	142.08	43	5
P56537|IF6_HUMAN	Eukaryotic translation initiation factor 6	141.86	45	5
P08590|MYL3_HUMAN	Myosin light chain 3 OS=Homo sapiens	141.71	54	5
P28838|AMPL_HUMAN	Cytosol aminopeptidase OS=Homo sap	141.63	19	5
Q13619|CUL4A_HUMAN	Cullin-4A OS=Homo sapiens GN=CUL4	141.56	22	5
Q6GMV3|CB079_HUMAN	Uncharacterized protein C2orf79 OS=H	140.53	47	5
P35520|CBS_HUMAN	Cystathionine beta-synthase OS=Homo	139.65	30	5
P04818|TYSY_HUMAN	Thymidylate synthase OS=Homo sapier	137.73	42	5
P10599|THIO_HUMAN	Thioredoxin OS=Homo sapiens GN=TX	137.64	55	5
P62304|RUXE_HUMAN	Small nuclear ribonucleoprotein E OS=I	137.16	73	5
Q13616|CUL1_HUMAN	Cullin-1 OS=Homo sapiens GN=CUL1 I	136.98	27	5
Q07021|C1QBP_HUMAN	Complement component 1 Q subcompo	136.76	26	5
P28070|PSB4_HUMAN	Proteasome subunit beta type-4 OS=Ho	136.62	39	5
Q15046|SYK_HUMAN	Lysyl-tRNA synthetase OS=Homo sapie	136.46	19	5
Q13011|ECH1_HUMAN	Delta(3,5)-Delta(2,4)-dienoyl-CoA isome	135.78	26	5
P42766|RL35_HUMAN	60S ribosomal protein L35 OS=Homo s	135.76	31	5
Q9BRX8|CJ058_HUMAN	UPF0765 protein C10orf58 OS=Homo s	135.53	57	5
Q9UHV9|PFD2_HUMAN	Prefoldin subunit 2 OS=Homo sapiens (	135.52	63	5
Q96AE4|FUBP1_HUMAN	Far upstream element-binding protein 1	135.35	31	5
P30520|PURA2_HUMAN	Adenylosuccinate synthetase isozyme 2	134.92	25	5
P26196|DDX6_HUMAN	Probable ATP-dependent RNA helicase	134.91	32	5
Q9UBQ5|EIF3K_HUMAN	Eukaryotic translation initiation factor 3	134.67	38	5
Q99622|C10_HUMAN	Protein C10 OS=Homo sapiens GN=C1	134.51	48	5
Q15417|CNN3_HUMAN	Calponin-3 OS=Homo sapiens GN=CNI	133.86	29	5
P63208|SKP1_HUMAN	S-phase kinase-associated protein 1 OS	133.12	34	5
P30566|PUR8_HUMAN	Adenylosuccinate lyase OS=Homo sapi	132.58	24	5
Q08257|QOR_HUMAN	Quinone oxidoreductase OS=Homo sap	131.97	36	5
Q9NZJ9|NUDT4_HUMAN	Diphosphoinositol polyphosphate phosp	131.71	53	5
Q9H910|HN1L_HUMAN	Hematological and neurological express	131.22	41	5
Q9Y4Z0|LSM4_HUMAN	U6 snRNA-associated Sm-like protein L	130.73	55	5
Q99873|ANM1_HUMAN	Protein arginine N-methyltransferase 1 (	128.61	20	5
Q13868|EXOS2_HUMAN	Exosome complex component RRP4 O	128.58	36	5
P23381|SYWC_HUMAN	Tryptophanyl-tRNA synthetase, cytoplas	128.08	36	5
Q9Y5Y2|NUBP2_HUMAN	Cytosolic Fe-S cluster assembly factor N	127.96	46	5

Q53GQ0|DHB12_HUMAN	Estradiol 17-beta-dehydrogenase 12 OS	126.82	29	5
P36542|ATPG_HUMAN	ATP synthase subunit gamma, mitocho	126.11	20	5
P51571|SSRD_HUMAN	Translocon-associated protein subunit d	125.65	36	5
P23142|FBLN1_HUMAN	Fibulin-1 OS=Homo sapiens GN=FBLN	125.2	10	5
P36871|PGM1_HUMAN	Phosphoglucomutase-1 OS=Homo sap	125.04	25	5
P42574|CASP3_HUMAN	Caspase-3 OS=Homo sapiens GN=CAS	124.36	34	5
Q14847|LASP1_HUMAN	LIM and SH3 domain protein 1 OS=Hor	124.13	22	5
O00233|PSMD9_HUMAN	26S proteasome non-ATPase regulator	122.79	24	5
O75083|WDR1_HUMAN	WD repeat-containing protein 1 OS=Ho	122.74	27	5
P17858|K6PL_HUMAN	6-phosphofructokinase, liver type OS=H	122.52	29	5
P56385|ATP5I_HUMAN	ATP synthase subunit e, mitochondrial	121.73	62	5
P48739|PIPNB_HUMAN	Phosphatidylinositol transfer protein bet	121.53	33	5
Q02952|AKA12_HUMAN	A-kinase anchor protein 12 OS=Homo s	121.52	17	5
P19623|SPEE_HUMAN	Spermidine synthase OS=Homo sapien	121.36	31	5
P23193|TCEA1_HUMAN	Transcription elongation factor A protein	121.15	34	5
P14735|IDE_HUMAN	Insulin-degrading enzyme OS=Homo sa	120.41	18	5
P49419|AL7A1_HUMAN	Alpha-aminoadipic semialdehyde dehyd	120.33	22	5
P33316|DUT_HUMAN	Deoxyuridine 5'-triphosphate nucleotido	120.29	33	5
P83731|RL24_HUMAN	60S ribosomal protein L24 OS=Homo s	120.2	38	5
P61221|ABCE1_HUMAN	ATP-binding cassette sub-family E mem	119.89	26	5
Q07866|KLC1_HUMAN	Kinesin light chain 1 OS=Homo sapiens	119.79	24	5
P62310|LSM3_HUMAN	U6 snRNA-associated Sm-like protein L	119.72	71	5
Q9BUL8|PDC10_HUMAN	Programmed cell death protein 10 OS=	119.72	29	5
O76094|SRP72_HUMAN	Signal recognition particle 72 kDa prote	119.34	31	5
Q00341|VIGLN_HUMAN	Vigilin OS=Homo sapiens GN=HDLBP	119.28	21	5
P62306|RUXF_HUMAN	Small nuclear ribonucleoprotein F OS=H	117.29	58	5
Q9NR31|SAR1A_HUMAN	GTP-binding protein SAR1a OS=Homo	117.12	25	5
P20340|RAB6A_HUMAN	Ras-related protein Rab-6A OS=Homo	117.06	39	5
P49458|SRP09_HUMAN	Signal recognition particle 9 kDa protein	116.38	57	5
O15143|ARC1B_HUMAN	Actin-related protein 2/3 complex subun	116.24	29	5
Q96C36|P5CR2_HUMAN	Pyrroline-5-carboxylate reductase 2 OS	115.93	32	5
P48061|SDF1_HUMAN	Stromal cell-derived factor 1 OS=Homo	115.65	42	5
P35249|RFC4_HUMAN	Replication factor C subunit 4 OS=Hom	115.58	22	5
Q8NFF5|FAD1_HUMAN	FAD synthase OS=Homo sapiens GN=F	115.43	27	5
Q9BPW8|NIPS1_HUMAN	Protein NipSnap homolog 1 OS=Homo	114.5	26	5
Q13242|SRSF9_HUMAN	Serine/arginine-rich splicing factor 9 OS	114.01	34	5
Q16543|CDC37_HUMAN	Hsp90 co-chaperone Cdc37 OS=Homo	113.75	27	5
Q15102|PA1B3_HUMAN	Platelet-activating factor acetylhydrolas	113.18	35	5
Q14203|DCTN1_HUMAN	Dynactin subunit 1 OS=Homo sapiens G	112.77	27	5
P49591|SYSC_HUMAN	Seryl-tRNA synthetase, cytoplasmic OS	112.66	24	5
P06730|IF4E_HUMAN	Eukaryotic translation initiation factor 4E	108.68	20	5
P08243|ASNS_HUMAN	Asparagine synthetase [glutamine-hydr	108.57	19	5
P13798|ACPH_HUMAN	Acylamino-acid-releasing enzyme OS=H	108.49	12	5
P41091|IF2G_HUMAN	Eukaryotic translation initiation factor 2	108.11	31	5
P07203|GPX1_HUMAN	Glutathione peroxidase 1 OS=Homo sa	107.71	36	5
P55786|PSA_HUMAN	Puromycin-sensitive aminopeptidase OS	102.38	12	5
Q9UIJ7|KAD3_HUMAN	GTP:AMP phosphotransferase, mitocho	99.68	24	5
O60925|PFD1_HUMAN	Prefoldin subunit 1 OS=Homo sapiens G	99.18	38	5
Q9UKM9|RALY_HUMAN	RNA-binding protein Raly OS=Homo sa	97.85	32	5
P35612|ADDB_HUMAN	Beta-adducin OS=Homo sapiens GN=A	97.71	21	5
Q15459|SF3A1_HUMAN	Splicing factor 3A subunit 1 OS=Homo	94.15	13	5
Q9BVK6|TMED9_HUMAN	Transmembrane emp24 domain-contain	92.8	26	5
Q13509|TBB3_HUMAN	Tubulin beta-3 chain OS=Homo sapiens	295.38	75	4
P62140|PP1B_HUMAN	Serine/threonine-protein phosphatase P	226.21	49	4
P16403|H12_HUMAN	Histone H1.2 OS=Homo sapiens GN=H	216.11	54	4
Q99877|H2B1N_HUMAN	Histone H2B type 1-N OS=Homo sapien	197.21	66	4

P62807|H2B1C_HUMAN	Histone H2B type 1-C/E/F/G/I OS=Hom	197.21	57	4
P58876|H2B1D_HUMAN	Histone H2B type 1-D OS=Homo sapier	197.21	57	4
Q93079|H2B1H_HUMAN	Histone H2B type 1-H OS=Homo sapier	197.21	57	4
O60814|H2B1K_HUMAN	Histone H2B type 1-K OS=Homo sapier	197.21	57	4
Q99879|H2B1M_HUMAN	Histone H2B type 1-M OS=Homo sapie	197.21	57	4
Q5QNW6|H2B2F_HUMAN	Histone H2B type 2-F OS=Homo sapier	197.21	57	4
P57053|H2BFS_HUMAN	Histone H2B type F-S OS=Homo sapier	197.21	52	4
P18085|ARF4_HUMAN	ADP-ribosylation factor 4 OS=Homo sa	187.48	81	4
P35241|RADI_HUMAN	Radixin OS=Homo sapiens GN=RDX P	179.37	32	4
Q13162|PRDX4_HUMAN	Peroxiredoxin-4 OS=Homo sapiens GN	179	38	4
Q96FJ2|DYL2_HUMAN	Dynein light chain 2, cytoplasmic OS=H	174.74	65	4
P31943|HNRH1_HUMAN	Heterogeneous nuclear ribonucleoprote	159.81	38	4
P26583|HMGB2_HUMAN	High mobility group protein B2 OS=Hom	157.67	33	4
P38919|IF4A3_HUMAN	Eukaryotic initiation factor 4A-III OS=Ho	157.14	33	4
O00425|IF2B3_HUMAN	Insulin-like growth factor 2 mRNA-bindi	155.79	30	4
P39687|AN32A_HUMAN	Acidic leucine-rich nuclear phosphoprot	154.16	31	4
Q9NUQ9|FA49B_HUMAN	Protein FAM49B OS=Homo sapiens GN	151.38	41	4
Q15436|SC23A_HUMAN	Protein transport protein Sec23A OS=H	149.19	27	4
P31153|METK2_HUMAN	S-adenosylmethionine synthase isoform	147.82	32	4
P43490|NAMPT_HUMAN	Nicotinamide phosphoribosyltransferase	146.85	54	4
P30085|KCY_HUMAN	UMP-CMP kinase OS=Homo sapiens G	146.6	44	4
P09455|RET1_HUMAN	Retinol-binding protein 1 OS=Homo sap	146.33	44	4
Q99729|ROAA_HUMAN	Heterogeneous nuclear ribonucleoprote	145.1	36	4
P38159|HNRPG_HUMAN	Heterogeneous nuclear ribonucleoprote	144.1	46	4
Q15366|PCBP2_HUMAN	Poly(rC)-binding protein 2 OS=Homo sa	143.12	51	4
Q9NWU2|CT011_HUMAN	Protein C20orf11 OS=Homo sapiens G	141.57	48	4
Q9ULZ3|ASC_HUMAN	Apoptosis-associated speck-like protein	141.54	40	4
P62847|RS24_HUMAN	40S ribosomal protein S24 OS=Homo s	138.89	44	4
P61923|COPZ1_HUMAN	Coatomer subunit zeta-1 OS=Homo sap	138.84	40	4
Q9UI30|TR112_HUMAN	tRNA methyltransferase 112 homolog C	137.88	56	4
P49411|EFTU_HUMAN	Elongation factor Tu, mitochondrial OS=	136.06	23	4
Q9BRA2|TXD17_HUMAN	Thioredoxin domain-containing protein	135.66	43	4
Q9UBQ0|VPS29_HUMAN	Vacuolar protein sorting-associated pro	135.66	45	4
P34897|GLYM_HUMAN	Serine hydroxymethyltransferase, mitoc	135.37	23	4
P05386|RLA1_HUMAN	60S acidic ribosomal protein P1 OS=Ho	135.35	66	4
P04216|THY1_HUMAN	Thy-1 membrane glycoprotein OS=Hom	134.55	30	4
O75608|LYPA1_HUMAN	Acyl-protein thioesterase 1 OS=Homo s	134.27	37	4
P13716|HEM2_HUMAN	Delta-aminolevulinic acid dehydratase C	133.85	38	4
P62834|RAP1A_HUMAN	Ras-related protein Rap-1A OS=Homo	133.82	27	4
P61224|RAP1B_HUMAN	Ras-related protein Rap-1b OS=Homo	133.82	27	4
P08579|RU2B_HUMAN	U2 small nuclear ribonucleoprotein B" C	133.69	30	4
Q9BS26|ERP44_HUMAN	Endoplasmic reticulum resident protein	133.02	33	4
P55010|IF5_HUMAN	Eukaryotic translation initiation factor 5	132.77	34	4
Q96AG4|LRC59_HUMAN	Leucine-rich repeat-containing protein 5	131.75	33	4
Q16629|SRSF7_HUMAN	Serine/arginine-rich splicing factor 7 OS	131.7	20	4
Q9UGI8|TES_HUMAN	Testin OS=Homo sapiens GN=TES PE	131.58	17	4
Q9Y3B4|PM14_HUMAN	Pre-mRNA branch site protein p14 OS=	131.55	42	4
Q9BZZ5|API5_HUMAN	Apoptosis inhibitor 5 OS=Homo sapiens	130.78	34	4
P41567|EIF1_HUMAN	Eukaryotic translation initiation factor 1	130.36	63	4
Q9NY33|DPP3_HUMAN	Dipeptidyl peptidase 3 OS=Homo sapie	130.1	23	4
Q00688|FKBP3_HUMAN	Peptidyl-prolyl cis-trans isomerase FKB	129.99	38	4
Q8NBS9|TXND5_HUMAN	Thioredoxin domain-containing protein	129.86	21	4
Q8IXM2|BAP18_HUMAN	Chromatin complexes subunit BAP18 C	129.54	44	4
P61026|RAB10_HUMAN	Ras-related protein Rab-10 OS=Homo	129	52	4
Q9ULC4|MCTS1_HUMAN	Malignant T cell-amplified sequence 1 C	128.22	51	4
P84090|ERH_HUMAN	Enhancer of rudimentary homolog OS=	127.9	53	4

Q96IZ0|PAWR_HUMAN	PRKC apoptosis WT1 regulator protein	127.53	34	4
Q9UBT2|SAE2_HUMAN	SUMO-activating enzyme subunit 2 OS	127.48	23	4
Q7L1Q6|BZW1_HUMAN	Basic leucine zipper and W2 domain-co	127.41	23	4
P36639|8ODP_HUMAN	7,8-dihydro-8-oxoguanine triphosphatas	127.23	29	4
P13489|RINI_HUMAN	Ribonuclease inhibitor OS=Homo sapie	126.94	15	4
Q9C005|DPY30_HUMAN	Protein dpy-30 homolog OS=Homo sap	126.61	65	4
Q13158|FADD_HUMAN	Protein FADD OS=Homo sapiens GN=F	126.59	50	4
P11216|PYGB_HUMAN	Glycogen phosphorylase, brain form OS	126.5	16	4
P41208|CETN2_HUMAN	Centrin-2 OS=Homo sapiens GN=CETN	125.68	42	4
Q07666|KHDR1_HUMAN	KH domain-containing, RNA-binding, si	125.54	41	4
Q13347|EIF3I_HUMAN	Eukaryotic translation initiation factor 3	125.45	34	4
Q7L5N1|CSN6_HUMAN	COP9 signalosome complex subunit 6 (	124.89	42	4
Q99584|S10AD_HUMAN	Protein S100-A13 OS=Homo sapiens G	124.64	71	4
P67809|YBOX1_HUMAN	Nuclease-sensitive element-binding pro	124.46	35	4
P11766|ADHX_HUMAN	Alcohol dehydrogenase class-3 OS=Ho	124.39	15	4
P62942|FKB1A_HUMAN	Peptidyl-prolyl cis-trans isomerase FKB	124.26	56	4
P35237|SPB6_HUMAN	Serpin B6 OS=Homo sapiens GN=SER	124.21	25	4
O14745|NHRF1_HUMAN	Na(+)/H(+) exchange regulatory cofacto	124.14	24	4
Q96CT7|CC124_HUMAN	Coiled-coil domain-containing protein 12	123.93	35	4
O14979|HNRDL_HUMAN	Heterogeneous nuclear ribonucleoprote	123.03	19	4
Q9GZT3|SLIRP_HUMAN	SRA stem-loop-interacting RNA-binding	122.52	59	4
O75340|PDCD6_HUMAN	Programmed cell death protein 6 OS=H	122.24	21	4
Q9Y6A5|TACC3_HUMAN	Transforming acidic coiled-coil-containir	120.35	16	4
O95456|PSMG1_HUMAN	Proteasome assembly chaperone 1 OS	120.27	43	4
O00264|PGRC1_HUMAN	Membrane-associated progesterone rec	120.06	29	4
P46776|RL27A_HUMAN	60S ribosomal protein L27a OS=Homo	119.89	43	4
P10768|ESTD_HUMAN	S-formylglutathione hydrolase OS=Hom	118.79	32	4
O75964|ATP5L_HUMAN	ATP synthase subunit g, mitochondrial (	118.21	48	4
O95816|BAG2_HUMAN	BAG family molecular chaperone regula	117.96	28	4
Q8TCD5|NT5C_HUMAN	5'(3')-deoxyribonucleotidase, cytosolic t	117.95	38	4
P35244|RFA3_HUMAN	Replication protein A 14 kDa subunit OS	117.26	51	4
P15121|ALDR_HUMAN	Aldose reductase OS=Homo sapiens G	116.57	32	4
Q12905|ILF2_HUMAN	Interleukin enhancer-binding factor 2 OS	116.36	26	4
O75368|SH3L1_HUMAN	SH3 domain-binding glutamic acid-rich-	116.19	61	4
P61326|MGN_HUMAN	Protein mago nashi homolog OS=Homo	115.68	32	4
Q96A72|MGN2_HUMAN	Protein mago nashi homolog 2 OS=Hor	115.68	32	4
Q9P2M7|CING_HUMAN	Cingulin OS=Homo sapiens GN=CGN F	115.57	14	4
P51659|DHB4_HUMAN	Peroxisomal multifunctional enzyme typ	115.3	23	4
Q92520|FAM3C_HUMAN	Protein FAM3C OS=Homo sapiens GN=	114.77	33	4
Q8N1G4|LRC47_HUMAN	Leucine-rich repeat-containing protein 4	114.53	22	4
P10606|COX5B_HUMAN	Cytochrome c oxidase subunit 5B, mito	113.36	59	4
P51991|ROA3_HUMAN	Heterogeneous nuclear ribonucleoprote	112.56	33	4
Q8NC51|PAIRB_HUMAN	Plasminogen activator inhibitor 1 RNA-b	112.55	32	4
P12830|CADH1_HUMAN	Cadherin-1 OS=Homo sapiens GN=CD	112.39	9	4
O95372|LYPA2_HUMAN	Acyl-protein thioesterase 2 OS=Homo s	111.76	40	4
P35613|BASI_HUMAN	Basigin OS=Homo sapiens GN=BSG P	110.96	20	4
Q8IZQ5|SELH_HUMAN	Selenoprotein H OS=Homo sapiens GN	110.76	30	4
O00743|PPP6_HUMAN	Serine/threonine-protein phosphatase 6	110.46	21	4
O43252|PAPS1_HUMAN	Bifunctional 3'-phosphoadenosine 5'-ph	109.93	16	4
P38606|VATA_HUMAN	V-type proton ATPase catalytic subunit	109.75	21	4
P12081|SYHC_HUMAN	Histidyl-tRNA synthetase, cytoplasmic (	108.91	18	4
P33992|MCM5_HUMAN	DNA replication licensing factor MCM5 (	108.62	18	4
P48449|ERG7_HUMAN	Lanosterol synthase OS=Homo sapiens	107.72	15	4
Q9NX63|CHCH3_HUMAN	Coiled-coil-helix-coiled-coil-helix domair	107.59	22	4
O00303|EIF3F_HUMAN	Eukaryotic translation initiation factor 3	106.68	25	4
Q8IYD1|ERF3B_HUMAN	Eukaryotic peptide chain release factor	106.49	24	4

O75475|PSIP1_HUMAN	PC4 and SFRS1-interacting protein OS	105.59	22	4
Q92522|H1X_HUMAN	Histone H1x OS=Homo sapiens GN=H1	103.64	42	4
Q8IXM3|RM41_HUMAN	39S ribosomal protein L41, mitochondri	103.23	41	4
Q8N8S7|ENAH_HUMAN	Protein enabled homolog OS=Homo sa	103.14	20	4
Q92896|GSLG1_HUMAN	Golgi apparatus protein 1 OS=Homo sa	103.11	12	4
P40429|RL13A_HUMAN	60S ribosomal protein L13a OS=Homo	102.57	26	4
Q9H0D6|XRN2_HUMAN	5'-3' exoribonuclease 2 OS=Homo sapi	102.57	13	4
Q9NSD9|SYFB_HUMAN	Phenylalanyl-tRNA synthetase beta cha	102.47	10	4
P14314|GLU2B_HUMAN	Glucosidase 2 subunit beta OS=Homo	102.28	16	4
Q86V81|THOC4_HUMAN	THO complex subunit 4 OS=Homo sapi	102.08	28	4
Q99988|GDF15_HUMAN	Growth/differentiation factor 15 OS=Ho	101.63	27	4
O14618|CCS_HUMAN	Copper chaperone for superoxide dismu	101.48	16	4
Q08752|PPID_HUMAN	Peptidyl-prolyl cis-trans isomerase D OS	101.47	24	4
P26640|SYVC_HUMAN	Valyl-tRNA synthetase OS=Homo sapie	101.13	17	4
Q9BRG1|VPS25_HUMAN	Vacuolar protein-sorting-associated pro	100.97	30	4
Q13561|DCTN2_HUMAN	Dynactin subunit 2 OS=Homo sapiens G	100.02	26	4
P47914|RL29_HUMAN	60S ribosomal protein L29 OS=Homo s	98.91	21	4
Q9BVG4|CX026_HUMAN	UPF0368 protein Cxorf26 OS=Homo sa	98.87	24	4
P31689|DNJA1_HUMAN	DnaJ homolog subfamily A member 1 O	98.39	16	4
O15355|PPM1G_HUMAN	Protein phosphatase 1G OS=Homo sap	98.26	20	4
P63165|SUMO1_HUMAN	Small ubiquitin-related modifier 1 OS=H	98.05	57	4
Q99417|MYCBP_HUMAN	C-Myc-binding protein OS=Homo sapie	97.87	58	4
P46379|BAG6_HUMAN	Large proline-rich protein BAG6 OS=Ho	97.72	11	4
P29279|CTGF_HUMAN	Connective tissue growth factor OS=Ho	93.72	15	4
Q14008|CKAP5_HUMAN	Cytoskeleton-associated protein 5 OS=	93.41	14	4
P62993|GRB2_HUMAN	Growth factor receptor-bound protein 2	93.17	29	4
Q9Y3U8|RL36_HUMAN	60S ribosomal protein L36 OS=Homo s	91.98	31	4
Q07065|CKAP4_HUMAN	Cytoskeleton-associated protein 4 OS=	91.64	21	4
P47897|SYQ_HUMAN	Glutaminyl-tRNA synthetase OS=Homo	90.69	27	4
P62070|RRAS2_HUMAN	Ras-related protein R-Ras2 OS=Homo	90.49	33	4
Q9UHD8|SEPT9_HUMAN	Septin-9 OS=Homo sapiens GN=SEPT	90.49	22	4
P04181|OAT_HUMAN	Ornithine aminotransferase, mitochondr	90.38	24	4
P46939|UTRO_HUMAN	Utrophin OS=Homo sapiens GN=UTRN	88.37	9	4
Q9Y376|CAB39_HUMAN	Calcium-binding protein 39 OS=Homo s	86.83	20	4
Q4VC31|CCD58_HUMAN	Coiled-coil domain-containing protein 58	86.34	27	4
Q99436|PSB7_HUMAN	Proteasome subunit beta type-7 OS=Ho	86.09	34	4
P61313|RL15_HUMAN	60S ribosomal protein L15 OS=Homo s	83.42	11	4
Q9UDR5|AASS_HUMAN	Alpha-aminoadipic semialdehyde syntha	81.96	10	4
P22307|NLTP_HUMAN	Non-specific lipid-transfer protein OS=H	81.42	11	4
Q9BRF8|CPPED_HUMAN	Calcineurin-like phosphoesterase doma	81.31	37	4
P02452|CO1A1_HUMAN	Collagen alpha-1(I) chain OS=Homo sa	76.55	28	4
Q15369|ELOC_HUMAN	Transcription elongation factor B polype	75.23	45	4
P49189|AL9A1_HUMAN	4-trimethylaminobutyraldehyde dehydro	73.78	12	4
P40616|ARL1_HUMAN	ADP-ribosylation factor-like protein 1 OS	67.07	42	4
P09496|CLCA_HUMAN	Clathrin light chain A OS=Homo sapien	57.3	19	4
Q7L7L0|H2A3_HUMAN	Histone H2A type 3 OS=Homo sapiens	220.39	68	3
P04908|H2A1B_HUMAN	Histone H2A type 1-B/E OS=Homo sap	220.39	63	3
P10412|H14_HUMAN	Histone H1.4 OS=Homo sapiens GN=H	216.2	69	3
P61586|RHOA_HUMAN	Transforming protein RhoA OS=Homo s	207.08	68	3
P19105|ML12A_HUMAN	Myosin regulatory light chain 12A OS=H	198.03	57	3
O14950|ML12B_HUMAN	Myosin regulatory light chain 12B OS=H	198.03	56	3
Q02539|H11_HUMAN	Histone H1.1 OS=Homo sapiens GN=H	186.73	48	3
P84085|ARF5_HUMAN	ADP-ribosylation factor 5 OS=Homo sa	185.14	69	3
P35749|MYH11_HUMAN	Myosin-11 OS=Homo sapiens GN=MYH	179.32	39	3
P05141|ADT2_HUMAN	ADP/ATP translocase 2 OS=Homo sap	178.45	48	3
P63167|DYL1_HUMAN	Dynein light chain 1, cytoplasmic OS=H	173.27	65	3

O00571|DDX3X_HUMAN	ATP-dependent RNA helicase DDX3X (	170.74	30	3
P61254|RL26_HUMAN	60S ribosomal protein L26 OS=Homo s	153.08	52	3
P62873|GBB1_HUMAN	Guanine nucleotide-binding protein G(I)	149.03	29	3
P17844|DDX5_HUMAN	Probable ATP-dependent RNA helicase	147.94	22	3
Q92688|AN32B_HUMAN	Acidic leucine-rich nuclear phosphoprot	145.49	39	3
Q12931|TRAP1_HUMAN	Heat shock protein 75 kDa, mitochondri	139.38	23	3
P48735|IDHP_HUMAN	Isocitrate dehydrogenase [NADP], mito	137.56	22	3
Q9P1F3|CF115_HUMAN	Costars family protein C6orf115 OS=Ho	134.83	64	3
P42677|RS27_HUMAN	40S ribosomal protein S27 OS=Homo s	134.49	40	3
Q93062|RBPMS_HUMAN	RNA-binding protein with multiple splici	134.46	39	3
Q9NX02|NALP2_HUMAN	NACHT, LRR and PYD domains-contai	133.77	24	3
Q16836|HCDH_HUMAN	Hydroxyacyl-coenzyme A dehydrogenas	133.68	48	3
Q71UM5|RS27L_HUMAN	40S ribosomal protein S27-like OS=Hor	133.64	40	3
P80723|BASP1_HUMAN	Brain acid soluble protein 1 OS=Homo	130.23	48	3
P47755|CAZA2_HUMAN	F-actin-capping protein subunit alpha-2	129.41	23	3
P68402|PA1B2_HUMAN	Platelet-activating factor acetylhydrolas	129.2	44	3
Q9NZL9|MAT2B_HUMAN	Methionine adenosyltransferase 2 subu	128.96	42	3
Q13526|PIN1_HUMAN	Peptidyl-prolyl cis-trans isomerase NIM	128.58	48	3
P51148|RAB5C_HUMAN	Ras-related protein Rab-5C OS=Homo	128.3	39	3
P11047|LAMC1_HUMAN	Laminin subunit gamma-1 OS=Homo sa	128.29	12	3
Q9H3R5|CENPH_HUMAN	Centromere protein H OS=Homo sapier	126.82	49	3
P47813|IF1AX_HUMAN	Eukaryotic translation initiation factor 1A	126.09	45	3
O14602|IF1AY_HUMAN	Eukaryotic translation initiation factor 1A	126.09	45	3
Q96IX5|USMG5_HUMAN	Up-regulated during skeletal muscle gro	125.63	47	3
Q13151|ROA0_HUMAN	Heterogeneous nuclear ribonucleoprote	125.54	29	3
O75607|NPM3_HUMAN	Nucleoplasmin-3 OS=Homo sapiens GN	124.93	29	3
Q99613|EIF3C_HUMAN	Eukaryotic translation initiation factor 3	124.89	26	3
Q9NYL9|TMOD3_HUMAN	Tropomodulin-3 OS=Homo sapiens GN	124.12	26	3
O75390|CISY_HUMAN	Citrate synthase, mitochondrial OS=Hor	123.78	18	3
Q9P289|MST4_HUMAN	Serine/threonine-protein kinase MST4 (	123.44	28	3
P62854|RS26_HUMAN	40S ribosomal protein S26 OS=Homo s	123.28	42	3
P17812|PYRG1_HUMAN	CTP synthase 1 OS=Homo sapiens GN	123.12	21	3
P54687|BCAT1_HUMAN	Branched-chain-amino-acid aminotrans	123	26	3
P52434|RPAB3_HUMAN	DNA-directed RNA polymerases I, II, ar	122.62	25	3
Q8WUM4|PDC6I_HUMAN	Programmed cell death 6-interacting pro	122.37	23	3
Q9BY32|ITPA_HUMAN	Inosine triphosphate pyrophosphatase (	120.89	35	3
Q96AC1|FERM2_HUMAN	Fermitin family homolog 2 OS=Homo sa	119.86	22	3
O43396|TXNL1_HUMAN	Thioredoxin-like protein 1 OS=Homo sa	119.7	40	3
Q9Y3C6|PPIL1_HUMAN	Peptidyl-prolyl cis-trans isomerase-like	119.47	31	3
Q9UQE7|SMC3_HUMAN	Structural maintenance of chromosome	118.55	22	3
Q00796|DHSO_HUMAN	Sorbitol dehydrogenase OS=Homo sap	118.03	25	3
P62877|RBX1_HUMAN	E3 ubiquitin-protein ligase RBX1 OS=H	117.05	33	3
P04080|CYTB_HUMAN	Cystatin-B OS=Homo sapiens GN=CST	116.74	65	3
O60869|EDF1_HUMAN	Endothelial differentiation-related factor	116.26	43	3
Q9H773|DCTP1_HUMAN	dCTP pyrophosphatase 1 OS=Homo sa	116.15	39	3
Q9UQ80|PA2G4_HUMAN	Proliferation-associated protein 2G4 OS	115.83	22	3
Q13618|CUL3_HUMAN	Cullin-3 OS=Homo sapiens GN=CUL3	115.72	15	3
P04179|SODM_HUMAN	Superoxide dismutase [Mn], mitochondr	115.24	25	3
P16083|NQO2_HUMAN	Ribosyldihydronicotinamide dehydroger	114.81	30	3
O00273|DFFA_HUMAN	DNA fragmentation factor subunit alpha	114.55	35	3
Q96DE0|NUD16_HUMAN	U8 snoRNA-decapping enzyme OS=Ho	114.52	56	3
Q9P000|COMD9_HUMAN	COMM domain-containing protein 9 OS	114.3	31	3
Q9UIL1|SCOC_HUMAN	Short coiled-coil protein OS=Homo sapi	113.32	29	3
Q9NQP4|PFD4_HUMAN	Prefoldin subunit 4 OS=Homo sapiens (	113.22	38	3
P23919|KTHY_HUMAN	Thymidylate kinase OS=Homo sapiens	112.9	33	3
P61201|CSN2_HUMAN	COP9 signalosome complex subunit 2 (	112.11	32	3

Q15717|ELAV1_HUMAN	ELAV-like protein 1 OS=Homo sapiens	112.02	20	3
Q86UP2|KTN1_HUMAN	Kinectin OS=Homo sapiens GN=KTN1	111.99	11	3
Q8TEA8|DTD1_HUMAN	D-tyrosyl-tRNA(Tyr) deacylase 1 OS=H	111.97	32	3
Q6ZRY4|RBPS2_HUMAN	RNA-binding protein with multiple splicir	111.74	32	3
O43143|DHX15_HUMAN	Putative pre-mRNA-splicing factor ATP-	111.74	21	3
P62910|RL32_HUMAN	60S ribosomal protein L32 OS=Homo s	111.73	45	3
Q9NR45|SIAS_HUMAN	Sialic acid synthase OS=Homo sapiens	111.51	20	3
P62266|RS23_HUMAN	40S ribosomal protein S23 OS=Homo s	111.48	16	3
P32321|DCTD_HUMAN	Deoxycytidylate deaminase OS=Homo	111.13	20	3
P35080|PROF2_HUMAN	Profilin-2 OS=Homo sapiens GN=PFN2	110.75	57	3
O14773|TPP1_HUMAN	Tripeptidyl-peptidase 1 OS=Homo sapie	110.66	31	3
P45880|VDAC2_HUMAN	Voltage-dependent anion-selective cha	110.22	22	3
P29966|MARCS_HUMAN	Myristoylated alanine-rich C-kinase sub	109.99	14	3
P39023|RL3_HUMAN	60S ribosomal protein L3 OS=Homo sa	109.82	15	3
P98095|FBLN2_HUMAN	Fibulin-2 OS=Homo sapiens GN=FBLN	109.77	12	3
P06737|PYGL_HUMAN	Glycogen phosphorylase, liver form OS	109.33	13	3
Q16527|CSRP2_HUMAN	Cysteine and glycine-rich protein 2 OS=	108.45	25	3
Q9NRV9|HEBP1_HUMAN	Heme-binding protein 1 OS=Homo sapi	108.16	46	3
O14880|MGST3_HUMAN	Microsomal glutathione S-transferase 3	108.14	26	3
P14923|PLAK_HUMAN	Junction plakoglobin OS=Homo sapiens	107.99	21	3
P62318|SMD3_HUMAN	Small nuclear ribonucleoprotein Sm D3	107.82	37	3
P46087|NOP2_HUMAN	Putative ribosomal RNA methyltransfera	107.14	13	3
Q969H8|CS010_HUMAN	UPF0556 protein C19orf10 OS=Homo s	106.3	21	3
P29373|RABP2_HUMAN	Cellular retinoic acid-binding protein 2 O	106.07	51	3
Q9Y5J9|TIM8B_HUMAN	Mitochondrial import inner membrane tr	105.86	52	3
O75190|DNJB6_HUMAN	DnaJ homolog subfamily B member 6 O	105.52	18	3
Q86X76|NIT1_HUMAN	Nitrilase homolog 1 OS=Homo sapiens	105.47	13	3
P60228|EIF3E_HUMAN	Eukaryotic translation initiation factor 3	105.39	24	3
P41223|BUD31_HUMAN	Protein BUD31 homolog OS=Homo sap	105.37	38	3
P52789|HXK2_HUMAN	Hexokinase-2 OS=Homo sapiens GN=H	104.68	18	3
O75663|TIPRL_HUMAN	TIP41-like protein OS=Homo sapiens G	104.43	24	3
Q8TBC4|UBA3_HUMAN	NEDD8-activating enzyme E1 catalytic s	104.42	18	3
Q96P16|RPR1A_HUMAN	Regulation of nuclear pre-mRNA domai	104.32	28	3
P30626|SORCN_HUMAN	Sorcin OS=Homo sapiens GN=SRI PE=	104.25	30	3
O43805|SSNA1_HUMAN	Sjoegren syndrome nuclear autoantiger	104.04	21	3
P11279|LAMP1_HUMAN	Lysosome-associated membrane glycop	103.74	14	3
O75821|EIF3G_HUMAN	Eukaryotic translation initiation factor 3	103.54	22	3
P51911|CNN1_HUMAN	Calponin-1 OS=Homo sapiens GN=CNI	103.35	22	3
Q14974|IMB1_HUMAN	Importin subunit beta-1 OS=Homo sapi	102.69	14	3
Q15363|TMED2_HUMAN	Transmembrane emp24 domain-contair	102.61	30	3
Q9Y5K5|UCHL5_HUMAN	Ubiquitin carboxyl-terminal hydrolase is	102.46	19	3
O75391|SPAG7_HUMAN	Sperm-associated antigen 7 OS=Homo	102.31	27	3
Q7L190|DPPA4_HUMAN	Developmental pluripotency-associated	102.08	25	3
Q56VL3|OCAD2_HUMAN	OCIA domain-containing protein 2 OS=	101.96	24	3
Q8NCW5|AIBP_HUMAN	Apolipoprotein A-I-binding protein OS=H	101.91	36	3
Q16795|NDUA9_HUMAN	NADH dehydrogenase [ubiquinone] 1 a	101.49	20	3
Q9Y5J7|TIM9_HUMAN	Mitochondrial import inner membrane tr	101.22	45	3
Q9NPJ3|ACO13_HUMAN	Acyl-coenzyme A thioesterase 13 OS=H	100.73	22	3
O00622|CYR61_HUMAN	Protein CYR61 OS=Homo sapiens GN=	100.58	16	3
Q8WU90|ZC3HF_HUMAN	Zinc finger CCCH domain-containing pr	100.56	18	3
Q2Q1W2|LIN41_HUMAN	Tripartite motif-containing protein 71 OS	100.38	9	3
Q14157|UBP2L_HUMAN	Ubiquitin-associated protein 2-like OS=H	100.19	7	3
Q92979|NEP1_HUMAN	Ribosomal RNA small subunit methyltra	99.69	34	3
Q9UBW8|CSN7A_HUMAN	COP9 signalosome complex subunit 7a	99.23	18	3
Q6P2Q9|PRP8_HUMAN	Pre-mRNA-processing-splicing factor 8	99.16	16	3
Q08431|MFGM_HUMAN	Lactadherin OS=Homo sapiens GN=MF	98.91	12	3

P09012|SNRPA_HUMAN	U1 small nuclear ribonucleoprotein A O	98.54	21	3
O60762|DPM1_HUMAN	Dolichol-phosphate mannosyltransferas	97.75	39	3
P54886|P5CS_HUMAN	Delta-1-pyrroline-5-carboxylate synthas	97.38	13	3
P78330|SERB_HUMAN	Phosphoserine phosphatase OS=Homo	97.17	29	3
Q14683|SMC1A_HUMAN	Structural maintenance of chromosome	96.89	13	3
P10620|MGST1_HUMAN	Microsomal glutathione S-transferase 1	96.84	30	3
Q9H444|CHM4B_HUMAN	Charged multivesicular body protein 4b	96.69	24	3
P51970|NDUA8_HUMAN	NADH dehydrogenase [ubiquinone] 1 a	96.5	23	3
P35659|DEK_HUMAN	Protein DEK OS=Homo sapiens GN=DE	96.28	18	3
P49023|PAXI_HUMAN	Paxillin OS=Homo sapiens GN=PXN PE	96.09	11	3
Q16891|IMMT_HUMAN	Mitochondrial inner membrane protein O	95.78	11	3
Q8NBT2|SPC24_HUMAN	Kinetochore protein Spc24 OS=Homo s	95.76	34	3
P19388|RPAB1_HUMAN	DNA-directed RNA polymerases I, II, ar	95.69	25	3
Q8WWM7|ATX2L_HUMAN	Ataxin-2-like protein OS=Homo sapiens	95.21	13	3
P51858|HDGF_HUMAN	Hepatoma-derived growth factor OS=Ho	94.92	26	3
Q96CN7|ISOC1_HUMAN	Isochorismatase domain-containing pro	94.28	29	3
P98179|RBM3_HUMAN	Putative RNA-binding protein 3 OS=Hor	93.74	42	3
O14974|MYPT1_HUMAN	Protein phosphatase 1 regulatory subur	93.67	16	3
P67812|SC11A_HUMAN	Signal peptidase complex catalytic subu	93.53	26	3
Q01860|PO5F1_HUMAN	POU domain, class 5, transcription fact	93.19	14	3
O15212|PFD6_HUMAN	Prefoldin subunit 6 OS=Homo sapiens G	93.17	53	3
P60468|SC61B_HUMAN	Protein transport protein Sec61 subunit	93.17	49	3
O43447|PPIH_HUMAN	Peptidyl-prolyl cis-trans isomerase H OS	93.05	24	3
Q15637|SF01_HUMAN	Splicing factor 1 OS=Homo sapiens GN	92.68	9	3
P61011|SRP54_HUMAN	Signal recognition particle 54 kDa prote	92.52	18	3
P35637|FUS_HUMAN	RNA-binding protein FUS OS=Homo sa	92.41	25	3
P21741|MK_HUMAN	Midkine OS=Homo sapiens GN=MDK P	92.16	23	3
Q9UHD1|CHRD1_HUMAN	Cysteine and histidine-rich domain-cont	92.01	18	3
Q9NRN7|ADPPT_HUMAN	L-aminoadipate-semialdehyde dehydrog	91.89	18	3
Q8WXX5|DNJC9_HUMAN	DnaJ homolog subfamily C member 9 O	91.37	17	3
P11413|G6PD_HUMAN	Glucose-6-phosphate 1-dehydrogenase	91.14	10	3
Q9HAV7|GRPE1_HUMAN	GrpE protein homolog 1, mitochondrial	90.4	27	3
Q9NQW7|XPP1_HUMAN	Xaa-Pro aminopeptidase 1 OS=Homo s	89.9	11	3
O15230|LAMA5_HUMAN	Laminin subunit alpha-5 OS=Homo sap	88.56	7	3
P53618|COPB_HUMAN	Coatomer subunit beta OS=Homo sapie	88.36	12	3
Q9H7C9|CK067_HUMAN	UPF0366 protein C11orf67 OS=Homo s	88.3	50	3
Q14498|RBM39_HUMAN	RNA-binding protein 39 OS=Homo sapi	88.2	16	3
Q9BWJ5|SF3B5_HUMAN	Splicing factor 3B subunit 5 OS=Homo	87.94	59	3
O14561|ACPM_HUMAN	Acyl carrier protein, mitochondrial OS=H	87.93	34	3
O00487|PSDE_HUMAN	26S proteasome non-ATPase regulator	87.85	39	3
Q9UJ70|NAGK_HUMAN	N-acetyl-D-glucosamine kinase OS=Ho	87.78	27	3
Q13867|BLMH_HUMAN	Bleomycin hydrolase OS=Homo sapien	87.64	11	3
P11441|UBL4A_HUMAN	Ubiquitin-like protein 4A OS=Homo sap	87.52	23	3
P05556|ITB1_HUMAN	Integrin beta-1 OS=Homo sapiens GN=	87.25	10	3
Q9BYD1|RM13_HUMAN	39S ribosomal protein L13, mitochondri	86.76	34	3
Q53GG5|PDLI3_HUMAN	PDZ and LIM domain protein 3 OS=Hor	86.38	13	3
Q9UNE7|CHIP_HUMAN	E3 ubiquitin-protein ligase CHIP OS=Ho	86.31	19	3
Q9NQ48|LZTL1_HUMAN	Leucine zipper transcription factor-like p	86.21	22	3
Q02750|MP2K1_HUMAN	Dual specificity mitogen-activated prote	85.56	13	3
Q14980|NUMA1_HUMAN	Nuclear mitotic apparatus protein 1 OS=	85.56	12	3
Q9NYU2|UGGG1_HUMAN	UDP-glucose:glycoprotein glucosyltrans	85.38	8	3
O00483|NDUA4_HUMAN	NADH dehydrogenase [ubiquinone] 1 a	84.09	37	3
P61599|NAA20_HUMAN	N-alpha-acetyltransferase 20, NatB cata	83.25	17	3
O15305|PMM2_HUMAN	Phosphomannomutase 2 OS=Homo sa	82.68	14	3
Q8WVJ2|NUDC2_HUMAN	NudC domain-containing protein 2 OS=	82.57	19	3
P82930|RT34_HUMAN	28S ribosomal protein S34, mitochondri	82.32	31	3

Q9P0J0|NDUAD_HUMAN	NADH dehydrogenase [ubiquinone] 1 a	81.88	19	3
P00918|CAH2_HUMAN	Carbonic anhydrase 2 OS=Homo sapie	81.64	24	3
P61457|PHS_HUMAN	Pterin-4-alpha-carbinolamine dehydrata	81.29	49	3
Q9NX24|NHP2_HUMAN	H/ACA ribonucleoprotein complex subu	80.98	19	3
O75935|DCTN3_HUMAN	Dynactin subunit 3 OS=Homo sapiens (	80.82	16	3
O43776|SYNC_HUMAN	Asparaginyl-tRNA synthetase, cytoplasr	78.81	12	3
Q9BV57|MTND_HUMAN	1,2-dihydroxy-3-keto-5-methylthiopente	78.58	31	3
O14776|TCRG1_HUMAN	Transcription elongation regulator 1 OS	78.46	8	3
O60716|CTND1_HUMAN	Catenin delta-1 OS=Homo sapiens GN=	78.31	13	3
Q32P28|P3H1_HUMAN	Prolyl 3-hydroxylase 1 OS=Homo sapie	77.96	8	3
O94760|DDAH1_HUMAN	N(G),N(G)-dimethylarginine dimethylam	77.81	13	3
O00762|UBE2C_HUMAN	Ubiquitin-conjugating enzyme E2 C OS=	77.44	22	3
P62861|RS30_HUMAN	40S ribosomal protein S30 OS=Homo s	76.48	20	3
P39060|COIA1_HUMAN	Collagen alpha-1(XVIII) chain OS=Hom	75.9	14	3
O60613|SEP15_HUMAN	15 kDa selenoprotein OS=Homo sapier	75.78	22	3
O14744|ANM5_HUMAN	Protein arginine N-methyltransferase 5 (	75.63	15	3
Q96HQ2|C2AIL_HUMAN	CDKN2AIP N-terminal-like protein OS=	75.18	24	3
Q12841|FSTL1_HUMAN	Follistatin-related protein 1 OS=Homo s	74.92	23	3
P36543|VATE1_HUMAN	V-type proton ATPase subunit E 1 OS=	73.98	16	3
O60256|KPRB_HUMAN	Phosphoribosyl pyrophosphate synthas	73.54	22	3
O75937|DNJC8_HUMAN	DnaJ homolog subfamily C member 8 C	73.14	29	3
Q7LBC6|KDM3B_HUMAN	Lysine-specific demethylase 3B OS=Ho	72.5	12	3
Q9NPE3|NOP10_HUMAN	H/ACA ribonucleoprotein complex subu	72.2	62	3
P62253|UB2G1_HUMAN	Ubiquitin-conjugating enzyme E2 G1 OS	71.77	15	3
Q8NFU3|TSTD1_HUMAN	Thiosulfate sulfurtransferase/rhodanese	69.82	21	3
Q9BR76|COR1B_HUMAN	Coronin-1B OS=Homo sapiens GN=CO	69.77	10	3
Q9Y547|HSB11_HUMAN	Heat shock protein beta-11 OS=Homo s	67.64	49	3
Q8WUW1|BRK1_HUMAN	Protein BRICK1 OS=Homo sapiens GN	67.4	37	3
Q00325|MPCP_HUMAN	Phosphate carrier protein, mitochondria	66.68	17	3
Q13564|ULA1_HUMAN	NEDD8-activating enzyme E1 regulator	62.1	11	3
Q5T0N5|FBP1L_HUMAN	Formin-binding protein 1-like OS=Homo	61.49	16	3
Q8NF91|SYNE1_HUMAN	Nesprin-1 OS=Homo sapiens GN=SYN	61.01	6	3
P52788|SPSY_HUMAN	Spermine synthase OS=Homo sapiens	59.64	17	3
P49916|DNLI3_HUMAN	DNA ligase 3 OS=Homo sapiens GN=L	59.01	5	3
P84098|RL19_HUMAN	60S ribosomal protein L19 OS=Homo s	58.49	24	3
P54727|RD23B_HUMAN	UV excision repair protein RAD23 homo	54.59	15	3
O14949|QCR8_HUMAN	Cytochrome b-c1 complex subunit 8 OS	50.95	39	3
P24043|LAMA2_HUMAN	Laminin subunit alpha-2 OS=Homo sap	36.38	8	3
Q5T5P2|SKT_HUMAN	Sickle tail protein homolog OS=Homo s	36.23	9	3
Q9UMZ3|PTPRQ_HUMAN	Phosphotidylinositol phosphatase PTPF	36.05	5	3
Q9BVA1|TBB2B_HUMAN	Tubulin beta-2B chain OS=Homo sapie	330.95	80	2
Q13885|TBB2A_HUMAN	Tubulin beta-2A chain OS=Homo sapie	329.55	80	2
P04350|TBB4_HUMAN	Tubulin beta-4 chain OS=Homo sapiens	302.6	76	2
P07951|TPM2_HUMAN	Tropomyosin beta chain OS=Homo sap	286.14	58	2
Q9BQE3|TBA1C_HUMAN	Tubulin alpha-1C chain OS=Homo sapi	275.14	76	2
P62979|RS27A_HUMAN	Ubiquitin-40S ribosomal protein S27a C	249.3	73	2
P36873|PP1G_HUMAN	Serine/threonine-protein phosphatase F	230.3	53	2
P16402|H13_HUMAN	Histone H1.3 OS=Homo sapiens GN=H	208.58	66	2
P11940|PABP1_HUMAN	Polyadenylate-binding protein 1 OS=Ho	197.97	41	2
Q99867|TBB4Q_HUMAN	Putative tubulin beta-4q chain OS=Hom	195.25	59	2
P08134|RHOC_HUMAN	Rho-related GTP-binding protein RhoC	192.52	59	2
A6NKZ8|YI016_HUMAN	Putative tubulin beta chain-like protein E	188.29	48	2
Q14240|IF4A2_HUMAN	Eukaryotic initiation factor 4A-II OS=Ho	180.35	35	2
P30154|2AAB_HUMAN	Serine/threonine-protein phosphatase 2	178.49	55	2
Q9H4B7|TBB1_HUMAN	Tubulin beta-1 chain OS=Homo sapiens	172.85	30	2
P12235|ADT1_HUMAN	ADP/ATP translocase 1 OS=Homo sap	168.81	39	2

O43390|HNRPR_HUMAN	Heterogeneous nuclear ribonucleoprote	149.02	26	2
O00292|LFTY2_HUMAN	Left-right determination factor 2 OS=Ho	135.99	34	2
Q16576|RBBP7_HUMAN	Histone-binding protein RBBP7 OS=Ho	132.75	30	2
P62191|PRS4_HUMAN	26S protease regulatory subunit 4 OS=	125.52	41	2
P61020|RAB5B_HUMAN	Ras-related protein Rab-5B OS=Homo	123.52	35	2
P61077|UB2D3_HUMAN	Ubiquitin-conjugating enzyme E2 D3 OS	123.06	31	2
Q96RU2|UBP28_HUMAN	Ubiquitin carboxyl-terminal hydrolase 28	122.59	12	2
P62879|GBB2_HUMAN	Guanine nucleotide-binding protein G(I)	119.57	27	2
Q13404|UB2V1_HUMAN	Ubiquitin-conjugating enzyme E2 varian	117.06	39	2
Q15819|UB2V2_HUMAN	Ubiquitin-conjugating enzyme E2 varian	116.9	45	2
O00764|PDXK_HUMAN	Pyridoxal kinase OS=Homo sapiens GN	116.49	35	2
Q09028|RBBP4_HUMAN	Histone-binding protein RBBP4 OS=Ho	115.76	16	2
P20339|RAB5A_HUMAN	Ras-related protein Rab-5A OS=Homo	115.52	26	2
P61163|ACTZ_HUMAN	Alpha-centractin OS=Homo sapiens GN	114.53	26	2
O96008|TOM40_HUMAN	Mitochondrial import receptor subunit T	110.41	33	2
O60763|USO1_HUMAN	General vesicular transport factor p115	109.9	23	2
Q9NVD7|PARVA_HUMAN	Alpha-parvin OS=Homo sapiens GN=P	109.79	26	2
P49902|5NTC_HUMAN	Cytosolic purine 5'-nucleotidase OS=Ho	108.62	29	2
P18859|ATP5J_HUMAN	ATP synthase-coupling factor 6, mitoch	107.86	41	2
Q9NXH9|TRM1_HUMAN	N(2),N(2)-dimethylguanosine tRNA met	106.8	24	2
P31942|HNRH3_HUMAN	Heterogeneous nuclear ribonucleoprote	106.42	37	2
Q14166|TTL12_HUMAN	Tubulin--tyrosine ligase-like protein 12 O	106.11	26	2
P62330|ARF6_HUMAN	ADP-ribosylation factor 6 OS=Homo sa	105.77	18	2
P63172|DYLT1_HUMAN	Dynein light chain Tctex-type 1 OS=Hor	104.88	51	2
Q9NUG6|PDRG1_HUMAN	p53 and DNA damage-regulated protein	104.32	23	2
O60502|NCOAT_HUMAN	Bifunctional protein NCOAT OS=Homo	102.68	21	2
P48507|GSH0_HUMAN	Glutamate--cysteine ligase regulatory su	102.5	24	2
O95983|MBD3_HUMAN	Methyl-CpG-binding domain protein 3 O	102.05	18	2
Q9H2U2|IPYR2_HUMAN	Inorganic pyrophosphatase 2, mitochon	102.01	20	2
Q9UBI1|COMD3_HUMAN	COMM domain-containing protein 3 OS	101.68	31	2
P51153|RAB13_HUMAN	Ras-related protein Rab-13 OS=Homo s	101.47	26	2
Q86Y39|NDUAB_HUMAN	NADH dehydrogenase [ubiquinone] 1 a	101.07	32	2
P43034|LIS1_HUMAN	Platelet-activating factor acetylhydrolase	100.5	23	2
Q9NRX4|PHP14_HUMAN	14 kDa phosphohistidine phosphatase O	100.38	42	2
P32322|P5CR1_HUMAN	Pyrroline-5-carboxylate reductase 1, mi	100.32	20	2
P55957|BID_HUMAN	BH3-interacting domain death agonist O	100.01	38	2
Q9NZT2|OGFR_HUMAN	Opioid growth factor receptor OS=Hom	99.66	18	2
P55036|PSMD4_HUMAN	26S proteasome non-ATPase regulator	99.41	19	2
P80294|MT1H_HUMAN	Metallothionein-1H OS=Homo sapiens O	99.38	66	2
P47895|AL1A3_HUMAN	Aldehyde dehydrogenase family 1 mem	99.32	19	2
P14543|NID1_HUMAN	Nidogen-1 OS=Homo sapiens GN=NID	99.03	9	2
Q9UJZ1|STML2_HUMAN	Stomatin-like protein 2 OS=Homo sapie	98.98	29	2
Q9Y3C4|TPRKB_HUMAN	TP53RK-binding protein OS=Homo sap	98.86	31	2
Q9H4G4|GAPR1_HUMAN	Golgi-associated plant pathogenesis-re	98.79	34	2
Q13418|ILK_HUMAN	Integrin-linked protein kinase OS=Hom	98.7	18	2
Q9Y2V2|CHSP1_HUMAN	Calcium-regulated heat stable protein 1	98.48	44	2
Q15024|EXOS7_HUMAN	Exosome complex component RRP42 O	98.12	25	2
P50995|ANX11_HUMAN	Annexin A11 OS=Homo sapiens GN=A	98.04	18	2
P07919|QCR6_HUMAN	Cytochrome b-c1 complex subunit 6, mi	97.86	60	2
P49006|MRP_HUMAN	MARCKS-related protein OS=Homo sa	97.19	29	2
Q92769|HDAC2_HUMAN	Histone deacetylase 2 OS=Homo sapie	97.1	15	2
Q9H299|SH3L3_HUMAN	SH3 domain-binding glutamic acid-rich-	97.09	31	2
Q6DKJ4|NXN_HUMAN	Nucleoredoxin OS=Homo sapiens GN=	96.92	17	2
O43488|ARK72_HUMAN	Aflatoxin B1 aldehyde reductase memb	96.74	22	2
O43852|CALU_HUMAN	Calumenin OS=Homo sapiens GN=CAL	96.52	16	2
Q9Y3Y2|CHTOP_HUMAN	Chromatin target of PRMT1 protein OS=	96.03	27	2

Q9UK76|HN1_HUMAN	Hematological and neurological express	95.88	32	2
P14854|CX6B1_HUMAN	Cytochrome c oxidase subunit 6B1 OS=	95.77	40	2
P61966|AP1S1_HUMAN	AP-1 complex subunit sigma-1A OS=Ho	95.37	28	2
Q9UBK9|UXT_HUMAN	Protein UXT OS=Homo sapiens GN=UX	95.24	35	2
A0AVT1|UBA6_HUMAN	Ubiquitin-like modifier-activating enzyme	94.73	18	2
Q9UBP6|TRMB_HUMAN	tRNA (guanine-N(7)-)-methyltransferase	94.63	17	2
Q9P0S9|TM14C_HUMAN	Transmembrane protein 14C OS=Homo	94.07	62	2
Q15427|SF3B4_HUMAN	Splicing factor 3B subunit 4 OS=Homo	93.81	26	2
P35250|RFC2_HUMAN	Replication factor C subunit 2 OS=Hom	93.74	12	2
Q9UBC3|DNM3B_HUMAN	DNA (cytosine-5)-methyltransferase 3B	93.71	9	2
P06132|DCUP_HUMAN	Uroporphyrinogen decarboxylase OS=H	93.6	24	2
O60888|CUTA_HUMAN	Protein CutA OS=Homo sapiens GN=C	93.52	36	2
Q16540|RM23_HUMAN	39S ribosomal protein L23, mitochondri	93.41	31	2
P42167|LAP2B_HUMAN	Lamina-associated polypeptide 2, isofo	92.93	20	2
P42166|LAP2A_HUMAN	Lamina-associated polypeptide 2, isofo	92.93	14	2
O14907|TX1B3_HUMAN	Tax1-binding protein 3 OS=Homo sapie	92.73	31	2
O43237|DC1L2_HUMAN	Cytoplasmic dynein 1 light intermediate	92.59	21	2
Q13232|NDK3_HUMAN	Nucleoside diphosphate kinase 3 OS=H	92	40	2
Q9H993|CF211_HUMAN	UPF0364 protein C6orf211 OS=Homo s	91.98	13	2
O95232|LC7L3_HUMAN	Luc7-like protein 3 OS=Homo sapiens G	91.9	18	2
Q9NXG2|THUM1_HUMAN	THUMP domain-containing protein 1 OS	91.29	18	2
Q12849|GRSF1_HUMAN	G-rich sequence factor 1 OS=Homo sap	90.84	26	2
O75688|PPM1B_HUMAN	Protein phosphatase 1B OS=Homo sap	89.87	10	2
Q04323|UBXN1_HUMAN	UBX domain-containing protein 1 OS=H	89.79	32	2
P14406|CX7A2_HUMAN	Cytochrome c oxidase subunit 7A2, mit	89.65	39	2
Q9H6S3|ES8L2_HUMAN	Epidermal growth factor receptor kinase	89.64	14	2
Q9BSD7|NTPCR_HUMAN	Cancer-related nucleoside-triphosphata	89.21	24	2
P41214|EIF2D_HUMAN	Eukaryotic translation initiation factor 2D	89.15	20	2
A6NDU8|CE051_HUMAN	UPF0600 protein C5orf51 OS=Homo sa	88.97	15	2
Q14061|COX17_HUMAN	Cytochrome c oxidase copper chaperon	88.94	48	2
Q9NYL4|FKB11_HUMAN	Peptidyl-prolyl cis-trans isomerase FKB	88.82	15	2
P19387|RPB3_HUMAN	DNA-directed RNA polymerase II subun	88.77	20	2
Q96GK7|FAH2A_HUMAN	Fumarylacetoacetate hydrolase domain	88.33	13	2
Q15642|CIP4_HUMAN	Cdc42-interacting protein 4 OS=Homo s	88.04	16	2
Q9BT73|PSMG3_HUMAN	Proteasome assembly chaperone 3 OS	88.01	23	2
Q9Y5B9|SP16H_HUMAN	FACT complex subunit SPT16 OS=Hom	87.4	7	2
P56134|ATPK_HUMAN	ATP synthase subunit f, mitochondrial G	87.36	26	2
P62273|RS29_HUMAN	40S ribosomal protein S29 OS=Homo s	87.36	48	2
P10619|PPGB_HUMAN	Lysosomal protective protein OS=Homo	87.22	10	2
O60518|RNBP6_HUMAN	Ran-binding protein 6 OS=Homo sapien	87.07	7	2
Q9Y3D6|FIS1_HUMAN	Mitochondrial fission 1 protein OS=Hom	86.95	28	2
Q9HBM1|SPC25_HUMAN	Kinetochore protein Spc25 OS=Homo s	86.86	21	2
P19367|HXK1_HUMAN	Hexokinase-1 OS=Homo sapiens GN=H	86.41	8	2
Q96EK6|GNA1_HUMAN	Glucosamine 6-phosphate N-acetyltrans	86.41	18	2
Q9H4M9|EHD1_HUMAN	EH domain-containing protein 1 OS=Ho	86.24	15	2
P15374|UCHL3_HUMAN	Ubiquitin carboxyl-terminal hydrolase is	86.23	37	2
O95813|CER1_HUMAN	Cerberus OS=Homo sapiens GN=CER1	86.12	21	2
P40937|RFC5_HUMAN	Replication factor C subunit 5 OS=Hom	86.1	25	2
P55039|DRG2_HUMAN	Developmentally-regulated GTP-binding	86.02	14	2
P20338|RAB4A_HUMAN	Ras-related protein Rab-4A OS=Homo	85.98	35	2
Q15293|RCN1_HUMAN	Reticulocalbin-1 OS=Homo sapiens GN	85.72	24	2
A2VDF0|FUCM_HUMAN	Fucose mutarotase OS=Homo sapiens	85.71	26	2
P23588|IF4B_HUMAN	Eukaryotic translation initiation factor 4B	85.61	17	2
Q7Z2W9|RM21_HUMAN	39S ribosomal protein L21, mitochondri	85.6	27	2
Q92905|CSN5_HUMAN	COP9 signalosome complex subunit 5 O	85.48	19	2
Q7RTV0|PHF5A_HUMAN	PHD finger-like domain-containing prote	85.47	32	2

Q16774|KGUA_HUMAN	Guanylate kinase OS=Homo sapiens G	84.97	12	2
O60783|RT14_HUMAN	28S ribosomal protein S14, mitochondri	84.75	27	2
Q04637|IF4G1_HUMAN	Eukaryotic translation initiation factor 4	84.69	9	2
Q05209|PTN12_HUMAN	Tyrosine-protein phosphatase non-rece	84.65	16	2
Q9H2J4|PDCL3_HUMAN	Phosducin-like protein 3 OS=Homo sap	84.64	29	2
O60884|DNJA2_HUMAN	DnaJ homolog subfamily A member 2 C	84.63	18	2
P67870|CSK2B_HUMAN	Casein kinase II subunit beta OS=Hom	84.56	9	2
Q9ULV4|COR1C_HUMAN	Coronin-1C OS=Homo sapiens GN=CO	84.23	22	2
P49643|PRI2_HUMAN	DNA primase large subunit OS=Homo s	84.03	17	2
Q7Z2Z2|ETUD1_HUMAN	Elongation factor Tu GTP-binding doma	83.91	11	2
Q9BW83|IFT27_HUMAN	Intraflagellar transport protein 27 homol	83.84	17	2
Q13951|PEBB_HUMAN	Core-binding factor subunit beta OS=H	83.76	23	2
Q8WTX7|GATL3_HUMAN	GATS-like protein 3 OS=Homo sapiens	83.64	20	2
P00568|KAD1_HUMAN	Adenylate kinase isoenzyme 1 OS=Hon	83.62	14	2
Q96H20|SNF8_HUMAN	Vacuolar-sorting protein SNF8 OS=Hon	83.59	16	2
P54105|ICLN_HUMAN	Methylosome subunit pICln OS=Homo s	83.25	11	2
Q9NR28|DBLOH_HUMAN	Diablo homolog, mitochondrial OS=Hon	83.12	25	2
Q9NS69|TOM22_HUMAN	Mitochondrial import receptor subunit T	83.03	37	2
Q9BX68|HINT2_HUMAN	Histidine triad nucleotide-binding protei	82.54	34	2
O43617|TPPC3_HUMAN	Trafficking protein particle complex subu	82.46	34	2
P46109|CRKL_HUMAN	Crk-like protein OS=Homo sapiens GN=	82.28	12	2
O15116|LSM1_HUMAN	U6 snRNA-associated Sm-like protein L	82.24	31	2
P15927|RFA2_HUMAN	Replication protein A 32 kDa subunit OS	82.12	33	2
P09486|SPRC_HUMAN	SPARC OS=Homo sapiens GN=SPARC	82.12	10	2
O95373|IPO7_HUMAN	Importin-7 OS=Homo sapiens GN=IPO7	81.84	8	2
Q16186|ADRM1_HUMAN	Proteasomal ubiquitin receptor ADRM1	81.75	13	2
Q13442|HAP28_HUMAN	28 kDa heat- and acid-stable phosphop	81.62	24	2
P48444|COPD_HUMAN	Coatomer subunit delta OS=Homo sapi	81.29	12	2
O75380|NDUS6_HUMAN	NADH dehydrogenase [ubiquinone] iron	81.2	27	2
A8MWD9|RUXGL_HUMAN	Small nuclear ribonucleoprotein G-like p	81.11	37	2
P62308|RUXG_HUMAN	Small nuclear ribonucleoprotein G OS=	81.11	17	2
Q96HE7|ERO1A_HUMAN	ERO1-like protein alpha OS=Homo sap	81.11	15	2
P55854|SUMO3_HUMAN	Small ubiquitin-related modifier 3 OS=H	80.97	24	2
P30049|ATPD_HUMAN	ATP synthase subunit delta, mitochondr	80.77	27	2
Q9UKY7|CDV3_HUMAN	Protein CDV3 homolog OS=Homo sapie	80.75	16	2
Q3LXA3|DHAK_HUMAN	Bifunctional ATP-dependent dihydroxya	80.72	25	2
P29218|IMPA1_HUMAN	Inositol monophosphatase 1 OS=Homo	80.63	8	2
P61803|DAD1_HUMAN	Dolichyl-diphosphooligosaccharide--pro	80.51	34	2
O96000|NDUBA_HUMAN	NADH dehydrogenase [ubiquinone] 1 b	80.43	27	2
Q9Y5S9|RBM8A_HUMAN	RNA-binding protein 8A OS=Homo sap	80.42	21	2
Q15833|STXB2_HUMAN	Syntaxin-binding protein 2 OS=Homo sa	80.37	19	2
Q99447|PCY2_HUMAN	Ethanolamine-phosphate cytidylyltransf	80.21	23	2
Q96C90|PP14B_HUMAN	Protein phosphatase 1 regulatory subun	80.1	59	2
P15954|COX7C_HUMAN	Cytochrome c oxidase subunit 7C, mito	79.92	41	2
P35611|ADDA_HUMAN	Alpha-adducin OS=Homo sapiens GN=	79.78	16	2
P52758|UK114_HUMAN	Ribonuclease UK114 OS=Homo sapien	79.42	31	2
O95793|STAU1_HUMAN	Double-stranded RNA-binding protein S	79.38	16	2
Q01081|U2AF1_HUMAN	Splicing factor U2AF 35 kDa subunit OS	79.3	11	2
P00390|GSHR_HUMAN	Glutathione reductase, mitochondrial O	79.25	9	2
Q8N0X7|SPG20_HUMAN	Spartin OS=Homo sapiens GN=SPG20	79.24	5	2
Q86SZ2|TPC6B_HUMAN	Trafficking protein particle complex subu	79.01	17	2
O75431|MTX2_HUMAN	Metaxin-2 OS=Homo sapiens GN=MTX	78.94	13	2
P49589|SYCC_HUMAN	Cysteinyl-tRNA synthetase, cytoplasmic	78.77	17	2
Q9H944|MED20_HUMAN	Mediator of RNA polymerase II transcrip	78.61	21	2
Q9Y285|SYFA_HUMAN	Phenylalanyl-tRNA synthetase alpha ch	78.51	13	2
P78344|IF4G2_HUMAN	Eukaryotic translation initiation factor 4	78.49	10	2

P07311|ACYP1_HUMAN	Acylphosphatase-1 OS=Homo sapiens	78.49	23	2
Q9UQ35|SRRM2_HUMAN	Serine/arginine repetitive matrix protein	78.46	9	2
P25391|LAMA1_HUMAN	Laminin subunit alpha-1 OS=Homo sap	78.39	9	2
Q9Y6M9|NDUB9_HUMAN	NADH dehydrogenase [ubiquinone] 1 b	78.27	18	2
Q06481|APLP2_HUMAN	Amyloid-like protein 2 OS=Homo sapier	78	11	2
Q9ULA0|DNPEP_HUMAN	Aspartyl aminopeptidase OS=Homo sa	77.95	17	2
Q9UNH7|SNX6_HUMAN	Sorting nexin-6 OS=Homo sapiens GN=	77.94	19	2
P04439|1A03_HUMAN	HLA class I histocompatibility antigen, A	77.85	18	2
P56192|SYMC_HUMAN	Methionyl-tRNA synthetase, cytoplasmi	77.47	8	2
P61086|UBE2K_HUMAN	Ubiquitin-conjugating enzyme E2 K OS=	77.36	39	2
O60841|IF2P_HUMAN	Eukaryotic translation initiation factor 5E	77.17	13	2
Q5TDH0|DDI2_HUMAN	Protein DDI1 homolog 2 OS=Homo sap	77.15	6	2
P52815|RM12_HUMAN	39S ribosomal protein L12, mitochondri	76.8	21	2
Q92572|AP3S1_HUMAN	AP-3 complex subunit sigma-1 OS=Hor	76.56	10	2
O00170|AIP_HUMAN	AH receptor-interacting protein OS=Hor	76.24	25	2
Q9NTX5|ECHD1_HUMAN	Enoyl-CoA hydratase domain-containing	76.14	15	2
Q9Y3D9|RT23_HUMAN	28S ribosomal protein S23, mitochondri	76.04	18	2
P53365|ARFP2_HUMAN	Arfaptin-2 OS=Homo sapiens GN=ARF	75.97	14	2
A6NK07|IF2BL_HUMAN	Eukaryotic translation initiation factor 2	75.91	13	2
P20042|IF2B_HUMAN	Eukaryotic translation initiation factor 2	75.91	13	2
P10155|RO60_HUMAN	60 kDa SS-A/Ro ribonucleoprotein OS=	75.88	11	2
P55060|XPO2_HUMAN	Exportin-2 OS=Homo sapiens GN=CSE	75.51	13	2
Q14CX7|NAA25_HUMAN	N-alpha-acetyltransferase 25, NatB aux	75.31	9	2
Q13148|TADBP_HUMAN	TAR DNA-binding protein 43 OS=Homo	74.94	14	2
Q96SM3|CPXM1_HUMAN	Probable carboxypeptidase X1 OS=Hor	74.86	10	2
Q99426|TBCB_HUMAN	Tubulin-folding cofactor B OS=Homo sa	74.55	9	2
Q92890|UFD1_HUMAN	Ubiquitin fusion degradation protein 1 h	74.47	14	2
P37268|FDFT_HUMAN	Squalene synthase OS=Homo sapiens	74.35	15	2
Q9UMY4|SNX12_HUMAN	Sorting nexin-12 OS=Homo sapiens GN	74.31	17	2
Q9UL25|RAB21_HUMAN	Ras-related protein Rab-21 OS=Homo	74.11	28	2
Q9NPH2|INO1_HUMAN	Inositol-3-phosphate synthase 1 OS=H	73.91	8	2
Q16706|MA2A1_HUMAN	Alpha-mannosidase 2 OS=Homo sapie	73.43	9	2
Q9UJC5|SH3L2_HUMAN	SH3 domain-binding glutamic acid-rich-	73.32	25	2
Q02978|M2OM_HUMAN	Mitochondrial 2-oxoglutarate/malate car	73.19	21	2
Q9Y3B7|RM11_HUMAN	39S ribosomal protein L11, mitochondri	73.04	46	2
Q9BU89|DOHH_HUMAN	Deoxyhypusine hydroxylase OS=Homo	73.02	18	2
P11233|RALA_HUMAN	Ras-related protein Ral-A OS=Homo sa	72.88	22	2
O00625|PIR_HUMAN	Pirin OS=Homo sapiens GN=PIR PE=1	72.82	16	2
Q9UHB9|SRP68_HUMAN	Signal recognition particle 68 kDa prote	72.49	11	2
Q99543|DNJC2_HUMAN	DnaJ homolog subfamily C member 2 C	72.4	12	2
P63272|SPT4H_HUMAN	Transcription elongation factor SPT4 OS	72.32	21	2
Q9H8S9|MOL1B_HUMAN	Mps one binder kinase activator-like 1B	72.25	19	2
Q7L9L4|MOL1A_HUMAN	Mps one binder kinase activator-like 1A	72.25	14	2
Q9UBV8|PEF1_HUMAN	Peflin OS=Homo sapiens GN=PEF1 PE	72.06	11	2
Q9NV35|NUD15_HUMAN	Probable 7,8-dihydro-8-oxoguanine trip	71.94	7	2
Q5TZA2|CROCC_HUMAN	Rootletin OS=Homo sapiens GN=CRO	71.86	9	2
Q14671|PUM1_HUMAN	Pumilio homolog 1 OS=Homo sapiens	71.78	5	2
Q5SSJ5|HP1B3_HUMAN	Heterochromatin protein 1-binding prote	71.74	12	2
Q96HR9|REEP6_HUMAN	Receptor expression-enhancing protein	71.42	29	2
P01116|RASK_HUMAN	GTPase KRas OS=Homo sapiens GN=	70.95	17	2
P01111|RASN_HUMAN	GTPase NRas OS=Homo sapiens GN=	70.95	17	2
Q9NVA2|SEP11_HUMAN	Septin-11 OS=Homo sapiens GN=SEP	70.48	17	2
Q8TDP1|RNH2C_HUMAN	Ribonuclease H2 subunit C OS=Homo	70.4	15	2
Q9UH65|SWP70_HUMAN	Switch-associated protein 70 OS=Homo	70.06	12	2
Q13153|PAK1_HUMAN	Serine/threonine-protein kinase PAK 1	69.67	6	2
P56747|CLD6_HUMAN	Claudin-6 OS=Homo sapiens GN=CLD	69.55	13	2

Q6IQ22|RAB12_HUMAN	Ras-related protein Rab-12 OS=Homo	69.4	13	2
Q7Z4H3|HDDC2_HUMAN	HD domain-containing protein 2 OS=Ho	69.3	22	2
O00629|IMA4_HUMAN	Importin subunit alpha-4 OS=Homo sap	69.15	8	2
Q8NC69|KCTD6_HUMAN	BTB/POZ domain-containing protein KC	68.94	19	2
Q8IZ83|A16A1_HUMAN	Aldehyde dehydrogenase family 16 mer	68.93	12	2
P29083|T2EA_HUMAN	General transcription factor IIE subunit	68.87	11	2
Q9Y6E0|STK24_HUMAN	Serine/threonine-protein kinase 24 OS=	68.56	15	2
P23378|GCSP_HUMAN	Glycine dehydrogenase [decarboxylatin	68.21	4	2
Q5TFE4|NT5D1_HUMAN	5'-nucleotidase domain-containing prote	68.2	11	2
Q9UKF6|CPSF3_HUMAN	Cleavage and polyadenylation specificit	67.53	8	2
O95218|ZRAB2_HUMAN	Zinc finger Ran-binding domain-contain	67.15	9	2
P04183|KITH_HUMAN	Thymidine kinase, cytosolic OS=Homo	66.94	14	2
Q16718|NDUA5_HUMAN	NADH dehydrogenase [ubiquinone] 1 a	66.93	30	2
P60510|PP4C_HUMAN	Serine/threonine-protein phosphatase 4	66.73	10	2
P61225|RAP2B_HUMAN	Ras-related protein Rap-2b OS=Homo	66.56	21	2
Q03426|KIME_HUMAN	Mevalonate kinase OS=Homo sapiens	66.39	13	2
O00154|BACH_HUMAN	Cytosolic acyl coenzyme A thioester hy	66.35	22	2
O95235|KI20A_HUMAN	Kinesin-like protein KIF20A OS=Homo	65.81	13	2
Q14011|CIRBP_HUMAN	Cold-inducible RNA-binding protein OS	65.66	22	2
O43583|DENR_HUMAN	Density-regulated protein OS=Homo sa	65.64	19	2
P20585|MSH3_HUMAN	DNA mismatch repair protein Msh3 OS=	65.59	17	2
Q8N5K1|CISD2_HUMAN	CDGSH iron-sulfur domain-containing p	65.57	34	2
P52888|THOP1_HUMAN	Thimet oligopeptidase OS=Homo sapie	65.26	4	2
Q9GZQ8|MLP3B_HUMAN	Microtubule-associated proteins 1A/1B	65.03	23	2
A6NCE7|MP3B2_HUMAN	Microtubule-associated proteins 1A/1B	65.03	23	2
O75534|CSDE1_HUMAN	Cold shock domain-containing protein E	65.03	9	2
Q9BZL1|UBL5_HUMAN	Ubiquitin-like protein 5 OS=Homo sapie	64.94	25	2
O14925|TIM23_HUMAN	Mitochondrial import inner membrane tr	64.93	13	2
Q5SRD1|TI23B_HUMAN	Putative mitochondrial import inner mem	64.93	11	2
Q9Y3B2|EXOS1_HUMAN	Exosome complex component CSL4 OS	64.87	13	2
Q13636|RAB31_HUMAN	Ras-related protein Rab-31 OS=Homo	64.3	19	2
P05204|HMGN2_HUMAN	Non-histone chromosomal protein HMG	64.24	56	2
P56377|AP1S2_HUMAN	AP-1 complex subunit sigma-2 OS=Hor	64.03	17	2
P61960|UFM1_HUMAN	Ubiquitin-fold modifier 1 OS=Homo sap	63.89	27	2
P18065|IBP2_HUMAN	Insulin-like growth factor-binding protein	63.87	8	2
Q9BRJ7|SDOS_HUMAN	Protein syndesmos OS=Homo sapiens	63.48	17	2
O00217|NDUS8_HUMAN	NADH dehydrogenase [ubiquinone] iron	63.33	18	2
Q96QK1|VPS35_HUMAN	Vacuolar protein sorting-associated pro	63.32	13	2
Q13155|AIMP2_HUMAN	Aminoacyl tRNA synthase complex-inte	63.04	10	2
Q07812|BAX_HUMAN	Apoptosis regulator BAX OS=Homo sap	62.59	19	2
P52732|KIF11_HUMAN	Kinesin-like protein KIF11 OS=Homo sa	62.44	5	2
O00115|DNS2A_HUMAN	Deoxyribonuclease-2-alpha OS=Homo	61.62	7	2
P49406|RM19_HUMAN	39S ribosomal protein L19, mitochondri	61.61	11	2
Q9H9J2|RM44_HUMAN	39S ribosomal protein L44, mitochondri	61.5	10	2
P49756|RBM25_HUMAN	RNA-binding protein 25 OS=Homo sapi	61.38	3	2
Q6NVY1|HIBCH_HUMAN	3-hydroxyisobutyryl-CoA hydrolase, mit	61.25	11	2
P19404|NDUV2_HUMAN	NADH dehydrogenase [ubiquinone] flav	61.16	16	2
Q96BM9|ARL8A_HUMAN	ADP-ribosylation factor-like protein 8A	61.03	15	2
Q9NVJ2|ARL8B_HUMAN	ADP-ribosylation factor-like protein 8B	61.03	15	2
O75251|NDUS7_HUMAN	NADH dehydrogenase [ubiquinone] iron	60.96	8	2
Q9Y2R0|CCD56_HUMAN	Coiled-coil domain-containing protein 5	60.9	27	2
O94826|TOM70_HUMAN	Mitochondrial import receptor subunit T	59.92	9	2
P14927|QCR7_HUMAN	Cytochrome b-c1 complex subunit 7 OS	59.92	27	2
P63098|CANB1_HUMAN	Calcineurin subunit B type 1 OS=Homo	59.79	11	2
P14866|HNRPL_HUMAN	Heterogeneous nuclear ribonucleoprote	58.35	12	2
P21281|VATB2_HUMAN	V-type proton ATPase subunit B, brain	58.26	10	2

Q02218|ODO1_HUMAN	2-oxoglutarate dehydrogenase, mitocho	58.05	8	2
Q9Y2Q9|RT28_HUMAN	28S ribosomal protein S28, mitochondri	57.96	13	2
P31930|QCR1_HUMAN	Cytochrome b-c1 complex subunit 1, mi	57.88	13	2
P56556|NDUA6_HUMAN	NADH dehydrogenase [ubiquinone] 1 a	57.21	31	2
O43678|NDUA2_HUMAN	NADH dehydrogenase [ubiquinone] 1 a	57.14	20	2
Q96K17|BT3L4_HUMAN	Transcription factor BTF3 homolog 4 O	56.73	33	2
O43865|SAHH2_HUMAN	Putative adenosylhomocysteinase 2 OS	56.61	16	2
Q9Y530|CF130_HUMAN	Uncharacterized protein C6orf130 OS=	56.26	26	2
O15498|YKT6_HUMAN	Synaptobrevin homolog YKT6 OS=Hom	55.34	10	2
Q14677|EPN4_HUMAN	Clathrin interactor 1 OS=Homo sapiens	55.24	6	2
Q92747|ARC1A_HUMAN	Actin-related protein 2/3 complex subur	54.89	26	2
Q99661|KIF2C_HUMAN	Kinesin-like protein KIF2C OS=Homo s	54.64	11	2
Q9NVM6|DJC17_HUMAN	DnaJ homolog subfamily C member 17	54.21	22	2
O75718|CRTAP_HUMAN	Cartilage-associated protein OS=Homo	53.78	6	2
Q02880|TOP2B_HUMAN	DNA topoisomerase 2-beta OS=Homo	53.64	5	2
Q13428|TCOF_HUMAN	Treacle protein OS=Homo sapiens GN=	52.99	13	2
Q8WZA0|LZIC_HUMAN	Protein LZIC OS=Homo sapiens GN=L	52.68	23	2
Q9H7Z7|PGES2_HUMAN	Prostaglandin E synthase 2 OS=Homo	52.65	12	2
O95881|TXD12_HUMAN	Thioredoxin domain-containing protein	51.81	14	2
P61513|RL37A_HUMAN	60S ribosomal protein L37a OS=Homo	51.22	28	2
P56381|ATP5E_HUMAN	ATP synthase subunit epsilon, mitochor	51.1	53	2
O75438|NDUB1_HUMAN	NADH dehydrogenase [ubiquinone] 1 b	51.05	48	2
Q7Z4W1|DCXR_HUMAN	L-xylulose reductase OS=Homo sapien	50.8	14	2
Q9UPG8|PLAL2_HUMAN	Zinc finger protein PLAGL2 OS=Homo	50.6	3	2
Q8TE73|DYH5_HUMAN	Dynein heavy chain 5, axonemal OS=H	50.53	7	2
O00754|MA2B1_HUMAN	Lysosomal alpha-mannosidase OS=Ho	50.45	5	2
O75822|EIF3J_HUMAN	Eukaryotic translation initiation factor 3	50.25	9	2
Q9BYN0|SRXN1_HUMAN	Sulfiredoxin-1 OS=Homo sapiens GN=S	49.96	61	2
Q96HF1|SFRP2_HUMAN	Secreted frizzled-related protein 2 OS=	48.73	8	2
O15484|CAN5_HUMAN	Calpain-5 OS=Homo sapiens GN=CAP	48.49	4	2
P49207|RL34_HUMAN	60S ribosomal protein L34 OS=Homo s	48.49	13	2
Q9NYF8|BCLF1_HUMAN	Bcl-2-associated transcription factor 1 C	48.31	5	2
P38117|ETFB_HUMAN	Electron transfer flavoprotein subunit be	47.14	20	2
Q8WVB6|CTF18_HUMAN	Chromosome transmission fidelity prote	46.84	8	2
P61916|NPC2_HUMAN	Epididymal secretory protein E1 OS=Ho	46.16	28	2
Q8IUR0|TPPC5_HUMAN	Trafficking protein particle complex sub	44.87	27	2
Q86UW8|HPLN4_HUMAN	Hyaluronan and proteoglycan link prote	42.29	10	2
P09038|FGF2_HUMAN	Heparin-binding growth factor 2 OS=Ho	41.24	15	2
Q9Y5Z4|HEBP2_HUMAN	Heme-binding protein 2 OS=Homo sapi	40.86	16	2
P06703|S10A6_HUMAN	Protein S100-A6 OS=Homo sapiens GN	40.68	17	2
Q9NRC6|SPTN5_HUMAN	Spectrin beta chain, brain 4 OS=Homo	39.95	8	2
Q6IQ55|TTBK2_HUMAN	Tau-tubulin kinase 2 OS=Homo sapiens	39.21	7	2
P49454|CENPF_HUMAN	Centromere protein F OS=Homo sapien	39.1	4	2
Q8IVF4|DYH10_HUMAN	Dynein heavy chain 10, axonemal OS=	38.62	6	2
Q5JWR5|DOP1_HUMAN	Protein dopey-1 OS=Homo sapiens GN	38.37	7	2
Q8NE71|ABCF1_HUMAN	ATP-binding cassette sub-family F mem	38.26	6	2
Q14669|TRIPC_HUMAN	Probable E3 ubiquitin-protein ligase TR	38.23	8	2
Q9BXM0|PRAX_HUMAN	Periaxin OS=Homo sapiens GN=PRX P	38.04	9	2
Q7Z5P9|MUC19_HUMAN	Mucin-19 OS=Homo sapiens GN=MUC	37.93	6	2
Q9HB07|MYG1_HUMAN	UPF0160 protein MYG1, mitochondrial	37.63	10	2
Q9Y4W2|LAS1L_HUMAN	Protein LAS1 homolog OS=Homo sapie	36.25	9	2
P20929|NEBU_HUMAN	Nebulin OS=Homo sapiens GN=NEB P	36.01	5	2
Q86TB3|ALPK2_HUMAN	Alpha-protein kinase 2 OS=Homo sapie	35.61	6	2
O75179|ANR17_HUMAN	Ankyrin repeat domain-containing prote	35.5	4	2
Q4G0P3|HYDIN_HUMAN	Hydrocephalus-inducing protein homolo	34.73	3	2
Q8N6I1|EID2_HUMAN	EP300-interacting inhibitor of differentia	33.82	14	2

O14815|CAN9_HUMAN	Calpain-9 OS=Homo sapiens GN=CAP	33.32	7	2
Q07157|ZO1_HUMAN	Tight junction protein ZO-1 OS=Homo s	33.22	8	2
P08123|CO1A2_HUMAN	Collagen alpha-2(I) chain OS=Homo sa	33.2	26	2
Q5K651|SAMD9_HUMAN	Sterile alpha motif domain-containing pr	31.36	3	2
Q17RW2|COOA1_HUMAN	Collagen alpha-1(XXIV) chain OS=Hom	30.94	9	2
O75145|LIPA3_HUMAN	Liprin-alpha-3 OS=Homo sapiens GN=P	30.5	4	2
Q07954|LRP1_HUMAN	Prolow-density lipoprotein receptor-rela	29.94	6	2
Q96FE5|LIGO1_HUMAN	Leucine-rich repeat and immunoglobulin	29.17	12	2
Q9H6A0|DEN2D_HUMAN	DENN domain-containing protein 2D OS	28.18	14	2
Q8IXJ9|ASXL1_HUMAN	Putative Polycomb group protein ASXL1	27.93	8	2
Q70EL4|UBP43_HUMAN	Ubiquitin carboxyl-terminal hydrolase 43	27.56	7	2
P49761|CLK3_HUMAN	Dual specificity protein kinase CLK3 OS	27.5	5	2

Table A1.11 BJ-1D hiPSC CMTX Protein Identifications. List of all proteins identified in CMTX from BJ-1D hiPSCs with corresponding accession, description, PEAKS score, unique peptide numbers, and coverage (in %).

Accession	Description	Score	Coverage (%)	#Unique
Q13813|SPTA2_HUMAN	Spectrin alpha chain, brain OS=Homo sap	415.57	69	88
P18206|VINC_HUMAN	Vinculin OS=Homo sapiens GN=VCL PE=	406.76	75	88
P21333|FLNA_HUMAN	Filamin-A OS=Homo sapiens GN=FLNA P	420.58	60	83
P49327|FAS_HUMAN	Fatty acid synthase OS=Homo sapiens GN	404.62	54	77
P04406|G3P_HUMAN	Glyceraldehyde-3-phosphate dehydrogena	393.33	80	59
P08670|VIME_HUMAN	Vimentin OS=Homo sapiens GN=VIM PE=	376.46	88	57
P13639|EF2_HUMAN	Elongation factor 2 OS=Homo sapiens GN	376.7	74	56
P14618|KPYM_HUMAN	Pyruvate kinase isozymes M1/M2 OS=Hon	388.34	84	55
P06733|ENOA_HUMAN	Alpha-enolase OS=Homo sapiens GN=EN	378.09	91	53
P55072|TERA_HUMAN	Transitional endoplasmic reticulum ATPas	320.9	66	48
Q01082|SPTB2_HUMAN	Spectrin beta chain, brain 1 OS=Homo sap	340.04	53	47
P29401|TKT_HUMAN	Transketolase OS=Homo sapiens GN=TK	341.77	71	46
P35579|MYH9_HUMAN	Myosin-9 OS=Homo sapiens GN=MYH9 P	359.17	55	43
P68104|EF1A1_HUMAN	Elongation factor 1-alpha 1 OS=Homo sap	382.81	83	41
P04075|ALDOA_HUMAN	Fructose-bisphosphate aldolase A OS=Ho	363.24	90	40
P07737|PROF1_HUMAN	Profilin-1 OS=Homo sapiens GN=PFN1 PE	331.51	97	40
P18669|PGAM1_HUMAN	Phosphoglycerate mutase 1 OS=Homo sa	327.03	87	36
P35580|MYH10_HUMAN	Myosin-10 OS=Homo sapiens GN=MYH10	346.9	57	35
P78371|TCPB_HUMAN	T-complex protein 1 subunit beta OS=Hom	336.45	73	34
P46940|IQGA1_HUMAN	Ras GTPase-activating-like protein IQGAP	291.2	45	34
P60174|TPIS_HUMAN	Triosephosphate isomerase OS=Homo sa	321.71	95	33
P62805|H4_HUMAN	Histone H4 OS=Homo sapiens GN=HIST1	297.26	62	33
P50454|SERPH_HUMAN	Serpin H1 OS=Homo sapiens GN=SERPIN	335.1	84	32
Q01995|TAGL_HUMAN	Transgelin OS=Homo sapiens GN=TAGLN	303.06	85	32
Q14152|EIF3A_HUMAN	Eukaryotic translation initiation factor 3 sub	272.93	40	32
P30101|PDIA3_HUMAN	Protein disulfide-isomerase A3 OS=Homo	266.77	59	32
P12814|ACTN1_HUMAN	Alpha-actinin-1 OS=Homo sapiens GN=AC	366.51	67	31
P22626|ROA2_HUMAN	Heterogeneous nuclear ribonucleoproteins	315.99	68	31
P00558|PGK1_HUMAN	Phosphoglycerate kinase 1 OS=Homo sap	304.57	86	31
P61978|HNRPK_HUMAN	Heterogeneous nuclear ribonucleoprotein	290.36	61	31
O75874|IDHC_HUMAN	Isocitrate dehydrogenase [NADP] cytoplas	327.63	82	30
P07355|ANXA2_HUMAN	Annexin A2 OS=Homo sapiens GN=ANXA	315.97	72	30
P53396|ACLY_HUMAN	ATP-citrate synthase OS=Homo sapiens G	293.91	42	30
P12956|XRCC6_HUMAN	X-ray repair cross-complementing protein 6	290.56	63	30
P07814|SYEP_HUMAN	Bifunctional aminoacyl-tRNA synthetase O	283.37	42	30
P50395|GDIB_HUMAN	Rab GDP dissociation inhibitor beta OS=H	323.5	73	29
Q06830|PRDX1_HUMAN	Peroxiredoxin-1 OS=Homo sapiens GN=P	312.03	81	29
P05455|LA_HUMAN	Lupus La protein OS=Homo sapiens GN=S	308.2	74	29
P48643|TCPE_HUMAN	T-complex protein 1 subunit epsilon OS=H	283.95	73	29
P62937|PPIA_HUMAN	Peptidyl-prolyl cis-trans isomerase A OS=H	279.13	81	28
Q00610|CLH1_HUMAN	Clathrin heavy chain 1 OS=Homo sapiens	346.23	61	27
P13010|XRCC5_HUMAN	X-ray repair cross-complementing protein 5	301.23	64	27
P30041|PRDX6_HUMAN	Peroxiredoxin-6 OS=Homo sapiens GN=P	297.01	85	27
P26038|MOES_HUMAN	Moesin OS=Homo sapiens GN=MSN PE=	289.19	70	27
P50990|TCPQ_HUMAN	T-complex protein 1 subunit theta OS=Hon	261.43	57	27
P14625|ENPL_HUMAN	Endoplasmin OS=Homo sapiens GN=HSP	257.85	45	27
P08238|HS90B_HUMAN	Heat shock protein HSP 90-beta OS=Hom	381.28	73	26

P23528|COF1_HUMAN	Cofilin-1 OS=Homo sapiens GN=CFL1 PE	351.29	93	26
P62328|TYB4_HUMAN	Thymosin beta-4 OS=Homo sapiens GN=T	311.08	93	26
O75369|FLNB_HUMAN	Filamin-B OS=Homo sapiens GN=FLNB P	275.65	31	26
P34932|HSP74_HUMAN	Heat shock 70 kDa protein 4 OS=Homo sa	270.13	55	26
P52272|HNRPM_HUMAN	Heterogeneous nuclear ribonucleoprotein	265.99	81	26
Q86UP2|KTN1_HUMAN	Kinectin OS=Homo sapiens GN=KTN1 PE	259.22	43	26
O43707|ACTN4_HUMAN	Alpha-actinin-4 OS=Homo sapiens GN=AC	340.07	62	25
P40926|MDHM_HUMAN	Malate dehydrogenase, mitochondrial OS=	321.36	87	25
Q99832|TCPH_HUMAN	T-complex protein 1 subunit eta OS=Homo	297.49	76	25
P23246|SFPQ_HUMAN	Splicing factor, proline- and glutamine-rich	281.88	51	25
P49368|TCPG_HUMAN	T-complex protein 1 subunit gamma OS=H	262.99	61	25
P62258|1433E_HUMAN	14-3-3 protein epsilon OS=Homo sapiens (	316.26	73	24
P62158|CALM_HUMAN	Calmodulin OS=Homo sapiens GN=CALM	288.06	73	24
P00338|LDHA_HUMAN	L-lactate dehydrogenase A chain OS=Hom	272.17	80	24
O00231|PSD11_HUMAN	26S proteasome non-ATPase regulatory su	270.46	60	24
P61604|CH10_HUMAN	10 kDa heat shock protein, mitochondrial (	264.25	97	24
P11586|C1TC_HUMAN	C-1-tetrahydrofolate synthase, cytoplasmic	261.8	48	24
P11142|HSP7C_HUMAN	Heat shock cognate 71 kDa protein OS=H	343.82	71	23
P09211|GSTP1_HUMAN	Glutathione S-transferase P OS=Homo sa	311.37	67	23
P63104|1433Z_HUMAN	14-3-3 protein zeta/delta OS=Homo sapien	309.6	75	23
Q14315|FLNC_HUMAN	Filamin-C OS=Homo sapiens GN=FLNC P	269.23	28	23
P11021|GRP78_HUMAN	78 kDa glucose-regulated protein OS=Hom	268.24	55	23
Q9P2E9|RRBP1_HUMAN	Ribosome-binding protein 1 OS=Homo sap	264.54	35	23
P49321|NASP_HUMAN	Nuclear autoantigenic sperm protein OS=H	264.04	52	23
P08758|ANXA5_HUMAN	Annexin A5 OS=Homo sapiens GN=ANXA	263.47	61	23
P10809|CH60_HUMAN	60 kDa heat shock protein, mitochondrial (	254.47	72	23
Q9P2J5|SYLC_HUMAN	Leucyl-tRNA synthetase, cytoplasmic OS=	249.98	34	23
P27816|MAP4_HUMAN	Microtubule-associated protein 4 OS=Hom	246.38	48	23
P06748|NPM_HUMAN	Nucleophosmin OS=Homo sapiens GN=NI	297.11	57	22
P04083|ANXA1_HUMAN	Annexin A1 OS=Homo sapiens GN=ANXA	293.21	82	22
O60664|PLIN3_HUMAN	Perilipin-3 OS=Homo sapiens GN=PLIN3 P	286.02	68	22
P07195|LDHB_HUMAN	L-lactate dehydrogenase B chain OS=Hom	280.74	70	22
P19338|NUCL_HUMAN	Nucleolin OS=Homo sapiens GN=NCL PE	279.66	70	22
P37802|TAGL2_HUMAN	Transgelin-2 OS=Homo sapiens GN=TAG	265.75	90	22
P23396|RS3_HUMAN	40S ribosomal protein S3 OS=Homo sapie	264.34	79	22
P25398|RS12_HUMAN	40S ribosomal protein S12 OS=Homo sapi	255.07	87	22
P61247|RS3A_HUMAN	40S ribosomal protein S3a OS=Homo sapi	237.12	67	22
Q00839|HNRPU_HUMAN	Heterogeneous nuclear ribonucleoprotein	235.34	38	22
P67936|TPM4_HUMAN	Tropomyosin alpha-4 chain OS=Homo sap	337.21	92	21
Q01469|FABP5_HUMAN	Fatty acid-binding protein, epidermal OS=H	310.82	91	21
P52209|6PGD_HUMAN	6-phosphogluconate dehydrogenase, deca	302.27	67	21
P22314|UBA1_HUMAN	Ubiquitin-like modifier-activating enzyme 1	287.66	52	21
P15311|EZRI_HUMAN	Ezrin OS=Homo sapiens GN=EZR PE=1 S	275.31	62	21
P08133|ANXA6_HUMAN	Annexin A6 OS=Homo sapiens GN=ANXA	263.46	54	21
P06744|G6PI_HUMAN	Glucose-6-phosphate isomerase OS=Hom	260.96	53	21
Q9UQE7|SMC3_HUMAN	Structural maintenance of chromosomes p	246.91	43	21
Q9Y617|SERC_HUMAN	Phosphoserine aminotransferase OS=Hom	235	63	21

Q13263|TIF1B_HUMAN	Transcription intermediary factor 1-beta OS	229.1	41	21
P07900|HS90A_HUMAN	Heat shock protein HSP 90-alpha OS=Hor	354.61	61	20
P25205|MCM3_HUMAN	DNA replication licensing factor MCM3 OS	241	43	20
P22102|PUR2_HUMAN	Trifunctional purine biosynthetic protein ad	236.14	44	20
P43243|MATR3_HUMAN	Matrin-3 OS=Homo sapiens GN=MATR3 P	234.49	38	20
P27348|1433T_HUMAN	14-3-3 protein theta OS=Homo sapiens GN	294.62	80	19
P09936|UCHL1_HUMAN	Ubiquitin carboxyl-terminal hydrolase isozy	288.93	72	19
P62826|RAN_HUMAN	GTP-binding nuclear protein Ran OS=Hom	265.32	67	19
P62333|PRS10_HUMAN	26S protease regulatory subunit 10B OS=H	253.46	62	19
Q05682|CALD1_HUMAN	Caldesmon OS=Homo sapiens GN=CALD	247.38	42	19
P31948|STIP1_HUMAN	Stress-induced-phosphoprotein 1 OS=Hon	245.14	54	19
Q14566|MCM6_HUMAN	DNA replication licensing factor MCM6 OS	232.1	40	19
P07237|PDIA1_HUMAN	Protein disulfide-isomerase OS=Homo sap	223.79	52	19
P36578|RL4_HUMAN	60S ribosomal protein L4 OS=Homo sapie	196.33	53	19
O43175|SERA_HUMAN	D-3-phosphoglycerate dehydrogenase OS	270.54	53	18
P40227|TCPZ_HUMAN	T-complex protein 1 subunit zeta OS=Hom	265.84	67	18
P33993|MCM7_HUMAN	DNA replication licensing factor MCM7 OS	260.76	58	18
P28074|PSB5_HUMAN	Proteasome subunit beta type-5 OS=Homo	245.18	59	18
Q15691|MARE1_HUMAN	Microtubule-associated protein RP/EB fam	238.96	62	18
P62081|RS7_HUMAN	40S ribosomal protein S7 OS=Homo sapie	197.73	68	18
P12270|TPR_HUMAN	Nucleoprotein TPR OS=Homo sapiens GN	196.85	25	18
P07910|HNRPC_HUMAN	Heterogeneous nuclear ribonucleoproteins	261.66	66	17
P05387|RLA2_HUMAN	60S acidic ribosomal protein P2 OS=Homo	260.83	84	17
P61981|1433G_HUMAN	14-3-3 protein gamma OS=Homo sapiens	253.74	81	17
P32119|PRDX2_HUMAN	Peroxiredoxin-2 OS=Homo sapiens GN=P	249.71	42	17
Q99623|PHB2_HUMAN	Prohibitin-2 OS=Homo sapiens GN=PHB2	241.91	71	17
Q16851|UGPA_HUMAN	UTP--glucose-1-phosphate uridylyltransfer	240.68	59	17
P17174|AATC_HUMAN	Aspartate aminotransferase, cytoplasmic O	239.08	62	17
P31939|PUR9_HUMAN	Bifunctional purine biosynthesis protein PU	235.43	46	17
P63244|GBLP_HUMAN	Guanine nucleotide-binding protein subuni	234.94	62	17
P39019|RS19_HUMAN	40S ribosomal protein S19 OS=Homo sapi	227.91	77	17
P62277|RS13_HUMAN	40S ribosomal protein S13 OS=Homo sapi	216.5	60	17
Q9Y4L1|HYOU1_HUMAN	Hypoxia up-regulated protein 1 OS=Homo	215.56	43	17
P48681|NEST_HUMAN	Nestin OS=Homo sapiens GN=NES PE=1	208.5	26	17
O00232|PSD12_HUMAN	26S proteasome non-ATPase regulatory su	197.18	41	17
O75347|TBCA_HUMAN	Tubulin-specific chaperone A OS=Homo sa	252.01	79	16
P09874|PARP1_HUMAN	Poly [ADP-ribose] polymerase 1 OS=Homo	250.38	39	16
Q9HB71|CYBP_HUMAN	Calcyclin-binding protein OS=Homo sapien	245.55	75	16
Q9BWD1|THIC_HUMAN	Acetyl-CoA acetyltransferase, cytosolic OS	237.68	63	16
Q15008|PSMD6_HUMAN	26S proteasome non-ATPase regulatory su	232.3	62	16
Q96KP4|CNDP2_HUMAN	Cytosolic non-specific dipeptidase OS=Hon	224.69	47	16
P05556|ITB1_HUMAN	Integrin beta-1 OS=Homo sapiens GN=ITG	223.84	34	16
Q08211|DHX9_HUMAN	ATP-dependent RNA helicase A OS=Hom	213.57	33	16
P54136|SYRC_HUMAN	Arginyl-tRNA synthetase, cytoplasmic OS=	182	37	16
P02794|FRIH_HUMAN	Ferritin heavy chain OS=Homo sapiens GN	181.41	64	16
P62701|RS4X_HUMAN	40S ribosomal protein S4, X isoform OS=H	178.24	63	16
P35221|CTNA1_HUMAN	Catenin alpha-1 OS=Homo sapiens GN=C	271.34	55	15

P26599|PTBP1_HUMAN	Polypyrimidine tract-binding protein 1 OS=	259.33	46	15
P62195|PRS8_HUMAN	26S protease regulatory subunit 8 OS=Hor	257.2	70	15
P02792|FRIL_HUMAN	Ferritin light chain OS=Homo sapiens GN=	256.12	69	15
P09972|ALDOC_HUMAN	Fructose-bisphosphate aldolase C OS=Ho	253.88	72	15
Q15084|PDIA6_HUMAN	Protein disulfide-isomerase A6 OS=Homo	244.61	60	15
Q16658|FSCN1_HUMAN	Fascin OS=Homo sapiens GN=FSCN1 PE	238.45	51	15
P31949|S10AB_HUMAN	Protein S100-A11 OS=Homo sapiens GN=	232.54	89	15
P25705|ATPA_HUMAN	ATP synthase subunit alpha, mitochondria	227.18	46	15
Q92499|DDX1_HUMAN	ATP-dependent RNA helicase DDX1 OS=H	225.41	50	15
P29692|EF1D_HUMAN	Elongation factor 1-delta OS=Homo sapier	224.66	70	15
P30044|PRDX5_HUMAN	Peroxiredoxin-5, mitochondrial OS=Homo	222.4	72	15
Q9BXP5|SRRT_HUMAN	Serrate RNA effector molecule homolog O	220.57	40	15
P08865|RSSA_HUMAN	40S ribosomal protein SA OS=Homo sapie	220.51	64	15
P17980|PRS6A_HUMAN	26S protease regulatory subunit 6A OS=H	218.83	59	15
P62316|SMD2_HUMAN	Small nuclear ribonucleoprotein Sm D2 OS	215.67	87	15
Q01581|HMCS1_HUMAN	Hydroxymethylglutaryl-CoA synthase, cyto	215.52	46	15
O43242|PSMD3_HUMAN	26S proteasome non-ATPase regulatory s	214.44	43	15
Q8NC51|PAIRB_HUMAN	Plasminogen activator inhibitor 1 RNA-bind	206.55	56	15
P33991|MCM4_HUMAN	DNA replication licensing factor MCM4 OS	206.07	39	15
P10599|THIO_HUMAN	Thioredoxin OS=Homo sapiens GN=TXN P	201.64	78	15
P02649|APOE_HUMAN	Apolipoprotein E OS=Homo sapiens GN=A	192.7	65	15
P10909|CLUS_HUMAN	Clusterin OS=Homo sapiens GN=CLU PE=	190.18	30	15
Q12906|ILF3_HUMAN	Interleukin enhancer-binding factor 3 OS=H	182.82	23	15
P07437|TBB5_HUMAN	Tubulin beta chain OS=Homo sapiens GN=	436.88	80	14
P12268|IMDH2_HUMAN	Inosine-5'-monophosphate dehydrogenase	255.92	46	14
P63220|RS21_HUMAN	40S ribosomal protein S21 OS=Homo sapi	250.13	84	14
Q9NZI8|IF2B1_HUMAN	Insulin-like growth factor 2 mRNA-binding p	249.44	38	14
P13796|PLSL_HUMAN	Plastin-2 OS=Homo sapiens GN=LCP1 PE	239.04	50	14
Q99497|PARK7_HUMAN	Protein DJ-1 OS=Homo sapiens GN=PARK	233.87	65	14
P27695|APEX1_HUMAN	DNA-(apurinic or apyrimidinic site) lyase O	232.53	49	14
P22234|PUR6_HUMAN	Multifunctional protein ADE2 OS=Homo sa	226.99	58	14
P43686|PRS6B_HUMAN	26S protease regulatory subunit 6B OS=H	226.07	53	14
P62424|RL7A_HUMAN	60S ribosomal protein L7a OS=Homo sapi	223.33	47	14
Q9H9Z2|LN28A_HUMAN	Protein lin-28 homolog A OS=Homo sapier	219.49	56	14
P37837|TALDO_HUMAN	Transaldolase OS=Homo sapiens GN=TAL	205.72	54	14
P47897|SYQ_HUMAN	Glutaminyl-tRNA synthetase OS=Homo sa	204.3	38	14
P78417|GSTO1_HUMAN	Glutathione S-transferase omega-1 OS=H	200.85	49	14
P11717|MPRI_HUMAN	Cation-independent mannose-6-phosphate	198.8	14	14
P41250|SYG_HUMAN	Glycyl-tRNA synthetase OS=Homo sapiens	196.4	37	14
Q02878|RL6_HUMAN	60S ribosomal protein L6 OS=Homo sapie	189.81	50	14
P62269|RS18_HUMAN	40S ribosomal protein S18 OS=Homo sapi	182.87	73	14
P18124|RL7_HUMAN	60S ribosomal protein L7 OS=Homo sapie	172.62	58	14
P60842|IF4A1_HUMAN	Eukaryotic initiation factor 4A-I OS=Homo	272.09	70	13
Q04917|1433F_HUMAN	14-3-3 protein eta OS=Homo sapiens GN=	272.01	78	13
P30086|PEBP1_HUMAN	Phosphatidylethanolamine-binding protein	237.8	79	13
Q9Y265|RUVB1_HUMAN	RuvB-like 1 OS=Homo sapiens GN=RUVB	236.18	66	13
P18084|ITB5_HUMAN	Integrin beta-5 OS=Homo sapiens GN=ITG	235.94	44	13

P23526|SAHH_HUMAN	Adenosylhomocysteinase OS=Homo sapie	234.94	57	13
Q9UNM6|PSD13_HUMAN	26S proteasome non-ATPase regulatory s	234.76	63	13
P25789|PSA4_HUMAN	Proteasome subunit alpha type-4 OS=Hom	229.68	68	13
P16152|CBR1_HUMAN	Carbonyl reductase [NADPH] 1 OS=Homo	226.77	69	13
Q14103|HNRPD_HUMAN	Heterogeneous nuclear ribonucleoprotein	225.83	52	13
P50991|TCPD_HUMAN	T-complex protein 1 subunit delta OS=Hon	225.14	44	13
P07108|ACBP_HUMAN	Acyl-CoA-binding protein OS=Homo sapie	219.18	90	13
P17987|TCPA_HUMAN	T-complex protein 1 subunit alpha OS=Ho	213.66	48	13
P16401|H15_HUMAN	Histone H1.5 OS=Homo sapiens GN=HIST	211.69	52	13
P43487|RANG_HUMAN	Ran-specific GTPase-activating protein OS	205.19	75	13
Q92626|PXDN_HUMAN	Peroxidasin homolog OS=Homo sapiens G	198.67	21	13
P14174|MIF_HUMAN	Macrophage migration inhibitory factor OS	195.3	79	13
Q9BQG0|MBB1A_HUMAN	Myb-binding protein 1A OS=Homo sapiens	182.01	25	13
P09493|TPM1_HUMAN	Tropomyosin alpha-1 chain OS=Homo sap	324.63	87	12
P09651|ROA1_HUMAN	Heterogeneous nuclear ribonucleoprotein A	308.23	68	12
O14818|PSA7_HUMAN	Proteasome subunit alpha type-7 OS=Hom	266.6	79	12
P22392|NDKB_HUMAN	Nucleoside diphosphate kinase B OS=Hon	255.67	93	12
P80723|BASP1_HUMAN	Brain acid soluble protein 1 OS=Homo sap	243.12	71	12
Q99536|VAT1_HUMAN	Synaptic vesicle membrane protein VAT-1	237.69	51	12
P35998|PRS7_HUMAN	26S protease regulatory subunit 7 OS=Hon	223.13	43	12
P60900|PSA6_HUMAN	Proteasome subunit alpha type-6 OS=Hom	216.15	49	12
P49756|RBM25_HUMAN	RNA-binding protein 25 OS=Homo sapiens	214.61	31	12
P00491|PNPH_HUMAN	Purine nucleoside phosphorylase OS=Hon	207.86	60	12
P46777|RL5_HUMAN	60S ribosomal protein L5 OS=Homo sapie	206.63	56	12
P62888|RL30_HUMAN	60S ribosomal protein L30 OS=Homo sapi	201.88	86	12
O00299|CLIC1_HUMAN	Chloride intracellular channel protein 1 OS	201.7	56	12
P62263|RS14_HUMAN	40S ribosomal protein S14 OS=Homo sapi	201.49	42	12
Q00341|VIGLN_HUMAN	Vigilin OS=Homo sapiens GN=HDLBP PE	201.21	37	12
Q8N163|K1967_HUMAN	Protein KIAA1967 OS=Homo sapiens GN=	199.82	28	12
P49773|HINT1_HUMAN	Histidine triad nucleotide-binding protein 1	198.96	87	12
P53621|COPA_HUMAN	Coatomer subunit alpha OS=Homo sapien	197.87	23	12
Q01518|CAP1_HUMAN	Adenylyl cyclase-associated protein 1 OS=	193.62	42	12
Q15233|NONO_HUMAN	Non-POU domain-containing octamer-bind	192.37	35	12
Q9Y224|CN166_HUMAN	UPF0568 protein C14orf166 OS=Homo sa	191.72	52	12
P00505|AATM_HUMAN	Aspartate aminotransferase, mitochondrial	189.9	44	12
P26641|EF1G_HUMAN	Elongation factor 1-gamma OS=Homo sap	186.2	23	12
P23142|FBLN1_HUMAN	Fibulin-1 OS=Homo sapiens GN=FBLN1 P	164.33	26	12
P46781|RS9_HUMAN	40S ribosomal protein S9 OS=Homo sapie	156.63	41	12
P54577|SYYC_HUMAN	Tyrosyl-tRNA synthetase, cytoplasmic OS=	156.42	41	12
P00441|SODC_HUMAN	Superoxide dismutase [Cu-Zn] OS=Homo	248.33	75	11
Q01105|SET_HUMAN	Protein SET OS=Homo sapiens GN=SET	245.06	41	11
Q9UHB9|SRP68_HUMAN	Signal recognition particle 68 kDa protein C	241.29	45	11
P20618|PSB1_HUMAN	Proteasome subunit beta type-1 OS=Hom	227.06	60	11
P53999|TCP4_HUMAN	Activated RNA polymerase II transcriptiona	226.58	76	11
Q9UBC3|DNM3B_HUMAN	DNA (cytosine-5)-methyltransferase 3B OS	225.72	35	11
O75531|BAF_HUMAN	Barrier-to-autointegration factor OS=Homo	224.18	78	11
P16949|STMN1_HUMAN	Stathmin OS=Homo sapiens GN=STMN1	221.6	56	11

O60506|HNRPQ_HUMAN	Heterogeneous nuclear ribonucleoprotein (	221.25	53	11
P63313|TYB10_HUMAN	Thymosin beta-10 OS=Homo sapiens GN=	220.92	84	11
Q14697|GANAB_HUMAN	Neutral alpha-glucosidase AB OS=Homo s	220.41	30	11
Q16555|DPYL2_HUMAN	Dihydropyrimidinase-related protein 2 OS=	208.62	48	11
P14868|SYDC_HUMAN	Aspartyl-tRNA synthetase, cytoplasmic OS	208.43	39	11
P14866|HNRPL_HUMAN	Heterogeneous nuclear ribonucleoprotein I	198.09	40	11
P17096|HMGA1_HUMAN	High mobility group protein HMG-I/HMG-Y	196.9	82	11
P08708|RS17_HUMAN	40S ribosomal protein S17 OS=Homo sapi	195.24	73	11
P38646|GRP75_HUMAN	Stress-70 protein, mitochondrial OS=Homo	193.13	37	11
P41091|IF2G_HUMAN	Eukaryotic translation initiation factor 2 sub	191.66	50	11
P23284|PPIB_HUMAN	Peptidyl-prolyl cis-trans isomerase B OS=H	189.48	45	11
P60866|RS20_HUMAN	40S ribosomal protein S20 OS=Homo sapi	188.77	50	11
Q7KZF4|SND1_HUMAN	Staphylococcal nuclease domain-containin	187.48	28	11
Q02790|FKBP4_HUMAN	Peptidyl-prolyl cis-trans isomerase FKBP4	186.94	35	11
P46783|RS10_HUMAN	40S ribosomal protein S10 OS=Homo sapi	186.53	58	11
P13693|TCTP_HUMAN	Translationally-controlled tumor protein OS	182.69	74	11
P62829|RL23_HUMAN	60S ribosomal protein L23 OS=Homo sapi	182.08	60	11
Q14019|COTL1_HUMAN	Coactosin-like protein OS=Homo sapiens (	178.96	65	11
P62280|RS11_HUMAN	40S ribosomal protein S11 OS=Homo sapi	171.23	73	11
A0MZ66|SHOT1_HUMAN	Shootin-1 OS=Homo sapiens GN=KIAA15	168.93	37	11
P02545|LMNA_HUMAN	Prelamin-A/C OS=Homo sapiens GN=LMN	154.33	22	11
P13797|PLST_HUMAN	Plastin-3 OS=Homo sapiens GN=PLS3 PE	241.79	51	10
A6NL28|TPM3L_HUMAN	Putative tropomyosin alpha-3 chain-like pr	237.92	47	10
P61158|ARP3_HUMAN	Actin-related protein 3 OS=Homo sapiens	213.13	49	10
P42166|LAP2A_HUMAN	Lamina-associated polypeptide 2, isoform	211.37	35	10
Q04760|LGUL_HUMAN	Lactoylglutathione lyase OS=Homo sapien	209.72	63	10
P19367|HXK1_HUMAN	Hexokinase-1 OS=Homo sapiens GN=HK1	208.28	28	10
Q9Y262|EIF3L_HUMAN	Eukaryotic translation initiation factor 3 sub	206.56	35	10
O00429|DNM1L_HUMAN	Dynamin-1-like protein OS=Homo sapiens	206.48	49	10
P60981|DEST_HUMAN	Destrin OS=Homo sapiens GN=DSTN PE=	205.47	47	10
Q9NR30|DDX21_HUMAN	Nucleolar RNA helicase 2 OS=Homo sapie	204.61	33	10
P51991|ROA3_HUMAN	Heterogeneous nuclear ribonucleoprotein A	203.9	43	10
O95336|6PGL_HUMAN	6-phosphogluconolactonase OS=Homo sa	202.04	59	10
P04792|HSPB1_HUMAN	Heat shock protein beta-1 OS=Homo sapie	199.56	66	10
Q9UHV9|PFD2_HUMAN	Prefoldin subunit 2 OS=Homo sapiens GN	196.4	82	10
P07093|GDN_HUMAN	Glia-derived nexin OS=Homo sapiens GN=	195.88	49	10
P56192|SYMC_HUMAN	Methionyl-tRNA synthetase, cytoplasmic O	195.28	26	10
Q15843|NEDD8_HUMAN	NEDD8 OS=Homo sapiens GN=NEDD8 P	192.98	59	10
P35613|BASI_HUMAN	Basigin OS=Homo sapiens GN=BSG PE=	191.53	32	10
Q9BXJ9|NAA15_HUMAN	N-alpha-acetyltransferase 15, NatA auxilia	188.31	32	10
P12429|ANXA3_HUMAN	Annexin A3 OS=Homo sapiens GN=ANXA	187.54	46	10
Q08J23|NSUN2_HUMAN	tRNA (cytosine(34)-C(5))-methyltransferas	184.54	34	10
Q8NBS9|TXND5_HUMAN	Thioredoxin domain-containing protein 5 O	180.98	36	10
P31942|HNRH3_HUMAN	Heterogeneous nuclear ribonucleoprotein H	179.33	39	10
P54819|KAD2_HUMAN	Adenylate kinase 2, mitochondrial OS=Hor	177.28	66	10
Q9BT78|CSN4_HUMAN	COP9 signalosome complex subunit 4 OS=	174.7	46	10
O60701|UGDH_HUMAN	UDP-glucose 6-dehydrogenase OS=Homo	173.53	29	10

Q7Z478|DHX29_HUMAN	ATP-dependent RNA helicase DHX29 OS=	168.63	23	10
Q9Y624|JAM1_HUMAN	Junctional adhesion molecule A OS=Homo	160.72	31	10
P07339|CATD_HUMAN	Cathepsin D OS=Homo sapiens GN=CTSD	160.67	35	10
P27635|RL10_HUMAN	60S ribosomal protein L10 OS=Homo sapi	159.37	35	10
O14776|TCRG1_HUMAN	Transcription elongation regulator 1 OS=H	158.41	21	10
P49591|SYSC_HUMAN	Seryl-tRNA synthetase, cytoplasmic OS=H	148.36	36	10
P06753|TPM3_HUMAN	Tropomyosin alpha-3 chain OS=Homo sap	328.7	86	9
P31946|1433B_HUMAN	14-3-3 protein beta/alpha OS=Homo sapie	231.54	59	9
P35241|RADI_HUMAN	Radixin OS=Homo sapiens GN=RDX PE=	226.95	57	9
Q06323|PSME1_HUMAN	Proteasome activator complex subunit 1 O	224.08	59	9
P12277|KCRB_HUMAN	Creatine kinase B-type OS=Homo sapiens	215.57	64	9
P60660|MYL6_HUMAN	Myosin light polypeptide 6 OS=Homo sapie	213.37	76	9
Q99729|ROAA_HUMAN	Heterogeneous nuclear ribonucleoprotein A	203.41	42	9
Q15365|PCBP1_HUMAN	Poly(rC)-binding protein 1 OS=Homo sapie	201.77	59	9
Q9Y3I0|RTCB_HUMAN	tRNA-splicing ligase RtcB homolog OS=Ho	198.78	42	9
P30084|ECHM_HUMAN	Enoyl-CoA hydratase, mitochondrial OS=H	197.31	47	9
O76003|GLRX3_HUMAN	Glutaredoxin-3 OS=Homo sapiens GN=GL	193.53	54	9
P14550|AK1A1_HUMAN	Alcohol dehydrogenase [NADP+] OS=Hom	189.89	51	9
Q07955|SRSF1_HUMAN	Serine/arginine-rich splicing factor 1 OS=H	188.29	62	9
P61289|PSME3_HUMAN	Proteasome activator complex subunit 3 O	187.73	48	9
Q9UL46|PSME2_HUMAN	Proteasome activator complex subunit 2 O	187.62	53	9
Q13618|CUL3_HUMAN	Cullin-3 OS=Homo sapiens GN=CUL3 PE=	186.78	47	9
Q14195|DPYL3_HUMAN	Dihydropyrimidinase-related protein 3 OS=	183	30	9
Q15417|CNN3_HUMAN	Calponin-3 OS=Homo sapiens GN=CNN3	182.31	31	9
P30040|ERP29_HUMAN	Endoplasmic reticulum resident protein 29	182.2	42	9
O14737|PDCD5_HUMAN	Programmed cell death protein 5 OS=Hom	181.55	56	9
P15880|RS2_HUMAN	40S ribosomal protein S2 OS=Homo sapie	178.29	36	9
P29966|MARCS_HUMAN	Myristoylated alanine-rich C-kinase substra	175.91	34	9
Q9Y230|RUVB2_HUMAN	RuvB-like 2 OS=Homo sapiens GN=RUVB	175.67	39	9
Q9BZZ5|API5_HUMAN	Apoptosis inhibitor 5 OS=Homo sapiens G	175.1	36	9
P34897|GLYM_HUMAN	Serine hydroxymethyltransferase, mitocho	172.74	26	9
P62249|RS16_HUMAN	40S ribosomal protein S16 OS=Homo sapi	172.1	45	9
Q9NTJ3|SMC4_HUMAN	Structural maintenance of chromosomes p	171.69	19	9
P25786|PSA1_HUMAN	Proteasome subunit alpha type-1 OS=Hom	169.93	46	9
O76094|SRP72_HUMAN	Signal recognition particle 72 kDa protein	168.49	35	9
O60502|NCOAT_HUMAN	Bifunctional protein NCOAT OS=Homo sap	166.84	25	9
Q8N8S7|ENAH_HUMAN	Protein enabled homolog OS=Homo sapie	164.96	31	9
Q9Y5X3|SNX5_HUMAN	Sorting nexin-5 OS=Homo sapiens GN=SN	163.57	34	9
P62750|RL23A_HUMAN	60S ribosomal protein L23a OS=Homo sap	156.73	54	9
Q9NY33|DPP3_HUMAN	Dipeptidyl peptidase 3 OS=Homo sapiens	154.57	24	9
P49915|GUAA_HUMAN	GMP synthase [glutamine-hydrolyzing] OS	151.81	18	9
P61088|UBE2N_HUMAN	Ubiquitin-conjugating enzyme E2 N OS=Ho	149.84	61	9
P50453|SPB9_HUMAN	Serpin B9 OS=Homo sapiens GN=SERPIN	139.99	36	9
P78347|GTF2I_HUMAN	General transcription factor II-I OS=Homo	117.84	21	9
P06454|PTMA_HUMAN	Prothymosin alpha OS=Homo sapiens GN	202.36	44	8
P09429|HMGB1_HUMAN	High mobility group protein B1 OS=Homo s	197.6	53	8
P68036|UB2L3_HUMAN	Ubiquitin-conjugating enzyme E2 L3 OS=H	195.56	73	8

Q99439|CNN2_HUMAN	Calponin-2 OS=Homo sapiens GN=CNN2	194.23	38	8
P51665|PSD7_HUMAN	26S proteasome non-ATPase regulatory s	190.42	48	8
P62191|PRS4_HUMAN	26S protease regulatory subunit 4 OS=Ho	185.03	43	8
P49736|MCM2_HUMAN	DNA replication licensing factor MCM2 OS	180.21	25	8
P06737|PYGL_HUMAN	Glycogen phosphorylase, liver form OS=H	179.54	27	8
P07741|APT_HUMAN	Adenine phosphoribosyltransferase OS=H	179.19	68	8
P63173|RL38_HUMAN	60S ribosomal protein L38 OS=Homo sapi	178.86	57	8
Q13126|MTAP_HUMAN	S-methyl-5'-thioadenosine phosphorylase	178.21	35	8
P22061|PIMT_HUMAN	Protein-L-isoaspartate(D-aspartate) O-met	178.09	63	8
Q9Y696|CLIC4_HUMAN	Chloride intracellular channel protein 4 OS	177.26	66	8
O00244|ATOX1_HUMAN	Copper transport protein ATOX1 OS=Hom	174.55	76	8
P27797|CALR_HUMAN	Calreticulin OS=Homo sapiens GN=CALR	172.97	46	8
P50552|VASP_HUMAN	Vasodilator-stimulated phosphoprotein OS	172.41	42	8
P62244|RS15A_HUMAN	40S ribosomal protein S15a OS=Homo sa	172.26	72	8
P23381|SYWC_HUMAN	Tryptophanyl-tRNA synthetase, cytoplasmi	172.23	46	8
Q15019|SEPT2_HUMAN	Septin-2 OS=Homo sapiens GN=SEPT2 P	169.9	46	8
P17844|DDX5_HUMAN	Probable ATP-dependent RNA helicase D	168.46	35	8
Q9Y266|NUDC_HUMAN	Nuclear migration protein nudC OS=Homo	167.43	45	8
Q13561|DCTN2_HUMAN	Dynactin subunit 2 OS=Homo sapiens GN	166.59	32	8
Q7L2H7|EIF3M_HUMAN	Eukaryotic translation initiation factor 3 sub	164.07	41	8
P62913|RL11_HUMAN	60S ribosomal protein L11 OS=Homo sapi	163.63	44	8
Q9UKK9|NUDT5_HUMAN	ADP-sugar pyrophosphatase OS=Homo sa	163.22	30	8
P62633|CNBP_HUMAN	Cellular nucleic acid-binding protein OS=H	161.71	31	8
Q9Y6G9|DC1L1_HUMAN	Cytoplasmic dynein 1 light intermediate cha	161.68	36	8
Q9UKM9|RALY_HUMAN	RNA-binding protein Raly OS=Homo sapie	160.61	32	8
P60903|S10AA_HUMAN	Protein S100-A10 OS=Homo sapiens GN=	160.34	58	8
P62241|RS8_HUMAN	40S ribosomal protein S8 OS=Homo sapie	159	51	8
Q9H910|HN1L_HUMAN	Hematological and neurological expressed	158.93	60	8
O15347|HMGB3_HUMAN	High mobility group protein B3 OS=Homo s	158.66	51	8
P48444|COPD_HUMAN	Coatomer subunit delta OS=Homo sapiens	156.83	22	8
P23921|RIR1_HUMAN	Ribonucleoside-diphosphate reductase lar	155.77	27	8
P35268|RL22_HUMAN	60S ribosomal protein L22 OS=Homo sapi	155.7	51	8
Q96AE4|FUBP1_HUMAN	Far upstream element-binding protein 1 OS	155.34	35	8
P18621|RL17_HUMAN	60S ribosomal protein L17 OS=Homo sapi	155.25	44	8
P31153|METK2_HUMAN	S-adenosylmethionine synthase isoform ty	155.08	22	8
P39023|RL3_HUMAN	60S ribosomal protein L3 OS=Homo sapie	155	37	8
Q99471|PFD5_HUMAN	Prefoldin subunit 5 OS=Homo sapiens GN	152.78	68	8
Q99459|CDC5L_HUMAN	Cell division cycle 5-like protein OS=Homo	152.12	30	8
O15372|EIF3H_HUMAN	Eukaryotic translation initiation factor 3 sub	149.94	36	8
P13667|PDIA4_HUMAN	Protein disulfide-isomerase A4 OS=Homo	148.57	22	8
Q9P258|RCC2_HUMAN	Protein RCC2 OS=Homo sapiens GN=RC	147.38	34	8
P60228|EIF3E_HUMAN	Eukaryotic translation initiation factor 3 sub	147.21	25	8
Q9GZZ1|NAA50_HUMAN	N-alpha-acetyltransferase 50, NatE catalyt	145.55	53	8
P02751|FINC_HUMAN	Fibronectin OS=Homo sapiens GN=FN1 P	139.94	9	8
P62851|RS25_HUMAN	40S ribosomal protein S25 OS=Homo sapi	139.67	50	8
Q14683|SMC1A_HUMAN	Structural maintenance of chromosomes p	137.71	16	8
P14678|RSMB_HUMAN	Small nuclear ribonucleoprotein-associated	137.1	55	8

P78344|IF4G2_HUMAN	Eukaryotic translation initiation factor 4 gar	136.91	19	8
Q09666|AHNK_HUMAN	Neuroblast differentiation-associated prote	136.7	9	8
Q6PKG0|LARP1_HUMAN	La-related protein 1 OS=Homo sapiens GN	136.3	26	8
P53634|CATC_HUMAN	Dipeptidyl peptidase 1 OS=Homo sapiens	136.19	24	8
P56385|ATP5I_HUMAN	ATP synthase subunit e, mitochondrial OS	133.41	71	8
P62899|RL31_HUMAN	60S ribosomal protein L31 OS=Homo sapi	132.46	43	8
O43491|E41L2_HUMAN	Band 4.1-like protein 2 OS=Homo sapiens	130.34	24	8
Q15907|RB11B_HUMAN	Ras-related protein Rab-11B OS=Homo sa	127.85	39	8
P23193|TCEA1_HUMAN	Transcription elongation factor A protein 1	125.98	42	8
P27144|KAD4_HUMAN	Adenylate kinase isoenzyme 4, mitochondr	122.02	51	8
Q6FI13|H2A2A_HUMAN	Histone H2A type 2-A OS=Homo sapiens (	272.39	84	7
Q16777|H2A2C_HUMAN	Histone H2A type 2-C OS=Homo sapiens (	272.39	77	7
P15531|NDKA_HUMAN	Nucleoside diphosphate kinase A OS=Hon	243.59	73	7
O00571|DDX3X_HUMAN	ATP-dependent RNA helicase DDX3X OS=	209.3	54	7
P25787|PSA2_HUMAN	Proteasome subunit alpha type-2 OS=Hom	208.64	56	7
P28066|PSA5_HUMAN	Proteasome subunit alpha type-5 OS=Hom	207.79	55	7
P20290|BTF3_HUMAN	Transcription factor BTF3 OS=Homo sapie	190.87	67	7
Q92598|HS105_HUMAN	Heat shock protein 105 kDa OS=Homo sa	187.69	29	7
Q16181|SEPT7_HUMAN	Septin-7 OS=Homo sapiens GN=SEPT7 P	185.01	46	7
P06493|CDK1_HUMAN	Cyclin-dependent kinase 1 OS=Homo sapi	184.69	40	7
P50502|F10A1_HUMAN	Hsc70-interacting protein OS=Homo sapie	181.9	27	7
P26196|DDX6_HUMAN	Probable ATP-dependent RNA helicase DI	180.68	37	7
O43809|CPSF5_HUMAN	Cleavage and polyadenylation specificity fa	180.06	60	7
Q15185|TEBP_HUMAN	Prostaglandin E synthase 3 OS=Homo sap	179.35	54	7
P54578|UBP14_HUMAN	Ubiquitin carboxyl-terminal hydrolase 14 O	178.35	40	7
Q13765|NACA_HUMAN	Nascent polypeptide-associated complex s	177.65	30	7
P32969|RL9_HUMAN	60S ribosomal protein L9 OS=Homo sapie	175.75	52	7
Q92945|FUBP2_HUMAN	Far upstream element-binding protein 2 OS	175.63	24	7
Q99460|PSMD1_HUMAN	26S proteasome non-ATPase regulatory su	175.02	27	7
O75368|SH3L1_HUMAN	SH3 domain-binding glutamic acid-rich-like	171.67	71	7
P11216|PYGB_HUMAN	Glycogen phosphorylase, brain form OS=H	170.16	17	7
Q15046|SYK_HUMAN	Lysyl-tRNA synthetase OS=Homo sapiens	169.41	26	7
Q96P16|RPR1A_HUMAN	Regulation of nuclear pre-mRNA domain-c	168.28	47	7
Q9NP97|DLRB1_HUMAN	Dynein light chain roadblock-type 1 OS=Ho	167.74	90	7
Q04837|SSBP_HUMAN	Single-stranded DNA-binding protein, mito	166.94	62	7
P49903|SPS1_HUMAN	Selenide, water dikinase 1 OS=Homo sapi	165.04	39	7
P49588|SYAC_HUMAN	Alanyl-tRNA synthetase, cytoplasmic OS=H	163.95	25	7
P33992|MCM5_HUMAN	DNA replication licensing factor MCM5 OS	162.73	28	7
Q16543|CDC37_HUMAN	Hsp90 co-chaperone Cdc37 OS=Homo sa	160.96	32	7
P61758|PFD3_HUMAN	Prefoldin subunit 3 OS=Homo sapiens GN	160.86	64	7
O43399|TPD54_HUMAN	Tumor protein D54 OS=Homo sapiens GN	160.49	41	7
P30520|PURA2_HUMAN	Adenylosuccinate synthetase isozyme 2 O	160.19	26	7
P62753|RS6_HUMAN	40S ribosomal protein S6 OS=Homo sapie	159.71	37	7
Q00688|FKBP3_HUMAN	Peptidyl-prolyl cis-trans isomerase FKBP3	158.13	44	7
Q9Y295|DRG1_HUMAN	Developmentally-regulated GTP-binding pr	157.98	37	7
Q08752|PPID_HUMAN	Peptidyl-prolyl cis-trans isomerase D OS=H	156.48	37	7
Q9UK76|HN1_HUMAN	Hematological and neurological expressed	155.3	54	7

O95347|SMC2_HUMAN	Structural maintenance of chromosomes p	154.66	21	7
P63279|UBC9_HUMAN	SUMO-conjugating enzyme UBC9 OS=Ho	154.41	28	7
P36405|ARL3_HUMAN	ADP-ribosylation factor-like protein 3 OS=H	153.13	62	7
P05198|IF2A_HUMAN	Eukaryotic translation initiation factor 2 sub	152.12	33	7
P61586|RHOA_HUMAN	Transforming protein RhoA OS=Homo sap	151.4	50	7
Q07065|CKAP4_HUMAN	Cytoskeleton-associated protein 4 OS=Ho	151.13	24	7
Q9Y3F4|STRAP_HUMAN	Serine-threonine kinase receptor-associate	150.82	44	7
Q15121|PEA15_HUMAN	Astrocytic phosphoprotein PEA-15 OS=Ho	149.34	71	7
Q9C005|DPY30_HUMAN	Protein dpy-30 homolog OS=Homo sapien	148.58	57	7
O00273|DFFA_HUMAN	DNA fragmentation factor subunit alpha OS	148.43	47	7
P62760|VISL1_HUMAN	Visinin-like protein 1 OS=Homo sapiens G	147.75	59	7
P37108|SRP14_HUMAN	Signal recognition particle 14 kDa protein (	147.44	44	7
Q9HC38|GLOD4_HUMAN	Glyoxalase domain-containing protein 4 OS	147.33	39	7
P12081|SYHC_HUMAN	Histidyl-tRNA synthetase, cytoplasmic OS=	147.27	28	7
P54727|RD23B_HUMAN	UV excision repair protein RAD23 homolog	144.2	22	7
Q15717|ELAV1_HUMAN	ELAV-like protein 1 OS=Homo sapiens GN	143.63	32	7
P04843|RPN1_HUMAN	Dolichyl-diphosphooligosaccharide--protein	142.15	20	7
Q15404|RSU1_HUMAN	Ras suppressor protein 1 OS=Homo sapie	141.75	34	7
Q14204|DYHC1_HUMAN	Cytoplasmic dynein 1 heavy chain 1 OS=H	141.6	13	7
P46926|GNPI1_HUMAN	Glucosamine-6-phosphate isomerase 1 OS	141.14	40	7
P06132|DCUP_HUMAN	Uroporphyrinogen decarboxylase OS=Hom	140.74	45	7
P62857|RS28_HUMAN	40S ribosomal protein S28 OS=Homo sapi	140.12	86	7
Q14980|NUMA1_HUMAN	Nuclear mitotic apparatus protein 1 OS=Ho	139.98	17	7
P52701|MSH6_HUMAN	DNA mismatch repair protein Msh6 OS=Ho	137.38	14	7
P50914|RL14_HUMAN	60S ribosomal protein L14 OS=Homo sapi	135.86	33	7
Q9H0D6|XRN2_HUMAN	5'-3' exoribonuclease 2 OS=Homo sapiens	133.65	20	7
P09661|RU2A_HUMAN	U2 small nuclear ribonucleoprotein A' OS=	132.84	37	7
P23588|IF4B_HUMAN	Eukaryotic translation initiation factor 4B O	132.64	15	7
P48556|PSMD8_HUMAN	26S proteasome non-ATPase regulatory su	129.93	32	7
P35249|RFC4_HUMAN	Replication factor C subunit 4 OS=Homo s	127.73	31	7
P14314|GLU2B_HUMAN	Glucosidase 2 subunit beta OS=Homo sap	127.34	19	7
P15927|RFA2_HUMAN	Replication protein A 32 kDa subunit OS=H	126.98	33	7
P08243|ASNS_HUMAN	Asparagine synthetase [glutamine-hydrolyz	125.23	17	7
Q9UHD8|SEPT9_HUMAN	Septin-9 OS=Homo sapiens GN=SEPT9 P	124.38	26	7
P61254|RL26_HUMAN	60S ribosomal protein L26 OS=Homo sapi	123.1	39	7
Q5T0N5|FBP1L_HUMAN	Formin-binding protein 1-like OS=Homo sa	123.01	19	7
P62312|LSM6_HUMAN	U6 snRNA-associated Sm-like protein LSm	119.5	91	7
Q15370|ELOB_HUMAN	Transcription elongation factor B polypepti	117.43	37	7
P48061|SDF1_HUMAN	Stromal cell-derived factor 1 OS=Homo sa	116.68	44	7
P61353|RL27_HUMAN	60S ribosomal protein L27 OS=Homo sapi	114.35	61	7
P50570|DYN2_HUMAN	Dynamin-2 OS=Homo sapiens GN=DNM2	114.2	17	7
P18077|RL35A_HUMAN	60S ribosomal protein L35a OS=Homo sap	98.79	30	7
P40222|TXLNA_HUMAN	Alpha-taxilin OS=Homo sapiens GN=TXLN	84.34	21	7
Q9BUF5|TBB6_HUMAN	Tubulin beta-6 chain OS=Homo sapiens G	262.48	62	6
P55209|NP1L1_HUMAN	Nucleosome assembly protein 1-like 1 OS=	199.97	34	6
P61204|ARF3_HUMAN	ADP-ribosylation factor 3 OS=Homo sapie	196.38	77	6
P84077|ARF1_HUMAN	ADP-ribosylation factor 1 OS=Homo sapie	196.38	72	6

Q92841|DDX17_HUMAN	Probable ATP-dependent RNA helicase DI	192.35	29	6
P06576|ATPB_HUMAN	ATP synthase subunit beta, mitochondrial	190.16	37	6
P67809|YBOX1_HUMAN	Nuclease-sensitive element-binding protein	190.09	44	6
O00487|PSDE_HUMAN	26S proteasome non-ATPase regulatory su	181.88	54	6
Q9Y5J9|TIM8B_HUMAN	Mitochondrial import inner membrane trans	180.61	65	6
P30566|PUR8_HUMAN	Adenylosuccinate lyase OS=Homo sapiens	180.24	47	6
O00425|IF2B3_HUMAN	Insulin-like growth factor 2 mRNA-binding p	177.95	36	6
P30046|DOPD_HUMAN	D-dopachrome decarboxylase OS=Homo s	177.9	67	6
P60983|GMFB_HUMAN	Glia maturation factor beta OS=Homo sapi	174.53	58	6
Q9Y333|LSM2_HUMAN	U6 snRNA-associated Sm-like protein LSm	174.34	81	6
P49720|PSB3_HUMAN	Proteasome subunit beta type-3 OS=Homo	172.88	57	6
P30050|RL12_HUMAN	60S ribosomal protein L12 OS=Homo sapi	169.81	59	6
P14324|FPPS_HUMAN	Farnesyl pyrophosphate synthase OS=Hor	169.63	31	6
P35520|CBS_HUMAN	Cystathionine beta-synthase OS=Homo sa	167.32	37	6
P33176|KINH_HUMAN	Kinesin-1 heavy chain OS=Homo sapiens	166.59	17	6
Q12905|ILF2_HUMAN	Interleukin enhancer-binding factor 2 OS=H	166.12	24	6
P62318|SMD3_HUMAN	Small nuclear ribonucleoprotein Sm D3 OS	162.13	67	6
Q15056|IF4H_HUMAN	Eukaryotic translation initiation factor 4H O	159.32	50	6
O95372|LYPA2_HUMAN	Acyl-protein thioesterase 2 OS=Homo sapi	154.42	51	6
O00303|EIF3F_HUMAN	Eukaryotic translation initiation factor 3 sub	153.11	48	6
Q8WVM8|SCFD1_HUMAN	Sec1 family domain-containing protein 1 O	152.53	24	6
O14979|HNRDL_HUMAN	Heterogeneous nuclear ribonucleoprotein D	152.45	23	6
O95816|BAG2_HUMAN	BAG family molecular chaperone regulator	152.41	30	6
Q71UI9|H2AV_HUMAN	Histone H2A.V OS=Homo sapiens GN=H2	151.34	31	6
P0C0S5|H2AZ_HUMAN	Histone H2A.Z OS=Homo sapiens GN=H2	151.34	31	6
P31350|RIR2_HUMAN	Ribonucleoside-diphosphate reductase sul	150.92	25	6
P45974|UBP5_HUMAN	Ubiquitin carboxyl-terminal hydrolase 5 OS	150.74	25	6
P55265|DSRAD_HUMAN	Double-stranded RNA-specific adenosine d	150.64	19	6
P05388|RLA0_HUMAN	60S acidic ribosomal protein P0 OS=Homo	150.45	36	6
P55769|NH2L1_HUMAN	NHP2-like protein 1 OS=Homo sapiens GN	150.36	55	6
O60264|SMCA5_HUMAN	SWI/SNF-related matrix-associated actin-d	148.81	17	6
P20700|LMNB1_HUMAN	Lamin-B1 OS=Homo sapiens GN=LMNB1	148.41	28	6
Q5T7N2|LITD1_HUMAN	LINE-1 type transposase domain-containin	147.44	19	6
O15212|PFD6_HUMAN	Prefoldin subunit 6 OS=Homo sapiens GN	146.76	75	6
Q96AG4|LRC59_HUMAN	Leucine-rich repeat-containing protein 59 O	146	42	6
O75223|GGCT_HUMAN	Gamma-glutamylcyclotransferase OS=Hor	144.87	36	6
O15067|PUR4_HUMAN	Phosphoribosylformylglycinamidine syntha	144.82	25	6
P22413|ENPP1_HUMAN	Ectonucleotide pyrophosphatase/phospho	140.99	18	6
P47756|CAPZB_HUMAN	F-actin-capping protein subunit beta OS=H	139.26	33	6
Q13283|G3BP1_HUMAN	Ras GTPase-activating protein-binding pro	138.61	22	6
P49411|EFTU_HUMAN	Elongation factor Tu, mitochondrial OS=Ho	138.54	28	6
Q13616|CUL1_HUMAN	Cullin-1 OS=Homo sapiens GN=CUL1 PE=	137.46	27	6
P62841|RS15_HUMAN	40S ribosomal protein S15 OS=Homo sapi	136.41	57	6
O43143|DHX15_HUMAN	Putative pre-mRNA-splicing factor ATP-de	136.26	22	6
Q9NZL4|HPBP1_HUMAN	Hsp70-binding protein 1 OS=Homo sapien	136.07	29	6
Q8N474|SFRP1_HUMAN	Secreted frizzled-related protein 1 OS=Hor	135.61	26	6
P84090|ERH_HUMAN	Enhancer of rudimentary homolog OS=Hor	135.37	38	6

O15145|ARPC3_HUMAN	Actin-related protein 2/3 complex subunit 3	132.65	38	6
Q8N0X7|SPG20_HUMAN	Spartin OS=Homo sapiens GN=SPG20 PE	130.8	22	6
Q86V81|THOC4_HUMAN	THO complex subunit 4 OS=Homo sapiens	130.58	44	6
P59998|ARPC4_HUMAN	Actin-related protein 2/3 complex subunit 4	128.79	55	6
O14974|MYPT1_HUMAN	Protein phosphatase 1 regulatory subunit 1	128.79	21	6
P26373|RL13_HUMAN	60S ribosomal protein L13 OS=Homo sapi	128.59	32	6
P51659|DHB4_HUMAN	Peroxisomal multifunctional enzyme type 2	128.3	24	6
Q8IVW6|ARI3B_HUMAN	AT-rich interactive domain-containing prote	127.95	32	6
O75489|NDUS3_HUMAN	NADH dehydrogenase [ubiquinone] iron-su	127.71	26	6
Q13085|ACACA_HUMAN	Acetyl-CoA carboxylase 1 OS=Homo sapie	127.4	13	6
P30153|2AAA_HUMAN	Serine/threonine-protein phosphatase 2A 6	127.29	24	6
Q8IZQ5|SELH_HUMAN	Selenoprotein H OS=Homo sapiens GN=S	127.24	39	6
P48047|ATPO_HUMAN	ATP synthase subunit O, mitochondrial OS	127.13	41	6
P25788|PSA3_HUMAN	Proteasome subunit alpha type-3 OS=Hom	126.49	25	6
O75947|ATP5H_HUMAN	ATP synthase subunit d, mitochondrial OS	125.19	45	6
Q15369|ELOC_HUMAN	Transcription elongation factor B polypepti	123.91	41	6
Q9UKV3|ACINU_HUMAN	Apoptotic chromatin condensation inducer	121.49	12	6
Q9UBE0|SAE1_HUMAN	SUMO-activating enzyme subunit 1 OS=H	120.57	32	6
Q16891|IMMT_HUMAN	Mitochondrial inner membrane protein OS=	120.48	12	6
Q9Y2X3|NOP58_HUMAN	Nucleolar protein 58 OS=Homo sapiens G	114.23	25	6
P15121|ALDR_HUMAN	Aldose reductase OS=Homo sapiens GN=	112.92	39	6
P55145|MANF_HUMAN	Mesencephalic astrocyte-derived neurotrop	112.85	47	6
P06730|IF4E_HUMAN	Eukaryotic translation initiation factor 4E O	110.98	28	6
P62273|RS29_HUMAN	40S ribosomal protein S29 OS=Homo sapi	109.59	52	6
P61081|UBC12_HUMAN	NEDD8-conjugating enzyme Ubc12 OS=H	109.41	37	6
P99999|CYC_HUMAN	Cytochrome c OS=Homo sapiens GN=CY	101.03	28	6
P28340|DPOD1_HUMAN	DNA polymerase delta catalytic subunit OS	99.12	12	6
P09669|COX6C_HUMAN	Cytochrome c oxidase subunit 6C OS=Hor	88.88	49	6
Q93077|H2A1C_HUMAN	Histone H2A type 1-C OS=Homo sapiens	262.76	75	5
P31947|1433S_HUMAN	14-3-3 protein sigma OS=Homo sapiens G	189.81	56	5
Q15366|PCBP2_HUMAN	Poly(rC)-binding protein 2 OS=Homo sapie	177.41	42	5
Q8N1G4|LRC47_HUMAN	Leucine-rich repeat-containing protein 47	172.96	34	5
Q9P289|MST4_HUMAN	Serine/threonine-protein kinase MST4 OS=	163.93	32	5
Q9P1F3|CF115_HUMAN	Costars family protein C6orf115 OS=Homo	163.39	80	5
Q9UBQ7|GRHPR_HUMAN	Glyoxylate reductase/hydroxypyruvate redu	158.58	28	5
Q13151|ROA0_HUMAN	Heterogeneous nuclear ribonucleoprotein A	158.36	38	5
P11388|TOP2A_HUMAN	DNA topoisomerase 2-alpha OS=Homo sa	157.26	18	5
Q13907|IDI1_HUMAN	Isopentenyl-diphosphate Delta-isomerase	156.78	45	5
P11279|LAMP1_HUMAN	Lysosome-associated membrane glycoprot	156.01	37	5
P20962|PTMS_HUMAN	Parathymosin OS=Homo sapiens GN=PTM	155.16	24	5
P24534|EF1B_HUMAN	Elongation factor 1-beta OS=Homo sapien	154.83	44	5
P26583|HMGB2_HUMAN	High mobility group protein B2 OS=Homo s	153.44	52	5
Q9Y2B0|CNPY2_HUMAN	Protein canopy homolog 2 OS=Homo sapi	152.97	58	5
Q16643|DREB_HUMAN	Drebrin OS=Homo sapiens GN=DBN1 PE=	152.54	21	5
Q99598|TSNAX_HUMAN	Translin-associated protein X OS=Homo s	149.52	36	5
Q07020|RL18_HUMAN	60S ribosomal protein L18 OS=Homo sapi	149.43	31	5
Q9NTK5|OLA1_HUMAN	Obg-like ATPase 1 OS=Homo sapiens GN	148.08	29	5

P52565|GDIR1_HUMAN	Rho GDP-dissociation inhibitor 1 OS=Hom	147.64	38	5
Q15942|ZYX_HUMAN	Zyxin OS=Homo sapiens GN=ZYX PE=1 S	147.47	17	5
P62314|SMD1_HUMAN	Small nuclear ribonucleoprotein Sm D1 OS	146.59	56	5
Q15181|IPYR_HUMAN	Inorganic pyrophosphatase OS=Homo sap	145.07	34	5
Q9UQ80|PA2G4_HUMAN	Proliferation-associated protein 2G4 OS=H	143.18	26	5
Q14166|TTL12_HUMAN	Tubulin--tyrosine ligase-like protein 12 OS=	142.77	22	5
P38159|HNRPG_HUMAN	Heterogeneous nuclear ribonucleoprotein (	142.73	40	5
P62993|GRB2_HUMAN	Growth factor receptor-bound protein 2 OS	142.24	33	5
Q4V328|GRAP1_HUMAN	GRIP1-associated protein 1 OS=Homo sap	142.03	20	5
O75475|PSIP1_HUMAN	PC4 and SFRS1-interacting protein OS=H	141.93	23	5
P05067|A4_HUMAN	Amyloid beta A4 protein OS=Homo sapien	140.83	19	5
Q9P2M7|CING_HUMAN	Cingulin OS=Homo sapiens GN=CGN PE=	140.29	18	5
Q9H9Q2|CSN7B_HUMAN	COP9 signalosome complex subunit 7b OS	139.8	37	5
P29762|RABP1_HUMAN	Cellular retinoic acid-binding protein 1 OS=	139.76	53	5
O60256|KPRB_HUMAN	Phosphoribosyl pyrophosphate synthase-a	139.74	30	5
P40121|CAPG_HUMAN	Macrophage-capping protein OS=Homo sa	139.14	25	5
Q99613|EIF3C_HUMAN	Eukaryotic translation initiation factor 3 sub	137.87	15	5
P47813|IF1AX_HUMAN	Eukaryotic translation initiation factor 1A, X	137.72	36	5
O14602|IF1AY_HUMAN	Eukaryotic translation initiation factor 1A, Y	137.72	36	5
P36871|PGM1_HUMAN	Phosphoglucomutase-1 OS=Homo sapien	137.46	20	5
O43776|SYNC_HUMAN	Asparaginyl-tRNA synthetase, cytoplasmic	136.71	16	5
P55327|TPD52_HUMAN	Tumor protein D52 OS=Homo sapiens GN	136.6	41	5
P62847|RS24_HUMAN	40S ribosomal protein S24 OS=Homo sapi	135.34	30	5
O60220|TIM8A_HUMAN	Mitochondrial import inner membrane trans	134.53	44	5
Q6IBS0|TWF2_HUMAN	Twinfilin-2 OS=Homo sapiens GN=TWF2 P	134.5	28	5
P54709|AT1B3_HUMAN	Sodium/potassium-transporting ATPase su	134.47	41	5
Q8N1F7|NUP93_HUMAN	Nuclear pore complex protein Nup93 OS=H	134.36	18	5
Q9NYL9|TMOD3_HUMAN	Tropomodulin-3 OS=Homo sapiens GN=TI	134.17	25	5
O00151|PDLI1_HUMAN	PDZ and LIM domain protein 1 OS=Homo	134.16	30	5
P83731|RL24_HUMAN	60S ribosomal protein L24 OS=Homo sapi	133.95	22	5
P83916|CBX1_HUMAN	Chromobox protein homolog 1 OS=Homo s	133.15	36	5
Q9BPW8|NIPS1_HUMAN	Protein NipSnap homolog 1 OS=Homo sap	132.84	36	5
P14854|CX6B1_HUMAN	Cytochrome c oxidase subunit 6B1 OS=Ho	132.84	50	5
P28072|PSB6_HUMAN	Proteasome subunit beta type-6 OS=Homo	131.74	31	5
Q9Y3B8|ORN_HUMAN	Oligoribonuclease, mitochondrial OS=Hom	131.32	39	5
P35080|PROF2_HUMAN	Profilin-2 OS=Homo sapiens GN=PFN2 PE	131.06	54	5
Q9BUL8|PDC10_HUMAN	Programmed cell death protein 10 OS=Hor	130.56	49	5
Q99417|MYCBP_HUMAN	C-Myc-binding protein OS=Homo sapiens (	130.13	46	5
P49458|SRP09_HUMAN	Signal recognition particle 9 kDa protein O	129.82	63	5
Q9Y2V2|CHSP1_HUMAN	Calcium-regulated heat stable protein 1 OS	129.71	35	5
P35611|ADDA_HUMAN	Alpha-adducin OS=Homo sapiens GN=AD	128.57	15	5
Q13098|CSN1_HUMAN	COP9 signalosome complex subunit 1 OS=	128.2	22	5
Q93062|RBPMS_HUMAN	RNA-binding protein with multiple splicing (	127.94	42	5
P28070|PSB4_HUMAN	Proteasome subunit beta type-4 OS=Homo	127.88	29	5
P21796|VDAC1_HUMAN	Voltage-dependent anion-selective channe	127.14	27	5
Q7L190|DPPA4_HUMAN	Developmental pluripotency-associated pr	127.02	34	5
Q15637|SF01_HUMAN	Splicing factor 1 OS=Homo sapiens GN=S	126.72	14	5

Q9UGI8|TES_HUMAN	Testin OS=Homo sapiens GN=TES PE=1	125.18	20	5
P55010|IF5_HUMAN	Eukaryotic translation initiation factor 5 OS	124.23	22	5
Q9Y4Z0|LSM4_HUMAN	U6 snRNA-associated Sm-like protein LSm	124.15	45	5
P61916|NPC2_HUMAN	Epididymal secretory protein E1 OS=Homo	124	48	5
P62942|FKB1A_HUMAN	Peptidyl-prolyl cis-trans isomerase FKBP1A	123.45	64	5
Q93009|UBP7_HUMAN	Ubiquitin carboxyl-terminal hydrolase 7 OS	122.55	12	5
P33316|DUT_HUMAN	Deoxyuridine 5'-triphosphate nucleotidohyd	121.34	30	5
P32321|DCTD_HUMAN	Deoxycytidylate deaminase OS=Homo sap	121.14	42	5
Q13242|SRSF9_HUMAN	Serine/arginine-rich splicing factor 9 OS=H	120.63	38	5
P63165|SUMO1_HUMAN	Small ubiquitin-related modifier 1 OS=Hom	119.88	50	5
O43795|MYO1B_HUMAN	Myosin-Ib OS=Homo sapiens GN=MYO1B	119.86	15	5
P51114|FXR1_HUMAN	Fragile X mental retardation syndrome-rela	119.51	12	5
P26639|SYTC_HUMAN	Threonyl-tRNA synthetase, cytoplasmic OS	119.35	17	5
Q9NVP1|DDX18_HUMAN	ATP-dependent RNA helicase DDX18 OS=	118.06	19	5
P36404|ARL2_HUMAN	ADP-ribosylation factor-like protein 2 OS=H	117.48	30	5
P24539|AT5F1_HUMAN	ATP synthase subunit b, mitochondrial OS	115.66	30	5
P45973|CBX5_HUMAN	Chromobox protein homolog 5 OS=Homo s	115.4	43	5
Q9P0J0|NDUAD_HUMAN	NADH dehydrogenase [ubiquinone] 1 alph	114.53	31	5
P17677|NEUM_HUMAN	Neuromodulin OS=Homo sapiens GN=GA	114.53	26	5
Q9BRP8|WIBG_HUMAN	Partner of Y14 and mago OS=Homo sapie	114.21	24	5
O95865|DDAH2_HUMAN	N(G),N(G)-dimethylarginine dimethylamino	112.71	26	5
Q14847|LASP1_HUMAN	LIM and SH3 domain protein 1 OS=Homo	111.79	29	5
Q92878|RAD50_HUMAN	DNA repair protein RAD50 OS=Homo sapi	109.33	10	5
Q9BQ04|RBM4B_HUMAN	RNA-binding protein 4B OS=Homo sapiens	109.23	17	5
Q9BWF3|RBM4_HUMAN	RNA-binding protein 4 OS=Homo sapiens	109.23	16	5
Q15020|SART3_HUMAN	Squamous cell carcinoma antigen recogniz	109.09	16	5
Q9UBQ0|VPS29_HUMAN	Vacuolar protein sorting-associated protein	108.11	32	5
P39748|FEN1_HUMAN	Flap endonuclease 1 OS=Homo sapiens G	106.17	26	5
O43447|PPIH_HUMAN	Peptidyl-prolyl cis-trans isomerase H OS=H	103.73	40	5
P82979|SARNP_HUMAN	SAP domain-containing ribonucleoprotein	103.56	29	5
Q15075|EEA1_HUMAN	Early endosome antigen 1 OS=Homo sapi	101.05	9	5
Q9BVG4|CX026_HUMAN	UPF0368 protein Cxorf26 OS=Homo sapie	100.76	31	5
P20674|COX5A_HUMAN	Cytochrome c oxidase subunit 5A, mitocho	100.34	37	5
Q99436|PSB7_HUMAN	Proteasome subunit beta type-7 OS=Homo	97.33	24	5
O75643|U520_HUMAN	U5 small nuclear ribonucleoprotein 200 kD	95.25	4	5
P78330|SERB_HUMAN	Phosphoserine phosphatase OS=Homo sa	95.03	24	5
P55957|BID_HUMAN	BH3-interacting domain death agonist OS=	94.65	33	5
Q14978|NOLC1_HUMAN	Nucleolar and coiled-body phosphoprotein	92.44	22	5
P11413|G6PD_HUMAN	Glucose-6-phosphate 1-dehydrogenase O	92.21	13	5
Q96PY5|FMNL2_HUMAN	Formin-like protein 2 OS=Homo sapiens G	88.46	9	5
P98160|PGBM_HUMAN	Basement membrane-specific heparan sul	84.39	4	5
P61326|MGN_HUMAN	Protein mago nashi homolog OS=Homo sa	83.83	40	5
Q96A72|MGN2_HUMAN	Protein mago nashi homolog 2 OS=Homo	83.83	39	5
P29373|RABP2_HUMAN	Cellular retinoic acid-binding protein 2 OS=	83.11	61	5
Q9NPE3|NOP10_HUMAN	H/ACA ribonucleoprotein complex subunit	78.6	70	5
Q4VC31|CCD58_HUMAN	Coiled-coil domain-containing protein 58 O	77.49	47	5
P19388|RPAB1_HUMAN	DNA-directed RNA polymerases I, II, and I	71.27	23	5

P63241|IF5A1_HUMAN	Eukaryotic translation initiation factor 5A-1	286.42	81	4
P11940|PABP1_HUMAN	Polyadenylate-binding protein 1 OS=Homo	242.19	43	4
P08107|HSP71_HUMAN	Heat shock 70 kDa protein 1A/1B OS=Hon	217.74	44	4
P62140|PP1B_HUMAN	Serine/threonine-protein phosphatase PP1	195.3	47	4
P31943|HNRH1_HUMAN	Heterogeneous nuclear ribonucleoprotein H	184.88	44	4
Q06210|GFPT1_HUMAN	Glucosamine--fructose-6-phosphate aminc	175.37	28	4
P41567|EIF1_HUMAN	Eukaryotic translation initiation factor 1 OS	164.11	79	4
P04216|THY1_HUMAN	Thy-1 membrane glycoprotein OS=Homo s	154.44	25	4
Q9UI30|TR112_HUMAN	tRNA methyltransferase 112 homolog OS=	153.69	42	4
Q8IXM2|BAP18_HUMAN	Chromatin complexes subunit BAP18 OS=	149.65	54	4
Q13185|CBX3_HUMAN	Chromobox protein homolog 3 OS=Homo s	148.56	39	4
P51858|HDGF_HUMAN	Hepatoma-derived growth factor OS=Hom	148.24	49	4
P43246|MSH2_HUMAN	DNA mismatch repair protein Msh2 OS=Ho	147.07	20	4
Q9H3K6|BOLA2_HUMAN	BolA-like protein 2 OS=Homo sapiens GN=	144.1	43	4
Q16630|CPSF6_HUMAN	Cleavage and polyadenylation specificity fa	143.95	20	4
Q13347|EIF3I_HUMAN	Eukaryotic translation initiation factor 3 sub	143.07	18	4
P17812|PYRG1_HUMAN	CTP synthase 1 OS=Homo sapiens GN=C	139.55	21	4
Q9NQT4|EXOS5_HUMAN	Exosome complex component RRP46 OS=	139.28	33	4
P84103|SRSF3_HUMAN	Serine/arginine-rich splicing factor 3 OS=H	138.96	30	4
P61970|NTF2_HUMAN	Nuclear transport factor 2 OS=Homo sapie	138.45	69	4
P52907|CAZA1_HUMAN	F-actin-capping protein subunit alpha-1 OS	138.21	31	4
P36969|GPX4_HUMAN	Phospholipid hydroperoxide glutathione pe	138.12	29	4
Q9Y2Z0|SUGT1_HUMAN	Suppressor of G2 allele of SKP1 homolog	136.71	24	4
Q9BRA2|TXD17_HUMAN	Thioredoxin domain-containing protein 17	136.32	42	4
P62917|RL8_HUMAN	60S ribosomal protein L8 OS=Homo sapie	136.01	24	4
Q15029|U5S1_HUMAN	116 kDa U5 small nuclear ribonucleoprotei	135.96	12	4
Q14444|CAPR1_HUMAN	Caprin-1 OS=Homo sapiens GN=CAPRIN1	135.89	24	4
O75607|NPM3_HUMAN	Nucleoplasmin-3 OS=Homo sapiens GN=N	135.26	41	4
O43765|SGTA_HUMAN	Small glutamine-rich tetratricopeptide repe	135.11	23	4
P11177|ODPB_HUMAN	Pyruvate dehydrogenase E1 component su	134.41	16	4
Q9NRX4|PHP14_HUMAN	14 kDa phosphohistidine phosphatase OS	131.26	56	4
Q13619|CUL4A_HUMAN	Cullin-4A OS=Homo sapiens GN=CUL4A P	131.24	21	4
Q9Y3B4|PM14_HUMAN	Pre-mRNA branch site protein p14 OS=Ho	129.85	35	4
P35232|PHB_HUMAN	Prohibitin OS=Homo sapiens GN=PHB PE	126.82	37	4
P30048|PRDX3_HUMAN	Thioredoxin-dependent peroxide reductase	125.71	36	4
P62306|RUXF_HUMAN	Small nuclear ribonucleoprotein F OS=Hon	124.69	56	4
Q9Y5L4|TIM13_HUMAN	Mitochondrial import inner membrane trans	124.68	54	4
P00492|HPRT_HUMAN	Hypoxanthine-guanine phosphoribosyltran	124.39	25	4
O75348|VATG1_HUMAN	V-type proton ATPase subunit G 1 OS=Ho	124.33	42	4
Q9NPH2|INO1_HUMAN	Inositol-3-phosphate synthase 1 OS=Hom	123.91	17	4
P36639|8ODP_HUMAN	7,8-dihydro-8-oxoguanine triphosphatase	123.84	19	4
P10606|COX5B_HUMAN	Cytochrome c oxidase subunit 5B, mitocho	123.61	60	4
O00622|CYR61_HUMAN	Protein CYR61 OS=Homo sapiens GN=CY	122.93	20	4
Q5VYJ4|RUEL1_HUMAN	Putative small nuclear ribonucleoprotein p	122.73	62	4
P62304|RUXE_HUMAN	Small nuclear ribonucleoprotein E OS=Hon	122.73	62	4
Q9UNZ2|NSF1C_HUMAN	NSFL1 cofactor p47 OS=Homo sapiens GI	122.61	35	4
P12004|PCNA_HUMAN	Proliferating cell nuclear antigen OS=Hom	121.45	20	4

Q9UNH7|SNX6_HUMAN	Sorting nexin-6 OS=Homo sapiens GN=SN	120.33	18	4
Q9BQI0|AIF1L_HUMAN	Allograft inflammatory factor 1-like OS=Ho	119.91	38	4
Q96AC1|FERM2_HUMAN	Fermitin family homolog 2 OS=Homo sapie	119.84	15	4
P35244|RFA3_HUMAN	Replication protein A 14 kDa subunit OS=H	119.22	40	4
Q92896|GSLG1_HUMAN	Golgi apparatus protein 1 OS=Homo sapie	118.67	9	4
Q8WUM4|PDC6I_HUMAN	Programmed cell death 6-interacting protei	118.37	19	4
Q9NUQ9|FA49B_HUMAN	Protein FAM49B OS=Homo sapiens GN=F	118.02	19	4
P07203|GPX1_HUMAN	Glutathione peroxidase 1 OS=Homo sapie	117.92	34	4
Q13158|FADD_HUMAN	Protein FADD OS=Homo sapiens GN=FAD	117.5	53	4
O60888|CUTA_HUMAN	Protein CutA OS=Homo sapiens GN=CUT	117.22	43	4
Q13442|HAP28_HUMAN	28 kDa heat- and acid-stable phosphoprot	116.43	24	4
Q14011|CIRBP_HUMAN	Cold-inducible RNA-binding protein OS=H	116.32	43	4
P09525|ANXA4_HUMAN	Annexin A4 OS=Homo sapiens GN=ANXA	116.04	31	4
Q9H299|SH3L3_HUMAN	SH3 domain-binding glutamic acid-rich-like	115.58	52	4
P31930|QCR1_HUMAN	Cytochrome b-c1 complex subunit 1, mitoc	115	23	4
Q9Y371|SHLB1_HUMAN	Endophilin-B1 OS=Homo sapiens GN=SH3	114.92	11	4
Q96SM3|CPXM1_HUMAN	Probable carboxypeptidase X1 OS=Homo	114.6	17	4
P14735|IDE_HUMAN	Insulin-degrading enzyme OS=Homo sapie	114.59	14	4
P46779|RL28_HUMAN	60S ribosomal protein L28 OS=Homo sapi	114.42	28	4
Q99873|ANM1_HUMAN	Protein arginine N-methyltransferase 1 OS	114.31	18	4
Q07666|KHDR1_HUMAN	KH domain-containing, RNA-binding, signa	114.08	27	4
Q9H444|CHM4B_HUMAN	Charged multivesicular body protein 4b OS	113.93	43	4
P40937|RFC5_HUMAN	Replication factor C subunit 5 OS=Homo s	113.69	22	4
Q14CX7|NAA25_HUMAN	N-alpha-acetyltransferase 25, NatB auxilia	113.62	12	4
P39687|AN32A_HUMAN	Acidic leucine-rich nuclear phosphoprotein	113.27	31	4
Q15257|PTPA_HUMAN	Serine/threonine-protein phosphatase 2A a	112.87	24	4
Q99584|S10AD_HUMAN	Protein S100-A13 OS=Homo sapiens GN=	112.84	45	4
P42285|SK2L2_HUMAN	Superkiller viralicidic activity 2-like 2 OS=H	112.73	17	4
P30626|SORCN_HUMAN	Sorcin OS=Homo sapiens GN=SRI PE=1 S	112.51	22	4
Q99961|SH3G1_HUMAN	Endophilin-A2 OS=Homo sapiens GN=SH3	112.33	16	4
Q9H1E3|NUCKS_HUMAN	Nuclear ubiquitous casein and cyclin-depe	111.79	27	4
P63208|SKP1_HUMAN	S-phase kinase-associated protein 1 OS=H	111.35	27	4
P09382|LEG1_HUMAN	Galectin-1 OS=Homo sapiens GN=LGALS	110.41	39	4
Q9ULC4|MCTS1_HUMAN	Malignant T cell-amplified sequence 1 OS=	109.93	38	4
O75821|EIF3G_HUMAN	Eukaryotic translation initiation factor 3 sub	109.22	21	4
Q8WWY3|PRP31_HUMAN	U4/U6 small nuclear ribonucleoprotein Prp	109.11	33	4
P24666|PPAC_HUMAN	Low molecular weight phosphotyrosine pro	108.01	22	4
P35637|FUS_HUMAN	RNA-binding protein FUS OS=Homo sapie	107.92	29	4
O60925|PFD1_HUMAN	Prefoldin subunit 1 OS=Homo sapiens GN	107.79	24	4
P52788|SPSY_HUMAN	Spermine synthase OS=Homo sapiens GN	107.68	23	4
O75312|ZPR1_HUMAN	Zinc finger protein ZPR1 OS=Homo sapien	107.14	19	4
O75955|FLOT1_HUMAN	Flotillin-1 OS=Homo sapiens GN=FLOT1 P	106.47	26	4
Q9Y285|SYFA_HUMAN	Phenylalanyl-tRNA synthetase alpha chain	105.83	18	4
P05937|CALB1_HUMAN	Calbindin OS=Homo sapiens GN=CALB1	104.54	31	4
P35606|COPB2_HUMAN	Coatomer subunit beta' OS=Homo sapiens	104.41	6	4
P09455|RET1_HUMAN	Retinol-binding protein 1 OS=Homo sapien	104.33	51	4
P55786|PSA_HUMAN	Puromycin-sensitive aminopeptidase OS=H	104.15	7	4

Q07866|KLC1_HUMAN	Kinesin light chain 1 OS=Homo sapiens GI	102.84	18	4
P51149|RAB7A_HUMAN	Ras-related protein Rab-7a OS=Homo sap	102.73	36	4
P05204|HMGN2_HUMAN	Non-histone chromosomal protein HMG-17	102.58	51	4
Q9Y376|CAB39_HUMAN	Calcium-binding protein 39 OS=Homo sap	102.37	23	4
O43324|MCA3_HUMAN	Eukaryotic translation elongation factor 1 e	102.05	39	4
Q13308|PTK7_HUMAN	Inactive tyrosine-protein kinase 7 OS=Hom	101.96	9	4
P12830|CADH1_HUMAN	Cadherin-1 OS=Homo sapiens GN=CDH1	101.75	7	4
P40429|RL13A_HUMAN	60S ribosomal protein L13a OS=Homo sap	101.69	29	4
O43252|PAPS1_HUMAN	Bifunctional 3'-phosphoadenosine 5'-phosp	101.48	19	4
P63000|RAC1_HUMAN	Ras-related C3 botulinum toxin substrate 1	100.68	26	4
P19623|SPEE_HUMAN	Spermidine synthase OS=Homo sapiens G	100.49	24	4
Q9GZT3|SLIRP_HUMAN	SRA stem-loop-interacting RNA-binding pr	100.31	55	4
Q9BYT8|NEUL_HUMAN	Neurolysin, mitochondrial OS=Homo sapie	99.07	13	4
Q9NSD9|SYFB_HUMAN	Phenylalanyl-tRNA synthetase beta chain (	98.12	11	4
P51148|RAB5C_HUMAN	Ras-related protein Rab-5C OS=Homo sap	97.15	31	4
Q9BS26|ERP44_HUMAN	Endoplasmic reticulum resident protein 44	95.98	16	4
P61086|UBE2K_HUMAN	Ubiquitin-conjugating enzyme E2 K OS=Ho	95.94	36	4
Q99426|TBCB_HUMAN	Tubulin-folding cofactor B OS=Homo sapie	95.64	16	4
Q02543|RL18A_HUMAN	60S ribosomal protein L18a OS=Homo sap	94.95	29	4
A6NDG6|PGP_HUMAN	Phosphoglycolate phosphatase OS=Homo	94.5	15	4
A8MWD9|RUXGL_HUMAN	Small nuclear ribonucleoprotein G-like prot	94.4	26	4
P62308|RUXG_HUMAN	Small nuclear ribonucleoprotein G OS=Hor	94.4	26	4
Q32P28|P3H1_HUMAN	Prolyl 3-hydroxylase 1 OS=Homo sapiens	94.24	7	4
Q969H8|CS010_HUMAN	UPF0556 protein C19orf10 OS=Homo sap	93.93	26	4
Q14203|DCTN1_HUMAN	Dynactin subunit 1 OS=Homo sapiens GN=	91.52	11	4
Q9UKY7|CDV3_HUMAN	Protein CDV3 homolog OS=Homo sapiens	90.41	19	4
P25325|THTM_HUMAN	3-mercaptopyruvate sulfurtransferase OS=	88.59	24	4
O00154|BACH_HUMAN	Cytosolic acyl coenzyme A thioester hydrol	86.47	12	4
Q03701|CEBPZ_HUMAN	CCAAT/enhancer-binding protein zeta OS=	83.82	8	4
Q5TZA2|CROCC_HUMAN	Rootletin OS=Homo sapiens GN=CROCC	83.36	7	4
Q9Y2S6|CCD72_HUMAN	Coiled-coil domain-containing protein 72 O	83.29	36	4
P36542|ATPG_HUMAN	ATP synthase subunit gamma, mitochondr	83.27	27	4
P38117|ETFB_HUMAN	Electron transfer flavoprotein subunit beta	82.51	29	4
P13073|COX41_HUMAN	Cytochrome c oxidase subunit 4 isoform 1,	81.1	32	4
P61221|ABCE1_HUMAN	ATP-binding cassette sub-family E membe	73.47	15	4
Q8WWM7|ATX2L_HUMAN	Ataxin-2-like protein OS=Homo sapiens GI	73.05	7	4
Q13435|SF3B2_HUMAN	Splicing factor 3B subunit 2 OS=Homo sap	71.02	8	4
Q04637|IF4G1_HUMAN	Eukaryotic translation initiation factor 4 gar	68.82	6	4
Q96PK6|RBM14_HUMAN	RNA-binding protein 14 OS=Homo sapiens	68.35	10	4
Q86X55|CARM1_HUMAN	Histone-arginine methyltransferase CARM1	58.7	16	4
Q8TDI0|CHD5_HUMAN	Chromodomain-helicase-DNA-binding prot	57.07	6	4
Q9HCM1|CL035_HUMAN	Uncharacterized protein C12orf35 OS=Hor	56.46	5	4
P35659|DEK_HUMAN	Protein DEK OS=Homo sapiens GN=DEK	52.16	11	4
Q8WZ42|TITIN_HUMAN	Titin OS=Homo sapiens GN=TTN PE=1 SV	50.28	4	4
Q8IZC6|CORA1_HUMAN	Collagen alpha-1(XXVII) chain OS=Homo s	46.19	10	4
Q13509|TBB3_HUMAN	Tubulin beta-3 chain OS=Homo sapiens G	328.66	65	3
P16403|H12_HUMAN	Histone H1.2 OS=Homo sapiens GN=HIST	246.08	54	3

P19105|ML12A_HUMAN	Myosin regulatory light chain 12A OS=Hom	218.29	64	3
O14950|ML12B_HUMAN	Myosin regulatory light chain 12B OS=Hom	218.29	63	3
P62136|PP1A_HUMAN	Serine/threonine-protein phosphatase PP1	214.64	50	3
P36873|PP1G_HUMAN	Serine/threonine-protein phosphatase PP1	207.58	51	3
P80297|MT1X_HUMAN	Metallothionein-1X OS=Homo sapiens GN	173.44	93	3
O00292|LFTY2_HUMAN	Left-right determination factor 2 OS=Homo	171.99	39	3
Q13526|PIN1_HUMAN	Peptidyl-prolyl cis-trans isomerase NIMA-in	157.53	56	3
P84085|ARF5_HUMAN	ADP-ribosylation factor 5 OS=Homo sapie	155.55	56	3
Q9Y6M1|IF2B2_HUMAN	Insulin-like growth factor 2 mRNA-binding p	152.9	22	3
P13804|ETFA_HUMAN	Electron transfer flavoprotein subunit alpha	145.32	53	3
Q9BUT1|BDH2_HUMAN	3-hydroxybutyrate dehydrogenase type 2 O	138.72	40	3
P22087|FBRL_HUMAN	rRNA 2'-O-methyltransferase fibrillarin OS=	138.49	42	3
P61163|ACTZ_HUMAN	Alpha-centractin OS=Homo sapiens GN=A	138.07	57	3
P42677|RS27_HUMAN	40S ribosomal protein S27 OS=Homo sapi	137.93	40	3
Q5VTR2|BRE1A_HUMAN	E3 ubiquitin-protein ligase BRE1A OS=Ho	136.26	19	3
Q6GMV3|CB079_HUMAN	Uncharacterized protein C2orf79 OS=Hom	135.56	52	3
Q16629|SRSF7_HUMAN	Serine/arginine-rich splicing factor 7 OS=H	135.25	20	3
P12829|MYL4_HUMAN	Myosin light chain 4 OS=Homo sapiens GN	135.23	70	3
O43768|ENSA_HUMAN	Alpha-endosulfine OS=Homo sapiens GN=	133.61	69	3
P14923|PLAK_HUMAN	Junction plakoglobin OS=Homo sapiens G	132.84	17	3
Q9BX68|HINT2_HUMAN	Histidine triad nucleotide-binding protein 2,	132.21	40	3
P04080|CYTB_HUMAN	Cystatin-B OS=Homo sapiens GN=CSTB P	130.76	55	3
Q92769|HDAC2_HUMAN	Histone deacetylase 2 OS=Homo sapiens	129.78	22	3
Q15437|SC23B_HUMAN	Protein transport protein Sec23B OS=Hom	129.03	16	3
Q9BQ52|RNZ2_HUMAN	Zinc phosphodiesterase ELAC protein 2 O	128.98	14	3
P48735|IDHP_HUMAN	Isocitrate dehydrogenase [NADP], mitocho	128.95	25	3
P62873|GBB1_HUMAN	Guanine nucleotide-binding protein G(I)/G(	128.14	17	3
P46782|RS5_HUMAN	40S ribosomal protein S5 OS=Homo sapie	128.04	30	3
P49006|MRP_HUMAN	MARCKS-related protein OS=Homo sapien	127.99	28	3
Q9Y3C6|PPIL1_HUMAN	Peptidyl-prolyl cis-trans isomerase-like 1 O	127.31	39	3
Q7L1Q6|BZW1_HUMAN	Basic leucine zipper and W2 domain-conta	126.41	28	3
P54920|SNAA_HUMAN	Alpha-soluble NSF attachment protein OS=	126.36	25	3
O76021|RL1D1_HUMAN	Ribosomal L1 domain-containing protein 1	125.66	32	3
Q6P2Q9|PRP8_HUMAN	Pre-mRNA-processing-splicing factor 8 OS	124.22	15	3
Q9NPJ3|ACO13_HUMAN	Acyl-coenzyme A thioesterase 13 OS=Hom	124.06	21	3
Q96PU8|QKI_HUMAN	Protein quaking OS=Homo sapiens GN=Q	122.86	48	3
Q9H0A0|NAT10_HUMAN	N-acetyltransferase 10 OS=Homo sapiens	122.86	14	3
Q15833|STXB2_HUMAN	Syntaxin-binding protein 2 OS=Homo sapie	122.7	20	3
P10768|ESTD_HUMAN	S-formylglutathione hydrolase OS=Homo s	122.62	29	3
O00264|PGRC1_HUMAN	Membrane-associated progesterone recep	122.35	36	3
Q12996|CSTF3_HUMAN	Cleavage stimulation factor subunit 3 OS=	121.58	17	3
Q99733|NP1L4_HUMAN	Nucleosome assembly protein 1-like 4 OS=	120.55	26	3
P19784|CSK22_HUMAN	Casein kinase II subunit alpha' OS=Homo	120.09	22	3
P11172|PYR5_HUMAN	Uridine 5'-monophosphate synthase OS=H	119.61	34	3
P62854|RS26_HUMAN	40S ribosomal protein S26 OS=Homo sapi	118.32	31	3
O00567|NOP56_HUMAN	Nucleolar protein 56 OS=Homo sapiens G	118.13	20	3
A6NDU8|CE051_HUMAN	UPF0600 protein C5orf51 OS=Homo sapie	116.57	50	3

P05386|RLA1_HUMAN	60S acidic ribosomal protein P1 OS=Homo	115.59	49	3
O43278|SPIT1_HUMAN	Kunitz-type protease inhibitor 1 OS=Homo	115.29	7	3
P46776|RL27A_HUMAN	60S ribosomal protein L27a OS=Homo sap	114.98	39	3
Q9NRN7|ADPPT_HUMAN	L-aminoadipate-semialdehyde dehydrogen	114.55	21	3
Q15555|MARE2_HUMAN	Microtubule-associated protein RP/EB fam	114.43	29	3
P0CG34|TB15A_HUMAN	Thymosin beta-15A OS=Homo sapiens GN	113.57	36	3
P0CG35|TB15B_HUMAN	Thymosin beta-15B OS=Homo sapiens GN	113.57	36	3
Q9H0U4|RAB1B_HUMAN	Ras-related protein Rab-1B OS=Homo sap	113.53	31	3
Q92928|RAB1C_HUMAN	Putative Ras-related protein Rab-1C OS=H	113.53	30	3
P16422|EPCAM_HUMAN	Epithelial cell adhesion molecule OS=Hom	113.42	10	3
P46109|CRKL_HUMAN	Crk-like protein OS=Homo sapiens GN=CR	111.98	17	3
Q08431|MFGM_HUMAN	Lactadherin OS=Homo sapiens GN=MFGE	111.36	14	3
Q12874|SF3A3_HUMAN	Splicing factor 3A subunit 3 OS=Homo sap	110.95	13	3
Q96IZ0|PAWR_HUMAN	PRKC apoptosis WT1 regulator protein OS	110.95	25	3
Q9Y6E2|BZW2_HUMAN	Basic leucine zipper and W2 domain-conta	110.32	16	3
O00764|PDXK_HUMAN	Pyridoxal kinase OS=Homo sapiens GN=P	110.13	23	3
P52888|THOP1_HUMAN	Thimet oligopeptidase OS=Homo sapiens	110.12	15	3
O75494|SRS10_HUMAN	Serine/arginine-rich splicing factor 10 OS=	109.44	30	3
P49589|SYCC_HUMAN	Cysteinyl-tRNA synthetase, cytoplasmic OS	108.74	12	3
O75340|PDCD6_HUMAN	Programmed cell death protein 6 OS=Hom	108.64	26	3
Q13451|FKBP5_HUMAN	Peptidyl-prolyl cis-trans isomerase FKBP5	108.23	13	3
Q01081|U2AF1_HUMAN	Splicing factor U2AF 35 kDa subunit OS=H	108.04	17	3
Q71UM5|RS27L_HUMAN	40S ribosomal protein S27-like OS=Homo	107.95	40	3
P54687|BCAT1_HUMAN	Branched-chain-amino-acid aminotransfera	107.36	18	3
P40925|MDHC_HUMAN	Malate dehydrogenase, cytoplasmic OS=H	106.84	24	3
Q9NV70|EXOC1_HUMAN	Exocyst complex component 1 OS=Homo	106.75	18	3
P62906|RL10A_HUMAN	60S ribosomal protein L10a OS=Homo sap	106.18	31	3
Q9H4M9|EHD1_HUMAN	EH domain-containing protein 1 OS=Homo	104.8	25	3
Q9NZL9|MAT2B_HUMAN	Methionine adenosyltransferase 2 subunit	104.76	24	3
P04179|SODM_HUMAN	Superoxide dismutase [Mn], mitochondrial	104.75	17	3
P09960|LKHA4_HUMAN	Leukotriene A-4 hydrolase OS=Homo sapi	104.56	9	3
Q15785|TOM34_HUMAN	Mitochondrial import receptor subunit TOM	104.54	24	3
P23919|KTHY_HUMAN	Thymidylate kinase OS=Homo sapiens GN	104.02	25	3
P42766|RL35_HUMAN	60S ribosomal protein L35 OS=Homo sapi	103.1	39	3
P52434|RPAB3_HUMAN	DNA-directed RNA polymerases I, II, and I	102.78	21	3
O75608|LYPA1_HUMAN	Acyl-protein thioesterase 1 OS=Homo sapi	102.13	27	3
Q86U42|PABP2_HUMAN	Polyadenylate-binding protein 2 OS=Homo	102.09	22	3
Q14677|EPN4_HUMAN	Clathrin interactor 1 OS=Homo sapiens GN	102.05	17	3
Q9Y5Z4|HEBP2_HUMAN	Heme-binding protein 2 OS=Homo sapiens	101.95	20	3
Q96K17|BT3L4_HUMAN	Transcription factor BTF3 homolog 4 OS=H	101.61	36	3
Q9UMY4|SNX12_HUMAN	Sorting nexin-12 OS=Homo sapiens GN=S	101.15	40	3
P61201|CSN2_HUMAN	COP9 signalosome complex subunit 2 OS=	100.4	21	3
P58546|MTPN_HUMAN	Myotrophin OS=Homo sapiens GN=MTPN	100.02	25	3
O43805|SSNA1_HUMAN	Sjoegren syndrome nuclear autoantigen 1	99.99	28	3
O60841|IF2P_HUMAN	Eukaryotic translation initiation factor 5B O	99.32	12	3
P49023|PAXI_HUMAN	Paxillin OS=Homo sapiens GN=PXN PE=1	98.54	14	3
Q9Y6Y8|S23IP_HUMAN	SEC23-interacting protein OS=Homo sapie	98.24	13	3

Q96CT7|CC124_HUMAN	Coiled-coil domain-containing protein 124 (	97.64	26	3
P51511|MMP15_HUMAN	Matrix metalloproteinase-15 OS=Homo sap	97.07	8	3
Q8NFU3|TSTD1_HUMAN	Thiosulfate sulfurtransferase/rhodanese-lik	96.82	31	3
O75330|HMMR_HUMAN	Hyaluronan mediated motility receptor OS=	96.74	24	3
Q9Y2W1|TR150_HUMAN	Thyroid hormone receptor-associated prote	96.6	12	3
O75400|PR40A_HUMAN	Pre-mRNA-processing factor 40 homolog A	96.29	7	3
Q9H0S4|DDX47_HUMAN	Probable ATP-dependent RNA helicase DI	96.18	25	3
P62861|RS30_HUMAN	40S ribosomal protein S30 OS=Homo sapi	96.07	34	3
Q5T6F2|UBAP2_HUMAN	Ubiquitin-associated protein 2 OS=Homo s	95.19	7	3
Q16186|ADRM1_HUMAN	Proteasomal ubiquitin receptor ADRM1 OS	95.01	11	3
P49902|5NTC_HUMAN	Cytosolic purine 5'-nucleotidase OS=Homo	94.73	15	3
P49721|PSB2_HUMAN	Proteasome subunit beta type-2 OS=Homo	94.17	19	3
P53367|ARFP1_HUMAN	Arfaptin-1 OS=Homo sapiens GN=ARFIP1	94.01	14	3
Q05086|UBE3A_HUMAN	Ubiquitin-protein ligase E3A OS=Homo sap	93.97	11	3
Q9H9A6|LRC40_HUMAN	Leucine-rich repeat-containing protein 40 (	93.81	10	3
O60869|EDF1_HUMAN	Endothelial differentiation-related factor 1 (	93.76	41	3
Q9UQ35|SRRM2_HUMAN	Serine/arginine repetitive matrix protein 2 (	93.59	11	3
Q15435|PP1R7_HUMAN	Protein phosphatase 1 regulatory subunit 7	93.13	23	3
P27694|RFA1_HUMAN	Replication protein A 70 kDa DNA-binding	93.02	15	3
P08579|RU2B_HUMAN	U2 small nuclear ribonucleoprotein B'' OS=	93.01	28	3
P38606|VATA_HUMAN	V-type proton ATPase catalytic subunit A (	92.51	9	3
Q96TA1|NIBL1_HUMAN	Niban-like protein 1 OS=Homo sapiens GN	92.31	10	3
Q9NQP4|PFD4_HUMAN	Prefoldin subunit 4 OS=Homo sapiens GN	91.87	22	3
P49419|AL7A1_HUMAN	Alpha-aminoadipic semialdehyde dehydrog	91.7	11	3
Q8WVJ2|NUDC2_HUMAN	NudC domain-containing protein 2 OS=Ho	91.06	19	3
Q9BY32|ITPA_HUMAN	Inosine triphosphate pyrophosphatase OS	90.55	28	3
Q13895|BYST_HUMAN	Bystin OS=Homo sapiens GN=BYSL PE=1	90.54	5	3
Q9NZD2|GLTP_HUMAN	Glycolipid transfer protein OS=Homo sapie	90.2	17	3
Q7L014|DDX46_HUMAN	Probable ATP-dependent RNA helicase DI	90.09	11	3
Q14914|PTGR1_HUMAN	Prostaglandin reductase 1 OS=Homo sapi	89.81	16	3
P13489|RINI_HUMAN	Ribonuclease inhibitor OS=Homo sapiens	89.8	14	3
Q15393|SF3B3_HUMAN	Splicing factor 3B subunit 3 OS=Homo sap	89.75	7	3
Q8WW12|PCNP_HUMAN	PEST proteolytic signal-containing nuclear	89.66	15	3
Q8IXM3|RM41_HUMAN	39S ribosomal protein L41, mitochondrial (	89.42	36	3
Q16527|CSRP2_HUMAN	Cysteine and glycine-rich protein 2 OS=Ho	89.24	13	3
P20042|IF2B_HUMAN	Eukaryotic translation initiation factor 2 sub	88.58	25	3
A6NK07|IF2BL_HUMAN	Eukaryotic translation initiation factor 2 sub	88.58	20	3
Q99622|C10_HUMAN	Protein C10 OS=Homo sapiens GN=C12o	88.42	48	3
Q96RU2|UBP28_HUMAN	Ubiquitin carboxyl-terminal hydrolase 28 O	88.14	13	3
O15514|RPB4_HUMAN	DNA-directed RNA polymerase II subunit F	88.11	37	3
O60341|KDM1A_HUMAN	Lysine-specific histone demethylase 1A OS	88.07	11	3
Q8IX90|SKA3_HUMAN	Spindle and kinetochore-associated protei	87.95	10	3
P62266|RS23_HUMAN	40S ribosomal protein S23 OS=Homo sapi	87.56	23	3
O60716|CTND1_HUMAN	Catenin delta-1 OS=Homo sapiens GN=CT	87.52	16	3
Q56VL3|OCAD2_HUMAN	OCIA domain-containing protein 2 OS=Hor	87.45	42	3
O75822|EIF3J_HUMAN	Eukaryotic translation initiation factor 3 sub	87.24	20	3
P18859|ATP5J_HUMAN	ATP synthase-coupling factor 6, mitochond	87.1	31	3

Q9Y5K6|CD2AP_HUMAN	CD2-associated protein OS=Homo sapiens	87.04	15	3
O60749|SNX2_HUMAN	Sorting nexin-2 OS=Homo sapiens GN=SN	86.95	13	3
Q92522|H1X_HUMAN	Histone H1x OS=Homo sapiens GN=H1FX	86.88	31	3
P49643|PRI2_HUMAN	DNA primase large subunit OS=Homo sap	86.84	9	3
Q16204|CCDC6_HUMAN	Coiled-coil domain-containing protein 6 OS	86.7	14	3
Q9UII2|ATIF1_HUMAN	ATPase inhibitor, mitochondrial OS=Homo	86.28	25	3
Q9BTE3|MCMBP_HUMAN	Mini-chromosome maintenance complex-b	86.04	9	3
Q8WUW1|BRK1_HUMAN	Protein BRICK1 OS=Homo sapiens GN=C	85.16	40	3
O00159|MYO1C_HUMAN	Myosin-Ic OS=Homo sapiens GN=MYO1C	84.93	6	3
Q96G03|PGM2_HUMAN	Phosphoglucomutase-2 OS=Homo sapiens	84.79	17	3
O60306|AQR_HUMAN	Intron-binding protein aquarius OS=Homo	84.76	9	3
Q15642|CIP4_HUMAN	Cdc42-interacting protein 4 OS=Homo sap	84.55	14	3
O94760|DDAH1_HUMAN	N(G),N(G)-dimethylarginine dimethylamino	83.98	32	3
P11047|LAMC1_HUMAN	Laminin subunit gamma-1 OS=Homo sapie	83.87	6	3
O43264|ZW10_HUMAN	Centromere/kinetochore protein zw10 hom	83.24	12	3
Q9UMS4|PRP19_HUMAN	Pre-mRNA-processing factor 19 OS=Homo	82.92	10	3
Q8N6M0|OTU6B_HUMAN	OTU domain-containing protein 6B OS=Ho	82.7	25	3
Q15293|RCN1_HUMAN	Reticulocalbin-1 OS=Homo sapiens GN=R	82.62	16	3
Q92917|GPKOW_HUMAN	G patch domain and KOW motifs-containir	82.51	18	3
Q8NCW5|AIBP_HUMAN	Apolipoprotein A-I-binding protein OS=Hor	82.16	14	3
Q86XP3|DDX42_HUMAN	ATP-dependent RNA helicase DDX42 OS=	82.1	13	3
Q14008|CKAP5_HUMAN	Cytoskeleton-associated protein 5 OS=Hor	81.36	9	3
O14618|CCS_HUMAN	Copper chaperone for superoxide dismuta	80.6	25	3
O43865|SAHH2_HUMAN	Putative adenosylhomocysteinase 2 OS=H	79.39	16	3
P07311|ACYP1_HUMAN	Acylphosphatase-1 OS=Homo sapiens GN	78.94	35	3
Q9HB07|MYG1_HUMAN	UPF0160 protein MYG1, mitochondrial OS	78.78	12	3
Q15102|PA1B3_HUMAN	Platelet-activating factor acetylhydrolase IB	77.77	11	3
Q52LJ0|FA98B_HUMAN	Protein FAM98B OS=Homo sapiens GN=F	77.62	12	3
O60832|DKC1_HUMAN	H/ACA ribonucleoprotein complex subunit	77.26	18	3
Q13868|EXOS2_HUMAN	Exosome complex component RRP4 OS=	77.13	30	3
Q14061|COX17_HUMAN	Cytochrome c oxidase copper chaperone C	77.09	75	3
Q9NQ48|LZTL1_HUMAN	Leucine zipper transcription factor-like prot	76.86	9	3
Q8IV08|PLD3_HUMAN	Phospholipase D3 OS=Homo sapiens GN=	76.83	12	3
P09496|CLCA_HUMAN	Clathrin light chain A OS=Homo sapiens G	76.59	11	3
P10155|RO60_HUMAN	60 kDa SS-A/Ro ribonucleoprotein OS=Ho	74	12	3
P62330|ARF6_HUMAN	ADP-ribosylation factor 6 OS=Homo sapie	72.99	18	3
Q9Y3U8|RL36_HUMAN	60S ribosomal protein L36 OS=Homo sapi	72.72	29	3
O43237|DC1L2_HUMAN	Cytoplasmic dynein 1 light intermediate cha	72.09	9	3
Q9Y2Q9|RT28_HUMAN	28S ribosomal protein S28, mitochondrial C	71.69	31	3
P35237|SPB6_HUMAN	Serpin B6 OS=Homo sapiens GN=SERPIN	71.25	19	3
Q9BWJ5|SF3B5_HUMAN	Splicing factor 3B subunit 5 OS=Homo sap	71.1	41	3
O95239|KIF4A_HUMAN	Chromosome-associated kinesin KIF4A OS	70.97	6	3
P30419|NMT1_HUMAN	Glycylpeptide N-tetradecanoyltransferase 1	70.75	11	3
Q9Y3D9|RT23_HUMAN	28S ribosomal protein S23, mitochondrial C	70.5	17	3
Q7LBC6|KDM3B_HUMAN	Lysine-specific demethylase 3B OS=Homo	70.24	3	3
O00762|UBE2C_HUMAN	Ubiquitin-conjugating enzyme E2 C OS=Ho	69.93	36	3
Q14157|UBP2L_HUMAN	Ubiquitin-associated protein 2-like OS=Hor	69.67	8	3

Q92879|CELF1_HUMAN	CUGBP Elav-like family member 1 OS=Ho	68.9	8	3
Q9NQW7|XPP1_HUMAN	Xaa-Pro aminopeptidase 1 OS=Homo sap	68.7	9	3
Q5TFE4|NT5D1_HUMAN	5'-nucleotidase domain-containing protein	68.33	8	3
Q86V88|MGDP1_HUMAN	Magnesium-dependent phosphatase 1 OS	67.49	27	3
P07686|HEXB_HUMAN	Beta-hexosaminidase subunit beta OS=Ho	67.18	12	3
O94973|AP2A2_HUMAN	AP-2 complex subunit alpha-2 OS=Homo s	67.1	12	3
P62253|UB2G1_HUMAN	Ubiquitin-conjugating enzyme E2 G1 OS=H	66.99	11	3
P24752|THIL_HUMAN	Acetyl-CoA acetyltransferase, mitochondria	66.66	16	3
Q9Y4C1|KDM3A_HUMAN	Lysine-specific demethylase 3A OS=Homo	65.93	7	3
Q9C0C9|UBE2O_HUMAN	Ubiquitin-conjugating enzyme E2 O OS=H	64.65	11	3
P47985|UCRI_HUMAN	Cytochrome b-c1 complex subunit Rieske,	64.15	20	3
P0C7P4|UCRIL_HUMAN	Putative cytochrome b-c1 complex subunit	64.15	19	3
O00115|DNS2A_HUMAN	Deoxyribonuclease-2-alpha OS=Homo sap	63.14	9	3
P10253|LYAG_HUMAN	Lysosomal alpha-glucosidase OS=Homo s	62.42	8	3
P16083|NQO2_HUMAN	Ribosyldihydronicotinamide dehydrogenas	61.65	18	3
Q9UHD1|CHRD1_HUMAN	Cysteine and histidine-rich domain-contain	61.41	15	3
Q92485|ASM3B_HUMAN	Acid sphingomyelinase-like phosphodieste	60.83	9	3
Q6DKJ4|NXN_HUMAN	Nucleoredoxin OS=Homo sapiens GN=NX	60.58	13	3
Q8NE71|ABCF1_HUMAN	ATP-binding cassette sub-family F membe	56.4	8	3
Q9HAV7|GRPE1_HUMAN	GrpE protein homolog 1, mitochondrial OS	56.04	28	3
Q9H1B7|I2BPL_HUMAN	Interferon regulatory factor 2-binding prote	54.33	11	3
Q01970|PLCB3_HUMAN	1-phosphatidylinositol-4,5-bisphosphate ph	46.82	5	3
P36406|TRI23_HUMAN	E3 ubiquitin-protein ligase TRIM23 OS=Ho	42.95	13	3
Q5U5R9|HECD2_HUMAN	Probable E3 ubiquitin-protein ligase HECT	40.01	5	3
P25391|LAMA1_HUMAN	Laminin subunit alpha-1 OS=Homo sapien	35.67	5	3
P68371|TBB2C_HUMAN	Tubulin beta-2C chain OS=Homo sapiens	424.6	82	2
P63261|ACTG_HUMAN	Actin, cytoplasmic 2 OS=Homo sapiens GN	415.2	86	2
Q9BVA1|TBB2B_HUMAN	Tubulin beta-2B chain OS=Homo sapiens	407.9	80	2
P04350|TBB4_HUMAN	Tubulin beta-4 chain OS=Homo sapiens G	389.06	76	2
Q9BQE3|TBA1C_HUMAN	Tubulin alpha-1C chain OS=Homo sapiens	327.76	74	2
P62979|RS27A_HUMAN	Ubiquitin-40S ribosomal protein S27a OS=	291.21	63	2
P0CG48|UBC_HUMAN	Polyubiquitin-C OS=Homo sapiens GN=UB	279.3	75	2
P0CG47|UBB_HUMAN	Polyubiquitin-B OS=Homo sapiens GN=UB	279.3	93	2
P35749|MYH11_HUMAN	Myosin-11 OS=Homo sapiens GN=MYH11	207.27	34	2
Q8TAA3|PSA7L_HUMAN	Proteasome subunit alpha type-7-like OS=	205.77	54	2
Q13310|PABP4_HUMAN	Polyadenylate-binding protein 4 OS=Homo	201.17	41	2
P68431|H31_HUMAN	Histone H3.1 OS=Homo sapiens GN=HIST	182.91	72	2
Q71DI3|H32_HUMAN	Histone H3.2 OS=Homo sapiens GN=HIST	182.91	72	2
P13929|ENOB_HUMAN	Beta-enolase OS=Homo sapiens GN=ENO	176.46	51	2
P56545|CTBP2_HUMAN	C-terminal-binding protein 2 OS=Homo sap	174.47	37	2
Q13162|PRDX4_HUMAN	Peroxiredoxin-4 OS=Homo sapiens GN=P	157.8	25	2
P63167|DYL1_HUMAN	Dynein light chain 1, cytoplasmic OS=Hom	157.64	61	2
O75610|LFTY1_HUMAN	Left-right determination factor 1 OS=Homo	157.28	31	2
Q13363|CTBP1_HUMAN	C-terminal-binding protein 1 OS=Homo sap	153.58	32	2
Q96FJ2|DYL2_HUMAN	Dynein light chain 2, cytoplasmic OS=Hom	152.48	40	2
O43390|HNRPR_HUMAN	Heterogeneous nuclear ribonucleoprotein	147.99	24	2
P52597|HNRPF_HUMAN	Heterogeneous nuclear ribonucleoprotein	136.85	27	2

Q15436|SC23A_HUMAN	Protein transport protein Sec23A OS=Hom	133.71	12	2
P38919|IF4A3_HUMAN	Eukaryotic initiation factor 4A-III OS=Homo	132.82	26	2
Q13404|UB2V1_HUMAN	Ubiquitin-conjugating enzyme E2 variant 1	130.6	50	2
Q96FW1|OTUB1_HUMAN	Ubiquitin thioesterase OTUB1 OS=Homo s	127.92	17	2
P18085|ARF4_HUMAN	ADP-ribosylation factor 4 OS=Homo sapie	127.46	48	2
O60282|KIF5C_HUMAN	Kinesin heavy chain isoform 5C OS=Homo	125.8	14	2
P46778|RL21_HUMAN	60S ribosomal protein L21 OS=Homo sapi	125.05	35	2
Q15819|UB2V2_HUMAN	Ubiquitin-conjugating enzyme E2 variant 2	124.61	44	2
Q9ULZ3|ASC_HUMAN	Apoptosis-associated speck-like protein co	124.37	32	2
P04899|GNAI2_HUMAN	Guanine nucleotide-binding protein G(i) su	121.44	24	2
P61160|ARP2_HUMAN	Actin-related protein 2 OS=Homo sapiens	121.32	14	2
Q9Y6E0|STK24_HUMAN	Serine/threonine-protein kinase 24 OS=Ho	119.76	26	2
Q96C90|PP14B_HUMAN	Protein phosphatase 1 regulatory subunit 1	118.44	48	2
Q13155|AIMP2_HUMAN	Aminoacyl tRNA synthase complex-interac	116.73	33	2
Q9UHY1|NRBP_HUMAN	Nuclear receptor-binding protein OS=Hom	113.38	14	2
P62910|RL32_HUMAN	60S ribosomal protein L32 OS=Homo sapi	111.91	24	2
P61077|UB2D3_HUMAN	Ubiquitin-conjugating enzyme E2 D3 OS=H	109.06	35	2
Q9P287|BCCIP_HUMAN	BRCA2 and CDKN1A-interacting protein C	108.56	17	2
Q9BSD7|NTPCR_HUMAN	Cancer-related nucleoside-triphosphatase	108.32	45	2
Q9UJQ4|SALL4_HUMAN	Sal-like protein 4 OS=Homo sapiens GN=S	106.89	21	2
O14579|COPE_HUMAN	Coatomer subunit epsilon OS=Homo sapie	105.69	23	2
P09234|RU1C_HUMAN	U1 small nuclear ribonucleoprotein C OS=	105.67	19	2
P68402|PA1B2_HUMAN	Platelet-activating factor acetylhydrolase IB	104.35	17	2
P48739|PIPNB_HUMAN	Phosphatidylinositol transfer protein beta is	102.3	22	2
Q96IX5|USMG5_HUMAN	Up-regulated during skeletal muscle growth	101.49	45	2
Q9H6R4|NOL6_HUMAN	Nucleolar protein 6 OS=Homo sapiens GN	101.44	6	2
O43598|RCL_HUMAN	Deoxyribonucleoside 5'-monophosphate N	101.42	26	2
Q9BRG1|VPS25_HUMAN	Vacuolar protein-sorting-associated protein	101.28	14	2
Q8WXF1|PSPC1_HUMAN	Paraspeckle component 1 OS=Homo sapi	99.71	22	2
P67775|PP2AA_HUMAN	Serine/threonine-protein phosphatase 2A c	99.63	16	2
Q07021|C1QBP_HUMAN	Complement component 1 Q subcompone	98.8	15	2
Q99567|NUP88_HUMAN	Nuclear pore complex protein Nup88 OS=H	98.75	14	2
Q13177|PAK2_HUMAN	Serine/threonine-protein kinase PAK 2 OS	97.58	21	2
Q92922|SMRC1_HUMAN	SWI/SNF complex subunit SMARCC1 OS=	97.06	8	2
Q8NBT2|SPC24_HUMAN	Kinetochore protein Spc24 OS=Homo sapi	96.91	24	2
P15954|COX7C_HUMAN	Cytochrome c oxidase subunit 7C, mitocho	96.87	52	2
Q9BPX5|ARP5L_HUMAN	Actin-related protein 2/3 complex subunit 5	96.72	27	2
P47755|CAZA2_HUMAN	F-actin-capping protein subunit alpha-2 OS	96.54	20	2
Q9UIL1|SCOC_HUMAN	Short coiled-coil protein OS=Homo sapiens	96.47	32	2
P63151|2ABA_HUMAN	Serine/threonine-protein phosphatase 2A 5	95.89	24	2
Q5JWF2|GNAS1_HUMAN	Guanine nucleotide-binding protein G(s) su	95.78	9	2
Q9UJZ1|STML2_HUMAN	Stomatin-like protein 2 OS=Homo sapiens	94.74	23	2
O95989|NUDT3_HUMAN	Diphosphoinositol polyphosphate phospho	94.72	18	2
Q12904|AIMP1_HUMAN	Aminoacyl tRNA synthase complex-interac	94.7	15	2
Q8IUD2|RB6I2_HUMAN	ELKS/Rab6-interacting/CAST family memb	94.12	20	2
P04632|CPNS1_HUMAN	Calpain small subunit 1 OS=Homo sapiens	93.86	18	2
Q14766|LTBP1_HUMAN	Latent-transforming growth factor beta-bind	93.84	6	2

Q15631|TSN_HUMAN	Translin OS=Homo sapiens GN=TSN PE=	93.49	25	2
Q15397|K0020_HUMAN	Pumilio domain-containing protein KIAA00	93.09	18	2
Q3KQU3|MA7D1_HUMAN	MAP7 domain-containing protein 1 OS=Ho	92.59	15	2
Q8TEA8|DTD1_HUMAN	D-tyrosyl-tRNA(Tyr) deacylase 1 OS=Hom	90.6	25	2
P60953|CDC42_HUMAN	Cell division control protein 42 homolog OS	90.45	28	2
Q9UBI6|GBG12_HUMAN	Guanine nucleotide-binding protein G(I)/G(	90.45	36	2
Q9Y263|PLAP_HUMAN	Phospholipase A-2-activating protein OS=H	90.34	11	2
O75934|SPF27_HUMAN	Pre-mRNA-splicing factor SPF27 OS=Hom	89.59	18	2
P08195|4F2_HUMAN	4F2 cell-surface antigen heavy chain OS=H	89.5	8	2
P50281|MMP14_HUMAN	Matrix metalloproteinase-14 OS=Homo sap	89.06	10	2
P68400|CSK21_HUMAN	Casein kinase II subunit alpha OS=Homo s	88.78	19	2
Q02952|AKA12_HUMAN	A-kinase anchor protein 12 OS=Homo sap	88.6	11	2
O15042|SR140_HUMAN	U2 snRNP-associated SURP motif-contain	87.91	11	2
Q8NDC0|MISSL_HUMAN	MAPK-interacting and spindle-stabilizing p	87.78	12	2
P07919|QCR6_HUMAN	Cytochrome b-c1 complex subunit 6, mitoc	87.64	27	2
O00499|BIN1_HUMAN	Myc box-dependent-interacting protein 1 O	87.42	24	2
Q5TAP6|UT14C_HUMAN	U3 small nucleolar RNA-associated protein	87.38	10	2
Q15276|RABE1_HUMAN	Rab GTPase-binding effector protein 1 OS	86.97	9	2
Q04323|UBXN1_HUMAN	UBX domain-containing protein 1 OS=Hom	86.92	16	2
Q9NV35|NUD15_HUMAN	Probable 7,8-dihydro-8-oxoguanine triphos	86.9	13	2
O75152|ZC11A_HUMAN	Zinc finger CCCH domain-containing prote	86.73	10	2
Q9Y5A9|YTHD2_HUMAN	YTH domain family protein 2 OS=Homo sa	86.69	8	2
O75391|SPAG7_HUMAN	Sperm-associated antigen 7 OS=Homo sa	86.47	27	2
P09012|SNRPA_HUMAN	U1 small nuclear ribonucleoprotein A OS=	86.26	11	2
P42574|CASP3_HUMAN	Caspase-3 OS=Homo sapiens GN=CASP3	85.84	18	2
Q13011|ECH1_HUMAN	Delta(3,5)-Delta(2,4)-dienoyl-CoA isomeras	85.79	15	2
P00568|KAD1_HUMAN	Adenylate kinase isoenzyme 1 OS=Homo s	85.73	13	2
Q9Y520|PRC2C_HUMAN	Protein PRRC2C OS=Homo sapiens GN=P	85.45	7	2
Q9NR19|ACSA_HUMAN	Acetyl-coenzyme A synthetase, cytoplasmi	85.41	7	2
P21291|CSRP1_HUMAN	Cysteine and glycine-rich protein 1 OS=Ho	85.25	25	2
O60258|FGF17_HUMAN	Fibroblast growth factor 17 OS=Homo sapi	85.07	21	2
O75390|CISY_HUMAN	Citrate synthase, mitochondrial OS=Homo	84.95	14	2
Q9NR28|DBLOH_HUMAN	Diablo homolog, mitochondrial OS=Homo s	84.46	13	2
Q7Z2W4|ZCCHV_HUMAN	Zinc finger CCCH-type antiviral protein 1 O	83.81	4	2
Q9BUJ2|HNRL1_HUMAN	Heterogeneous nuclear ribonucleoprotein U	83.64	7	2
Q969V3|NCLN_HUMAN	Nicalin OS=Homo sapiens GN=NCLN PE=	83.57	13	2
Q14181|DPOA2_HUMAN	DNA polymerase alpha subunit B OS=Hom	83.52	9	2
Q13148|TADBP_HUMAN	TAR DNA-binding protein 43 OS=Homo sa	82.87	14	2
Q9UBT2|SAE2_HUMAN	SUMO-activating enzyme subunit 2 OS=H	82.82	14	2
O95218|ZRAB2_HUMAN	Zinc finger Ran-binding domain-containing	82.24	13	2
Q5SSJ5|HP1B3_HUMAN	Heterochromatin protein 1-binding protein	82.15	18	2
P09132|SRP19_HUMAN	Signal recognition particle 19 kDa protein	81.87	32	2
Q9NRF8|PYRG2_HUMAN	CTP synthase 2 OS=Homo sapiens GN=C	81.59	8	2
Q9Y3E1|HDGR3_HUMAN	Hepatoma-derived growth factor-related pr	81.54	18	2
O00233|PSMD9_HUMAN	26S proteasome non-ATPase regulatory s	81.3	13	2
P00390|GSHR_HUMAN	Glutathione reductase, mitochondrial OS=H	81.01	14	2
P62875|RPAB5_HUMAN	DNA-directed RNA polymerases I, II, and I	80.88	30	2

P61956|SUMO2_HUMAN	Small ubiquitin-related modifier 2 OS=Hom	80.85	43	2
Q9UJC3|HOOK1_HUMAN	Protein Hook homolog 1 OS=Homo sapien	80.74	8	2
Q9NVA2|SEP11_HUMAN	Septin-11 OS=Homo sapiens GN=SEPT11	80.42	13	2
Q15007|FL2D_HUMAN	Pre-mRNA-splicing regulator WTAP OS=H	80.32	18	2
O43290|SNUT1_HUMAN	U4/U6.U5 tri-snRNP-associated protein 1 (	80.28	15	2
P41227|NAA10_HUMAN	N-alpha-acetyltransferase 10, NatA catalyt	80.28	21	2
Q15126|PMVK_HUMAN	Phosphomevalonate kinase OS=Homo sap	80.19	20	2
A6NIZ1|RP1BL_HUMAN	Ras-related protein Rap-1b-like protein OS	79.86	22	2
P61224|RAP1B_HUMAN	Ras-related protein Rap-1b OS=Homo sap	79.86	17	2
P62834|RAP1A_HUMAN	Ras-related protein Rap-1A OS=Homo sap	79.86	8	2
P56134|ATPK_HUMAN	ATP synthase subunit f, mitochondrial OS=	79.85	26	2
Q7Z739|YTHD3_HUMAN	YTH domain family protein 3 OS=Homo sa	79.7	7	2
Q9UBW8|CSN7A_HUMAN	COP9 signalosome complex subunit 7a OS	79.56	17	2
P51571|SSRD_HUMAN	Translocon-associated protein subunit delt	79.5	23	2
Q15363|TMED2_HUMAN	Transmembrane emp24 domain-containing	79.08	9	2
Q9P2I0|CPSF2_HUMAN	Cleavage and polyadenylation specificity fa	79	13	2
Q9H3R5|CENPH_HUMAN	Centromere protein H OS=Homo sapiens (	78.83	17	2
O95793|STAU1_HUMAN	Double-stranded RNA-binding protein Stau	78.65	6	2
Q93034|CUL5_HUMAN	Cullin-5 OS=Homo sapiens GN=CUL5 PE=	78.64	12	2
Q13464|ROCK1_HUMAN	Rho-associated protein kinase 1 OS=Hom	77.86	5	2
Q16706|MA2A1_HUMAN	Alpha-mannosidase 2 OS=Homo sapiens (	77.77	4	2
Q14738|2A5D_HUMAN	Serine/threonine-protein phosphatase 2A 5	77.77	11	2
P55263|ADK_HUMAN	Adenosine kinase OS=Homo sapiens GN=	77.29	9	2
P18065|IBP2_HUMAN	Insulin-like growth factor-binding protein 2	77.23	27	2
P62310|LSM3_HUMAN	U6 snRNA-associated Sm-like protein LSm	77.04	34	2
O60885|BRD4_HUMAN	Bromodomain-containing protein 4 OS=Ho	76.79	9	2
P55039|DRG2_HUMAN	Developmentally-regulated GTP-binding pr	76.74	20	2
P31483|TIA1_HUMAN	Nucleolysin TIA-1 isoform p40 OS=Homo s	76.61	9	2
Q9P0K7|RAI14_HUMAN	Ankycorbin OS=Homo sapiens GN=RAI14	76.54	9	2
Q9NQG5|RPR1B_HUMAN	Regulation of nuclear pre-mRNA domain-c	76.47	23	2
O75190|DNJB6_HUMAN	DnaJ homolog subfamily B member 6 OS=	76.03	8	2
Q86YP4|P66A_HUMAN	Transcriptional repressor p66-alpha OS=H	75.65	12	2
P67870|CSK2B_HUMAN	Casein kinase II subunit beta OS=Homo sa	75.58	13	2
Q9H223|EHD4_HUMAN	EH domain-containing protein 4 OS=Homo	75.44	9	2
Q9UJC5|SH3L2_HUMAN	SH3 domain-binding glutamic acid-rich-like	75.06	25	2
O60346|PHLP1_HUMAN	PH domain leucine-rich repeat-containing p	74.43	9	2
Q9NR45|SIAS_HUMAN	Sialic acid synthase OS=Homo sapiens GN	74.15	15	2
Q9BV57|MTND_HUMAN	1,2-dihydroxy-3-keto-5-methylthiopentene	74.05	15	2
Q9NUP9|LIN7C_HUMAN	Protein lin-7 homolog C OS=Homo sapiens	74.02	36	2
O43678|NDUA2_HUMAN	NADH dehydrogenase [ubiquinone] 1 alph	73.91	32	2
P60510|PP4C_HUMAN	Serine/threonine-protein phosphatase 4 ca	73.7	16	2
Q01780|EXOSX_HUMAN	Exosome component 10 OS=Homo sapien	73.54	6	2
Q9Y5S9|RBM8A_HUMAN	RNA-binding protein 8A OS=Homo sapiens	72.87	25	2
Q12765|SCRN1_HUMAN	Secernin-1 OS=Homo sapiens GN=SCRN	72.58	7	2
Q9UNF1|MAGD2_HUMAN	Melanoma-associated antigen D2 OS=Hon	72.46	11	2
Q00796|DHSO_HUMAN	Sorbitol dehydrogenase OS=Homo sapien	72.11	15	2
Q99829|CPNE1_HUMAN	Copine-1 OS=Homo sapiens GN=CPNE1	71.96	12	2

O95456|PSMG1_HUMAN	Proteasome assembly chaperone 1 OS=H	71.94	20	2
P30837|AL1B1_HUMAN	Aldehyde dehydrogenase X, mitochondrial	71.86	7	2
Q08257|QOR_HUMAN	Quinone oxidoreductase OS=Homo sapien	71.79	17	2
Q9NQ88|TIGAR_HUMAN	Probable fructose-2,6-bisphosphatase TIG	71.65	7	2
Q9HCD5|NCOA5_HUMAN	Nuclear receptor coactivator 5 OS=Homo s	71.43	7	2
Q9C0C2|TB182_HUMAN	182 kDa tankyrase-1-binding protein OS=H	71.43	9	2
Q96QK1|VPS35_HUMAN	Vacuolar protein sorting-associated protein	71.43	10	2
O60613|SEP15_HUMAN	15 kDa selenoprotein OS=Homo sapiens (	71.28	23	2
O00754|MA2B1_HUMAN	Lysosomal alpha-mannosidase OS=Homo	70.84	4	2
O75937|DNJC8_HUMAN	DnaJ homolog subfamily C member 8 OS=	70.81	20	2
Q13867|BLMH_HUMAN	Bleomycin hydrolase OS=Homo sapiens G	70.58	15	2
Q92979|NEP1_HUMAN	Ribosomal RNA small subunit methyltransf	70.53	17	2
P22307|NLTP_HUMAN	Non-specific lipid-transfer protein OS=Hom	69.7	9	2
Q16718|NDUA5_HUMAN	NADH dehydrogenase [ubiquinone] 1 alph	69.22	38	2
P55036|PSMD4_HUMAN	26S proteasome non-ATPase regulatory s	69.05	15	2
Q71RC2|LARP4_HUMAN	La-related protein 4 OS=Homo sapiens GN	68.92	5	2
Q9Y6M9|NDUB9_HUMAN	NADH dehydrogenase [ubiquinone] 1 beta	68.86	13	2
Q9BW83|IFT27_HUMAN	Intraflagellar transport protein 27 homolog	68.69	13	2
Q99661|KIF2C_HUMAN	Kinesin-like protein KIF2C OS=Homo sapi	68.2	6	2
Q02818|NUCB1_HUMAN	Nucleobindin-1 OS=Homo sapiens GN=NU	68.14	13	2
P52292|IMA2_HUMAN	Importin subunit alpha-2 OS=Homo sapien	67.93	8	2
Q9NUQ6|SPS2L_HUMAN	SPATS2-like protein OS=Homo sapiens G	67.55	6	2
Q9H4A6|GOLP3_HUMAN	Golgi phosphoprotein 3 OS=Homo sapiens	67.46	13	2
Q9UHX1|PUF60_HUMAN	Poly(U)-binding-splicing factor PUF60 OS=	67.43	24	2
Q9H074|PAIP1_HUMAN	Polyadenylate-binding protein-interacting p	67.38	10	2
Q9ULV4|COR1C_HUMAN	Coronin-1C OS=Homo sapiens GN=CORO	67.35	12	2
O00471|EXOC5_HUMAN	Exocyst complex component 5 OS=Homo	67.21	3	2
Q9NPJ6|MED4_HUMAN	Mediator of RNA polymerase II transcriptio	67.18	22	2
Q14155|ARHG7_HUMAN	Rho guanine nucleotide exchange factor 7	67.04	9	2
P42704|LPPRC_HUMAN	Leucine-rich PPR motif-containing protein,	67	10	2
O95232|LC7L3_HUMAN	Luc7-like protein 3 OS=Homo sapiens GN=	66.75	8	2
Q9NR31|SAR1A_HUMAN	GTP-binding protein SAR1a OS=Homo sa	66.74	21	2
Q9Y6B6|SAR1B_HUMAN	GTP-binding protein SAR1b OS=Homo sa	66.74	17	2
Q13596|SNX1_HUMAN	Sorting nexin-1 OS=Homo sapiens GN=SN	66.53	11	2
Q96MW1|CCD43_HUMAN	Coiled-coil domain-containing protein 43 O	66.27	18	2
Q9Y2R0|CCD56_HUMAN	Coiled-coil domain-containing protein 56 O	65.91	21	2
Q9P0V9|SEP10_HUMAN	Septin-10 OS=Homo sapiens GN=SEPT10	65.67	7	2
Q8WVB6|CTF18_HUMAN	Chromosome transmission fidelity protein 1	65.6	8	2
P12955|PEPD_HUMAN	Xaa-Pro dipeptidase OS=Homo sapiens G	65.51	4	2
Q12849|GRSF1_HUMAN	G-rich sequence factor 1 OS=Homo sapien	65.37	13	2
Q13492|PICAL_HUMAN	Phosphatidylinositol-binding clathrin assem	65.24	10	2
Q96C01|F136A_HUMAN	Protein FAM136A OS=Homo sapiens GN=	64.59	14	2
Q9BU89|DOHH_HUMAN	Deoxyhypusine hydroxylase OS=Homo sa	64.54	14	2
Q9NX63|CHCH3_HUMAN	Coiled-coil-helix-coiled-coil-helix domain-c	64.42	21	2
O14929|HAT1_HUMAN	Histone acetyltransferase type B catalytic s	64.35	13	2
Q03426|KIME_HUMAN	Mevalonate kinase OS=Homo sapiens GN	64.12	7	2
P08473|NEP_HUMAN	Neprilysin OS=Homo sapiens GN=MME P	64.01	3	2

Q15750|TAB1_HUMAN	TGF-beta-activated kinase 1 and MAP3K7	63.83	7	2
P62070|RRAS2_HUMAN	Ras-related protein R-Ras2 OS=Homo sap	63.79	18	2
P61960|UFM1_HUMAN	Ubiquitin-fold modifier 1 OS=Homo sapien	63.63	35	2
P49755|TMEDA_HUMAN	Transmembrane emp24 domain-containing	63.6	13	2
Q12841|FSTL1_HUMAN	Follistatin-related protein 1 OS=Homo sapi	63.48	7	2
Q13153|PAK1_HUMAN	Serine/threonine-protein kinase PAK 1 OS	63.03	14	2
Q08379|GOGA2_HUMAN	Golgin subfamily A member 2 OS=Homo s	62.85	6	2
Q13564|ULA1_HUMAN	NEDD8-activating enzyme E1 regulatory su	62.68	6	2
P19525|E2AK2_HUMAN	Interferon-induced, double-stranded RNA-a	62.6	5	2
P54886|P5CS_HUMAN	Delta-1-pyrroline-5-carboxylate synthase O	62.58	9	2
Q9NX40|OCAD1_HUMAN	OCIA domain-containing protein 1 OS=Hor	61.98	11	2
Q8N983|RM43_HUMAN	39S ribosomal protein L43, mitochondrial O	61.98	20	2
P32322|P5CR1_HUMAN	Pyrroline-5-carboxylate reductase 1, mitoch	61.29	14	2
P51003|PAPOA_HUMAN	Poly(A) polymerase alpha OS=Homo sapie	60.84	7	2
Q9NRJ5|PAPOB_HUMAN	Poly(A) polymerase beta OS=Homo sapien	60.84	6	2
Q07960|RHG01_HUMAN	Rho GTPase-activating protein 1 OS=Hom	60.52	12	2
Q13428|TCOF_HUMAN	Treacle protein OS=Homo sapiens GN=TC	60.45	7	2
Q8IZ83|A16A1_HUMAN	Aldehyde dehydrogenase family 16 membe	60.3	8	2
P56537|IF6_HUMAN	Eukaryotic translation initiation factor 6 OS	60.12	18	2
P21281|VATB2_HUMAN	V-type proton ATPase subunit B, brain isof	59.64	12	2
Q96P48|ARAP1_HUMAN	Arf-GAP with Rho-GAP domain, ANK repe	59.42	6	2
Q9NX58|LYAR_HUMAN	Cell growth-regulating nucleolar protein OS	59.29	13	2
O00217|NDUS8_HUMAN	NADH dehydrogenase [ubiquinone] iron-su	58.56	13	2
P46060|RAGP1_HUMAN	Ran GTPase-activating protein 1 OS=Hom	58.21	16	2
Q9BXF3|CECR2_HUMAN	Cat eye syndrome critical region protein 2 O	58	5	2
A6NHR9|SMHD1_HUMAN	Structural maintenance of chromosomes fl	57.73	5	2
Q96RE7|NACC1_HUMAN	Nucleus accumbens-associated protein 1 O	57.73	7	2
Q9BRP1|PDD2L_HUMAN	Programmed cell death protein 2-like OS=H	57.11	12	2
Q14498|RBM39_HUMAN	RNA-binding protein 39 OS=Homo sapiens	56.94	6	2
Q05519|SRS11_HUMAN	Serine/arginine-rich splicing factor 11 OS=	56.7	15	2
P19404|NDUV2_HUMAN	NADH dehydrogenase [ubiquinone] flavopr	56.23	17	2
O75251|NDUS7_HUMAN	NADH dehydrogenase [ubiquinone] iron-su	56.15	8	2
Q9BZL1|UBL5_HUMAN	Ubiquitin-like protein 5 OS=Homo sapiens	55.86	25	2
Q00059|TFAM_HUMAN	Transcription factor A, mitochondrial OS=H	55.73	16	2
P35612|ADDB_HUMAN	Beta-adducin OS=Homo sapiens GN=ADD	54.77	15	2
Q9Y5K5|UCHL5_HUMAN	Ubiquitin carboxyl-terminal hydrolase isozy	54.46	8	2
Q9UPT5|EXOC7_HUMAN	Exocyst complex component 7 OS=Homo	54.28	4	2
P19387|RPB3_HUMAN	DNA-directed RNA polymerase II subunit R	54.09	12	2
P60468|SC61B_HUMAN	Protein transport protein Sec61 subunit be	53.55	36	2
O00479|HMGN4_HUMAN	High mobility group nucleosome-binding do	53.51	33	2
P45880|VDAC2_HUMAN	Voltage-dependent anion-selective channe	53.49	7	2
Q9UHY7|ENOPH_HUMAN	Enolase-phosphatase E1 OS=Homo sapie	53.36	13	2
P46939|UTRO_HUMAN	Utrophin OS=Homo sapiens GN=UTRN PE	53.05	4	2
Q86X76|NIT1_HUMAN	Nitrilase homolog 1 OS=Homo sapiens GN	52.26	14	2
Q92520|FAM3C_HUMAN	Protein FAM3C OS=Homo sapiens GN=FA	51.99	15	2
P21912|DHSB_HUMAN	Succinate dehydrogenase [ubiquinone] iro	51.74	7	2
P20936|RASA1_HUMAN	Ras GTPase-activating protein 1 OS=Hom	51.56	4	2

Q9H3S7|PTN23_HUMAN	Tyrosine-protein phosphatase non-recepto	51.35	5	2
P52732|KIF11_HUMAN	Kinesin-like protein KIF11 OS=Homo sapie	51.09	4	2
Q9H4B8|DPEP3_HUMAN	Dipeptidase 3 OS=Homo sapiens GN=DPE	50.87	7	2
Q9NYJ1|CHCH8_HUMAN	Coiled-coil-helix-coiled-coil-helix domain-co	50.55	48	2
Q15545|TAF7_HUMAN	Transcription initiation factor TFIID subunit	50.54	9	2
P35968|VGFR2_HUMAN	Vascular endothelial growth factor recepto	50.16	3	2
Q96A26|F162A_HUMAN	Protein FAM162A OS=Homo sapiens GN=	49.71	20	2
P61513|RL37A_HUMAN	60S ribosomal protein L37a OS=Homo sap	49.06	39	2
Q9Y530|CF130_HUMAN	Uncharacterized protein C6orf130 OS=Hor	48.84	21	2
Q14690|RRP5_HUMAN	Protein RRP5 homolog OS=Homo sapiens	48.67	3	2
Q9UIJ7|KAD3_HUMAN	GTP:AMP phosphotransferase, mitochond	48.44	19	2
Q9Y2W2|WBP11_HUMAN	WW domain-binding protein 11 OS=Homo	48.14	4	2
Q7L4E1|FA73B_HUMAN	Protein FAM73B OS=Homo sapiens GN=F	47.7	5	2
Q13416|ORC2_HUMAN	Origin recognition complex subunit 2 OS=H	47.54	7	2
Q15388|TOM20_HUMAN	Mitochondrial import receptor subunit TOM	47.43	24	2
P49792|RBP2_HUMAN	E3 SUMO-protein ligase RanBP2 OS=Hom	47.42	6	2
P20585|MSH3_HUMAN	DNA mismatch repair protein Msh3 OS=Ho	47.22	10	2
O94906|PRP6_HUMAN	Pre-mRNA-processing factor 6 OS=Homo	47.09	8	2
P46013|KI67_HUMAN	Antigen KI-67 OS=Homo sapiens GN=MKI	46.36	5	2
O15144|ARPC2_HUMAN	Actin-related protein 2/3 complex subunit 2	46.29	22	2
P46821|MAP1B_HUMAN	Microtubule-associated protein 1B OS=Ho	45.98	3	2
Q9Y6A5|TACC3_HUMAN	Transforming acidic coiled-coil-containing p	45.75	6	2
Q9UPG8|PLAL2_HUMAN	Zinc finger protein PLAGL2 OS=Homo sap	45.47	3	2
Q9UK45|LSM7_HUMAN	U6 snRNA-associated Sm-like protein LSm	44.9	22	2
Q9Y2R5|RT17_HUMAN	28S ribosomal protein S17, mitochondrial (	44.81	20	2
P43490|NAMPT_HUMAN	Nicotinamide phosphoribosyltransferase O	43.41	12	2
Q9NY12|GAR1_HUMAN	H/ACA ribonucleoprotein complex subunit	42.8	20	2
Q9Y4F1|FARP1_HUMAN	FERM, RhoGEF and pleckstrin domain-cor	42.61	5	2
P49207|RL34_HUMAN	60S ribosomal protein L34 OS=Homo sapi	42.29	13	2
Q9P2P6|STAR9_HUMAN	StAR-related lipid transfer protein 9 OS=H	42.21	4	2
O95139|NDUB6_HUMAN	NADH dehydrogenase [ubiquinone] 1 beta	41.56	21	2
O00562|PITM1_HUMAN	Membrane-associated phosphatidylinositol	41.45	5	2
O75155|CAND2_HUMAN	Cullin-associated NEDD8-dissociated prote	41	7	2
P82933|RT09_HUMAN	28S ribosomal protein S9, mitochondrial O	39.74	8	2
A8MVX0|ARG33_HUMAN	Rho guanine nucleotide exchange factor 3	39.66	7	2
P60891|PRPS1_HUMAN	Ribose-phosphate pyrophosphokinase 1 C	38.75	9	2
P11908|PRPS2_HUMAN	Ribose-phosphate pyrophosphokinase 2 C	38.75	9	2
P20929|NEBU_HUMAN	Nebulin OS=Homo sapiens GN=NEB PE=	38.67	2	2
Q8NHP8|PLBL2_HUMAN	Putative phospholipase B-like 2 OS=Homo	38.66	13	2
P61599|NAA20_HUMAN	N-alpha-acetyltransferase 20, NatB catalyt	38.53	20	2
Q9Y618|NCOR2_HUMAN	Nuclear receptor corepressor 2 OS=Homo	38.36	3	2
Q8NF91|SYNE1_HUMAN	Nesprin-1 OS=Homo sapiens GN=SYNE1	38.27	6	2
Q92833|JARD2_HUMAN	Protein Jumonji OS=Homo sapiens GN=JA	37.86	7	2
P20930|FILA_HUMAN	Filaggrin OS=Homo sapiens GN=FLG PE=	37.59	2	2
Q6Q759|SPG17_HUMAN	Sperm-associated antigen 17 OS=Homo s	37.51	3	2
Q0VF96|CGNL1_HUMAN	Cingulin-like protein 1 OS=Homo sapiens (	37.38	8	2
Q99541|PLIN2_HUMAN	Perilipin-2 OS=Homo sapiens GN=PLIN2 F	36.46	14	2

Q8IWZ3|ANKH1_HUMAN	Ankyrin repeat and KH domain-containing	36.02	5	2
Q9NRV9|HEBP1_HUMAN	Heme-binding protein 1 OS=Homo sapiens	35.77	11	2
Q15027|ACAP1_HUMAN	Arf-GAP with coiled-coil, ANK repeat and P	35.73	5	2
Q5JPE7|NOMO2_HUMAN	Nodal modulator 2 OS=Homo sapiens GN=	35.63	3	2
O60488|ACSL4_HUMAN	Long-chain-fatty-acid--CoA ligase 4 OS=H	35.57	8	2
O95613|PCNT_HUMAN	Pericentrin OS=Homo sapiens GN=PCNT	35.1	3	2
O43157|PLXB1_HUMAN	Plexin-B1 OS=Homo sapiens GN=PLXNB1	34.97	4	2
O00555|CAC1A_HUMAN	Voltage-dependent P/Q-type calcium chan	33.97	3	2
Q9Y566|SHAN1_HUMAN	SH3 and multiple ankyrin repeat domains p	33.87	4	2
Q9H2Z4|NKX24_HUMAN	Homeobox protein Nkx-2.4 OS=Homo sap	32.67	8	2
Q702N8|XIRP1_HUMAN	Xin actin-binding repeat-containing protein	32.65	3	2
Q92630|DYRK2_HUMAN	Dual specificity tyrosine-phosphorylation-re	32.04	4	2
O95935|TBX18_HUMAN	T-box transcription factor TBX18 OS=Hom	31.95	5	2
Q13490|BIRC2_HUMAN	Baculoviral IAP repeat-containing protein 2	31.77	7	2
O14802|RPC1_HUMAN	DNA-directed RNA polymerase III subunit	31.77	4	2
Q7Z3I7|ZN572_HUMAN	Zinc finger protein 572 OS=Homo sapiens	31.45	4	2
Q7L2E3|DHX30_HUMAN	Putative ATP-dependent RNA helicase DH	31.4	8	2
Q9NRS4|TMPS4_HUMAN	Transmembrane protease serine 4 OS=Ho	31.25	8	2
P31689|DNJA1_HUMAN	DnaJ homolog subfamily A member 1 OS=	30.78	13	2
Q9UJU5|FOXD3_HUMAN	Forkhead box protein D3 OS=Homo sapie	30.14	10	2
Q15543|TAF13_HUMAN	Transcription initiation factor TFIID subunit	29.7	22	2
Q8N9L9|ACOT4_HUMAN	Acyl-coenzyme A thioesterase 4 OS=Hom	29.08	5	2
Q13206|DDX10_HUMAN	Probable ATP-dependent RNA helicase DI	28.86	7	2
Q5JRC9|FA47A_HUMAN	Protein FAM47A OS=Homo sapiens GN=F	28.76	4	2
Q9NYF0|DACT1_HUMAN	Dapper homolog 1 OS=Homo sapiens GN=	28.41	6	2
Q8N302|AGGF1_HUMAN	Angiogenic factor with G patch and FHA d	28.11	5	2
Q9Y485|DMXL1_HUMAN	DmX-like protein 1 OS=Homo sapiens GN=	28.08	2	2
Q6ZQQ6|WDR87_HUMAN	WD repeat-containing protein 87 OS=Hom	27.55	5	2
Q96A46|MFRN2_HUMAN	Mitoferrin-2 OS=Homo sapiens GN=SLC25	27.52	11	2
Q9C0G0|ZN407_HUMAN	Zinc finger protein 407 OS=Homo sapiens	27.46	4	2
Q96M20|CT152_HUMAN	Uncharacterized protein C20orf152 OS=H	26.88	6	2
Q9NRL3|STRN4_HUMAN	Striatin-4 OS=Homo sapiens GN=STRN4 P	26.4	6	2
Q96PK2|MACF4_HUMAN	Microtubule-actin cross-linking factor 1, iso	26.39	6	2
Q92616|GCN1L_HUMAN	Translational activator GCN1 OS=Homo sa	25.57	5	2

Table A1.12 H9 hESC Extracellular and Cell Surface Protein Identifications. List of all proteins identified in CMTX from H9 hESCs that are classified as ‘extracellular’ or ‘cell surface’ by cellular component gene ontology. Corresponding accession, description, unique peptide numbers are shown.

UniProt ID	Name	# Unique Peptides
P18206	Vinculin	46
P21333	Filamin-A	32
P02649	Apolipoprotein E	28
P04075	Fructose-bisphosphate aldolase A	20
P23142	Fibulin-1	18
P62805	Histone H4	18
P07355	Annexin A2	17
P11021	78 kDa glucose-regulated protein	15
P12814	Alpha-actinin-1	15
Q92626	Peroxidasin homolog	14
P62937	Peptidyl-prolyl cis-trans isomerase A	13
P11142	Heat shock cognate 71 kDa protein	12
P10909	Clusterin	12
P05067	Amyloid beta A4 protein	11
P04792	Heat shock protein beta-1	9
Q9Y490	Talin-1	9
P11047	Laminin subunit gamma-1	9
P25391	Laminin subunit alpha-1	9
P07942	Laminin subunit beta-1	8
O43707	Alpha-actinin-4	8
Q92598	Heat shock protein 105 kDa	8
P02751	Fibronectin	7
P54577	Tyrosyl-tRNA synthetase, cytoplasmic	7
P09486	SPARC	7
P10809	60 kDa heat shock protein, mitochondrial	6
P67809	Nuclease-sensitive element-binding protein 1	6
P84243	Histone H3.3	6
P68431	Histone H3.1	6
Q71DI3	Histone H3.2	6
P09429	High mobility group protein B1	5
Q8N474	Secreted frizzled-related protein 1	5
P50395	Rab GDP dissociation inhibitor beta	5
P08195	4F2 cell-surface antigen heavy chain	5
P06744	Glucose-6-phosphate isomerase	5
P98160	Basement membrane-specific heparan sulfate proteoglycan c	5
P39060	Collagen alpha-1(XVIII) chain	5
P62158	Calmodulin	4
P98095	Fibulin-2	4
Q12904	Aminoacyl tRNA synthase complex-interacting multifunctional	4
P07339	Cathepsin D	4
P27797	Calreticulin	4
P11717	Cation-independent mannose-6-phosphate receptor	3
O75487	Glypican-4	3
P23352	Anosmin-1	3
P07093	Glia-derived nexin	3
P29279	Connective tissue growth factor	3
O75610	Left-right determination factor 1	3
P52907	F-actin-capping protein subunit alpha-1	3
P51858	Hepatoma-derived growth factor	3
P38159	Heterogeneous nuclear ribonucleoprotein G	3
Q92820	Gamma-glutamyl hydrolase	3
O43852	Calumenin	3
Q8WZ42	Titin	3
P12109	Collagen alpha-1(VI) chain	3

P07237	Protein disulfide-isomerase	2
P14174	Macrophage migration inhibitory factor	2
O00264	Membrane-associated progesterone receptor component 1	2
P06576	ATP synthase subunit beta, mitochondrial	2
P54578	Ubiquitin carboxyl-terminal hydrolase 14	2
O15078	Centrosomal protein of 290 kDa	2
Q15046	Lysyl-tRNA synthetase	2
Q00341	Vigilin	2
Q96HF1	Secreted frizzled-related protein 2	2
Q9BYX7	Putative beta-actin-like protein 3	2
O00292	Left-right determination factor 2	2
P50453	Serpin B9	2
P21741	Midkine	2
P53621	Coatomer subunit alpha	2
P18065	Insulin-like growth factor-binding protein 2	2
Q96S86	Hyaluronan and proteoglycan link protein 3	2
P02768	Serum albumin	2

Table A1.13 CA1 hESC Extracellular and Cell Surface Protein Identifications. List of all proteins identified in CMTX from CA1 hESCs that are classified as ‘extracellular’ or ‘cell surface’ by cellular component gene ontology. Corresponding accession, description, unique peptide numbers are shown.

UniProt ID	Name	# Unique Peptides
P21333	Filamin-A	72
P18206	Vinculin	51
P04075	Fructose-bisphosphate aldolase A	33
P07355	Annexin A2	33
P12814	Alpha-actinin-1	28
P11142	Heat shock cognate 71 kDa protein	27
P10809	60 kDa heat shock protein, mitochondrial	26
P62805	Histone H4	26
O43707	Alpha-actinin-4	24
Q9Y490	Talin-1	23
P62937	Peptidyl-prolyl cis-trans isomerase A	23
P02649	Apolipoprotein E	22
P06576	ATP synthase subunit beta, mitochondrial	19
P84243	Histone H3.3	18
P11021	78 kDa glucose-regulated protein	17
P50395	Rab GDP dissociation inhibitor beta	16
P04792	Heat shock protein beta-1	16
P06744	Glucose-6-phosphate isomerase	15
P00441	Superoxide dismutase [Cu-Zn]	13
P54577	Tyrosyl-tRNA synthetase, cytoplasmic	13
P50453	Serpin B9	12
P62328	Thymosin beta-4	12
P62158	Calmodulin	11
P07093	Glia-derived nexin	11
Q92598	Heat shock protein 105 kDa	11
P07237	Protein disulfide-isomerase	10
Q9Y696	Chloride intracellular channel protein 4	10
Q00839	Heterogeneous nuclear ribonucleoprotein U	10
P31947	14-3-3 protein sigma	10
P09429	High mobility group protein B1	9
P38646	Stress-70 protein, mitochondrial	9
P09382	Galectin-1	9
P10909	Clusterin	8
P05067	Amyloid beta A4 protein	7
P02751	Fibronectin	7
P07602	Proactivator polypeptide	7
P27797	Calreticulin	7
P52907	F-actin-capping protein subunit alpha-1	7
Q92626	Peroxidasin homolog	7
Q12904	Aminoacyl tRNA synthase complex-interacting multifunctional p	7
P55145	Mesencephalic astrocyte-derived neurotrophic factor	7
P14174	Macrophage migration inhibitory factor	6
P54578	Ubiquitin carboxyl-terminal hydrolase 14	6
P07942	Laminin subunit beta-1	6
P13693	Translationally-controlled tumor protein	6
P07339	Cathepsin D	6
Q8WZ42	Titin	6
P14735	Insulin-degrading enzyme	5
Q15046	Lysyl-tRNA synthetase	5
Q00341	Vigilin	5
P10599	Thioredoxin	5
Q9BRX8	Redox-regulatory protein PAMM	5
P23142	Fibulin-1	5
O75083	WD repeat-containing protein 1	5

P48061	Stromal cell-derived factor 1	5
O00264	Membrane-associated progesterone receptor component 1	4
P29279	Connective tissue growth factor	4
P02452	Collagen alpha-1(I) chain	4
P26583	High mobility group protein B2	4
P38159	Heterogeneous nuclear ribonucleoprotein G	4
P13489	Ribonuclease inhibitor	4
Q99584	Protein S100-A13	4
P67809	Nuclease-sensitive element-binding protein 1	4
P15121	Aldose reductase	4
Q92520	Protein FAM3C	4
Q99988	Growth/differentiation factor 15	4
P05556	Integrin beta-1	3
P47755	F-actin-capping protein subunit alpha-2	3
P11047	Laminin subunit gamma-1	3
Q9UQE7	Structural maintenance of chromosomes protein 3	3
Q00796	Sorbitol dehydrogenase	3
P98095	Fibulin-2	3
Q9NRV9	Heme-binding protein 1	3
Q969H8	UPF0556 protein C19orf10	3
Q8NCW5	Apolipoprotein A-I-binding protein	3
O00622	Protein CYR61	3
P51858	Hepatoma-derived growth factor	3
P21741	Midkine	3
O15230	Laminin subunit alpha-5	3
Q32P28	Prolyl 3-hydroxylase 1	3
P39060	Collagen alpha-1(XVIII) chain	3
Q12841	Follistatin-related protein 1	3
P24043	Laminin subunit alpha-2	3
P11233	Ras-related protein Ral-A	2
O75145	Liprin-alpha-3	2
Q96HF1	Secreted frizzled-related protein 2	2
P08123	Collagen alpha-2(I) chain	2
O00292	Left-right determination factor 2	2
Q9H4G4	Golgi-associated plant pathogenesis-related protein 1	2
O43852	Calumenin	2
O95813	Cerberus	2
P09486	SPARC	2
P25391	Laminin subunit alpha-1	2
P18065	Insulin-like growth factor-binding protein 2	2
O75718	Cartilage-associated protein	2
P61916	Epididymal secretory protein E1	2
Q86UW8	Hyaluronan and proteoglycan link protein 4	2
P09038	Heparin-binding growth factor 2	2
Q7Z5P9	Mucin-19	2
Q17RW2	Collagen alpha-1(XXIV) chain	2

Table A1.14 BJ-1D hiPSC Extracellular and Cell Surface Protein Identifications. List of all proteins identified in CMTX from BJ-1D hiPSCs that are classified as ‘extracellular’ or ‘cell surface’ by cellular component gene ontology. Corresponding accession, description, unique peptide numbers are shown.

Uniprot ID	Name	# Unique Peptides
P18206	Vinculin	88
P21333	Filamin-A	83
P04075	Fructose-bisphosphate aldolase A	40
P62805	Histone H4	33
P12814	Alpha-actinin-1	31
P07355	Annexin A2	30
P50395	Rab GDP dissociation inhibitor beta	29
P62937	Peptidyl-prolyl cis-trans isomerase A	28
P62328	Thymosin beta-4	26
O43707	Alpha-actinin-4	25
P62158	Calmodulin	24
P10809	60 kDa heat shock protein, mitochondrial	23
P11142	Heat shock cognate 71 kDa protein	23
P11021	78 kDa glucose-regulated protein	23
Q00839	Heterogeneous nuclear ribonucleoprotein U	22
P06744	Glucose-6-phosphate isomerase	21
Q9UQE7	Structural maintenance of chromosomes protein 3	21
P07237	Protein disulfide-isomerase	19
P05556	Integrin beta-1	16
P10599	Thioredoxin	15
P02649	Apolipoprotein E	15
P10909	Clusterin	15
P11717	Cation-independent mannose-6-phosphate receptor	14
Q92626	Peroxidasin homolog	13
P14174	Macrophage migration inhibitory factor	13
Q00341	Vigilin	12
P53621	Coatomer subunit alpha	12
P23142	Fibulin-1	12
P54577	Tyrosyl-tRNA synthetase, cytoplasmic	12
P00441	Superoxide dismutase [Cu-Zn]	11
P13693	Translationally-controlled tumor protein	11
P38646	Stress-70 protein, mitochondrial	11
P07093	Glia-derived nexin	10
P07339	Cathepsin D	10
P04792	Heat shock protein beta-1	10
P50453	Serpin B9	9
P27797	Calreticulin	8
P02751	Fibronectin	8
P09429	High mobility group protein B1	8
Q9Y696	Chloride intracellular channel protein 4	8
Q15046	Lysyl-tRNA synthetase	7
Q92598	Heat shock protein 105 kDa	7
P48061	Stromal cell-derived factor 1	7
P40222	Alpha-taxilin	7
P54578	Ubiquitin carboxyl-terminal hydrolase 14	7
P67809	Nuclease-sensitive element-binding protein 1	6
P15121	Aldose reductase	6
P55145	Mesencephalic astrocyte-derived neurotrophic factor	6
P22413	Ectonucleotide pyrophosphatase/phosphodiesterase family member	6
Q8N474	Secreted frizzled-related protein 1	6
P06576	ATP synthase subunit beta, mitochondrial	6
P98160	Basement membrane-specific heparan sulfate proteoglycan core pr	5
P31947	14-3-3 protein sigma	5
P26583	High mobility group protein B2	5

P38159	Heterogeneous nuclear ribonucleoprotein G	5
P61916	Epididymal secretory protein E1	5
P05067	Amyloid beta A4 protein	5
P51858	Hepatoma-derived growth factor	4
P52907	F-actin-capping protein subunit alpha-1	4
O00622	Protein CYR61	4
Q99584	Protein S100-A13	4
P09382	Galectin-1	4
Q32P28	Prolyl 3-hydroxylase 1	4
Q969H8	UPF0556 protein C19orf10	4
Q8WZ42	Titin	4
P14735	Insulin-degrading enzyme	4
P51511	Matrix metalloproteinase-15	3
O00292	Left-right determination factor 2	3
O43278	Kunitz-type protease inhibitor 1	3
P13489	Ribonuclease inhibitor	3
P11047	Laminin subunit gamma-1	3
Q8NCW5	Apolipoprotein A-I-binding protein	3
Q92485	Acid sphingomyelinase-like phosphodiesterase 3b	3
P25391	Laminin subunit alpha-1	3
O00264	Membrane-associated progesterone receptor component 1	3
O75330	Hyaluronan mediated motility receptor	3
Q9UII2	ATPase inhibitor, mitochondrial	3
P50281	Matrix metalloproteinase-14	2
Q99541	Perilipin-2	2
O43157	Plexin-B1	2
P68431	Histone H3.1	2
Q71DI3	Histone H3.2	2
O75610	Left-right determination factor 1	2
P47755	F-actin-capping protein subunit alpha-2	2
Q12904	Aminoacyl tRNA synthase complex-interacting multifunctional protei	2
Q14766	Latent-transforming growth factor beta-binding protein 1	2
O60258	Fibroblast growth factor 17	2
P18065	Insulin-like growth factor-binding protein 2	2
Q00796	Sorbitol dehydrogenase	2
Q02818	Nucleobindin-1	2
Q12841	Follistatin-related protein 1	2
Q92520	Protein FAM3C	2
Q9NRV9	Heme-binding protein 1	2
Q8N302	Angiogenic factor with G patch and FHA domains 1	2
P08195	4F2 cell-surface antigen heavy chain	2

Table A1.15 Real Time PCR Primer Information. List of all primers used in real-time PCR experiments in this thesis with corresponding target, assay identification, and NCBI gene reference.

Target	Assay ID	NCBI Gene Reference
SRY (sex determining region Y)-box 1	Hs01057642_s1	NM_005986.2
alpha-fetoprotein	Hs00173490_m1	NM_001134.1
GATA binding protein 4	Hs00171403_m1	NM_002052.3
T, brachyury homolog (mouse)	Hs00610080_m1	NM_003181.2
GATA binding protein 6	Hs00232018_m1	NM_005257.3
paired box 6	Hs01088112_m1	NM_001127612.1
neurogenic differentiation 1	Hs00159598_m1	NM_002500.2
caudal type homeobox 2	Hs01078080_m1	NM_001265.3
Nanog homeobox	Hs02387400_g1	NM_024865.2
Pou class 5 homeobox 1	Hs00742896_s1	NM_203289.3
Secreted frizzled related protein - 1	Hs00610060_m1	NM_003012.4
Secreted frizzled related protein - 2	Hs00293258_m1	NM_003013.2
Wingless-type MMTV Integration Site Family Member 3A	Hs00263977_m1	NM_033131.3
Goosecoid	Hs00418279_m1	NM_173849.2
Mix paired-like homeobox 1	Hs00430824_g1	NM_031944.1

Table A1.16 shRNA Sequence Information. List of all short hairpin sequences used in transient knockdown experiments in this thesis with corresponding sequence and oligo name shown.

Oligo sequence (5' to 3')	Oligo name
GATCCGGGCCATTTAGATTAGGAATTCAAGAGATTCCTAATCTAAATGGCCCTTTTTTC	sFRP1 shRNA Top
TCGAGAAAAAAGGGCCATTTAGATTAGGAATCTCTTGAATTCCTAATCTAAATGGCCCG	sFRP1 shRNA Bottom
GATCCGCCCACCCGAATCTTGTAGTTCAAGAGACTACAAGATTCGGGTGGGCTTTTTTC	sFRP2 shRNA Top
TCGAGAAAAAAGCCCACCCGAATCTTGTAGTCTCTTGAACTACAAGATTCGGGTGGGCG	sFRP2 shRNA Bottom
GATCCGCTTGAACCGCCAGATCTATTCAAGAGATAGATCTGGCGGTTCAAGCTTTTTTC	Control Top
TCGAGAAAAAAGCTTGAACCGCCAGATCTATCTCTTGAATAGATCTGGCGGTTCAAGCG	Control Bottom

Appendix II

Copyright Permissions

For Molecular and Cellular Proteomics:

http://mcponline.org/site/misc/Copyright_Permission.xhtml

These guidelines apply to the reuse of articles, figures, charts and photos in the ***Journal of Biological Chemistry***, ***Molecular & Cellular Proteomics*** and the ***Journal of Lipid Research***.

For authors reusing their own material:

Authors need **NOT** contact the journal to obtain rights to reuse their own material. They are automatically granted permission to do the following:

- Reuse the article in print collections of their own writing.
- Present a work orally in its entirety.
- Use an article in a thesis and/or dissertation.
- Reproduce an article for use in the author's courses. (If the author is employed by an academic institution, that institution also may reproduce the article for teaching purposes.)
- Reuse a figure, photo and/or table in future commercial and noncommercial works.
- Post a copy of the paper in PDF that you submitted via BenchPress.
    - Only authors who published their papers under the "Author's Choice" option may post the final edited PDFs created by the publisher to their own/departmental/university Web sites.
    - All authors may link to the journal site containing the final edited PDFs created by the publisher.

Please note that authors must include the following citation when using material that appeared in an ASBMB journal:

"This research was originally published in Journal Name. Author(s). Title. *Journal Name*. Year; Vol:pp-pp. © the American Society for Biochemistry and Molecular Biology."

For the Journal of Proteomics:

http://www.blackwellpublishing.com/permis.asp?ref=0962-1075&site=1

Permission to reproduce Wiley journal Content:

Authors - If you wish to reuse your own article (or an amended version of it) in a new publication of which you are the author, editor or co-editor, prior permission is not required (with the usual acknowledgements). However, a formal grant of license can be downloaded free of charge from Rightslink if required.

For Methods in Molecular Biology:

This is a License Agreement between Christopher Hughes ("You") and Springer ("Springer") provided by Copyright Clearance Center ("CCC"). The license consists of your order details, the terms and conditions provided by Springer, and the payment terms and conditions.

All payments must be made in full to CCC. For payment instructions, please see information listed at the bottom of this form.

License Number	2863840437193
License date	Mar 07, 2012
Licensed content publisher	Springer
Licensed content publication	Springer eBook
Licensed content title	De Novo Sequencing Methods in Proteomics
Licensed content author	Christopher Hughes
Licensed content date	Dec 16, 2009
Type of Use	Thesis/Dissertation
Portion	Excerpts
Author of this Springer article	Yes and you are the sole author of the new work
Order reference number	
Title of your thesis / dissertation	Mass Spectrometry-Based Proteomics Analysis of the Matrix Microenvironment in Pluripotent Stem Cell

	Culture
Expected completion date	Apr 2012
Estimated size(pages)	350
Total	0.00 USD
Terms and Conditions	

If you would like to pay for this license now, please remit this license along with your payment made payable to "COPYRIGHT CLEARANCE CENTER" otherwise you will be invoiced within 48 hours of the license date. Payment should be in the form of a check or money order referencing your account number and this invoice number RLNK500734946.
Once you receive your invoice for this order, you may pay your invoice by credit card. Please follow instructions provided at that time.

Make Payment To:
Copyright Clearance Center
Dept 001
P.O. Box 843006
Boston, MA 02284-3006

For suggestions or comments regarding this order, contact RightsLink Customer Support:customercare@copyright.com or +1-877-622-5543 (toll free in the US) or +1-978-646-2777.

Gratis licenses (referencing $0 in the Total field) are free. Please retain this printable license for your reference. No payment is required.

Christopher Hughes

Education

PhD in Biochemistry – University of Western Ontario, London, Canada (Jan 2009 – Current)

Masters of Biochemistry – University of Western Ontario, London, Canada (May 2007 – Jan 2009)

Honors Bachelor of Science – University of Waterloo, Waterloo, Canada (Sept 2002 – May 2007)

Stem Cell Training Course – Stem Cell Technologies, Vancouver, Canada (April 2010)

Quantitative Proteomics Workshop Short Course – ASMS 2009

FT-ICR Mass Spectrometry Workshop Short Course – ASMS 2008

Achievements and Publications

Publications:

Hughes, C.S. *et al.* (2012) Mass Spectrometry-Based Proteomics Analysis of the Matrix Microenvironment in Pluripotent Stem Cell Culture. (In preparation)

Liu, S. and **Hughes, C.S.** (2011) Recent Advances and Special Considerations for the Analysis of Phosphorylated Peptides by LC-ESI-MS/MS. *Current Anal. Chem.* (accepted - in press)

Hughes, C.S. *et al.* (2011) Proteomic analysis of matrices used in the growth of human embryonic stem cells. *Proteomics* (accepted - in press)

Hughes, C.S. and Nuhn, A. *et al.* (2011) Proteomics of human embryonic stem cells. *Proteomics* 11:4, 675-690

Hughes, C. S. *et al.* (2010) Matrigel: A complex protein mixture required for optimal growth of cell culture. *Proteomics* 10:9,1886-1890

Hughes, C.S. *et al.* (2010) De novo sequencing methods in proteomics. *Methods in Mol. Biol.* 604, 105-121

Bendall, S.C., **Hughes, C.S.** *et al.* (2009) An Enhanced Mass Spectrometry Approach Reveals Human Embryonic Stem Cell Growth Factors in Culture. *Mol. Cell. Proteomics.* 8; 3, 421-432

Bendall, S.C. and **Hughes, C.S.** *et al.* (2008) Prevention of amino acid conversion in SILAC experiments with embryonic stem cells. *Mol. Cell. Prot.* 7:9,1587 - 1597

Wu, J., **Hughes, C.S.** *et al.* (2007) High-throughput cytochrome P450 inhibition assays using laser diode thermal desorption-atmospheric pressure chemical ionization-tandem mass spectrometry. *Anal. Chem.* 79:12, 4657 – 4665

Presentations:

Hughes, C.S. *et al.* (2011) – HUPO 2011 – Analysis of Human Embryonic Stem Cell Depositome (Poster Number – P1346)

Hughes, C.S. *et al.* (2011) – ISSCR – Analysis of Human Embryonic Stem Cell Depositome (Poster Number – 2219)

Hughes, C.S. *et al.* (2010) – Canadian National Proteomics Network Conference – Analysis of Human Embryonic Stem Cell Depositome (Poster)

Hughes, C.S. *et al.* (2010) – HUPO 2010 – Matrigel: A complex mixture required for optimal growth of cell culture (Poster)

Hughes, C.S. *et al.* (2010) – HUPO 2010 – Analysis and quantitation of a glycogen synthase kinase-3 knockout embryonic stem cell line to a depth of >3500 proteins (Poster Number)

Hughes, C.S. *et al.* (2009) – ASMS 2009 – Analysis and quantitation of a glycogen synthase kinase-3 knockout embryonic stem cell line to a depth of >3500 proteins (Poster)

Hughes, C.S. *et al.* (2008) – ASMS 2008 – Prevention of amino acid conversion in SILAC experiments with embryonic stem cells (Oral presentation)

Awards:

NSERC Canadian Graduate Scholarship – Doctoral (May 2009 – Current)
NSERC Canadian Graduate Scholarship – Masters (May 2008 – May 2009)
NSERC Undergraduate Research Scholarship – (Jan 2006 – May 2006)
USC Excellence in Teaching Award – (2009, 2011)
Young Investigator Award – HUPO 2010
CSMS Student Travel Award – ASMS 2009

Professional Experience

Apr. - Sept. 2006 **Merck Frosst Canada –** Pointe-Claire, QC

I spent a single work term at Merck Frosst working on the drug metabolism team. My main project while at Merck involved testing and validating a new mass spectrometer ion source based on thermal desorption. I was involved in all aspects of the project from sample and instrument preparation, analysis, interpretation, and manuscript authoring. My work at Merck resulted in a publication: Wu, J. (2007) *Anal. Chem.* 79:12, 4657 – 4665.

Jan. - Apr. 2006 **Radient Technologies Inc. –** Burlington, ON

I spent a single work term at Radient working in the drug purification division. While there I would perform large column (80L) purification and separation of an active drug ingredient from natural sources. I was part of all stages of the process from crude product to purified form. My main duties were running, maintenance, packing of the large columns, and purification post-column.

Sept. 2004 - Sept. 2005 **MDS Sciex –** Concord, ON

I spent two work terms in the demo and projects laboratory department. While at MDS, I worked with all types of MDS Sciex mass spectrometry hardware and software as well as on HPLC hardware from a wide range of manufacturers. I completed a project profiling carcinogenic food dyes found in spices from around the world. As well, I completed another project profiling excipients from analgesic drugs in an attempt to identify counterfeit drugs. Both of these reports have been presented at conferences and are frequently used as sales information for instrumentation. I also acted in a support role providing worldwide technical support on Sciex hardware and software.

Jan. - Apr. 2004 **Agriculture and Agri-Food Canada –** Harrow, ON

While at Agri-food, I worked in the dry beans division. I studied bean plants under various diseased conditions in an attempt to isolate resistant varieties. Inoculated plants were analyzed visually as well as at the DNA level for changes. A secondary project I was part of involved the results of mechanical damage to seedling growth and maturity.